



Die Küste

ARCHIV FÜR FORSCHUNG UND TECHNIK
AN DER NORD- UND OSTSEE

ARCHIVE FOR RESEARCH AND TECHNOLOGY
ON THE NORTH SEA AND BALTIC COAST

Modellierung der Küstengewässer in Deutschland –
Leistungsfähigkeit und Anwendungsbeispiele

Models of Coastal Waters in Germany –
Performance and Application Examples

Die Küste

ARCHIV FÜR FORSCHUNG UND TECHNIK
AN DER NORD- UND OSTSEE

ARCHIVE FOR RESEARCH AND TECHNOLOGY
ON THE NORTH SEA AND BALTIC COAST

MODELS OF COASTAL WATERS IN GERMANY -
PERFORMANCE AND APPLICATION EXAMPLES

Heft 81 · Jahr 2014

Herausgeber: Kuratorium für Forschung im Küsteningenieurwesen

Verlag:
Bundesanstalt für Wasserbau (BAW)
Kußmaulstraße 17, 76187 Karlsruhe
Postfach 21 02 53, 76152 Karlsruhe
Telefon: 0721 9726-0 Telefax: 0721 9726-4540
E-Mail: info@baw.de, www.baw.de
Druck: Bonifatius GmbH

Gefördert durch:



Bundesministerium für
Ernährung, Landwirtschaft
und Verbraucherschutz

aufgrund eines Beschlusses
des Deutschen Bundestages

ISSN 0452-7739
ISBN 978-3-939230-28-1

Die Verfasser sind für den Inhalt der Aufsätze allein verantwortlich. Nachdruck aus dem Inhalt nur mit Genehmigung des Herausgebers gestattet: Kuratorium für Forschung im Küsteningenieurwesen, Geschäftsstelle, Wedeler Landstraße 157, 22559 Hamburg.
Vorsitzender des Kuratoriums: TRDir STEFAN HAUSER, Bundesministerium für Verkehr und digitale Infrastruktur, Robert-Schuman-Platz 1, 53175 Bonn
Geschäftsführer: Dr.-Ing. RAINER LEHFELDT, Wedeler Landstraße 157, 22559 Hamburg
Lektorat: Prof. Dr. JÜRGEN SÜNDERMANN, Universität Hamburg, Bundestraße 53, 20146 Hamburg

Contents

Introduction: Motivation, Objectives, Target

Harro Heyer

- Models of Coastal Waters in Germany –
Performance and Application Examples 1

Existing Data Base

Ralf Weisse, Lidia Gaslikova, Beate Geyer, Nikolaus Groll and Elke Meyer
coastDat – Model Data for Science and Industry 5

Angela Schäfer and Roland Koppe

- The Marine Network of Integrated Data Access and the Data Portal
German Marine Research 19

Rainer Lehfeldt and Johannes Melles

- MDI-DE – German Marine Data Infrastructure 29

Ronny Beyer, Axel Orths and Lothar Neumann

- Data Management Centre of the Federal Waterways and Shipping Agency,
Northern Region Office 45

Oliver Lojek, Knut Krämer, Anna Zorndt, Nils Goseberg and Torsten Schlurmann

- Velocity and Turbulence Measurements at the Ems Barrage 55

Modelling Foundations

Hans Burchard, Ulf Gräbe, Peter Holtermann, Knut Klingbeil and Lars Umlauf

- Turbulence Closure Modelling in Coastal Waters 69

Bert Putzar and Andreas Malcherek

- Modelling of Sediment Transport and Morphodynamics 89

Arne Hammrich and Dagmar Schuster

- Fundamentals on Ecological Modelling in Coastal Waters Including an
Example from the River Elbe 107

Livia Mittelbach, Martin Pohl, Peter Schulze and Heinz Konietzky

- Numerical Simulation of Rip-Rap Revetments in Tidal Areas 119

<i>Emil Stanev and Johannes Schulz-Stellenfleth</i> Methods of Data Assimilation	133
<i>Cordula Berkenbrink and Hans Dieter Niemeyer</i> Analysis of Salinity Alterations due to Estuarine Waterway Deepening by Artificial Neural Networks	153
<i>Anja Brüning and Elimar Precht</i> Statistical Analyses of Metocean Data for Offshore Wind Design in German Waters	167
<i>Marko Kastens</i> Statistical Estuary Data Analysis in Models and Measurements – Some Methods and their Limitations	185
<i>Andreas Schöl, Birte Hein, Jens Wyrwa and Volker Kirchesch</i> Modelling Water Quality in the Elbe and its Estuary – Large Scale and Long Term Applications with Focus on the Oxygen Budget of the Estuary	203
Applied Modelling: Hydrodynamics	
<i>Joanna Staneva, Arno Behrens and Nikolaus Groll</i> Recent Advances in Wave Modelling for the North Sea and German Bight	233
<i>Silvia Maßmann, Frank Janssen, Thorger Brüning, Eckhard Kleine, Hartmut Komo, Inge Menzenhauer-Schumacher and Stephan Dick</i> An Operational Oil Drift Forecasting System for German Coastal Waters	255
<i>Thorger Brüning, Frank Janssen, Eckhard Kleine, Hartmut Komo, Silvia Maßmann, Inge Menzenhauer-Schumacher, Simon Jandt and Stephan Dick</i> Operational Ocean Forecasting for German Coastal Waters	273
<i>Elisabeth Rudolph</i> Storm Surges in the Elbe, Jade-Weser and Ems Estuaries	291
<i>Jana Kristandt, Benedict Brecht, Helmut Frank and Heiko Knaack</i> Optimization of Empirical Storm Surge Forecast – Modelling of High Resolution Wind Fields	301
<i>Mohamed Tayel and Hocine Oumeraci</i> Extreme Storm Surge Prediction Using Hydrodynamic Modelling and Artificial Neural Networks	319

- Guntram Seif*
Hydrodynamic Numerical Models Suitable for Application to the
German Fairways and Ports at the Baltic Sea Coast 343
- Gerald Herrling, Johanna Elsebach and Anne Ritzmann*
Evaluation of Changes in the Tidal Regime of the Ems-Dollard and
Lower Weser Estuaries by Mathematical Modelling 353

Applied Modelling: Sediment Transport

- Manfred Zeiler, Peter Milbradt, Andreas Pliß and Jennifer Valerius*
Modelling Large Scale Sediment Transport in the German Bight (North Sea) 369
- Frank Kösters, Iris Grabemann and Reiner Schubert*
On SPM Dynamics in the Turbidity Maximum Zone of the Weser Estuary 393
- Holger Weilbeer*
Sediment Transport and Sediment Management in the Elbe Estuary 409
- Dennis Oberrecht and Andreas Wurpts*
Impact of Controlled Tidal Barrier Operation on Tidal Dynamics
in the Ems Estuary 427
- Monika Donner and Oliver Stoschek*
Simulation of High Suspended Sediment Concentrations and
Options for a Reduction in the Lower Ems 435
- Dennis Oberrecht and Andreas Wurpts*
Investigations of Rheological Flow Properties Based on Lab Data of
Fluid Mud Samples and an Extended Model Approach 455
- Denise Wehr*
A Numerical Model for Fluid Mud Dynamics in Estuarine Systems –
Overview and Outlook 463

Applied Modelling: Coastal Defense

- Jan-Moritz Müller and Gabriele Gönner*
Recent Developments in Hamburg's Coastal Protection 473
- Ulrich Winkowsky and Birgit Matelski*
Model-Based Verification of Dikes along the West Coast of Schleswig-Holstein 481

<i>Cordula Berkenbrink and Hans Dieter Niemeyer</i> Integrated Design of Sea- and Estuarine Dikes	491
<i>H. Oumeraci, A. Kortenhaus, A. Burzel, M. Naulin, D. R. Dassanayake, J. Jensen, T. Wahl, C. Mudersbach, G. Gönner, S. Thumm, B. Gerkenmeier, P. Fröhle, K.-F. Daemrich, E. Pasche and G. Ujeyl</i> XtremRisK – Integrated Flood Risk Analysis for Extreme Storm Surges at Open Coasts and in Estuaries: Key Results and Lessons Learned	503

The Coast Under Global Change

<i>Arne Arns, Jürgen Jensen and Thomas Wahl</i> A Consistent Return Level Assessment Considering Present Day and Future Mean Sea Level Conditions	525
<i>Anna C. Zornidt and Torsten Schlurmann</i> Investigating Impacts of Climate Change on the Weser Estuary	541
<i>Rita Seiffert and Fred Hesser</i> Investigating Climate Change Impacts and Adaptation Strategies in German Estuaries	551
<i>Hans Dieter Niemeyer, Cordula Berkenbrink, Anne Ritzmann, Heiko Knaack, Andreas Wurpts and Ralf Kaiser</i> Evaluation of Coastal Protection Strategies in Respect of Climate Change Impacts	565

Authorindex	579
--------------------	-----

Models of Coastal Waters in Germany – Performance and Application Examples

Harro Heyer

Foreword

This publication is a contribution to ICHE 2014, the 11th International Conference on Hydrosience and Engineering. “Hydro-Engineering for Environmental Challenges” will be the topic with which the international scientific and professional water-related community assembled at the conference will discuss in Hamburg. In general “hydro-engineering” is regarded as the science and the associated technology of water management, the management of natural systems and of resources influenced by water-related processes. Demand for the design and development of technical and environmental measures for marine, coastal and estuarine systems has been growing worldwide, with a view to meeting and mastering present and future economic needs and environmental challenges. In the recent past, this growing demand has meant that there has also been an increasing need for work on fundamental hydraulic principles, data driven methods, process-oriented computer models and numerical techniques as well as on practical applications. Germany is no exception in this respect. This publication focuses on current research topics relating to the German coastal zone.

The science and technology of “hydro-engineering” is mainly based on natural phenomena. It studies fundamental forces and the dynamics of water bodies as they are influenced by the geometry and roughness of their boundaries. Interaction with the atmosphere above and with the sea bed below dynamic water bodies plays a major role in this scientific field. An improved quantitative understanding of how marine, coastal and estuarine systems function, how they have changed in the past, evolved to their present state and how they can be changed in the future, both by natural processes and by engineering structures, is an important goal of scientific work in Germany. The knowledge and understanding of systems obtained to date are based on observable phenomena, on special tools for data analysis as well as and increasingly on sophisticated numerical models. As there are many scientific institutions in Germany working on topics related to the science and technology of “hydro-engineering”, our country is able to offer a great deal of professional expertise as regards improvements in the validity of methods and tools. Over the last decade in particular, there has been an increasing demand for water related model studies in Germany.

We report in this publication on many efforts to improve fluids-related research on special natural phenomena and on computational aspects of fluid flow, on large- and small-scale hydraulic modelling including monitoring data and, last but not least, about engineering practice for safety and security on the coast.

The science and technology of “hydro-engineering” increasingly incorporates the ideal of “hydromorphology”. This deals with the structure, evolution, and dynamic morphology of hydrologic systems at nearly all spatial and temporal scales and is driven by natural and anthropogenic influences. Hydrologic systems have been transformed for more than a century by human activities that impact water use, land use, and climate. The hydrologic

response of a natural system to specific transformation measures can be monitored directly in terms of water levels, fluid flow and salinity. To date, however, quantifying the exact values of changes in state variables due to the natural variability of coastal systems has remained a problem. One real challenge, therefore, is to predict the hydromorphologic response of the system to anthropogenic impacts. The natural morphodynamics of the system are generally disturbed by human measures. System transformations due to human activities can induce creeping processes affecting the long term natural morphologic evolution of the system. The uncertainty and non-stationarity of coastal systems may therefore increase in times of such transformations.

There are numerous factors which make tidal estuaries extremely complex hydrologic systems: the dilution of sea water with varying fresh water discharges, complex advection and mixing processes, variation of friction in tidal flows affected by different water depths, river training structures and bed roughness as well as varying density fields in the water body influenced by longitudinal and transverse salinity gradients. An increasingly intertwined world economy has resulted in huge growth in ship capacities, not only for oil, but also and mainly for container-shipment around the world. Deeper and wider fairways are needed in coastal regions to accommodate larger vessels. This unavoidable waterborne coastal transport has influenced the hydromorphologic situation of large German estuaries. Human interventions have affected stratification and gravitational circulation processes and have impacted the mass transport of suspended and bed load material as well as the dynamics and location of the turbidity zone. Tidal pumping phenomena have also been intensified due to an increased imbalance in barotropic pressure gradients during flood and ebb current phases. An upstream shift in main dredging areas and the formation of highly concentrated mud suspensions up to fluid mud layers was the byproduct in some areas of German estuaries located at the German Bight. A change in residual tidal processes is often responsible for non-balanced morphological developments. In particular a non-balanced budget of fine sediments in suspension can lead to low oxygen conditions and to a modified distribution of the substrate within the system.

We have learned that human interventions in water systems can cause profound impacts on system dynamics in terms of alterations to nearly all the physical, chemical and biological parameters describing the state of a system. A very important hydro-engineering task today is therefore to advise all stakeholders in water-related projects in the most transparent manner possible. Verified answers to general and special questions are important for planners and also for society as a whole: what is the current system state, which processes have determined this system state, what is the plausible future of the system state in times of increased flooding due to extreme weather conditions and climate change, how will the system-state be changed by economically driven measures, what is the best strategy to improve the system state and to protect against flooding? One overridingly important issue is ensuring that business and environmental stakeholders can remain in contact with each other and continue to discuss issues as equals. Environmental objectives have become, and will continue to become, increasingly important, particularly for policy makers and NGOs. The people who actually live behind coastal protection structures are also forming their own opinions more directly via internet platforms, and this means that the role of public media will gradually decline.

Coastal waters are fundamental natural resources in Germany and all over the world. For many years now, hydro-engineers have been confronted with the major challenge of working on strategies and techniques to protect and improve the environment of coastal water systems. Today, it is of vital importance to society as a whole to retain possession and to achieve sustainable development. The EU Water Framework Directive (2000) and the EU Marine Strategy Framework Directive (2008) were established to this end. These formulate several obligations for the EU Member States with regard to monitoring. The EU implemented the INSPIRE Directive (2007) to facilitate these reporting obligations and to support the development of a European spatial data infrastructure relying on interoperable Web based software components. This has also become a very important task within the realm of hydro-engineering work.

Deep scientific knowledge and technical understanding, combined with specialized skills in discussions and communications as well as transparent state-of-the-art methods and models for the different coastal systems, are needed. This is an extremely demanding task in the field of hydrosience and engineering. This task can best be fulfilled by acting within a national and international collaborative framework.

Harro Heyer
20. Mai 2014

coastDat – Model Data for Science and Industry

Ralf Weisse, Lidia Gaslikova, Beate Geyer, Nikolaus Groll and Elke Meyer

Summary

The coastDat data set is a compilation of regional meteo-marine hindcasts and scenarios of possible future developments derived from numerical models. The core of the data set comprises high-resolution wind, wind wave and tide-surge hindcasts mostly for the North Sea. Other areas progressively become available. Depending on parameter, the hindcast period covers the last five to six decades of years including the most recent ones. The data set was successfully applied for a variety of scientific as well as more practically oriented applications comprising, for example, naval architecture or offshore wind farms. Here the data set and the history leading to its development are briefly described, validation is reviewed, and an overview about recent uses of the data is provided. Eventually access to the data is briefly sketched.

Keywords

coastDat, hindcast, met-ocean data, meteo-marine data, North Sea

Zusammenfassung

Der coastDat Datensatz ist eine Zusammenstellung meteo-mariner Rekonstruktionen und von Szenarierechnungen für die Zukunft, die mit Hilfe numerischer Modelle erstellt wurden. Die Kernstücke des Datensatzes umfassen hoch aufgelöste Wind-, Seegang- und Wasserstandsrekonstruktionen (Hindcasts), die bisher hauptsächlich für die Nordsee entwickelt wurden. Rekonstruktionen und Szenarien für andere Gebiete werden jedoch zunehmend verfügbar und in den Datensatz integriert. Je nach Parameter umfassen die rekonstruierten Zeiträume die letzten etwa 50-60 Jahre. Daten aus coastDat wurden erfolgreich sowohl zur Untersuchung wissenschaftlicher Fragestellungen als auch zur Betrachtung von mehr praxisorientierten Anwendungen z. B. im Schiffbau oder der Offshore Windindustrie eingesetzt. In diesem Beitrag werden der Datensatz und die notwendigen Entwicklungen kurz vorgestellt sowie ein Überblick über Validierungsergebnisse gegeben. Anschließend werden eine kurze Übersicht über derzeit existierende Anwendungen gegeben und die Zugangsmöglichkeiten zu den Daten beschrieben.

Schlagwörter

coastDat, Hindcast, meteo-marine Daten, Nordsee

Contents

1	Introduction	6
2	History	7
3	coastDat-1 and coastDat-2	8

4	Validation	10
5	Applications	12
6	Accessing coastDat.....	13
7	Summary.....	14
8	References	15

1 Introduction

Assessing statistics such as the mean, the variability or the extremes of marine environmental conditions and their long-term changes are essential for both, marine science and a variety of commercial offshore activities. Marine scientists are interested, for example, in the understanding of the processes, their variability and changes. Authorities or industry may need comparable information for planning, designing or maintaining for example, coastal defences or offshore structures. Often data to derive such statistics are unavailable for various reasons. In many cases observational records are too short to cover the full spectrum of time scales. In some cases, sampling in space and time is insufficient or data for the parameters of interest are unavailable. Frequently, longer records are not homogeneous; that is, technical changes, for example in measurement techniques, exist and may introduce artificial variability or spurious trends in the data (e.g. WEISSE and VON STORCH 2009).

The coastDat approach was developed to address such problems. It uses quasi-realistic numerical models of the marine atmosphere, tide-surges or wind waves to optimally exploit existing observations and to reconstruct the marine climate providing detailed hourly descriptions of changing marine environmental conditions from 1948/1958 up to now. Scenarios of potential future developments in a changing climate are also available, complementing the reconstruction of past conditions in a consistent way. For the North Sea, the coastDat approach was developed over more than 10 years and was successfully applied, for example, for providing assessments of the effectiveness of political measures to reduce chronic oil pollutions (e.g. CHRASTANSKY et al. 2009; CHRASTANSKY and CALLIES 2009) or changes in wind (e.g. WEISSE et al. 2005) and storm surge climate (e.g. WEISSE and PLUESS 2006). Industrial applications comprise, for example, uses in ship design, oil risk modelling and assessment, or the construction and operation of offshore wind farms (WEISSE et al. 2009). As of mid-2014 the coastDat data set is used by more than 80 users with about 46 % of them located in industry, 15 % in authorities and 39 % in other research institutes. In the following we briefly introduce this data set. In section 2 some background informations are provided, in particular on how the approach developed over time and the major achievements and milestones eventually leading to the development of coastDat. In section 3 a brief comparison is made between the first version of coastDat (the origins of which are dating back to the late 1990s) and a newer version that is gradually and progressively replacing the first one. Validation aspects are touched in section 4 and in section 5 a brief overview of scientific and more practically oriented applications is given. In section 6 we describe how coastDat data may be located and accessed and in section 7 a short summary and discussion are provided.

2 History

Using numerical models to hindcast or to reconstruct specific events such as an extreme storm or storm surge has a long tradition. The objective of such studies was twofold. In some cases hindcasts were performed to reproduce extreme events that caused severe damages. Examples comprise, for instance, the simulation of the so-called Halloween storm in 1991 (CARDONE et al. 1996) or the simulation of the severe wave conditions causing the abandonment of five yachts in the 1998 Sydney to Hobart yacht race (GREENSLADE 2001). In other cases hindcasts were used to validate the models under extreme conditions (e.g. HOPE et al. 2013; DIETRICH et al. 2009).

In the course of time as models matured and computers became more efficient, hindcasts covering longer periods or a large number of selected extreme events became more popular. The purpose of such studies usually was to generate data bases from which climatologies of environmental conditions in data sparse regions could be derived. In particular for wind waves, the efforts were often driven by demands from naval and offshore (mostly oil) industry and as a consequence many of the studies were classified and unavailable for further research (WEISSE and GÜNTHER 2011). An example of such a study is the seasonal wave climatology for the North Sea based on a wave hindcast of 16 years forced by winds calculated from a quasi-geostrophic model using digitized analyzed surface pressure maps (N.N. 1987).

In the early 1990s there was considerable concern about an intensification of the extra-tropical storm climate and the offshore industry was confronted with reports on waves higher than had ever been observed (WASA 1998). In this atmosphere, the European project WASA (Waves and Storms in the North Atlantic) was inspired and implemented to prove or disprove hypotheses about a worsening storm and wave climate in the North Atlantic (WASA 1998). One approach taken by the project was to *continuously* hindcast waves and surges over more than four decades of year. To our knowledge, this provided the first *multi-decadal* hindcast aiming at assessing *long-term changes*. The project also the first time emphasized the need for homogeneity in multi-decadal hindcasts; that is, in-homogeneities caused, for example, by changes in the observational network or measurement techniques may introduce artificial trends making the hindcasts unsuitable for assessing long-term changes (WASA 1998). For a detailed discussion see e.g. WEISSE and VON STORCH (2009).

A major conclusion from the WASA project was the need for a more homogeneous wind forcing of the storm surge and wave hindcasts that was unavailable at the time the project was running. The situation improved considerably when global atmospheric reanalyses became available at the mid-1990's aiming at providing gridded atmospheric data sets and reducing effects from in-homogeneities. A particular useful product which is still continuously updated was provided by the National Center for Environmental Prediction (NCEP) (KALNAY et al. 1996; KISTLER et al. 2001). In this reanalysis 6-hourly data are available from 1948 onwards until now at about 210 km x 210 km spatial resolution (KALNAY et al. 1996).

While the latter was very useful for studies at the global or continental scale, the spatial and temporal resolution remained too coarse for many regional or smaller scale studies and a number of attempts were therefore undertaken to further downscale global reanalyses. To fully exploit the information contained in the global product, VON STORCH

et al. (2000) proposed a special technique called spectral nudging for dynamically downscaling of global reanalysis. The idea behind the approach is the following: The skill of the global reanalyses is scale dependent with higher confidence in the larger scales supported by data assimilation. Consequently, at larger scales the downscaling solution should be more strongly confined to the global solution while at smaller scales (where added value can be expected) the regional model should be less constrained. The approach is sometimes also referred to as regional data assimilation without observations (VON STORCH et al. 2000). It is nowadays widely used (for an overview see e.g. WEISSE and VON STORCH 2009) and it was demonstrated to provide substantial added value when compared to the standard approach (e.g. WEISSE and FESER 2003; FESER et al. 2011).

The availability of global reanalyses, the development of the spectral nudging technique to improve downscaling, and the need for consistent and high-resolution met-ocean hindcasts paved the way for the set-up of the HIPOCAS (Hindcast of Dynamic Processes of the Oceans and the Coastal Areas of Europe) project in the late 1990's. Based on the aforementioned developments this project, for the first time, aimed at providing a detailed, high-resolution, and consistent met-ocean hindcast for European shelf seas and coastal areas. Typically, hindcasts were performed from 1958-1998 at grids varying from 50 km x 50 km for the atmosphere to about 5 km x 5 km for waves and up to a few hundred metres for storm surges (SOARES et al. 2002). Data were stored every hour, allowing for both, a detailed validation and assessment of long-term changes (e.g. WEISSE and GÜNTHER 2007; CIEŚLIKIEWICZ and PAPLIŃSKA-SWERPEL 2008; MUSIĆ and NICKOVIĆ 2008). As the project terminated, the data set produced became rapidly outdated. Because of existing demands and requests, both from the scientific community and offshore industry, the effort was, for the North Sea, routinely continued and extended at the Helmholtz-Zentrum Geesthacht (HZG) using the model system and techniques implemented during the HIPOCAS project. As the effort became increasingly comprehensive further including scenarios of potential future developments in the course of the expected anthropogenic climate change or hindcasts for the Baltic Sea area, the effort was renamed and continued as coastDat.

The effort was finally terminated around 2007, when model developments and computational efficiency allowed the set-up of a new coastDat-2 system for which the entire period from 1948 until now (presently 2013) is simulated and continuously updated. The original coastDat data set is now referred to as coastDat-1 and still available but no longer updated. In the following the similarities and differences between the two data sets are briefly described.

3 coastDat-1 and coastDat-2

In the following we limit ourselves to the core simulations and data available from both coastDat products; that is, wind, waves and tide-surge hindcasts for the North Sea. Note that additional products are available such as climate change scenarios (e.g. WOTH et al. 2006) and temperature and salinity hindcasts (MEYER et al. 2014) for the North Sea or tide-surge reconstructions for the Baltic Sea (WEIDEMANN 2014). As this list is continuously increasing, an up-to-date-list is maintained the coastDat Website (see section 6 for details).

Both data sets used the National Centers for Environmental Prediction–National Center for Atmospheric Research (NCEP-NCAR) global reanalysis (KALNAY et al. 1996) in combination with spectral nudging (VON STORCH et al. 2000) to first drive a regional atmosphere model (Tab. 1) for an area covering most of Europe and the adjacent seas. For coastDat-1, the regional atmosphere model REMO (JACOB and PODZUN 1997; FESER et al. 2001) at a spatial resolution of approximately 50 km x 50 km was used to hindcast the period 1948-2007. For coastDat-2, this model was replaced by the COSMO model in CLimate Mode (COSMO-CLM) version 4.8_clm_11 (ROCKEL et al. 2008; BALDAUF et al. 2011; STEPELER et al. 2003). Compared to REMO, the COSMO model is a non-hydrostatic operational weather prediction model that is developed and applied by a number of national weather services affiliated in the COnsortium for SMall-scale MOdelling (COSMO). The climate mode of this model is developed and applied by the Climate Limited-area Modelling Community (<http://www.clm-community.eu>). For coastDat-2, the model was run at a spatial resolution of about 24 km x 24 km to hindcast the period 1948-2013. For both, coastDat-1 and coastDat-2 full atmosphere model output was stored every hour. While the production of coastDat-1 terminated in 2007, coastDat-2 is continuously extended and updated.

From the atmospheric simulations in coastDat-1 and coastDat-2, near-surface marine wind fields and atmospheric sea level pressure were used to drive high-resolution wave and tide-surge models (Tab. 1). For the waves, changes in the modelling system from coastDat-1 to coastDat-2 are minor. In both cases the most recent release of the wave model WAM at the time when production started was used. In both cases, the model was run in a nested mode with a coarse grid (approximately 50 km x 50 km) covering most of the Northeast Atlantic and a fine grid (about 5.5 km x 5.5 km) covering the North Sea south of 56N in coastDat-1 and the entire North Sea in coastDat-2. Apart from some technical modifications such as grid restructuring or introducing parallelized code, depth induced wave breaking was introduced in coastDat-2, limiting the wave heights in extreme shallow waters that were sometimes reported too high in coastDat-1. For both, coastDat-1 and coastDat-2 full wave model output was stored every hour. While the production of coastDat-1 terminated in 2007, coastDat-2 is continuously extended and updated.

For tide-surges in coastDat-1 a 2D version of TELEMAC (HERVOUET and HAREN 1996) was used. The model was run on an unstructured grid with typical spatial resolutions of about 5 km in the open North Sea increasing up to about 100 m near the coasts. In coastDat-2, the model was replaced by a 2D version of TRIM-NP (KAPITZA 2008), a nested non-hydrostatic shelf sea model with spatial resolutions increasing from 12.8 km x 12.8 km in the North Atlantic to 1.6 km x 1.6 km in the German Bight. In both cases, the models were forced with amplitudes and phases from a global tidal data set (LYARD et al. 2006). While in coastDat-1 external surges were accounted for by assimilating tide-surge data from Aberdeen, they were explicitly accounted for in coastDat-2 by using boundaries from a coarse grid simulation covering the Northeast Atlantic. For both, coastDat-1 and coastDat-2 full tide-surge model output was stored every hour. While the production of coastDat-1 terminated in 2002, coastDat-2 is continuously extended and updated.

Table 1: Comparison of set-ups and hindcast periods for coastDat-1 and coastDat-2.

Hindcast period	Model (Model Reference; Set-up reference)	Model area	Grid distance	Forcing data
coastDat-1				
1948-2007	REMO (JACOB and PODZUN 1997; FESER et al. 2001)	Western Europe; Adjacent seas	50 x 50 km	NCEP/NCAR reanalysis
1948-2007	WAM (WAMDI 1988; WEISSE and GÜNTHER 2007)	Northeast Atlantic; North Sea south of 56N	50 x 50 km 5.5 x 5.5 km	Near-surface winds from REMO
1958-2002	TELEMAC2D (HERVOUET and HAREN 1996; WEISSE and PLUESS 2006)	North Sea	Unstructured grid from approx. 5 km to 100 m	Near-surface wind and pressure from REMO
coastDat-2				
1948-2013	COSMO-CLM (ROCKEL et al. 2008; GEYER 2014)	Europe; Adjacent seas	24 x 24 km	NCEP/NCAR reanalysis
1948-2013	WAM (WAMDI 1988)	Northeast Atlantic; North Sea	50 x 50 km 5.5 x 5.5 km	Near-surface winds from COSMO-CLM
1948-2013	TRIM-NP (KAPITZA 2008)	Northeast Atlantic; North Sea	12.8 x 12.8 km 6.4 x 6.4 km 3.2 x 3.2 km 1.6 x 1.6 km	Near-surface wind and pressure from COSMO-CLM

4 Validation

Validation of wind, tide-surge and waves from coastDat-1 are comprehensively described in the peer-reviewed literature. WEISSE et al. (2005) compared wind speed percentiles and storm counts derived from North Sea station data with data obtained from coastDat-1 and generally found a good agreement for both, average conditions and variability. Similar results for tide-surges and wind waves are inferred and described in WEISSE and PLUESS (2006) and WEISSE and GÜNTHER (2007). In particular WEISSE and PLUESS (2006) showed that high water levels and surges are reasonably reproduced while a tendency to overestimate the lowest water levels was reported. WEISSE and GÜNTHER (2007) in general demonstrated a good agreement between observed and modelled wave parameters but found the highest waves to be somewhat overestimated in very shallow areas where bathymetry effects could not adequately be resolved by the model, a finding also confirmed in GASLIKOVA and WEISSE (2006). Both WEISSE and PLUESS (2006) and

WEISSE and GÜNTHER (2007) found the interannual and decadal variability to be reasonably reproduced within coastDat-1. Using both, in-situ wind speed measurements from a series of buoys and wind speeds derived from different satellite products WINTERFELDT et al. (2011, 2010) and WINTERFELDT and WEISSE (2009) assessed the added value of coastDat-1 compared to the driving global NCEP/NCAR reanalysis and found that wind speeds from coastDat-1 are improved, in particular in coastal areas and along coastlines with complex orography.

Since data from coastDat-2 are relatively new, less comprehensive results for validation are available so far. Validation of the atmospheric hindcast is described in GEYER (2014) focusing mostly on the validation of near-surface temperatures and precipitation. For near-surface wind speeds GEYER (2014) compared results from coastDat-2 with observations from two buoys confirming the good offshore quality of coastDat-2 wind fields and the findings of WINTERFELDT et al. (2011) regarding the added value of coastDat.

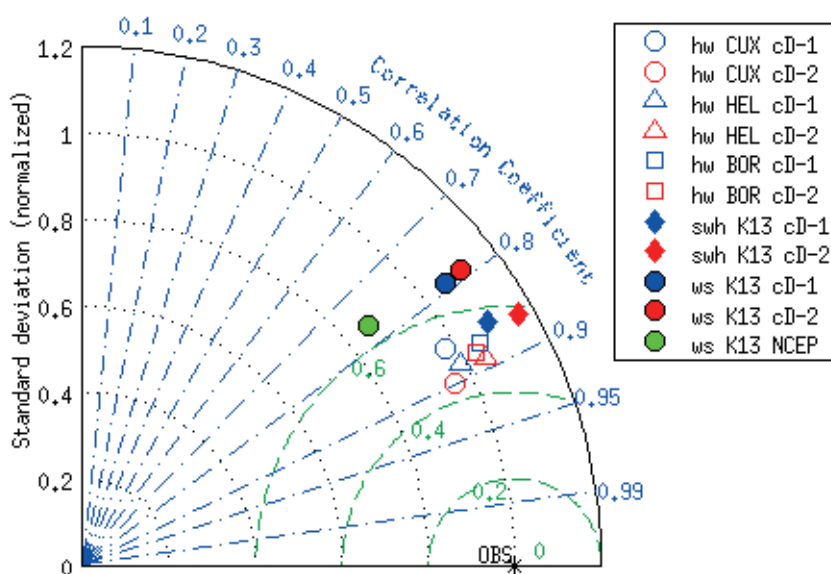


Figure 1: Taylor diagram for wind speed (filled circles) and significant wave height (filled diamonds) at platform K13 as well as for high water levels at Cuxhaven (open circles), Helgoland (open triangles) and Borkum (open squares) for 2000-2002 comparing results from coastDat-1 (blue) and coastDat-2 (red) with observations. For wind speed, also a comparison with the driving global NCEP reanalysis is shown (green). The black star denotes the location of a data set that would perfectly match observations.

Fig. 1 shows some additional validation of wind speed, significant wave heights and tide-surges from coastDat-2. The so-called Taylor diagram shows a comparison of validation statistics between modelled and measured data in terms of correlation (blue lines), centered root mean square error (green lines) and standard deviation (black lines). The latter two are normalized by the standard deviation of the corresponding observational datasets. In general, correlations between hindcast and modelled data vary between about 0.8 for wind speeds and 0.9 for high water levels for both, coastDat-1 and coastDat-2.

Centered root mean square errors range from about 0.4 for tide-surges to 0.6 for wave heights and they are somewhat larger for wind speeds. For high water levels, the standard deviation of the modelled data is close to the observed values, while for wave height and wind speed it appears to be somewhat larger with a tendency towards higher values in coastDat-2. Generally, however, both versions of coastDat are hardly distinguishable in the diagram indicating comparable qualities. The added value of the coastDat approach is further illustrated by a comparison with wind speeds derived directly from the driving global NCEP reanalysis which show too small variability compared to observations.

5 Applications

Being available for more than 15 years, coastDat was used in a large variety of scientific and more practically oriented applications. While quite different in detail, all applications require long, consistent and mostly homogeneous time series.

A substantial fraction of studies is related to long-term changes in marine environmental conditions. For example, WEISSE et al. (2005) studied the variability and long-term trends in storm activity over the Northeast Atlantic and Northern Europe. Similarly, changes in the frequency of polar lows (ZAHN et al. 2008) or tropical cyclones (BARCIKOWSKA et al. 2012) were studied. Changes and variability in storm surge and wind wave climate were addressed, for example, in WEISSE and PLUESS (2006), GASLIKOVA and WEISSE (2006), or WEISSE and GÜNTHER (2007) while MEYER et al. (2011) studied thermodynamic variability and change. Future changes in storm surge and wind wave climate were considered, for example, in WOTH et al. (2006) and GRABEMANN and WEISSE (2008).

The coastDat data set was also used extensively to investigate methodical aspects of the approach. For example, the review provided by FESER et al. (2011) summarizes the findings from a number of studies analysing the added value of the dynamical downscaling. Moreover, KRUEGER and VON STORCH (2011, 2012) used the data base to systematically investigate the informational content of proxy based indicators for storm activity and FESER and VON STORCH (2008) systematically assessed the performance of the spectral nudging approach for the case of typhoons in Southeast Asia.

There are also some studies dealing with different aspects of risk assessment. For example, CHRASTANSKY and CALLIES (2009) coupled a Lagrangeian transport and an oil chemistry module with coastDat. By assuming a constant frequency of oil releases, a large number of simulations (hypothetical oil spills) at different locations was initialized with constant time lags (28 h) between them. Subdividing the German North Sea coast into a couple of receptor regions, results provided a proper description of both the mean risk exposure of different coastal areas and corresponding variability. CHRASTANSKY et al. (2009) were successful in using these data for a more in-depth interpretation of monitoring data. CHRASTANSKY and CALLIES (2009) summarized the results in terms of probabilistic relationships that describe spatial dependences and sensitivities between parameters addressed in the study. Coupling storm surges from coastDat with a loss model, GASLIKOVA et al. (2011) investigated future storm surge impacts on insurable losses for the North Sea region. Superimposing different mean sea level changes GASLIKOVA et al. (2011) found a nonlinear response at the country level, as the future storm surge changes were found to be higher for Germany and Denmark emphasizing the necessity to assess

the socio-economic impacts of coastal flooding by combining expected sea level rise with storm surge projections.

Data from coastDat were also used for addressing questions related to the use of renewable marine energy. For example, WIESE (2008) used data from coastDat to simulate the impacts of offshore wind production on the national grid for a scenario in which all planned offshore wind farms in the German exclusive economic zone in the North Sea are fully operational. MARX (2010) analyzed long-term variability of the wave energy potential in the North Sea and the report by BÖMER et al. (2012) contains a description of the theoretical potential from various sources based on coastDat.

Data from coastDat have been used extensively for example for designing, planning and installation of offshore wind farms. Return periods of extreme wind speed, surge and wave heights are used by a variety of users involved in the design and construction of offshore wind parks. Moreover, planning of installation and maintenance requires the estimation of probabilities of fair weather windows; that is, for example the probability of an extended period with wave heights below a given threshold to enable installation and/or maintenance. Data from coastDat were frequently used in such cases as observational data are too often too short to derive reliable statistics. Other examples comprise the use in naval architecture or coastal protection and adaptation. For a more detailed description we refer to the summary provided in WEISSE et al. (2009).

6 Accessing coastDat

The unique entry point for accessing coastDat data is the central coastDat webpage <http://www.coastdat.de> from which all data sets in coastDat-1 and coastDat-2 are locatable. For some of the more frequently used and requested data online access was realized that can be reached from the central coastDat webpage. Physically these data are stored at the World Data Center for Climate (WDCC) in Hamburg and the online access is generally realized via their CERA data interface. Each of the data sets was assigned with a unique doi simplifying referencing and identification of data sets. Fig. 2 shows an example of the usage of the online data access by external users. It illustrates that the access is increasingly used and that, in terms of volume and counts, coastDat-1 and coastDat-2 in total are among the top products downloaded from the WDCC.

Additionally, an interface allowing for a visualisation of the gridded model data is available at <http://vis.coastdat.de>. Initially, parameters such as wind speed, significant wave height, currents and water levels were introduced at hourly resolution so that visualization or animation of extreme events such as storms or storm surges is possible. Simple statistics such as monthly maximum wind speed or seasonal cycles are also available.

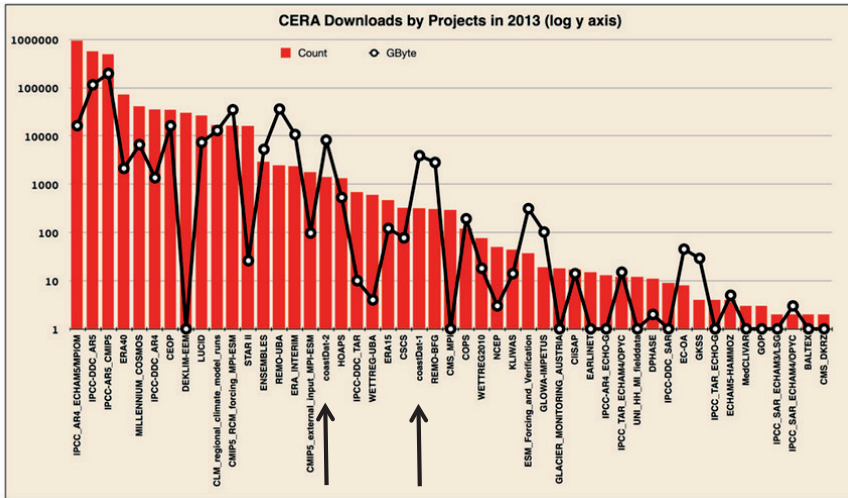


Figure 2: Downloads in 2013 from major products and data bases available from the CERA data base at the World Data Center for Climate.

7 Summary

The coastDat data base, its development and validation together with a brief summary of recent uses were briefly described. Data from coastDat were successfully used for both, research and more practically oriented questions sharing similar data needs. Both require long, consistent and homogeneous data sets to derive statistics such as the mean, the variability or the extremes of marine environmental conditions and their long-term changes. Frequently such data are unavailable and the approach described here provides one possibility to address such issues.

The need and the success of both, the approach and data base derived are illustrated by the large number and variety of users applying coastDat for their own research or practical questions. As of mid-2014, there are presently about 80 external registered users with about 45 % of them coming from the industrial sector while about 40 % are from academic and 15 % from authorities. Added values derived are manifold, ranging from assessments of long-term changes to improvements in ship designs, risk assessments, or planning of logistics for offshore wind farms.

Climate information plays a crucial role for many purposes and the dissemination of climate information to the public or a specific user is often referred to as climate services (http://www.wmo.int/pages/themes/climate/climate_services.php – last accessed: 23.05.2014). Implicitly such services are associated with atmospheric parameters such as temperature or precipitation from scenarios of future developments in the course of anthropogenic climate change. Related parameters such as storm surges or wind waves as well as recent climate and climate variability traditionally receive less attention. Based on our experiences and on feedbacks from users it is concluded that hindcasts of past decades of years and derived products such as waves or surges are just as important. While scenarios are mostly important for sectors planning for long time horizons (e.g. coastal protection, policy regulations), hindcasts are more often requested from sectors planning

for shorter periods or operating in data sparse regions (e.g. offshore wind, naval architecture). So far the latter is frequently unaccounted for from climate service perspectives and we proposed that their value may be substantially enhanced taking shorter time scales and natural climate variability into account.

8 References

- BALDAUF, M.; SEIFERT, A.; FÖRSTNER, J.; MAJEWSKI, D.; RASCHENDORFER, M. and REINHARDT, T.: Operational Convective-Scale Numerical Weather Prediction with the COSMO Model: Description and Sensitivities. *Mon. Weather Rev.*, 139, 3887-3905, doi:10.1175 / MWR-D-10-05013.1, 2011.
- BARCIKOWSKA, M.; FESER, F. and VON STORCH, H.: Usability of best track data in climate statistics in the western North Pacific *Mon. Weather Rev.*, 140, 2818–2830, doi:10.1175/MWR-D-11-00175.1, 2012.
- BÖMER, J.; BRODERSEN, N.; HUNKE, D.; SCHÜLER, V.; GÜNTHER, H.; WEISSE, R.; FISCHER, J.; SCHÄFFER, M. and GABNER, H.: Ocean Energy in Germany, Final Rep. Project number PPSMDE082434, Federal Ministry for the Environment, Nature Conservation and Nuclear Safety, 2012.
- CARDONE, V.; JENSEN, R.; RESIO, T.; SWAIL, V. and COX, A.: Evaluation of Contemporary Ocean Wave Models in Rare Extreme Events: The "Halloween Storm" of October 1991 and the "Storm of the Century" of March 1993. *J. Atmos. Oceanic Technol.*, 13, 198-230, 1996.
- CHRASTANSKY, A. and CALLIES, U.: Model-based long-term reconstruction of weather-driven variations in chronic oil pollution along the German North Sea coast. *Marine Pollution Bulletin*, 58, 967-975, doi:10.1016/j.marpolbul.2009.03.009, 2009.
- CHRASTANSKY, A.; CALLIES, U. and FLEET, D.M.: Estimation of the impact of prevailing weather conditions on the occurrence of oil-contaminated dead birds on the German North Sea coast. *Environmental Pollution*, 157, 194-198, doi:10.1016/j.envpol.2008.07.004, 2009.
- CIEŚLIKIEWICZ, W. and PAPLIŃSKA-SWERPEL, B.: A 44-year hindcast of wind wave fields over the Baltic Sea, *Coastal Engineering*, 55, 894-905, doi:10.1016/j.coastaleng.2008.02.017, 2008.
- DIETRICH, J.C.; WESTERINK, J.J.; KENNEDY, A.B.; SMITH, J.M.; JENSEN, R.E.; ZIJLEMA, M.; HOLTHUIJSEN, L.H.; DAWSON, C.; LUETTICH JR., R.A.; POWELL, M.D.; CARDONE, V.J.; COX, A.T.; STONE, G.W.; POURTAHERI, H.; HOPE, M.E.; TANAKA, S.; WESTERINK, L.G.; WESTERINK, H.J. and Cobell, Z.: Hurricane Gustav (2008) waves and storm surge: hindcast, synoptic analysis, and validation in southern Louisiana. *Mon. Weather Rev.*, 139, 2488-2522, doi:10.1175/2011MWR3611.1, 2011.
- FESER, F.; ROCKEL, B.; VON STORCH, H.; WINTERFELDT, J. and ZAHN, M.: Regional Climate Models add Value to Global Model Data: A Review and selected Examples. *Bull. Amer. Meteor. Soc.*, 92, 1181-1192, doi:10.1175/2011BAMS3061.1, 2011.
- FESER, F. and VON STORCH, H.: Regional modelling of the western Pacific typhoon season 2004, *Meteorolog. Z.*, 17, 519-528, 2008.

- FESER, F.; WEISSE, R. and VON STORCH, H.: Multi-decadal Atmospheric Modeling for Europe Yields Multi-purpose Data. EOS, Transactions American Geophysical Union, 82, 305+310, 2001.
- GASLIKOVA, L.; SCHWERZMANN, A.; RAIBLE, C. and STOCKER, T.: Future storm surge impacts on insurable losses for the North Sea region. Nat. Hazards Earth Syst. Sci., 11, doi:10.5194/nhess-11-1205-2011, 2011.
- GASLIKOVA, L. and WEISSE, R.: Estimating near-shore wave statistics from regional hindcasts using downscaling techniques. Ocean Dynamics, 56, 26-35, 2006.
- GEYER, B.: High-resolution atmospheric reconstruction for Europe 1948–2012: coast-Dat2. Earth Syst. Sci. Data, 6, 147-164, 2014.
- GRABEMANN, I. and WEISSE, R.: Climate change impact on extreme wave conditions in the North Sea: an ensemble study. Ocean Dynamics, 58, 199-212, 2008.
- GREENSLADE, D.: A Wave Modelling Study of the 1998 Sydney to Hobart Yacht Race. Aust. Met. Mag., 50, 53-63, 2001.
- HERVOUET J. and HAREN L.V.: TELEMAC2D Version 3.0 Principle Note. Rapport EDF HE-4394052B, Electricité de France, Département Laboratoire National d'Hydraulique, Chatou CEDEX, 1996.
- HOPE, M.E.; WESTERINK, J.J.; KENNEDY, A.B.; KERR, P.C.; DIETRICH, J.C.; DAWSON, C.; BENDER, C.; SMITH, J.M.; JENSEN, R.E.; ZIJLEMA, M.; HOLTHUIJSEN, L.H.; LUETTICH JR., R.A.; POWELL, M.D.; CARDONE, V.J.; COX, A.T.; POURTAHERI, H.; ROBERTS, H.J.; ATKINSON, J.H.; TANAKA, S.; WESTERINK, H.J. and WESTERINK, L.G.: Hindcast and validation of Hurricane Ike (2008) waves, forerunner, and storm surge. J. Geophys. Res., 118, 4424-4460, doi:10.1002/jgrc.20314, 2013.
- JACOB, D. and PODZUN, R.: Sensitivity studies with the regional climate model REMO. Meteorol. Atmos. Phys., 63, 119-129, 1997.
- KALNAY, E.; KANAMITSU, M.; KISTLER, R.; COLLINS, W.; DEAVEN, D.; GANDIN, L.; IREDELL, M.; SAHA, S.; WHITE, G.; WOOLLEN, J.; ZHU, Y.; CHELLIAH, M.; EBISUZAKI, W.; HIGGINS, W.; JANOWIAK, J.; MO, K.; ROPELEWSKI, C.; WANG, J.; LEETMAA, A.; REYNOLDS, R.; JENNE, R. and JOSEPH, D.: The NCEP/NCAR Reanalysis Project. Bull. Amer. Meteor. Soc., 77, 437-471, 1996.
- KAPITZA, H.: Mops - a morphodynamical prediction system on cluster computers. In: High performance computing for computational science - VECPAR 2008, Laginha, J. M.; Palma, M.; Amestoy, P.R.; Dayde, M.; Mattoso, M. and Lopez J. (Eds.), 63-68. Lecture Notes in Computer Science, Springer Verlag, 2008
- KISTLER, R.; KALNAY, E.; COLLINS, W.; SAHA, S.; WHITE, G.; WOLLEN, J.; CHELLIAH, M.; EBISUZAKI, W.; KANAMITSU, M.; KOUSKY, V.; VAN DEN DOOL, H.; JENNE, R. and FIORIONO, M.: The NCEP/NCAR 50-year Reanalysis: Monthly means CD-ROM and documentation. Bull. Amer. Meteor. Soc., 82, 247-267, 2001.
- KRUEGER, O. and VON STORCH, H.: The Informational Value of Pressure-Based Single-Station Proxies for Storm Activity. J. Atmos. Oceanic Technol., 29, 569-580, doi:10.1175/JTECH-D-11-00163.1, 2012.
- KRUEGER, O. and VON STORCH, H.: Evaluation of an Air Pressure-Based Proxy for Storm Activity. J. Climate, 24, 2612-2619. doi:10.1175/2011JCLI3913.1, 2011.
- LYARD F.; LEFEVRE F.; LETELLIER T. and FRANCIS, O.: Modelling the global ocean tides: modern insights from FES2004. Ocean Dynamics, 56, 394-415, 2006.

- MARX, J.: Langzeitige Variabilität des Wellenenergiepotenzials in der Nordsee, Master Thesis, Univ. Basel, Institut für Physiogeographie und Umweltwandel, Basel, 2010.
- MEYER, E.; POHLMANN, T. and WEISSE, R.: Thermodynamic variability and change in the North Sea (1948-2007) derived from a multidecadal hindcast. *Journal of Marine Systems*, 86, 35-44, 2011.
- MUSIĆ, S. and NICKOVIĆ, S.: 44-year wave hindcast for the Eastern Mediterranean, *Coastal Engineering*, 55, 872-880, doi:10.1016/j.coastaleng.2008.02.024, 2008.
- N. N.: Seasonal Climatology for the North Sea, Allied Naval Engineering Publication, ANEP 14, NATO International Staff, Defence Support Division, 1987.
- ROCKEL, B.; Will, A. and Hense, A. 2008: The Regional Climate Model COSMO-CLM (CCLM), *Meteorol. Z.*, 17, 347-348.
- SOARES, C.; WEISSE, R.; CARRETERO, J. and ALVAREZ, E.: A 40 years hindcast of wind, sea level and waves in European Waters. Proc. 21st International Conference on Offshore Mechanics and Arctic Engineering, 23-28 June 2002, Norway, Oslo, 2002
- STEPPELER, J.; DOMS, G.; SCHÄTTLER, U.; BITZER, H.; GASSMANN, A.; DAMRATH, U. and GREGORIC, G.: Meso-gamma scale forecasts using the nonhydrostatic model LM. *Meteorol. Atmos. Phys.*, 82, 75-96, doi:10.1007/s00703-001-0592-9, 2003.
- VON STORCH, H.; LANGENBERG, H. and FESER, F.: A Spectral Nudging Technique for Dynamical Downscaling Purposes. *Mon. Weather Rev.*, 128, 3664-3673, 2000.
- WAMDI-Group: The WAM Model – a Third Generation Ocean Wave Prediction Model. *J. Phys. Oceanogr.*, 18, 1776-1810, 1988.
- WASA-Group: Changing waves and storms in the Northeast Atlantic? *Bull. Amer. Meteor. Soc.*, 79, 741-760, 1998.
- WEIDEMANN, H.: Klimatologie der Ostseewasserstände: Eine Rekonstruktion 1948-2011. PhD Thesis, Universität Hamburg, 2014.
- WEISSE, R. and GÜNTHER, H.: Wave Hindcasting. In: Soares, C.; Garbatov, Y.; Fonseca, N. and Teixeira, A. (Eds.), *Marine Technology and Engineering*, Taylor & Francis Group, London, 2011, 1, 279-285, 2011.
- WEISSE, R.; VON STORCH, H.; CALLIES, U.; CHRASTANSKY, A.; FESER, F.; GRABEMANN, I.; GÜNTHER, H.; PLUESS, A.; STOYE, T.; TELLKAMP, J.; WINTERFELDT, J. and WOTH, K.: Regional Meteorological-Marine Reanalyses and Climate Change Projections: Results for Northern Europe and Potential for Coastal and Offshore Applications. *Bull. Amer. Meteor. Soc.*, 90, 849-860, 2009.
- WEISSE, R. and VON STORCH, H.: Marine Climate and Climate Change. Storms, Wind Waves and Storm Surges. Springer Praxis, 219pp, doi: 10.1007/978-3-540-68491-6, 2009.
- WEISSE, R. and PLUESS, A.: Storm-related sea level variations along the North Sea coast as simulated by a high-resolution model 1958-2002. *Ocean Dynamics*, 56, 16-25, 2006.
- WEISSE, R. and GÜNTHER, H.: Wave climate and long-term changes for the Southern North Sea obtained from a high-resolution hindcast 1958-2002. *Ocean Dynamics*, 57, 161-172, 2007.
- WEISSE, R.; VON STORCH, H. and FESER, F.: Northeast Atlantic and North Sea storminess as simulated by a regional climate model during 1958-2001 and comparison with observations *Journal of Climate*, 18, 465-479, 2005.

- WEISSE, R. and FESER, F.: Evaluation of a method to reduce uncertainty in wind hindcasts performed with regional atmosphere models. *Coastal Engineering*, 48, 211-225, 2003.
- WIESE, F.: Auswirkungen der Offshore-Windenergie auf den Betrieb von Kohlekraftwerken in Brunsbüttel. Master Thesis, Universität und Fachhochschule Flensburg, Energie- und Umweltmanagement, Flensburg, 2008.
- WINTERFELDT, J.; GEYER, B. and WEISSE, R.: Using QuikSCAT in the added value assessment of dynamically downscaled wind speed. *International Journal of Climatology*, 31, 1028-1039, 2011.
- WINTERFELDT, J.; ANDERSSON, A.; KLEPP, C.; BAKAN, S. and WEISSE, R.: Comparison of HOAPS, QuikSCAT, and Buoy Wind Speed in the Eastern North Atlantic and the North Sea. *IEEE Transactions on Geoscience and Remote Sensing*, 48, 338-348, 2010.
- WINTERFELDT, J. and WEISSE, R.: Assessment of Value Added for Surface Marine Wind Speed Obtained from Two Regional Climate Models. *Mon. Weather Rev.*, 137, 2955-2965, 2009.
- WOTH, K.; WEISSE, R. and VON STORCH, H.: Climate change and North Sea storm surge extremes: an ensemble study of storm surge extremes expected in a changed climate projected by four different regional climate models. *Ocean Dynamics*, 56, 3-15, 2006.
- ZAHN, M.; VON STORCH, H. and BAKAN, S.: Climate mode simulation of North Atlantic polar lows in a limited area model *Tellus A*, 60, 620-631, 2008.

The Marine Network of Integrated Data Access and the Data Portal German Marine Research

Angela Schäfer and Roland Koppe

Summary

The linkage of data beyond disciplinary boundaries is essential for marine research. Sufficient national and international data infrastructures are fundamental for central and easy access to the variety of existing, but distributed datasets in marine science. The Marine Network for Integrated Data Access (MaNIDA) provides a national networked approach in accessing and mining of federated marine research data infrastructures together with data management strategies and data workflows. In that course the MaNIDA consortium conceptualized and developed the “Data Portal German Marine Research” for coherent discovery, view, download and dissemination of scientific data and publications. The data portal is based on a central harvesting and interfacing approach by connecting distributed data sources. Here we inform about the specific details of the portal in terms of content, functionality, services, architecture, interfaces, standards and the contributing data providers.

Keywords

data infrastructures, data portal, marine research data, data access, data retrieval, portal architecture, standards, interfaces, web services, data providers, data management, data workflows, data publication, data citation

Zusammenfassung

Für die marine Forschung ist die Verknüpfung von interdisziplinären Daten essentiell. Um dahingehend einen zentralen und leichten Zugriff auf die existierenden und vielfältigen, jedoch verteilten Daten der marinen Forschung zu ermöglichen, sind gut funktionierende nationale und internationale Infrastrukturen fundamental wichtig.

In diesem Sinne entwickelt das “Marine Network for Integrated Data Access” (MaNIDA) einen nationalen und vernetzten Ansatz für die Auffindbarkeit und den Zugriff auf verteilte marine Forschungsdateninfrastrukturen mit entsprechenden Datenmanagementstrategien und Arbeitsabläufen. Um sowohl eine kohärente Datenauffindbarkeit, Visualisierung und einen einfachen Datenzugriff als auch die Veröffentlichung von wissenschaftlichen Daten und Publikationen zu ermöglichen, entwickelt das MaNIDA-Konsortium das zentrale „Datenportal Deutsche Meeresforschung“. Durch ein zentrales, automatisiertes Harvesting-Verfahren und standardisierte Schnittstellen verknüpft dieses Datenportal unterschiedliche und verteilte Datenquellen. In diesem Artikel werden sowohl die speziellen Aspekte des Portals zum Thema Inhalte, Funktionalität, Dienste, Architektur, Schnittstellen und Standards als auch die beitragenden Datenanbieter vorgestellt.

Schlagwörter

Dateninfrastruktur, Datenportal, marine Forschungsdaten, Datenzugriff, Datenabfrage, Portalarchitektur, Standards, Schnittstellen, Webdienste, Datenanbieter, Datenprovider, Datenmanagement, Datenarbeitsabläufe, Datenpublikation, Datenzitierbarkeit

Contents

1	Introduction	20
2	The MaNIDA Consortium	21
2.1	Development of data workflows and data curation.....	22
3	The Data Portal German Marine Research	23
3.1	Content and functionalities	23
3.2	Value-added services	24
3.3	Data providers	24
3.4	Architecture.....	25
3.5	Interfaces and standards	26
3.6	Terms of data access and good scientific practice.....	27
4	Acknowledgement	27
5	References	27

1 Introduction

In earth system research major achievements in scientific knowledge increasingly depend on the availability of data. Especially the linkage of data beyond disciplinary boundaries is essential for global change research. Major observations and new insights on global environmental change can only be obtained if data is collected over long periods and with easy access in a coherent manner. Compared to other fields of research (astronomy, high-energy physics, genetics) neither sufficient national nor international data infrastructure exists that enables central and easy access to the variety of existing, but distributed datasets in marine science.

The Marine Network for Integrated Data Access (MANIDA 2014), co-financed by the Helmholtz Association and several participating marine research institutes and universities in Germany, provides a networked approach in accessing and mining of federated marine research data infrastructures together with management strategies targeting long-term sustainability. The network aims to create a new paradigm in respect to integration, harmonization and aggregation of quality-controlled marine research data and related data products.

One of the main tasks of MaNIDA is the implementation and maintenance of a sustainable e-infrastructure for coherent discovery, view, download and dissemination of scientific data and publications in the form of a central data portal – the DATA PORTAL GERMAN MARINE RESEARCH (2014). For the first time a large amount of marine research datasets from nationally operated research platforms and monitoring facilities are made searchable and accessible through a single portal.

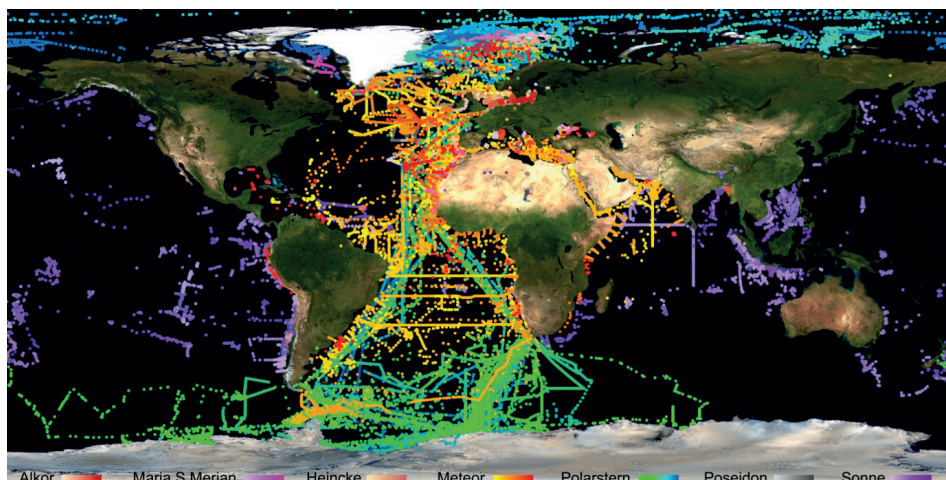


Figure 1: Recent status of sampling stations and cruises by major German research vessels (source PANGAEA 2013).

2 The MaNIDA Consortium

The Marine Network for Integrated Data Access started in February 2012 as an Impulse and Networking Fund project financed cooperatively by the Helmholtz Association and the partner institutions. Currently the consortium consists of five partner institutions and two associated universities that are engaged in marine research and in establishing research data infrastructures. The initial partners are:

- AWI – Alfred-Wegener-Institut, Helmholtz-Zentrum für Polar- und Meeresforschung, Bremerhaven
- MARUM – Zentrum für Marine Umweltwissenschaften, Universität Bremen
- BSH – Bundesamt für Seeschifffahrt und Hydrographie, Hamburg und Rostock-Warnemünde
- GEOMAR – Helmholtz-Zentrum für Ozeanforschung Kiel
- HZG – Helmholtz-Zentrum Geesthacht, Zentrum für Material- und Küstenforschung GmbH
- CAU – Christian-Albrechts-Universität zu Kiel, Institut für Informatik (associated)
- UHH – Universität Hamburg, Leitstelle Deutsche Forschungsschiffe (associated)

MaNIDA and the “Data Portal German Marine Research” are coordinated by the Alfred Wegener Institute. A steering committee and several cross-partner working groups (comprising more than twenty scientific staff members mainly by own resources) have been installed. They are working jointly on data workflows, harmonization, standards, technical concepts and the practical implementation of the central data portal, interfaces and the structural adaption of the participating distributed data providers.

After the initial phase ending in July 2014 the MaNIDA consortium is open to integrate additional national partner institutions that are willing to engage in establishing joint research data workflows, standards and a common e-infrastructure for marine research data.

2.1 Development of data workflows and data curation

Central search and access to marine research data will only work out in a satisfying manner if data contents are well provided and made accessible in a reliable and re-usable way. Therefore MaNIDA not only focuses on technical solutions alone but on developing data relevant workflows and curation procedures for scientific data as well. This approach comprises

- validated expedition and campaign information on German research vessels and platforms,
- archived, quality controlled primary data, near real time data and data products,
- persistent citability and re-usability of data and
- scientific publications and reports.

In order to achieve these intentions the cross-partner working groups of MaNIDA are also involved in the generation of outlines for best practices in terms of data validation, archival and dissemination of marine research data as well as proposals for decision-makers und committees for marine research infrastructures.

In the long run additional benefit for the research community will be improved procedures for data ingestion, data quality assurance and user support, thereby achieving substantial enhancements in the lifecycle management of marine scientific data. Explicitly, the creation of a Data Curation Center is planned for the next project phase along with the implementation of technical and organizational structures and ways to sustain the infrastructure financially. The main tasks for a joint Data Curation Center for marine research data are:

- support of workflows and user support,
- contact point and editorial system for standardized vocabularies and ontologies and
- structured data management.

In that term MaNIDA reaches out to stakeholders in the academic sector and government agencies so as to create acceptable and reliable workflows.



Figure 2: Simplified workflow schema for well curated research data.

The work of MaNIDA and the central data portal does not only enhance data mining in various disciplines and improve planning of future expeditions, via easy identification of missing data, but also provides means for combining various data types (underway data, post cruise data, satellite gridded products, modeling data, etc.) into enhanced data products.

Hence cross-partner working groups have been established by members according to their expertise as they are involved in the following topics:

- Data portal architecture, interfaces and implementation towards international standards and requirements for participating data providers
- Expedition catalogue – centrally maintained for up-to-date and past expeditions' metadata linked to research data and publications

- Underway data – validation and harmonization via an improved data acquisition and information system (DSHIP 2014) for recording of technical, nautical and scientific data taken at sea on board of all major German research vessels
- Cruise Summary Reports – semi-automated generation and interfacing via DSHIP for national data providers and international alignment of major German research vessels and platforms
- Vocabularies, ontologies, quality assurance – harmonization and establishment of international standards
- Joint data curation center and ticketing system – requirements, concept and establishment
- Adequate handling of marine research data – joint data policies and data management plans

3 The Data Portal German Marine Research

3.1 Content and functionalities

The “Data Portal German Marine Research” offers an integrative “one-stop-shop” framework for coherent discovery, view, download and dissemination of marine research data (research vessels, observatories, gliders, etc.). Its content originates from distinct data and publication repositories offered by the German marine research partner institutions. As Figure 3 illustrates, the portal integrates cruise-related metadata (expeditions), reports, publications, archived data and near real time data as well as data products of the whole marine and earth science community of Germany and their international projects. The portal focuses on published datasets along with necessary metadata and global persistent identifiers (e.g. DOI 2014) for proper citability to facilitate the general attitude of data sharing and data re-use as well as the acknowledgment of the original data provider.



Figure 3: The Data Portal German Marine Research and its integrated content.

Up to now the following search functionalities are implemented in the data portal:

- Generally data and publications are searchable by keywords described in the metadata of datasets collected from data provider repositories. Additional constrains like

temporal or geographical coverage either by regional gazetteers or graphical boundary boxes can be set.

- Also datasets can be found by faceted search and via prepared categories like data providers (repositories), regions (gazetteer), authors, platforms, expeditions/campaigns, projects, devices, parameters and others.
- Along with datasets, data products and near real time data the portal allows for searchable and interlinked access to scientific publications, reports and documentations from institutional publication repositories aligned with accessible datasets.

3.2 Value-added services

Case studies for improved and enhanced data retrieval are developed within MaNIDA and offered as value-added services in the data portal. These case studies are prototypical and will evolve over time with user feedback. So far three additional services are offered by the data portal:

- A module that enables direct access to the data sources of PANGAEA (2014, AWI/MARUM), COSYNA (2014, HZG) und DOD (2014, BSH). Distinct measurements can be requested by defining a temporal and geographical extent for harmonized parameters, e.g. salinity or temperature. The requested and integrated data is then available for download. This direct access service will be extended as more parameters are mapped and made available between the data providers via international vocabularies.
- Validated bathymetry data of the partner institutes are pooled together for the first time with a well-defined extended and harmonized metadata description for central retrievability.
- Near real time data in the German Bight are visualized and retrievable within the data portal by comparison of current vector fields (surface sea water velocity).

3.3 Data providers

The datasets accessible in the “Data Portal German Marine Research” are physically drawn from different sources and are maintained and updated at different institutes. Hence datasets are delivered directly in a provider specific manner – but presently accessible and up-to-date.

Harmonization of data content, parameters, vocabularies, etc. is a major ongoing issue while technically connecting the distributed data holdings of partner institutions that have developed solitarily for the last decades. Together with our scientific community and our data providers we work continuously on standardization, classification and the linking with international initiatives like ICSU World Data System (ICSU WDS 2014), Global Earth Observation System of Systems (GEOSS 2014), Global Biodiversity Information Facility (GBIF 2014), World Register of Marine Species (WORMS 2014) and EU initiatives such as the European Marine Observation and Data Network (EMODNET 2014), SEADATANET (2014) with BODC NERC (2014) and CF-standardizations (CFC 2014) as well as EUROFLEETS (2014).

The participating data providers for the “Data Portal German Marine Research” are:

- PANGAEA (2014) – Data Publisher for Earth & Environmental Science is an information system for long-term archiving and publication of data from earth & environmental sciences operated by AWI and MARUM as an Open Access library for geo-referenced data since 1993. PANGAEA is accredited by the “International Council for Science” (ICSU) as World Data Center and by the “World Meteorological Organization” (WMO). Each dataset can be identified, shared, published and cited by using persistent Digital Object Identifier (DOI). Data are archived as discrete and citable data collections or as supplements to publications. As a data library PANGAEA links primary data related to articles in earth and environmental science journals of the ELSEVIER (2014) portfolio and COPERNICUS PUBLICATIONS (2014) freely available in SCIENCE DIRECT (2014). Currently PANGAEA serves more than 350.000 datasets and 8 billion measurements.
- COSYNA (2014) – “Coastal Observing System for Northern and Arctic Seas” is an operational, integrated observational system that combines observations and numerical modelling. It measures key physical, sedimentary, geochemical and biological parameters at high temporal resolution in the water column and at the sediment and atmospheric boundaries. Data products range from real time or near real time datasets and web services generated from in-situ observation or remote sensing systems to forecasts resulting from operative modelling. COSYNA data management organizes the data streams between observational and central storage systems at the Helmholtz-Zentrum Geesthacht and partner sites, the data documentation and the user interfaces for data retrieval and presentation. Around 15.000 datasets of COSYNA are integrated in the portal.
- DOD (2014) – The German Oceanographic Data Centre was established in 1967 between the German Hydrographic Institute (BSH) and the DFG, the German Research Foundation. The national oceanographic database comprises currently data and information on German cruises and almost 300.000 stations with more than 45 million data values of about 900 parameters. These are mainly oceanographic variables such as temperature and salinity, chemical variables with nutrients, organic, inorganic and radioactive components in seawater, sediments and biota (fish and mussels).
- Aligned with the accessible datasets by the data providers the data portal provides access to scientific publications, reports and documentations. The participating institutional publication repositories are EPIC (2014) at AWI, OCEANREP (2014) at GEOMAR and publications from HZG (2014) and MARUM (2014).

3.4 Architecture

Fig. 4 depicts the underlying architecture of the “Data Portal German Marine Research” The integration of federated content is realized by harvesting and indexing metadata offered by our data providers. The harvesting and indexing approach allows searching of scientific content with high performance based on an APACHE LUCENE (2014) ELASTIC SEARCH (2014) cluster. Since the systems of data providers offer different metadata formats via distinct interfaces the following metadata fields are defined as minimal requirement:

- Persistent identifier
- Title
- Publication date
- Authors, principal investigators
- Begin and end date of data
- Platform or research vessel
- Expedition
- Measured parameters

Furthermore the metadata contains dissemination links to data download services or dynamic services, e.g. Sensor Observation Services (SOS) or Web Map Services (WMS). To present users harmonized (metadata) content a Feature Catalogue is used to align different vocabularies of parameter names to standard names and to annotate original metadata with marine region names based on a standardized Gazetteer.

Next to the metadata delivered by data providers, the portal holds a database on expedition metadata (Expedition Catalogue). The Expedition Catalogue combines metadata about expeditions (e.g., IDs, begin, end, ports, persons) from distinct sources and is therefore used as master catalogue for the portal. The contents of Feature Catalogue and Expedition Catalogue are edited by the mentioned data curation center.

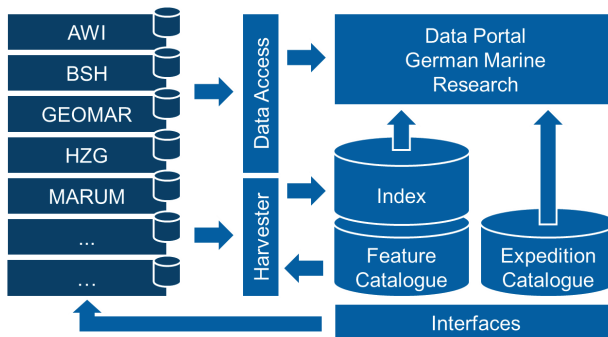


Figure 4: Architecture of the “Data Portal German Marine Research”.

Additionally, the portal provides interfaces in form of web services for the Feature Catalogue and the Expedition Catalogue. Therefore data providers can use curated information and metadata for their own catalogues.

3.5 Interfaces and standards

The harvesting approach supports different standards for metadata collection. Three of the supported protocols are:

- OAI-PMH (2014) – Open Archives Initiative Protocol for Metadata Harvesting,
- OGC CSW (2014) – Open Geospatial Consortium Catalogue Service for Web and
- OGC WFS (2014) – Open Geospatial Consortium Web Feature Service.

Metadata is expected in form of XML serializations. If provided INSPIRE (2014) compliant ISO 19115 / 19139 format is recommended. Dissemination of data described by

metadata datasets are defined by the data provider. Typical data delivery formats are tab-delimited (TSV) or comma separated values (CSV), possibly packed as ZIP archives as well as portable document format (PDF) for publications and reports. Provided web services ranges from OPENDAP (2014) based files, Sensor Observation Service (SOS 2014) to OGC Web Feature Services (WFS) and Web Map Services (WMS 2014).

For direct data access the portal performs concurrent requests to data providers. For data requests and transport the portal supports direct reading SQL access, e.g. the data warehouse of PANGAEA (2014), and Web Feature Service (WFS) requests, e.g. data retrieved from COSYNA (2014) and DOD (2014).

3.6 Terms of data access and good scientific practice

The data portal is based on open technologies and access is freely available for scientists, funding agencies and the public. So far no registration is required and user feedback is very welcome to further improve the functionality and content of the joint data portal.

Data citation is considered as good scientific practice. In this respect the downloaded datasets should always be cited and used with the appropriate citation given by the data provider. To that effect the dataset handle or DOI should always be provided along with the data citation for sustainable tracking.

4 Acknowledgement

The core team of the MaNIDA consortium consists of more than twenty scientific coworkers from all partner institutions and cooperation beyond, who mainly dedicate their own engagement and resources to shape and establish shared data infrastructures and workflows – a service oriented endeavor to the benefit of science. This continuous effort receives our full recognition and thank, especially in the context that data management and data publication usually do not gain sufficient incentives or awards by the scientific rating system of success. Thanks to the efforts of all MaNIDA cooperators the “Data Portal German Marine Research” could be realized and connects distributed data providers and major repositories for earth system and marine research in Germany. The MaNIDA project is mainly funded by the Initiative and Networking Fund of the Helmholtz Association (SO-071) and by a notable portion of own resources of all partners.

5 References

APACHE LUCENE: last visited: 2014-06-14.

BODC NERC (British Oceanographic Data Centre – Natural Environment Research Council): http://www.bodc.ac.uk/products/web_services/vocab/, last visited: 2014-06-14.

CFC (Climate and Forecast Conventions): <http://cfconventions.org/>, last visited: 2014-06-14.

COPERNICUS PUBLICATIONS: <http://publications.copernicus.org/>, last visited: 2014-06-14.

COSYNA (Costal Observing System for Northern and Arctic Seas): <http://www.cosyna.de/>, last visited: 2014-06-14.

- DATA PORTAL GERMAN MARINE RESEARCH: <http://manida.awi.de>, last visited: 2014-06-14.
- DOD (German Oceanographic Data Centre): http://www.bsh.de/en/Marine_data/Observations/DOD_Data_Centre/, last visited: 2014-06-14.
- DOI (Digital Object Identifier): <http://www.doi.org/>, last visited: 2014-06-14.
- DSHIP Data Acquisition System: <http://www.werum.de/plattformen/dship.jsp>, last visited: 2014-06-14.
- ELASTICSEARCH: <http://www.elasticsearch.org/>, last visited: 2014-06-14.
- ELSEVIER: <http://www.elsevier.com/>, last visited: 2014-06-14.
- EMODNET (European Marine Observation and Data Network): <http://www.emodnet.eu/>, last visited: 2014-06-14.
- EPIC (electronic publication information center): <http://epic.awi.de/>, last visited: 2014-06-14.
- EUROFLEETS: <http://www.eurofleets.eu/>, last visited: 2014-06-14.
- GBIF (Global Biodiversity Information Facility): <http://www.gbif.org/>, last visited: 2014-06-14.
- GEOSS (Global Earth Observation System): <https://www.earthobservations.org/geoss.shtml>, last visited: 2014-06-14.
- HZG – Publication database: <http://141.4.217.215/fmi/xsl/publikat/Search.xml>, last visited: 2014-06-14.
- ICSU WDS (International Council for Science World Data System): <https://www.icsu-wds.org/>, last visited: 2014-06-14.
- INSPIRE (Infrastructure for Spatial Information in the European Community): <http://inspire.ec.europa.eu/index.cfm/pageid/101>, last visited: 2014-106-14.
- MANIDA (Marine Network for Integrated Data Access): <http://manida.org>, last visited: 2014-06-14.
- MARUM PUBLICATIONS: <http://publications.marum.de/>, last visited: 2014-06-14.
- OAI-PMH (Open Archives Initiative Protocol for Metadata Harvesting): <http://www.openarchives.org/pmh/>, last visited: 2014-06-14.
- OCEANREP: <http://oceanrep.geomar.de/>, last visited: 2014-06-14.
- OGC CSW (Open Geospatial Consortium Catalogue Service for Web): <http://www.opengeospatial.org/standards/cat>, last visited: 2014-06-14.
- OGC WFS (Open Geospatial Consortium Web Feature Service): <http://www.opengeospatial.org/standards/wfs>, last visited: 2014-06-14.
- OPENDAP: <http://www.opendap.org/>, last visited: 2014-06-14.
- PANGAEA – Data Publisher for Earth & Environmental Science: <http://www.pangaea.de/>, last visited: 2014-06-14.
- SCIENCE DIRECT: <http://www.sciencedirect.com/>, last visited: 2014-06-14.
- SEADATANET: <http://www.seadatanet.org/>, last visited: 2014-06-14.
- SOS (Open Geospatial Consortium Sensor Observation Service): <http://www.opengeospatial.org/standards/sos>, last visited: 2014-06-14.
- WMS (Open Geospatial Consortium Web Map Service): <http://www.opengeospatial.org/standards/wms>, last visited: 2014-06-14.
- WORMS (World Register of Marine Species): <http://www.marinespecies.org/>, last visited: 2014-06-14.

MDI-DE – German Marine Data Infrastructure

Rainer Lehfeldt and Johannes Melles

Summary

Driven by the growing interest in marine spatial data and reporting obligations of the European Union with respect to effective framework directives, a novel marine data infrastructure has been established in Germany. 11 Federal and State agencies provide coastal and marine data which are documented with metadata according to the ISO standard and presented with OGC Web services. A new Web portal serves as central access point for spatial data and information from the German coastal zone and the adjacent marine waters. This facilitates intersectoral views of resources by providing technological solutions of networking and distributed data management and for meeting service based reporting obligations. The MDI-DE infrastructure is permanently maintained at BSH as a joint project of Federal and State ministries under the guidance of a steering group.

Keywords

MDI-DE, Web portal, marine data, coastal data, data mining, data access, visualization

Zusammenfassung

Durch das wachsende Interesse an marinen Geodaten und Berichtspflichten der Europäischen Union für geltende Rahmenrichtlinien veranlasst, wurde eine neuartige Infrastruktur für marine Daten in Deutschland aufgebaut. 11 Bundes- und Landesbehörden bieten Küsten- und Meeresdaten an, die mit Metadaten nach dem ISO-Standard dokumentiert und mit OGC Web Services präsentiert werden. Ein neues Web-Portal dient als zentraler Zugangspunkt für räumliche Daten und Informationen aus der deutschen Küstenzone und den angrenzenden Meeresgebieten. Eine sektorübergreifende Sicht auf Ressourcen wird durch die Bereitstellung technischer Lösungen mit Netzwerken und verteiltem Datenmanagement erleichtert und hilft bei der Erfüllung von Berichtspflichten mit Diensten. Die MDI-DE-Infrastruktur wird dauerhaft beim BSH als gemeinsames Projekt von Bundes- und Landesministerien unter der Leitung einer Lenkungsgruppe betrieben.

Schlagwörter

MDI-DE, Web-Portal, Meeresdaten, Küstendaten, Datenrecherche, Datenzugang, Visualisierung

Contents

1	Introduction	30
1.1	Motivation for a new data infrastructure	31
2	The MDI-DE network.....	34
2.1	Partners in the German coastal zone.....	34
2.1.1	Coastal engineering and coastal water protection	34
2.1.2	Marine environmental protection.....	35
2.1.3	Marine nature conservation.....	36
2.1.4	Scientific accompanying research.....	36
2.1.5	Sustainable platform for conceptual and technical operation	36
2.2	Technical infrastructure	37
3	Metadata and spatial data from the German coastal zone	38
3.1	Metadata elements.....	38
3.1.1	The German coastal zone metadata profile.....	39
3.2	Web services	40
4	The MDI-DE Web portal	40
5	Conclusions.....	41
6	Acknowledgements.....	42
7	References	42

1 Introduction

The marine data infrastructure for Germany MDI-DE has been conceptually developed and technically implemented in the period from 2010 until 2013 when funding was provided by the Federal Ministry of Education and Research BMBF. A total of 11 Federal and State agencies were involved which are responsible for coastal engineering and coastal water protection, marine environmental protection, marine nature conservation and accompanying scientific/technical research. A total of 12 scientists have been working on the integration of coastal and marine data.

The project aimed at providing spatial data and information from the mentioned areas of responsibility for policy, economy and the public which could be accessed through a central Internet portal www.mdi-de.org (LEHFELDT und MELLES 2011). Methods and technologies have been developed and implemented in order to meet national and international reporting obligations. Lead partners were the Federal Waterways and Engineering Research Institute, Hamburg Office, BAW, the Federal Maritime and Hydrographic Agency Hamburg BSH and the Federal Agency for Nature Conservation, Vilm Office, BfN.

The search for data, data products and their use is supported by using metadata and Web services. The MDI-DE assists authorities in the German coastal zone in fulfilling their reporting requirements with respect to the EU Framework Directives INSPIRE, Infrastructure for Spatial Information in Europe, 2007/2/EC (European Parliament and Council 2007a) and MSFD, European Marine Strategy Framework Directive,

2008/56/EC (European Parliament and Council 2008). It also supports the continuous reporting obligations for the Water Framework Directive WFD, 2000/60/EC (European Parliament and Council 2000) and NATURA 2000 sites, 97/266/EC (COMMISSION 1997).



Figure 1: The network of the Marine Data Infrastructure MDI-DE in the German coastal zone. Lead partners: A1: BAW, A2: BSH, A3: BfN, A4: Uni Rostock. Partners: P1: LKN, P2: LWKN, P3: NLPV, P4: WSD NW, P5: WSD N, P6: LLUR, P7: LUNG.

The new MDI-DE Web portal provides standardized access to specialized data. It implements a uniform technical data base and relieves the partner offices from routine service work. The information integrated in MDI-DE represents quality-assured official information on the German coastal zone of the North and Baltic Sea and the adjacent marine regions supplied by the responsible Federal and State authorities.

In particular, the interfaces to provide data for INSPIRE and for the German Spatial Data Infrastructure, GDI-DE (GEODATENINFRASTRUKTUR DEUTSCHLAND 2008), are essential components of this infrastructure. Following international technical standards facilitates widespread dissemination of information offered by the participating partners.

1.1 Motivation for a new data infrastructure

Federal and State agencies collecting information and data from monitoring and surveying programs for different objectives use their respective authorities' portals to present their sectoral data. Coastal data usually play only a minor role for the higher Federal authorities Federal Waterways and Engineering Research Institute BAW (www.baw.de), Federal Maritime and Hydrographic Agency BSH (www.bsh.de) and Federal Agency for Nature Conservation BfN (www.bfn.de) as well as for the Waterways and Shipping Administration of the Federal Government WSV (www.wsv.de).

The same situation is found in the State portals of the Lower Saxony Water Management, Coastal Defence and Nature Conservation Agency (NLWKN, www.nlwkn.de), the Administration of the Wadden Sea National Park of Lower Saxony (NLPV, www.nationalpark-wattenmeer.de/nds), the Schleswig-Holstein State Agency for Coastal Defence, National Park and Marine Conservation (LKN, www.schleswig-holstein.de/LKN), the State Agency for agriculture, environment and rural areas of the State of Schleswig-Holstein (LLUR, www.schleswig-holstein.de/LLUR), and the State Agency of Environment, Nature conservation and Geology in Mecklenburg-Western Pomerania (LUNG, www.lung.mv-regierung.de).

The Geodata Portal of the Federal government (www.geoportal.de) and the Environmental Information Portal of the Federal government (www.portalu.de) provide integrative views of existing data from thematic perspectives. Here the available data are retrievable in search portals through standardized metadata and standardized Web services are used for visualization and download. Especially for the coastal zone, there were only the GeoSeaPortal (MELLES 2009) at BSH using OGC-compliant Web services (OGC 2011) and the coastal metadata information system NOKIS (LEHFELDT et al. 2008) jointly operated by BSH and BAW using ISO 19115-compliant metadata.

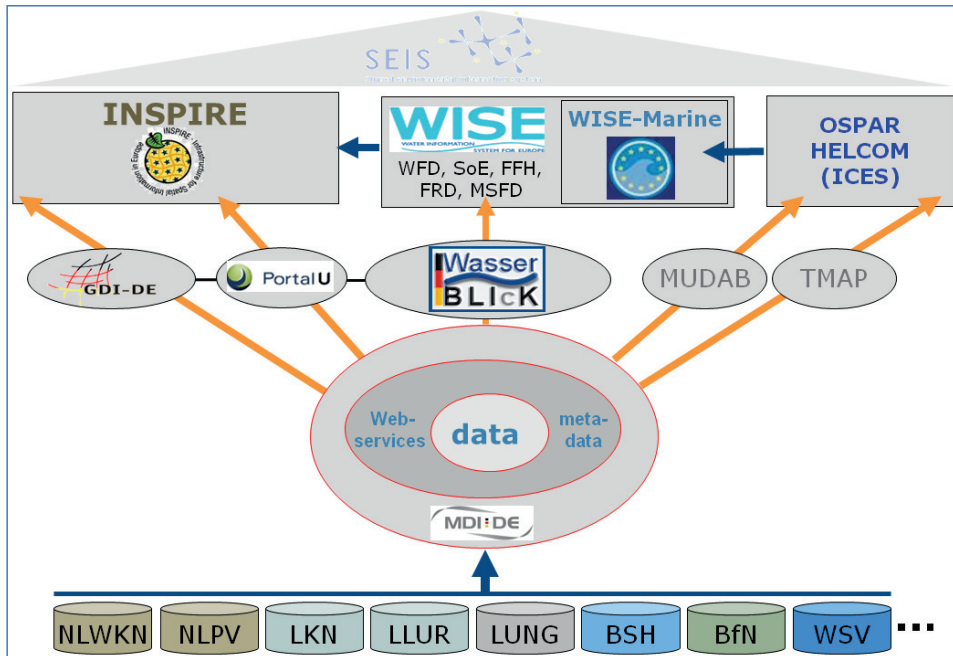


Figure 2: Data flow and reporting within the MDI-DE information network.

Fig. 2 illustrates the data flow from the distributed source systems in the MDI-DE information network to existing national and international target systems, which have to be supplied with data and metadata by the Federal and State authorities. To ensure an efficient task completion in this context, first a data infrastructure for the networking of existing source systems must be built. The demands from government, academia, politics, industry and the public require integration of marine data from the existing heterogeneous portals. The new MDI-DE portal benefits from the technical experience with NOKIS and the GeoSeaPortal.

The demand for cross-thematic data analysis is constantly growing. The reasons for this are the increasing complexity of current issues in connection with anthropogenic changes in marine ecosystems and global climate change. So there are new demands from coastal protection and increasing legal requirements for reporting obligations by the Marine Strategy MSFD, the Flood Risk Directive FRD (EUROPEAN PARLIAMENT AND COUNCIL 2007b) and the INSPIRE framework directives. At the same time the technical developments in the World Wide Web and by the Open Geospatial Consortium (OGC

2011) enhance conditions for developing modern information infrastructures. Quality and performance of appropriate infrastructure forms an important basis for the optimization of cooperation, to increase productivity and to fulfill legal duties.

The currently available tools do not meet these requirements. Important building blocks for the necessary networking have already been developed by NOKIS and the implementation of local spatial data infrastructures in various departments. There is still a considerable need for research and for standardization at national and European level in setting up functioning networks, which allow the use of harmonized and interoperable spatial data on the various administrative levels.

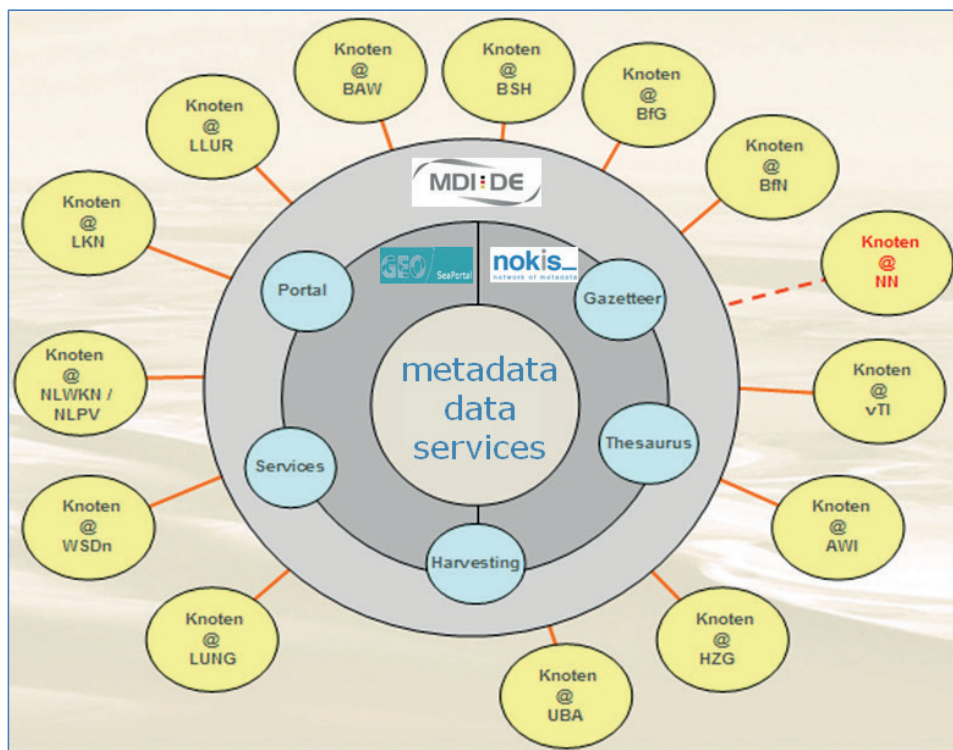


Figure 3: MDI-DE infrastructure.

VOGT (2002) highlights the importance of harmonization of data from different sources in the case of river basin analysis in the Guidelines for the implementation of the Water Framework Directive. It is a prerequisite for interoperable provision of geo-information by services to use interdisciplinary and distributed geodata (ARBEITSKREIS ARCHITEKTUR der GDI-DE 2007). The INSPIRE Directive establishes a strict time frame until 2014, in which documentation of data with metadata and data access with standardized network services for searching, visualization and download shall be implemented in stages. The MDI-DE project has been working on prototype solutions in this context. Section 2.1.5 describes the sustainable platform for future conceptual and technical operation of MDI-DE.

2 The MDI-DE network

The marine data infrastructure for Germany MDI-DE contributes to the achievement of these objectives. All participating Federal and State agencies benefit from this network, which established information technology to be used in the future for data dissemination and for meeting reporting requirements.

2.1 Partners in the German coastal zone

Coastal engineering and coastal water protection

BAW Hamburg - Federal Waterways and Engineering Research Institute

LKN Husum and Tönning - Schleswig-Holstein State Agency for Coastal Defence, National Park and Marine Conservation

NLWKN Norden-Norderney and Brake-Oldenburg - Lower Saxony Water Management, Coastal Defence and Nature Conservation Agency

NLPV Wilhelmshaven - Administration of the Wadden Sea National Park of Lower Saxony

WSD Nordwest in Aurich / Nord in Kiel - Waterways and Shipping Directorate North-WSD-N and Northwest WSD-NW

Marine environmental protection

BSH Hamburg - Federal Maritime and Hydrographic Agency Hamburg BSH

LLUR Flintbek - State Agency for agriculture, environment and rural areas of the State of Schleswig-Holstein

LUNG Güstrow - State Agency of Environment, Nature conservation and Geology in Mecklenburg-Western Pomerania

Marine nature conservation

BfN Insel Vilm - Federal Agency for Nature Conservation, Vilm Office, BfN

Scientific accompanying research

Universität Rostock - Chair of Geodesy and Geoinformatics at the University of Rostock

2.1.1 Coastal engineering and coastal water protection

A key objective of the research work at BAW was to support the data management for numerical modelling. To this end, harmonization of data sets maintained in distributed data bases and interoperability of field data and modelling data through the use of web services have been studied. Similarly, the standardized documentation of data and models with metadata for identifying scenarios and for intersectoral data mining has been focused on.

The project partner at the Administration of the Wadden Sea National Park of Lower Saxony NLPV and at the Lower Saxony Water Management, Coastal Defence and Nature Conservation Agency NLWKN has actively participated in the metadata working group of the GDI-DE (GEODATENINFRASTRUKTUR DEUTSCHLAND 2008). Another work package concerning a coastal gazetteer carried on the longstanding collaboration between NOKIS with the Federal Agency for Cartography and Geodesy BKG. There is an expression of interest by the government in a detailed gazetteer for the entire German coastal zone, which is to be established as part of the MDI-DE in cooperation with the Schleswig-Holstein State Agency for Coastal Defence, National Park and Marine Conservation LKN in Tönning. Important steps have been taken to merge preexisting wordlists from BAW and KFKI into a coastal thesaurus by a joint effort of BAW and the Chair of Geodesy and Geoinformatics at the University of Rostock.

The German Coastal Engineering Research Council KFKI has a working group on surveying coastal waters at regular intervals in order to provide up to date bathymetry data for numerical modelling purposes. Since 1973, this group organizes the division of work between the Federal and State authorities in the coastal zone to produce area-wide data sets. A Web based planning tool has been developed in cooperation with the Waterways and Shipping Directorate North WSD-N in Kiel, which visualizes past, present and planned surveying campaigns. As it is based on the coastal zone metadata profile (see section 3.1.1) and uses OGC Web services it is integrated in the MDI-DE network.

2.1.2 Marine environmental protection

The lead partner Federal Maritime and Hydrographic Agency BSH in Hamburg has carried out research and development work for marine environment protection in cooperation with project partners in the State Agency for agriculture, environment and rural areas of the State of Schleswig-Holstein LLUR in Flintbek and the State Agency of Environment, Nature conservation and Geology in Mecklenburg-Western Pomerania LUNG in Güstrow. Earlier cooperations of BSH, LLUR and LUNG concerning the marine environment database MUDAB and the EU Water Framework Directive WFD led to developments of data interfaces that were used for the exchange of spatial data. These results were further developed in the MDI-DE project.

The Federal Institute of Hydrology BfG with its information portal WasserBLiCK was a major project partner. The Federal Environmental Agency UBA in Dessau was also involved with its responsibility for MUDAB. During the project runtime contacts for possible cooperation were made with the Institute for Coastal Research at the Helmholtz-Zentrum Geesthacht HZG, the Leibniz Institute of Marine Sciences at Kiel University IFM-GEOMAR, the Leibniz Institute for Baltic Sea Research IOW Warnemünde, the Centre for Geoinformation at Christian Albrechts University of Kiel ZfG, and the Alfred Wegener Institute, Helmholtz Centre for Polar and Marine Research, AWI in Bremerhaven.

BSH has been working with BAW at merging GDI-BSH and NOKIS. The technical integration of the existing systems was realized first, followed by building the common infrastructure for maps, map tools and charts that are now used by all project partners. The existing services of GDI-BSH and NOKIS were taken into account.

The primary aim of the work was to establish an innovative Web portal for marine data and an infrastructure in which distributed harmonized and interoperable data are made available. This platform can develop into a one-stop portal for marine data from the German coastal zone (see section 2.1.5). It promotes the dissemination of marine information, improves the transparency of existing data and can help to avoid duplication of work.

2.1.3 Marine nature conservation

The department "Marine and coastal conservation" of the Federal Agency for Nature Conservation BfN on the Isle of Vilm concentrated on research and development work regarding marine nature conservation. All partners from Federal and State agencies are working together in Natura 2000 and MSFD issues to serve the national and international information and reporting systems.

Additional scientific cooperation partners are involved such as the Research and Technology Centre FTZ in Büsum, the Leibniz Institute for Baltic Sea Research IOW in Warnemünde and the Alfred Wegener Institute AWI in Bremerhaven. This is also true for the State Agency for agriculture, environment and rural areas of the State of Schleswig-Holstein LLUR in Flintbek, the State Agency of Environment, Nature conservation and Geology in Mecklenburg-Western Pomerania LUNG in Güstrow and the Federal Environmental Agency UBA in Dessau.

BfN uses internal information systems for nature protection and landscape conservation as well as for the collection, documentation, administration and organization of nature conservation data. These are used for the reporting requirements of Natura 2000, for monitoring data, extensive ecological data and expert reports as well as for data that is collected with regard to the MSFD. A major basis is the professional thesaurus, which is supplemented on the basis of the UMTHESES Thesaurus of the Federal Environmental Agency and the PortalU by a microthesauri relating to nature conservation and to marine nature conservation. The data documented so far are to be exchanged via the new MDI-DE portal with all coastal offices and agencies and shall be reported to the EU in a further step.

2.1.4 Scientific accompanying research

The Chair of Geodesy and Geoinformatics at the University of Rostock has carried out scientifically and technically supporting research on MDI-DE. The system architecture was analyzed (RÜH et al. 2011) and implementation strategies were optimized. These include conformance and performance tests of the developed services concerning requirements of existing systems such as GDI-DE, PortalU and WasserBLICK as well as the set up for reporting requirements for MSFD and INSPIRE workflows.

2.1.5 Sustainable platform for conceptual and technical operation

Since March 2014, the former research and development partners are cooperating according to an administrative agreement, VKoopUIS MDI-DE, between Federal and State

Ministries responsible for the German coastal zone (STÄNDIGER AUSSCHUSS UMWELT-INFORMATIONSSYSTEME 2008).

The central components of the MDI-DE are hosted at BSH. These are the Web portal, which integrates harmonized data and services from Federal and State resources, a metadata management system for harvesting and archiving, a coastal gazetteer, a thesaurus for marine vocabularies, and central data assessment services. All partners maintain their distributed infrastructure nodes (see section 2.2) within the MDI-DE network and contribute to necessary maintenance, update and development expenditures based on an allocation key.

2.2 Technical infrastructure

Data and metadata of the MDI-DE partners are maintained in local infrastructure nodes. This denotes the hardware and software of a local server architecture, with which spatial data and metadata are managed and deployed via standardized services. According to the Publish-Find-Bind-principle the individual components interact with each other by services compliant with OpenGeospatial Consortium (OGC 2011) standards. BINDER (2012) gives a comprehensive description of infrastructure nodes from which Fig.4 is taken as a prototype example.

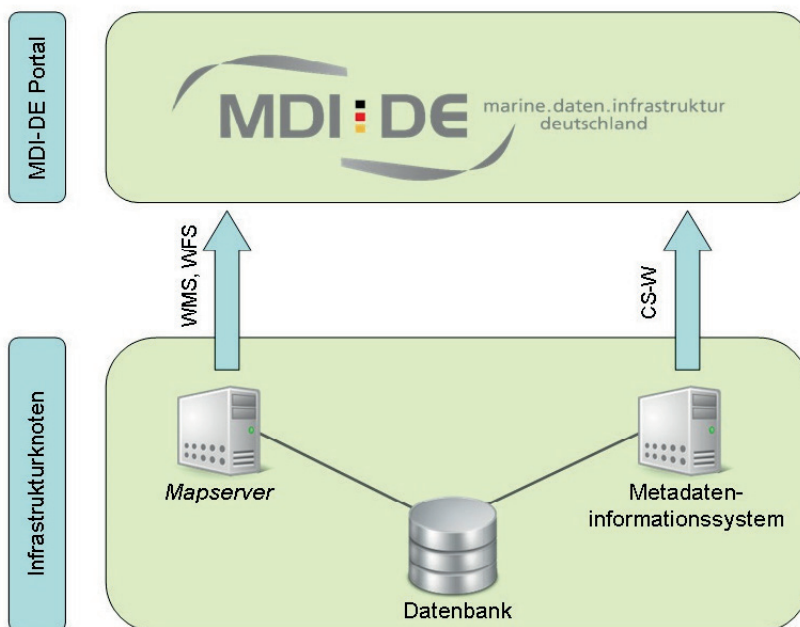


Figure 4: The elements of a prototype MDI-DE infrastructure node.

Any information flow is directed towards the MDI-DE Web portal, which is the central node of the MDI-DE network. Being implemented by standardized OGC Web services for mapping WMS, download WFS and searching CS-W, the information hosted at

distributed infrastructure nodes can thus be used in other connections, which also rely on these standards.

In order to speed up response times in the Web portal, the distributed metadata is harvested at the central node using the CS-W interfaces. The services provided are currently available free of charge and there are no plans to introduce a billing system.

3 Metadata and spatial data from the German coastal zone

The implementation of the European Water Framework Directive adopted by the EUROPEAN PARLIAMENT AND COUNCIL (2000) calls for novel information management in the member states and for automated workflows to meet reporting requirements. LEHFELDT and REIMERS (2004) point out the importance of standardized metadata for these obligations, which help to discover and share relevant and timely information from distributed data sources. The Water Information System for Europe WISE maintains a Web portal, water.europa.eu, presenting the current status and activities within this thematic network.

Cross-boundary information exchange becomes an important issue when considering catchment areas, for example. Apart from producing seamless geographic data, there may be diverse vertical reference systems in place, and different units or measurement methods may be applied. These must be documented so as to be able to harmonize available data with transformation algorithms for an integrated view and analysis.

Already in 2003, the NOKIS group (LEHFELDT and HEIDMANN 2003) agreed on a metadata profile for the coastal zone, which addresses these issues in much detail. The selected metadata elements put equal emphasis on horizontal information flow between the actors involved in collecting data and creating data products for public information and vertical information flow between either hierarchical or cascading information systems (see Fig. 2).

The agreed Coastal Zone Metadata Profile meets all requirements of existing German information systems (German Environmental Information Portal, www.portalu.de, Federal Spatial Data Portal, www.geoportal.de). Therefore, once an information resource such as a dataset, a map, an image, etc. has been documented with this profile it can be discovered by these national portals and by the MDI-E portal, in particular. Without further editing its metadata are valid in multiple environments and, most importantly, they comply with the European INSPIRE.

3.1 Metadata elements

The INTERNATIONAL STANDARD ORGANIZATION (2003) published the ISO19115 Metadata Standard which provides some 300 metadata elements grouped into 13 categories of information about a resource. These address the essential questions of “what, where, when, who and how” for documentation of geographic information. The full standard is a generic approach for describing resources. User communities are encouraged to select those elements necessary for their specific purposes and reduce the volume of information to a manageable amount.

However, there is a Recommended Core, which is mandatory in order to ensure communication between different applications. This minimum set of metadata is a key-stone for interdepartmental information exchange and intersectoral views implemented in

networks for integrated thematic information systems. It consists of eight elements: dataset title, dataset reference date, dataset responsible party, geographic location of the dataset (by four coordinates or by geographic identifiers), dataset topic category, abstract describing the dataset, metadata language, metadata point of contact.

3.1.1 The German coastal zone metadata profile

Details on the selection of metadata elements for the coastal zone metadata profile have been published by LEHFELDT and HEIDMANN (2003). With applications such as gazetteer and tools for planning, sediment classification, and EU reporting in mind, there are more elements of the ISO 19115 Metadata Standard declared mandatory than in the ISO Core or Recommended Core element sets. In order to support automated discovery services, it is essential to have detailed information on the temporal and geographical extents associated with the resources to be documented. Descriptive keywords preferably taken from controlled vocabularies maintained by user communities or from thesauri are also needed in order to optimize functionalities of discovery services built with these metadata. Automated workflows can be controlled by the status description of a dataset and limitations placed upon the access or use of the data. In such applications the context for data must be provided by specifications of the scope of data and the scope to which the metadata applies.

As the ISO 19115 standard provides for metadata extensions adapted to the specific needs of user communities, the coastal zone metadata profile incorporates elements of elsewhere existing profiles. Our common metadata model thus contains a “shore line” profile for surveying in intertidal domains, which adopts metadata elements first published by the FEDERAL GEOGRAPHIC DATA COMMITTEE (2001). Information about tidal and marine weather conditions at the time of surveying are recorded so that details for the correct interpretation of data are available. Viewed, in particular, from a synoptic point of view of planning or modelling, the additional metadata elements serve as quality assurance parameters to be used in harmonization procedures of complementary datasets.

The European Directory of Marine Environmental Research Projects EDMERP as described by SCHAAP (2000) defines metadata elements which are applied in the coastal zone metadata profile for projects. These are mapped on the ISO19115 Metadata Standard and contain the temporal and geographical limits as well as the related publications with links to online resources when available. All projects of the German Coastal Engineering Research Council (KFKI) are documented with this metadata profile and registered at www.kfki.de/de/projekte.

Another important source of information, which needs structured documentation results from scenarios investigated with computational models. A Content Standard for Computational Models has been published by HILL et al. (2001), which introduces a number of metadata elements to document important features of applied models and input data used in the study of scenarios. The NOKIS group is working on mapping these elements on the ISO19115 Metadata Standard for a coastal zone metadata profile for models.

3.2 Web services

Preparation, maintenance and use of metadata in the MDI-DE are described in a Metadata Guide by WOSNIOK and RÄDER (2013). The INSPIRE directive provides for metadata of both geo-data sets and Web services related to these data. The target system GDI-DE (GEODATENINFRASTRUKTUR DEUTSCHLAND 2008) has designed appropriate conventions for metadata for this purpose. GDI-DE also makes available a test suite in order to assure compliance of all metadata within its network including MDI-DE with the technical form and content required by INSPIRE.

Efficient search clients implemented in Web portals rely on consistent metadata for geo-data and services. An index is used in the portals of GDI-DE and MDI-DE to first register all existing metadata records within the network and then associate data and services in a second step. This mechanism allows result lists on the portals to display the found records together with related services for their visualization and download.

4 The MDI-DE Web portal

According to the concept of the new Web portal for marine and coastal data, the MDI-DE Web portal serves as the central access point for data and information from the German coastal zone and the adjacent marine waters. It provides the following functionality:

- Simple and expert search using a metadata catalogue, a thesaurus for controlled vocabulary and a coastal gazetteer for geographic names in the marine environment,
- Intersectorally consistent data structures for interdisciplinary views on marine data,
- Web services and download services for visualization and data access,
- Implementation of prototype services for data analysis and automatic report generation with respect to the requirements put forward in EU framework directives.

The MDI-DE portal relies on a network for marine data, connecting local nodes at the major data sources of Federal and State agencies, which provide a wide range of data types. The experience gained in the research and development project will be used for further implementations in the coastal States of Germany.

The future Web services provided by the new Marine Data Infrastructure will support system analysis applications related to coastal engineering, spatial planning, nature conservation, science and ecology.



Figure 5: MDI-DE portal www.mdi-de.org.

5 Conclusions

The new, highly-innovative information and communication technology of MDI-DE provides a common marine spatial data infrastructure for management of marine data:

- Integration and access to data with services for policy, business, administration, science and the public via a single and common web-portal,
- Harmonization, standardization and quality assurance of available and in future to be collected data,
- Consideration of metadata and services for modeling scenarios,
- Technological implementation by using the most current standards and developments (ISO standards, specifications by the Open Geospatial Consortium OGC and World Wide Web W3C),
- Compliance with European and national guidelines (Infrastructure for Spatial Information in Europe INSPIRE, Water Framework Directive WFD, Natura 2000, the Marine Strategy Framework Directive MSFD or at the Federal level, the Spatial Data Infrastructure Germany GDI-DE and the environmental Information Portal of the Federal government PortalU).

In all partner authorities investments have been made to use MDI-DE in operational mode. The continuous operation is ensured by an administrative agreement between Federal and State ministries.

6 Acknowledgements

The co-operative research and development project MDI-DE was funded by the German Federal Ministry of Education and Research BMBF through the project management of Projektträger Jülich PTJ under grant numbers 03KIS089, 3KIS090, 03KIS091 and 03KIS092. The authors gratefully acknowledge this support as well as the many contributions from students, co-workers and other partners of these research projects.

7 References

- ARBEITSKREIS ARCHITEKTUR der GDI-DE (Hrsg.) (2007): Architektur der Geodateninfrastruktur Deutschland. Koordinierungsstelle GD I-DE. <http://www.geoportal.de/SharedDocs/Downloads/DE/GDI-DE/GDI-DE%20Architekturkonzeptv1.html>. Last visited: June 19, 2014.
- BINDER, K.(Hg.): Leitfaden zur Anbindung eines Infrastrukturknotens an die MDI-DE. 37S., 2012. http://projekt.mdi-de.org/images/mdi-de/Publikationen/plugin-mdi-de_leit_faden_isk_2_0_publish.pdf. Last visited June 19, 2014.
- EUROPEAN PARLIAMENT AND COUNCIL: Directive 2008/56/EC establishing a framework for community action in the field of marine environmental policy (Marine Strategy Framework Directive). Official Journal of the European Union L 164, 19-40, 2008.
- EUROPEAN PARLIAMENT AND COUNCIL: Directive 2007/60/EC on the assessment and management of flood risks. Official Journal of the European Union L 288, 27-34, 2007.
- EUROPEAN PARLIAMENT AND COUNCIL: Directive 2007/2/EC establishing an Infrastructure for Spatial Information in the European Community (INSPIRE). Official Journal of the European Union L108, 1-14, 2007.
- EUROPEAN PARLIAMENT AND COUNCIL: Directive 2000/60/EC of the establishing a frame-work for the Community action in the field of water policy (EU Water Framework Directive). Official Journal of the European Communities L 327, 1-72, 2000.
- COMMISSION: 97/266/EC Commission Decision of 18 December 1996 concerning a site information format for proposed Natura 2000 sites. Official Journal of the European Communities, L 107, 24 April 1997.
- FEDERAL GEOGRAPHIC DATA COMMITTEE: Shoreline Metadata Profile of the Content Standards for Digital Geospatial Metadata. FGDC-STD-001.2-2001, 75p, 2001.
- GEODATENINFRASTRUKTUR DEUTSCHLAND: Auftrag GDI-DE. 2008. <http://www.geoportal.de/DE/GDI-DE/Organisation/Aufgaben/aufgaben.html>. Last visited: June 19, 2014.
- HILL, L.L., CROSIER, S.J., SMITH, T.R. and GOODCHILD, M.: A Content Standard for Computational Models. D-Lib Magazine, 7 (6), 2001. <http://www.dlib.org/dlib/june01/hill/06hill.html>. Last visited: June 19, 2014.

- INTERNATIONAL STANDARD ORGANIZATION: Geographic information: ISO 19115 - Metadata; ISO 19119 - Services. 2003. <http://www.iso.ch/iso/>. Last visited: May 24, 2006.
- LEHFELDT, R. und MELLES, J.: Die Marine Dateninfrastruktur Deutschland MDI-DE. In: TRAUB, K.-P., KOHLUS, J. und LÜLLWITZ, T. (Hg.): Geoinformationen für die Küstenzone. Norden Halmstad: Points Verlag (3), 107-116, 2011.
- LEHFELDT, R.; REIMERS, H.-C.; KOHLUS, J. and SELLERHOFF, F.: A Network of Metadata and Web Services for Integrated Coastal Zone Management. COPEDEC VII, Dubai, UAE, Cyber-proceedings, paper 207, 2008.
- LEHFELDT, R. and REIMERS, H.-C.: The WFD Reporting Process - A German Approach to Information Management in the Coastal Zone. In: GARCÍA de JALÓN, D., VIZCAINO, P. (eds): 5th International Symposium on Ecohydraulics. Aquatic Habitats: Analysis & Restoration, September 12-17. IAHR, Madrid, Spain, 175-181, 2004.
- LEHFELDT, R. and HEIDMANN, C.: Information Infrastructure for Integrated Coastal Zone Management. In: GANOULIS, J. and PRINOS, P. (eds): XXX IAHR Congress Proceedings. Theme A. Coastal Environment: Processes and Integrated Management. 465-472, 2003.
- MELLES, J.: GeoSeaPortal - die GDI für marine Geoinformationen. Schriftenreihe des DVW, 58, 125-130, Wißner-Verlag, Augsburg, 2009.
- OGC - OPEN GEOSPATIAL CONSORTIUM (ed.) (2011): Implementierungsspezifikationen für Geodatendienste. <http://www.opengeospatial.org/>. Last visited: June 19, 2014.
- RÜH, C.; KORDUAN, P. and BILL, R.: Development of the reference model for the marine spatial data infrastructure Germany (MDI-DE). In: PILLMANN, W.; SCHADE, S. and SMITS, P. (eds): Innovations in sharing environmental observation and information. Proceedings of the 25th International Conference EnviroInfo, October 5 – 7. Joint Research Centre Ispra, Institute for Environment and Sustainability. Aachen: Shaker. 419-425, 2011.
- SCHAAP, D.: European Directory of Marine Environmental Research projects (ED-MERP). A key resource of the SEA-SEARCH network. 2000. <http://www.ifremer.fr/sismer/program/seasearch/doc/EDMERP1.doc>. Last visited: June 19, 2014.
- STÄNDIGER AUSSCHUSS UMWELTINFORMATIONSSYSTEME StA UIS: Aufgaben und Ziele. 2008. <http://www.laga-online.de/servlet/is/103/>. Last visited June 19, 2014.
- VOGT, J.V. (Ed.): GUIDANCE DOCUMENT ON IMPLEMENTING THE GIS ELEMENTS OF THE WATER FRAMEWORK DIRECTIVE. EC-JRC, (EUR 20544 EN) LUXEMBOURG, 166 p, 2002.
- WOSNIOK, C. and RÄDER, M. (Hg.): Leitfaden zur Pflege und Erstellung von Metadaten in der MDI-DE und Mappingtabelle. 86 Seiten, 2013. http://projekt.mdi-de.org/images/mdi-de/Dokumente/MDI-DE_Leitfaden_Metadaten_v1.0.1.pdf. Last visited: June 19, 2014.

Data Management Centre of the Federal Waterways and Shipping Agency, Northern Region Office

Romy Beyer, Axel Orths and Lotbar Neumann

Summary

The Data Management Centre (Zentrales Datenmanagement, ZDM) has been operating the portal system www.kuestendaten.de since 2008 as an information platform for the northern coastal area, including the estuaries, rivers and canals under the competence of the Federal Government. The main task involved is documenting the construction works carried out on federal waterways within the sphere of competence of the Federal Waterways and Shipping Agency, Northern Region Office (GDWS, Northern Region Office). The ZDM is responsible for distributing technical data and information on hydrology, nature conservation, remote sensing technology and any additional environmental data that is commonly available.

In recent years it has been possible to further extend the range of data and information offered. It now also includes plausibility tested time series, complete and consistent digital terrain models, ecological data, data related to the documentation of existing conditions and a database of publications. In addition scoping papers, planning documents and plan approval decisions are provided on an area and project basis on the general entry portal and the five regional portals Tidal Elbe (Tideelbe), Kiel Canal (Nord-Ostsee-Kanal), North Sea Coast (Nordseeküste) and Baltic Sea Coast (Ostseeküste).

The provided data is made available both for manual research and for access through standardised interfaces like Web Mapping Service (WMS), Web Feature Service (WFS) and Sensor Observation Service (SOS).

The user can perform spatial searches using a map tool. For visualising a time series a state-of-the-art Sensor Web Client is available.

Keywords

extension, existing conditions documentation, German coast, data provisioning, Elbe estuary, extension of the River Elbe, deepening of the Elbe, extension of the River Ems, GDWS Northern Region Office, geospatial data, new construction projects, North Sea coast, Baltic Sea coast, planning approval, planning documents, Tidal Elbe, Tidal Ems, WSV, time series, ZDM, German Bight

Zusammenfassung

Das Zentrale Datenmanagement (ZDM) betreibt das Portalsystem www.kuestendaten.de seit 2008 als Informationsplattform für den norddeutschen Küstenbereich, seine Ästuarie, Flüsse und Kanäle im Zuständigkeitsbereich des Bundes. Die wesentliche Aufgabe besteht in der Dokumentation von Baumaßnahmen an Bundeswasserstraßen innerhalb des Zuständigkeitsbereichs der Generaldirektion Wasserstraßen und Schifffahrt - Außenstelle Nord (GDWS Ast. Nord). Das ZDM übernimmt die

Verbreitung von Fachdaten und Informationen aus den Bereichen Gewässerkunde, Naturschutz, Fernerkundung und weiterer allgemein verfügbarer Umweltdaten.

Das Angebot an Daten und Informationen konnte in den letzten Jahren immer weiter ausgebaut werden und beinhaltet u.a. plausibilisierte Zeitreihen, komplette konsistente digitale Geländemodelle, ökologische Daten, Beweissicherungsdaten und eine Publikationsdatenbank. Dazu kommen Scopingpapiere, Planunterlagen, genehmigte Planfeststellungsbeschlüsse, die gebiets- und projektbezogen auf dem Einstiegsportal und den fünf regionalen Portalen Tideems, Tideelbe, Nord-Ostsee-Kanal, Nordseeküste, Ostseeküste bereitstehen.

Die angebotenen Daten werden sowohl für die manuelle Recherche als auch über standardisierte Schnittstellen, wie Web Mapping Service (WMS), Web Feature Service (WFS) und Sensor Observation Service (SOS) zur Verfügung gestellt.

Eine räumliche Suche über ein Kartentool ist möglich und zur Visualisierung von Zeitreihen ist ein moderner Sensor Web Client im Einsatz.

Schlagwörter

Ausbau, Beweissicherung, Deutsche Küste, Datenbereitstellung, Elbeästuar, Elbausbau, Elbvertiefung, Emsausbau, GDWS Ast. Nord, Geodaten, Neubauvorhaben, Nordseeküste, Ostseeküste, Planfeststellung, Planunterlagen, Tideelbe, Tideems, WSV, Zeitreihen, ZDM, Deutsche Bucht

Contents

1	Introduction	46
2	Centre for data provisioning and publishing.....	47
3	Collaboration with the Information Technology Service Centre in Ilmenau.....	48
4	Regional portal Tidal Elbe.....	48
4.1	Project information.....	49
4.2	Map.....	50
4.2.1	Web Map Service and Web Feature Service.....	50
4.3	Time series.....	50
4.3.1	Provision of time series - Sensor Observation Service.....	51
4.3.2	Display of time series - Sensor Web Client	52
4.4	Data download - available data.....	53
5	Metadata	54
6	References	54

1 Introduction

Since October 2008, all data and digital documents related to the complete range of new and ongoing construction and extension projects falling under the competence of the Federal Waterways and Shipping Agency, Northern Region Office (GDWS Northern Region Office) have been captured and merged by using standardised criteria and made available over the Internet at the Data Management Centre (ZDM). Thus the offices of

the GDWS, Northern Region Office can use the ZDM as a new service facility that takes on an additional role as information centre for external users against the background of freedom of information and environmental information laws.

The database of the ZDM is available at www.kuestendaten.de. This is the entry page to the regional portals for the North Sea (www.portalnsk.de), Kiel Canal (www.portalnok.de), Tidal Elbe (www.portal-tideelbe.de) and Baltic Sea (www.portalosk.de), which are also directly accessible through their respective web addresses. The regionally organised portals document specific data and information on construction works carried out by the Waterways and Shipping Offices in that particular region. The Tidal Ems portal (www.tideems.de) is unique in so far as it falls outside the competence of the GDWS, Northern Region Office. The area boundaries (see Fig. 1) are approximate points of reference for the regional portals' study areas; the lines do not represent areas of responsibility within the structures of the Waterways and Shipping Administration.

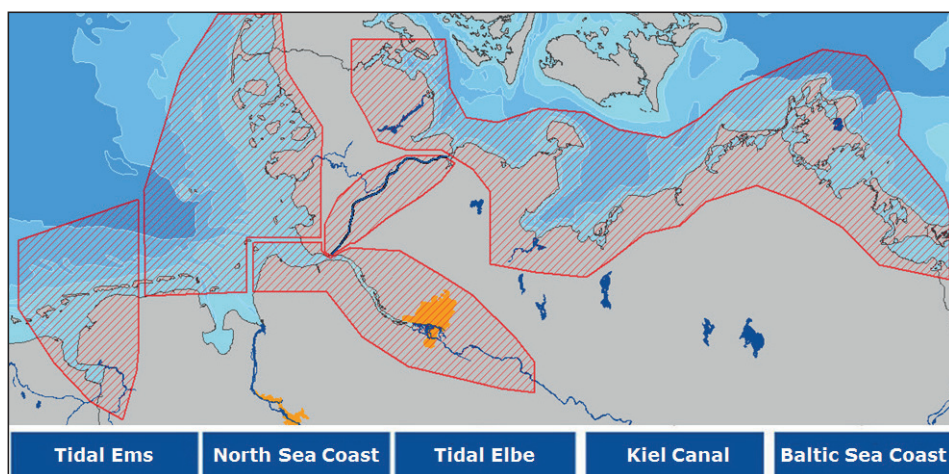


Figure 1: The regional subportals of www.kuestendaten.de.

2 Centre for data provisioning and publishing

The ZDM originated from the data collection centre established for measuring and documenting existing conditions in connection with the adjustment of the Lower and Outer Elbe fairways to the requirements of container ships. The data collection centre was set up in compliance with a provision in the plan approval notice of 02/22/1999 stipulating free access to the database of existing conditions for the regulatory authorities (*Einvernehmensbehörden*) of the federal states. In addition to merging data of new construction projects, the ZDM is now responsible for supporting the authorities in all aspects of specialised IT-supported data storage and visualisation. By pooling specialised and IT knowledge in the GIS, CAD and database areas and by ensuring free access to information and data repositories the requirements of the regulations of both the Environmental Information Act (Umweltinformationsgesetz, UIG) and the Freedom of Information Act (Informationsfreiheitsgesetz, IDf) are met at the same time. The services

provided by the ZDM also include the development and provision of formatting and layout specifications that can serve as templates for tender issuing offices.

3 Collaboration with the Information Technology Service Centre in Ilmenau

In fulfilling its tasks the ZDM is supported by the centralized server hardware and the IT contracting authority of the Information Technology Service Centre (DLZ-IT) in Ilmenau. This collaboration, which is designed as a long-term project, started as early as 2002 with the ZDM's predecessor, the data collection centre, and has been continued successfully since.

The static content is managed using the WSV Content Management System and thus seamlessly fits in with the corporate design of the WSV. The dynamic content is implemented by an external service provider.

The ZDM hardware infrastructure is completely embedded in the local network structure of the DLZ-IT and the intranet of the WSV and can therefore provide general and fast access to the central services offered by the DLZ-IT. This simplifies the integration of central services provided for federal and other waterways by the WSV in the ZDM portals. In future this network will be used, for example, to access data in the water resources management information system KISTERS (WISKI) and to eliminate complex exports and imports of data. If changes are made to data, they can be used directly by the hydrological divisions with no additional efforts by the ZDM and no need for redundant data storage.

4 Regional portal Tidal Elbe

The regional portal Tidal Elbe was the first web portal to start operation. It was set up together with the data collection centre which was used in the survey of existing conditions during the last fairway adjustment in 1999/2000. The data and content provided on this portal therefore exceed what is available on the other regional portals. The functionality and content of the portal Tidal Elbe is representative of the other four regional portals of the ZDM.

The area under observation in this portal (see Fig. 1) roughly follows the regime of the Elbe estuary, extending from the weir at Geesthacht (Elbe km 588) to the mouth of the Elbe (Elbe km 760) (BOEHLICH and STROTMANN, 2008). In addition, the subareas of the tributaries at the Lower Elbe and the Binnenelbe as far as Neu Darchau are included.

The web site is divided into four areas (see Fig. 2) where the following information and data is available, as described below:

- Project information ("Projekte" (projects))
- Map ("Kartentool" (map tool))
- Time series ("Messwertassistent" (measurement wizard))
- Downloads ("Datendownload")

The closely interlinked pages can each serve as an entry point for navigating to the information and data on the individual portals. The user can easily and conveniently navigate from a map view of an oxygen monitoring network to a time series presentation and a

page where data on the oxygen parameter can be downloaded. The reverse path is just as easy. If the user enters the web page via the data download section, the map retrieval from there is equally simple.



Figure 2: Homepage of www.Portal-Tideelbe.de.

4.1 Project information

This page holds static content of projects organised in new constructions and extensions. The static content comprises scoping papers, planning documents and plan approvals presented systematically in a repetitive pattern and in a manner which is easy to follow. For larger projects a short project profile is followed by further technical content, sorted by project phase:

- Preliminary studies
- Planning
- Planning approval
- Existing conditions documentation
- Measures of compensation

On providing this information the ZDM seeks to offer the static content with the highest possible standards of accessibility and hereby ensuring that it complies with the ordinance on barrier-free information technology pursuant to the Act on Equal Opportunities for Disabled Persons (Behindertengleichstellungsgesetz (BITV 2.0)) which is applicable to the federal authorities.

There are many links leading from the areas with static content to the portals' dynamic areas, (e.g. the map tool, the data download pane, the database of publications or the presentation of time series), for example to complement a planning document with a corresponding map presentation.

4.2 Map

The display of maps is always an essential part of data portals. The ZDM portals use the map server of the Open Source Geospatial Foundation (OSGeo) which offers a variety of general functionalities. One of the most noteworthy features is the permalink which allows for permanent storage of map views and a free text search in all existing map topics.

Unlike many other geo portals the ZDM portals offer a wide spectrum of data, ranging from base geospatial data to data taken from hydrological and meteorological stations (point information) to the documentation of longitudinal and cross profiles (line data) and to large biotope type collections from High Resolution Stereo Camera (HRSC) data and comprehensive topographic models created from aerial laser scanning and hydrographical surveys (surface data).

The map topics cover the following subject areas:

- Base geospatial data
- Observational networks
- Topography
- Vegetation
- Sediment distribution
- Compensation areas
- Photo documentation
- Port documentation
- Estuary dams

4.2.1 Web Map Service and Web Feature Service

All map-related topics are freely available as a Web Map Service (WMS) and can be conveniently embedded in the user's own local GIS applications.

Each regional portal has its own separate WMS web address following the pattern set on the Tidal Elbe Portal:

<http://www.portal-tideelbe.de/cgi-bin/bs>

To improve the indexing capability of our maps for external and internal search engines a Web Feature Service (WFS) is used. With the WFS a description of all map topics is available so that the monitoring networks in particular can be found and presented in a better manner.

<http://www.portal-tideelbe.de/cgi-bin/wfs>

The standardised connection of the WISKI system (see section 3 Collaboration with the DLZ-IT Ilmenau) will use a Web Processing Service (WPS) in future to derive water level values, since this data is not stored in the WISKI database.

4.3 Time series

Among the topics dealt with in existing condition documentation great significance is attached to plausibility tested time series data related to parameters such as water level, current, electrical conductivity and oxygen. The principal focus of the portal is on

plausibility tested time series. They provide a sound basis for analyses regarding all river regime-related topics. Regular requests from research and industry prove their high value.

The following data is available in form of plausibility tested time series:

- Discharge
- Chloride content
- Electrical conductivity
- PH value
- Salinity
- Oxygen
- Flow velocity
- Flow direction
- Water temperature
- Water level data
- Meteorological data

Moreover, to ensure that the appropriate decisions are taken regarding water sampling in the *Alte Land* area, a system with near real-time capability is operated. It provides updated measurement data on electrical conductivity and temperature at currently 12 stations. Upon its completion it will enable the retrieval of data from 18 stations. The notification functionality of the Sensor Web Client used here (see section 4.3.2 Display of time series – Sensor Web Client) facilitates sending a notification via email if certain limits are exceeded.

4.3.1 Provision of time series - Sensor Observation Service

The Sensor Observation Service (SOS) is a web service interface maintained by the Open Geospatial Consortium (OGC) for accessing time series data in real time or for data archiving. The OGC SOS interface enables interoperable (pull-based) access to measurement and observation data. Analogous to the functions of other OGC services it offers operations for retrieving (or publishing, where appropriate) spatial measurement data and associated metadata (JIRKA et al. 2014).

The evaluation across applications of hydrological data from different sources is becoming increasingly important. In this field the ZDM has long been a pioneer in provisioning data from different providers. In the context of fairway extension at the Lower Elbe an essential task of the ZDM is the merging of time series data collected from the different authorities of the federal government and the federal states. Due to the fact that data producers like the Elbe River Basin Community (Flussgebietsgemeinschaft (FGG) Elbe) have not been using standardised interfaces such as the SOS interface for data provisioning, it is first of all necessary to transfer the data manually to the ZDM's database.

The Sensor Observation Service (SOS) serves as an abstraction layer to ensure data independence from specific databases. It publishes the time series data in a standardised format and deploys them on the web. Fig. 3 shows a typical configuration for the use of a SOS server. If other data providers use this interface in the future, time series data may be exchanged easily and without data duplication.

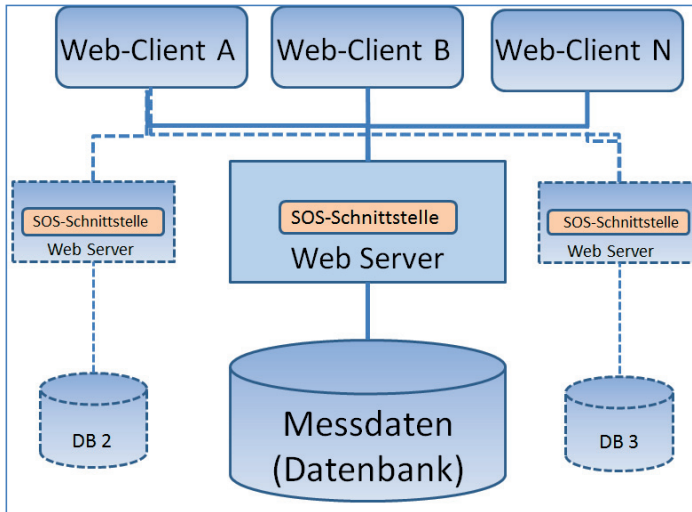


Figure 3: Typical SOS configuration.

4.3.2 Display of time series - Sensor Web Client

With the use of the Sensor Web Client (SWE Client) the ZDM aims at a user friendly presentation of different time series. The SWE Client enables a combined display of hydrographs (see Fig. 4) in an efficient and elegant manner. The version used by the ZDM is a customized version of the Open Source Client developed by the company 52 North. All changes made by the ZDM have been transferred back to the Open Source Community and are therefore openly available.

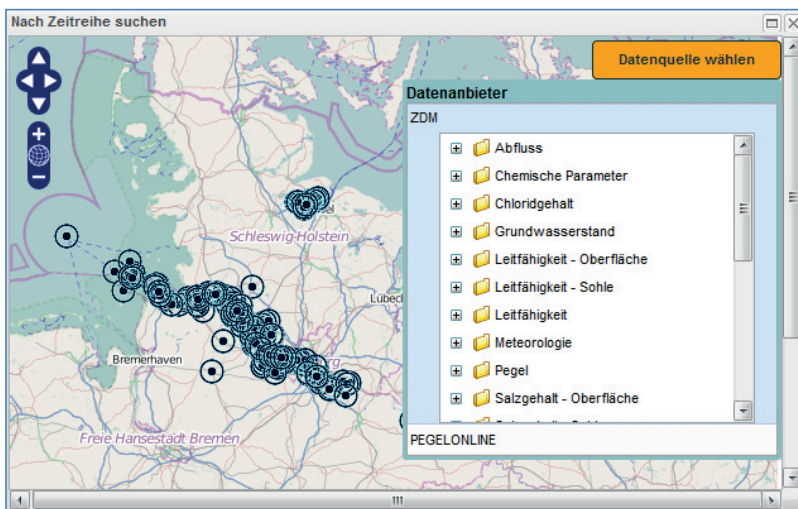


Figure 4: Sensor Web Client time series selected by measurement parameter.

A map component allows choosing a data provider (SOS interface) and one of the available parameters. A short profile of specifications presents the master data of the measuring station. If the data is of interest it can be included in the hydrographs displayed. Further time series can be loaded and combined provided the data extends over the same temporal range. As illustrated in the example of an extreme flood scenario (see Fig. 5) several different parameters can be considered in a particular period of time.

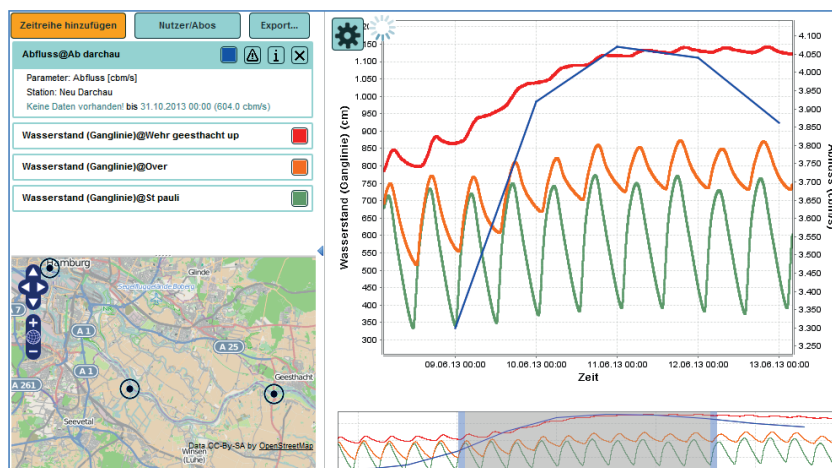


Figure 5: Sensor Web Client time series display – extreme flood event in Geesthacht on the River Elbe – water level and discharge parameters.

The following functions are available for the generation of an analytical visual display:

- Manual scaling of timeline
- Manual scaling of data axis for each parameter separately
- Customising of colours and line thickness in all hydrographs

The permalink feature enables permanent reproduction of user settings. The user only needs to save one link which contains the information required for restoring all the comprehensive adjustments made for a representation. The ZDM Web Client is available at: <http://www.portaltideelbe.de/SWC/>

4.4 Data download - available data

All the maps and plausibility tested time series are freely downloadable. The maps are offered in Esri shape file format and the time series in ASCII file format. In addition the user can download large data collections like a port or construction database.

Daten-Download

Ich habe die Nutzungsbedingungen gelesen und akzeptiere sie.

Portal

Erhebende Organisation

Bitte wählen Sie einen Themenbereich und wenn gewünscht, ein Einzelthema aus diesem Themenbereich aus.

Themenbereich

Einzelthema

Aktualisiert seit (tt.mm.JJJJ)

[Liste erstellen](#)

Figure 6: Data download – choices for portal, organisation and subject areas.

5 Metadata

Metadata about the available geospatial data and measuring stations of the ZDM portals are published in the German Portal for geospatial data Geoportal.de. Metadata are maintained in the WSV central metadata information system GeoKatalog.WSV and are transferred to Geoportal.de using the Catalogue Service Web (CSW) interface.

6 References

- BOEHLICH, M.J. and STROTMANN, T.: The Elbe Estuary, *Die Küste*, 74, 288-306, 2008.
- MAPSERVER.ORG: MapServer - open source web mapping. <http://mapserver.org/>, Stand: 22.04.2013.
- ORTHS, A. and NEUMANN, L.J.R.: Maritime Daten zentralisieren – Fachstelle Zentrales Datenmanagement, *Die Küste, Jahresbericht 2008 Wasser- und Schifffahrtsdirektion Nord*, http://www.wsd-nord.wsv.de/Service/Broschueren__Flyer_etc/Anlagen/Jahresbericht_2008_WSD-N.pdf, 32-33, 2008.
- OPENLAYERS.ORG: Free Maps for the Web. <http://www.openlayers.org>, last visited: 20.04.2013.
- OGCNETWORK.NET: OGC Network. Sensor Observation Service. <http://www.openlayers.org/SOS>, last visited: 20.04.2013.
- JIRKA, S.; REMKE, A.; BRÖRING, A. AND RIEKE, M.: Erfüllung von INSPIRE-Verpflichtungen zu Anhang II und III-Themen mit Hilfe von Sensor Web-Technologie (DGPF Tagungsband 23 / 2014), 2014.

Velocity and Turbulence Measurements at the Ems Barrage

Oliver Lojek, Knut Krümer, Anna Zorndt, Nils Goseberg and Torsten Schlurmann

Summary

From July 14th-16th, 2012 a joint measurement campaign was conducted at the Ems barrage in Gandersum, Germany, by The Lower Saxon State Department for Water, Coastal and Nature Conservation (NLWKN), the Water and Shipping Authority (WSA) Emden and the Franzius-Institute for Hydraulic, Waterways and Coastal Engineering (FI). Both, moored and mobile measurements were carried out.

Measurement results of mobile 3D-current velocities by Acoustic Doppler Current Profiler (ADCP), complemented by a conductivity, temperature and depth (CTD) sensor for vertical profiling are presented here. Results support the calibration and development of a hydro numerical model by the NLWKN.

Keywords

Ems, barrage, ADCP, CTD, Reynolds stresses, TKE, gradient Richardson number

Zusammenfassung

Vom 14. bis 16. Juli 2012 wurde am Emsperrwerk in Gandersum, Deutschland, von dem Niedersächsischer Landesbetrieb für Wasserwirtschaft, Küsten- und Naturschutz (NLWKN) zusammen mit der Wasser und Schifffahrtsverwaltung des Bundes (WSA/WSV) sowie dem Franzius-Institut für Wasserbau, Ästuar- und Küsteningenieurwesen (FI) eine gemeinsame Feldmesskampagne durchgeführt. Es wurden Messungen von vertäuten sowie mobilen Plattformen aus durchgeführt.

Messergebnisse von 3D-Strömungsgeschwindigkeiten gemessen mittels Ultraschall-Doppler-Profil-Strömungsmesser (engl.: Acoustic Doppler Current Profiler, ADCP), sowie ergänzende Leitfähigkeits-, Temperatur- und Tiefenmessungen im Profil mit einer gefierten CTD-Sonde werden hier vorgestellt. Die Ergebnisse eignen sich für die weitere Entwicklung und Kalibrierung eines hydro-numerischen Modells der Ems durch das NLWKN.

Schlagwörter

Ems, Sperrwerk, ADCP, CTD, Reynolds-Spannungen, TKE, Gradient Richardson Zahl

Contents

1	Introduction	56
2	Methods	57
2.1	Measuring equipment	57
2.2	Measuring schedule.....	58
2.3	Blending of ADCP- and CTD-data	59
3	Results	60
3.1	ADCP-measurements.....	60
3.1.1	Baseline measurement	61
3.1.2	Tidal control run	61
3.1.3	Comparison.....	62
3.2	CTD-measurements	62
3.2.1	Salinity.....	63
3.2.2	Turbidity.....	63
4	Turbulence parameters.....	64
5	Discussion and Conclusion	66
6	References	66

1 Introduction

The Lower Saxon State Department for Water, Coastal and Nature Conservation (NLWKN) is evaluating the use of an existing storm surge barrage in the lower river Ems in order to influence the estuaries sediment transport behaviour (see Fig. 1 OBERRECHT and WURPTS 2014). From July 14th-16th, 2012, a tidal control experiment was conducted at the Ems barrage in Gandersum, Germany. The aim of the series of experiments is the investigation of a possible manipulation of tidal- and sediment dynamics in the Ems estuary. Supplementing in-situ measurements, a numerical model of the estuary is developed by NLWKN. The model is capable of simulating the operation of the Ems barrage as well as the Ems-specific fluid-mud dynamics. Prerequisite for a successful calibration and operation of the model is the knowledge of the local current- and turbulence characteristics in the vicinity of the barrage. By means of a specific time-variable operation of the barrage gates, the tidal flow during the flood phase was slightly delayed in order to reduce tidal asymmetry.

The reduced water level gradient in combination with narrowing of the flow cross section was expected to minimize the flood momentum and therewith the sediment transport capacity. The tidal control experiment was complemented by a comprehensive measuring campaign.

2 Methods

A number of research vessels took various measurements of different characteristics in the area of the barrage. Measurement stations located both seaward and inland of the barrage were operated by the Water and Shipping Authority (WSA) Emden, moored NLWKN R/V Burchana performed stationary turbulence measurements employing Acoustic Doppler Current Profiler (ADCP)-Turbulence and – for reference – Acoustic Doppler Velocimetry (ADV). The NLWKN survey vessel Nynorder Oog, performed bathymetric soundings both. Furthermore, the research boat of the Franzius-Institute (FI) conducted current- and turbulence measurements in direct vicinity of the barrage by means of an ADCP complemented by a conductivity, temperature and depth (CTD) sensor. Over a period of five tidal cycles, the secondary barrage gates (Nebenöffnungen) were closed approximately 30 min before ebb slack water, and were kept shut during the flood period until the following high water. Measurements in 2009 already revealed that the narrowing of the flow cross section results in significantly increased current velocities within the proximity of the remaining two open weir gates. By means of ADCP measurements conducted by FI, the effect of the tide control experiment on current velocities and current fields were monitored.

2.1 Measuring equipment

Measurements evaluated here were conducted with the research boat of the Franzius-Institute. Vectorial 3D-current velocities were measured by means of an ADCP Work Horse Rio Grande by Teledyne TD Instruments with a working frequency of 600 kHz. The orientation of the ADPC is determined by internal sensors registering pitch and roll magnitudes. Absolute positioning of the vessel is obtained by its geodetic differential GPS-receiver by Trimble which features its own reference station allowing for real time kinematic (RTK) correction of the vessels position. This allows an absolute positioning within decimetre precision. The orientation of the vessel as well as the ADCP in the measuring plane is obtained by means of a GPS-compass rendering the method immune to ferromagnetic distortions such as could be present near the barrage gates or pile moorings at the Ems barrage. In case of failure of the GPS-compass yaw line-of-sight (LOS) rates were also recorded using the vessels gyroscopic system for a fail-safe determination of bearing information via dead reckoning. Vertical profiles of salinity, turbidity and temperature in the water column were measured utilizing a CTD-probe. The most important parameters of the operated instruments are summed up in Tab. 1 below.

Table 1: Overview of measurement instruments operated on the FI-vessel.

Instrument	Type	Manufacturer	Test frequency	Resolution
ADCP	WH Rio Grande	Teledyne RDI	2,5 Hz	0,25 m
dGPS	Trimble 5700	Trimble	1 Hz	0,1 m
Rotation rate sensor	Gyro Plus 2	Raymarine	10 Hz	0,1°
GPS-compass	LV 100	Hemisphere	10 Hz	0,1°
Conductivity, temperature and depth sensor (CTD)	ECO IV	Grisard	1 Hz	-

2.2 Measuring schedule

The tidal control experiment stretched over four tidal cycles ranging from July 14th to 16th, 2010. In order to evaluate the influence of the experimental tidal control run onto local current conditions supplemental unimpeded “zero-tides” have been measured before and aft. The measurement campaign was especially focused onto varying flood-current-velocities. Measurement times/periods were tied to the tidal control experiment from ebb slack tide to mean tide. Measurements were conducted in so called measurement cycles (mc) which are made up of profile groups featuring distinct procedures of ADCP-profiles and CTD-measurements. Measurement positions are depicted in Fig. 1.

One regular measurement cycle entails one longitudinal (P0) and five cross-sectional profiles (P1-5) landward and one profile seaward of the barrage. Additional CTD-measurements were conducted at the intersections of the cross-sectional profiles P1, P4 and P5 with the longitudinal profile as well as at the position of the NLWKN research vessel Burchana between the first and second rows of pile moorings at level with the southern pier of the main barrage opening (HSÖ) (V1-V4). In total 130 ADCP-profiles and 78 vertical CDT-profiles were measured, whereof 17 pairs rendered suitable for an advanced scientific investigation regarding possible turbulence parameters.

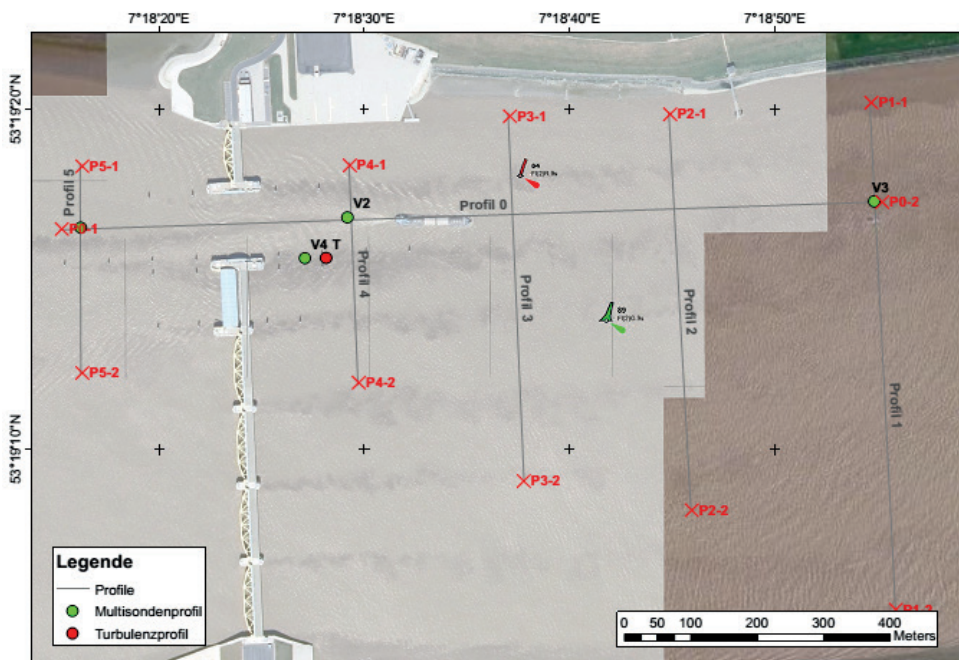


Figure 1: Overview of the measurement profiles (—) for the FI-boat with CTD-measurement positions (•) and turbulence measurement positions (•).

2.3 Blending of ADCP- and CTD-data

Standalone ADCP- and CTD-measurements form the basis upon which local current characteristics before and after the barrage under changing gate operation are evaluated. Furthermore a conjoint deployment of the ADCP and the CTD probe allow for a subsequent blending of the data for a specific location using the instrument timestamps. By interpolating the CTD data linearly onto the ADCP data (cf. Fig. 2) one value is obtained for salinity, temperature and pressure for every ADCP depth cell at a point in time.

This approach allows for turbulence parameters such as the turbulent kinetic energy (TKE) or gradient Richardson numbers (Ri) to be determined for specific positions.

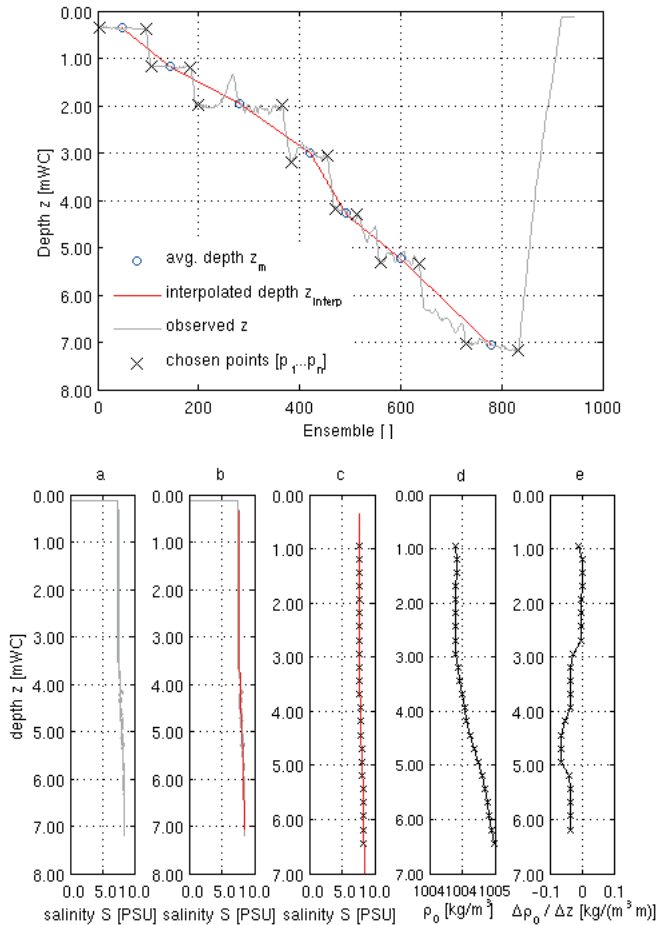


Figure 2: First panel: Linear interpolation of CTD-measurements for further blending with ADCP-measurements. Second panel: Stepwise generation of input data for determining turbulence parameters. Exemplary salinity data. a) CTD-measurements of salinity over the water column. b) PSU-function based upon averaged depth-values. c) interpolated PSU-cell-centre-values (x). d) Potential density in kg/m³ determined based upon the interpolated values (x). e) Change of the pot. density over the depth in kg/m³ (x).

3 Results

In-situ measurements of pressure, temperature and conductivity by CTD illustrate the evolution of the said parameters over the tidal cycle. In addition, blending the ADCP velocity measurement data with the CTD profile data obtained at the same locations allows for calculating turbulence parameters. Therefore, the CTD data was linearly interpolated onto the vertical positions of the ADCP bins, resulting in one value per variable (salinity, pressure, temperature) per ADCP depth cell. Reynolds stresses ($R_{i,j}$) have been determined using the variance technique described by LOHRMANN et al. (1990).

Turbulent kinetic energy (TKE) was calculated following the approach described in LOHRMANN et al. (1990), as well as STACEY et al. (1999a, 1999b). Finally, profiles of gradient Richardson numbers (Ri) were calculated, which serve as an indicator for stability of a stratification in the water column. The theoretical framework of LOHRMANN et al. (1990) has been used, which relates the stratification to the velocity shear. The investigations revealed a distinct influence of the tidal control experiment on the local turbulence regime. These observation-based results support the calibration of the numerical model of the river Ems and the barrage developed and operated by the NLWKN.

3.1 ADCP-measurements

3D-current velocity measurements were carried out with an ADCP which was operated on the FI-boat. Thus, current measurements have successfully been conducted over a wider area. Fig. 3 depicts the temporal distribution of conducted measurement cycles (mz02-19) with the underlying tide.

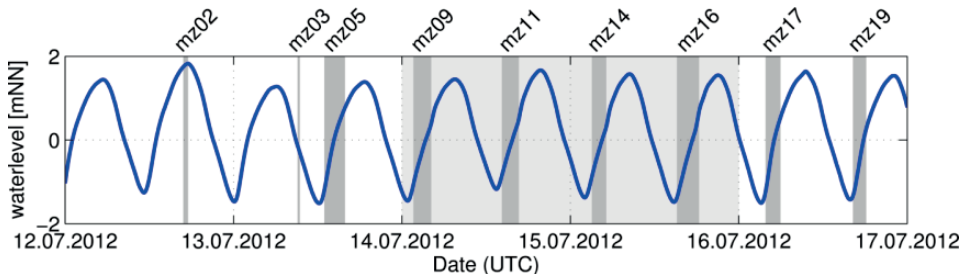


Figure 3: Overview of ADCP-measurements conducted with the FI-boat during the measurement campaign July 14th–16th, 2012. Turbulence measurement cycles (■), Tidal control experiment (□), Water level at the gauge Ems barrage (—).

3.1.1 Baseline measurement

The tidal control run was preceded by measurement cycle mc05 during which current velocities were recorded. For the baseline measurement all gates of the barrage were kept open. Three measurement cycles were conducted (mc05a - mc05c). Fig. 4 shows results for mc05c.

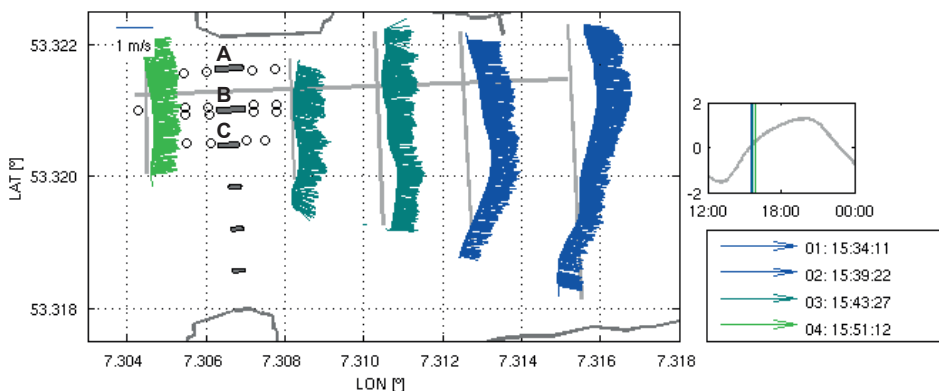


Figure 4: ADCP-velocity measurements during a "zero tide". mc05c, six profiles within the time period 15:34:11–15:53:59 UTC|13.07.2012. The Ems flows unimpeded and develops an approximately constant current field A) NÖ1, B) HSÖ, C) BSÖ.

The first mc05a, recorded on the 13.07.2012 from 12:57 to 13:34 UTC, captures the current velocity distribution near the barrage shortly after the flood stream flow began. Depth averaged flow velocities reach 0,3 - 0,6 m/s. Due to the larger flow cross section within the area of NÖ1 (A), HSÖ (B) and BSÖ (C) a reduction of the current velocities from the northern shore towards the southern shore can be observed. Mc05b was measured at fully developed flood stream between 14:25 and 15:00 UTC. Velocities range from 0,8 m/s to 1,2 m/s. The formerly mentioned reduction of the velocities from northern to southern shore is less distinctive. mc05c was captured during mean tide and features velocities ranging from 0,6 to 0,8 m/s (cf. Fig. 4).

3.1.2 Tidal control run

For visual assessment of the current velocity field influenced by the tidal control experiment during mc09, recorded the 14th of July 2012 with four full profile groups from 01:28 - 04:10 UTC, is presented here. Fig. 5 shows ADCP-measurement results for mc09b.

mc09a was recorded between 01:38 and 02:06 UTC, shortly after low tide. Current velocities within the area of the navigational sluices reach 0,7 m/s at the beginning and continuously rise during the mc and reach 1,5 m/s. Due to a reduction of the cross-section to the navigation openings a backflow develops downstream the closed gates. It reaches velocities of up to 0,6 m/s in the southern half of the river. In the course of the flood the current velocities rise up to 2,0 m/s in the main navigational openings during mc09b. Furthermore, the backflow intensifies and reaches up to 1,0 m/s.

During mc09d, velocities within the navigational channel still reach 2,0 m/s, whereas the backflow slightly diminishes to 0,6 m/s.

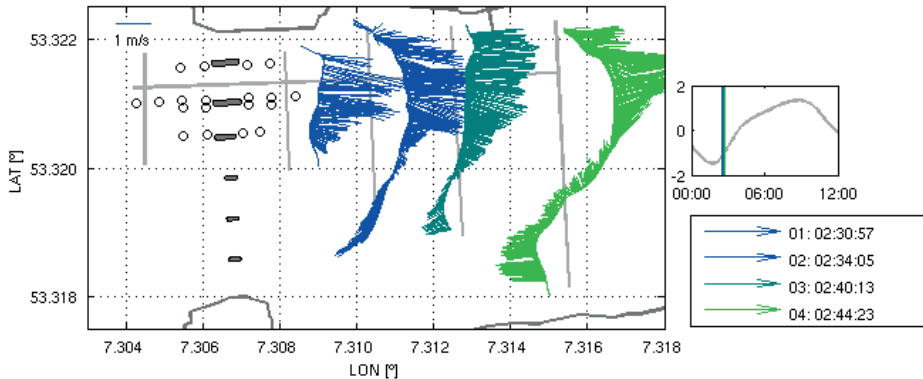


Figure 5: ADCP-velocity measurements during the tidal control run. mc09b, four profiles within the time period 02:30:57–02:44:23 UTC|14.07.2012. Landwards of the barrage towards the southern shore a distinct eddy and backflow develop.

3.1.3 Comparison

The baseline measurement preceding the tidal control experiment (mc02, mc03 and mc05), depicts a uniform current field with a tendency for slightly higher velocities in the navigational channel near the northern shore of the Ems. Compared to the baseline measurement the tidal control run clearly constricts the flood stream to the main and inland navigational gates, inducing an intense velocity shear between the northern and southern part of the river as well as the development of an eddy in the southern part of the river. Depth averaged maximum flood velocities reach 2,5 m/s in the navigational channel during the tidal control experiment with peak values above 3,0 m/s. Follow-up baseline measurements (mc17 and mc18) document that the previously measured uniform current field is re-established. Depth averaged velocity values are not altered by the foregone control run e.g. due to the retention of backwater.

3.2 CTD-measurements

Salinity and temperature have been measured by means of a CTD probe at various locations and intervals (cf. Fig. 1). The development of the variables over the tidal cycle, as anticipated, depicts a slight variability in time.

However, no stratification can be detected in the measurement data. Nevertheless, the salinity data reveals the development of a vertical salt gradient (cf. Fig. 6).

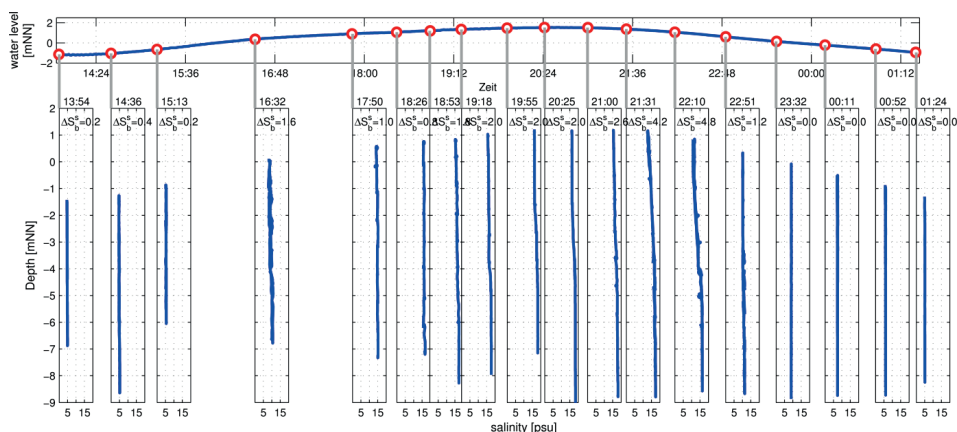


Figure 6: CTD measurements of salinity in PSU in the water column over the tide. mc11-13, 19 profiles within the time period from 13:51:59 14.07.2012–15.07.2012 13:27:03 UTC.

3.2.1 Salinity

The CTD-salinity-data shows four distinct phases. At low water the measured salinity reaches 5 PSU and the water column is completely mixed. Difference between top and bottom layer are 0,2 PSU. During flood stream the salinity values rise continuously until they reach 10 PSU at mean tide water. The difference reaches up to 1,2 PSU here. From mean tide to high water a slight layering of the salinity values within the water column can be seen. Values reach 15 PSU near the surface and 17 PSU near the bottom. With the initial ebb stream values decrease again due to the increasing influence of the headwater discharge, resulting in surface values of 10 PSU, maximising the internal gradient. From mean tide onwards the ebb stream shows a completely mixed water column again. Salinity values drop continuously from 10 to 5 PSU at low water.

3.2.2 Turbidity

The turbidity is measured by means of an optical attenuation sensor and describes the ratio of the emitted to absorbed and scattered light. A turbidity of 0 % is reached when 100 % of the emitted light is detected at the end of the measuring distance. A turbidity of 100 % results when 100 % of the emitted light is scattered and/or absorbed. The measurement values of the turbidity sensor have been evaluated by means of onsite collected water samples. These were stepwise diluted with fresh water afterwards in order to obtain a suitable calibration for the sensor. Accounting for the high turbidity in the Ems river, a customized measuring distance of 15 mm has been used instead of the 135 mm long standard distance.

The CTD turbidity data shows four distinct phases. From low tide to mean tide, high turbidity values around 95 % with a completely mixed water column were observed. From tide mean water to the subsequent high tide a reduction of the turbidity to 70 % was measured in the upper half of the water column. This results in a gradient within the water column, since the bottom values remain at about 90 %. At high tide the surface

values drop to 30-40 % and the bottom values to 50-60 %. During ebb current well-mixed conditions are re-established and the values rise continuously up to 95 % at the following low tide.

4 Turbulence parameters

Further blending the measurement data taken at the same time and location allows for Reynolds stresses as well as Turbulent kinetic energy (TKE) and gradient Richardson numbers (Ri) to be determined for these specific measurements. In total 17 mc rendered a blending possible. These parameters have been calculated based on the framework presented by LOHRMANN et al. (1990), STACEY et al. (1999a, 1999b), TRUCKENBRODT (2008), MCDUGALL et. al. (2010) and LU and LUECK (1999). Results for the baseline measurements depict an evolution of the parameters over the course of the flood stream. Reynolds stresses develop the typical Reynolds stress profile over the water column described in (not shown here). For the baseline measurements the values range from 0.005-0.02 m²/s². Values rise with the beginning of the flood stream and gradually sink again after mean tide. A similar behaviour was observed for the tidal control run, whilst the overall values were slightly larger ranging from 0.02-0.04 m²/s².

TKE-values develop in a similar way, for the baseline measurements the values rise with the initial flood stream and gradually drop when mean tide is reached. Values range from 0,1-0.15 W/m². During the tidal control run the values, similar to the Reynolds stresses, are bigger and range from 0.17-0.21 W/m². Nevertheless, the course of development remains the same, where the values gradually drop once mean tide is reached.

Finally the Richardson number Ri has been determined as a means to evaluate whether the turbulent energy present suffices to overcome potential stratifications within the water column. Ri describes a ratio the potential energy to the kinetic energy. The critical value lies at $Ri_{crit} = 0.25$, above which too little energy is present and a stratification could form. Values below Ri_{crit} feature enough energy to overcome a potential stratification within the water column. Ri-values have been normalized in accordance with int. literature, with $\log_{10}(Ri/0.25)$ shifting Ri_{crit} from 0.25 to 0.0, facilitating the interpretation of plots (STACEY et al. 1999a, 1999b).

Ri-values determined for the baseline measurement data exhibit a similar behaviour as the other two turbulence parameters determined, in that the values increase with the beginning flood stream and decrease again when the mean tide is reached. Values for the baseline measurements range from -3.0 to -5.3, indicating sufficient energy to overcome a potential stratification. For the tidal control run, values also rise over the course of the flood stream and decrease with mean tide. Ri-values for the tidal control run are more negative, ranging from -4.3 to -6.0, implicating a shift of the ratio towards the kinetic energy. Fig. 7a shows the result for a Ri-profile for mc09c with its measurement location (Fig. 7b) and time frame (Fig. 7c).

Finally, all Ri-values obtained are negative, and feature no sudden, large variances within their profiles, thus can be depth averaged without losing any vital data for an easier visual assessment (cf. Fig. 7d).

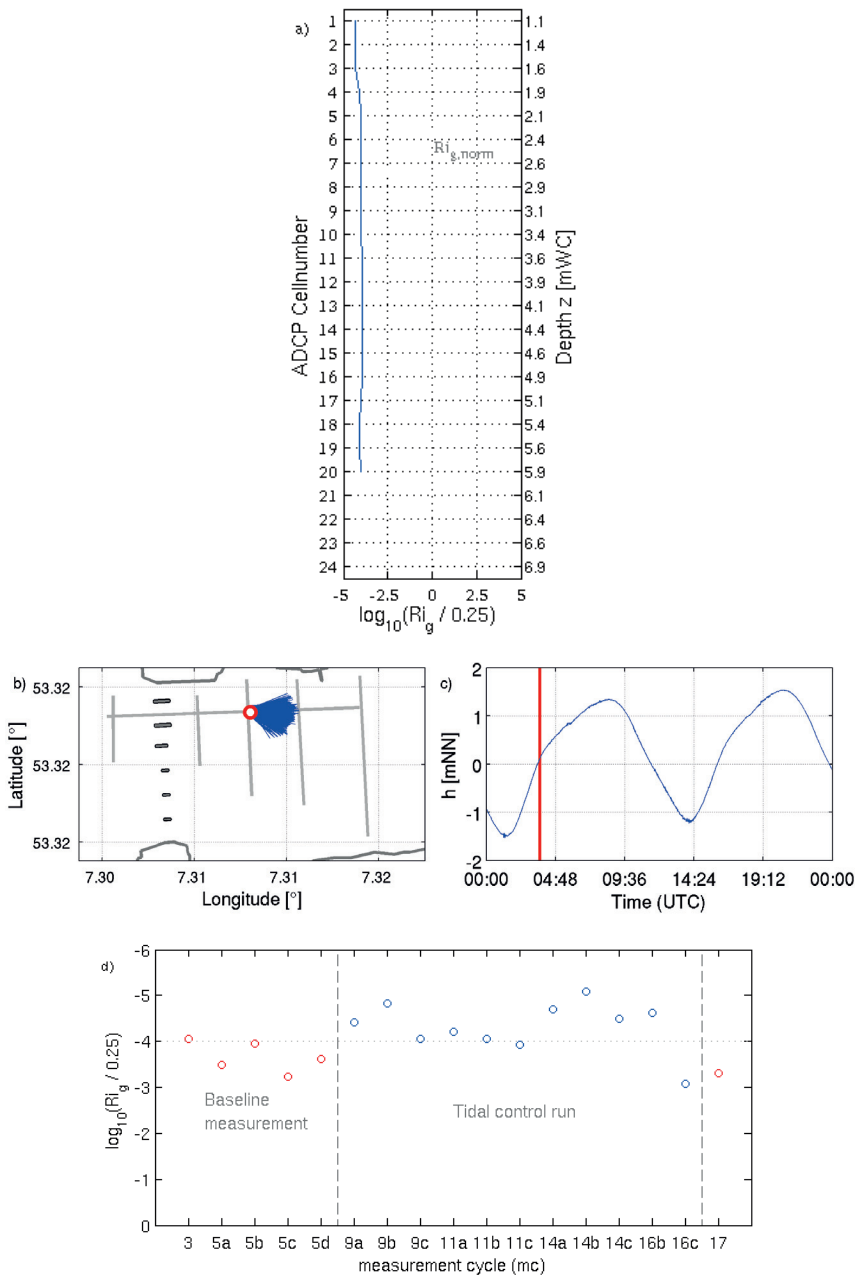


Figure 7: a) Normalized gradient Richardson number (\rightarrow) plotted over the profile mc09a CTD: 14.07.2012, 02:17:21–02:24:01 | ADCP: 14.07.2012, 02:15:49–02:25:57 UTC. b) Locations of the measurements in regards to the barrage with the position of the CTD-probe (\circ) as well as the supplemental ADCP-measurements (\rightarrow) c) Measurement period within the tide. d) Normalized depth averaged Gradient-Richardson-Numbers for the turbulence measurement cycles 3 to 17 originating from the blending of the ADCP-measurements with the CTD-data collected with the FI-boat on sight.

5 Discussion and Conclusion

During the tidal control experiment at the Ems barrage from the 14th to the 16th of July 2012, the Franzius-Institute conducted measurements of the 3D current velocities by ADCP as well as salinity and turbidity by CTD. Measurements were conducted from a mobile platform, operated in the fast flowing waters of the Ems river, and have successfully been evaluated. Measurement results presented here capture alterations in the local current field associated with the tidal control experiment.

Furthermore, collected data supports the calibration and validation of a hydro-numerical model of the Ems estuary developed and operated by NLWKN.

The ADCP measurements clearly depict an augmentation of the depth averaged current velocities by constricting the flow cross section to the navigation openings.

During flood current an eddy and backflow develop in the area of the closed secondary gates.

Vertical CTD measurements of salinity and turbidity showed a slight vertical gradient for water levels above mean water. The turbidity exhibits a maximum difference between top and bottom values of 30 %. Salinity values exhibit a maximum vertical gradient of 5 PSU.

Furthermore, in the area of the main navigational opening measurement deficiencies were encountered during baseline measurements due to non-detectable channel bed. This could be indicative of a near bed accumulation of suspended sediments or fluid mud is present within this area.

Turbulence parameters calculated by blending measurement data reveal an overall enhancement of already existent turbulences caused by the tidal control experiment. However, a significant increase in turbulence characteristics could not be detected. Nevertheless, the measurements help to assess the effects of the experimental gate operation procedure on hydrodynamics in the vicinity of the Ems barrage.

Finally, a new and mobile measurement method for turbulence parameters based on ADCP and CTD measurements, has been successfully applied.

6 References

- MCDUGALL, T.J.; FEISTEL, R.; MILLERO, F.J.; JACKETT, D.R.; WRIGHT, D.G.; KING, B.A.; MARION, G.M.; CHEN, C-T.A.; SPITZER, P. and SEITZ, S.: The International Thermodynamic Equation of Seawater 2010 (TEOS-10): Calculation and Use of Thermodynamic Properties. In: Global Ship-based Repeat Hydrography Manual, IOCCP Report No, 14, ICPO Publication Series No. 134, 2010.
- LOHRMANN, A.; HACKETT, B. and ROED, L.P.: High Resolution Measurements of Turbulence, Velocity and Stress Using a Pulse-to-Pulse coherent Sonar. In: Journal of Atmospheric and Oceanic Technology, 19-37, 1990.
- LU, Y. and LUECK, R.G.: Using a Broadband ADCP in a Tidal Channel. Part I: Mean Flow and Shear. In: Journal of Atmospheric and Oceanic Technology, 16, 1556-1567, 1998a.
- LU, Y. and LUECK, R.G.: Using a Broadband ADCP in a Tidal Channel. Part II: Turbulence. In: Journal of Atmospheric and Oceanic Technology, 16, 1568-1579, 1998b.

- OBERRECHT, D. and WURPTS, A.: Impact of Controlled Tidal Barrier Operation on Tidal Dynamics in the Ems Estuary. In: Die Küste, 81, 2014.
- STACEY, M.T.; MONISMITH, S.G. and BURAU, J.R.: Measurements of Reynolds stress profiles in unstratified tidal flow. In: Journal of Geophysical research, 104(C5), 10933-10949, 1999a.
- STACEY, M.T.; MONISMITH, S.G. and BURAU, J.R.: Observations of Turbulences in a Partially Stratified Estuary. In: Journal of Physical Oceanography, 29, 1959-1970, 1999b.
- TRUCKENBRODT, E.. Grundlagen und elementare Strömungsvorgänge dichtebeständiger Fluide. In: Fluidmechanik Band 1, doi: 10.1007/978-3-540-79018-1_3, 2008.

Turbulence Closure Modelling in Coastal Waters

Hans Burghard, Ulf Gräbe, Peter Holtermann, Knut Klingbeil and Lars Umlauf

Summary

In this paper the use of turbulence closure models in coastal ocean models is reviewed. Two-equation turbulence closure models are argued to be an optimal compromise between efficiency and accuracy for the purpose of calculating diapycnal fluxes of momentum, heat and tracers in coastal ocean modelling. They provide enough degrees of freedom to be calibrated to the most prominent properties of coastal ocean mixing, but are still numerically robust and computationally efficient. Isopycnal mixing schemes are briefly reviewed as well. Major implementational and numerical aspects are presented, with some focus on the inherent problem of numerically-induced mixing which together with the physically-induced mixing gives the effective mixing in ocean models. Vertically adaptive coordinates are presented as one possibility to reduce numerical mixing. Finally, three coastal ocean simulation examples from the General Estuarine Transport Model (GETM) which is coupled to the turbulence module of the General Ocean Turbulence Model (GOTM) are given. These examples include thermocline mixing in the Northern North Sea, physically and numerically induced mixing in the Western Baltic Sea as well as basin-wide mixing in the Central Baltic Sea. All three examples highlight the importance of using well-calibrated turbulence closure models together with vertically adaptive coordinates.

Keywords

coastal ocean modelling, turbulence closure modelling, numerical mixing, adaptive coordinates, General Ocean Turbulence Model (GOTM), General Estuarine Transport Model (GETM)

Zusammenfassung

In diesem Artikel wird die Anwendung von Turbulenzschließungsmodellen in numerischen Modellen für den Küstenozean dargestellt. Zwei-Gleichungs-Turbulenzschließungsmodelle stellen für die Berechnung von diapycnischen Impuls-, Wärme- und Konzentrationsflüssen im Küstenozean einen optimalen Kompromiss zwischen Effizienz und Genauigkeit dar. Diese Modelle gewährleisten ausreichende Freiheitsgrade, um sie für die wichtigsten Eigenschaften der Vermischung im Küstenozean zu kalibrieren, sind aber immer noch numerisch robust und effizient im Bedarf an Rechenzeit. Isopycnische Vermischungsschemata werden ebenfalls kurz dargestellt. Die wichtigsten Aspekte der Implementierung und Numerik werden diskutiert, wobei der Schwerpunkt auf der numerisch induzierten Vermischung liegt, die zusammen mit der physikalisch induzierten Vermischung erst die effektive Vermischung in Ozeanmodellen ergibt. Vertikal-adaptive Koordinaten werden als eine Möglichkeit dargestellt, die numerische Vermischung zu reduzieren. Abschließend werden Beispiele von Simulationen im Küstenozean mit dem General Estuarine Transport Model (GETM) in Kopplung mit dem Turbulenzmodul des General Ocean Turbulence Model (GOTM) gezeigt. Diese Beispiele umfassen Vermischung in der Thermokline der nördlichen

Nordsee, physikalisch und numerisch induzierte Vermischung in der westlichen Ostsee sowie beckenweite Vermischung in der zentralen Ostsee. Diese drei Beispiele zeigen, wie wichtig die Verwendung von gut kalibrierten Turbulenzschließungsmodellen zusammen mit vertikal-adaptiven Koordinaten in der Modellierung von Prozessen im Küstenozean ist.

Schlagwörter

Küstenozeanmodellierung, Turbulenzschließungsmodellierung, numerische Vermischung, adaptive Koordinaten, General Ocean Turbulence Model (GOTM), General Estuarine Transport Model (GETM)

Contents

1	Introduction	70
2	Turbulence closure modelling.....	72
2.1	Two-equation closure models as work horses for parameterising vertical turbulent fluxes.....	72
2.2	Parameterisations for horizontal turbulent fluxes	75
3	Numerical and implementation aspects	76
4	Coastal ocean modelling examples.....	77
4.1	Thermocline mixing in the Central North Sea.....	78
4.2	Physical and numerical mixing in the Western Baltic Sea.....	79
4.3	Basin-wide mixing in the Central Baltic Sea.....	81
5	Conclusions.....	83
6	References	84

1 Introduction

Turbulent dissipation and mixing is of tremendous importance for the dynamics of the coastal ocean and the associated transports of heat, salt, suspended matter and biogeochemical solutes. Direct observations of mixing and dissipation are hampered by the stochastic character of the turbulence and its strong spatial and temporal variability. Meaningful observations of turbulence can only be carried out at single locations and at relatively large instrumental effort. Typical instrumentation includes free-falling turbulence microstructure profilers, operated from board, as well as high-resolution acoustic Doppler velocity measurements on integrated moored platforms. Successful observations of this type in the coastal zone of the North Sea and the Baltic Sea have, for example, been carried out by BECHERER et al. (2011), UMLAUF et al. (2007) and VAN DER LEE and UMLAUF (2011). These observations are indispensable for process studies in coastal waters but, in view of the extreme spatial and temporal intermittency of turbulence, they are usually insufficient to assess the gross turbulent transport and mixing in entire coastal ocean areas such as the basins in the Baltic Sea, tidal estuaries or the German Bight. For such system-wide studies, realistic three-dimensional numerical models are applied, which parameterise the turbulent processes with statistical methods. The turbulence observa-

tions (which are typically accompanied by observations of currents and stratification) are then invaluable for model calibration and validation.

Major processes for which marine turbulence is essential are for example the annual cycle of mixed layer dynamics (on which the entire primary production depends), sediment transport in highly dynamic waters such as the Wadden Sea or tidal estuaries (on which for example the morphodynamic evolution of these waters depends), processes of estuarine circulation and residual currents in estuaries and tidal inlets (on which residual sediment and solute transports depend), entrainment of ambient waters into buoyant surface plumes (such as river plumes) or dense bottom currents such as the saline inflows into the Baltic Sea, just to name a few.

The three-dimensional shallow water (i.e., hydrostatic) momentum equations for the calculation of the velocity vector (u, v, w) are the basis of most coastal ocean models. Examples for such models are the structured-grid models ROMS (Regional Ocean Modelling System, www.myroms.org, see e.g. SHCHEPETKIN and MCWILLIAMS 2005) and GETM (General Estuarine Transport Model, www.getm.eu, see e.g. HOFMEISTER et al. 2010 and references therein) and the unstructured-grid models SELFE (http://www.stccmop.org/knowledge_transfer/software/selfe, ZHANG and BAPTISTA 2008) and FVCOM (Unstructured Grid Finite Volume Coastal Ocean Model, <http://fvcom.smast.umassd.edu/FVCOM/>, CHEN et al. 2002). The general form of the momentum equations in these models is as follows (see, e.g., BLUMBERG and MELLOR 1987):

$$\begin{aligned} \partial_t u + \partial_x(uu) + \partial_y(uv) + \partial_z(uw) - \partial_x(2A_h \partial_x u) - \partial_y(A_h(\partial_y u + \partial_x v)) - \partial_z(A_v \partial_z u) = \\ +fv - g\partial_x \eta + \int_z^\eta \partial_x b d\xi \end{aligned} \quad (1)$$

$$\begin{aligned} \partial_t v + \partial_x(vu) + \partial_y(vv) + \partial_z(vw) - \partial_y(2A_h \partial_y v) - \partial_x(A_h(\partial_y u + \partial_x v)) - \partial_z(A_v \partial_z v) = \\ -fu - g\partial_y \eta + \int_z^\eta \partial_y b d\xi \end{aligned} \quad (2)$$

where x and y denote the horizontal coordinates, z the vertical coordinate (positive upward), and t the time. f is the Coriolis parameter, $b = -g(\rho - \rho_0)/\rho_0$ is buoyancy (with gravitational acceleration g , reference density ρ_0 and potential density ρ), and η is surface elevation. Together with equations for temperature and salinity and an equation of state for the calculation of potential density, this system of equations is closed, apart from the determination of the vertical and horizontal eddy viscosities A_v and A_h , respectively, and the vertical and horizontal eddy diffusivities, K_v and K_h , respectively (the latter are required for the temperature, salinity and other tracer budget equations). For the determination of the vertical eddy viscosity and diffusivities, A_v and K_v , turbulence closure modelling is required for which complex and diverse theories are available. The coastal ocean models listed above all use directly coupled (or recoded as in the case of ROMS, see WARNER et al. 2005) versions of the turbulence closure modelling library GOTM (General Ocean Turbulence Model, www.gotm.net, UMLAUF and BURCHARD 2005), the underlying theory of which will be presented in Section 2.1. For the modelling of the horizontal eddy viscosity and diffusivity, A_h and K_h , typically relatively simple algebraic closures are used, which will briefly be discussed in Section 2.2.

2 Turbulence closure modelling

2.1 Two-equation closure models as work horses for parameterising vertical turbulent fluxes

Two-equation turbulence closure models have emerged as work horses of coastal ocean modelling during the last decades. The most prominent members of this class of models are the $k-\varepsilon$ model (RODI 1980; BURCHARD and BAUMERT 1995), the $k-\omega$ model (WILCOX 1988; UMLAUF et al. 2003), and the $k-kl$ model (MELLOR and YAMADA 1982), with the turbulent kinetic energy per unit mass (TKE), k , the dissipation rate of the TKE, ε , the turbulent frequency, $\omega = \varepsilon/k$ and the length scale of the energetic turbulent eddies, l . Key component of all models of this type is the so-called energy cascading relation,

$$\varepsilon = c_e \frac{k^{3/2}}{l} \tag{3}$$

which connects the energy-containing turbulent motions of scale l with the dissipation of kinetic energy at the smallest (Kolmogorov) scales (c_e is a proportionality constant). In analogy to the kinetic theory of ideal gases, the vertical eddy viscosity and eddy diffusivity are determined as proportional to the product of a turbulent length scale (here l) and a turbulent velocity scale (here $k^{1/2}$). Using the cascading law in (3), these relations can be re-expressed in their most commonly used forms

$$A_v = c_\mu \frac{k^2}{\varepsilon}; \quad K_v = c'_\mu \frac{k^2}{\varepsilon}, \tag{4}$$

with the non-dimensional stability functions c_μ and c'_μ which may in general be functions of a number of non-dimensional flow invariants (see below). It could be shown in a series of papers (BURCHARD et al. 1998; BAUMERT and PETERS 2000; UMLAUF et al. 2003; UMLAUF and BURCHARD 2003) that all two-equation models mentioned above are mathematically equivalent in situations where the (advective and turbulent) transport of turbulence quantities is negligible. As these situations determine the basic properties of the turbulence models used in coastal ocean modelling, we limit our following discussion to the most commonly used two-equation turbulence closure model: the $k-\varepsilon$ model. Within three-dimensional ocean models, the $k-\varepsilon$ model is generally applied in the following form:

$$\partial_t k + \partial_x(uk) + \partial_y(vk) + \partial_z(wk) - \partial_z \left(\frac{A_v}{\sigma_k} \partial_z k \right) = P + B - \varepsilon \tag{5}$$

$$\partial_t \varepsilon + \partial_x(u\varepsilon) + \partial_y(v\varepsilon) + \partial_z(w\varepsilon) - \partial_z \left(\frac{A_v}{\sigma_\varepsilon} \partial_z \varepsilon \right) = \frac{\varepsilon}{k} (c_1 P + c_3 B - c_2 \varepsilon) \tag{6}$$

with the 5 empirical parameters σ_k and σ_ε (turbulent Schmidt numbers) and c_1 , c_2 and c_3 . For the latter parameter, we distinguish between c_3^- for stable stratification and c_3^+ for unstable stratification. $P = A_v M^2$ with vertical shear squared $M^2 = (\partial_z u)^2 + (\partial_z v)^2$ is the shear production (converting mean kinetic energy into TKE), and $B = -K_v N^2$ with buoyancy frequency squared $N^2 = \partial_z b$ is the buoyancy production (converting potential

energy to TKE or vice versa). It should be noted that the TKE equation can be directly derived from Reynold-averaging the Navier-Stokes equations, with only one rather straight-forward closure assumption: the down-gradient parameterisation for the turbulent fluxes. The right hand side of the budget equation for the dissipation rate, however, is entirely empirical, assuming dimensional consistency, and a form of the source and sink terms that is analogous to that in the TKE budget.

The five free parameters of the $k - \varepsilon$ model provide sufficient degrees of freedom to calibrate this model to the most relevant standard flow situations. The basis for calibrating the three parameters on the right hand side of the dissipation rate equation is the assumption of a homogeneous turbulent flow for which all spatial gradients on the left hand side of (5) and (6) vanish, leaving a system of two ordinary differential equations (ODEs). To calibrate c_1 , (3) is used to derive an ODE for the length scale l from (5) and (6), which has the following form:

$$\partial_t l = c_e \frac{k^{1/2}}{\varepsilon} ((1.5 - c_1)P + (1.5 - c_3)B - (1.5 - c_2)\varepsilon) \quad (7)$$

Using the theoretical argument that shear, which has dimensions of an inverse time, should not determine a length scale (BAUMERT and PETERS 2000), $c_1 = 1.5$ is required to eliminate the corresponding shear production term on the right hand side of (7). To calibrate c_2 , freely decaying turbulence with $P = B = 0$ is assumed for which the ODEs for k and ε can be solved for large t as

$$\frac{k}{k_0} \propto \left(\frac{t}{t_0} \right)^d \quad (8)$$

with the decay rate $d = -1/(c_2 - 1)$. Experimentally, $-1.3 \leq d \leq -1$ has been determined, such that $1.77 \leq c_2 \leq 2$ is a realistic range for c_2 (see UMLAUF and BURCHARD 2003, for details).

A strategy for calibrating c_3^- is to consider steady-state solutions for the ODEs for k and ε to eliminate P . Defining the mixing efficiency as $\Gamma = -B/\varepsilon$, the following relation for calculating c_3^- is obtained:

$$\Gamma = \frac{c_2 - c_1}{c_1 - c_3^-} \quad (9)$$

Since for a stationary, stably stratified shear flow a mixing efficiency of $\Gamma \approx 0.2$ is a well-established result (OSBORN 1980), c_3^- can be considered as the calibration parameter for the mixing efficiency (BURCHARD and HETLAND 2010). It should be pointed out that the correct calibration of the model parameter c_3^- is essential for the performance of the model in stably stratified flows (e.g., in entrainment situations). Note that earlier approaches suggested using the steady-state Richardson number (which has been shown to be in the order of $1/4$) for the calibration of c_3^- (BURCHARD and BAUMERT 1995). For unstable stratification (convective turbulence with $B > 0$), HOLT and UMLAUF (2008) argued that for the length scale equation in (7) the second term on the right hand side must not be positive, since otherwise there would only be source terms for the length scale equation. This would result into a situation where the source terms could only be balanced by the turbulent transport term (which however would be zero or of the wrong

sign in parts of the water column). Therefore, HOLT and UMLAUF (2008) suggest $c_3^+ = 1.5$.

The Schmidt number for the dissipation rate, σ_ε , is calibrated by the requirement that the dissipation rate equation is consistent with law-of-the-wall scaling for steady-state solutions with $B = 0$, where the resulting relation is

$$\sigma_\varepsilon = \frac{\kappa^2}{(c_\mu^0)^{1/2} (c_2 - c_1)} \tag{10}$$

with the von Karman constant $\kappa = 0.4$ and the equilibrium (for $P = \varepsilon$) value of the viscosity stability function, c_μ^0 (with a typical value of $c_\mu^0 = 0.09$). Note that the bottom boundary conditions for the TKE and its dissipation rate are usually directly derived from the law of the wall (see BURCHARD and PETERSEN 1999 who could show that flux conditions are numerically more accurate than Dirichlet conditions). Surface boundary conditions are constructed in the same way, using the surface friction velocity as velocity scale. For situations where injection of TKE due to surface wave breaking is relevant, a downward TKE flux and a modified flux of the dissipation rate are applied (UMLAUF and BURCHARD 2003, 2005). Finally, the Schmidt number for the TKE equation, σ_k , can be used to calibrate the experimentally determined spatial decay rate of TKE for grid stirring experiments (UMLAUF and BURCHARD 2003), and should have a value of about unity. With these relations, a consistent parameter set would for example be:

$$c_1 = 1.5; \quad c_2 = 1.9; \quad c_3^- = -0.5; \quad c_3^+ = 1.5; \quad \sigma_k = 1.0; \quad \sigma_\varepsilon = 1.33. \tag{11}$$

The standard $k - \varepsilon$ model as it is described above is closed by a choice for the turbulent Prandtl number $P_r^t = A_v / K_v$ which is of the order of unity and may depend on stratification (BURCHARD and BAUMERT 1995). Two-equation models of higher complexity are obtained from so-called algebraic closures of the transport equations for the second moments (e.g., the Reynolds stresses and the turbulent heat fluxes). These models have been shown to result in significant improvements over the standard model, in particular in stratified situations, as discussed in detail e.g. in BURCHARD (2002) and UMLAUF and BURCHARD (2005). Successful algebraic second-moment closures have been provided by CANUTO et al. (2001) and adapted to two-equation models by BURCHARD and BOLDING (2001). In short, the result of these algebraic second moment closures is that the stability functions defined in (4) turn out as functions of the shear number $M^2 \tau^2$ and the buoyancy number $N^2 \tau^2$, with the turbulent time scale $\tau = k / \varepsilon$.

The way how the two-equation models are constructed, they are boundary layer models which would fail in the ocean interior where the interaction between turbulence and internal waves dominates mixing. Therefore, in the interior, where turbulence quantities predicted from solutions of the transport equations for k and ε tend to vanish, a lower threshold for k and ε is implemented. To this end, in stratified flow, the turbulent length scale l is limited by the Ozmidov scale $l_O = (\varepsilon / N^3)^{1/2}$, which can be reformulated as $\varepsilon > (c_e / c_{lim}) k N$ with $c_{lim} = 0.53$ as suggested by GALPERIN et al. (1988). In stably stratified turbulence, the TKE is assumed to be kept on certain levels due to the energy flux from the internal wave field to turbulence, where generally no information about this energy transfer is available in ocean models. Therefore, the TKE is simply limited by a minimum TKE level: $k \geq k_{min}$, where k_{min} basically is a calibration parameter for the

eddy viscosity in the stably stratified low energy flow. BURCHARD et al. (2002) could show that observed thermocline eddy viscosities in the Northern North Sea could be reproduced by using a value of $k_{\min} = 10^{-6}$ J/kg.

2.2 Parameterisations for horizontal turbulent fluxes

Whereas in ocean models a consistent theoretical framework for the vertical turbulent fluxes exists, such a rigorous closure for the horizontal fluxes is still missing. Two common approaches used in the coastal ocean modelling community are to either neglect horizontal diffusion (e.g., due to the excess of artificial numerical mixing, see BURCHARD and RENNAU 2008 and Section 3) or to set A_h to a constant value. The proper choice of A_h is determined by sensitivity studies. The major criticism against using a constant horizontal viscosity (diffusivity) is that this approach is not scale-sensitive. An increase in grid resolution should lead to a decrease in horizontal viscosity. In the limit of doing Direct Numerical Simulations (DNS) the value of A_h should vanish (the so far neglected molecular viscosity must be reconsidered in this case). A second drawback of using a constant A_h is that the spatial structure of the flow is not taken into account. For instance in regions with high horizontal shear or strain the horizontal turbulent fluxes should be higher than in regions of calm waters. Therefore a scale- and flow-sensitive sub-grid closure is needed.

A possible solution is the use of Large Eddy Simulations (LES). Here the energy containing eddies are resolved. However, for most oceanographic applications the numerical effort required for this technique is prohibitively large.

To close the gap, SMAGORINSKY (1963) proposed an LES-type closure for geophysical applications. He proposed a scaling for the horizontal eddy viscosity for a numerical model whose grid-scale lies in the forward energy cascade range of 3D turbulence as proposed by KOLMOGOROV (1941):

$$A_h = c(\Delta x \Delta y) \sqrt{(\partial_x u)^2 + \frac{1}{2}(\partial_y u + \partial_x v)^2 + (\partial_y v)^2} \quad (12)$$

with c being a constant in the order of $O(0.1)$, and Δx , Δy being the horizontal grid size. As required, this parameterisation is scale-sensitive but also takes the shear and strain of the flow field into account. The only free parameter c needs to be determined by sensitivity experiments. For instance, HOLT and JAMES (2006) could show that for their application a value of $c = 0.1$ gave a too rich eddy field (as compared to satellite observations). A value of $c = 0.4$ resulted in a too smooth velocity field. They concluded that a value of $c = 0.2$ gave best results.

Smagorinsky's viscosity was a leap forward in understanding the interaction of numerical resolution and physics, and has proven useful in engineering and coastal scale flows. Nevertheless in the last decade the validity of Smagorinsky's underlying assumptions were questioned (e.g., FOX-KEMPER et al. 2008).

The scaling in (12) was derived basing on the assumption that the spectral energy scales as $E(k) \propto k^{-5/3}$, with k being the wavenumber. Moreover, Kolmogorov envisioned a forward energy cascade from large scales to smaller scales. The same holds for the enstrophy. To resolve the Kolmogorov energy cascade in the ocean a resolution in the order of $O(1\text{cm})$ is necessary, which is far from being feasible today. Additionally,

CHARNEY (1971) showed that at geophysical scales, the turbulence is 2D (geostrophic turbulence) and not isotropic any more. He could show that the energy now scales as $E(k) \propto k^{-3}$. Since in most oceanographic applications the Rossby number (the ratio of vorticity and Coriolis frequency) is smaller than one, large parts of the flow are in geostrophic balance and thus described by geostrophic turbulence. Additionally, Charney could show that the enstrophy still shows a forward energy cascade. In contrast to Kolmogorov's 3D turbulence, 2D turbulence shows an inverse cascade of energy. Thus, energy is transferred from smaller scales to the larger scales. To take this fact into account, LEITH (1996) suggested an alternative scaling of the viscosity based on the vorticity.

During a numerical experiment, MENEMENLIS et al. (2006) compared the SMAGORINSKY (1963) and the LEITH (1996) parameterisations of the horizontal viscosity. They concluded that the viscosity scaling should be based on an enstrophy cascade that is reproduced by the LEITH (1996) scaling rather than the SMAGORINSKY (1963) scaling resulting from an inertial energy cascade. However, the LEITH (1996) scaling needs to be adapted such that divergent motions present in 3D simulations do not become unstable or too large such that the vertical advection Courant condition is violated.

The above discussed horizontal viscosities are expected to be less sensitive to subgrid-scale parameterisations than in coarse-resolution modelling exercises. Moreover, they outperform the still applied constant viscosities. However, even high-resolution ocean models are sensitive to subgrid-scale parameterisations, so parameterisation improvement is important. Of course, the range of scales in the ocean is vast and diverse. Phenomena that are substantially smaller than the grid-scale, for instance submesoscale eddies, the loss of geostrophic balance or even microstructure turbulence – will continue to require purely theoretical parameterisations in ocean models for the next few decades at least (e.g., FOX-KEMPER et al. 2008).

3 Numerical and implementation aspects

To obtain a modular coupling between a turbulence closure model and a three-dimensional hydrodynamic ocean model, well defined lists of parameters have to be exchanged between the two models. The 3D model needs to receive the eddy viscosity and the eddy diffusivity from the turbulence closure model. Furthermore, since typically turbulence closure models are formulated as one-dimensional water column models, the 3D model has to store the turbulent properties k and ε . In turn, the 1D turbulence closure model has to receive shear M and stratification N to calculate the production terms and the surface and bottom friction velocities (as well as the surface and bottom roughness lengths) to calculate the surface and bottom boundary conditions. These properties need to be exchanged at each time step. Since 3D models mostly are based on horizontally and vertically staggered grids, spatial interpolations are needed to locate the exchanged terms in the correct and numerically stable position. This is also essential for Finite Element Models (see, e.g., KÄRNÄ et al. 2012). Since the turbulent time scale is mostly much shorter than the time scales of the hydrodynamics, it is tempting to neglect the 3D advection of k and ε , which has to be managed by the 3D hydrodynamic model. The quality requirements to the applied advection schemes are high, since the turbulent quantities may vary over orders of magnitude on short distances and the resulting values must still be positive. Therefore, relatively expensive positive-definite advection schemes need to

be applied. Although 3D model results neglecting advection of turbulent quantities may often be sufficiently accurate, numerical instabilities may occur due to this neglect. Therefore, in complex realistic flow situations, turbulence advection should be included.

One other essential numerical aspect of turbulence closure modelling is the discretization of the dissipation terms for k and ε to ensure their positivity (which is mathematically guaranteed). The method which is generally used, is the source term linearisation (PATANKAR 1980), see the detailed discussion by BURCHARD et al. (2005).

Finally, it should be noted that the effective dissipation and mixing in ocean modelling generally is higher than the physically calculated mixing based on the turbulence closure. Dissipation and mixing are defined as the decay of variance of velocity or tracers, respectively. As an example the temperature mixing is locally calculated as

$$\chi_{\theta} = 2K_v(\partial_z \theta)^2 + 2K_h(\partial_x \theta)^2 + 2K_h(\partial_y \theta)^2 \quad (13)$$

with the potential temperature θ . It is, however, known that numerical advection of tracers (such as temperature, salinity, suspended matter) generally leads to artificial numerical mixing, which may be of the same order of magnitude as the physical mixing. Methods to exactly quantifying numerical mixing have been developed by BURCHARD and RENNAU (2008) and KLINGBEIL et al. (2014). The latter authors have shown how to extend the numerical mixing analysis to a numerical dissipation analysis. In summary, to assess effective mixing and dissipation in numerical models, the numerical variance decay must be quantified as well. Numerical dissipation and mixing can be reduced by choosing accurate advection schemes, high resolution or adaptive coordinates (HOFMEISTER et al. 2010).

4 Coastal ocean modelling examples

In this section, results from coastal ocean example simulations are shown which demonstrate the essential role of turbulence closure modelling for such regions. All simulations are carried out with the General Estuarine Transport Model (GETM, see e.g. HOFMEISTER et al. 2011), which is coupled to the turbulence closure module of the General Ocean Turbulence Model (GOTM, see UMLAUF and BURCHARD 2005). Details of the turbulence closures included are presented in detail in Section 2.1. For all simulations, bottom and surface following vertically adaptive coordinates (HOFMEISTER et al. 2011) were used to provide high vertical resolutions in (temporally and spatially variable) regions of strong shear or stratification. In the horizontal, spherical coordinates with a staggered C-grid were used. Surface forcing was provided from the German Weather Service local model, while lateral boundary conditions were prescribed from a 1nm GETM simulation for the entire North Sea and Baltic Sea region. Fig. 1 shows the complete model domain for this simulation, of which results along a transect in the North Sea (green line) are discussed in Section 4.1. This North Sea transect demonstrates the relevance of accurate thermocline resolution and diapycnal mixing rates for realistic North Sea modelling. Results for a nested Western Baltic Sea (WBS) simulation with a resolution of about 600 m with focus on numerical mixing are shown in Section 2.2. Finally, results from a 600 m resolution nested simulation of the Central Baltic Sea (CBS) to study effective basin-wide mixing are presented in Section 4.3. The model domains for the WBS and the CBS models are shown in Fig. 1 as well.

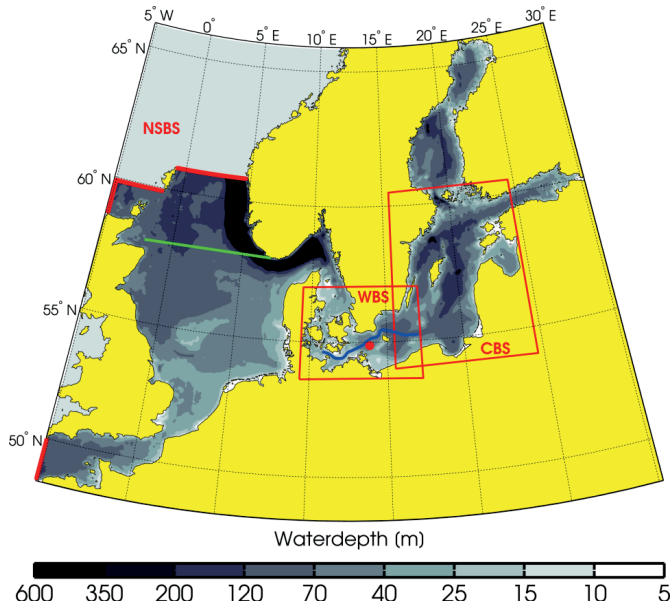


Figure 1: Map auf the North Sea / Baltic Sea 1nm model setup (NSBS). The two red boxes indicate the boundaries of the nested Western Baltic Sea model (WBS) and the Central Baltic Sea (CBS). Additionally, the green line marks the location of the temperature transect in Fig. 2. The blue line indicates the transect as shown in Fig. 4. The red dot shows the position of the MARNET Arkona buoy the data of which is used here for model validation (see Fig. 3).

4.1 Thermocline mixing in the Central North Sea

The Central North Sea is temperature-stratified during summer and well-mixed during winter. Summer stratification starts in spring when turbulent mixing due to tides and wind is sufficiently suppressed by the stratifying effect of the downward surface heat fluxes. Mixing also plays a pivotal role in the primary production of the North Sea. Once in late spring surface nutrients are depleted, nutrient supply to the euphotic zone is limited to upward diapycnal nutrient fluxes from the nutrient-rich bottom waters across the thermocline. The intensity of these fluxes depends largely on the values of eddy diffusivity K_p in the strongly stratified thermocline region. As discussed in Section 2.1, the eddy viscosity and the eddy diffusivity in this region are controlled by the value for the minimum TKE level, κ_{min} . Fig. 2 shows observed and simulated summer temperature stratification along a 58°N transect across the North Sea. The agreement between the observations (which are limited to a depth range between 10 m and 70 m) and model results is good. Even details of the temperature structure such as a decrease in near-surface temperature and stratification from east to west and the sharpness of the temperature jump in the thermocline region are well-reproduced. The latter is only possible due to the strong accumulation of coordinate layers in the thermocline region which allows for a vertical resolution of locally below 0.2 m (Fig. 2c). The eddy viscosity in the sharp thermocline region is generally above values of $10^{-6}\text{m}^2\text{s}^{-1}$. Apart from the high vertical resolution, the use of vertically adaptive coordinates is strongly reducing artificial numeri-

cal mixing (see also Section 4.2), which would in models with geopotential coordinates dominate the diapycnal mixing and the associated fluxes of nutrients.

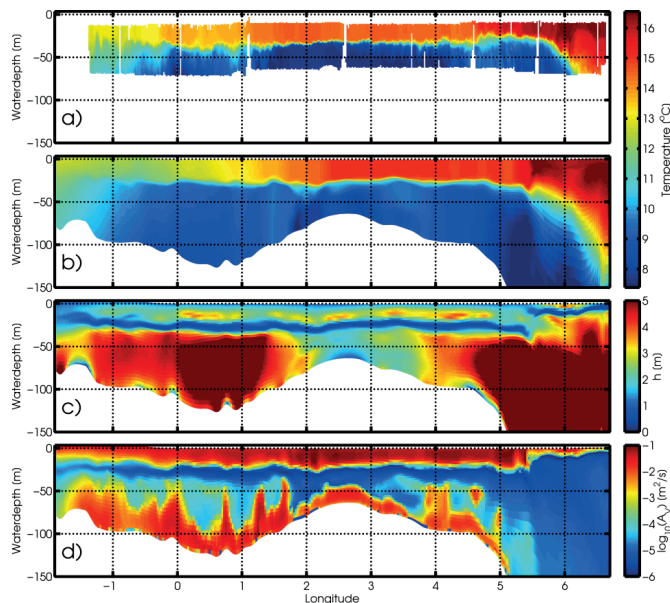


Figure 2: Simulations and model results along a 58°N transect across the North Sea (see the green line in Fig. 1 for the location) on September 03, 2009. a: temperature observed by an undulating CTD profiler (courtesy Bundesamt für Seeschifffahrt und Hydrographie); b: simulated temperature; c: local thickness of adaptive coordinates; d: eddy viscosity.

4.2 Physical and numerical mixing in the Western Baltic Sea

Numerical modelling of the Baltic Sea is a challenging task. Simulations of the Baltic Sea must reproduce the water mass exchange through the narrow and shallow Danish Straits, the irregular overflows over the Darss Sill and the Drogden Sill, the emerging bottom gravity currents into the chain of basins in the Baltic proper, the interleaving of inflows at the correct density level, and low mixing levels during stagnation periods in the deep basins. These different demands require a well-designed ocean circulation model with a well-calibrated turbulence closure (Section 2.1). In several studies, it was shown that the General Estuarine Transport Model (GETM) equipped with the General Ocean Turbulence Model (GOTM) provides an excellent numerical model suite to tackle these demands (BURCHARD et al. 2009; HOFMEISTER et al. 2011). For example, HOFMEISTER et al. (2011) presented a validated model for the whole Baltic Sea with a resolution of 1 nm. In order to study local and submesoscale processes, models with higher resolution can be nested into such coarse-grid models. In this section results from a 600 m model of the Western Baltic Sea are presented (see Fig. 1 for the model domain). At the open boundaries in the Kattegat and east of the Bornholm Basin the free surface elevation, depth-integrated velocities and profiles of temperature and salinity are prescribed from the coarse-resolution NSBS model. The simulation was performed with 40 adaptive layers, providing high vertical resolution in boundary layers but also at the evolving

thermo- and haloclines. With these settings the dynamics in the Western Baltic Sea were accurately simulated. Fig. 3 shows a validation against mooring data in the Arkona basin (see Fig. 1 for the location of this autonomous buoy). However, as argued in Section 3, the simulated effective mixing and dissipation is not only a result of the parameterised subgrid-scale effects (physical contribution), but also of the truncation errors of the discrete advection terms (numerical contribution), see Klingbeil et al. 2014. In Fig. 4 the ratios of numerical to physical salt mixing and kinetic energy dissipation are shown along the transect depicted in Fig. 1. In large areas the numerically induced mixing had the same order of magnitude as the physical one. In contrast, the numerically induced dissipation of kinetic energy was at least one order of magnitude smaller than the physical dissipation. These results emphasise the need of accurate advection schemes with reduced numerical mixing and the relevance of well-calibrated turbulence parameterisations for the (physical) dissipation of kinetic energy.

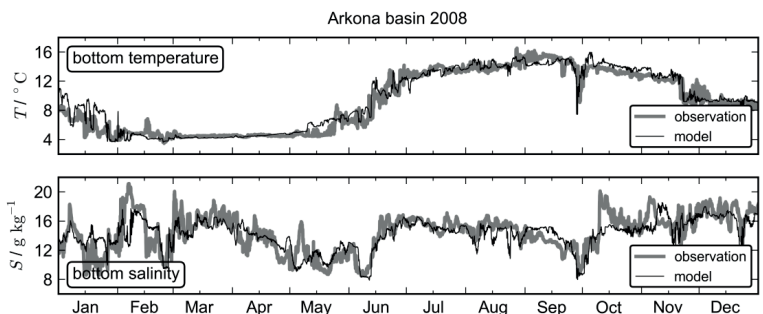


Figure 3: Comparison of time series for observed and simulated bottom temperature and bottom salinity in the Arkona Basin for the year 2008. The observations are from near-bottom (48 m depth) CTD sensor of the MARNET Arkona buoy located in the central Arkona basin (see Fig. 1 for the location).

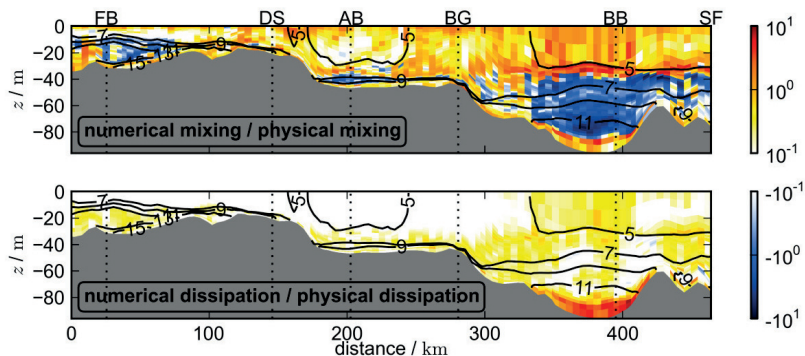


Figure 4: Ratios of numerical to physical salt mixing and kinetic energy dissipation along the transect shown in Fig. 1. Isopycnals are depicted by contour lines. The data are averaged over the period 19-28 Sep 2008. Vertical lines indicate the positions of Fehmarn Belt (FB), Darss Sill (DS), Arkona Basin (AB), Bornholmsgat (BG), Bornholm Basin (BB) and Slupsk Furrow (SF).

4.3 Basin-wide mixing in the Central Baltic Sea

The Central Baltic Sea is, similar to the Baltic Sea in general, defined by a chain of basins which are interconnected through sills. The dominant basin is the Gotland Basin which is one of the deepest (up to 240 m depth) and, in terms of the water volume, largest basin of the Baltic Sea.

In contrast to the North Sea, tides are virtually absent in the Central Baltic Sea (FEISTEL et al. 2008), leaving wind forcing as the major energy source for mixing. While the upper water column is directly influenced by wind and atmospheric temperature changes, stratification suppresses turbulence and mixing in the deeper parts of the water column; even during winter, surface mixing extends only down to the halocline, located in approx. 80 m depth. The halocline is defined by the transition of the fresher upper layer waters with salinities of about 8 g/kg to the deeper areas with salinities of up to 13 g/kg. The heating of the surface waters during spring and summer creates a second density interface, the thermocline. The thermocline strongly inhibits the mixing between the colder winter water above the halocline and below the thermocline due to direct atmospheric forcing.

Mixing below the halocline and thermocline, respectively, differs thus, in terms of the processes driving the mixing, from near-surface mixing. The effects of a wind event such as a storm, start, from the perspective of deep water mixing, with the excitation of different types of deep-water motions (e.g., internal and topographic waves). These motions lose their energy by bottom and interior friction, and, to a smaller amount, by mixing (i.e., conversion of kinetic into background potential energy). Different from surface layer mixing, deep-water mixing is therefore only indirectly linked to the wind forcing via the chain of processes described above. AXELL (1998) could show that the deep water mixing in the Gotland Basin increased during the stormier winter season, and HOLTERMANN and UMLAUF (2012) correlated single storm events to increased mixing rates. Numerous deep-water processes are known, see for example Fig. 2 by REISSMANN et al. (2009) for a good overview of the mixing processes in the Baltic Sea. Less well-known is the importance of the different processes to deep-water mixing.

An experiment to study the major mixing processes and mixing rates in the deeper parts of the Central Baltic Sea has been conducted in 2007 by releasing a passive tracer in 200 m depth in the Central Gotland Basin (approx. at C1 in Fig. 5). This experiment was called the Baltic Sea Tracer Release Experiment (BaTRE). The use of the inert tracer gas CF_3SF_5 , detectable at very low concentrations, allowed following the tracer patch over a time span of two years. In combination with the tracer release, several moorings had been deployed in the Gotland Basin, and turbulence microstructure measurements had been conducted during the same time (UMLAUF et al. 2008; HOLTERMANN et al. 2012; HOLTERMANN and UMLAUF 2012). One of the key results of the experiment were the substantially different vertical turbulent diffusivities felt by the tracer patch during the initial and later phases of the experiment, respectively. These differences were attributed to the effect of boundary mixing processes that started acting on the tracer cloud after the first boundary contact such that the vertical spread of the tracer increased dramatically. This result was found to be in agreement with direct measurements of the turbulent dissipation rate using a free falling shear-microstructure profiler.

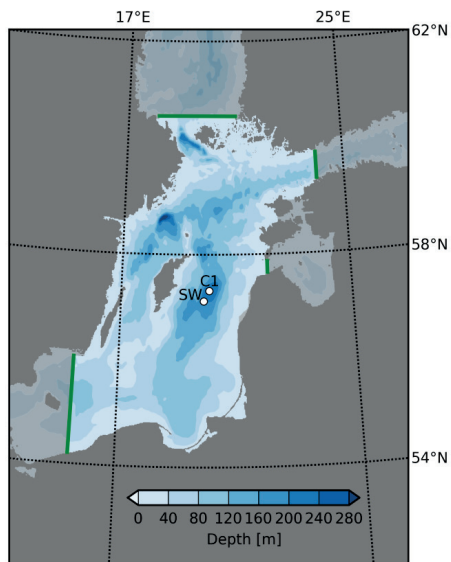


Figure 5: Model domain of the Central Baltic Sea GETM model. Green lines depict the open boundaries. White dots represent the locations of two moorings deployed in the Gotland Basin.

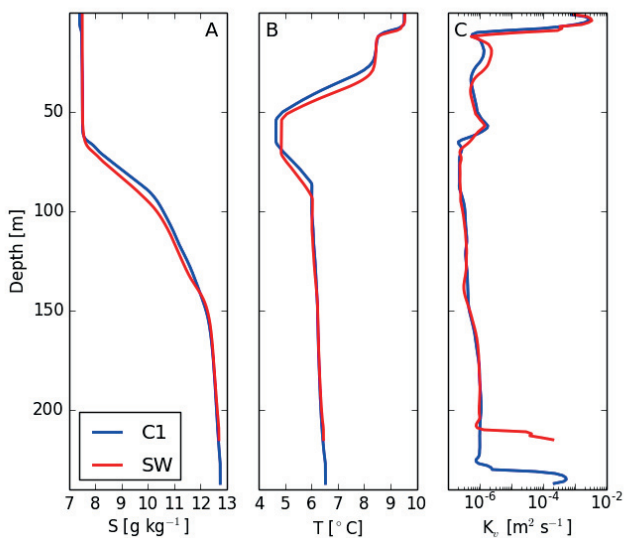


Figure 6: Salinity (A), temperature (B) and turbulent diffusivity (C) at C1 (blue) and SW (red), see as well Fig. 5 for the location of the stations. Data is taken from the GETM model of the Central Baltic Sea at midnight of June 1, 2008.

The consequence of this result, in terms of numerical modelling, is that in the best case, the model should be able to reproduce these different mixing regimes. Good results in that respect have been achieved by a setup for the Central Baltic Sea using the GETM model with 200 vertically adaptive layers and a horizontal resolution of 600 m, see HOLTERMANN et al. (2014). This resolution is rather high in comparison to commonly used models of the Baltic Sea which typically have horizontal grid sizes of 1 nm to 2 nm or coarser (see, e.g., FENNEL et al. 2010). The model was able to reproduce the differences between the low mixing in the interior of the water column and the increased mixing at the basin boundaries and thus the evolution of the tracer cloud.

Fig. 6 shows model results for salinity, temperature and turbulent diffusivity at the stations C1 and SW for a typical summer situation. Clearly visible is the heated upper water column above a layer with colder winter water sandwiched between the thermocline and halocline. Turbulent diffusivities in the upper layers range between $1 \cdot 10^{-6} \text{m}^2 \text{s}^{-1}$ and $5 \cdot 10^{-3} \text{m}^2 \text{s}^{-1}$. Below the winter water, turbulent diffusivities rarely exceed $10^{-6} \text{m}^2 \text{s}^{-1}$, illustrating the mechanical insulation of deeper layers from direct atmospheric forcing. Directly above the bottom, however, the turbulent diffusivities increase again as a result of bottom friction. As it can be nicely seen by comparing the eddy diffusivity profiles of the SW and C1 stations in Fig. 6c, the increased bottom boundary turbulent diffusivities occur at different depths. This lateral inhomogeneity between the low K_p at C1 and the increased K_p at SW in 210 m is a major reason for the different spreading rates of the passive tracer before and after touching the basin's boundary. Using model results that have been carefully validated against a wealth of observations from the BaTRE experiment, it could be shown that the atmospheric forcing triggered a spectrum of internal waves and sub-inertial motions, which in turn were found to be the main drivers of boundary layer mixing. By successfully reproducing the tracer experiment, the results demonstrated as well the complex interaction between the water masses mixed at the boundaries and the interior water column.

5 Conclusions

This study demonstrates the necessity of using sufficiently realistic turbulence closure models as well as sufficiently accurate numerical schemes in models of the coastal ocean. Two-equation turbulence closure models have been demonstrated to provide an optimal solution to this task. Simpler parametric turbulence closure models such as the KPP model (LARGE et al. 1994) as they are often used in large scale ocean models would properly reproduce dynamics such as stratification and de-stratification in proper accuracy. More complex models are typically only applied in idealised situations and have been reported for realistic 3D models of the coastal ocean. For most coastal ocean applications, the physically correct reproduction of the mixing efficiency is key to the predictability for the state of the coastal ocean. In the model applications shown in the present paper, this included suppression of mixing in the seasonal thermocline, entrainment in dense bottom currents and basin-wide mixing. Other coastal ocean processes critically connected to mixing efficiency are for example estuarine circulation, sediment-flow interactions for high sediment concentrations and entrainment of ambient waters into river plumes. The required numerical resolution is here mainly obtained by vertically adaptive coordinates which allow high resolution in regions of high shear and stratification, a pro-

cedure which is of course only effective together with sufficiently accurate advection schemes. Other (non-adaptive) ways of obtaining a high vertical resolution would be simply using a high number of vertical layers (which may often not be affordable) or the use of geopotential coordinates with lateral variation in resolution (BACKHAUS 2008) which however has not yet been tested with coupling to turbulence closure models. One may also use unstructured adaptive Finite Elements in the vertical (PIGGOTT et al. 2008), a method which is still in its infancy in ocean modelling.

Acknowledgements: The German part of the Baltic Monitoring Programme (COMBINE) and the operation of the measuring stations of the German Marine Monitoring Network (MARNET) in the Baltic Sea are conducted by the Baltic Sea Research Institute Warnemünde (IOW) on behalf of the Bundesamt für Seeschifffahrt und Hydrographie (BSH), financed by the Bundesministerium für Verkehr, Bau und Stadtentwicklung (BMVBS). The authors are grateful for the persistent support by Karsten Bolding (Asperup, Denmark) in the development and maintenance of GETM.

6 References

- AXELL, L.B.: On the variability of Baltic Sea deep water mixing, *J. Geophys. Res.*, 103(C10), 21,667-21,682, doi:10.1029/98JC01714, 1998.
- BACKHAUS, J.O.: Improved representation of topographic effects by a vertical adaptive grid in vector-ocean-model (VOM). Part I: Generation of adaptive grids, *Ocean Modelling*, 22, 114-127, 2008.
- BAUMERT, H. and PETERS, H.: Second-moment closures and length scales for weakly stratified turbulent shear flows, *J. Geophys. Res.*, 105, 6453-6468, 2000.
- BECHERER, J.; BURCHARD, H.; FLÖSER, G.; MOHRHOLZ, V. and UMLAUF, L.: Evidence of tidal straining in well-mixed channel flow from micro-structure observations, *Geophys. Res. Lett.*, 38, L17611, doi: 10.1029/2011GL049005, 2011.
- BLUMBERG, A.F. and MELLOR, G.L.: A description of a coastal ocean circulation model. In: Heaps, N.S. (Ed.), *Three Dimensional Ocean Models*. American Geophysical Union, Washington, D.C., pp. 1-16, 1987.
- BURCHARD, H.: Applied turbulence modelling in marine waters, vol. 100 of *Lecture Notes in Earth Sciences*, Springer, Berlin, Heidelberg, New York, 229 pp., 2002.
- BURCHARD, H. and BAUMERT, H.: On the performance of a mixed layer model based on the k-e turbulence closure, *J. Geophys. Res.*, 100, 8523-8540, 1995.
- BURCHARD, H. and BOLDING, K.: Comparative analysis of four second-moment turbulence closure models for the oceanic mixed layer. *J. Phys. Oceanogr.*, 31, 1943-1968, 2001.
- BURCHARD, H.; BOLDING, K.; RIPPETH, T.P.; STIPS, A.; SIMPSON, J.H. and SÜNDERMANN, J.: Microstructure of turbulence in the northern North Sea: a comparative study of observations and model simulations, *J. Sea. Res.*, 47, 223-238, 2002.
- BURCHARD, H.; DELEERSNIJDER, E. and STOYAN, G.: Some numerical aspects of turbulence-closure models, pp. 197-206. In: BAUMERT, H.Z.; SIMPSON, J.H. and SÜNDERMANN, J. (eds.), *Marine Turbulence: Theories, Observations and Models*, Cambridge University Press, Cambridge, 630 pp., 2005.

- BURCHARD, H. and HETLAND, R.D.: Quantifying the contributions of tidal straining and gravitational circulation to residual circulation in periodically stratified tidal estuaries, *J. Phys. Oceanogr.*, 40, 1243-1262, 2010.
- BURCHARD, H.; JANSSEN, F.; BOLDING, K.; UMLAUF, L. and RENNAU, H.: Model simulations of dense bottom currents in the Western Baltic Sea. *Cont. Shelf Res.*, 29, 205-220. 2009.
- BURCHARD, H. and PETERSEN, O.: Models of turbulence in the marine environment – a comparative study of two-equation turbulence models, *J. Mar. Syst.*, 21, 29-53, 1999.
- BURCHARD, H.; PETERSEN, O. and RIPPETH, T.P.: Comparing the performance of the k- ϵ and the Mellor-Yamada two-equation turbulence models, *J. Geophys. Res.*, 103, 10543-10554, 1998.
- BURCHARD, H. and RENNAU, H.: Comparative quantification of physically and numerically induced mixing in ocean models, *Ocean Modelling*, 20, 293-311, 2008.
- CANUTO, V.M.; HOWARD, A.; CHENG, Y. and DUBOVIKOV, M.S.: Ocean turbulence. Part I: one-point closure model. Momentum and heat vertical diffusivities. *J. Phys. Oceanogr.*, 31, 1413-1426, 2001.
- CHARNEY, J.G.: Geostrophic Turbulence, *J. Atmos. Sci.*, 28, 1087-1095, 1971.
- CHEN, C.; LIU, H. and BEARDSLEY, R.C.: An unstructured, finite-volume, three-dimensional, primitive equation ocean model: application to coastal ocean and estuaries. *J. Atmos. Ocean. Tech.*, 20, 159-186, 2002.
- FEISTEL, R.; NAUSCH, G. and WASMUND, N. (Eds.): State and Evolution of the Baltic Sea, 1952-2005. A detailed 50-year survey of meteorology and climate, physics, chemistry, biology, and marine environment, 703 pp., Wiley-Interscience, Hoboken, NJ, USA, 2008.
- FENNEL, W.; RADTKE, H.; SCHMIDT, M. and Neumann, T.: Transient upwelling in the central Baltic Sea, *Cont. Shelf Res.*, 30(19), 2015-2026, doi:10.1016/j.csr.2010.10.002, 2010.
- FOX-KEMPER, B.; FERRARI, R. and HALLBERG, R.: Parameterization of mixed layer eddies. Part I: Theory and diagnosis, *J. Phys. Oceanogr.*, 38, 1145-1165, 2008.
- GALPERIN, B.; KANTHA, L.H.; HASSID, S. and ROSATI, A.: A quasi-equilibrium turbulent energy model for geophysical flows. *J. Atmos. Sci.*, 45, 55-62, 1988.
- HOFMEISTER, R.; BECKERS, J.-M. and BURCHARD, H.: Realistic modelling of the exceptional inflows into the central Baltic Sea in 2003 using terrain-following coordinates. *Ocean Modelling*, 39, 233-247, 2011.
- HOFMEISTER, R.; BURCHARD, H. and BECKERS, J.-M.: Non-uniform adaptive vertical grids for 3D numerical ocean models, *Ocean Modelling*, 33, 70-86, 2010.
- HOLT, J.T. and JAMES, I.D.: An assessment of the fine-scale eddies in a high-resolution model of the shelf seas west of Great Britain, *Ocean Modelling*, 13, 271-291, 2006.
- HOLT, J. and UMLAUF, L.: Modelling the tidal mixing fronts and seasonal stratification of the Northwest European Continental shelf, *Cont. Shelf Res.*, 28, 887-903, 2008.
- HOLTERMANN, P.; UMLAUF, L.; TANHUA, T.; SCHMALE, O.; REHDER, G. and WANIEK, J.: The Baltic Sea Tracer Release Experiment. Part 1: Mixing rates, *J. Geophys. Res.*, 117, C01,021, doi:10.1029/2011JC007439, 2012.

- HOLTERMANN, P. and UMLAUF, L.: The Baltic Sea Tracer Release Experiment. Part 2: Mixing processes, *J. Geophys. Res.*, 117, C01,022, doi:10.1029/2011JC007445, 2012.
- HOLTERMANN, P.; BURCHARD, H.; GRÄWE, U.; KLINGBEIL, K. and UMLAUF, L.: Deep-water dynamics and boundary mixing in a non-tidal stratified basin. A modeling study of the Baltic Sea, *J. Geophys. Res. Oceans*, 119, doi:10.1002/2013JC009483, 2014.
- KÄRNÄ, T.; LEGAT, V.; DELEERSNIJDER, E. and BURCHARD, H.: Coupling of a discontinuous Galerkin finite element marine model with a finite difference turbulence closure model, *Ocean Modelling*, 47, 55-64, 2012.
- KLINGBEIL, K.; MOHAMMADI-ARAGH, M.; GRÄWE, U. and BURCHARD, H.: Quantification of spurious dissipation and mixing – Discrete Variance Decay in a Finite-Volume framework, *Ocean Modelling*, doi:10.1016/j.ocemod.2014.06.001, 2014.
- KOLMOGOROV, A.N.: The local structure of turbulence in incompressible viscous fluid for very large Reynolds numbers, *Dokl. Akad. Nauk SSSR*, 30, 301-305, 1941. Reprinted in: *Proc. R. Soc. Lond. A*, 434, 9-13, 1991.
- LARGE, W.G.; MCWILLIAMS, J.C. and DONEY, S.C.: Oceanic vertical mixing: a review and a model with nonlocal boundary layer parameterisation, *Rev. Geophys.*, 32, 363-403, 1994.
- LEITH, C.E.: Stochastic models of chaotic systems, *Physica D*, 98, 481-491, 1996.
- MELLOR, G.L. and YAMADA, T.: Development of a turbulence closure model for geophysical fluid problems. *Rev. Geophys. Space Phys.* 20, 851-875, 1982.
- MENEMENLIS, D.; HILL, C.; ADCROFT, A.; CAMPIN, J.-M.; CHENG, B.; CIOTTI, B.; FUKUMORI, I.; HEIMBACH, P.; HENZE, C.; KÖHL, A.; LEE, T.; STAMMER, D.; TAFT, J. and ZHANG, J.: NASA supercomputer improves prospects for ocean climate research, *Am. Geophys. Union*, 86(9), 95-96, 2005.
- OSBORN, T.R.: Estimates of the local rate of vertical diffusion from dissipation measurements. *J. Phys. Oceanogr.*, 10, 83-89, 1980.
- PATANKAR, S.V.: *Numerical Heat Transfer and Fluid flow*. McGraw-Hill, New York, 1980.
- PIGGOTT, M.D.; GORMAN, G.J.; PAIN, C.C.; ALLISON, P.A.; CANDY, A.S.; MARTIN, B.T. and WELL, M.R.: A new computational framework for multi-scale ocean modelling-based on adapting unstructured meshes, *Int. J. Numer. Meth. Fluids*, 56, 1003-1015, 2008.
- REISSMANN, J.; BURCHARD, H.; FEISTEL, R.; HAGEN, E.; LASS, H.U.; MOHRHOLZ, V.; NAUSCH, G.; UMLAUF, L. and WIECZOREK, G.: State-of-the-art review on vertical mixing in the Baltic Sea and consequences for eutrophication, *Progr. Oceanogr.*, 82, 47-80, 2009.
- RODI, W.: *Turbulence models and their applications in hydraulics*, Tech. Rep., Int. Assoc. for Hydraul. res., Delft, The Netherlands, 1980.
- SHCHEPETKIN, A.F. and MCWILLIAMS, J.C.: The Regional Ocean Modeling System: A split-explicit, free-surface, topography following coordinates ocean model, *Ocean Modelling*, 9, 347-404, 2005.
- SMAGORINSKY, J.: General circulation experiments with the primitive equations, *Month. Weather Rev.*, 91, 99-164, 1963.

- UMLAUF, L.; ARNEBORG, L.; BURCHARD, H.; FIEKAS, V.; LASS, H.U.; MOHRHOLZ, V. and PRANDKE, H.: The transverse structure of turbulence in a rotating gravity current, *Geophys. Res. Lett.*, 34, L08601, doi:10.1029/2007GL029521, 2007.
- UMLAUF, L. and BURCHARD, H.: A generic length-scale equation for geophysical turbulence models, *J. Mar. Res.*, 61, 235-265, 2003.
- UMLAUF, L. and BURCHARD, H.: Second-order turbulence closure models for geophysical boundary layers. A review of recent work, *Cont. Shelf Res.*, 25, 795-827, 2005.
- UMLAUF, L.; BURCHARD, H. and HUTTER, K.: Extending the k-omega turbulence model towards oceanic applications, *Ocean Modelling*, 5, 195-218, 2003.
- UMLAUF, L.; TANHUA, T.; WANIEK, J.J.; SCHMALE, O.; HOLTERMANN, P. and REHDER, G.: Hunting a new tracer, *EOS, Transactions American Geophysical Union*, 89(43), 419-419, 2008.
- VAN DER LEE, E.M. and UMLAUF, L.: Internal-wave mixing in the Baltic Sea: Near-inertial waves in the absence of tides. *J. Geophys. Res.*, 116, C10016, doi:10.1029/2011JC007072, 2011.
- WARNER, J.C.; SHERWOOD, C.R.; ARANGO, H.G. and SIGNELL, R.P.: Performance of four turbulence closure models implemented using a generic length scale method, *Ocean Modelling*, 8, 81-113, 2005.
- WILCOX, D.C.: Reassessment of the scale-determining equation for advanced turbulence models. *AIAA Journal*, 26, 1299-1310, 1988.
- ZHANG, Y. and BAPTISTA, A.M.: SELFE: A semi-implicit Eulerian-Lagrangian finite-element model for cross-scale ocean circulation. *Ocean Modelling*, 21, 71-96, 2008.

Modelling of Sediment Transport and Morphodynamics

Bert Putzar and Andreas Malcherek

Summary

This article summarizes general concepts for morphodynamic modelling and sediment transport in the coastal zone. Firstly, basic concepts with respect to non-cohesive sediments are introduced. The following sections describe techniques to model fractionated sediment transport and to predict bed forms, as well as the related bed roughness. The last section is devoted to the simulation of dredging and dumping activities in the context of long term morphodynamic simulations.

Keywords

sediment transport, morphodynamics, bed evolution, coastal zone, fractionated sediment transport, dunes, ripples, bed roughness, dredging and dumping, long-term morphodynamic modelling

Zusammenfassung

Es werden die grundlegenden Konzepte der Soblevolution und des Sedimenttransports nicht-kohäsiver Sedimente eingeführt. Anhand von Beispielen werden Ansätze zur Behandlung von Sedimentklassen und zur Prädiktion von Soblformen vorgestellt. Der Einfluss von Unterhaltungsmaßnahmen in Seeschiff-fahrtsstraßen auf die langfristige Soblentwicklung wird im Rahmen eines Langfristmodells aufgezeigt.

Schlagwörter

Sedimenttransport, Morphodynamik, Soblevolution, Küstenzone, fraktionierter Sedimenttransport, Dünen, Riffel, Sobhraubeit, Unterhaltungsmaßnahmen, Langfristmodellierung

Contents

1	Introduction	90
2	Fundamental Concepts of Natural Sediment Transport	90
2.1	The Bed-Evolution Equation	91
2.2	Bottom Shear Stress and Transport Initiation	92
2.3	Bed Load Transport	94
2.4	Suspended Sediment Transport	95
3	Fractionated Sediment Transport	97
3.1	Vertical Discretization of the Hydrographic Bed	97

3.2	Sediment Separation in a Tide-affected Bight.....	98
4	Prediction of Dunes and Ripples	99
4.1	Grain and Bed Roughness.....	99
4.2	Predicted Heights of Bed Forms and Resulting Roughness.....	100
5	Effect of Maintenance Measures on Bed Evolution.....	102
5.1	Modelling of Maintenance Measures.....	102
5.2	Long-term Bed Evolution in the Elbe Estuary.....	102
6	References	104

1 Introduction

Even today, modelling of the continuous changes in the elevation of the hydrographic bottom and the structure of the corresponding subsurface of coastal waters is a tremendous scientific challenge. Primary cause is the large number of processes involved. These range from the different scales of the currents involved, like turbulences, swell, tides and long-range currents (MALCHEREK 2010a), via the composition of the present sediments and biological processes, right up to anthropogenic encroachment like, for instance, dredging and dumping as maintenance measures or resource extraction.

This article aims to introduce the approaches established today and implemented in most current sediment transport models. Emphasis is placed on non-cohesive sediments, which, in coastal regions, are primarily represented through sandy sediment distribution. The multitude of empirical formulations and dedicated models regarding individual processes can and will not be covered. Rather, the emphasis is placed on outlining the premises pertaining to the various process models and their associated problems, limitations and knowledge deficits.

The mechanisms that apply to cohesive sediments are different than those applying to sandy sediments. An introduction to this topic and further research is given by MALCHEREK (2010b), MALCHEREK and CHA (2011), as well as WEHR and MALCHEREK (2012), in which an isopycnic numerical model for the simulation of cohesive transport processes in tidal regions was presented. Sediment mixtures constitute a further field of research. For an introduction to modelling of the interaction of cohesive and non-cohesive beds see DONG (2007) and JACOBS et al. (2010).

2 Fundamental Concepts of Natural Sediment Transport

As a rule, the beds of natural channels consist of a mixture of grains of sediment with varying properties, as well as miscellaneous biological components. They form a framework whose cavities are filled with in-situ water and whose structural cohesiveness may be influenced by chemical as well as biological processes. Separation processes and the geological history of the substratum lead to horizontal as well as vertical structuring.

This complex structure cannot be precisely described in a deterministic manner. Therefore, within the numerical model the mobile sediment of the bed and the adjoining bodies of water will be considered as a continuum (Fig. 1) and its physics described

through mathematical models. Particularly size, shape and the properties of the sediment particles, as well as the water content, apply to its specific classification.

The most basic case occurs with uniform sediment distribution of spherical sediment particles with a diameter of no more than 64 μm . This presumes a case of non-cohesive sediment, where the electro-chemical forces in relation to the weight force per grain are negligible. This concept forms the basis for the subsequent comments in this paragraph. Sediment particles with varying diameters represent an enlargement on the basic scenario. Sediment fractions can then be developed according to the grain distribution curve and models for the physical processes of inhomogeneous sediment distribution can be established. These approaches will be discussed in paragraph 3.

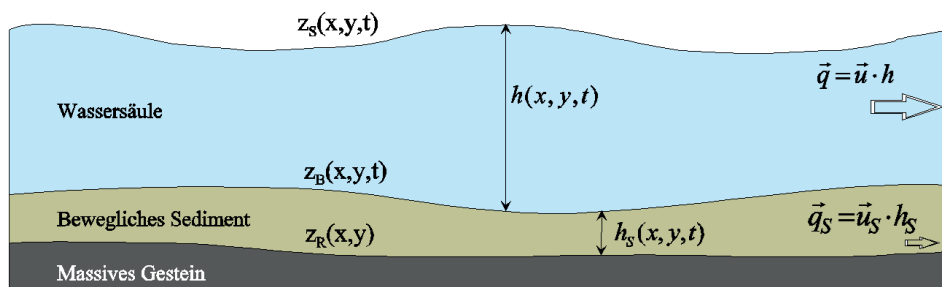


Figure 1: Conceptual design of a body of water with mobile bed.

2.1 The Bed-Evolution Equation

Almost all morphodynamic numerical models utilize the Bed-Evolution or Exner-equation as a basis for conceptual modelling. It describes the changes in the geodetic location of the bed z_B in dependence of the time t through the transport of bed and suspended load:

$$(1-n) \frac{\partial z_B}{\partial t} = -\text{div} \vec{q}_S + \frac{\Phi_S}{\rho_S} \tag{1}$$

In this equation the dimensionless parameter n represents the porosity, $\vec{q}_S = (q_{Sx}, q_{Sy})^T$ the horizontal volumetric bed load transport in $[\text{m}^2/\text{s}]$, Φ_S in $[\text{kg}/\text{m}^2\text{s}]$ the vertical sediment flow of suspended sediment and ρ_S in $[\text{kg}/\text{m}^3]$ the sediment density. The porosity represents the relation between water volume and the total volume of water and sediment and carries an approximate value of 0.3 for sandy sediment. A prediction of this parameter was presented in MALCHEREK and PIECHOTTA (2004). The dry density of the sediment is generally given as $\rho_S = 2650 \text{ kg}/\text{m}^3$.

As has been described, the movement of sediment can be differentiated as bed load transport and suspended sediment transport. In the former, sediment particles move along the bed in a rolling or skipping motion. Suspended sediment transport is achieved when turbulences near the bed are high enough to prevent the particles from settling. Particles are detached from the bed and transported within the current.

To interpret the bed evolution equation, both transport types will be considered separately in a one-dimensional scenario. For bed load transport in direction x the right side

of the equation is reduced to $-\partial q_{sx} / \partial x$. Accordingly, the bed does not undergo any changes assuming the bed load transport rate also remains at a constant volume. An equilibrium exists. If, however, q_{sx} increases in the x-vector, less sediment is introduced than discharged. The bed is degraded. Correspondingly, a deposition scenario results when the bed load transport is decreased and, thus, $\partial q_{sx} / \partial x$ is negative. In the case of suspended sediment, the exchange of sediment between the water column and the bed is decisive. If the sediment flow is balanced, $\Phi_s = 0$ applies and the bed is not affected. In the case of a negative balance more sediment is discharged than being supplied to the bed. It deepens. The deposition scenario is reinstated when the sediment flow is positive.

These observations show that the gradient of sediment transport and the balance of the vertical exchange are decisive for bed evolution. In addition, sediment transport can take place, even without changes in the bed. Therefore, it has to be determined as of which current load sediment is transported and how it may be quantified in terms of bed load transport and suspended sediment transport.

2.2 Bottom Shear Stress and Transport Initiation

The interaction between current and the bed is modelled via the bottom shear stress $\overline{\tau_B}$ in [N/m²]. Assuming a logarithmic velocity profile and the equivalent bed roughness κ_s in [m] for hydraulically rough beds, it is formulated as follows:

$$\overline{\tau_B} = \rho \frac{\kappa^2}{\left(\ln \frac{12b}{\kappa_s}\right)^2} \|\vec{u}\| \vec{u} \tag{2}$$

These are the water density ρ in [kg/m³], the dimensionless von-Karman constant κ , the mean flow velocity $\vec{u} = (u_x, u_y)^T$ in [m/s] and the water depth b in [m]. According to Nikuradse, the equivalent bed roughness κ_s can be set in relation to the in-situ sediment. A multitude of formulae exist in regard to their calculation, which essentially depends on a characteristic grain diameter, as well as a scaling factor. One example is the correlation $\kappa_s = 3d_{90}$. To achieve three-dimensional current modelling, the bottom shear stress needs to be inserted in place of equation 2.

Natural channels often exhibit bed forms which dissipate additional flow energies. According to VAN RIJN (1993), the bed roughness may in this case be considered as the sum of grain coarseness κ_s^g and bed form κ_s^f . This will be discussed in more detail in paragraph 4. The stresses acting on the sediment particles are of importance regarding sediment transport. These can be calculated through inserting the grain roughness in place of the bed roughness in equation 2. Accordingly, the variable for the effective bottom shear stress can be expressed as:

$$\overline{\tau_B} = \rho \frac{\kappa^2}{\left(\ln \frac{12b}{\kappa_s^g}\right)^2} \|\vec{u}\| \vec{u} \tag{3}$$

It represents the morphologically active bottom shear stress and is of essential importance for the calculation of sediment transport.

The central question concerning transport calculations is, as at what level of bottom shear stress transport of mobile sediment is initiated. A popular approach in morphodynamic modelling is based on research by Shields regarding critical bottom shear stress. It assumes that sediment only becomes mobile after a critical value, the dimensionless Shields-Parameter θ_{cr} , has been exceeded. Shields does not supply a functional correlation, presenting his findings graphically in dependence of dimensionless parameters instead. In follow-up articles, this data was supported by curves. A number of functional correlations for the calculation of θ_{cr} can be found in the appropriate technical literature. One example, the approach by BROWNLIE (1981), is shown in Fig. 2.

The course of the curve or, rather, the Shields diagram is commonly known and has been adequately discussed (BUFFINGTON and MONTGOMERY 1997; VAN RIJN 2007). It should be mentioned that this curve fit naturally represents Shields' data, but is intended to overestimate θ_{cr} , particularly for coarse sediment. Therefore, Figure 2 plots the approach according to PARKER et al. (2003), scaling the approach by BROWNLIE (1981) to 0.5. This should better represent the initiation of sediment transport. These two formulae alone demonstrate the range necessary to calculate the critical bottom shear stress. In addition, turbulent currents, which can be assumed in natural bodies of water, represent a stochastic process (ZANKE 2002). Stress peaks on single grains caused by turbulent fluctuations are not represented by the functional sequences shown in Figure 2. The approach using θ_{cr} has nevertheless been proven successful, as it represents a critical value whose exceedance points out that significant amounts of sediment are transported and not only scant particles.

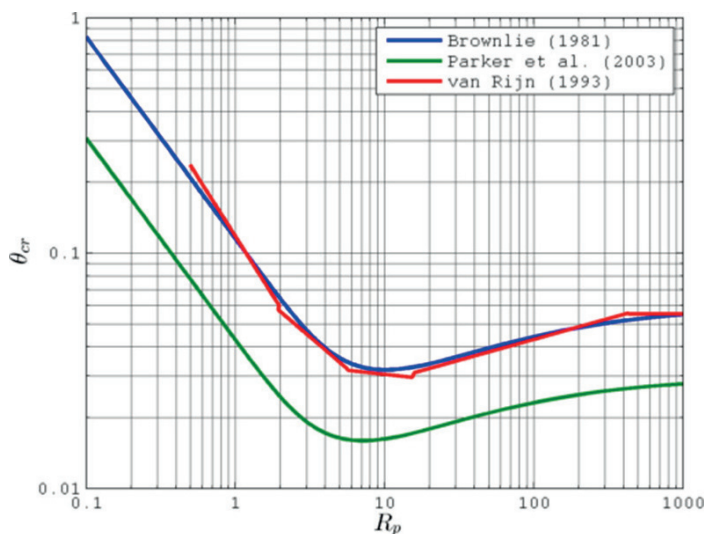


Figure 2: Critical bottom shear stress θ_{cr} of the transport initiation in dependence of the Grain-Reynolds-Number.

Fig. 2 displays a further curve. Shown is the partial parameterization according to VAN RIJN (1993), which is frequently used in numerical models. It should be noted, that it is a

good reflection of the critical bottom shear stress, while showing discontinuities along the transitions, though. These could lead to numerical instabilities and should not be applied, according to its authors. Approaches like those by BROWNLIE (1981), PARKER et al. (2003) or ZANKE (2001) are to be preferred.

2.3 Bed Load Transport

Calculating sediment transport along the bottom is a decisive step toward morphodynamic simulation. Technical literature offers a nearly overwhelming number of more or less empirically derived formulae, which have been previously examined extensively, for instance in ZANKE (1982). These have a certain validity based on the data applied, so that new approaches regarding different problems are still being published today, for instance regarding wave and tide influenced transport (CAMENEN and LARSON 2005; MALCHEREK and KNOCH 2005; VAN DER A et al. 2013).

The majority of bed load transport formulae can be divided into two classes. There are the marginal value formulae, in which sediment is not transported until the critical bottom shear stress has been exceeded. In general terms, many of these approaches can be described as

$$q_s = m(\theta' - \theta_{cr})^n a \quad (4)$$

Here q_s represents the amount of the bed load transport capacity in [m²/s], m and n are formula-dependent parameters and $\theta' = \tau'_B / ((\rho_s - \rho)gd_{50})$ is the effective dimensionless bottom shear stress with the gravitation acceleration g in [m/s²] and the grain diameter d_{50} in [m]. Furthermore, $a = ((s-1)gd_{50}^3)^{1.5}$ in [m²/s] with the specific density $s = \rho_s / \rho$. The vector transport rate is derived from the flow field along the x and y axes. The classic transport formula according to MEYER-PETER and MÜLLER (1948) is equally relevant as is, for instance, a formula based on data re-analysis by NIELSEN (1992). In addition, other formulae were developed that did not factor in this critical value, like the probabilistic approach by EINSTEIN (1950), or BIJKER's (1968) formula for coastal longitudinal transport.

In the case of large bed gradients, gravitation exercises a considerable effect on the amount and direction of bed load transport. To be able to consider this effect, a number of approaches have been developed, which modify the transport vector, the critical bottom shear stress or the entire transport formula (for instance SOULSBY 1997; CHENG et al. 2010). Is the bed gradient higher than the inner angle of friction, slope slides will occur, which have to be treated separately.

To characterize coastal bed load transport, a simulation result using the formula according to Meyer-Peter and Müller (with $m=8$ and $n=1.5$ in equation 4) for the flood-tide current is shown in Fig. 3 as an example. Only the tide was factored in as a load factor and fine sand assigned for the sediment. The results show large-scale mobilization of sediments within the German Bight. However, the transport rates are lower by several magnitudes in relation to the peak values. These occur in the inlets and estuaries, where bottom shear stresses are high. Therefore, large-scale bed load transports can be expected in these areas. The transport rate decreases markedly in the shallower areas. Within the

Wadden areas the model does not simulate any substantial transport due to the tidal load alone.

The example shown can merely give a general overview into the bed load dynamics of coastal regions, as the simulated results depend strongly on the applied transport formula and further sediment characteristics, as well as the applied loads. Depending on the selected approach, the bed load transport rates can vary by several magnitudes and may, therefore, lead to a different bed evolution. In addition, the simulation presumes the availability of a constant and sufficient quantity of sediment for the predicted transport capacity according to equation 4 and that this quantity is directly introduced into the bed evolution equation as the actual bed load transport rate. Numerically, limited sediment transport is much more difficult to model (MALCHEREK 1997).

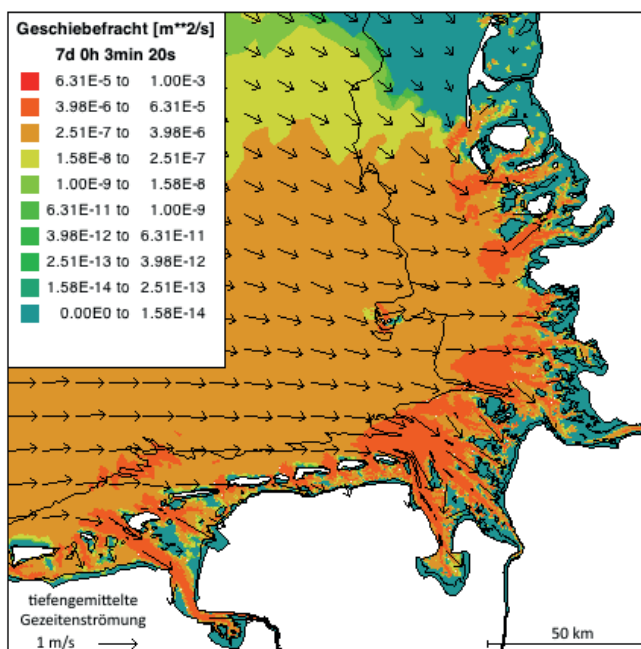


Figure 3: Example of bed load transport rate in the German Bight during incoming tide according to the Meyer-Peter-and- Müller formula.

2.4 Suspended Sediment Transport

The three-dimensional transport of suspended sediment can be described with the following scalar advection/ diffusion equation:

$$\frac{\partial c}{\partial t} + \text{div}(c \vec{u}_S) = \text{div}(\varepsilon_S \text{grad} c) \quad (5)$$

Here c is the volumetric sediment concentration in the water in $[\text{m}^3/\text{m}^3]$, $\vec{u}_S = (u, v, w - w_S)^T$ is the velocity vector with which sediment is carried, w_S the sink rate

in [m/s] and ε_s the sediment diffusivity in m^2/s (JULIEN 2010). The sink rate can be calculated through formulae like, for instance, VAN RIJN (1993). It must be noted, however, that, especially in coastal zones, effects like flocculation (MALCHEREK 1994) or sediment mixtures exacerbate precise determination of sink rates considerably.

It is assumed as a marginal condition along the water surface that no sediment passes through the surface. Close to the bed, however, a vertical sediment flow between the body of water and its bed may occur. It is defined in a definite height above the bed, which represents the strength of the load-carrying layer. The sediment flow depends on the qualities of the sediment, the bed characteristics and the effective bottom shear stress. It is further divided into an erosion and a deposit flow. Several different approaches exist for its modelling. The erosion flow is commonly described in terms of a power law in dependence of the excess bottom shear stress $\max(0, \tau'_B - \tau_{cr})$ (for instance according to Partheniades), while the deposit flow, in the simplest case, is dependent on the concentration close to the bed and the sink rate.

When determining the mean of the three-dimensional suspended particle transport equation (equation 5), the two-dimensional transport equation is achieved. It displays the erosion and deposit flows as source and sink terms. The definition of the deposit flow is problematic, as it technically depends on the sediment concentration near the bed. One possibility is the assumption that an equilibrium concentration will occur, during which the erosion and deposit flows cancel each other out. This is the basis upon which the necessary net flow for achieving this condition is calculated in the numerical model.

The result of a mean suspended particle transport equation is shown in Fig. 4. For comparison with the bed load transport rate, the suspended particle transport rate was calculated from the sediment concentration. Fine sand was defined as the mobile sediment for the entire modelling area and only the tidal currents were simulated. Furthermore, an equilibrium concentration was assumed in order to model the erosion and deposit flows. This transportation mode, too, incurs large-scale mobilization of sediment due to the floodtide current. The highest suspended sediment transport rates are generated in the estuaries and channels, where the current produces an elevated bottom shear stress and large quantities of sediment are transported in the water column. In the Wadden areas, however, only a limited mobilization of sediments can be detected for the generated current condition. Part of the suspended sediment transported by the tide is deposited here.

Decisive in both, the three-dimensional and two-dimensional, transport equations is the amount of sediment introduced into or discharged from the body of water along its bed. The net flow appears in the bed evolution equation and may possibly lead to a change in the bed. The formulations used for the deposit and erosion flows, as well as for the sink rate, are essential factors, which may alter the morphodynamic results considerably. It is interesting to note that the transported amounts can be higher by several magnitudes than during bed load transport and play a critical role in the overall sediment dynamics. Particular attention should therefore be paid to the modelling of suspended sediment transport.

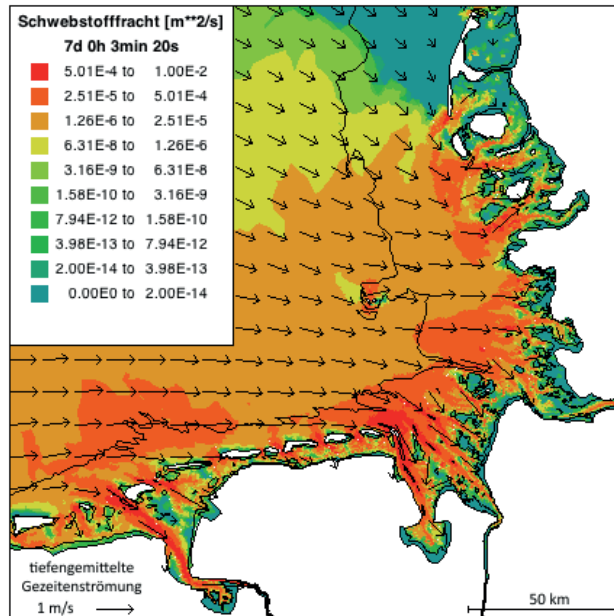


Figure 4: Example of mean suspended sediment transport during incoming tide.

3 Fractionated Sediment Transport

The bottom of natural channels generally consists of a mixture of different sediments. Since bottom shear stress, transport initiation and sediment transport are influenced by grain size, more advanced concepts than those already discussed are required. The composition of the bed can be discretized by way of sediment classes, to which a characteristic grain diameter will be assigned, saved as an initial sediment configuration. Another possibility would be to presume a lognormal distribution of the sediment classes. The statistical parameters for the description of the function profile would be saved and may change during the course of the simulation. This concept will not be discussed further here.

3.1 Vertical Discretization of the Hydrographic Bed

Grain size-dependent sediment transport leads to a separation within the uppermost sediment layer bordering on the body of water.

A modelling concept for this phenomenon is the Active-Layer-Concept. The hydrographic bed is divided into an active layer (the layer bordering on the body of water) and an underlying inactive layer. Further layers may follow up to a non-erodible soil horizon. Horizontal sediment transport and the exchange of sediments with the water column only take place within the active layer. Its strength is defined by the user or calculated, for instance dependent on grain diameter or the bottom shear stress.

Fractionated bed load transport can, for example, be modeled by calculating transport initiation and bed load transport rate with a grain diameter characteristic for the sediment mixture. The transport rate is then proportionally distributed on the existing sediment fractions and the bed evolution equation is solved. For suspended sediment transport, the calculated erosion and deposit flows can be determined similarly. Through fractionation of the sediment, effects like Hiding/Exposure can be considered.

Both in the active layer as well as all potential substratum layers, an initial sediment distribution has to be provided. Due to bed load and suspended sediment transport in the sediment classes, not only the composition but also the position of the bed changes over the course of the simulation.

3.2 Sediment Separation in a Tide-affected Bight

Fig. 5 shows an abstract of a separation study for the Jadebusen Bay by MALCHEREK and KNOCH (2004), utilizing seven different sediment fractions ranging from medium silt to very coarse sand. It incorporates bottom shear stress from tides as well as from wave effects. Fine sand was assigned as the initial sediment load. It was generated through the interpolation of measurement data and shows distinct artifacts. The actual water body structure, which is characterized by a multitude of tidal gullies and channels, is only superficially represented.

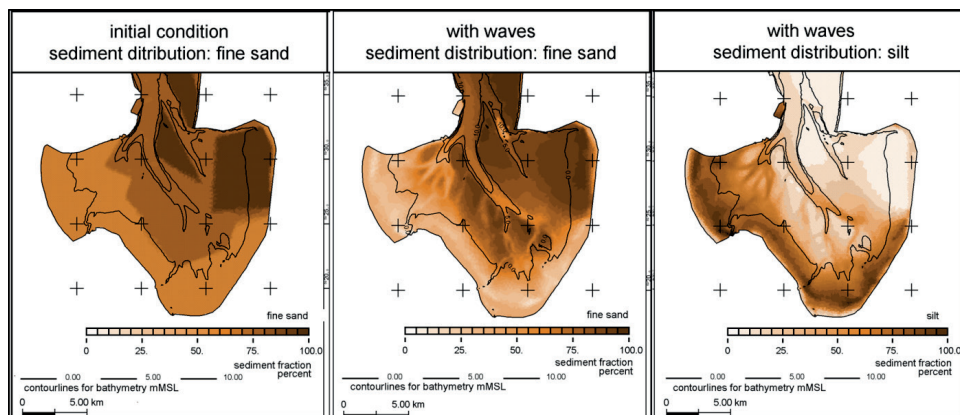


Figure 5: Initial distribution of fine sand, as well as fine sand and silt after 9 simulated days.

After a period of 9 days, a distinct transformation in the sediment composition can be detected. A structuring corresponding to the morphological structure can be recognized. The prevailing Westerly wind direction results in a lower wave load in the West and a higher wave load in the East of the bay. This leads to a higher percentage of fine sediment in the tidal change zone in the Western part of the Jadebusen, as outlined by the silt example. In contrast, the percentage of fine sand is reduced at the same location. The bottom shear stress in the Eastern part is so high that the sediment primarily consists of fine sand.

The results emphatically demonstrate the performance capabilities of morphodynamic modelling. The disadvantage of the Active-Layer-Concept, though, is the fact that data concerning the layering of sediment are lost during the simulation run. New developments attempt to correct this via a bookkeeping algorithm (MERKEL and KOPMANN 2012).

4 Prediction of Dunes and Ripples

If the bottom consists of mobile sediment, bed forms such as dunes and ripples may develop under certain current conditions and with the appropriate bottom substrate (YALIN 1992). In relation to the bed load stress, we need to distinguish between different stages of development, current status and decay. In coastal regions, roughness-induced bed forms can be classically divided into dunes and ripples. The latter may be generated through either tidal currents or wave load. In addition, dunes and ripples can occur simultaneously and may be superimposed.

4.1 Grain and Bed Roughness

If bottom forms are present, the roughness of the bottom increases significantly in relation to the pure grain roughness. In this case, a distinction must be made between the roughness of the grains, which have been selected for the calculation of sediment transport, and the current-related roughness. According to VAN RIJN (1993), the equivalent bed roughness can be partitioned as follows:

$$k_S = k_S^g + k_S^f \quad (6)$$

Accordingly, k_S is made up of the sediment-related grain roughness k_S^g and the bed form k_S^f , which is dependent on the extent of shaping of the bottom. The bed form can be further subdivided into ripple form k_S^r and dune form k_S^d . According to van Rijn, the individual form can be calculated as:

- The grain roughness: $k_S^g = 3d_{90}$
- The bed form due to ripples: $k_S^r = a_r \gamma_r \Delta_r^2 / \lambda_r$
- The bed form due to dunes: $k_S^d = 1.1 \gamma_d \Delta_d (1 - \exp(-25 \Delta_d / \lambda_d))$

Here, a_r and γ_r are weighting factors. For a_r , literature indicates values between 8.0 (VAN RIJN 1993), 20.0 (NIELSEN 1992) and up to 27.7 (GRANT and MADSEN 1982). For superimposed ripples and dunes or sand waves, VAN RIJN (1993) gives a value of $\gamma_r = 0.7$, otherwise 1. Furthermore, Δ_r is the ripple height, λ_r the ripple length, Δ_d the dune height and λ_d the dune length. For natural conditions, a value of 0.7 needs to be applied for γ_d .

Thus, the definition of the bed form can be traced back to the prediction of length and height of the sediment bodies. For a detailed study on the prediction of dunes and ripples see MALCHEREK and PUTZAR (2004), as well as PUTZAR and MALCHEREK (2010). The methods described therein not only consider flow conditions and the in-situ sediment, but also include modelling of the temporal development.

4.2 Predicted Heights of Bed Forms and Resulting Roughness

In the following, the results of a morphodynamic simulation with fractionated sediment transport, tidal load, waves and wind is presented, that also considered the roughness of dunes and ripples. This simulation is based on the long-term model of the German Bight (in HEYER and SCHROTTKE 2012).

Fig. 6 shows the time-dependent ripple height. In comparison with the sediment distribution from HEYER and SCHROTTKE (2012), which is the basis of the simulation, it becomes apparent that these bed forms do not appear (or at least only negligibly) in areas with primarily cohesive sediment. Examples for this are the silt lens at Heligoland and the Dollart. On sandy soils, however, ripple heights of up to a maximum of 2 cm can be observed. But here too, there are areas in which ripples do not occur. Here the bottom shear stress of tides and waves is so high that the critical value of ripple existence is exceeded and the ripples disappear. Equally, there are areas in which the bed load is insufficient to generate ripples. The predicted dune height (Fig. 7), on the other hand, demonstrates a different spatial distribution. These bed forms can be found in channels and estuaries with sandy sediment. The predicted dune height also varies from only a few centimeters up to approximately 2 m. This results in the bed form k_s according to equation 4, as shown in Fig. 8. Not only is it significantly higher, as compared to the grain roughness k_s^d , but also demonstrates a larger spatial and temporal variability.

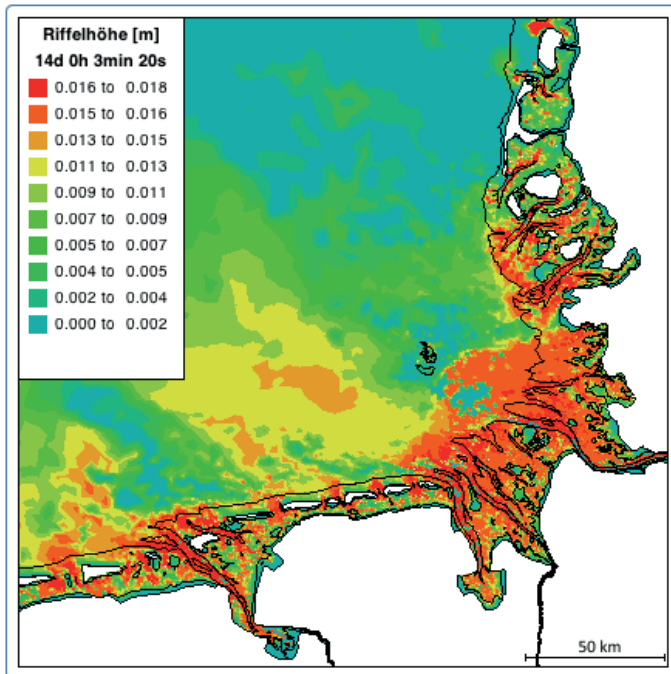


Figure 6: Predicted ripple height.

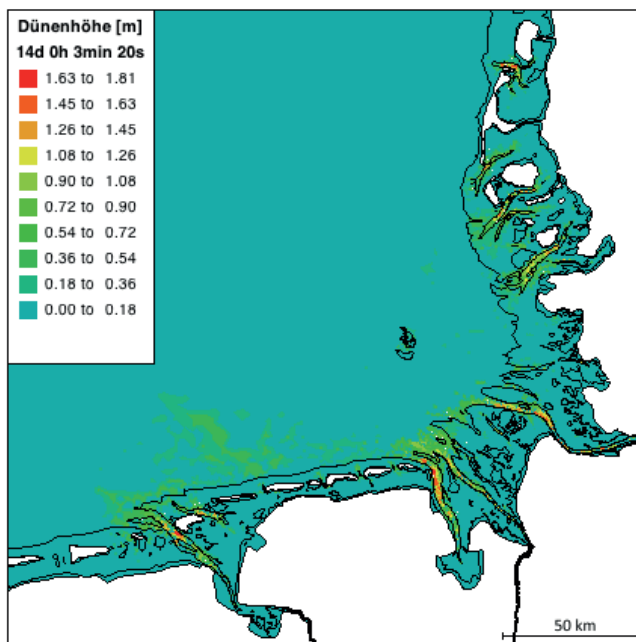


Figure 7: Predicted dune height.

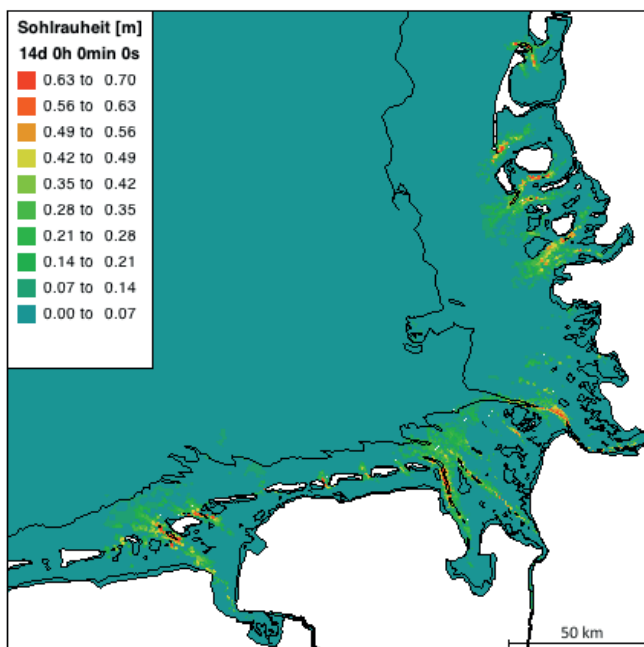


Figure 8: Bed roughness calculated from ripple and dune measurements.

The simulation results shown represent initial results towards a large-scale prognosis of bed forms and are still being actively researched. The results of the dune and ripple predictions depend on the hydrodynamic and sedimentological input data. In principle, the predictors need to be calibrated in order to attain naturalistic results. In particular, it must be noted that the predicted bed forms need to be assessed critically in regard to the effect of their roughness. VAN RIJN (1993) refers to the fact that a value $k_s^f = 0$ applies to symmetrical sediment waves. Future challenges will lie in the reliable prognosis of actual profile-related bed geometries.

5 Effect of Maintenance Measures on Bed Evolution

Whereas the previous paragraphs were dedicated to natural sediment transport, the following outlines the anthropogenic influences by example of maintenance measures on waterways. Through the extraction and dumping of dredged material, they can play a decisive role in sediment dynamics.

5.1 Modelling of Maintenance Measures

Dredging and dumping can be realistically modeled with the DredgeSim module (MAERKER and MALCHEREK 2010), which was developed by the German Federal Waterways and Research Institute in Karlsruhe in cooperation with the University of the German Federal Armed Forces in Munich, Institute of Hydrosociences. It is coupled with a morphodynamic-numerical model, for instance into the TELEMAC simulation system (HERVOUET and BATES 2000), and offers the option of optimizing sediment management and to make its planning more efficient.

As part of the AufMod project/sub-project 4 (HEYER and SCHROTTKE 2012), dredging criteria were developed for the three major German estuaries, the Elbe, Weser and Ems rivers. All of these contained maintenance strategies and were incorporated into a long-term model of the German Bight (PUTZAR and MALCHEREK 2012; HEYER and SCHROTTKE 2012). Essentially, a minimum required depth for the navigation channel was determined, whose exceedance would ensue the extraction of sediment. The minimum depth is checked at intervals of one year and dredging operations are initiated as required. The extracted sediment can then be dumped in closely defined areas or removed entirely from the simulation model. A detailed description of the sub-project 4 can be found in HEYER and SCHROTTKE (2012).

5.2 Long-term Bed Evolution in the Elbe Estuary

As an example for the analysis of the effects of maintenance measures, two simulations are outlined, each with a simulated run-time of 100 years, one with, the other without sediment extraction within the Elbe estuary. For both simulation runs a grain diameter of 0.375 mm was used and the sole load on the bed was the tidal current. The maintenance measures on the tidal Elbe were considered by way of a defined minimum required depth. Dumping of the extracted sediment was dispensed with.

The effect of the maintenance measure on the simulated morphodynamics can be demonstrated particularly well in the area of the Elbe mouth. Without maintenance measures, the navigation channel of the Outer Elbe between the banks of Großer Vogelsand and the Gelbsand would shift toward the Northeast, as shown in Fig. 9. For the sake of orientation, the dredging areas are represented as yellow polygons. The navigable channel would fill in on a length of 14 km, making it impossible to guarantee the consistency and safety of the waterway.

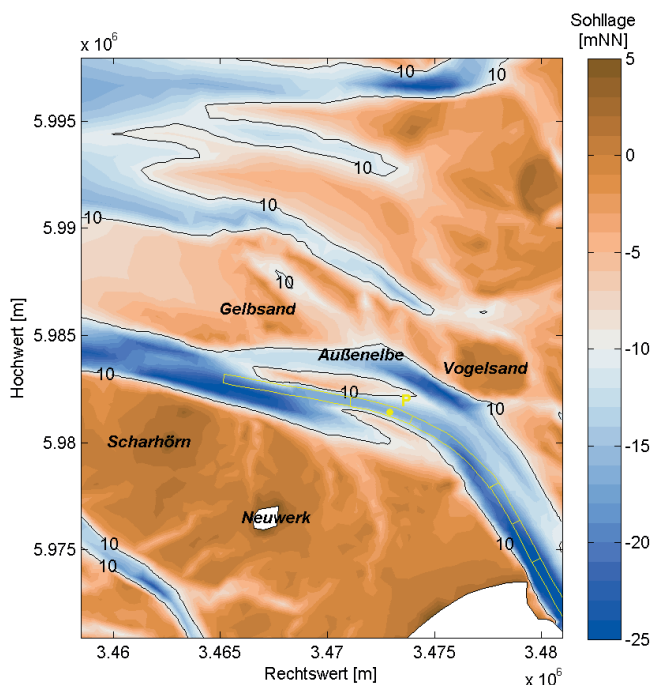


Figure 9: Simulated bed geometry, without dredging, after 100 years, in the Elbe estuary in the German Bight. Those areas of the shipping channel on which maintenance measures were carried out in the simulation, are marked yellow and are intended to ease comparison of the two simulations.

If dredging is to be simulated, the bed elevation is corrected in accordance with the minimum required depth and sediment is extracted from the shipping channel (Fig. 10), thereby creating a massive influence on the morphodynamic development. Even though sediment is still transported towards the Northeast in this simulation, it can be extracted from the navigation channel once the minimum required depth is undercut. The natural tendency of the navigation channel to drift towards the Northeast is reduced, as simulated in the model. The resulting differences in bed elevation from both simulations amount to up to 17 m.

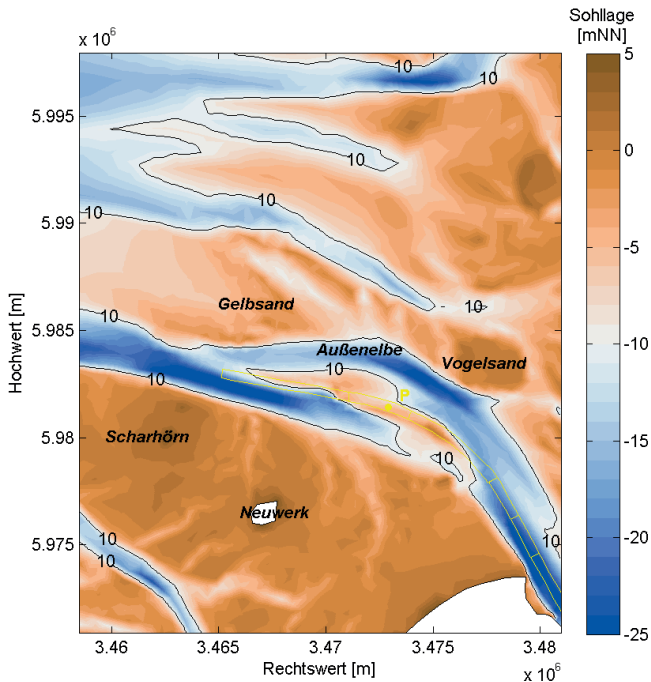


Figure 10: Simulated bed geometry, including dredging, after 100 years, in the Elbe estuary in the German Bight. The regions of sediment extraction in the navigation channel are marked yellow.

6 References

- BIJKER, E.W.: Mechanics of sediment transport by the combination of waves and current Design and Reliability of Coastal Structures, 23rd Int. Conf. on Coastal Engineering, 147-173, 1968.
- BROWNLIE, W.R.: Prediction of flow depth and sediment discharge in open channels, Report No. KH-R-43A, W. M. Keck Laboratory of Hydraulics and Water Resources, California Institute of Technology, Pasadena, Kalifornien, USA, 1981.
- BUFFINGTON, J.M. and MONTGOMERY, D.R.: A systematic analysis of eight decades of incipient motion studies, with special reference to gravel-bedded rivers. *Water Resources Research*, 33(8):1993-2029, 1997.
- CAMENEN, B. and LARSON, M.: A general formula for non-cohesive bed load sediment transport. *Estuarine, Coastal and Shelf Science*, 63(1-2):249-260, 2005.
- CHEN, X; MA, J. and DEY, S.: Sediment Transport on Arbitrary Slopes: Simplified Model, *Journal of Hydraulic Engineering*, 136(5), 311-317, 2010.
- DONG, P: Two-Fraction Formulation of Critical Shear Stresses for Sand and Silt Mixtures. *J. Waterway, Port, Coastal, Ocean Eng.*, 133(3), 238-241, 2007.
- GRANT, W.D. and MADSEN, O.S.: Movable bed roughness in unsteady oscillatory flow, *Journal of Geophysical Research* 87(C1), 469-481, 1982.

- HERVOUET, J.M. and BATES, P. (Ed.): The TELEMAC Modeling System, Sonderausgabe Hydrological Processes, Jg. 14, 2000.
- HEYER, H. and SCHROTTKE, K.: Aufbau von integrierten Modellsystemen zur Analyse der langfristigen Morphodynamik in der Deutschen Bucht (AufMod). Gemeinsamer Abschlussbericht für das Gesamtprojekt mit Beiträgen aus allen 7 Teilprojekten, 2012.
- JACOBS, W.; LE HIR, P.; VAN KESTEREN, W. and CANN, P.: Erosion threshold of sand-mud mixtures. *Continental Shelf Research*, 31, 10: S14-25, 2011.
- JULIEN, P.Y.: *Erosion and Sedimentation*, Cambridge University Press; Updated edition edition, 2010.
- MALCHEREK, A.: Numerical Modeling of Cohesive Settling Velocities. *International Journal of Sediment Research*, 9(3), 97-106, 1994.
- MALCHEREK, A.: Application of Bed Evolution Models Over Loose and Rigid Areas, *International Journal of Sediment Research*, 12(2), 291-299, 1997.
- MALCHEREK, A. and PIECHOTTA, F.: Investigations on the Porosity as a Parameter for Sediment Erodibility. *Proc. 9th Int. Symp. River Sedimentation*, Vol III, 1913-1918, 2004.
- MALCHEREK, A. and KNOCH, D.: The influence of waves on the sediment composition in a tidal bay. In: SPAULDING, M.L. (Ed.), *Estuarine and Coastal Modeling – Proceedings of the 9th International Conference*, New York, 2005, ASCE.
- MALCHEREK, A. and PUTZAR, B.: The Prediction of Dunes and Their Related Roughness in Estuarine Morphological Models. In *Proceedings of the 8th Int. Conference on Estuarine and Coastal Modeling*, Monterey, California, 2004.
- MALCHEREK, A.: *Gezeiten und Wellen - Die Hydromechanik der Küstengewässer*. Vieweg & Teubner, Wiesbaden 2010a.
- MALCHEREK, A.: Zur Beschreibung der rheologischen Eigenschaften von Flüssigschlickten. *Die Küste* 77, S. 135-178, 2010b.
- MALCHEREK, A and CHA, H.: *Zur Rheologie von Flüssigschlickten*. Mitteilungen des Instituts für Wasserwesen der Universität der Bundeswehr München, Heft 111/2011, Shaker-Verlag, Aachen, 2011.
- MAERKER, C. and MALCHEREK, A.: Die Analyse von Baggern und Verklappen. Teil 1: Das Softwarepaket DredgeSim, *Korrespondenz Wasserwirtschaft*, 3 (10), 550-555, 2010.
- MERKEL, U. and KOPMANN, R.: Continuous Vertical Grain Sorting for TELEMAC & SISYPHE v6p2. BOURBAN, S.; DURAND, N. and HERVOUET, J-M. (Hrsg.): XIXth TELEMAC-MASCARET Users Conference, 2012.
- MEYER-PETER, E. and MÜLLER, R.: Formulas for Bed-Load Transport, *Proceedings 2nd Meeting Int. As. Hydraulic Structure Research*, 1-26, 1948.
- NIELSEN, P.: *Coastal bottom boundary layers and sediment transport*, World Science, Singapore. 1992.
- PARKER, G.; TORO-ESCOBAR, C.; RAMEY, M. and BECK, S.: Effect of floodwater extraction on mountain stream morphology. *Journal of Hydraulic Engineering*, 129(11):885-95, 2003.
- PUTZAR, B. and MALCHEREK, A.: Numerical Prediction of Ripple Dimensions and Related Roughness for Tidal Environments. In *Proceedings of ninth International Conference on Hydro-Science and Engineering*, ICHE, 2010.

- PUTZAR, B. and MALCHEREK, A.: Development of a Long Term Morphodynamic Model of the German Bight. In: BOURBAN, S.; DURAND, N. and HERVOUET, J.-M. (Hrsg.): XIXth TELEMAC-MASCARET Users Conference, 2012.
- SOULSBY, R.: Dynamics of marine sands, Thomas Thelford Edition, 1997.
- WEHR, D and MALCHEREK, A.: Numerical Simulation of Fluid Mud Dynamics – The Isopycnical Model MudSim. Die Küste, 79: 1-52, 2012.
- VAN DER A, D.A.; RIBBERINK, J.S.; VAN DER WERF, J.J.; O'DONOGHUE, T.; BUIJSROGGE, R.H. and KRANENBURG, W.M.: Practical sand transport formula for non-breaking waves and currents. Coastal Engineering, 76(0):26-42, 2013.
- VAN RIJN, L.C.: Principles of Sediment Transport in Rivers, Estuaries and Coastal Seas. Aqua Publications, Amsterdam, 1993.
- VAN RIJN, L.C.: Unified view of sediment transport by currents and waves. i: Initiation of motion, bed roughness, and bed-load transport. Journal of Hydraulic Engineering, 133(6):649-667, 2007.
- YALIN, M.S.: River Mechanics, Pergamon Press, Oxford, New York, Seoul, Tokyo, 1992.
- ZANKE, U.C.E.: Grundlagen der Sedimentbewegung. Springer Verlag, Berlin, Heidelberg, New York, 1982.
- ZANKE, U.C.E.: Zum Einfluss der Turbulenz auf den Beginn der Sedimentbewegung. Mitteilungen, Institut für Wasserbau und Wasserwirtschaft (Heft 120): 24, 2001.
- ZANKE, U.C.E.: Hydromechanik der Gerinne und Küstengewässer. Parey Buchverlag, Berlin, 2002.

Fundamentals on Ecological Modelling in Coastal Waters Including an Example from the River Elbe

Arne Hammrich and Dagmar Schuster

Summary

Modelling dissolved oxygen in water encompasses a range of requirements and process descriptions. Among a good representation of hydraulic, including advection/dispersion, the processes in the ecological part of the model are crucial for a reliable model.

A MIKE 21 (DHI 2013) flexible mesh model was used to simulate the hydrodynamic conditions in the River Elbe around Hamburg. The model is based on the numerical solution of twodimensional incompressible Reynolds averaged Navier-Stokes equations subject to the assumptions of Boussinesq and of hydrostatic pressure. Thus, the model consists of continuity, momentum, temperature and density equations and is solved by a turbulent closure scheme. The spatial discretisation is performed using a cell-centred finite volume method. In the horizontal plane an unstructured mesh is used.

This hydrodynamic model was coupled to the ecological module (ECO Lab) to form the basis for the water quality model. ECO Lab (DHI 2013) is a numerical lab for ecological modelling. It is an open and generic tool for customising aquatic ecosystem models to describe water quality. The module is mostly used for modelling water quality as part of an environmental impact assessment.

In the present case a eutrophication model was used to describe the concentrations of phytoplankton, chlorophyll-a, zooplankton, organic matter (detritus), inorganic nutrients and oxygen in the river Elbe in Hamburg. Rooted vegetation and macroalgae were not implemented as their influence in this part of the Elbe is negligible. The eutrophication module is integrated within the advection-dispersion module which describes the physical transport processes at each node in the model domain.

The model was used to describe the oxygen conditions in the Port of Hamburg, especially the change of dissolved oxygen in the Reiherstieg, a lateral channel which is usually closed with a sluice at the southern end to prevent suspended solids to deposit in the port. Due to plans for a new sluice gate the Hamburg Port Authority tested if a temporary opening of the gate could improve the oxygen conditions in the port. The model showed that resuspension and mineralization of organic material play an important role in this system. The balance between opening the gates to flush oxygen rich water into the port and preventing the introduction of organic material is crucial for better oxygen balance in the Reiherstieg.

Keywords

oxygen, nutrients, water quality, Elbe, model, MIKE21, ECO Lab

Zusammenfassung

Die mathematische Modellierung von Sauerstoff im Gewässer umfasst zahlreiche Prozesse. Neben einer präzisen Berechnung der Hydraulik, sowie der Advektion/Dispersion, sind die formulierten Prozesse im Wasserqualitätsmodell eine wichtige Voraussetzung für ein verlässliches Modell.

Ein MIKE 21 (DHI, 2013) flexible Mesh Modell wurde in der vorliegenden Untersuchung verwendet, um die hydraulischen Bedingung im Hafen von Hamburg und der angrenzenden Tideelbe zu berechnen. Das Modell basiert Reynolds-gemittelten Navier-Stokes Gleichungen unter Berücksichtigung der Annahmen von Boussinesq und unter Annahme einer hydrostatischen Druckverteilung. Impuls- und Massenerhaltung auch für die Inhaltsstoffe wie z. B. Salz und Temperatur sind in dem zugrunde liegenden Ansatz erfasst. Die räumliche Diskretisierung erfolgt über einen Element-zentrierten Finite Volumen Ansatz. Horizontal wird ein unstrukturiertes Mesh verwendet.

Das hydrodynamische Modell wurde an einen ökologischen Gleichungslöser (ECO Lab) als Basis für das Wasserqualitätsmodell gekoppelt. ECO Lab (DHI, 2013) ist eine numerischen Gleichungslöser zur Programmierung von ökologischen Modellen.

In der vorliegenden Untersuchung wurde ein Eutrophierungsmodell in ECO Lab verwendet, um die Konzentrationen von Phytoplankton, Chlorophyll-a, Zooplankton, Detritus, anorganischen Nährstoffen und Sauerstoff in der Elbe bei Hamburg zu berechnen. Makroalgen wurden im Modell nicht berücksichtigt, da ihr Einfluss in diesem Teil der Elbe vernachlässigbar ist. Das Eutrophierungsmodell ist in das Advektions/Dispersionsmodul integriert, welches den physikalischen Transport im Modell rechnet.

Das Modell wurde zur Berechnung der Sauerstoffkonzentration im Hafen von Hamburg verwendet. Speziell die Veränderungen der Sauerstoffkonzentration im Reiberstieg, einem Kanal im Süden Hamburgs, der normalerweise zur Süderelbe hin durch eine Schleuse verschlossen ist, sollte im Modell erfasst werden. Die geschlossene Schleuse soll vor allem den Eintrag und die Sedimentation von Schwebstoffen in das Hafengebiet verhindern. Im Rahmen der Planungen für eine neue Schleuse am Reiberstieg sollte mithilfe des Modells untersucht werden, ob durch eine zeitweilige Öffnung der Schleuse die Sauerstoffkonzentration im Reiberstieg verbessert werden kann. Die Untersuchung zeigt, dass die Resuspension und anschließende sauerstoffzehrende Mineralisation von organischem Material eine wichtige Rolle spielt. Eine optimale Steuerung der Schleuse muss ein Kompromiss sein, zwischen möglichst langer Öffnung der Schleusentore, um viel sauerstoffreiches Wasser in den Hafen zu spülen, und einer möglichst geringen Resuspension von organischem Material, da diese immer eine Sauerstoffzehrung durch Mineralisation nach sich zieht.

Schlagwörter

Sauerstoff, Nährstoff, Wasserqualität, Elbe, Modell, MIKE 21, ECO Lab

Contents

1	Introduction	109
2	Methods	110
2.1	Hydrodynamic Model	110
2.2	Ecological Model	111
3	Results	112
3.1	Hydrodynamic Model	112
3.2	Ecological Model	114
4	Discussion.....	118
5	References.....	118

1 Introduction

Although modelling hydrodynamics is well-established since years, ecological modelling rather plays a minor role. As ecological models are usually very complex, a major problem so far was computational time. But with decreasing prices for powerful computers ecological modelling more and more evolves into a tool for investigating anthropogenic impacts in coastal waters.

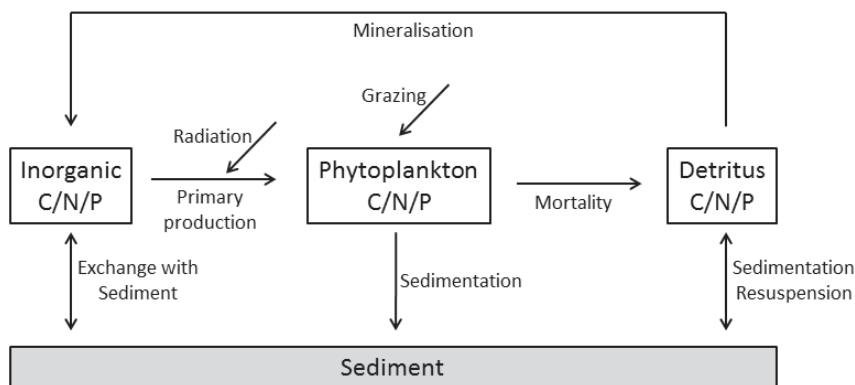


Figure 1: Typical conceptual ecological model.

The complexity of such models derives from tight interlocking biological and chemical processes, which highly depend on each other. The concentration of oxygen for example depends on temperature and the concentration of phytoplankton, whereas the phytoplankton concentration itself depends on light and the availability of nutrients. This in turn means, that an oxygen-model requires to model temperature and all nutrient cycles (especially for carbon, nitrogen and phosphorous) as well. A typical conceptual model which neglects the influence of benthic vegetation is shown in Fig. 1.

All phytoplankton is built up in primary production from inorganic matter under the influence of light. This primary production is the only oxygen producing process in water. All dead matter (detritus) in turn is mineralised under oxygen consumption to inorganic

matter. Both organic pools (phytoplankton and detritus) are subject to settling. Usually only the detritus fraction can resuspend again, as it is often assumed, that settled phytoplankton dies off.

As light is the superior driver in primary production, all factors that have an influence on light penetration, e.g. turbidity, directly impact the dissolved oxygen. Another important factor is that turbidity often enhances the biological oxygen demand (BOD), because organic compounds mineralise after resuspension, which consumes dissolved oxygen.

Here we present a study that deals with the problem of resuspended matter that caused strong oxygen depletions in the Port of Hamburg.

The so called “Reiherstieg” in the southern part of the Port of Hamburg is a port basin which is closed at its southern end by a sluice (Fig. 2). To prevent suspended solids from entering the Reiherstieg the sluice is usually closed, which causes long retention times and low oxygen concentrations. As this sluice is planned to be renewed, it was debated if an intermittent opening of the sluice gates could lower the retention time and improve the oxygen conditions within the port. Obviously any opening would lower the retention time, but it remained unclear, if sediments could resuspend due to increased current velocities and cause an increase of BOD in the Reiherstieg.

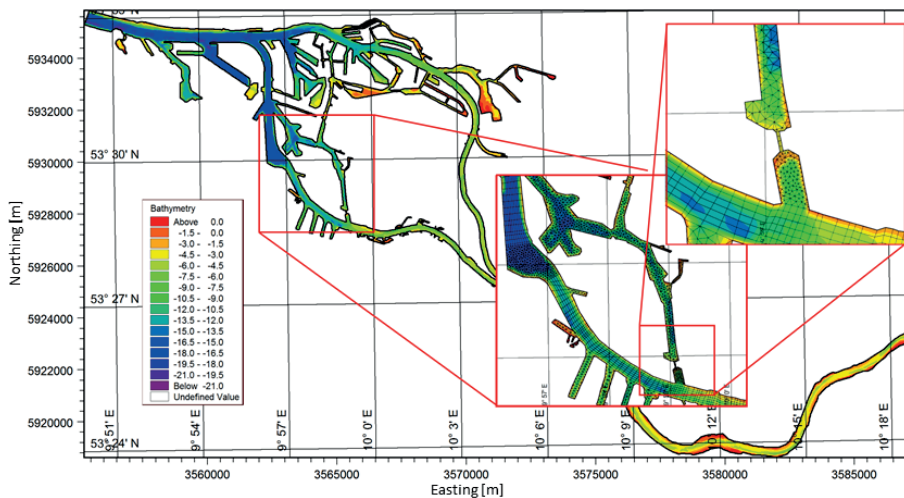


Figure 2: The “Reiherstieg” in the Port of Hamburg.

2 Methods

2.1 Hydrodynamic Model

A MIKE 21 (DHI 2013) flexible mesh model was used to simulate the hydrodynamic conditions in the River Elbe around Hamburg. The model is based on the numerical solution of twodimensional incompressible Reynolds averaged Navier-Stokes equations subject to the assumptions of Boussinesq and of hydrostatic pressure. Thus, the model consists of continuity, momentum, temperature and density equations and is solved by a

turbulent closure scheme. The spatial discretisation is performed using a cell-centred finite volume method. In the horizontal plane an unstructured mesh is used.

The model domain (Fig. 3) extends in the tidal part of the River Elbe from the weir in Geesthacht (upstream) to Blankenese (downstream).

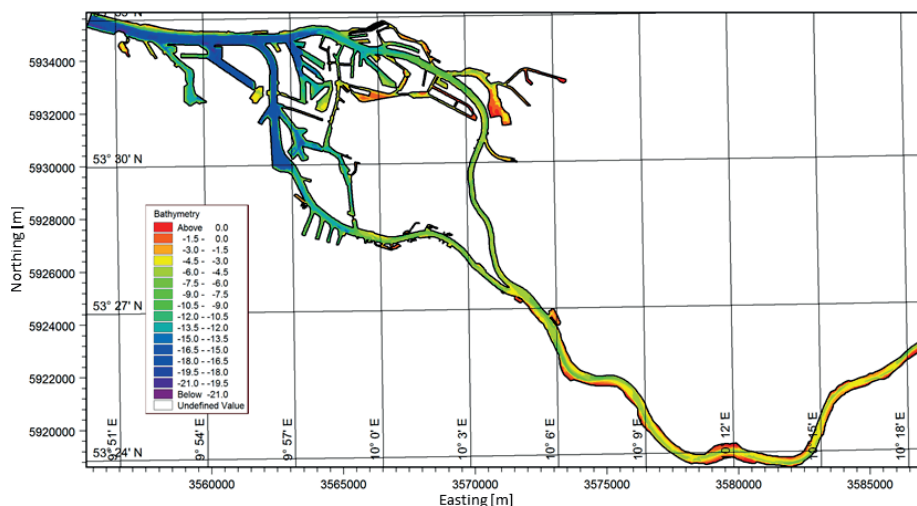


Figure 3: Model domain of the M21FM model.

2.2 Ecological Model

Into the 2D hydrodynamic model we embedded an ecological model, in order to simulate the simultaneous processes of transport, dispersion and biological/chemical processes. The ecological model is based on the DHI ECO Lab template “Eutrophication 1” (DHI 2013), which describes the following 11 state variables, which are subject to advection and dispersion:

- Phytoplankton Carbon (gC/m³)
- Phytoplankton Nitrogen (gN/m³)
- Phytoplankton phosphorous (gP/m³)
- Chlorophyll-a (g/m³)
- Zooplankton carbon (gC/m³)
- Detritus carbon (gC/m³)
- Detritus nitrogen (gN/m³)
- Detritus phosphorus (gP/m³)
- Inorganic nitrogen (gN/m³)
- Inorganic phosphorous (gP/m³)
- Dissolved oxygen (g/m³)

Benthic vegetation was considered to be negligible in this tidal part of the River Elbe and the Port of Hamburg.

A particular focus was set to the resuspension of sediments close to the sluice due to higher currents speeds when the gates are opened. Therefore sediment samples have been

taken at the sluice to measure the grain size distribution. Based on these measurements a correlation between current speed and resuspended sediment for different grain size classes was established (Fig. 4).

Additionally the biological oxygen demand (BOD) of the sediment samples was measured. The empiric correlations for resuspension and the BOD were then implemented into the ecological model. By this approach we ensured that the biological/chemical oxygen consumption caused by the mineralisation of resuspended sediments at the sluice gate is implemented appropriately in the model.

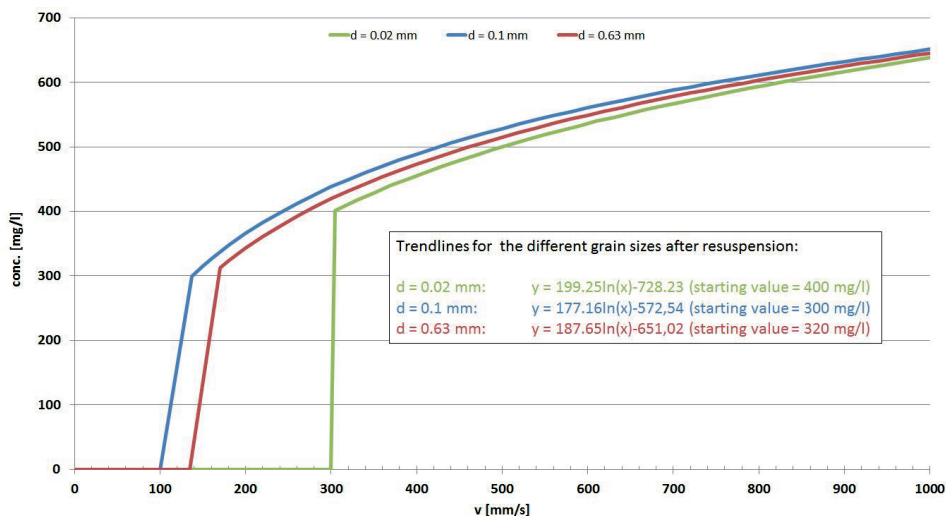


Figure 4: Correlation between current speed and resuspended sediment for different grain size classes.

3 Results

3.1 Hydrodynamic Model

The hydrodynamic model was calibrated against the water level at the gauging stations in St. Pauli (Fig. 5) and Bunthaus (Fig. 6). At tidal low water the model tends to overestimate the measured values, especially at Bunthaus, but in general there is a good accordance between measured and simulated water levels.

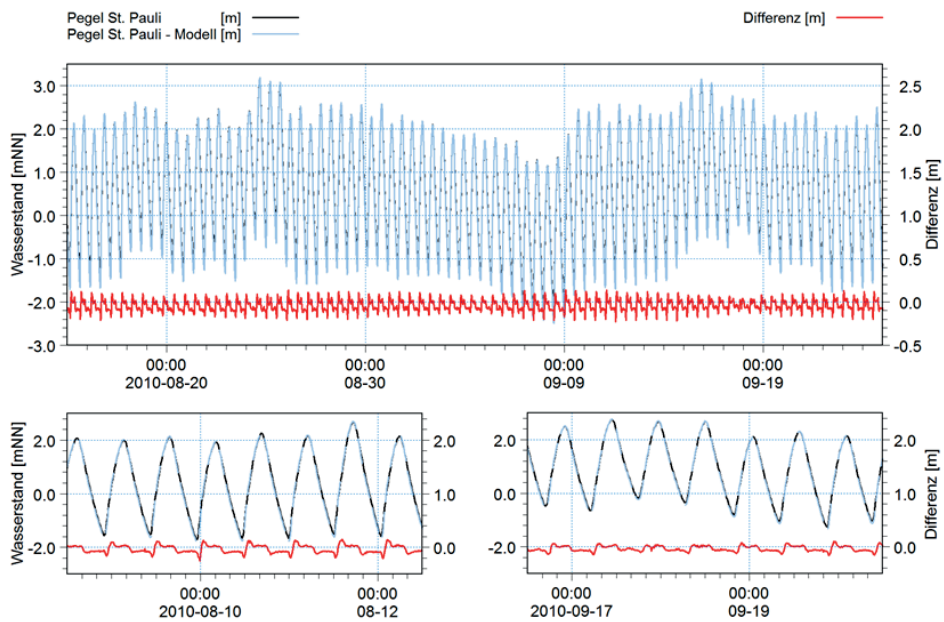


Figure 5: Measured (black line) and simulated (blue line) water levels at the gauging station St. Pauli. The red line denotes the difference between measured and simulated values.

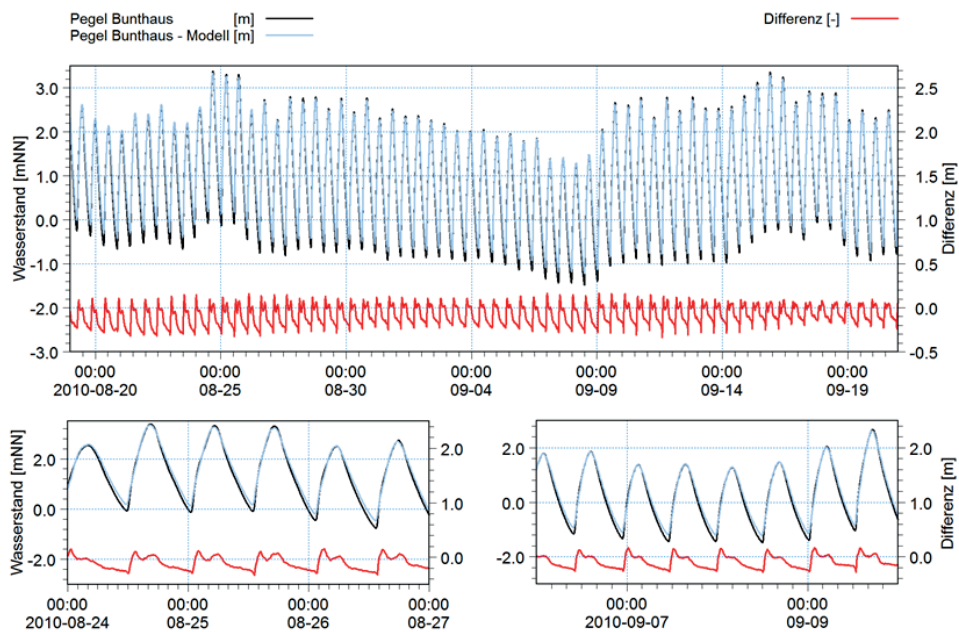


Figure 6: Measured (black line) and simulated (blue line) water levels at the gauging station Bunthaus. The red line denotes the difference between measured and simulated values.

3.2 Ecological Model

The oxygen concentrations were calibrated against measurements at two monitoring stations. One oxygen sensor was deployed south of the Reiherstieg-sluiice; the second sensor was deployed in the Reiherstieg north of the sluiice (Fig. 7).

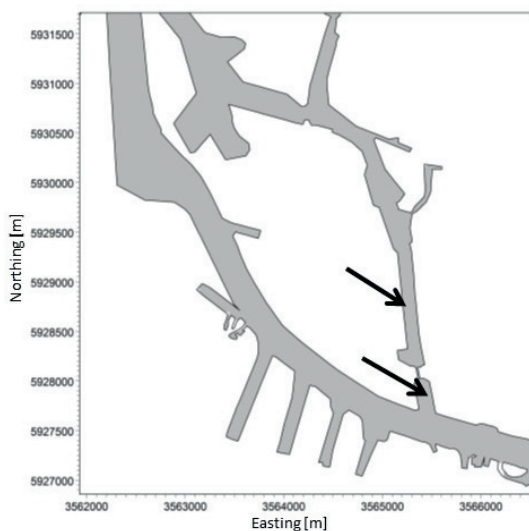


Figure 7: Positions of the two oxygen probes.

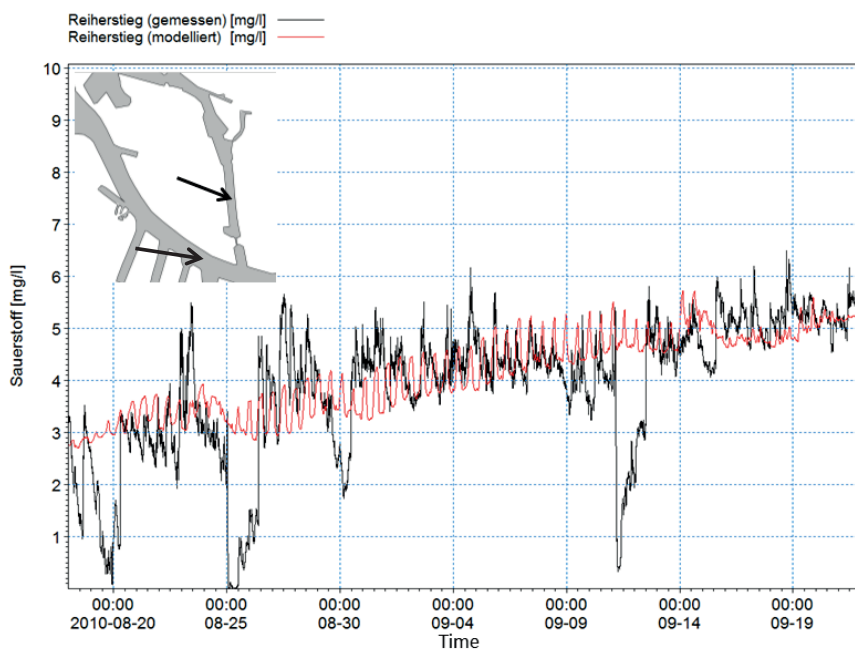


Figure 8: Measured (black) and simulated (red) oxygen concentrations in the Reiherstieg.

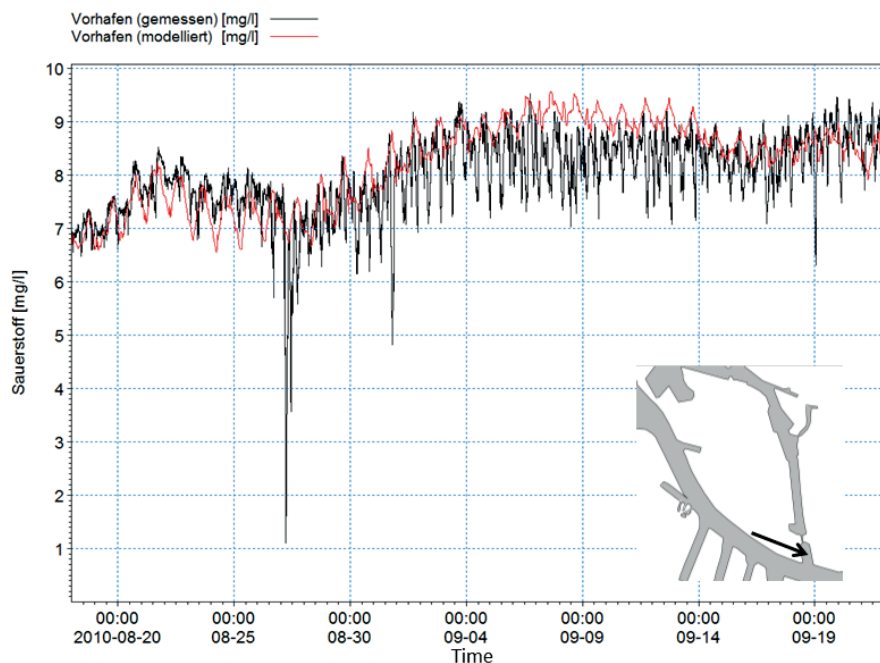


Figure 9: Measured (black) and simulated (red) oxygen concentrations south of the Reiherstieg-sludge.

The oxygen measurements showed strong fluctuations which did not coincide with a diurnal or tidal cycle (Fig. 8 and Fig. 9). It is likely that the strong decreases in the Reiherstieg could be caused by ship movements, where large amounts of sediments are resuspended. Another explanation could be local industrial discharges or introduced organic waste after rain events. However due to lacking data these possible explanations cannot be confirmed. Consequently these events cannot be reproduced by the present model. Apart from these unexplained events the model reproduces the general trends and diurnal and tidal cycles.

After calibration a scenario with intermittent open sluice gates was run. The model was set up in such way that the gates opened one hour after high tide, and closed one hour before low tide. The intention of this controlled strategy was, to pump as much water from the southern branch of the Elbe into the Reiherstieg. During flood period the gates were kept close to prevent water from downstream to enter the Reiherstieg. The downstream water usually has a lower dissolved oxygen concentration than the upstream water, therefore it was intended to pump as much water from upstream into the Reiherstieg, and prevent water from downstream to enter the Reiherstieg.

Fig. 10 shows the general development of dissolved oxygen, BOD and resuspended sediment over several tides. The time series depicts the situation directly at the sluice gates in the Reiherstieg. For dissolved oxygen a clear positive effect can be seen when the gates are opened. Large amounts of water with a high dissolved oxygen concentration enter the Reiherstieg, which immediately raises the dissolved oxygen concentration at the sluice gates.

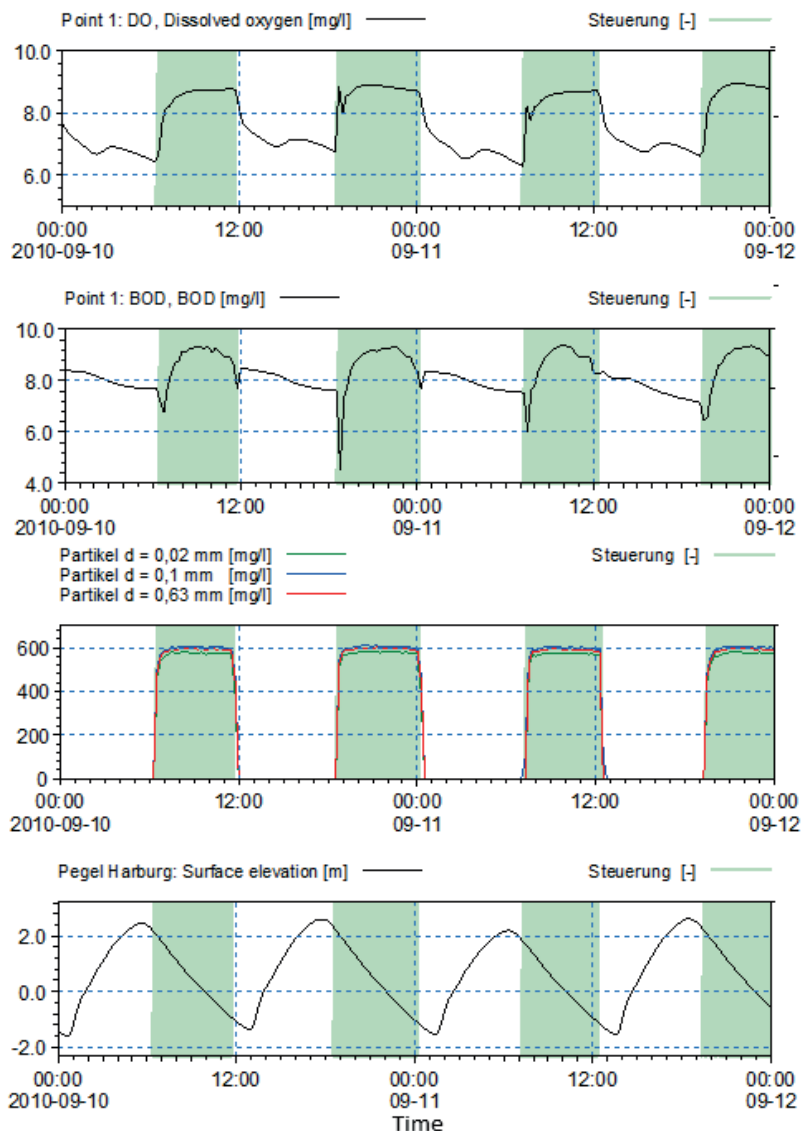


Figure 10: Characteristics of dissolved oxygen, BOD and resuspended sediments at the sluice gate during different tide periods. The lowest panel shows the water level. Periods when the sluice gates are opened are highlighted in green.

Synced with the entry of water and oxygen into the Reiherstieg, large amounts of sediments resuspend due to higher current speeds at the gate (Fig. 10). In consequence, the BOD rises as well.

In between, when the gates are closed, the BOD declines, because the organic compounds start to mineralise. This process is also reflected in the dropping concentration of dissolved oxygen, as the mineralisation is an oxygen consuming process.

Fig. 11 and Fig. 12 show the spatial effect of the intermittent opening for dissolved oxygen at high tide and low tide on 30.08.2010. At the initial state (Fig. 11) the lowest dissolved oxygen concentration in the Reiherstieg is around 1.5 mg/l. Depending on the tide the lowest concentration oscillates between the “Äußerer Schmidtkanal” and the “Mittlerer Reiherstieg”. The intermittent opening (Fig. 12) does not change the spatial pattern, but causes much lower dissolved oxygen concentrations around 0.5 mg/l caused by the oxygen consuming BOD. Only on the first few hundred metres north of the gate the positive effect of oxygen rich Elbe water is visible.

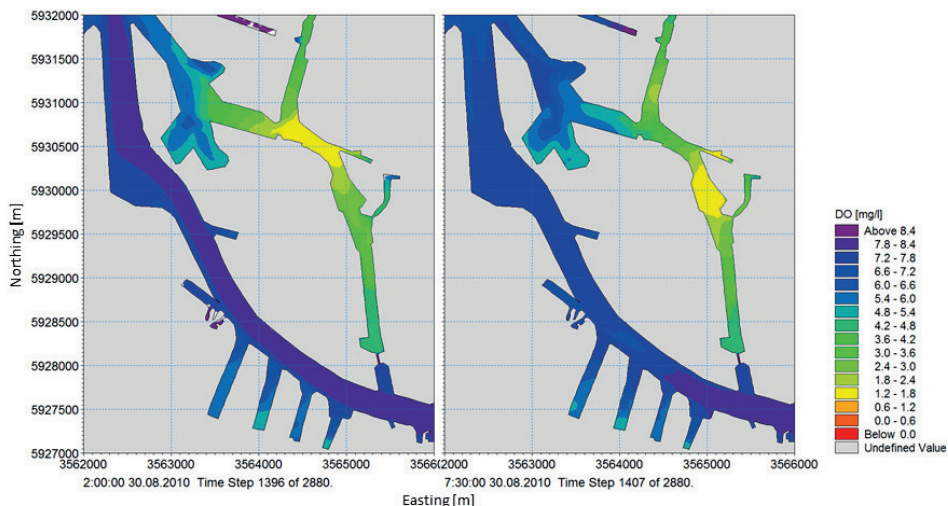


Figure 11: Dissolved oxygen concentration in the Reiherstieg in the scenario with permanently closed sluice gates. The left panel shows conditions at low tide, the right panel shows high tide.

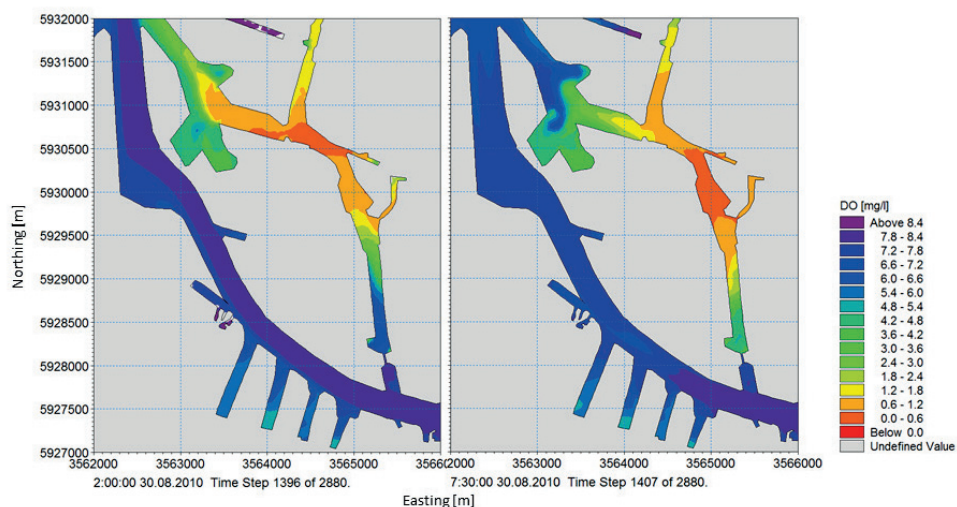


Figure 12: Dissolved oxygen concentration in the Reiherstieg in the scenario with intermittently opened sluice gates. The left panel shows conditions at low tide, the right panel shows high tide.

4 Discussion

The present study shows the influence of mineralising resuspended sediment. The aspired improvement for dissolved oxygen by intermittent opening of the sluice gates shows unexpectedly worth oxygen conditions in wide areas of the Reiherstieg. The positive effect of oxygen rich Elbe water vanishes after a few hundred metres in the Reiherstieg. North of this little zone the dissolved oxygen decreases to lower values than to the scenario with permanently closed gates. This decrease can be attributed to the strong oxygen consumption of mineralising material (BOD), which derives mainly from resuspended sediments due to high current speeds around the sluice gates. The material is transported northwards into the Reiherstieg and starts to mineralise, which causes strong oxygen consumptions in the centre of the Reiherstieg. Although large amounts of oxygen rich water enters the Reiherstieg, this positive effect is completely counteracted by the BOD in most areas of the Reiherstieg.

The present results show that a sustainable positive effect for the oxygen concentration in the Reiherstieg is a compromise between getting as much as possible oxygen rich Elbe water, but keeping the BOD as low as possible. Therefore the current has to be kept low to prevent sediments to resuspend.

5 References

- DHI: MIKE 21 & MIKE 3 Flow Model FM, Hydrodynamic and Transport Module, Scientific Documentation, 2013.
DHI: ECO Lab, Short scientific description, 2013.

Numerical Simulation of Rip-Rap Revetments in Tidal Areas

Livia Mittelbach, Martin Pohl, Peter Schulze and Heinz Konietzky

Summary

Rip-rap revetments are used to protect embankments and coastal shores against erosion. They are built to resist ship and wind induced waves, tidal and ship induced currents, tidally varying water levels and storm surges. In some areas the current basis of rip-rap design is inadequate for dealing with the complexity and variety of boundary conditions, especially in tidal zones. A numerical model has therefore been developed which is capable of simulating the resistance of rip-rap to hydraulic loads. Rip-rap-water-interaction is modelled holistically using two numerical methods.

Rip-rap is modelled using the Discrete Element Method (DEM) in three dimensions. The DEM can be used to model rip-rap stones as autonomous objects with all degrees of freedom and realistic movement. The DEM code is coupled with a computational fluid dynamics code (CFD) to account for the influence of the hydraulic loads. Waves and currents acting on the rip-rap stones as well as tidally varying water levels can be generated realistically using time dependent boundary conditions.

Additional physical model tests in a laboratory flume, field tests and measurements with instrumented rip-rap stones serve as validation for the numerical model.

Keywords

revetment, rip-rap, numerical simulation, discrete element method, computational fluid dynamics, model tests

Zusammenfassung

Deckwerke dienen dem Schutz der Uferböschungen von Schiffahrtsstraßen vor auftretenden hydraulischen Belastungen aus schiffs- und windinduzierten Wellen und Strömungen, wechselnden Tidewasserständen sowie Sturmfluten. Die derzeitigen Grundlagen zur Deckwerksbemessung sind für die vielfältigen und komplexen Randbedingungen insbesondere im Tidegebiet teilweise ungenügend. Daher wird ein numerisches Modell entwickelt, mit dem die Interaktion zwischen Deckwerk und hydraulischen Belastungen simuliert werden kann. Zur ganzheitlichen Simulation werden dabei zwei verschiedene numerische Methoden verwendet.

Das Deckwerk wird mit der Diskreten Elemente Methode (DEM) modelliert. Das Verhalten der einzelnen Deckwerkssteine kann somit realistisch mit allen Freiheitsgraden abgebildet werden. Die DEM wird mit einem Programm zur numerischen Strömungssimulation (CFD) gekoppelt, um die hydraulischen Einwirkungen zu berücksichtigen.

Zusätzliche Modellversuche in einer hydraulischen Rinne, Feldversuche und Messungen mit instrumentierten Deckwerkssteinen dienen zur Validierung des numerischen Modells.

Schlagwörter

Deckwerk, Numerische Simulation, Diskrete Elemente Methode, Computational Fluid Dynamics, Modellversuche

Contents

1	Introduction	120
2	Research project	121
3	Design of rip-rap	122
4	Modelling of rip-rap with the DEM	122
5	Modelling of hydraulic influences with CFD	125
6	CFD-DEM coupling	127
7	Armourstone equipped with sensor technology	128
8	Physical model tests	129
9	Field Tests	130
10	Conclusion and outlook	131
11	References	131

1 Introduction

Revetments are used to protect the banks of waterways and coastal shores against erosion. Because of the numerous advantages they offer, such as high flexibility and robustness against settlements, rip-rap revetments are used most frequently (Fig. 1). Revetments have to resist manifold influences. The main parameters affecting rip-rap design on inland waterways are ship-induced waves and currents as well as excess pore water pressures due to ship-induced water level drawdown. On waterways in coastal zones additional influences specific to the coast play an important role as well.



Figure 1: Rip-rap on the banks of the Ems River (Germany) as a protective layer to prevent erosion of bank slope by hydraulic loads.

The present guidelines used for rip-rap design in Germany are:

- BAW Code of Practice: “Principles for the Design of Bank and Bottom Protection for Inland Waterways” – GBB 2010 (BAW 2010)
- BAW Code of Practice: “Use of Standard Construction Methods for Bank and Bottom Protection on Inland Waterways” – MAR 2008 (BAW 2008)
- “Empfehlung für die Ausführung von Küstenschutzwerken” – EAK 2002 (KFKI 2007)
- “Wasserbausteine im Deckwerksbau” (HANSEN 1985)
- “The Rock Manual” (CIRIA et al. 2007)
- “Dikes and Revetments” / “Geosynthetics and Geosystems in Hydraulic and Coastal Engineering” (PILARCZYK 1998; PILARCZYK 2000)

The above criteria are mostly based on small-scale model tests or experience data from inland waterways. This means that, in some areas, these guidelines are of only limited applicability in view of the complex and diverse boundary conditions in tidal zones. Fig 2 gives an overview of the variety of influences which are relevant to rip-rap design for waterways in coastal areas. Larger, seagoing vessels with different geometries and increasing size instead of inland water vessels, different and irregular cross sectional areas of the waterway with varying slopes instead of a regular channel cross section, the influence of wind waves because of a larger, wind-exposed water surface, tidal currents in addition to ship-induced currents and tidal varying groundwater levels are just some of the factors that affect the different rip-rap design needed for inland and coastal waterways.

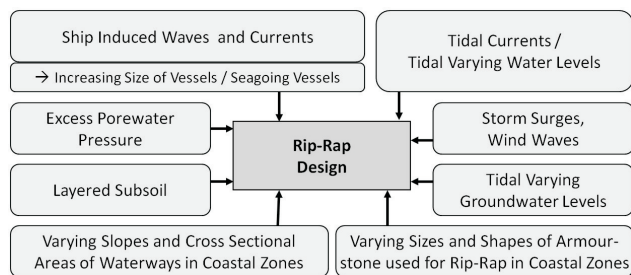


Figure 2: Influences on rip-rap design in tidal and coastal areas.

2 Research project

In the light of the insufficient basic criteria available for rip-rap design, especially in coastal zones, the aim is to develop a numerical model in 3D which is capable of simulating the rip-rap-water interaction. By coupling different numerical methods, the model takes the hydraulic part (waves and currents) as well as the mechanical part (the rip-rap) into consideration. Hence, a holistic numerical analysis of the stability of rip-rap revetments is possible.

The research project is divided into different parts: numerical simulation and model respectively field tests. The numerical modelling of the hydraulic part is done using a Computational Fluid Dynamics code (CFD), the simulation of the rip-rap is undertaken using the 3D Discrete Element Method (DEM). The holistic numerical modelling is carried out by a coupled computation of both codes. The numerical model is then validated

by model tests in a laboratory flume, measurement data from instrumented armourstones and measurement data of waves and currents from field tests.

The long-term objective of the research project is a suitable numerical tool for a safe and economic rip-rap design adapted to particular local conditions.

3 Design of rip-rap

The stability of rip-rap against hydraulic loads depends on the size and mass of the individual stones used as well as on the interaction of all the stones as an assembly. The interaction of all the stones in non-grouted rip-rap is achieved by means of interlocking effects between the armourstones. According to the BAW Code of Practice GBB (BAW 2010), the required individual stone size is determined in the hydraulic design of a revetment and depends on the acting hydraulic loads (waves, currents). The required mass per unit area (thickness of the rip-rap) is determined in the geotechnical design and is necessary to guarantee resistance to sliding failure, uplift and hydrodynamic soil displacement. Nonetheless, it is necessary for rip-rap to have a certain minimum thickness in order to ensure a stable armour layer with interlocking between the stones as referred to above. In addition to hydraulic and geotechnical design, the overall stability of the bank slope including the rip-rap is proved in the revetment design (BAW 2010).

Stone gradings according to the European standard for armourstone (DIN EN 13383-1) are used for rip-rap revetments. Light mass gradings (LMB_{5/40}, LMB_{10/60}) are mostly used on coastal waterways to produce appropriate and robust revetments.

In the numerical model the representation of the rip-rap should be realistic with regard to the particular armourstone grading category (size and mass of the stones) as well as the stability mechanism inside the rip-rap (interlocking effects).

4 Modelling of rip-rap with the DEM

The Discrete Element Method (DEM) is a numerical method which simulates the movement and interaction of particles of a discontinuous medium on the basis of Newton's second law of motion and a contact law. In a discontinuous medium, contacts or interfaces exist between the discrete bodies that make up the system (ITASCA 2014). An effective contact detection algorithm is therefore necessary in a DEM code in order to detect contacts, which are arising and breaking during the calculation progress, as well as corresponding contact laws that become active during interaction of particles (JAKOB and KONIETZKY 2012). The DEM was originally developed by CUNDALL and STACK (1979). Today it is widely used to examine engineering problems in granular and discontinuous materials.

The calculation cycle executed in the DEM is described in ITASCA (2014): "The calculations performed in the DEM alternate between the application of Newton's second law to the particles and a force-displacement law at the contacts. Newton's second law is used to determine the motion of each particle arising from the contact and body forces acting upon it, while the force-displacement law is used to update the contact forces arising from the relative motion at each contact." (Fig. 3)

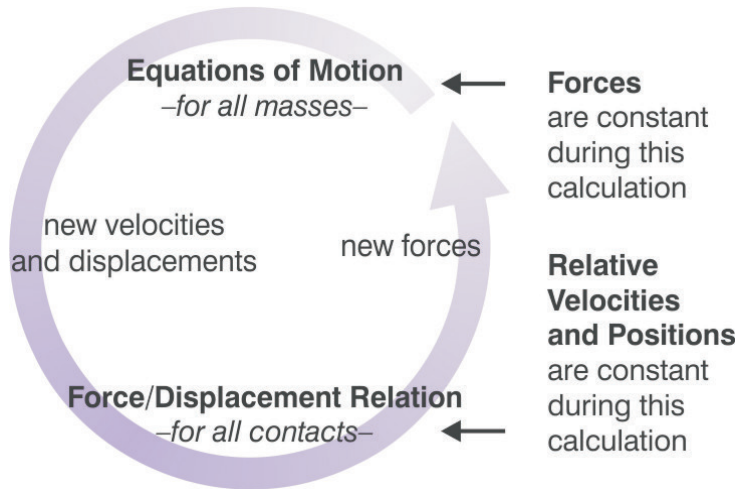


Figure 3: Calculation cycle DEM (ITASCA 2014).

The DEM allows rip-rap stones to be modelled as autonomous objects. The movement of stones with six degrees of freedom (three for translational and three for rotational movement) is represented realistically. In this research project the DEM part of the modelling is undertaken by using the three dimensional code PFC3D (Particle Flow Code 3D) developed by ITASCA CONSULTING GROUP INC. (2008a). This code is a simplified version of the general DEM because it utilises spherical particles (so-called balls) to make contact detection easier. However, arbitrary complex shapes can be produced by overlapping spheres (so-called clumps). This multi-sphere approach can be used to generate stone-like particles and the whole rip-rap (Fig. 4). Each clump acts as an independent object and cannot break during the calculation cycle (ITASCA 2008a).

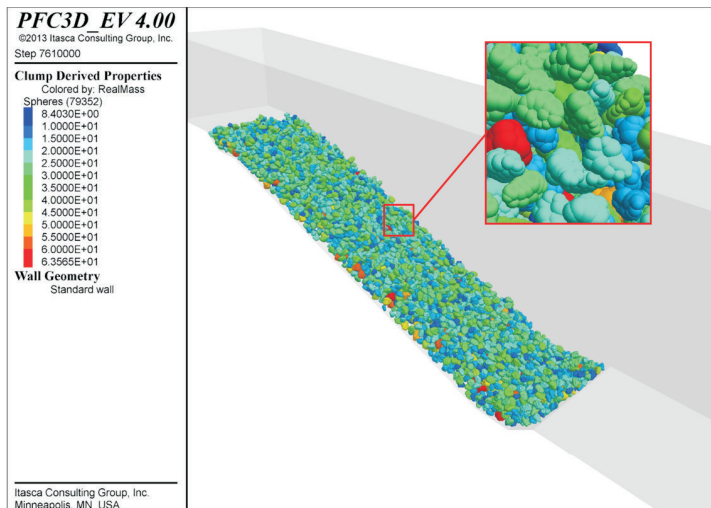


Figure 4: Rip-rap generated in PFC3D.

As referred to above the numerical rip-rap should be realistic with regard to the representation of interlocking effects between the stones as well as with regard to the particular armourstone grading category. This results in two important issues: the realistic representation of the particle shape of the individual stones and the realistic representation of the whole rip-rap with respect to the size and mass distribution of all stones in the numerical model.

The research project was carried out in cooperation with the Chair of Rock Mechanics and Rock Engineering, Geotechnical Institute, TU Bergakademie Freiberg, Germany. To reproduce the rip-rap in a realistic way, the stones were divided into different size and shape categories (platy, longish, compact) and a mixture of stones from all categories was used for the numerical model (HERBST et al. 2010). Several methods of generating irregular shaped particles and of representing rip-rap were also investigated, developed and tested (HERBST et al. 2010; YUAN 2012). The first method for the generation of rip-rap stones is a random algorithm developed on the basis of the procedure of LU and MCDOWELL (2007). The shape of the generated particles depends on six different parameters: the number of directions for ball generation, the probability of each direction, the number of balls generated in the chosen direction, the degree of reduction of radii and the degree of overlapping of balls. Another method for the generation of rip-rap stones with realistic shapes is the use of surface meshes from real stones (obtained by photo or 3D-Scan). With the help of a bubble-pack-algorithm contained in the DEM code the 3D surface mesh is filled with balls. In both cases the rip-rap can be represented realistically regarding the size and mass distribution of the corresponding armourstone grading category (Fig. 5).

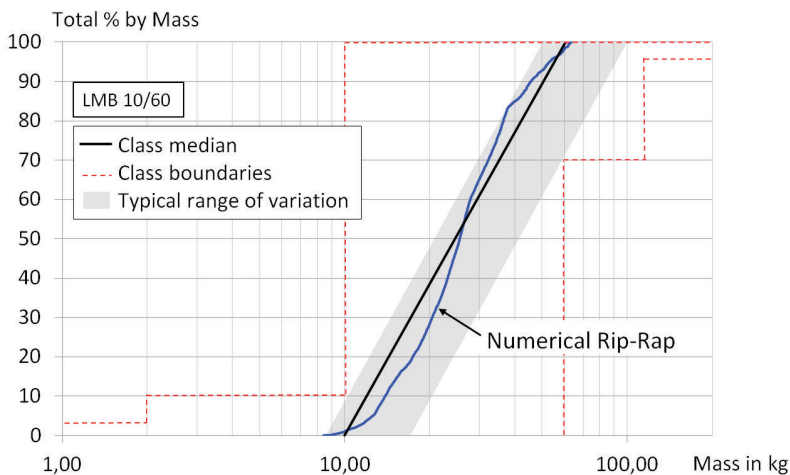


Figure 5: Typical range of variation of cumulative curve for armourstones class LMB_{10/60} (BAW 2008), cumulative curve of corresponding numerical rip-rap.

The stones in the numerical model can be represented in a detailed or simplified way (high or low resolution of particle shape), depending on the number of balls that are used to build one clump (Fig. 6). The more detailed the clumps are, the better the interaction of the stones is represented. However, the time required for the generation of the numerical rip-rap and the model calculation time in general increase exponentially if detailed

clumps are used. Besides the particle shape, the behaviour of the clumps during calculation is also affected by the friction coefficient on the particle surface and indirectly by the stiffness of the particles. The extent to which these properties affect the accuracy of the numerical modelling and the way the parameters should be chosen in order to produce the best match with reality is examined in physical model tests.

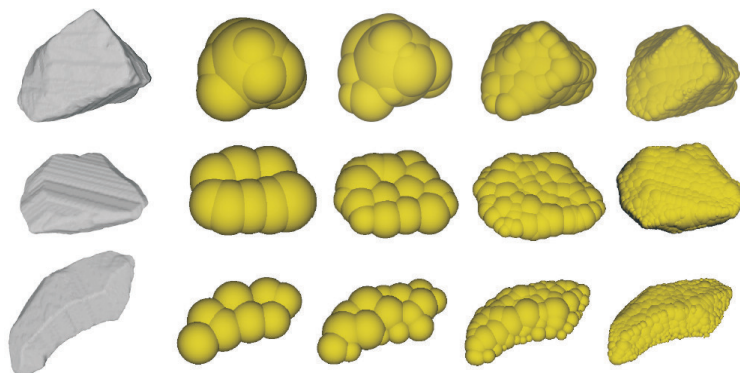


Figure 6: Representation of armourstones as clumps in simplified and detailed way (YUAN 2012).

5 Modelling of hydraulic influences with CFD

The modelling of the hydraulic part, such as waves and currents, is undertaken using a computational fluid dynamics (CFD) code. The hydrodynamic computation is done on the basis of the Navier-Stokes equations, which describe the motion of fluid substances. Together with the continuity equation they can be applied to solve all hydrodynamic problems.

In this research project the software “Coupled Computational Fluid Dynamics” (CCFD) is used, which is a product of ITOCHU Techno-Solution Corporation (ITASCA 2008b). CCFD solves the simplified incompressible Navier-Stokes equations (ITASCA 2008b, HERBST 2011):

$$\rho \frac{\partial \vec{v}}{\partial t} + \rho \vec{v} \cdot \nabla (\vec{v}) = -\nabla p + \eta \nabla^2 (\vec{v}) \quad (1)$$

and the continuity equation (HERBST 2011):

$$\nabla \cdot \vec{v} = 0 \quad (2)$$

with ρ as the fluid density, \vec{v} as the fluid velocity, p as the fluid pressure and η as the fluid dynamic viscosity with the help of a finite volume method in a 3D discretized domain (fluid element, hexahedron). The coupled computation of both codes – the mechanical DEM calculation in PFC3D and the hydraulic computation in CCFD – is possible (Fig. 7). The CCFD-solver is embedded in a graphic modeller (pre/post-processor) which serves to specify the model geometry and the initial and boundary conditions (INTERNATIONAL CENTER FOR NUMERICAL METHODS IN ENGINEERING 2008).

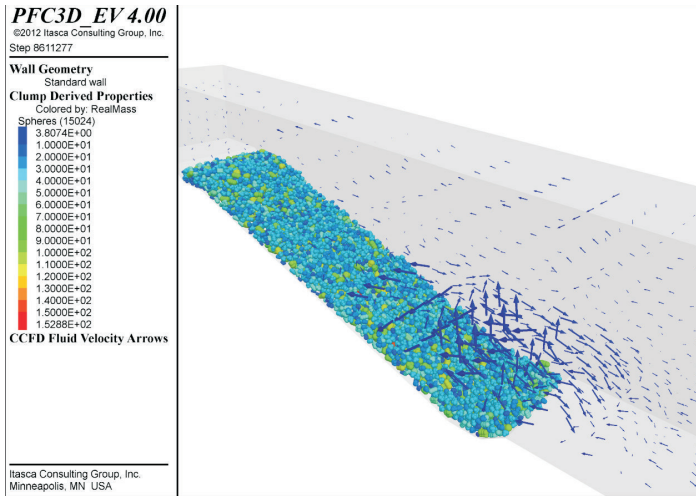


Figure 7: Coupled computation of wave impact on rip-rap.

In the numerical simulation the hydraulic loads can be generated by applying time-varying boundary conditions at the model boundary. Waves and currents are generated in the form of the water surface elevation and the horizontal and vertical orbital velocities described as a function of time. The data from the field tests will then be used as input data for the waves generated in the numerical model (Fig. 8). The measured water surface elevation (wave heights) and the deduced velocity field (development of horizontal and vertical velocity below the wave) are imported into the numerical model as time series for every time step. Hence, the measured wave is generated directly in the numerical simulation.

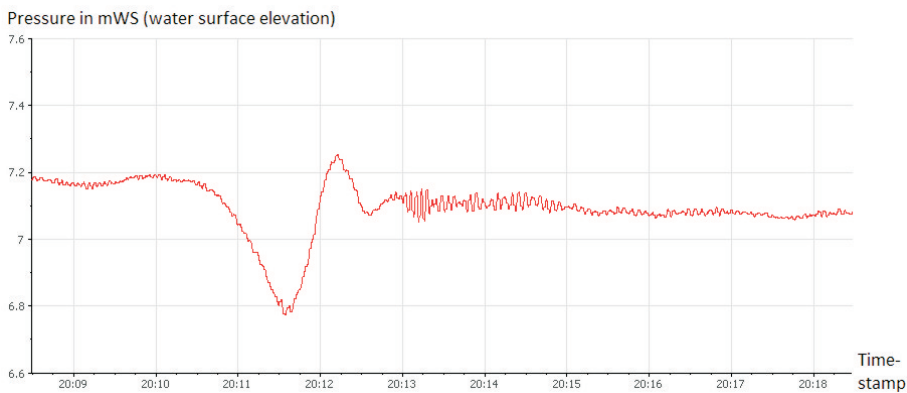


Figure 8: Example of measurement of ship-induced wave from field test.

The reaction of the rip-rap stones in the DEM code due to current and wave attack from the hydraulic calculation in CCFD can be recorded by using so called “histories” in PFC3D.

6 CFD-DEM coupling

The numerical codes used in this research project allow the two-way coupled computation of the mechanical DEM calculation and the hydraulic computation (see example Fig. 7). The displacement and the velocity of the particles are determined in PFC3D and the state variables of the flow in CCFD. During the coupled computation both programmes are executed using the procedure referred to above (section 4 and 5) with an additional data exchange at predefined time intervals. The DEM as well as the CFD code are formulated with additional terms to account for the fluid forces and the presence of particles in the flow.

In the DEM-part of the coupled computation a new term \vec{f}_{fluid} is added to the calculation to represent the force applied by the fluid (ITASCA 2008b):

$$\frac{\partial \vec{u}}{\partial t} = \frac{\vec{f}_{mech} + \vec{f}_{fluid}}{m} + \vec{g} \quad (3)$$

where \vec{u} is the particle velocity, m is the particle mass, \vec{f}_{fluid} is the total force applied by the fluid on the particle, \vec{f}_{mech} is the sum of additional forces and \vec{g} the acceleration of gravity. The force \vec{f}_{fluid} consists of three terms: the drag force, the force applied by the fluid pressure gradient and the buoyancy (ITASCA 2008b):

$$\vec{f}_{fluid} = \vec{f}_{drag} + \frac{4}{3} \pi r^3 (\nabla p - \rho \vec{g}) \quad (4)$$

with

$$\vec{f}_{drag} = \left(\frac{1}{2} C_d \rho \pi r^2 |\vec{u} - \vec{v}| (\vec{u} - \vec{v}) \right) \cdot n^{-\kappa} \quad (5)$$

where r is the particle radius, C_d is a drag coefficient and $n^{-\kappa}$ is an empirical factor to account for the local porosity. The current fluid velocity \vec{v} and the fluid pressure gradient ∇p necessary for this calculation are determined by CCFD and sent to PFC3D each time the coupling information are exchanged. The fluid force acting on the particles is applied to each particle (ITASCA 2008b).

In the hydraulic part of the computation the equations of motion of the fluid (1) and the continuity equation (2) are formulated with porosity terms and an additional body force due to the presence of particles in the flow (ITASCA 2008b):

$$\rho \frac{\partial n \vec{v}}{\partial t} + \rho \vec{v} \cdot \nabla (n \vec{v}) = -n \nabla p + \eta \nabla^2 (n \vec{v}) + \vec{f}_b \quad (6)$$

and

$$\frac{\partial n}{\partial t} + \nabla \cdot (n \vec{v}) = 0 \quad (7)$$

with n as the porosity and \vec{f}_b as the body force. The current porosity n in each fluid element and the body force \vec{f}_b is determined in PFC3D and sent to CCFD during the data exchange. The body force acting on the fluid due to the particles is given as an average value over one fluid element (ITASCA 2008b).

The calculation cycle described above is shown in Fig. 9.

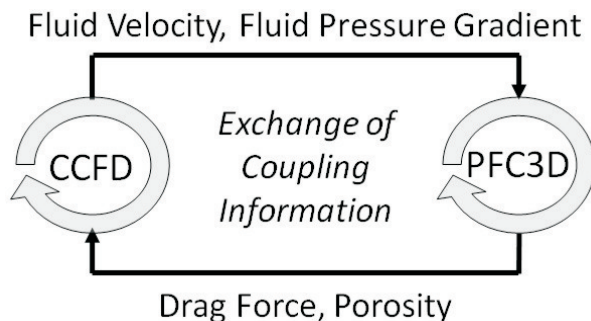


Figure 9: Calculation cycle of coupled DEM-CFD computation.

A limiting condition for the coupled computation is the minimum porosity of 1 % in each fluid element, in order to allow the flow of fluid. This means that a maximum of 99 % of the volume of one fluid element can be filled with particles. This affects the mesh resolution of the flow problem and results in fluid elements larger than the generated rip-rap stones.

7 Armourstone equipped with sensor technology

In the context of the research project a measurement device is developed to record the translational and rotational movements of armourstones due to current and wave attack. Several armourstones of different size, shape and density are bored and equipped with acceleration sensors and gyroscopes (Fig. 10). The corresponding circuit board for measuring acceleration and rotational speed is an in-house development. In this context the particular challenge was the limited space available, especially for the internal energy supply, as well as the minimisation of the electricity consumption of the system. Data can be registered by the stone for a period of up to one month and stored on a memory card. The displacements of the stone measured by the equipment in model or field tests can be compared to the displacements and the translational and angular velocities taken as histories from the particles in the numerical model. It is intended to determine the hydraulic loads and forces acting on the rip-rap from these measurements. Measurements with the equipped stones are carried out in the flume tests as well as in the field tests.

Fig. 11 shows the result of an equipped stone in the hydraulic flume embedded loosely in a rip-rap section during constant overflow with increasing flow velocity. The development of the angular velocity of roll, pitch and yaw angle during the test is shown. There is not stone movement at the beginning of the stepwise increase in flow velocity, but the stone starts shaking at a flow velocity of about 1.7 m/s to 2.0 m/s.



Figure 10: Example of armourstone equipped with sensor technology.

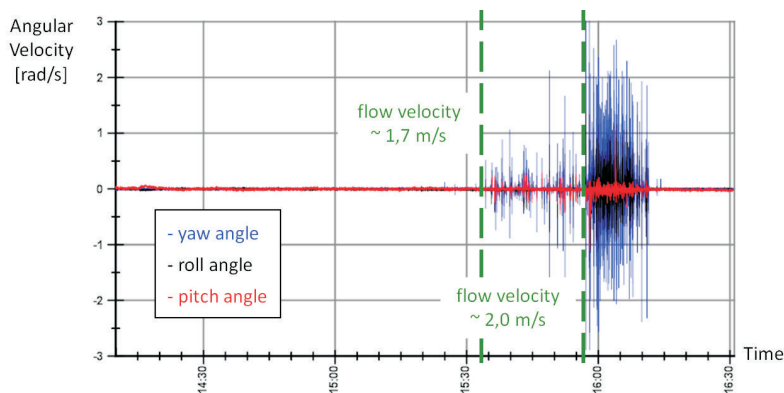


Figure 11: Example of measurement result from flume test.

8 Physical model tests

Physical model tests are used to validate the numerical model. The behaviour of the numerical armourstones depends primarily on the particle shape and the friction coefficient of the particle surface. Because a detailed representation of the stones raises the calculation time enormously, flume tests are performed to examine the extent to which these properties affect the accuracy of the numerical modelling and how the parameters should be chosen to achieve the best possible match with reality. The results of the physical tests with known boundary conditions are compared to an equivalent numerical model (Fig. 12).

The physical model tests are carried out in a hydraulic flume of the Federal Waterways Engineering and Research Institute, Hamburg. A rip-rap section on a scale of 1:1 with stones of the armourstone grading category CP_{90/250} is built into the flume (Fig. 12). There is an overflow parallel to the slope of the rip-rap section. The slope ratio of the rip-rap section is 1:1 respectively 1:3 in two different measurement campaigns. The flow in the zone of the rip-rap section is increased in four steps from about 1 m/s up to 2 m/s in several tests during one measurement campaign. The displacement of the stones due to the overflow is documented by a laser scan and a coloured surface of the rip-rap section.

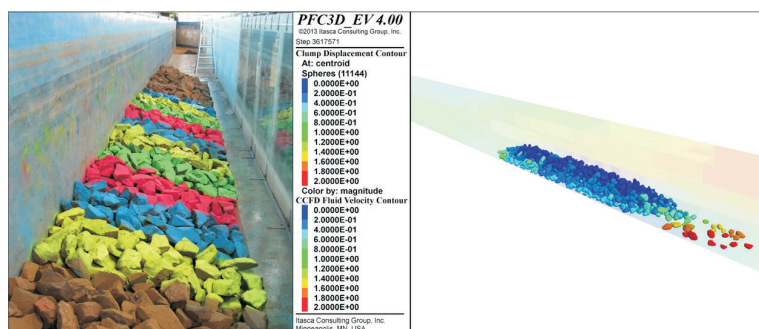


Figure 12: Rip-rap section in hydraulic flume and numerical simulation of physical model tests.

9 Field Tests

In addition to the physical model tests the numerical model is validated by field measurements executed as part of a project. Wave heights, flow velocities and to some extent pore water pressures in the subsoil are measured at the island “Lühesand” in the Lower Elbe River. The measurements are carried out at two different monitoring stations in exposed positions with varying slope ratios and varying distances to the navigation channel of the Elbe (Fig. 13). Stationary measurement systems and two flexible flow probes with independent power supply are applied. This equipment is placed at different positions over the entire slope of the bank and measures the acting hydraulic loads directly above the surface of the slope. Together with the measurement of the hydraulic loads, measurements with equipped armourstones are carried out as well.

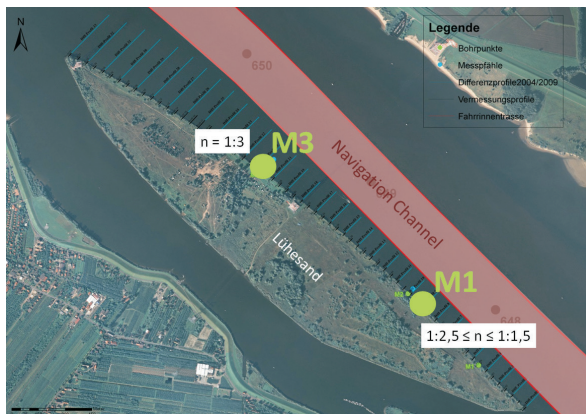


Figure 13: Monitoring positions M1 and M3 at island Lühesand, Elbe, Germany.

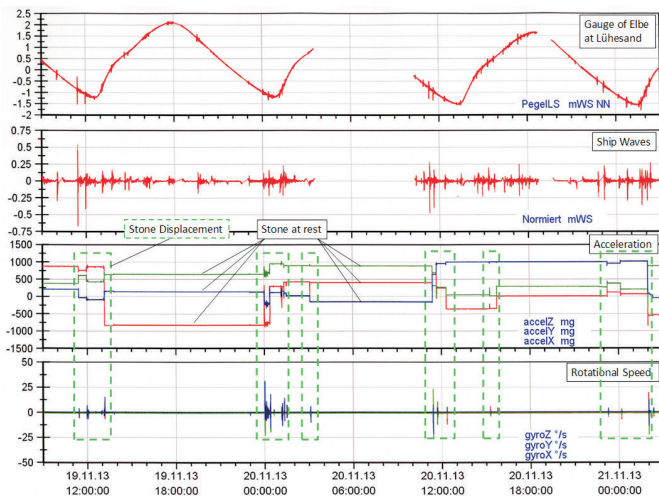


Figure 14: Example of measurements with equipped armourstones in field test.

Fig. 14 shows the measurement results with the equipped armourstone in the field tests over a period of 42 hours. From top to bottom the figure shows the tidally varying water level of the Elbe (gauge at Lühesand), the ship passages respectively the occurring ship waves, the acceleration in x-, y- and z-direction and the rotational speed in x-, y- and z-direction. This example taken from the first measurements demonstrates that displacements of single rip-rap stones mainly take place when ships are passing in periods of low tide.

10 Conclusion and outlook

The Discrete Element Method is a suitable method for the simulation of rip-raps with complex-shaped particles. The movement of single stones can be reproduced with any number of degrees of freedom. Together with a CFD-computation, the interaction of rip-rap and hydraulic loads is modelled holistically. The numerical particles representing rip-rap stones are calibrated using physical tests in a hydraulic flume and a measurement device for recording the movement of stones. The physical model tests and field tests will be continued and the modelling and validation of the numerical simulation will be adapted and improved to achieve the best possible match with reality.

11 References

- BUNDESANSTALT FÜR WASSERBAU (BAW): Anwendung von Regelbauweisen für Böschungs- und Sohlensicherungen an Binnenwasserstraßen (MAR). Eigenverlag, Karlsruhe, 2008.
- BUNDESANSTALT FÜR WASSERBAU (BAW): Grundlagen zur Bemessung von Böschungs- und Sohlensicherungen an Binnenwasserstraßen (GKB). Eigenverlag, Karlsruhe, 2010.
- CIRIA; CUR and CETMEF: The Rock Manual. The use of rock in hydraulic engineering (2nd edition). C683, CIRIA, London, 2007.
- CUNDALL, P.A. and STRACK, O.D.L.: A discrete numerical model for granular assemblies. In: Géotechnique, Vol. 29,1, 47-65, doi: 10.1680/geot.1979.29.1.47, 1979.
- DIN EN 13383-1: Wasserbausteine Teil 1: Anforderungen, 2002.
- HANSEN, U.A.: Wasserbausteine im Deckwerksbau. Bemessung und Konstruktion. Westholsteinische Verlagsanstalt Boyens & Co. Heide (Holstein), 1985.
- HERBST, M.; POHL, M. and KONIETZKY, H.: Numerische Simulation der Interaktion Wasser – Deckwerk im Tidegebiet. In: Dresdner Wasserbauliche Mitteilungen, Vol. 40. Dresden, 85-94, 2010.
- HERBST, M.: DEM-Fluid Coupling. Coupled CFD Add-on to PFC3D 4.0. Coupled CFD Training. Presentation, Freiberg, 23.-25.03.2011.
- INTERNATIONAL CENTER FOR NUMERICAL METHODS IN ENGINEERING: GiD. User Manual. Version 9. Barcelona, 2008.
- ITASCA CONSULTING GROUP INC.: PFC3D. Particle Flow Code in 3 Dimensions. User's Manual. Version 4.0. Minneapolis, 2008a.
- ITASCA CONSULTING GROUP INC.: PFC3D. Particle Flow Code in 3 Dimensions. CCFD Add-on. Version 1.0. Minneapolis, 2008b.

- ITASCA CONSULTING GROUP INC.: Distinct Element Method. <http://www.itascacg.com/software/pfc/distinct-element-method>, last visited: 13.05.2014.
- JAKOB, C. and KONIETZKY, H.: Partikelmethode. Eine Übersicht. Report. TU Bergakademie Freiberg, 2012. http://tu-freiberg.de/fakult3/gt/feme/studium/Handbuch_Partikelmethode.pdf, last visited: 13.05.2014.
- KURATORIUM FÜR FORSCHUNG IM KÜSTENINGENIEURWESEN (KFKI) (Ed.): Empfehlungen für die Ausführung von Küstenschutzwerken durch den Ausschuss für Küstenschutzwerke (EAK 2002, Korrigierte Ausgabe 2007). Die Küste, 65, 2007.
- LU, M. and MCDOWELL, G.R.: The importance of modelling ballast particle shape in the discrete element method. In: Granular Matter, Vol. 9, 1-2, 69-80, 2007.
- MITTELBACH, L.: Numerical Simulation of Rip-Raps with the Distinct Element Method. In: AIP Conf. Proc. 1542: Powders and Grains. Sydney, 1178-1181, doi: 10.1063/1.4812147, 2013.
- PILARCZYK, K.W.: Dikes and Revetments. Design, Maintenance and Safety Assessment. A.A.Balkema, Rotterdam, 1998.
- PILARCZYK, K.W.: Geosynthetics and Geosystems in Hydraulic and Coastal Engineering. A.A.Balkema, Rotterdam, 2000.
- YUAN, F.L.: Coupled CFD-DEM simulation of wind wave interaction with rock riprap on riverside slopes. Research Report. TU Bergakademie Freiberg (not published), 2012.

Methods of Data Assimilation

Emil Stanev and Johannes Schulz-Stellenfleth

Summary

An overview of ocean forecasting techniques amalgamating numerical models, observations and data assimilation methods is presented. The basics of data assimilation as an application of estimation theory or control theory is described and the corresponding statistical and numerical methods are introduced. Classical approaches like Kalman filter or optimal interpolation are explained as well as state of the art methods like reduced rank filters and smoother approaches. Problems and challenges of coastal ocean forecasting are identified, which are associated with the specific variables of interest for coastal applications, such as: complex physics complicating the assimilation of data; characteristic time scales; vigorous adjustment process arising in sequential data assimilation, when models are restarted; specific data and observational platforms in coastal ocean and maximising the outcome of synergies between different data types; model and observation error specification; coupling coastal and deep ocean models and seamless transition between coastal and open-ocean scales. Illustrations of some of the above challenges and their treatment in the area of the German Bight are given by describing a pre-operational HF radar data assimilation system using three WERA stations, as well as an assimilation system using FerryBox surface temperature and salinity measurements.

Keywords

Kalman filter, variational data assimilation, smoothers, coastal ocean forecasting, model and observation errors, German Bight

Zusammenfassung

Es wird eine Übersicht über Vorhersagemethoden in der Ozeanographie, die numerische Modelle, Beobachtungen und Datenassimilation verbinden, gegeben. Die Grundlagen der Datenassimilation als eine Anwendung der Schätz- und Kontrolltheorie werden beschrieben und die zugehörigen statistischen und numerischen Methoden eingeführt. Klassische Verfahren wie der Kalman Filter oder Optimale Interpolation werden ebenso wie neuartige Ansätze wie der „reduced rank filter“ oder „smoother“ erläutert. Probleme und Herausforderungen werden angesprochen, die charakteristisch sind für Vorhersagen im Küstenbereich. Dazu gehören die folgenden Punkte: komplexe Physik, die die Datenassimilation erschwert; charakteristische Zeitskalen; starke Schockeffekte bei der sequentiellen Datenassimilation, wenn Modelle neu gestartet werden; spezielle Daten- und Beobachtungsplattformen im Küstenbereich und optimale Nutzung von Synergien zwischen verschiedenen Daten; schwierige Spezifizierung von Modell- und Beobachtungsfehlern; Kopplung von Modellen für den Küsten- und den Tiefwasserbereich und der nahtlose Übergang zwischen den verschiedenen räumlichen Skalen. Einige dieser Herausforderungen und ihre Behandlung werden für den Bereich der Deutschen Bucht veranschaulicht durch die Beschreibung eines prä-operationellen HF Radar Datenassimilationsystems, das drei WERA Stationen verwendet, sowie ein

Assimilationsystem, das FerryBox Messungen von Temperatur und Salzgehalt an der Meeresoberfläche benutzt.

Schlagwörter

Kalman-Filter, 4D-VAR, Smoother, Vorhersagen im Küstenbereich, Modell- und Beobachtungsfehler, Deutsche Bucht

Contents

1	Introduction	134
2	Methods	136
2.1	Basic Concepts	136
2.2	Direct Insertion and Newtonian Relaxation	137
2.3	Sequential Approaches.....	138
2.3.1	Optimal Interpolation	138
2.3.2	Kalman Filter.....	138
2.3.3	Ensemble techniques.....	139
2.3.4	State and error sub-spaces reduction.....	139
2.3.5	The three-dimensional analysis (3D-VAR).....	140
2.4	Smoother Approaches	140
2.4.1	General presentation	140
2.4.2	The four-dimensional analysis (4D-VAR)	141
2.4.3	Ensemble smoother: optimization of boundary conditions and meteorological forcing.....	141
3	Data assimilation in coastal ocean: German Bight examples	142
3.1	Specific problems of data assimilation in coastal ocean	142
3.2	FerryBox Sea Surface Temperature and Salinity Assimilation	144
3.3	Spatio-temporal OI (STOI): A step towards “best surface current estimate”.....	146
3.4	Demonstration of the potential usefulness of operational surface current products.....	147
4	Conclusions and future challenges.....	148
5	Acknowledgements.....	148
6	References	148

1 Introduction

Ocean data assimilation combines observations and models with the aim to (1) improve our understanding of ocean circulation on all relevant temporal and spatial scales, (2) monitor and (3) predict the ocean state. This combination of observations and numerical simulations enables efficient, accurate and realistic state estimations. Furthermore, for sampling rates, spatial domains and time intervals of practical interest, state estimates

might not otherwise be feasible, because data acquisition in the ocean is difficult and costly in particular if done on a sustained basis. Thus, data assimilation can provide four-dimensional time series of dynamically adjusted fields, which can serve as high resolution and complete data sets (mix between observations and modelling) for dynamical studies. This goes beyond the classical methodology, where observations and theory were developing independently, or in the best case, when used in parallel, their synergy was not well exploited.

The challenge in data assimilation is to extract the most important information from relatively sparse and noisy observations, and to feed this information in an optimal way into numerical forecast models. The observation errors are due to instrumental noise, environmental noise, sampling, and possible misinterpretation of measurements. Numerical ocean models are obviously also not error-free; errors are originating from incomplete (non-perfect) model physics, insufficient grid resolution, problems in open boundary conditions, atmospheric or hydrological forcing. Even “perfect” ocean models will drift away from reality, which is known as loss of predictability beyond the predictability limit. This limit depends upon the type of geophysical fluids and dominating processes. For synoptic processes in the ocean it is of the order of weeks to months, for the coastal ocean it is of the order of hours and days. The loss of predictability is associated with the nonlinear transfer and growth of errors.

The above fundamental characteristics of geophysical systems inhibits accurate forecasts and calls for periodically correcting their evolution using observations with appropriate spatial coverage and at intervals less than the predictability limit. This correction process necessitates knowledge of multivariate aspects of model and observational data to be combined. A fundamental problem in data assimilation is the specification of the background and observation error covariance matrices, which determines how information is passed from the observations to the model. If this information is complete and used correctly, observations of one model variable can produce dynamically consistent corrections in other model variables or areas where no observations exist.

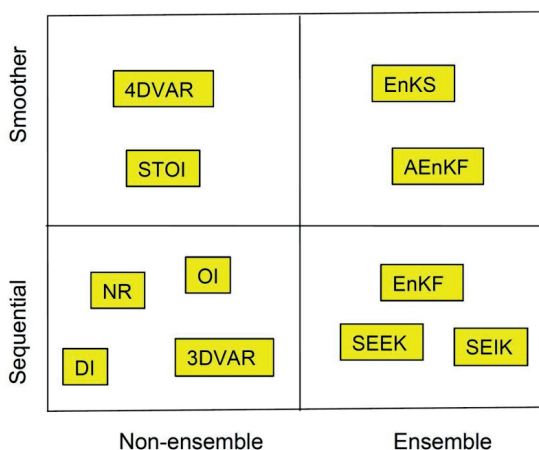


Figure 1: Schematic illustration of different assimilation methods. Used abbreviations are explained in Section 2. Direct insertion (DI) and Newtonian Relaxation (NR) methods are added to the bottom-left box although they are not typical representatives of sequential methods used nowadays.

During the last years ocean data assimilation and forecasting has reached an impressive level of maturity (CHASIGNET and VERRON 2006). One good example is the Global Ocean Data Assimilation Experiment (GODAE), where several systems have been developed and are operated by the Australian Bureau of Meteorology (BLUElink Ocean Data Assimilation System, BODAS), the Jet Propulsion Laboratory (Estimating the Circulation and Climate of the Ocean, ECCO), the UK Met Office (Forecast Ocean Assimilation Model, FOAM), the MyOcean system operated in several EU countries (Nucleus for European Modeling of the Ocean VARIational data assimilation, NEMOVAR), and some others (CUMMINGS et al. 2009). These GODAE systems assimilate various measurements such as sea level anomaly data provided by satellite altimeters, subsurface temperature and salinity data from Argo floats, moored and drifting buoys, expendable bathythermograph (XBT), and conductivity-temperature-depth (CTD) recorders, in situ and satellite sea surface temperature data, as well as satellite derived sea ice concentration and drift data.

So far ocean data assimilation techniques have been applied for operational forecasts, error analysis, parameter optimization, for ocean process studies, and observational network design. The latter, known as Observation System Simulation Experiments (OSSEs), enables the optimization of future experimental or operational monitoring networks. Compared to the methodologies used in meteorology and global oceanography, coastal forecasting techniques are still at a relatively early stage of development. This is because the specific problems of ocean data assimilation in coastal ocean are full of challenges, which are not sufficiently addressed in global or regional ocean data assimilation. This motivates us to present in the present study the basics of data assimilation, identify specific coastal problems and illustrate solutions of some of them. The area of applications used to illustrate different approaches is the German Bight, which is a shallow, tidally driven part of the southern North Sea.

The present paper describes in section 2 the theoretical background of ocean data assimilation. In Section 3 examples addressing applications for the German Bight area are demonstrated followed by short conclusions in section 4.

2 Methods

2.1 Basic Concepts

Ocean data assimilation deals with the spatial distribution and temporal evolution of state variables (e.g. velocity, pressure, density, temperature and salinity), that is with the state estimation in three dimensions and time. Ocean forecasting systems provide the future ocean state given its state at an initial time. The tool for such predictions is a dynamical (circulation) model. This is *the first component of prediction systems*, which numerically approximates a set of prognostic field equations for state variables. These equations include parameters (e.g., associated with unresolved physical processes or fundamental constants) and are initialized and forced by given initial and boundary condition data, respectively. Dynamical models used in data assimilation have to correctly represent internal dynamics and the ocean response to external forcing. i.e., their performance has to statistically agree with the statistics of real processes.

The second component of prediction systems is a data assimilation tool used to link the state variables of the dynamical model to the observations. Such a tool has to work as dynamical interpolation and extrapolation of the data and to combine observations and simulations with weights inversely proportional to their relative errors. Data assimilation uses statistical estimation theory or control theory (Fig. 1). One classical approach belonging to the first class is the Kalman Filter (KF), which is based on a probability maximization. The control theory deals with the behavior of dynamical systems where one or more output variables of a system need to follow a certain reference over time, therefore a manipulation is applied to the inputs to obtain the desired effect on the output. The 4DVAR technique is the most established method in this category. The third component of prediction systems consists of the used observational networks, which have to be adequate to capture dominating processes and to possess the required accuracies. In this paper we will concentrate on the second component of prediction systems.

We will denote in the following the state variables at time step k by a vector x_k of dimension n . The observations of dimension m at time k are denoted by y_k^O . We will assume that the evolution of the state variables is described through a dynamical (forecasting) model

$$x_{k+1}^f = Mx_k^a + \eta_k \quad (1)$$

where the index “f” stays for forecasting, M is a $n \times n$ matrix, which corresponds to the discrete scheme associated with a given numerical model, and η_k is Gaussian noise with covariance matrix Q_k .

The relation between the state variables and the measurements are described using a linear model

$$y_k^O = Hx_k + \epsilon_k \quad (2)$$

where H is the observation operator and ϵ_k is Gaussian noise with covariance R , which is often assumed as white. Observation errors consist of instrument noise and so called representation errors, which are model dependent. The magnitude of the observation error, in combination with the numerical model error, determines the relative weight given to the observation. The model errors are often specified by the error covariance matrix P .

In the following different approaches are described to find a so called analyzed state x^a , which represents an optimal combination of a first guess model state x^f and measurements y^O . Most of the approaches (Fig. 1) can be formulated as a cost function minimization problem, where on the one hand the mismatch between model and observations (the so called innovation) is reduced and on the other the departure from the first guess is not too big.

2.2 Direct Insertion and Newtonian Relaxation

The simplest assimilation approach, called Direct Insertion (DI), replaces in the observation points the forecast values by the observed ones. Because this can only be done if the data are consistent, which is hardly ever the case, this method is sub-optimal. In comparison, the Nudging or Newtonian Relaxation (NR) scheme introduces in the prognostic

equations terms proportional to the difference between the data and state variables (i.e., data residuals). This method “relaxes” the model towards the observations. The relaxation times should be consistent with the dominating time-scales, but cannot be too small to avoid model disruptions.

2.3 Sequential Approaches

In sequential data assimilation methods (BRASSEUR 2006) repeated forecast analysis cycles are performed, where at each analysis time step a new initial model state for the next forecast is computed based on the model state and the observations available at that time. In the following different approaches falling into that category are described.

2.3.1 Optimal Interpolation

Optimal interpolation (OI) (GANDIN 1963; LORENC 1981; DALEY 1991) is a simplification of the KF, where the forecast error covariance is replaced by the background error covariance. In simpler implementations the weights used in the filter are empirically assigned. The fundamental hypothesis of this method is that *for each model variable, only a few observations are important to determining the analysis increment*. P -matrix specification usually relies on the design of empirical auto-correlation functions (e.g. Gaussian), which are considered as time-independent. In the OI method significant weight is assigned to those observations which have significant background error covariance. In practice, the correlation radius limits the geometrical domain around model variables, which need to be considered.

2.3.2 Kalman Filter

The estimation of state vector can be formulated as the maximization of an *a posteriori* probability of the system state for given observations y_k^0 and for a given first guess model state x_k^f . Estimation theory (e.g., GELB 1974) states that the so called analysis x_k^a , which is the optimal combination of the model and observation is given by

$$x_k^a = x_k^f + K_k \left(y_k^0 - Hx_k^f \right) \tag{3}$$

where

$$K_k = P_k^f H^T \left(HP_k^f H^T + R \right)^{-1} \tag{4}$$

is the Kalman gain matrix. Thus, the filter can be considered as a two step process: (i) the forecast of the state vector and of its error covariance are computed as

$$x_k^f = Mx_{k-1}^a \tag{5}$$

$$P_k^f = MP_{k-1}^a M^T + Q_k \tag{6}$$

(ii) The analysis is derived from equations (3) and (4) and finally (iii) the a posteriori covariance is computed as

$$P_a^k = (I - K_k H) P_k^f \quad (7)$$

The analysis step is a linear combination of the dynamical forecast x_k^f with the difference between the data and model predictions $y_k^a - Hx_k^f$, which is called data residual.

In conclusion, the KF (KALMAN 1960) is a simplification of Bayesian estimation for the case of linear systems, i.e, it is only optimal for linear models. Linearization of the model around the state estimate leads to the so-called extended Kalman (EK) filter (JAZWINSKI 1970).

A KF analysis is obtained when errors associated with forecasts and observations are known and accurately specified. Since these statistics are not generally available, actual implementations of assimilation algorithms are always sub-optimal (DEE and DA SILVA 1998).

2.3.3 Ensemble techniques

A further variant of the Kalman filter based on ensemble techniques and Monte-Carlo methods was developed to avoid the linearization of the model required in the KF. This method known as ensemble KF (EnKF; EVENSEN 1994; BURGERS et al. 1998) uses an ensemble of model states to represent the error statistics given in the EK filter (the covariance is approximated by sample covariances). The estimation of the flow-dependent background error covariance makes this method a good alternative to the variational approaches (see section 2.3.4).

2.3.4 State and error sub-spaces reduction

A full KF cannot be implemented into realistic ocean models, because error forecast and analysis equations are too demanding (CPU and memory requirements are too high). On the other side OI over-simplifies the propagation of errors. In the filter proposed by CANE et al. (1996) the state space is reduced through the projection onto a linear subspace of basic functions using a limited number of empirical orthogonal functions (EOF).

Another approach to reduce the computational costs is based on a low-rank approximation of the state covariance matrix. Examples of low-rank filters are the reduced rank square-root (RRSQRT) algorithm (VERLAAN and HEEMINK 1995) and the singular evolutive extended Kalman (SEEK) filter (PHAM et al. 1998). In the SEEK filter the error covariance matrix is approximated by a singular low rank matrix. In practice the SEEK filter corrects the forecast in the directions for which the error is not sufficiently attenuated by the dynamics of the model. These 'directions of correction' evolve with time according to the model evolution. For an improved treatment of non-linear error evolution, the singular evolutive interpolated Kalman (SEIK) filter (PHAM et al. 1998) was introduced as a variant of the SEEK filter. It combines the low-rank approximation with an ensemble representation of the covariance matrix.

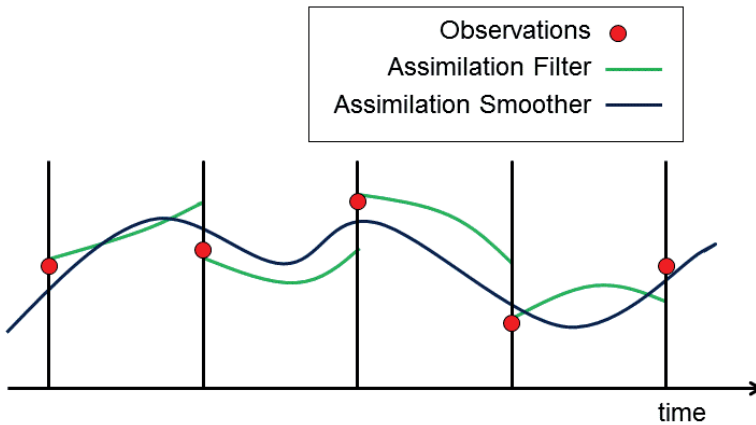


Figure 2: Trajectories of the model state during the data assimilation process in variational methods (blue line) and sequential methods (green lines). Red dots symbolize observations.

2.3.5 The three-dimensional analysis (3D-VAR)

The 3D-VAR was developed for the first time by SASAKI (1958). It was introduced into operational global numerical weather prediction by LORENC et al. (2000); recent applications in ocean forecasting are described by DOBRICIC and PINARDI (2008). Like in the 4D-VAR approach introduced in section 2.4.2 the computation of the gain matrix K (Eq. 4) is avoided. However, unlike to the 4D-VAR case, all observations (in the time-window around the analysis time) are assigned to analysis time. The solution is sought iteratively by performing several evaluations of the cost function

$$J(x) = (x - x_k^f)^T B^{-1} (x - x_k^f) + (y_k^o - H[x])^T R^{-1} (y_k^o - H[x]) \quad (8)$$

and of its gradient

$$\nabla J(x) = 2B^{-1}(x - x_k^f) - 2H^T R^{-1}(y_k^o - H[x]) \quad (9)$$

which is needed to find the minimum using a suitable descent algorithm. The estimated state x^a minimizing the cost function is then used as the initial state for the next forecast.

2.4 Smoother Approaches

2.4.1 General presentation

Important optimal control theory schemes (GHIL and MALANOTTE-RIZZOLI 1991) include the generalized inverse and adjoint methods. These methods, which are known as variational methods, seek to minimize the misfit between data and model trajectory over a given period. They were first developed by MARCHUK (1974) and further made popular in the environmental modelling by TALAGRAND and COURTIER (1987) and MOORE et al. (2011).

Variational methods assume that the analysis is at the initial time, and the individual observations at any given observation time t_i are distributed among n time steps over a given time interval. Like in the presentation of sequential methods we denote with y_i , x_i and x_{ii} the observations, the model and the true states at time t_i . The error covariance matrix for the observation errors $y_i - H(x_{ii}) - H(x_{ii})$ is R_i .

2.4.2 The four-dimensional analysis (4D-VAR)

The 4D-VAR minimizes the following cost function:

$$J(x) = (x - x_b)^T B^{-1} (x - x_b) + \sum_{i=1}^n (y_i - H_i[x_i])^T R_i^{-1} (y_i - H_i[x_i]) \quad (10)$$

This cost function, which is the sum of the squared deviations of the forecast fields and the analyzed fields weighted by the accuracy of the forecast (first term in the right hand side of 10) plus the sum of the squared deviations of the analysis values from the observations weighted by the accuracy of the observations (second term in the right hand side of 10), ensures that the analysis does not drift too far away from observations and forecasts. The significant advantage of the variational approaches is that the minimization problem is subject to the constraint that the sequence of model states x_i must be a solution of the model equations. Usually the gradient of the cost function is estimated using an adjoint model, which is quite demanding concerning the implementation and maintenance of the computer code. Furthermore, in a real-time forecasting the assimilation has “to wait” for the observations over the whole 4D-VAR time interval to be available. In sequential systems observations are used shortly after they become available.

2.4.3 Ensemble smoother: optimization of boundary conditions and meteorological forcing

A modification of the EnKF called ensemble Kalman smoother (EnKS) solves a smoothing problem (VAN LEEUWEN and EVENSEN 1996; EVENSEN and VAN LEEUWEN 2000; VAN LEEUWEN 2001; SAKOV et al. 2010). In order to estimate the ocean state at a certain time, it uses the data available before and after that time. Thus by propagating the future data information backward in time EnKS smooths the dynamical state ensuring a longer assimilation window, assimilating all collected observations in a single update and taking into account the evolution of the state and state error covariance over the length of the window.

BARTH et al. (2010; 2011) demonstrated the use of ensemble perturbation smoothers for optimizing tidal boundary conditions and correcting surface winds, respectively. In both cases assimilated data were HF radar surface currents in the German Bight. As stated in the previous section the situation is different from the open-ocean case because tides in coastal models are not generated within the domain, but are rather propagated inside the domain through the boundary conditions. For improving the modeled tidal variability it is therefore not sufficient to update the model state via data assimilation without updating the boundary conditions.

The used smoother assumes that all observations within the model integration period are grouped into a single observation vector (y^o) with their corresponding error covariance (R). To create an ensemble of dynamically realistic boundary conditions (BARTH et al. 2009), a cost function is formulated, which is directly related to the probability of each boundary condition perturbation. This cost function ensures that the perturbations have a finite energy, are smooth and satisfy a linear constraint. The approach is closely related to the asynchronous EnKF (AEnKF, SAKOV et al. 2010), where model trajectories (i.e. the model results in space and time), instead of model states, are optimized. For an increasing number of ensemble members, the Ensemble Smoother does converge to the AEnKF.

3 Data assimilation in coastal ocean: German Bight examples

3.1 Specific problems of data assimilation in coastal ocean

Complexity of data assimilation in the coastal ocean increases with the vast range of phenomena and the multitude of interactive scales in space and time (DE MEY et al. 2009; DE MEY and PROCTOR 2009). The spatial and temporal resolution required for realistic coastal predictions is much higher than the resolution required for the deep ocean. Processes, which are sometimes disregarded in the open-ocean data assimilation such as tides and the high-frequency barotropic response to atmospheric forcing, become dominant in the coastal ocean. The small temporal scales (hours) and horizontal scales (hundreds of meters) are both computationally and scientifically challenging.

Most methods described in section 2 are presently used to assimilate data in coastal models. Their diversity reflects the complexity of coastal processes and the status of forecasting systems, which are still dealing with research issues. Efforts are however underway to test and improve quality of data assimilation in operational practices (STANEV et al. 2011).

Several problems associated with coastal data assimilation are addressed below.

1. *The variables of interest* for coastal applications include the same physical properties as in the open-ocean models, but also near bottom currents, which are important for sediment transport and a large number of biogeochemical properties. This greatly increases the number of variables and the complexity of models and the assimilation schemes. Short time scales (e.g., minutes to hours for tides) increase not only the demand for high-quality observations, but also for specific data assimilation schemes.
2. *Vigorous adjustment process* arises in sequential data assimilation, when they are restarted (e.g. MALANOTTE-RIZZOLI et al. 1989). A too frequent assimilation of observations can even lead to the situation, where the assimilation degrades the model results due to the high-frequency motions generated by the assimilation (TALAGRAND 1972). One approach to overcome this problem will be illustrated in following sections.
3. *Data and observational platforms* differ from the ones in the open ocean. For example, satellite altimetry does not fully resolve all important coastal-ocean scales; data from profiling floats are not available in the shelf seas. However, data from high frequency (HF) radars and ADCP, sea level from coastal tide gauges and bottom

pressure gauges, water properties from fixed data stations and ferries (Fig. 3), gliders, and AUVs gives new perspectives and challenges. In particular, the assimilation of altimetry must also account for the aliasing of the tidal signal, which can well be compensated by using the synergy between altimeter, tide gauge and HF radar data.

4. *Complex physics* in the coastal zone complicates the assimilation of data and necessitates resolving the whole spectrum of free-surface variations (tides, storm surges), multiple scales, friction and mixing effects and associated tidal straining and fronts, dependency of solution of small-scale bathymetric channels and variations of bathymetry (which is not well known), control of straits for the inter-basin exchange and inlets for the exchange between tidal flats and open ocean, drying and flooding. The situation is further complicated by complex nonlinear processes (e.g. creating of over-tides) and other complex coupling of the variability at different frequencies.

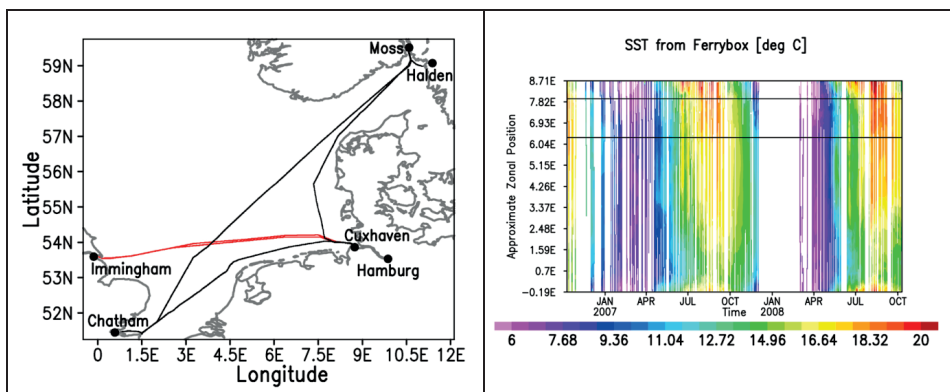


Figure 3: FerryBox routes in the North Sea with Cuxhaven – Immingham track in red (left) and FerryBox SST measurements (right) taken in 2007 and 2008 (from GRAYEK et al. 2011).

5. *Error specification* is extremely challenging in the coastal zone. Strong nonlinearities that couple variability at different frequencies (e.g., M2 tidal frequencies and lower frequency processes such as variation of stratification between neap and spring tides) necessitate using dynamically-consistent error prediction schemes. Furthermore, most existing assimilation schemes assume unbiased observations with Gaussian noise, which is often unrealistic. For many coastal observational platforms the determination of errors is also difficult, some platforms, e.g., satellite altimeters show larger errors in the coastal zone.
6. *Coupling coastal and deep ocean models* is still not a well-solved problem. Most coastal models are one-way nested; the model solution is strongly controlled by boundary forcing originating from larger-scale models. Two-way nested models enable that (assimilated) information from coastal observations, which is usually not assimilated by the larger-scale forecasting systems, is propagated out of the coastal region. These upscaling capabilities could become beneficial for regional models. One effective way to achieve a seamless transition is using unstructured-grid models representing much better the transition between coastal and open-ocean scales. In these models observations in the shelf sea would correct the deep ocean state and the deep ocean data would at the same time correct the coastal state. A good example of the potential of such capabilities tested in structured grid model is demonstrated

by STANEV et al. (2014). Available FerryBox and HF radar observations are used in the following sections as an enhancement of predictive modelling and to demonstrate solutions of some of problems described above.

3.2 FerryBox Sea Surface Temperature and Salinity Assimilation

In this section we will describe the assimilation of sea surface salinity (SSS) and surface temperature (SST) data acquired by a FerryBox system in a coastal area using a sequential filter approach. A FerryBox is an autonomous measurement, data logging and transmission system, which operates continuously while the carrying ship is on its way (PETERSEN et al. 2006). Measurements are made using devices, which are either in direct contact with or sample from a continuous flow of seawater taken at a water depth of 4–6 m. The basic sensors used in this study measure temperature, salinity, turbidity, and chlorophyll-a fluorescence.

The North Sea routes so far equipped with FerryBox systems are the ones between Büsum and Helgoland, Cuxhaven and Harwich, Cuxhaven and Immingham and recently between Hamburg, Cuxhaven, Chatham, Moss and Halden (Fig. 3 left). Depending on the travel distance, the routes provide the following revisit times: Büsum–Helgoland, daily, Cuxhaven–Immingham, less than 36 h, Hamburg–Cuxhaven–Chatham–Moss–Halden about 8 days. The route analyzed here is the one from Cuxhaven to Immingham (see the red line in Fig. 3 left) for the period 2007–2008.

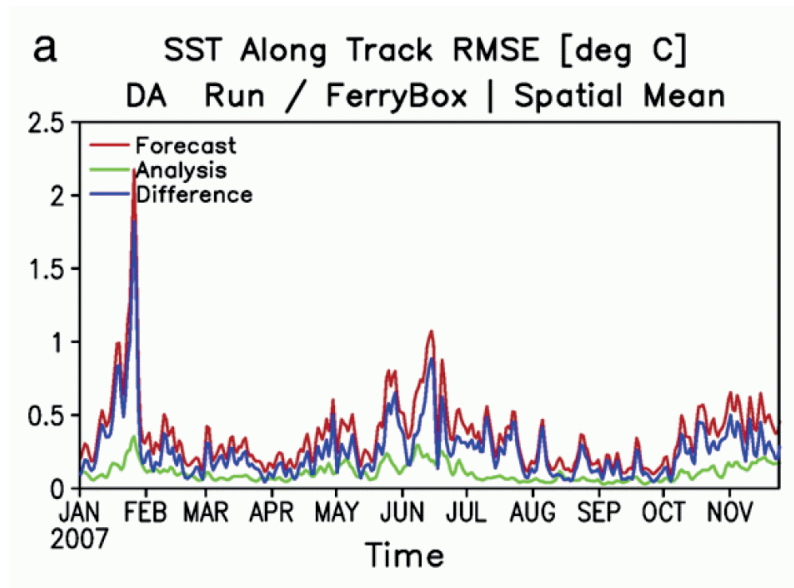


Figure 4: RMSE values of the SST forecast (red), SST analysis and the difference of the two (from GRAYEK et al. 2011).

The model used here is a 3-D primitive equation numerical model (BURCHARD and BOLDING 2002), in which the equations for the three velocity components u , v and w , and sea surface height ζ , as well as the equations for the turbulent kinetic energy and the

eddy dissipation rate due to viscosity are solved. The application of the model to the German Bight (Fig. 3) is described in STANEVA et al. (2009).

The potential of FerryBox data for forecast skill improvements was analyzed in GRAYEK et al. (2011). As already pointed out there are many assimilation methods described in literature, which are applicable for this problem (e.g., EVENSEN 2003; BRASSEUR 2006; NERGER et al. 2006; DOBRICIC and PINARDI 2008). For this study we decided to use a relatively simple assimilation approach based on optimal interpolation (OI) filter, because we wanted to make statements about the potential of FerryBox data for forecast skill improvements in general, rather than statements about specific assimilation techniques.

In the standard Kalman filter the forecast covariance matrix P has to be updated in each analysis step using either linearizations of the model operator or ensemble techniques. The OI method as used in this study avoids this complication by assuming that the forecast error statistics is stationary. Furthermore, the OI assimilation scheme uses a distance-dependent localization, which filters out long-range correlations in the background covariance matrix P . A Gaussian function with a width of 30 km is used for this purpose.

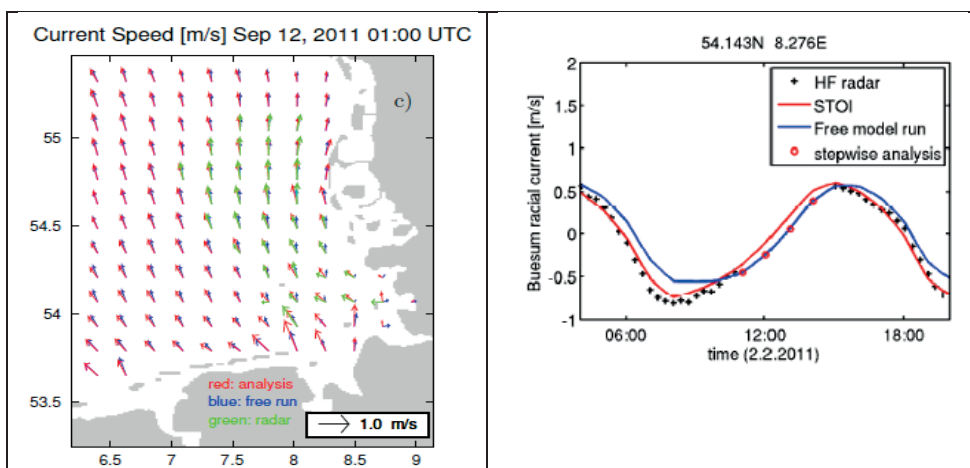


Figure 5: (Left) Illustration of differences between free run (blue), analysis (red) and HF-radar observations (green). (Right) Radial current velocity from HF radar (black crosses), the free model run (blue line), and the STOI analysis (red line) as well as an analysis obtained with a sequential approach (red circles).

Based on the OI scheme an assimilation system was implemented, which performs an analysis every day at 12:00. Fig. 4 shows a comparison of the free model run (red) with the analysis (green) in terms of spatially averaged SST RMSE errors. In this case satellite based SST measurements (OSTIA) were used as a reference. As one can see the analysis is able to decrease the errors most of the time.

3.3 Spatio-temporal OI (STOI): A step towards “best surface current estimate”

Here, we give an illustration of how to maximize the operational outcome of observations in the frame of the Coastal Observing SYstem for Northern and Arctic Seas (COSYNA), which was recently deployed in the area of the German Bight. This system uses three WERA stations and data from stationary platforms. A major challenge of HF radar assimilation is the treatment of tides. This issue is obviously of particular concern in areas like the German Bight, which are dominated by tidal currents. For HF radar data, which are typically acquired several times per hour, analysis and model restart each time new observations become available is not advisable, because models cannot reach equilibrium between two analysis time steps. The method called spatio temporal optimal interpolation (STOI, STANEV et al. 2014) uses elements of both classical assimilation filters and techniques, which use observations alone (FROLOV et al. 2012; WAHLE and STANEV 2011). The proposed data assimilation approach (see Fig. 1 which summarizes different methodologies) has similarities with the methods described in BARTH et al. (2010) and SAKOV (2010). However, it uses a simpler formulation of the model error covariance matrix, but at the same time addresses the forecast capability.

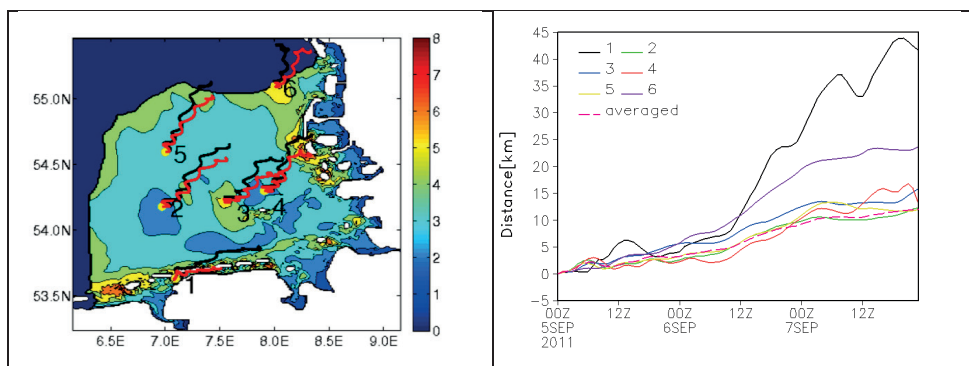


Figure 6: (Left) Using observations from COSYNA HF radars enables preparing useful data products applicable, e.g. for search and rescue operations. The figure on the left exemplifies the displacement of floating objects (in this case Lagrangean particles). Black lines give the results from the model free run, red trajectories visualize the results in the data assimilation run. Color coding gives the mean distance in km between position of Lagrangean particles in the analysis and free run for September 2011 after 24 h of integration. (Right) Distance of drifting particles in the assimilation run and the free run.

Surface currents are analyzed simultaneously using an analysis window of 13 or 24 hours. Using this approach a continuous surface current trajectory over one or two $M2$ tidal cycles is obtained. This block-wise analysis avoids the problem with HF-radar data, which are taken at short intervals (20 minutes for the radar system used in this study). Compared to a classical filter approach the method also has advantages concerning observation data gaps as illustrated in Fig. 5 (right). In this case the sequential method follows the free run when no observations are available, while the STOI method is able to correct a phase error also during this period. To increase the area with available measurements and to avoid any issues related to the processing of two dimensional current vectors from HF-radar data, radial components are used as input for the analysis instead of zonal and

meridional components. The main difference from implementations using ensemble Kalman smoother (BARTH et al. 2010; BARTH et al. 2011) and the technique described in SAKOV et al. (2010) is that the model error covariance matrix is estimated from the model background statistics, and not from an ensemble of model runs.

A reduced rank approximation of the state covariance matrix is estimated by EOF analysis of a period of model simulation (February-April 2011). The analysis window was progressed in hourly time steps. This method is different from the classical assimilation approach, where a model restart is performed for the forecast horizon using analyzed fields for initialization. The method also differs from classical statistical forecast methods (e.g. WAHLE and STANEV 2011), where forecasts are computed based on measurements alone. In the STOI-forecast mode we use the original free run as a prior estimate for the forecasts.

3.4 Demonstration of the potential usefulness of operational surface current products

The validation of STOI in STANEV et al. (2014) demonstrated that the HF-radar data can be not only interpolated, but also 'extended' in space, which makes possible to generate homogeneous mapped data series. The key difference of the STOI method to other techniques, which provide extrapolated surface current fields based on HF radar data alone is that the state estimates are dynamically consistent with a numerical model run. This is an important aspect when considering the use of such methods in operational systems, many of which have numerical models as their core part.

The following two experiments have been carried out: 33746 Lagrangean particles (this number equals the number of wet model points) have been released every day starting from 00:00 on September 1, 2011 at the surface in the center of every grid cell and were 2-D tracked with a Lagrangean model. Trajectories were computed over three days using hourly model output from either analysis or free model run. The trajectory simulations for the same initial positions of particles have been restarted every day for the same integration time of three days. The Lagrangean model output consisted of 33746x30x24 individual positions. In Fig. 6 (left) the monthly averaged distance between positions of particles in the two runs 24 hours after the release is shown. Release locations from where particles reached the model boundary were excluded from the statistical analysis.

This map gives an idea about the expected success of search and rescue operation if data from HF radar are used or not used. In the latter case the positioning of a lost object would be 3-6 km wrong after one day. Errors could be particularly big if release is in the proximity of barrier islands or close to the northern model boundary. The complicated mesoscale currents around the Helgoland Island could pose problems in the model and observations and explain larger spatial variability of the error pattern. Superimposed on the same figure are the trajectories from the two runs in 6 exemplary locations during three days of integration starting on September 5. They give an idea about the dominating propagation patterns, as well as an illustration that the coherence of tidal oscillations is lost relatively soon after the release. This illustrates the need for intra-tidal information from measurements to correct model trajectories.

The temporal evolution of the distance between particles released at the same positions (Fig. 6 (right)) demonstrates the rapid increase of the distances between trajectories

in the two runs. The averaged positioning error plotted by the dashed line gives an overall idea about accuracy in the search and rescue operations using output from the free run. In three days reduction of the error of positioning of an object due to the use of HF radar data is about 10 km on average. It is obvious that this is a relevant difference for applications like Search and Rescue.

4 Conclusions and future challenges

The economic implications of coastal forecasting provide a strong argument for enhancing coastal observing systems. Marine operations depend largely on the success of data assimilation methods, because applications like risk assessment require dynamically consistent data, which are close to available measurements. Regional ocean prediction and monitoring systems, designed by OSSEs, are about to be put in place, in which predictability error is an important part of products. Multi-model ensembles could be also very useful for practical applications.

The examples presented in this paper illustrate the application of data assimilation in the German coastal waters and give an idea of how to develop data assimilation methods appropriate for coastal areas dominated by tides. These methods address complex physics, and the respective characteristic time scales, the outcome of using specific coastal data (radial components of surface currents) from three WERA stations, as well as some pre-operational issues.

There is still a number of challenges in coastal ocean data assimilation. Diagnostics and metrics for assessing performance of the coastal assimilation models need further improvements. Coupling between coastal and open-ocean assimilation systems is still an open problem. Forecasting biogeochemistry state variables in the coastal ocean, although extremely important, is still in infancy. Treatment of river flows, mixing, bottom roughness and small-scale topography is still an issue. Non-homogeneity in space and time of model error statistics needs further consideration. Of particular importance is the optimal use of non-homogeneous data from different origins and platforms. Here, it is expected that 4D-VAR and EnKS could largely contribute to advancing practical applications.

5 Acknowledgements

We thank Alexander Barth, Sebastian Grayek, Joanna Staneva, and Xi Lu for inspiring discussions and support.

6 References

- BARTH, A.; ALVERA-AZCÁRATEM, A.; BECKERS, J.M.; STANEVA, J.; STANEV, E.V. and SCHULZ-STELLENFLETH, J.: Correcting surface winds by assimilating high-frequency radar surface currents in the German Bight, *Ocean Dyn.*, 61, 599-610, 2011.
- BARTH, A.; ALVERA-AZCÁRATE, A.; BECKERS, J.M.; WEISBERG, R.H.; VANDENBULCKE, L.; LENARTZ, F. and RIXEN, M.: Dynamically Constrained Ensemble Perturbations: Application to Tides on the West Florida Shelf, *Ocean Sci.*, 5, 259-270, 2009.

- BARTH, A.; ALVERA-AZCÁRATE, A.; GURGEL, K.-W.; STANEVA, J.; PORT, A.; BECKERS, J.-M. and STANEV, E.: Ensemble perturbation smoother for optimizing tidal boundary conditions by assimilation of High-Frequency radar surface currents – application to the German Bight, *Ocean Sci.*, 6, 161-178, 2010.
- BRASSEUR, P.: Ocean data assimilation using sequential methods base on the Kalman filter, in: CHASIGNET, E. and VERRON, J. (eds.): *Ocean weather forecasting: An integrated view of oceanography*, Springer, 271-316, 2006.
- BURCHARD, H. and BOLDING, K.: GETM – a General Estuarine Transport Model, No EUR 20253 EN, printed in Italy, European Commission, 2002.
- BURGERS, G.; VAN LEEUWEN, J. and EVENSEN, G.: Analysis scheme in the ensemble Kalman filter, *Mon. Weather Rev.*, 126 (6), 1719-1724, 1998.
- CANE, M.A.; KAPLAN, A.; MILLER, R.N.; TANG, B.; HACKERT, E.C. and BUSALACCHI, A.J.: Mapping tropical Pacific sea level: Data assimilation via a reduced state space Kalman filter, *J. Geophys. Res.*, 101 (C10), 22599-22617, 1996.
- CHASIGNET, E. and VERRON, J.: *Ocean Weather Forecasting: An Integrated View of Oceanography*, Springer, Dordrecht, 2006.
- CUMMINGS, J.; BERTINO, L.; BRASSEUR, P.; FUKUMORI, I.; KAMACHI, M.; MARTIN, M.; MOGENSEN, K.; OKE, P.; TESTUT, C.; VERRON, J. and others: Description of assimilation methods used in GODAE systems, *Oceanography Magazine*, 22, 96-109, 2009.
- DALEY, R.: *Atmospheric Data Analysis*, Cambridge University Press, 1991.
- DEE, D.P. and DA SILVA, A.M.: Data assimilation in the presence of forecast bias, *Q. J. R. Meteorol. Soc.*, 124 (545), 269-295, 1998.
- DE MEY, P.; CRAIG, P.; DAVIDSON, F.; EDWARDS, C.; ISHIKAWA, Y.; KINDLE, J.; PROCTOR, R.; THOMPSON, K.; ZHU, J.; the GODAE COASTAL and S.S.W.G.C. COMMUNITY: Applications in coastal modeling and forecasting, *Oceanography*, 22 (3), 198-205, 2009.
- DE MEY, P. and PROCTOR, R.: Assessing the value of GODAE products in coastal and shelf seas, *Ocean Dyn.*, 59, 1-2, 2009.
- DOBRICIC, S. and PINARDI, N.: An oceanographic three-dimensional variational data assimilation scheme, *Ocean Modelling*, 22, 89-105, 2008.
- EVENSEN, G.: The ensemble Kalman filter: theoretical formulation and practical implementation, *Ocean Dyn.*, 31, 961-981, 2003.
- EVENSEN, G.: Sequential data assimilation with a nonlinear quasi-geostrophic model using Monte Carlo methods to forecast error statistics, *J. Geophys. Res.*, 99, 10, 143-10, 162, 1994.
- EVENSEN, G. and VAN LEEUWEN, P.: An ensemble Kalman smoother for nonlinear dynamics., *Mon. Weather Rev.*, 128, 1852-1867, 2000.
- FROLOV, S.; PADUAN, J.; COOK, M. and BELLINGHAM, J.: Improved statistical prediction of surface currents based on historic HF-radar observations, *Ocean Dyn.*, 62, 1111-1122, 2012.
- GANDIN, L.: *Objective Analysis of Meteorological Fields*, Translated by Israel Program for Scientific Translations, Jerusalem, 242, 1963.
- GELB, A.: *Applied optimal estimation*, The MIT press, 1974.
- GHIL, M. and MALANOTTE-RIZZOLI, P.: Data assimilation in meteorology and oceanography, *Adv. Geophys.*, 33, 141-266, 1991.

- GRAYEK, S.; STANEVA, J.; SCHULZ-STELLENFLETH, J.; PETERSEN, W. and STANEV, E.: Use of FerryBox surface temperature and salinity measurements to improve model based state estimates for the German Bight, *J. Mar. Syst.*, 88, 45-59, 2011.
- JAZWINSKI, A.H.: *Stochastic Processes and Filtering Theory*, Academic Press, New York, 1970.
- KALMAN, R.: A new approach to linear filtering and prediction problems, *Journal of basic Engineering*, 82 (1), 35-45, 1960.
- LORENC, A.: A global three-dimensional multivariate statistical interpolation scheme, *Mon. Weather Rev.*, 109 (4), 701-721, 1981.
- LORENC, A.; BALLARD, S.; BELL, R.; INGLEBY, N.; ANDREWS, P.; BARKER, D.; BRAY, J.; CLAYTON, A.; DALBY, T.; LI, D. and others: The Met. Office global three-dimensional variational data assimilation scheme, *Q. J. R. Meteorol. Soc.*, 126 (570), 2991-3012, 2000.
- MALANOTTE-RIZZOLI, P., YOUNG, R.E. and HAIDVOGEL, D.B.: Initialization and data assimilation experiments with a primitive equation model, *Dyn. Atmos. Oceans*, 13 (3), 349-378, 1989.
- MARCHUK, G.: *Numerical methods in weather prediction*, Academic Press, 1974.
- MOORE, A.M.; ARANGO, H.G.; BROQUET, G.; POWELL, B.S.; WEAVER, A.T. and ZAVALA-GARAY, J.: The Regional Ocean Modeling System (ROMS) 4-dimensional variational data assimilation systems: part I—system overview and formulation, *Progress in Oceanography*, 91 (1), 34-49, 2011.
- NERGER, L.; DANILOV, S. and HILLER, W.: Using sea-level data to constrain a finite-element primitive-equation ocean model with a local SEIK filter, *Ocean Dyn.*, 56, 634-649, 2006.
- PETERSEN, W.: FerryBox: A mature system for operational monitoring, *Sea Technology*, 47, 53-57, 2006.
- PHAM, D.; VERRON, J. and ROUBAUD, M.: A singular evolutive extended Kalman filter for data assimilation in oceanography, *J. Mar. Syst.*, 16, 323-340, 1998.
- Sakov, P.; EVENSEN, G. and BERTINO, L.: Asynchronous data assimilation with the EnKF, *Tellus*, 62A, 24-29, 2010.
- SASAKI, T.: An objective analysis based on the variational analysis, *J. Meteorol. Soc. Japan*, 36, 738-742, 1958.
- STANEV, E.; SCHULZ-STELLENFLETH, J.; STANEVA, J.; Grayek, S.; SEEMANN, J. and PETERSEN, W.: Coastal Observing and Forecasting System for the German Bight. Estimates of Hydrophysical States, *Ocean Sci.*, 7, 1-15, 2011.
- STANEV, E.; ZIEMER, F.; SCHULZ-STELLENFLETH, J.; SEEMANN, J.; STANEVA, J. and GURGEL, K.: Blending surface currents from HF radar observations and numerical modelling: Tidal hindcasts and forecasts, Submitted to *J. Atmos. Ocean Techn.*, 2014.
- STANEVA, J.; STANEV, E.; WOLFF, J.-O.; BADEWIEN, T.H.; REUTER, R.; FLEMMING, B.; BARTHOLOMAE, A. and BOLDING, K.: Hydrodynamics and sediment dynamics in the German Bight. A focus on observations and numerical modeling in the East Frisian Wadden Sea, *Cont. Shelf Res.*, 29, 302-319, 2009.
- TALAGRAND, O.: On the Damping of High-Frequency Motions in Four-Dimensional Assimilation of Meteorological Data, *Journal of Atmospheric Sciences*, 29, 1571-1571, 1972.

- VAN LEEUWEN, P.: An Ensemble Smoother with Error Estimates, *Mon. Weather Rev.*, 129, 709-728, 2001.
- VAN LEEUWEN, P.J. and EVENSEN, G.: Data assimilation and inverse methods in terms of a probabilistic formulation, *Monthly Weather Review*, 124, 2898-2913, 1996.
- VERLAAN, M. and HEEMINK, A.: Reduced rank square root filters for large scale data assimilation problems. *Second International Symposium on Assimilation of Observations in Meteorology and Oceanography*, 1995.
- WAHLE, K. and STANEV, E.: Consistency and Complementarity of Different Coastal Ocean Observations, A Neural Network-based Analysis for the German Bight, *Geophys. Res. Lett.*, 38, 1-4, 2011.

Analysis of Salinity Alterations due to Estuarine Waterway Deepening by Artificial Neural Networks

Cordula Berkenbrink and Hans Dieter Niemeyer

Summary

Deepening of estuarine waterways effects primarily changes of tidal water levels and secondarily that of tidal volumes and salt intrusion. These effects are subject of Environmental Impact Assessments which are often checked by afterwards monitoring for preservation of evidence. After the deepening of the waterway in the Outer Weser estuary among others such measurements were carried out for salinity. Since the data indicated alterations of salt intrusion into the Weser estuary a reliable quantification of the changes by conventional procedures like e. g. nonlinear regression analysis failed. However test with Artificial Neural Networks (ANN) provided reliable results for the respective data sets gained before and after the waterway deepening. Whereas the application of the ANN which was trained with data before the deepening mismatched with the data gained after deepening. These differences provide a reliable measure for the increased salt intrusion into the Weser estuary due to the deepening of the Waterway.

Keywords

tide, salinity, artificial neural network (ANN), estuary, waterway deepening

Zusammenfassung

Fabrwasserausbauten in Ästuarien bewirken erstrangig Veränderungen des Tideregimes und nachfolgend auch die des Salzeintrags nach oberstrom. Diese potenziellen Auswirkungen werden in Umweltverträglichkeitsprüfungen untersucht, deren Ergebnisse hinsichtlich ihrer Verlässlichkeit durch Beweissicherung überprüft werden. Nachdem Ausbau des Fabrwassers in der Außenweser wurden entsprechend u. a. Messungen der Salzgehalte vorgenommen. Da die Daten Indizien für Änderungen des Salzgehalts aufzeigten und deren umfassende Quantifizierung mit Methoden wie nichtlinearer Regression fehlschlagen, wurden Analysen mit Hilfe Künstlicher Neuronaler Netzwerke (KNN) ausgeführt. Damit konnten die Salzgehalte jeweils vor und nach dem Ausbau mit hoher Qualität reproduziert werden. Es zeigte sich weiterhin, dass mit dem Künstlichen Neuronalen Netzwerk, das mit den Daten vor dem Ausbau trainiert worden war, für die nach dem Ausbau gewonnen Daten keine entsprechende Übereinstimmung erreichbar war. Die dabei offenbar werdenden Differenzen konnten zur Quantifizierung der ausbaubedingten Änderungen der Salzgehalte genutzt werden.

Schlagwörter

Tide, Salzgehalt, Ästuarien, Fabrwasserausbauten, Künstliche Neuronale Netzwerke (KNN)

Contents

1	Introduction	154
2	Investigation Area and Data Set	155
3	Methodology	155
4	Calculation by an ANN	158
4.1	Bremerhaven	158
4.2	Nordenham	160
4.3	Strohauser Plate	161
4.4	Brake	163
5	Evaluation of the methodology	164
6	Summary and Conclusions	166
7	References	166

1 Introduction

Major harbours are often located at tidal estuaries where as well large natural water depths as traffic links to the inland are available, in particular for inland navigation. The growth of container ships and their corresponding draft, the depth and sometimes also the width of the waterways in the estuaries had to be increased several times leading to changes in hydro- and morphodynamics. One of these effects is an increasing salt intrusion into the estuaries affecting on the one hand ecology and on the other the ability of the surrounding farms to use the water of the estuary or of connected channels for their animals or plants.

According to planning law important infrastructure measures have to be proven for an environmental assessment procedure. If these results provide only an uncertain foundation for a reliable and appropriate appraisal, the planning approval authority has the option to establish a conservation of evidence procedure.

This strategy was applied by the planning approval authority for the deepening of the waterway in the outer Weser estuary in 1997. In particular for hydro- and morphodynamics a detailed measuring programme and corresponding data analysis were constituted in the decision on the official planning approval. Part of the programme were among others measurements on salt content at distinct measuring station in the Weser estuary (Fig. 1) in order to detect any increase of salt intrusion into the estuary.

The first data analysis carried out by the project operator Federal Waterway Authority Bremerhaven showed no indications for a significant change of salt intrusion into the Weser estuary (WSA BREMERHAVEN 2010). In respect of the interests of the Federal State of Lower Saxony a reassessment nonlinear regression analyses were carried out by the Coastal Research Station. The results highlighted significant changes of salt intrusion into the estuary after the waterway deepening, but it was not possible to quantify these changes, particularly for low and high values of salinity. In order to overcome this deficit the data set was reanalysed by applying artificial neural networks, which allowed finally a reliable determination of increasing salt intrusion into the Weser estuary due to the waterway deepening of the outer Weser estuary.

2 Investigation Area and Data Set

The area of investigation extends from the Outer Weser estuary; where the channel deepening has almost no effect, up to Intschede upstream the tidal barrier in Bremen-Hemelingen. Between these locations the area of interest with the gauges Bremerhaven, Nordenham, Strohauser Plate and Brake is settled (Fig. 1).

For the calculation two datasets for salinity for each location are available (WSA BREMERHAVEN 2010). The first dataset contains the time series from 1997 to 1998. This is a time series which is not influenced by the deepening, because the salinity was measured before the dredging started. The second time series starts in 2006 and contains the data after the waterway deepening.



Figure 1: Investigation Area.

3 Methodology

Artificial neural networks (ANN) are computational models inspired from the thinking pattern of human brain. They can learn and generalize from experiences, and they can abstract essential information from data. The network is made of various single units -the neurons- which are connected to each other by simple arithmetical functions. For the quantification of the alteration in salinity a Multi-Layer-Feed-Forward-Network was chosen (BERKENBRINK and NIEMEYER 2011). This type of ANN connects the neurons to each other in just one direction. The neurons are arranged in several layers. The neurons in the input-layer get all information about the process governing parameters. The neurons in the output-layer represent the result. Between these layers the hidden-layers are settled (Fig. 2).

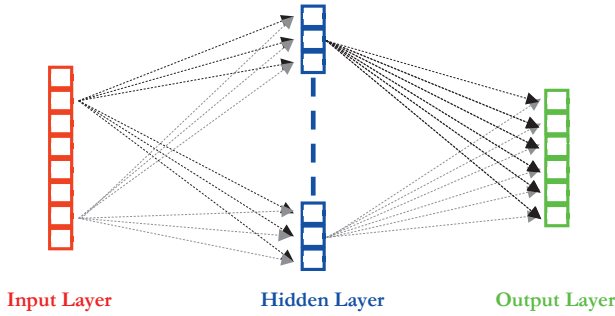


Figure 2: Illustration of the set-up.

These neurons change the values during the learning process till the output-layer get results with sufficient quality. For this kind of problem a supervised learning process was chosen. That means the output-layer is compared to measured data-sets and the neurons in the hidden-layer and the connection between all neurons are changed till the output-layer fits to the measured dataset. After this process the values for the hidden-neurons and the connection will be fixed and the ANN can calculate data of similar processes.

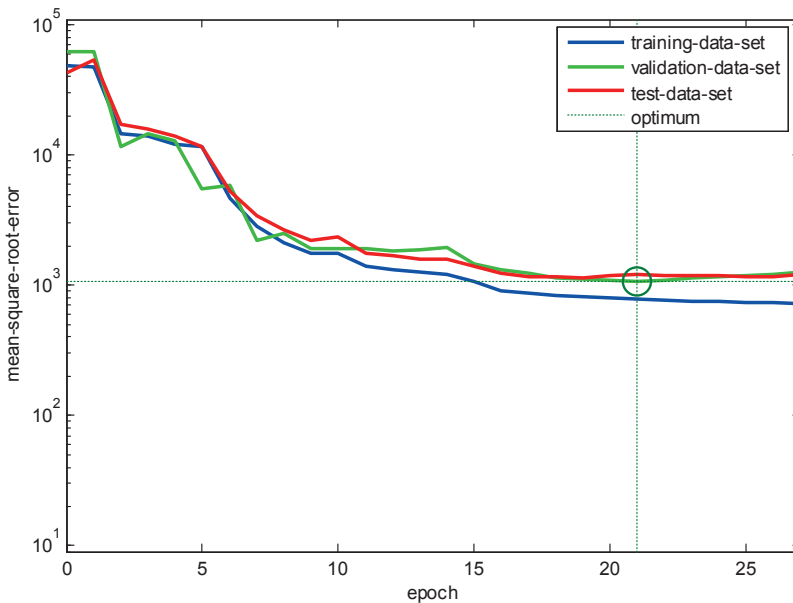


Figure 3: Training-process of the ANN.

To insure the generality the data set is split into three parts. 70 % of the data set is used for the training in order to fit the neurons and the connections of the ANN. Another 15 % of the data-set is used for validation. To be sure, that the ANN does not memorize the data, the learning process of the ANN is controlled by the validation data-set. During the training the mean-square-root-error between output and measured data is calculated for each training-epoch. The same procedure is carried out for the validation data-set.

While the mean-square-root-error for the training-data-sets getting smaller after each epoch, the validation- data-set reach the point, where this error gets bigger. This is the point, where the memorizing-process starts. Then the training-process has to be stopped and the ANN is fixed (Fig. 3).

The quality of the ANN is verified by regression-diagrams (Fig. 4). They show the functional correlation between calculated and measured data. There is a good agreement between calculated and measured data which is seen in the low distribution of the values around the regression line and this line is similar to the angle bisector, following called reference line, for which calculated and measured data are identical.

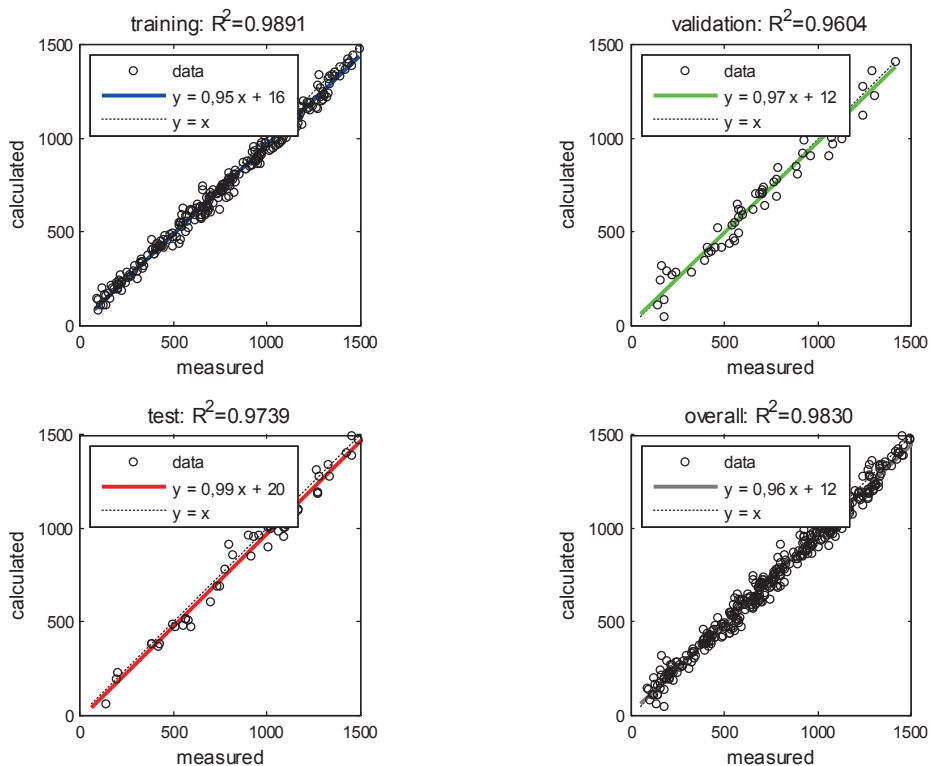


Figure 4: Results of a trained ANN [0,01 %] (example: Bremerhaven).

The ANN is now suitable for other data-sets for the same location under similar conditions. It will calculate like the test-data-set the salinity with the following boundary conditions: different time steps for the salinity, tidal range and tidal high water level in the Outer Weser (Aussenweser) and the freshwater discharge in Intschede, which represent the most important governing factors for salinity in the estuary. Seasonal effects such as storm surges or dry summers are implicitly included. The topography is not considered in the ANN. If there is a significant variation between the Outer Weser and the point of interest it can be identified and quantified by the results of the ANN.

4 Calculation by an ANN

4.1 Bremerhaven

The data set of 1998 for Bremerhaven does not cover the whole year and therefore the analysis by ANN may miss seasonal effects. 70 % of the 401 available data sets were used for the training of the ANN, the rest for testing and validation. The agreement between measured and calculated data is very close (Fig. 5). The distribution is very low and the regression and reference line fit nearly exact.

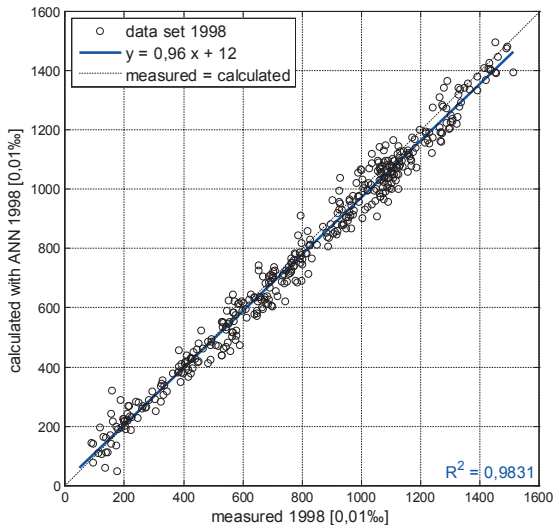


Figure 5: Scatter plot for calculated and measured salinities for gauge Bremerhaven: data set from 1998 before waterway deepening.

This ANN is afterwards used for calculating the salinity values after the waterway deepening and then compared with the measuring data being available for the years 2006-2008 after the deepening. The corresponding scatter plot highlights that the calculated salinity values underestimate the salt intrusion after the deepening the more the higher the values (Fig. 6). This indicates a significant change in the salt intrusion into the Weser estuary since the measurements in 1998, which data were used for the training process of the ANN. Obviously the deepening of the waterway has significantly changed the process of salt intrusion into the estuary. This is a physically absolutely plausible result for which no analysis by ANN is indispensably necessary, but it makes a reliable quantification possible.

The alterations are neither constant nor linear. Up to a value of about 4 ‰ the salinity remains nearly the same as before the deepening, though scattering gets stronger around the reference line (Fig. 6). Above that threshold the measured values are underestimated by the ANN which indicates an increase of the salinity after the deepening of the waterway which is represented by a nonlinear regression. The distance between both regression lines of the calculations with the data set from 1998 and the data set from 2006-2008 is the measure for the alteration in salinity caused by the waterway deepening (Fig. 7).

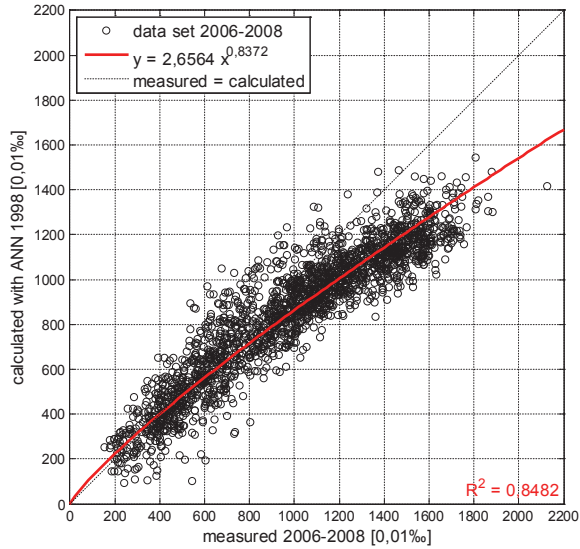


Figure 6: Scatter plot for calculated and measured salinities for gauge Bremerhaven: data set from 2006-2008 after waterway deepening.

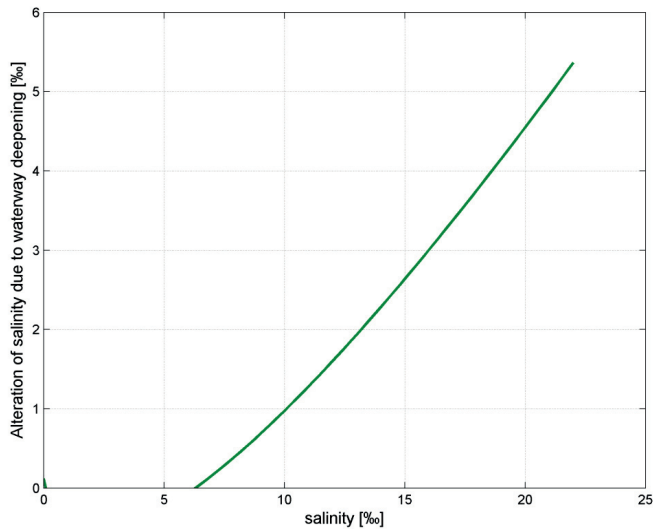


Figure 7: Alteration of salinity due to the waterway deepening at the location Bremerhaven.

For the complete time series this results in a difference of 1.1 ‰ increasing for salinities higher than 12 ‰ to values of 1.6 up to 4.2 ‰. The mean difference is determined by the difference between values calculated with the ANN established with data for the situation before the deepening of the waterway in comparison with the measured values after the deepening.

4.2 Nordenham

The longest time series with 701 values for the training are available for the gauge Nordenham which allows establishing an ANN with complete seasonal variations. The comparison of measured and calculated data shows a very good agreement (Fig. 8). There is only small scattering around the reference line.

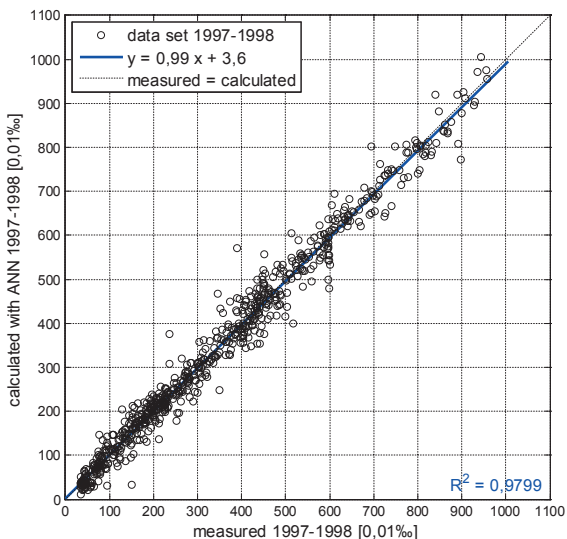


Figure 8: Scatter plot for calculated and measured salinities for the gauge Nordenham: data set from 1998 before waterway deepening.

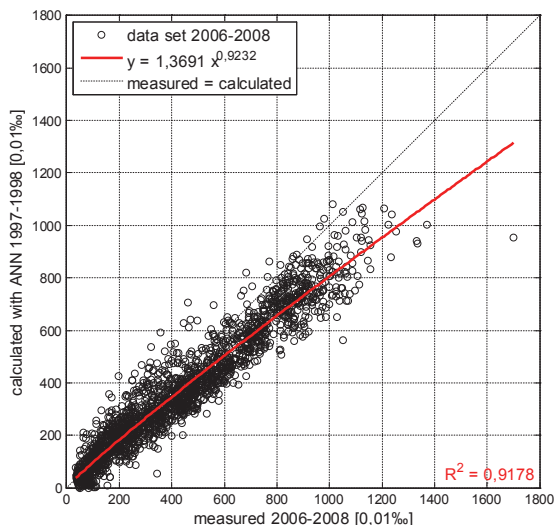


Figure 9: Scatter plot for calculated and measured salinities for gauge Nordenham: data set from 2006-2008 after waterway deepening.

Similar to the results for the location Bremerhaven the application of the ANN trained with the data set from 1998 for the data set of 2006-2008 results in an underestimation of the measured values. The impact of the waterway deepening is again represented by the differences between calculated and measured data for salinity. The effect of the waterway deepening is unknown to the ANN which therefore calculates lower salinity values than measured (Fig. 9). For the whole time series this results in a mean difference of 0.73 ‰ with maximum deviations from 1.8 ‰ up to 3.5 ‰ above a threshold of about 10 ‰ (Fig. 10).

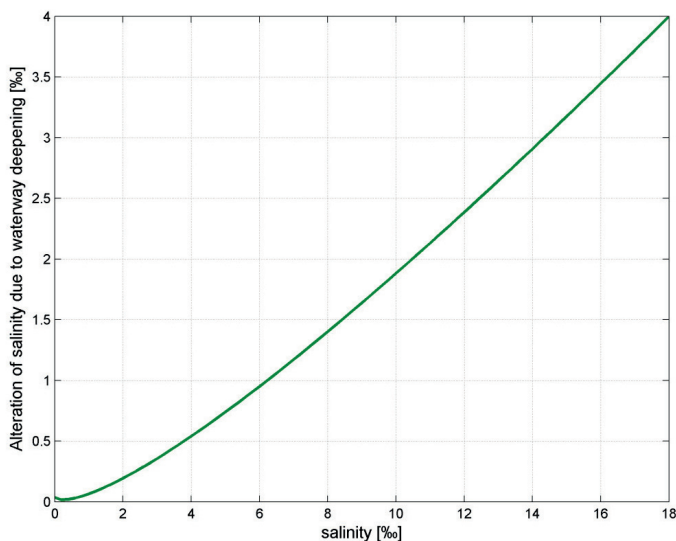


Figure 10: Alteration of salinity due to waterway deepening at the location Nordenham.

4.3 Strohauser Plate

The data set from the location Strohauser Plate is comparable to the data set of Bremerhaven. 70 % of the 484 measured values were used for the training of the ANN. Therefore it has to be taken into consideration that not all seasonal effects are implemented in the ANN. Anyway it shows similar reliable results like the ANN trained by the all-embracing data set of Nordenham. The correlation between measured and calculated data is nearly exact with a very small scatter (Fig. 11).

The application of the ANN trained for the data set from 1998 on the data set of 2006-2008 results here again in lower salinity values than measured (Fig. 12). In comparison to the results gained for the two locations further downstream the relative underestimation of the salinity values is higher and increases particularly for the higher ones. The mean value of the differences is 0.53 ‰ due to deepening of the waterway in the Outer Weser Estuary (Fig. 13).

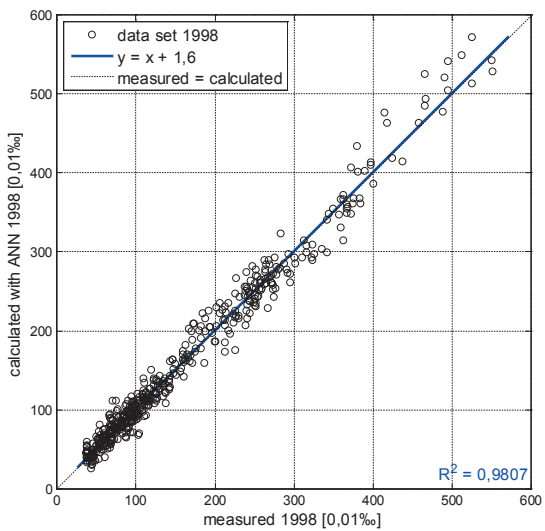


Figure 11: Scatter plot for calculated and measured salinities for gauge Strohauser Plate: data set from 1998 before waterway deepening.

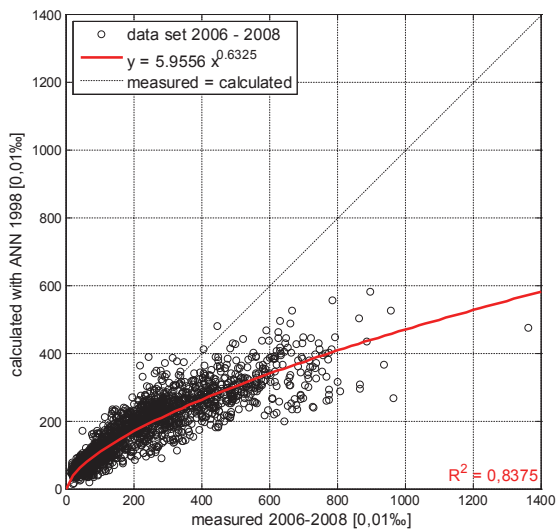


Figure 12: Scatter plot for calculated and measured salinities for gauge Strohauser Plate: data set from 2006-2008 after waterway deepening.

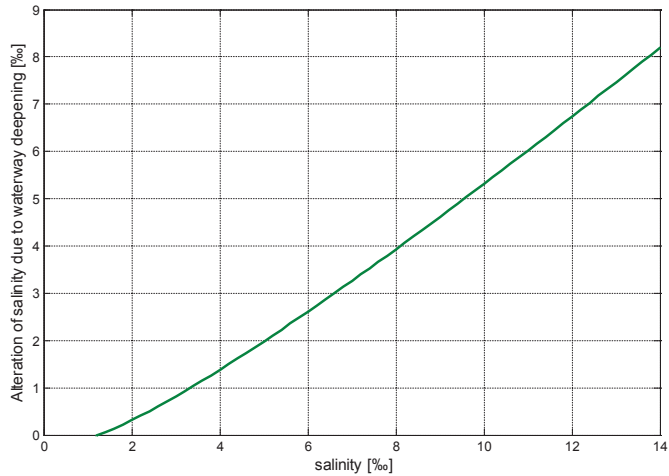


Figure 13: Alteration of salinity due to waterway deepening at the location Strohauser Plate.

4.4 Brake

For Brake a complete data set with 711 values covering all seasonal effects was available. There is a good agreement between the values calculated by the ANN and measured data (Fig. 14). The scatter is very low and the regression line fits nearly exactly with the reference line.

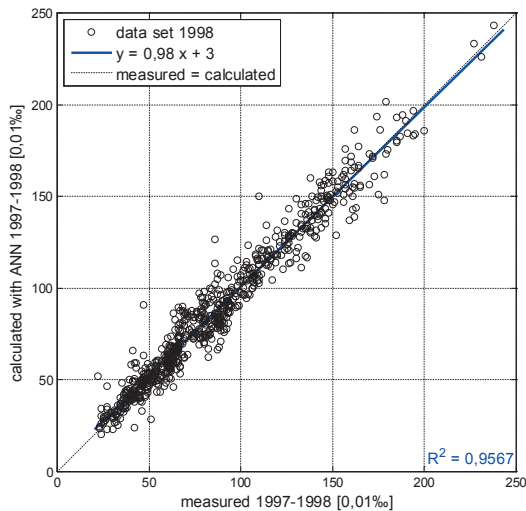


Figure 14: Scatter plot for calculated and measured salinities for gauge Brake: data set from 1998 before waterway deepening.

Applying the ANN to the data set from 2006-2008 the relative underestimation of the measured salinity values above a threshold of 1.5 ‰ is significant (Fig. 15). The intrusion of salt water from the North Sea ranges further upstream after the waterway deepening.

But this effect is only significant for the higher salinity values. The lower values scatter more which is an effect of the relatively small absolute values. Effects of the waterway deepening are at the location Brake are only significant for absolute values higher than 1.5 ‰ (Fig. 16).

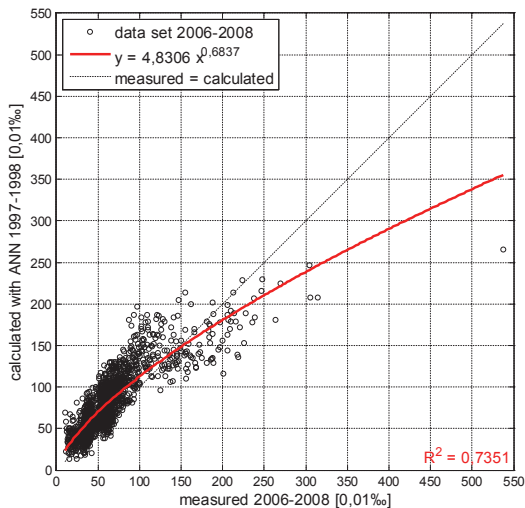


Figure 15: Scatter plot for calculated and measured salinities for gauge Brake: data set from 2006-2008 after waterway deepening.

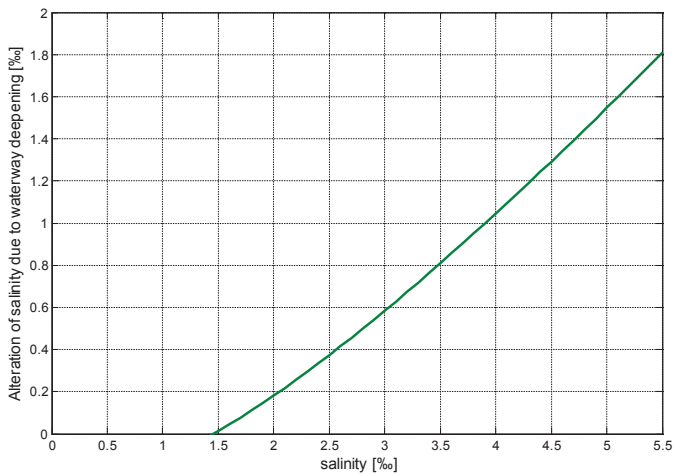


Figure 16: Alteration of salinity due to the waterway deepening at the location Brake.

5 Evaluation of the methodology

In order to prove suitability and reliability of ANNs control experiments were carried out with the data set from the location Nordenham -the one with the longest time series. Up to now the ANN were only trained with the data set from 1998 and then applied for the

one from 2006-2008. The disagreement between measured and calculated values must be induced by effects which are not included in the learning process of the ANN which are obviously the effects of the changed topography due to the waterway deepening after 1998 and before 2006. In order to prove the reliability of the ANN its training is carried out again by using only half of the data set (test data set 1). Afterwards this ANN is adapted to the other half of the data set (test data set 2).

The ANN provides reliable results for test data set 2. The scatter of sporadic values is a little bit higher, but the mean value of the calculated salinity fits to the measured ones. Both data sets are from the same period without any significant change of the estuarine topography and the ANN reproduces the salinity values correctly and consistently (Fig. 17).

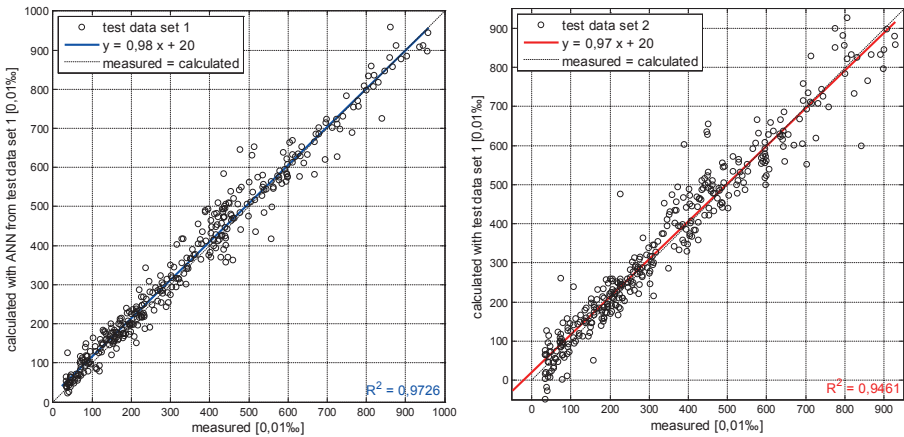


Figure 17: Training and application of the ANN for test data sets before waterway deepening.

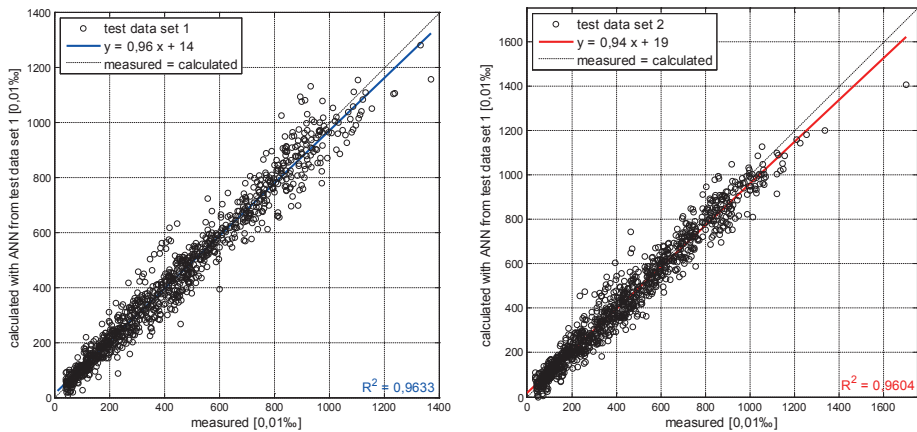


Figure 18: Training and application of the ANN for test data set after waterway deepening.

As an additional proof for the reliability of the methodology the same procedure was done with the data set of 2006-2008. Now the ANN learns the behavior of the salinity intrusion for the Weser Estuary after deepening of the waterway and provides results

with a similar reliability as gained by the calculations with the data set of 1998. Training and application of the ANN show very good and reliable results. Calculated and measured values are of the same magnitude with a small scattering (Fig. 18).

The results of both analyses illustrate the capability and reliability of the methodology to reproduce salinity values by Artificial Neural Networks if there is no significant change in boundary conditions which are not considered for the training.

6 Summary and Conclusions

The quantification of changes in salt intrusion in the Weser Estuary after deepening of the waterway has been carried out by application of Artificial Neural Networks. The study highlights the reliability of that methodology for this purpose. It allows the identification of significant patterns in data sets and their reproductions by functional relationships.

With the data set of 1998 -measured before the waterway deepening started- an ANN was set up for each station in the Weser Estuary. This ANN was adapted to the data set of 2006-2008, which was gathered after the deepening of the waterway. After training with the corresponding input values tidal range, water level, freshwater discharge and salinity in the Outer Weser, ANNs can reproduce the salinity for each location further upstream. These parameters govern dominantly salt intrusion into an estuary if there are no further impacts like a significant change in the topography of the estuary. This was demonstrated by plausibility tests which highlighted suitability and reliability of the methodology by application of ANNs.

Based on the ANN output the alteration in salinity can be quantified. For every location an increase of salinity above a certain threshold was identified with growing the more the higher the absolute values are. Salt intrusion further upstream takes place since the waterway deepening leads to larger flood volumes.

7 References

- BERKENBRINK, C. and NIEMEYER, H.D.: Salzgehaltsänderungen in der Unterweser nach 1998 - Quantifizierung mit künstlichen neuronalen Netzen. Forschungsbericht 01/2011 – NLWKN-Forschungsstelle Küste. Norderney, <http://www.nlwkn.niedersachsen.de/wasserwirtschaft/nordseekueste/FSK/kuesteningenieurwesen/kuesteningenieurwesen-106527.html>, 2011.
- WSA BREMERHAVEN: Dokumentation und Durchführung der im Planfeststellungsbeschluss für den Ausbau der Bundeswasserstraße Weser von km 65 bis km 130 zur Herstellung einer Mindesttiefe von 14 m unter Seekartennull angeordneten Beweissicherungsaufgaben und Bewertung der Ergebnisse – Abschlussbericht, <http://www.wsa-bremerhaven.de/medienarchiv>, 2010.

Statistical Analyses of Metocean Data for Offshore Wind Design in German Waters

Anja Brüning and Elimar Precht

Summary

This paper summarises how statistical analyses of hindcast MetOcean data can be applied to find optimal solutions for offshore windfarm projects. Models can be used to generate oceanographic conditions for large sea areas where long time series can be extracted from any position of interest. The results from analysis of normal and extreme conditions are favourable informations for the design, planning and operational process of an offshore windfarm project. Based on the level of detail benefits are the development of a cost effective design and operation process as well as a better understanding of the site conditions for the development of a risk assessment for the entire lifecycle of offshore wind farms.

Keywords

metocean data, offshore environments, extreme value analysis, probability distribution, joint probabilities

Zusammenfassung

Eine optimale Planung von Offshore Windparks setzt die bestmögliche Kenntnis der meteorologischen und ozeanographischen Rahmenbedingungen voraus. Dieser Artikel zeigt, wie statistische Auswertungen von Hindcastdaten zu diesem Zweck genutzt werden können. Numerische Modelle finden Anwendung, um die ozeanographischen Bedingungen großer Seegebiete zu berechnen und lange Ergebniszeitreihen an beliebigen Positionen aus der räumlichen Ergebnisdatei auszulesen. Die Ergebnisse der Analyse von Normal- und Extrembedingungen begünstigen den Entwurfs- und Planungsvorgang, sowie den betrieblichen Ablauf eines Windpark Projektes. Je nach Detailgrad kann zum Beispiel folgender Nutzen aus den Auswertungen gezogen werden: Die Entwicklung eines kosteneffektiven Entwurfs- und Betriebsplans oder eine Risikobewertung für den Lebenszyklus des Parks aufgrund eines verbesserten Verständnis der Umgebungsbedingungen.

Schlagwörter

Meteorologische und hydrographische Standortbedingungen, Offshore, Extremwertanalyse, Wahrscheinlichkeitsverteilung, Multivariate Eintrittswahrscheinlichkeit

Contents

1	Introduction	168
2	Database.....	169

3	Statistical analyses of metocean data.....	170
3.1	Normal conditions.....	170
3.1.1	Time series and statistics.....	170
3.1.2	Scatter diagrams and roses.....	171
3.1.3	Fatigue data.....	172
3.1.4	Wind wave misalignment.....	173
3.1.5	Operational parameters – weather windows/persistence statistics.....	174
3.2	Extreme conditions.....	176
3.2.1	Extreme value analysis.....	177
3.2.2	On probability distributions.....	177
3.2.3	Confidence limits.....	179
3.2.4	Individual wave and crest heights.....	179
3.2.5	Short-term distributions.....	179
3.2.6	Individual Waves (Modes).....	179
3.2.7	Subset-extremes.....	181
3.2.8	Optimized subsets (directional).....	181
3.2.9	Joint Probability Analysis (JPA).....	182
4	Summary and conclusions.....	183
5	References.....	183
6	Acknowledgements.....	184

1 Introduction

The development of offshore wind farms requires sound and reliable meteorologic-oceanographic (MetOcean) data. Learning from the oil and gas industry and looking at available offshore standards adaptations were necessary to account for site-specific and wind farm industry related requirements. While offshore standards for structural design (DNV 2011; GL 2012; IEC 2009) provide a guideline for the methodology to be used, particular analysis tools are often subject to changes due to scientific progress and individual assessment.

Methods were established by DHI/DHI-WASY in numerous studies to provide reliable MetOcean data and related statistical parameters for design, construction/installation and O&M purposes. An overview will be given on applied statistical analyses of site-specific oceanographic parameters for normal and extreme conditions. These results can be used for the design of offshore structures with respect to either fatigue limit state (FLS), related to the possibility of failure due to the cumulative damage effect of cyclic loading, or ultimate limit state (ULS), corresponding to the limit of the load-carrying capacity.

For practical applications, preferably long time series for the project sites are evaluated. These can be derived from hindcast modelling or observational data. Methods and tools for subsequent analyses will be illustrated. Furthermore, the sensitivity to the choice of methods will be discussed. Conclusions will be drawn on the applicability and accuracy of MetOcean data for offshore design in German waters.

2 Database

In order to conduct statistical analysis for normal and extreme conditions within an Off-shore Windfarm (OWF) preferably long time series of water levels, currents and waves should be evaluated for the project site. These can be derived either from available measurements close to the OWF or from extracted hindcast data time series within the project area.

To date most of the OWF in the German Bight and Baltic Sea were planned in areas where observational data was not or scarcely available. Observational data sets usually cover short periods of time and may be not consistent due to time gaps. Available long time series are typically not available for the project sites proper. In most cases these data are not suitable as a base for reliable site-specific statistical analyses. A possible solution is to use the hindcast approach in order to assess the MetOcean conditions at various sites.

The hindcast approach is based on the description of large sea areas, e.g. the entire North or Baltic Sea with numerical models that are able to simulate currents and water levels as well as waves (Fig. 1). The models are driven by long time series of meteorological data. It is crucial that available observational data is used to validate the models.

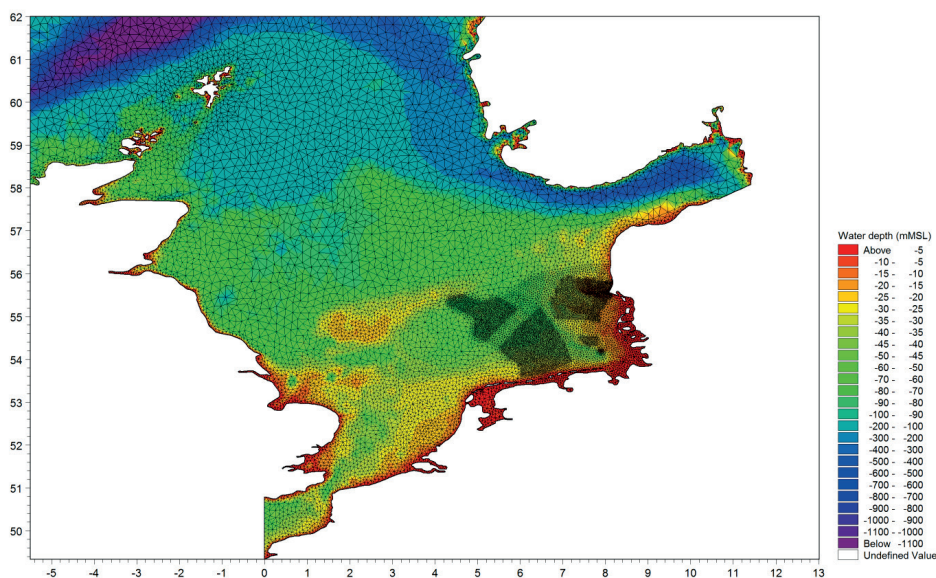


Figure 1: Bathymetry and mesh of the spectral wave model for the North Sea (focusing on the German Bight).

Modelling of currents and water levels is carried out with a hydrodynamic model, e.g. MIKE 21 HD FM (FM – flexible mesh), using long time series of astronomical tides, wind fields and atmospheric air pressure. Modelling of the waves is carried out with a last generation spectral wave model, like MIKE 21 SW FM. Boundary conditions for this model are again the wind fields and the currents and water levels from the hydrodynamic calculation, as those influence the wave field propagation and wave heights in shallow areas. Furthermore, wave spectra from a North Atlantic Model are integrated at the

model boundaries in order to account for the entering long period swell from the North Atlantic Ocean.

By means of these models it is possible to use the available long time series of wind fields to calculate waves, water levels and currents for long periods of time (hindcast). These time series can subsequently be subject to a thorough statistical analysis.

3 Statistical analyses of metocean data

For the design of wind turbines and their foundations, the hydrographic conditions at the location of the OWF in question are required. In order to assess the normal and extreme conditions of water levels, currents and waves, reference points for the area of interest are chosen to be analyzed. The choice depends on the size of the project area, the complexity of the bathymetry, and the level of detail required by the designer.

3.1 Normal conditions

A number of analyses are carried out on observations or the established MetOcean data detailing the operational and fatigue design conditions within the project site: Time series of hourly data are evaluated statistically to provide scatter tables and plots, as well as weather windows and downtimes.

3.1.1 Time series and statistics

Time series and general statistics represent the values of wind, water level, current and waves that are used for analyses of normal conditions. Parameters of interest that are directly extracted from the hindcast model are e.g. highest modelled wind speed 10 m above mean sea level (U_{10}), the total water level range (consisting of tidal and residual – surge induced- parts), the total current speed and wave parameters, namely significant wave height (H_{m0}), peak period (T_p) and zero-crossing period (T_{02}), of the total spectrum (including wind waves and swell).

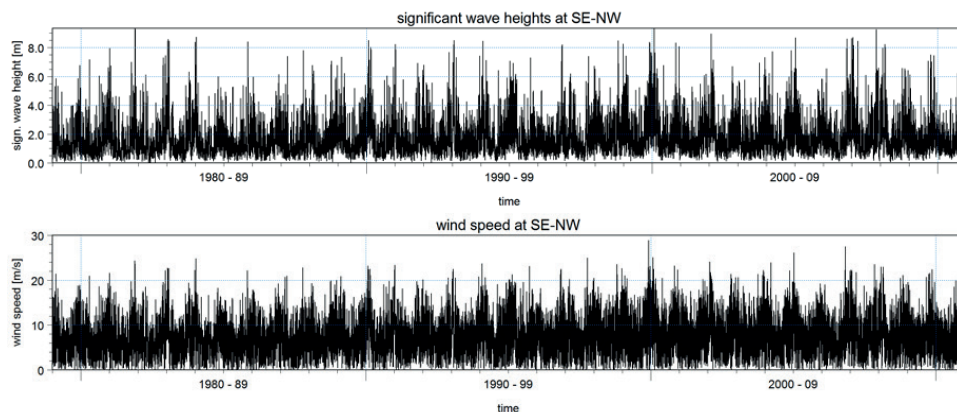


Figure 2: Long time series of modelled hindcast data for OWF Sandbank, significant wave height (top) and wind speed (bottom).

Fig. 2 exemplifies a time series of hindcast data (in this case significant wave height and wind speed at the Sandbank project site). These datasets for various parameters are the base for subsequent analyses.

3.1.2 Scatter diagrams and roses

Based on the metocean database, scatter diagrams/roses for the annual/omni, monthly and directional conditions can be conducted for combinations of e.g.: significant wave height vs. wave period (scatter) or wave direction (rose plot) as well as wind/current speed vs. direction. For monthly (Jan-Dec) and directional (based on MWD or D_{10}) conditions the data base is filtered by a third parameter.

Rose plots give a good overview of the general distribution of the parameter in question. The figure for annual/omni current conditions at the project site of Sandbank presented in Fig. 3 indicates the main current directions (going to) along the NW-SE axes and shows that highest currents can be observed for the Ebb tide.

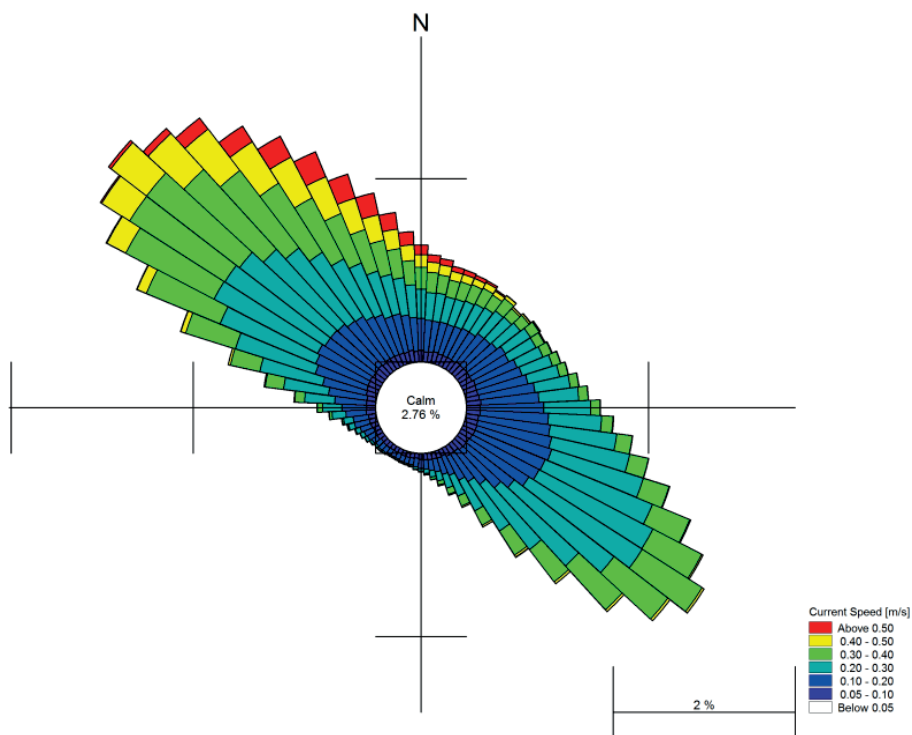
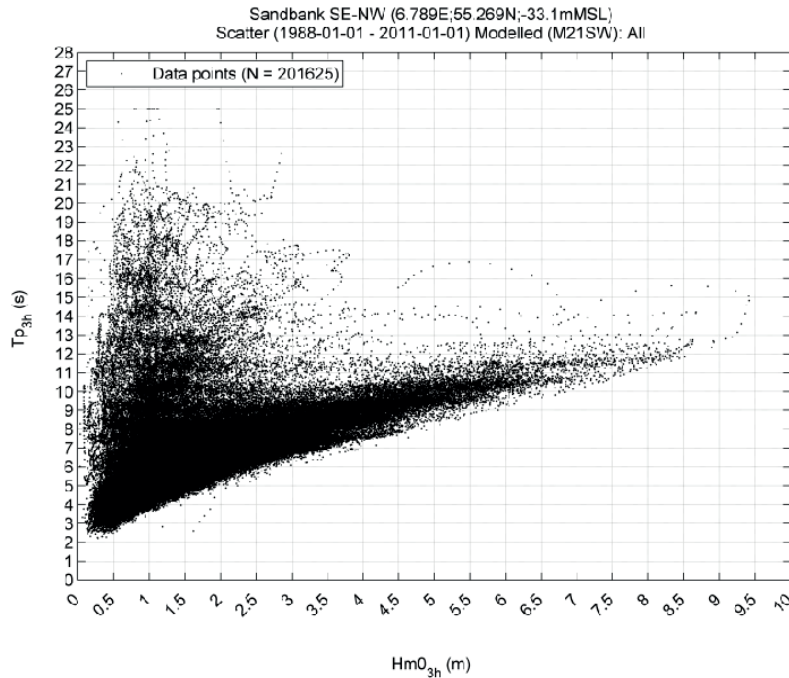


Figure 3: Current rose for Sandbank project site.

3.1.3 Fatigue data

For fatigue analysis, significant wave heights and their related wave periods are assessed from scatter plots and diagrams to identify the most important load cycles for e.g. the design of the foundation.

An omnidirectional scatter plot and associated diagram of significant wave height (H_{m0}) against peak wave period (T_p) for a 3h sea state at the Sandbank project site is presented in Fig. 4. Resolution of the scales are 1 s for T_p and 0.5 m for H_{m0} , respectively.



Reference Point Sandbank SE-NW - All Wind Directions

Sandbank SE-NW (6.789E;55.269N;-33.1mMSL)
Absolute Occurrence: -1 (08E-C1-01 - 2011-01-31) Modelled (M21SW): All
 H_{m0}_{3h} (m)

	[0-0.5]	[0.5-1]	[1-1.5]	[1.5-2]	[2-2.5]	[2.5-3]	[3-3.5]	[3.5-4]	[4-4.5]	[4.5-5]	[5-5.5]	[5.5-6]	[6-6.5]	[6.5-7]	[7-7.5]	[7.5-8]	[8-8.5]	[8.5-9]	[9-9.5]	[9.5-10]	Total	Accum.	
P-1	317	24	1																		344	374	
P-2	2097	1651	1116	3																		374	374
P-3	7472	13030	9053	416	2																	4467	35239
P-4	2781	13080	18685	5724	1189	37																51651	68481
P-5	590	3252	12024	19191	1419	3055	525	118														4421	13481
P-6	430	1318	5188	1585	4298	813	2059	182	207	14												5884	14238
P-7	337	729	2154	5238	2941	4669	820	3278	1210	277	85	15										12677	17242
P-8	218	628	107	776	748	150	17	1944	2300	1808	635	185	13	6								12369	16210
P-9	107	682	140	518	291	302	194	202	355	259	697	502	268	111	37	4						382	18112
P-10	190	469	820	371	233	129	86	156	75	23	117	120	180	126	108	36	10					3283	14527
P-11	118	304	523	420	138	82	41	27	11	12	24	38	34	7	30	26	31	16	2			1843	10700
P-12	54	127	240	208	129	52	23	14	3	3	8	18	2	5	16	4	8					1648	10646
P-13	28	311	203	133	138	60	14	13	6	4	5	2	2	9	2	2	3	2	3			1014	10620
P-14	18	247	209	82	65	31	19	4	1	3				2	1	1	1	2				859	20000
P-15	17	240	181	76	35	26	5	15														627	20046
P-16	3	9	189	36	16	24	10	9														359	20100
P-17	1	88	113	36	16	1																256	20134
P-18	3	21	88	26	11	1																227	20181
P-19	1	21	37	11	8	12																83	20154
P-20		2	8																			11	20166
P-21		2	3																			8	20166
P-22			2																			5	20110
P-23			8	2																		15	20125
P-24																							20125
P-25																							20125
P-26																							20125
P-27																							20125
P-28																							20125
P-29																							20125
Total	81.0	42544	47140	33381	240.7	1817	18110	6388	4285	2368	150	907	622	230	133	10300	201510	77	21	9		20122	
Accum.	81.0	53680	69468	124727	182724	174691	104711	110211	163260	182919	18947	204414	202308	202123	202000	223114	221821					20122	

Figure 4: Scatter plot and table for H_{m0} vs T_p – modelled data at OWF Sandbank.

Clear relations can be identified, this is in particular apparent during higher sea states as illustrated. However, lower sea states might include a significant fraction of longer-period waves associated with swell conditions as can be seen from the higher peak wave periods for $H_{m0} < 4$ m in Fig. 4. Through a polynomial fit to the 1 % highest waves a correlation between significant wave height and Wave period can be derived from the data. The polynom, which describe the correlation between H_{m0} and T_{02} , or T_p respectively, is in good agreement with relationships known from literature, e.g. JOURNÉE and MASSIE 2001, WMO 1998.

Further improvements of the used hindcast models allow to use their frequency spectra for each individual sea state to determine scatter data of individual wave heights, H , vs. wave period, T , for fatigue damage calculations, instead of simply using the original time series data from the model. These scatter tables are generated by inverse Fourier transform of the modelled frequency spectra for each individual sea state, assuming a Gaussian process. Individual wave heights and wave periods are found by a zero down-crossing analysis of the generated time series of sea surface elevation. The analyses are conducted for the total part of the wave spectrum, and sea states are sorted by mean wave direction MWD.

A least-square fit of the H_{max} and T_{Hmax} mean values (based on the single maximum H in each sea state and the associated T) is included in the applied method.

3.1.4 Wind wave misalignment

For wind turbine design, misalignment between the two most important dynamic forces (wind at hub height and waves) is a significant loading condition.

A scatter table between wind direction (D_{10}) and mean wave direction (MWD) indicates the wind-wave-misalignment in total values (Fig. 5). Typically analyses are separated for different wind speeds at hub height to allow a more detailed and thus optimized design. Design optimization based on thorough analysis may lead to substantial cost savings in the design of the wind turbines.

Sandbank SE-NW (6.789E:55.269N;-33.1mMSL)
Absolute Occurrence [-] (1988-01-01 - 2011-01-01): All
MWD_{3h} (°N-from)

Wind Direction (°N-from)	[15-15]	[15-45]	[45-75]	[75-105]	[105-135]	[135-165]	[165-195]	[195-225]	[225-255]	[255-285]	[285-315]	[315-345]	Total	Accum
[15-15]	2346	189	28	22	11	33	38	23	171	257	887	6599	10542	10542
[15-45]	3053	1540	122	51	23	12	9	14	97	199	509	2596	8236	18777
[45-75]	1754	2047	1792	424	113	48	18	20	118	188	387	1401	8270	28056
[75-105]	814	1134	2053	4314	2005	188	53	85	212	212	465	1122	12687	40743
[105-135]	433	348	401	1139	6578	2788	402	385	423	381	647	1418	15413	59156
[135-165]	247	124	89	193	691	4549	2520	1526	890	671	877	1030	13213	69369
[165-195]	139	36	42	85	146	785	2529	5702	2660	1316	966	890	15288	84657
[195-225]	100	29	27	22	83	161	552	8214	9719	2998	1885	1051	22648	107305
[225-255]	131	38	17	16	44	80	150	1445	12140	7898	3222	1386	26587	133872
[255-285]	142	12	9	13	18	51	75	329	3555	10628	6004	2415	24152	158024
[285-315]	222	16	4	4	16	21	38	132	714	3340	10878	7848	23230	181283
[315-345]	693	28	8	6	12	22	19	69	294	710	3914	14587	20362	201625
Total	10104	6421	4590	6271	9723	8728	6482	15953	30962	28791	31201	42369	201625	-
Accum	10104	18525	21115	27388	37109	45837	52319	68272	99284	128055	159256	201625	-	-

Figure 5: Scatter table for wind direction vs – mean wave direction at OWF Sandbank.

At present a slightly different approach is used to assess the misalignment.

The wind-wave misalignment is calculated as MWD minus D_{10} for each time step. For example, if the wind blows from south ($WD = 180^\circ N$) and the waves propagate from west ($MWD = 270^\circ N$), the misalignment is $+90^\circ$.

Scatter diagrams of the misalignment vs. U_{10} and H_{m0} and frequency distributions depict the general load incidents. For the total sea states, a significant misalignment is observed for low wind speeds (i.e. below about 10 m/s) or low H_{m0} (i.e. below 1.5 m). This is explained by the occurrence of mixed sea-states and the fact that waves propagate e.g. in the German Bight predominantly from the Northwest, while the occurrences of wind events are more evenly distributed over the directional sectors. For higher sea-states, the misalignment is reduced noticeable. The most extreme sea-states show a misalignment in the range close around 0° .

The sea-part of the wave spectrum is by definition fairly well correlated with the wind direction, while the swell-part of the wave spectrum shows dominating misalignment of -90 and $+90^\circ$.

3.1.5 Operational parameters – weather windows/persistence statistics

Operational parameters (weather windows and downtimes) are crucial during construction and operation of OWF's. Precise datasets and thorough analyses can be used to improve the planning and optimize the operations by e.g. choosing the right time slots or vessels.

Time series of hindcast data are analysed in order to estimate the probability of occurrence of weather windows and down times for offshore works within the project site. A persistence analysis provides information regarding the long term average of weather conditions within the project area. For this purpose weather windows and downtimes for operational parameters such as significant wave height H_{m0} and wind speed U_{10} are calculated.

A weather window is defined as a period of time during which an operational condition is continuously fulfilled, this means a certain parameter is constantly below a given threshold (e.g. significant wave height $H_{m0} < 3\text{m}$). The downtime period is defined as all other periods of time. Hence, the total of weather windows and downtimes for each considered weather condition corresponds to the length of the entire period of time. This definition follows the usual interpretation for logistic planning. Two different approaches, overlapping and non-overlapping can be applied when analysing weather windows.

When the non-overlapping approach is applied only total numbers of weather windows are counted. This means when a weather window beneath a parameter's threshold within a given period is counted, its number of occurrence is rounded down to an integer value instead of giving a decimal number (overlapping approach) as illustrated by Fig. 6.

Base for the analysis can be the mean value, but statistical percentiles such as the P50 (median) are used more frequently. For most of the resistant statistics the median aligns with the mean value (50 %). As long as more than half of the data do not reveal gaps, the median will lead to a correct result and a more robust statistic with regards to outliers.

The analyses can be conducted for different percentiles (e.g. P50, P75 and P90) based on a selection of thresholds for operational parameters (H_{m0} , U_{10}) for varying periods of time. Additionally a combination of both parameters based on their critical thresholds can be analyzed for defined durations like, e.g. 1; 3; 6; 9; 12; 18; 24; 48; and 96 hours.

The analyses are illustrated based on the P50 results at Sandbank for different thresholds of H_{m0} and duration of 12h (see Fig. 7).

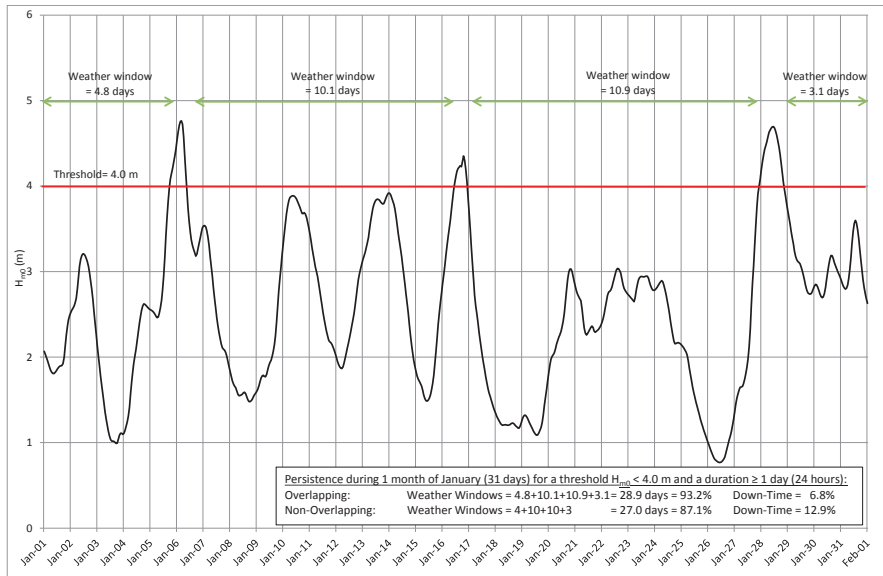


Figure 6: Weather window January (31 days) including an example for comparison between overlapping and non-overlapping methods. Both approaches refer to the definition Weather Windows + Down Times = 100%.

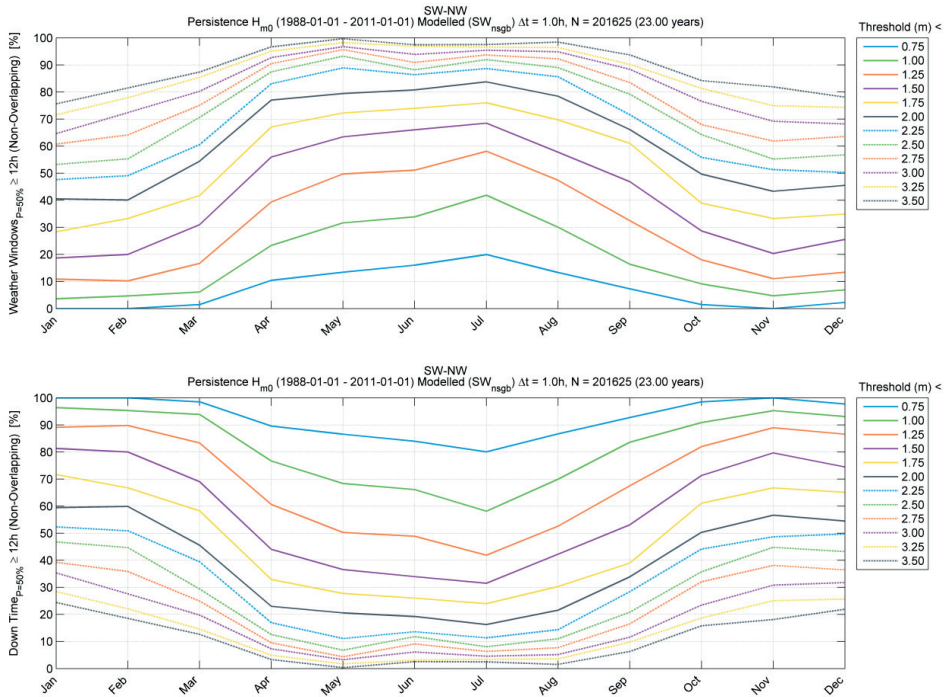


Figure 7: Diagram of weather window (top) and down time (bottom) for H_{m0} and duration of 12 h.

Seasonal results are additionally presented in Tab. 1 given as percentage of occurrence for each month. The standard deviation, which is per definition based on the mean value, is included in parenthesis to indicate the variance/scatter of each monthly bin value within a model period of 23 years.

Table 1: Table of weather window (top) and down time (bottom) for H_{m0} and duration of 12 h.

SW-NW Persistence H_{m0} (1988-01-01 - 2011-01-01) Modelled (SW_{nsgb}) $\Delta t = 1.0h$, $N = 201625$ (23.00 years) Weather Windows $p_{=50\%} \geq 12h$ (Non-Overlapping) [%]												
	Jan	Feb	Mar	Apr	May	Jun	Jul	Aug	Sep	Oct	Nov	Dec
0.75	0.0 (1.9)	0.0 (2.9)	1.5 (4.8)	10.4 (9.9)	13.4 (10.6)	16.0 (11.2)	20.0 (13.3)	13.3 (12.2)	7.3 (5.7)	1.5 (5.1)	0.0 (3.2)	2.3 (3.1)
1.00	3.6 (6.2)	4.7 (7.4)	6.1 (10.4)	23.3 (12.2)	31.7 (13.2)	33.9 (14.8)	41.9 (16.3)	30.0 (15.3)	16.4 (9.7)	9.1 (7.7)	4.7 (7.2)	6.9 (8.0)
1.25	10.9 (11.9)	10.2 (12.1)	16.7 (12.9)	39.4 (13.1)	49.7 (12.1)	51.1 (16.4)	58.1 (16.0)	47.4 (14.7)	32.5 (11.8)	18.0 (11.0)	11.0 (12.7)	13.4 (11.2)
1.50	18.7 (14.4)	20.0 (16.8)	31.0 (15.0)	56.0 (14.8)	63.4 (10.6)	66.0 (13.9)	68.5 (14.8)	57.7 (13.7)	46.9 (14.2)	28.7 (13.7)	20.3 (15.0)	25.5 (12.2)
1.75	28.4 (15.2)	33.3 (19.0)	41.7 (16.7)	67.1 (14.3)	72.2 (9.4)	74.0 (11.4)	76.0 (13.1)	69.7 (11.2)	61.0 (14.4)	38.9 (14.5)	33.3 (16.1)	34.9 (13.4)
2.00	40.5 (18.1)	40.1 (20.9)	54.4 (17.3)	77.0 (11.4)	79.4 (7.2)	80.8 (9.5)	83.7 (10.9)	78.4 (9.2)	66.1 (13.6)	49.7 (15.7)	43.3 (16.1)	45.5 (14.8)
2.25	47.6 (18.9)	49.1 (20.6)	60.6 (18.1)	83.1 (9.2)	88.9 (5.9)	86.4 (7.3)	88.6 (9.2)	85.6 (8.0)	71.6 (12.8)	55.6 (16.3)	51.3 (15.2)	50.3 (14.7)
2.50	53.2 (19.3)	55.3 (21.3)	70.6 (18.0)	87.4 (7.5)	93.2 (4.5)	88.2 (5.9)	91.9 (7.6)	89.0 (6.6)	79.2 (11.5)	64.2 (15.9)	55.2 (14.4)	56.8 (15.5)
2.75	60.8 (19.8)	64.1 (18.5)	75.1 (17.7)	90.5 (5.8)	95.6 (3.5)	90.9 (3.8)	93.7 (5.7)	92.3 (5.8)	83.5 (10.5)	67.9 (14.9)	61.9 (13.8)	63.6 (14.4)
3.00	64.7 (19.9)	72.4 (18.1)	80.2 (16.0)	92.7 (4.9)	96.7 (2.8)	93.9 (3.5)	95.4 (4.3)	94.8 (4.3)	88.4 (9.2)	76.5 (14.6)	69.2 (12.9)	68.2 (14.1)
3.25	71.6 (19.7)	77.9 (17.1)	85.4 (14.3)	95.1 (4.3)	98.3 (2.5)	96.9 (3.0)	96.6 (3.5)	96.4 (3.1)	90.2 (7.9)	81.3 (11.5)	74.9 (12.4)	74.3 (12.6)
3.50	75.6 (19.0)	81.5 (14.8)	87.4 (12.7)	96.7 (3.5)	99.7 (1.9)	97.4 (2.6)	97.5 (2.6)	96.5 (2.8)	93.7 (6.6)	84.2 (10.8)	81.9 (10.7)	78.1 (11.6)

SW-NW Persistence H_{m0} (1988-01-01 - 2011-01-01) Modelled (SW_{nsgb}) $\Delta t = 1.0h$, $N = 201625$ (23.00 years) Down Time $p_{=50\%} \geq 12h$ (Non-Overlapping) [%]												
	Jan	Feb	Mar	Apr	May	Jun	Jul	Aug	Sep	Oct	Nov	Dec
0.75	100.0 (1.9)	100.0 (2.9)	98.5 (4.6)	89.6 (9.9)	86.6 (10.6)	84.0 (11.2)	80.0 (13.3)	86.7 (12.2)	92.7 (5.7)	98.5 (5.1)	100.0 (3.2)	97.7 (3.1)
1.00	96.4 (6.2)	95.3 (7.4)	93.9 (10.4)	76.7 (12.2)	68.3 (13.2)	66.1 (14.8)	58.1 (16.3)	70.0 (15.3)	83.6 (9.7)	90.9 (7.7)	95.3 (7.2)	93.1 (8.0)
1.25	89.1 (11.9)	89.8 (12.1)	83.3 (12.9)	60.6 (13.1)	50.3 (12.1)	48.9 (16.4)	41.9 (16.0)	52.6 (14.7)	67.5 (11.8)	82.0 (11.0)	89.0 (12.7)	86.6 (11.2)
1.50	81.3 (14.4)	80.0 (16.8)	69.0 (15.0)	44.0 (14.8)	36.6 (10.6)	34.0 (13.9)	31.5 (14.8)	42.3 (13.7)	53.1 (14.2)	71.3 (13.7)	79.7 (15.0)	74.5 (12.2)
1.75	71.6 (15.2)	66.7 (19.0)	58.3 (16.7)	32.9 (14.3)	27.8 (9.4)	26.0 (11.4)	24.0 (13.1)	30.3 (11.2)	39.0 (14.4)	61.1 (14.5)	66.7 (16.1)	65.1 (13.4)
2.00	59.5 (18.1)	59.9 (20.9)	45.6 (17.3)	23.0 (11.4)	20.6 (7.2)	19.2 (9.5)	16.3 (10.9)	21.6 (9.2)	33.9 (13.6)	50.3 (15.7)	56.7 (16.1)	54.5 (14.8)
2.25	52.4 (18.9)	50.9 (20.6)	39.4 (18.1)	16.9 (9.2)	11.1 (5.9)	13.6 (7.3)	11.4 (9.2)	14.4 (8.0)	28.4 (12.8)	44.2 (16.3)	48.7 (15.2)	49.7 (14.7)
2.50	46.8 (19.3)	44.7 (21.3)	29.4 (18.0)	12.6 (7.5)	6.8 (4.5)	11.8 (5.9)	8.1 (7.6)	11.0 (6.6)	20.8 (11.5)	35.6 (15.9)	44.8 (14.4)	43.2 (15.5)
2.75	39.2 (19.8)	35.9 (18.5)	24.9 (17.7)	9.5 (5.8)	4.4 (3.5)	9.1 (3.8)	6.3 (5.7)	7.7 (5.8)	16.5 (10.5)	32.1 (14.9)	38.1 (13.8)	36.4 (14.4)
3.00	35.3 (19.9)	27.6 (18.1)	19.8 (16.0)	7.3 (4.9)	3.3 (2.8)	6.1 (3.5)	4.6 (4.3)	5.2 (4.3)	11.6 (9.2)	23.5 (14.6)	30.8 (12.9)	31.8 (14.1)
3.25	28.4 (19.7)	22.1 (17.1)	14.6 (14.3)	4.9 (4.3)	1.7 (2.5)	3.1 (3.0)	3.4 (3.5)	3.6 (3.1)	9.8 (7.9)	18.7 (11.5)	25.1 (12.4)	25.7 (12.6)
3.50	24.4 (19.0)	18.5 (14.8)	12.6 (12.7)	3.3 (3.5)	0.3 (1.9)	2.6 (2.6)	2.5 (2.6)	1.5 (2.8)	6.3 (6.6)	15.8 (10.8)	18.1 (10.7)	21.9 (11.6)

3.2 Extreme conditions

Extreme conditions of wind, wave, water levels and currents occurring at the site are determined in order to define design conditions for the ultimate limit state (ULS), corresponding to the limit of the load-carrying capacity. Precise assessment of extreme conditions is not only crucial for safety issues, a detailed and sound assessment can also be used for an optimised design which is safe and cost-efficient.

At DHI, extreme value analyses (EVA) for the parameters of interest are conducted based on sensitivity tests of a number of different distributions and thresholds, as well as fitting methods.

The assessment of individual wave heights within predefined storm sea states can be assessed based on the storm mode approach (TROMANS and VANDERSCHUREN 1995). This approach allows determining the maximum wave and/or cresting height (H_{max} , C_{max}) occurring during a storm based on short term distributions.

Furthermore, extreme value assessment can be constrained by monthly or directional subseries in order to account for directional or monthly variability.

3.2.1 Extreme value analysis

The first step in extreme value analysis is to identify the extreme events from the data, on which a probability distribution will be fitted. Various identification methods exist such as Annual Maximum Peak (AMP) or Peak Over Threshold (POT). The AMP method selects one peak per year of data, while the POT method selects all peaks above a given threshold. POT can also be referred to as the Average Annual Peak (AAP) method, if the threshold is defined by specifying an average number of peaks to be selected per year instead of a fixed threshold. The applied function and method are always very subjective depending on physical and site specific knowledge. Therefore, both AMP and AAP methods can be used in studies to perform sensitivity analyses for different distributions to find the most robust and more objective sustained estimate.

When the POT/AAP method is used, independence of the extreme events can be ensured by using an inter-event time of 36h and an inter-event level of 0.7. This means that two events can be selected as extremes only if they are separated by a minimum of 36 h and that the value ($WS, H_{m0} \dots$) went below 0.7 times the peak value of the smaller of the two events. Fig. 8 depicts the POT/AAP method.

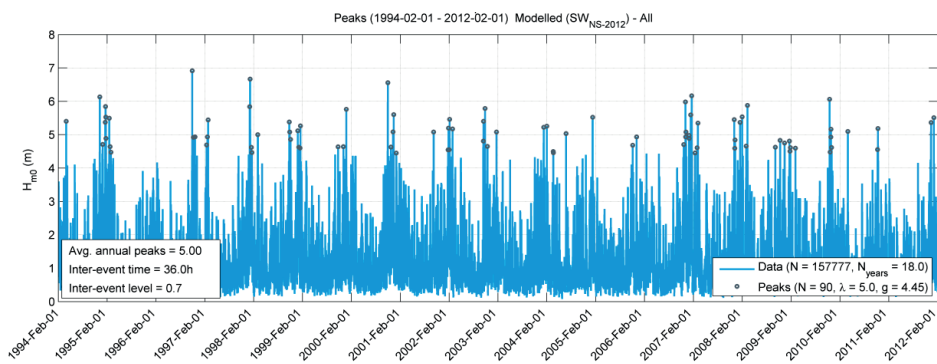


Figure 8: Time series of H_{m0} showing selected peaks using the AAP method.

3.2.2 On probability distributions

Extreme values with long return periods are estimated by fitting a probability distribution to historical data. A number of distributions, data selection and fitting techniques are available for estimation of extremes from historical data and the estimated extremes are often rather sensitive to the choice of method. However, it is not possible to choose a preferred method only based on its superior theoretical support or widespread acceptance within the industry. Hence, it is common practice to test a number of approaches and make the final decision based on goodness of fit. The following probability distributions are often used in connection with extreme value estimation: 2-parameter Weibull, the truncated Weibull and the Gumbel Distribution.

An example of the different fittings is given in Fig. 9 and Fig. 10 depicts an extreme distribution fit.

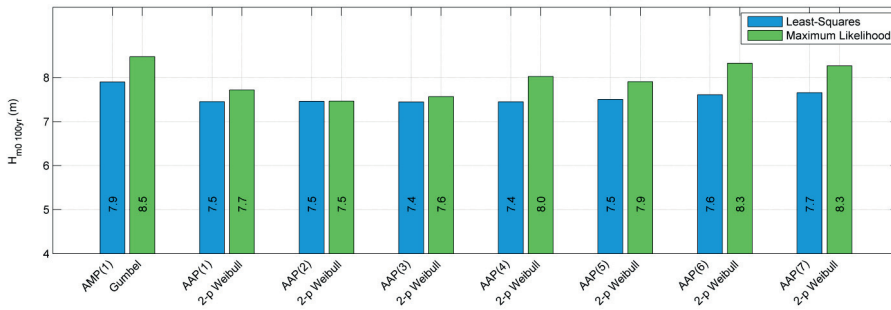


Figure 9: Omni-directional values of 100-year H_{m0} at a North Sea OWF site estimated using different distributions for a varying thresholds.

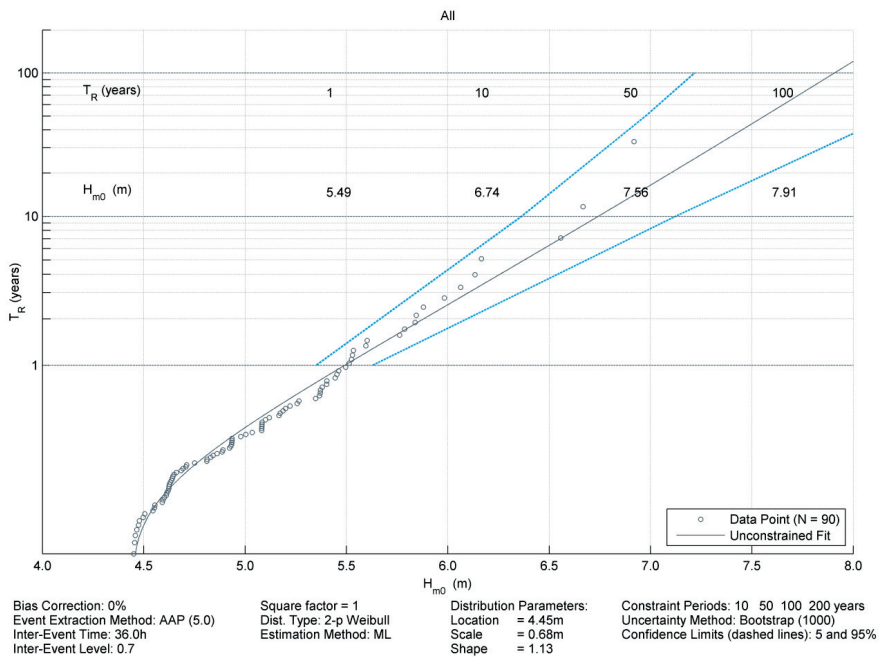


Figure 10: Extreme distribution of H_{m0} at a North Sea OWF site (UK EEZ) based on Weibull distribution (AAP = 5.0). Dots: data, black line: central estimate of extreme distribution. 5 % and 95 % confidence bounds are shown with dashed blue line.

3.2.3 Confidence limits

To estimate the uncertainty due to sampling errors, a bootstrap analysis is carried out on the omnidirectional extreme values. The bootstrap consists of the following steps:

- Construct a new set of extreme events by sampling randomly with replacement from the original data set of extremes
- Carry out an extreme value analysis on the new set to estimate T-year events.

An empirical distribution of the T-year event is obtained by looping step 1 and 2 many times. Quartiles are read from the empirical distribution.

The results are presented in terms of plots showing the estimated distribution and the 5 % and 95 % quartiles (dashed lines).

3.2.4 Individual wave and crest heights

For design purposes, the maximum wave and crest height occurring in a storm are of special interest e.g. in order to estimate the most severe ULS requiring the maximum wave height or to define the air gap at a substation based on the maximum crest height ULS. Based on hindcast data only the extreme values for significant wave heights are estimated for a certain sea state and the maximum individual wave height H_{\max} occurring in that particular storm is often derived by formulae, which does not account for the rare and rather asymptotic properties of extremes.

A more detailed approach used by DHI is to estimate the short term variability of the maximum individual wave and crest heights within a storm by using the convolution method supposed by (TROMANS and VANDERSCHUREN 1995). Here the long-term distribution of individual waves and crests is found by convolution of the long-term distribution of the modes with the short-term distribution of the maximum conditional on the mode.

3.2.5 Short-term distributions

The short-term distributions of individual wave heights and crests conditional on H_{m0} are assumed to follow the distributions proposed by FORRISTALL (1978 and 2000). The Forristall wave height distribution is based on Gulf of Mexico measurements, but experience from the North Sea has shown that these distributions may have a more general applicability. For this type of distribution, the distribution of the extremes of a given number of events, N, (waves or crests) converges towards the Gumbel distribution conditional on the most probable value of the extreme event, H_{mp} (or C_{mp} for crests).

3.2.6 Individual Waves (Modes)

The storm modes, or most probable values of the maximum wave or crest in the storm (H_{mp} or C_{mp}), are obtained by integrating the short-term distribution of wave heights conditional on H_{m0} over the entire number of sea states making up the storm. This produces a database of historical storms each characterized by its most probable maximum individual wave height which is used for further extreme value analysis.

Peak-over-threshold estimates of the 100 year maximum wave at a North Sea OWF site are plotted as a function of the average annual number of events over threshold in Fig. 11.

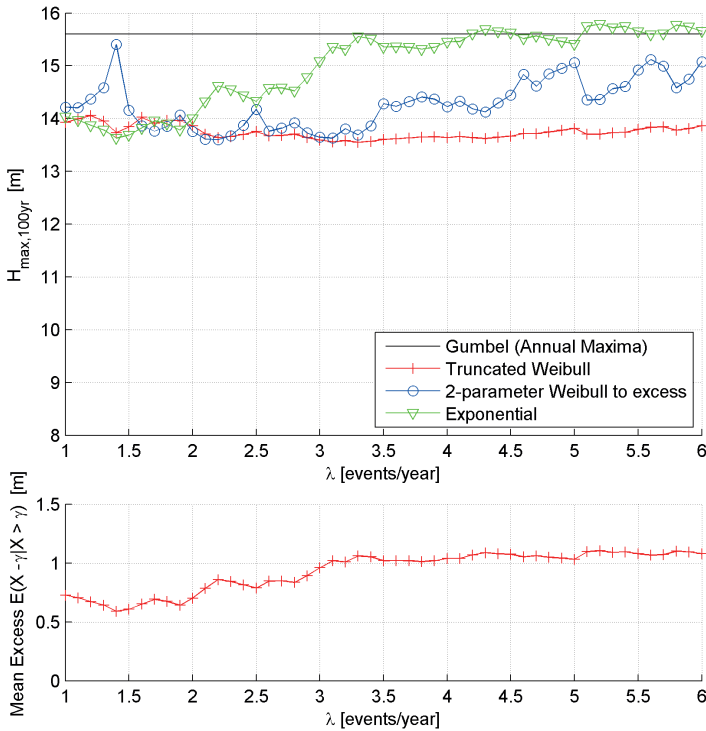


Figure 11: Omni-directional values of 100-year H_{max} at a North Sea OWF site estimated using different distributions for a varying number of selected peak events (AAP).

On-site analysis for individual crest heights follows the same approach using the short-term distribution proposed by FORRISTALL (2000). The analysis is carried out for the crest height above SWL (the instantaneous water level including effects of tide and surge).

The associated period for the maximum wave can be derived according to the recommendations in (DNV 2010) and (IEC, 2009). The stated relations are estimated for a specific area in the North Sea and therefore do not account for site specific conditions. A rather/more progressive way of estimating the relation between H_{max} and associated Period $T_{H_{max}}$ is to use the given spectral information from hindcast data. The periods associated with the maximum individual waves ($T_{H_{max}}$) are derived from pairs of maximum wave and associated period for each individual sea state simulation carried out to determine HT-scatter data (see Fatigue data). The joint probability model described later on is used to determine the relationship between H_{max} and its resulting median (50) periods as well as 5 and 95 percentiles (which may be used as upper and lower bounds).

3.2.7 Subset-extremes

Estimates of subset (e.g. directional and monthly) extremes are required for a number of parameters. These allow a better understanding of the site conditions; e.g. at a project site with highly directional extremes the developer can account for this directional extremes within the design process when e.g. boat landings or scour protection measures are planned.

In order to establish these extremes, a common practice is to fit extreme value distributions to data sampled from the modelled database that fulfil the specific requirement to direction, i.e. the extremes from each direction are extracted, and distributions fitted to each set of directional data in turn. By sampling an often relatively small number of values from the data set, each of these directional distributions is subject to uncertainty due to sampling error. This will often lead to the directional distributions being inconsistent with the omnidirectional distribution fitted to the maxima of the entire (omnidirectional) data set. Consistency between directional and omnidirectional distributions can e.g. be ensured by requiring that the product of the n directional annual non-exceedance probabilities equals the omnidirectional.

3.2.8 Optimized subsets (directional)

The directional extremes are derived FROM fits to each subseries data set meaning that a T_R year event from each direction will be exceeded once every T_R years on average. Having e.g. 8 directions this means that *one* of the directions will be exceeded once every $T_R/8$ years on average. A 100-year event would thus be exceeded once every $100/8 = 12.5$ years (on average) from *one* of the directions.

For design application, it is often required that the summed (overall) return period (probability) is T_R years. A simple way of fulfilling this would be to take the return value corresponding to the return period T_R times the number of directions, i.e. in this case the $8 \times 100 = 800$ -year event for each direction. However, this is often not optimal since it may lead to very high estimates for the strong sectors, while the weak sectors may still be insignificant.

Therefore, an optimized set of directional extreme values is produced for design purpose in addition to the individual values of directional extremes described above. The optimized values are derived by increasing (scaling) the individual T_R values of the directions to obtain a summed (overall) probability of T_R years while ensuring that the extreme values of the strong sector(s) become as close to the overall extreme value as possible. In practice, this is done by increasing the T_R of the weak directions more than that of the strong sectors but ensuring that the sum of the inverse directional T_R 's equals the inverse of the targeted return period, i.e.:

$$\sum_{i=1}^n \frac{1}{T_{R,i}} = \frac{1}{T_{R,omni}} \quad (1)$$

where n is the number of directional sectors and $T_{R,omni}$ is the targeted overall return period.

3.2.9 Joint Probability Analysis (JPA)

The probability of coincidence for two extreme parameters in question (e.g. WL and H_{m0}) is mostly required to evaluate the unlikely event of an extreme loading condition. As an example, in the North Sea, the probability of an extreme wave occurring jointly with a very low water level is negligible, as the former are associated to westerly storms and the latter to easterly winds. Therefore it is beneficial for the design to estimate, e.g., the association between extreme high water levels and extreme wave heights to derive the probability of a joint occurrence of the two parameters.

Values of U_{10} , WL and CS associated with extremes of one variable are estimated using the methodology proposed in (HEFFERNAN and TAWN 2004). This method consists in modelling the marginal distribution of each variable separately.

No restriction is given on the marginal model of the variables. A combination of the empirical distribution for the bulk of events and a parametric extreme value distribution function fitted to the extreme tail of data has been adopted here. For parameters which may have both a positive and a negative extreme such as the water level associated to wave height, both the positive and the negative extreme tail are modelled parametrically.

Fig. 12 shows an example of the modelled dependence structure for significant wave height H_{m0} and water level η in physical space. The model is clearly capable of describing the positive association between wave heights and water level for this condition and appears also to capture the relatively large spreading.

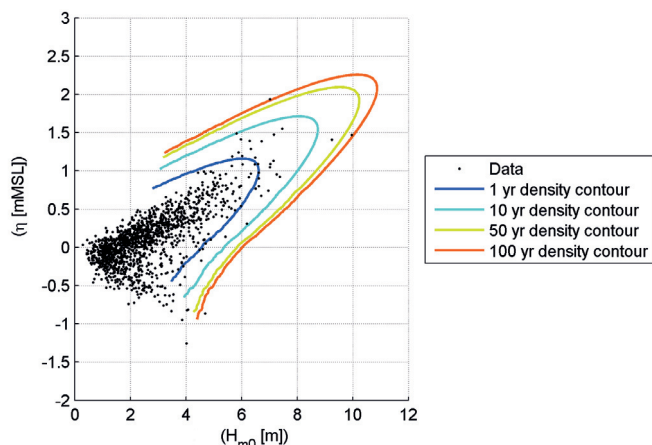


Figure 12: Dependence structure of H_{m0} and water level in physical space. Circle markers show data points and coloured lines mark the contours of constant probability density.

The applied joint probability model is event-based. This means that independent events of the conditioning parameter are extracted from the model data of hourly values. The combined inter-event time and inter-event level criterion was applied to isolate independent events of the conditioning parameter. The conditioned parameter was extracted from the model time series at the point in time of the peak of the conditioning parameter. Time averaging of the conditioned parameter is often carried out prior to data extraction in order to reduce the influence of phases in the analysis (the fact that the water level may not peak at exactly the same time as the peak wave height for instance).

4 Summary and conclusions

For design and operational purposes, detailed and sound knowledge of the site conditions at an OWF location are crucial for safe and cost-effective planning.

Long time series of reliable MetOcean conditions form the backbone of any sound statistical analysis. These long time series can be from measurements or from state-of-the-art numerical models that have been validated with measurements from different locations and for variable conditions.

Statistics on normal conditions give a good overview of the design-governing parameters with regards to their directional and monthly occurrence. Especially fatigue analyses based on scatter data and wind-wave-misalignment are important for the structural design. Weather statistics are a basic and most likely contractual document for the logistics planning of construction and operation of OWF's and may save costs during O&M operations as an optimised logistics approach can be chosen.

The extreme statistics presented here shows DHI's approach to determine the most severe loading conditions based on hindcast data, which are used for wind farms planned within the German EEZ waters. This ensures an optimized design including spatial and time variation of the extreme conditions as well as the joint occurrence of individual parameters.

In general the development of an offshore wind farm based on continuously improving MetOcean data and analysis will lead to a safe but not over-dimensioned and therefore cost effective construction which benefits a risk assessed planning.

5 References

- DHI: MIKE 21 & MIKE 3 FLOW MODEL FM Hydrodynamic and Transport Module Scientific Documentation. MIKE by DHI. Hørsholm, 2014.
- DHI: MIKE 21 Spectral Wave Module Scientific Documentation. MIKE by DHI. Hørsholm, 2014.
- DNV: Environmental Conditions and Environmental Loads, Offshore Standard DNV-RP-C205, Det Norske Veritas AS, 2010.
- DNV: Design of Offshore Wind Structures, Offshore Standard DNV-OS-J101, Det Norske Veritas AS, 2011.
- FORRISTALL, G.Z.: On the Statistical Distribution of Wave Heights in a Storm. *Journal of Geophysical Research*, Vol.83, p.2353-2358, 1978.
- FORRISTALL, G.Z.: Wave Crest Distributions: Observations and Second-Order Theory. *Journal of Physical Oceanography*, Vol.30, p.1931-1942, 2000.
- GL: Guideline for the Certification of Offshore Wind Turbines. Germanischer Lloyd, Hamburg, 2012.
- HEFFERNAN, J.E. and TAWN, J.A.: A conditional approach for multivariate extreme values. *Journal of the Royal Statistical Society*, p. 497-546, 2004.
- IEC: Design Requirements for Offshore Wind Turbines. IEC 61400-3, 2009.
- JOURNÉE, J.M.J. and MASSIE, W.W.: Offshore Hydromechanics, 1st Edition. Delft University of Technology, Maritime Technology Departement, Script. Delft, Netherlands, 2001.

- TROMANS, P. and VANDERSCHUREN, L.: Response Based Design Conditions in the North Sea: Application of a New Method, Offshore Technology Conference, Texas, USA, May 1995, OTC 7683, 1995.
- WMO: Guide to Wave Analysis and Forecasting, 2nd Edition. Secretariat of the World Meteorological Organisation, Genf, Schweiz, 1998.

6 Acknowledgements

Examples from OWF Sandbank presented in this paper with kind permission from Vattenfall Europe Windkraft GmbH.

Statistical Estuary Data Analysis in Models and Measurements – Some Methods and their Limitations

Marko Kastens

Summary

This paper considers the impact of people on a complex natural system like an estuary and how this influence can be assessed. The methods of mathematical modelling and analysis of measured data are briefly introduced and their advantages and shortcomings highlighted. The paper looks into statistical methods for time series analysis, using the example of the water level - a parameter that represents a mixed times series signal consisting of harmonic and non-harmonic components. Some spectral methods and the regression method are then chosen from the wide selection of methods available and their limitations and prerequisites are discussed. A procedure combining both methods is presented and applied to the example of the Elbe gauge in Hamburg-St. Pauli. The focus is on the method and its limitations; the results obtained are of secondary importance and are not discussed here. Reference is made to a relatively recent method of analysing non-stationary and nonlinear phenomena (Hilbert Huang Transform). The application of this method would, however, imply abandoning the classical view of the tidal wave as consisting of partial tides. Since it is hardly possible any more for one single person or institution to be familiar with the vast selection of analytical methods or to apply them, the analysis of and research into complex systems will require cooperative approaches in the future.

Keywords

statistical methods, regression method, spectral methods, FFT, LSSA, wavelet analysis, neural networks, water level development, estuary, Elbe, Hamburg-St. Pauli

Zusammenfassung

Anhand der Leitfrage, wie der Einfluss des Menschen auf ein komplexes natürliches System, wie dem Ästuar, beurteilt werden kann, werden die Methoden der mathematischen Modellierung und der Messdatenanalyse mit ihren Vor- und Nachteilen kurz dargestellt. Anhand des Parameters Wasserstand, der stellvertretend für ein aus harmonischen und nicht harmonischen Anteilen gemischtes Zeitreibensignal steht, werden statistische Methoden zur Zeitreihenanalyse behandelt. Aus der Fülle der Methoden werden einige Spektralmethoden und das Regressionsverfahren ausgewählt und ihre Limitierungen und Voraussetzungen besprochen. Ein aus beiden Methoden kombiniertes Verfahren wird vorgestellt und am Beispiel des Elbepegel Hamburg-St. Pauli angewendet. Im Vordergrund steht die Methode mit ihrer Begrenzung; die Ergebnisse sind sekundär und werden nicht weiter diskutiert. Eine relativ neue Analysemethode für nichtstationäre und nichtlineare Phänomene wird erwähnt (Hilbert-Huang-Transformation), die jedoch

die Aufgabe der klassischen Sicht der Tidewelle bestehend aus Partialtiden bedeutet. Die Fülle und Breite der vorhandenen Analysemethoden, die weder ein Mensch noch eine Institution kaum mehr überblicken oder anwenden kann, fordert zukünftig ein kooperatives Vorgehen in der Analyse und Erforschung komplexer Systeme.

Schlagwörter

Statistische Methoden, Regressionsverfahren, Spektrale Methoden, FFT, LSSA, Waveletanalyse, Neuronale Netze, Wasserstandsentwicklung, Ästuar, Elbe, Hamburg-St. Pauli

Contents

1	Introduction	186
1.1	Numerical simulation model:	187
1.2	Analysis of data gathered in field measurements:	187
2	Analysis of model results	188
3	Analysis of field measurements	188
4	The water level as the lead parameter	189
5	Methods of time series analysis	189
5.1	Harmonic analysis	190
5.1.1	Fast Fourier Transform (FFT):	190
5.1.2	Least-squares spectral analysis (LSSA):	194
5.1.3	Wavelet analysis	195
5.2	Regression analysis	195
5.2.1	Results	197
5.2.2	Evaluation of the results	198
5.3	Neural networks	199
5.4	Other methods	199
6	Conclusion	200
7	References	200

1 Introduction

The key question addressed in this paper is: How can we assess or, even better, quantify the past, current and future influence of humans on a natural system like an estuary? To answer this question, the system investigated (the estuary in this case) must be understood as comprehensively as possible.

An estuary is a highly dynamic and complex system, which is explained at length in the extensive literature, for example PUGH (2004), NIELSEN (2009) or MALCHEREK (2010)). It reacts time and again not only to external influences such as flood waves from upstream or changes in the sea connected to the estuary but also to human influence, and it is subject to permanent alteration and adaptation. It is of interest to understand how

phenomena such as the increase in the tidal range can be ascribed to certain events both regarding their cause and in quantitative terms?

Applying the following two methods helps - at least to some degree - to answer these questions. The first method is the numerical simulation model. Based on the relevant physical laws it endeavours to simulate estuarine dynamics on the computer. The second method is the analysis of data gathered in field measurements. Both methods come with their own major advantages and considerable deficiencies which are listed below.

1.1 Numerical simulation model:

- + is an internally consistent system which enables the user to vary just one parameter and observe the impact of the alteration on the overall system (system studies).
- + enables predictions about the system behaviour following complex changes of initial and boundary values.
- + provides a comprehensive view of the overall estuarine system.
- - maps natural processes only in an incomplete, model-based way. This results in inaccuracies in the calculations and related conclusions.
- - uses a discretisation and parameters adjusted to the former. If the discretisation is increased, which is in most cases due to a desire to reduce the inaccuracies, the two scales may no longer fit together (*up-/downscaling*) so that the effort of recalibrating the model is necessary. This requires considerable experience, knowledge and depending on the circumstances, also a lot of time.
- - always uses initial values (e.g. sediment covering of the bed) and boundary values (e.g. the water level at the seaward edge). These values are incomplete and/or inaccurate, which can also lead to increased inaccuracies in the calculations and predictions.

1.2 Analysis of data gathered in field measurements:

- + is based on reality. By contrast, model conditions are either purely hypothetical or they are *hindcasts* or *nowcasts* with the above mentioned inaccuracies.
- - is characterised by some inaccuracies in the measured values.
- - may have gaps due to the failure of measurement equipment or other adversities, resulting in time periods for which no data is available.
- - is often limited to individual spots. Since spatial representativeness has to be estimated, the informative value of field measurements has its limitations in many cases.
- - fails to distinguish between natural and anthropogenic influences, but only shows changes.
- - is incapable of providing forecasts. Extrapolating measurements into the future is only possible for short time periods and subject to uncertainties.

The above list of pros and cons shows that neither of the two methods is clearly superior to the other, but that their different perspectives rather complement each other and can open up a new dimension - as is the case with stereoscopic vision which requires two eyes.

The use of both methods depends on a fundamental understanding of the system. On the other hand, both methods can also enhance such understanding.

2 Analysis of model results

The overwhelming majority of mathematical simulation models yield large volumes of data which are then analysed, often with the aim of aggregating the data in order to reduce the data volume or elicit specific characteristics by which the model run can be distinguished from others. Generally speaking, this data constitutes characteristic numbers. The characteristic numbers are time and spatially referenced, in the latter instance to points, lines, surfaces and/or volumes, etc. Examples of such ratios are:

- Events in a time series: tidal low water, tidal high water, slack tide (zero velocity), ...
- Statistical parameters: mean values, global minima and maxima, standard deviation, variance
- Spectral characteristic numbers: amplitudes and phases of partial tides, spectrum of sea waves, periodograms
- Integrative parameters: sums, partial sums and balances
- Differential parameters: velocities and accelerations (for morphological parameters see MILBRADT (2011))

As many people find it easier to understand complex matters if they are represented by illustrations or animations, visualisation plays an important role in addition to these characteristic numbers.

A detailed description of the catalogue of characteristic numbers used by the BAW is provided in BAWiki (BAW 2014).

3 Analysis of field measurements

In principle, the aggregation examples listed above also apply to field measurements. However, preparing and harmonising the measurements requires significant additional work.

Preparing the measurements includes plausibility checks. Each measurement has to be verified, based on an individual error catalogue for the parameter (and for the measuring device, if necessary). If any errors are detected, the place affected must be marked, for example using a flag system. Some parameters will also need to be converted if the measurement relates to proxy information. The water level, for example, may be calculated based on pressure measurements after making adjustments for the atmosphere. Or: sediment concentration which is derived from turbidity after calibration using measurement samples.

In the next step, the measuring data from different data sources (measuring devices, companies, authorities), including meta data, are converted to a standardised data format (ASCII, XML, NetCDF, ...). Once the field data are harmonised and thus - in most cases - also standardised, they can be used for further analysis, although it is important to bear in mind that in contrast to model results measurements can have gaps because of missing data.

4 The water level as the lead parameter

After this general overview, a few methods of data analysis are employed in the following concrete examples. The parameter chosen as an example is the water level. Firstly, because it is an important lead parameter used in numerous environmental reports, and secondly because the German Federal Waterways and Shipping Administration (WSV) has been maintaining a gauge measurement network for many years - including databases and systems for storing and processing the data - so that at many gauges long time series are available which are sufficiently plausible and well documented.

The tidal Elbe and the gauge of Hamburg-St. Pauli which is located there, are used as the estuary example (for more information see Tide – Tidal River Development, EUROPEAN UNION (2014)). In addition, to compensate for the external influence factors (discharge and sea) the gauges of Helgoland and Neu Darchau are used.

5 Methods of time series analysis

Many of the model results and field measurements are available as time series. Time series analysis is a tool used almost on a daily basis in a multitude of disciplines. It is numbered among the statistical methods which are used everywhere: from simple descriptive statistics (e.g. mean values) via probabilities (e.g. expected values and confidences) through to statistical tests and distributions, regressions and, last but not least, time series analysis, (e.g. HARTUNG et al. (2005)) a broad array of statistical methods for evaluating and describing times series are available. Even spectral analysis may be considered a sub-field of statistics, although nowadays it tends to be regarded as a discipline in its own right. However, as consideration of statistics in general would exceed the narrow bounds of this paper, the following discussion focuses on harmonic and regression analysis.

An analysis often starts with a phenomenology or qualitative analysis: What are the relationships between the parameters; are there any correlations and are they strengthened or weakened by other factors, etc. The next step is to perform a quantitative analysis. A qualitative analysis is the first step and precondition for regression which is described below. It requires a model function to describe the interaction of all parameters involved in a qualitative way. In the subsequent regression analysis, these parameters are determined in quantitative terms.

Benchmarks are indispensable for verifying all the methods used. They enable verification of whether the respective method is suitable for the purpose of the analysis, which types of analysis may not work and what are the uncertainties inherent in the method. The time series analysis conducted here can be verified by a benchmark consisting of one or several completely artificial time series whose composition is 100 percent known (for example, the partial tides and their amplitudes and phases, the offset and, where applicable, the linear trend). When comparing the results obtained by different analysis methods, many insights can be gained as to whether or not a particular method is suitable for the purpose.

5.1 Harmonic analysis

The measurement of the water level in an estuary is influenced by the tide and by meteorological factors. The tides can be represented as partial tides with fixed frequencies. Each partial tide is a linear combination of the five basic frequencies of the sun-moon-earth system (e.g. GODIN (1988) and BAW (2007)). Hence, a tidal signal must have a certain harmonic component.

Harmonic analysis of the water level has a long tradition (CARTWRIGHT 2000), whereas spectral methods have been applied in rather more recent studies. In the German literature examples of spectral analysis methods can be found in GÖNNERT et al. (2004) or LIEBIG (1994) who uses the method to close gaps in water level recordings.

In view of the extensive literature, no introduction to the methods is provided here. Instead, this paper focuses on the special aspects of employing these methods for the analysis of tidal signals. The preconditions, limitations and recommendations relating to some harmonic analysis methods are outlined in the following sections.

5.1.1 Fast Fourier Transform (FFT):

The Fast Fourier Transform (FFT) is a standard spectral analysis method. This widely used method and its application can be found in numerous textbooks and reference books (BUTZ (2003) and OPPENHEIM et al. (2004), to name but a few).

In a spectral representation, partial tides become visible in an amplitude spectrum as lines which clearly stand out from their environment (Fig. 1). Besides the harmonic component, which expresses itself in the dominating spectral lines, there is an aperiodic component. The latter moves roughly along a decreasing exponential function (red line). The major share of the aperiodic signal's energy is located in the long-wave range (0 to 13 degrees/hour) before the first partial tide (Q1 in this case).

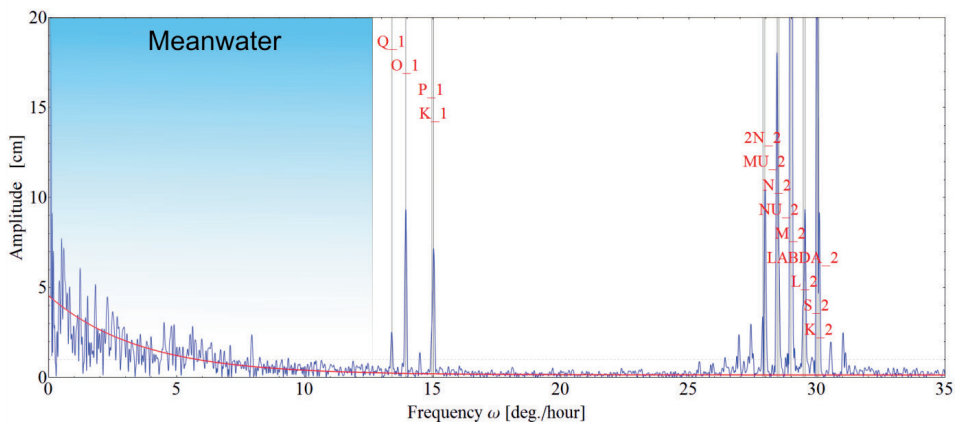


Figure 1: The beginning of an amplitude spectrum of a measured water level. The area of the mean water (0 to 13 degrees/hour) and several partial tides.

When applying FFT to analyse (tidal water level) time series, the following has to be taken into account:

General statements

- The signals caused by meteorological influences are mostly in the range of low frequencies (see Fig. 1). The influences decrease in power as the frequency increases. When considering the development of a spectrum over time, the peaks in the lower frequency band show variation, i.e. they are more of a stochastic nature. Partial tides form an almost constant peak in the amplitude spectrum over time.
- A low-pass filter enables the main aperiodic portion of the signal to be separated from the rest of the signal. This portion represents a kind of baseline for the tidal signal and is referred to as mean water in this paper. The remaining signal portion corresponds to the main tidal signal which varies on the baseline. From a physical perspective the separation is not complete because meteorological influences lead to signals which are also in range of the frequencies of the partial tides; and: long-wave partial tides are superimposed by the meteorological noise in the range of 0 to 13 degrees/hour (e.g. the partial tides SA and SSA).
- The fixed peaks in the amplitude spectrum allow the frequencies and thus partial tides to be determined. Peaks/partial tides that are not classified can be determined via a linear combination of the five astronomical basic frequencies.
- Since the frequencies of the meteorological signals are also those of the partial tides, these basic frequencies are also subject to natural variation. The amount of this variation can be estimated by using the spectral environment as a reference.

Prerequisites:

- Equidistant time series without any gaps are required. However, if the time grid is equidistant and zero padding is used where values are missing, it is also possible to use an incomplete time series. For the partial tide this means that the amplitude is diminished compared to the real amplitude, and that the phase information is incorrect. Where the gaps are small it is nevertheless possible to make a *qualitative* statement.
- The time distance between the samples determines the highest frequency (cut-off frequency Ω_{Nyq}) which is possible for this time series (derived from the Shannon/Nyquist sampling theorem in BUTZ (2003)). With a time distance of $dt = 600s$ the highest frequency is:

$$\Omega_{Nyq} = \frac{180 \text{ degrees} \cdot 3600 \text{ s/hr}}{600 \text{ s}} = 1080 \text{ degrees/hr} \quad (1)$$

This means that it is theoretically possible to detect the partial tide M74 (1072.41 degrees/hour).

- The degree to which partial tides - or general frequencies - can be resolved is determined by the length of the time series. For example, the resolution f_n of a one-year time series is:

$$f_n = \frac{360 \text{ degrees}}{365 \text{ days} \cdot 24 \text{ hrs}} \sim 0.041 \text{ degrees/hr} \quad (2)$$

The central peaks of the partial tides M2 (~ 28.984 degrees/hour) and S2 (30 degrees/hour) are thus $(30 \text{ degrees/hour} - 28.984 \text{ degrees/hour})/0.041 \text{ degrees/hour}$ located at a distance of ~ 25 grid points from each other on the discrete spectrum and can thus be sufficiently resolved or separated from each other.

- Resolvability also depends on the window function used (see below).

Recommendations:

Using window functions to reduce *sidelobes* (see Fig. 2). The rectangular window is inherent to the analysis in cases where only a limited set (e.g. an annual time series) of data is used. It is characterised by rather unfavourable properties (less than 100% of the energy in the central peak, unfavourable attenuation behaviour of the *sidelobes*, ...). The Hanning window employed in this example shows clearly improved properties in the central peak and regarding attenuation (see Fig. 2). No general recommendation regarding a specific window can be given. It is the signal's spectral composition and also the problem to be solved which determine the window functions to be used.

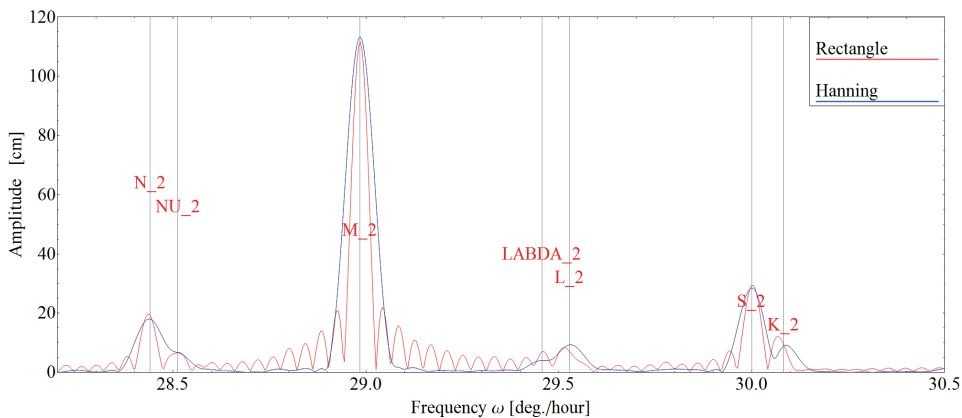


Figure 2: Amplitude spectrum without (rectangle) and with (Hanning) window function - the rectangular window has poor attenuation properties and it has a significant influence on the neighbouring amplitudes.

Using zero padding to hit the central peak A discrete data series yields a discrete spectrum whose frequencies are located on a specific grid (see above). It is rarely the case that the frequencies of the partial tides are located exactly on the grid of the discrete spectrum. By adding zeros (zero padding) to the data series, the frequency grid is changed (see above) without *information* being added to the data series. For example, if ten times the amount of zeros is added to the end of the data series, the grid in the frequency domain is refined by a factor of ten (interpolation, see Fig. 3). Eventually, the number of zeros to be added can be predicted, in order to resolve a specific frequency which is being searched as accurately as possible.

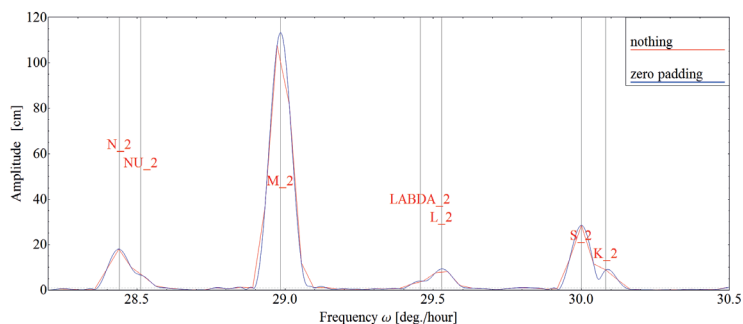


Figure 3: Amplitude spectrum with and without zero padding; while the latter increases the number of grid points, it does not add any information.

Time range analysed: 1 year. The length of the time series determines the resolution behaviour (see above). If the frequencies of two partial tides within one water level measurement are so close to each other that separate resolution is no longer possible, the following will happen: if the amplitudes are plotted over time (with an analysed time range of one month, for example, which is deferred by one day, respectively), the result is a modulation of the partial tides. Resolved partial tides show only minor variations over time. The time range analysed of one year has become the established time range for the gauges in the German Bight and its estuaries since it enables a good separation of all the partial tides.

Limitations/scenarios:

- How does the FFT react to a linear trend (e.g. an increase in the mean sea level (MSL))? The linearity theorem helps to answer this question: If a function can be decomposed into summands, the Fourier-transformed sum is the (complex!) sum of the Fourier-transformed summands. The following example refers to a data series which can be divided into a linear increase (trend for the mean sea level) and a sine wave (M2). The amplitude spectrum consists of the superposition of the Fourier-transformed lines and the Fourier-transformed sine (see Fig. 4). The lower part of the spectrum shows the trend; it can be easily separated from the partial tides (see above).

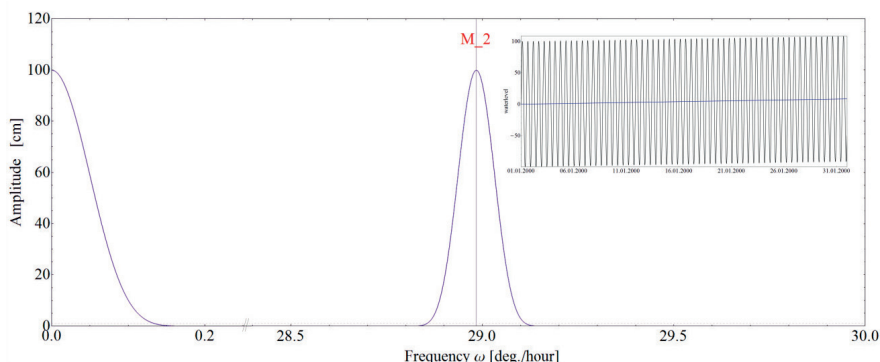


Figure 4: Amplitude spectrum of a linear trend with sine wave (M2) - the time series is depicted at the top right.

- How will the FFT be affected if a partial tide's amplitude varies or is subject to trends? The result reflects the mean of the amplitude over the time range analysed. It is possible to resolve long-term trends via annual analyses, for instance the nodal tide which has a period of roughly 18.6 years. Short-term fluctuations within a year cannot be represented and are averaged out.
- There is a dilemma: on the one hand, the time window for analysis needs to be reduced in size to increase the time resolution of the partial tides. On the other hand, the reduction in size results in a lower spectral resolution (see above) and the partial tides themselves are modulated by the neighbouring tides. Time resolution and spectral resolution are incompatible to a certain degree, similar to the *uncertainty principle* according to Heisenberg (BLATTER 2003).
- What, then, are the implications for the quality of the predictability of tide gauge levels based on partial tides? Predictions based on partial tides will be subject to minor errors if disturbances like the mean water and/or discharge have low dynamics and their influence on the specific area is low. This is the case in the summer, for example, when the dynamics of the mean water are low. If the location of the gauge is exposed to large discharge waves, the signal's prediction quality will be impaired by greater errors.

5.1.2 Least-squares spectral analysis (LSSA):

The most important technical drawback of FFT is that it requires equidistant time series. When time series are checked for plausibility this often results in numerous gaps in the time series so that the method can no longer be applied. To gain insights into the amplitudes and phases of the partial tides, however, use can be made of LSSA methods such as the Lomb periodogram (PRESS 2007). An even simpler method from the canon of LSSA methods is regression. The model function used is the sum of the partial tides to be analysed. The data are fitted to this model function. Just as with FFT, the resolution of the partial tides is a prerequisite. If this prerequisite is not fulfilled, the analysis will yield extremely high correlated amplitudes and phases which, depending on the initial value of the equation solver, can yield different values in a second analysis. Interpreting the analysis results is facilitated by information on the correlations, obtained through an analysis of variance and statistical tests, where appropriate. This also helps to ensure that the analysis is free from structural errors caused by an overparameterisation of the model function (PRESS 2007).

Besides its application to equidistant times series with data gaps the method described above can also be applied to long-term non-equidistant time series, for example tidal high water and tidal low water. These were used to estimate the amplitude of the nodal tide at the Helgoland gauge (here around 2.8 cm or approx. 2.5 percent of the tidal range, see Fig. 5).

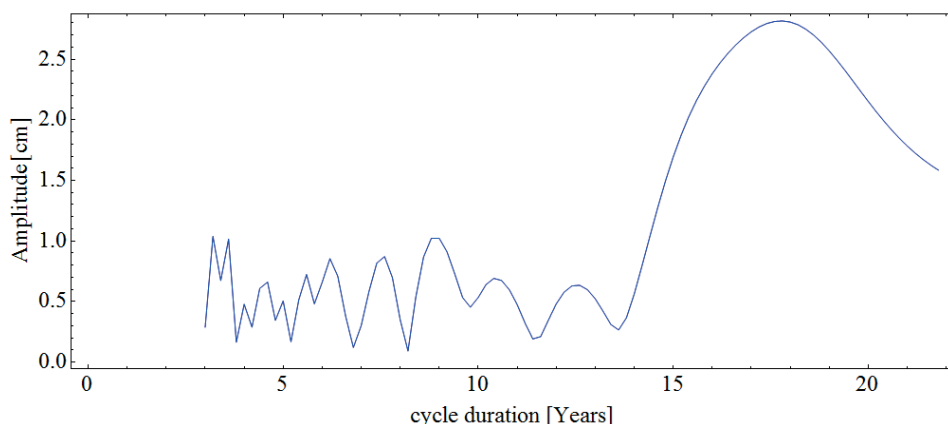


Figure 5: Amplitude spectrum based on a tidal range time series of approx. 61 years.

5.1.3 Wavelet analysis

The advantage of the wavelet analysis is that it allows for better localisation in time, i.e. a better time resolution of amplitudes. The Fourier transform, on the other hand, only yields a complex number at a frequency (amplitude and phase) for the analysed time range. Unfortunately, Heisenberg's *uncertainty principle* also plays a role in wavelet analysis (BLATTER (2003) and BERGH et al. (2007)). Since the localisation in time is achieved at the expense of resolvability in the domain of frequencies, the spectral representation of the separate partial tides can be lost. This is the case, for example, with measurements taken in estuaries where partial tides are numerous and their frequencies often are very close to each other (see Fig. 1). A wavelet analysis shows interference of the partial tides in the individual frequency ranges/bands; often these partial tides constitute a complex signal themselves which is difficult to interpret.

The wavelet analysis, but also the *short-time Fourier analysis* and/or filter banks (OPPENHEIM et al. 2004) can be used, if no decomposition into partial tides is required because the examination of spectral areas provides sufficient data.

5.2 Regression analysis

Regression analysis methods are more widely used than spectral methods in the German-speaking world. The regression method is not only easier to perform, the prerequisites for spectral methods (i.e. an equidistant time series without any data gaps) are also much more difficult to meet.

The relationships between the values recorded at the Elbe gauges on the one hand and discharge as well as the North Sea gauge at Helgoland on the other were determined by SIEFERT and JENSEN (1993) and SIEFERT (1998) as part of preliminary studies on a further extension of the River Elbe. They then tried to filter from the water level signals the relationships which had been determined via regression in order to obtain a better

view of the remaining signal dynamics. Their studies are mainly based on the annual mean values of discharge and tidal low and high water.

This approach is extended by NIEMEYER (2001) who describes a model function for the gauge's tidal low water and high water: The latter are proportional to the tidal low and high water levels at the Helgoland gauge, to the tidal range at the Helgoland gauge and to the discharge at the gauge of Neu Darchau. The regression is based on monthly means. While the influence of the mean water on extension works is mentioned, the parameter itself is excluded from the calculation.

The method developed by NIEMEYER (2001) was refined further by KASTENS (2007, 2009) and BAW (2007): instead of using monthly means it is now based on the individual values derived from the water level time series for tidal high and low water. The mean water is used in the model functions.

The method's findings and model functions are briefly outlined in the following:

- Tidal low water and tidal high water are a combination of mean water and tidal range. As a result, no conclusions concerning original influences can be drawn from the evolution of either. This is illustrated by the following two examples: a decrease in tidal low water can be caused by a lower mean water *or* an increase in the tidal range. The same is true for tidal high water: an increase can be due to either a greater tidal range *or* a higher mean water. Only the primary parameters mean water (potential) and tidal range (energy) are used in the following.
- The mean water can be derived as a regression line from the measured water level signal using a low-pass filter (see section 5.1.1). The rest of the time series (mainly the tidal signal) is used to obtain the tidal characteristic numbers (*tcn*): low/high water and tidal range. Thus, the measurement signal is divided in two parts which are analysed separately. Owing to this separation it is possible to determine the influence of the mean water on the tidal range. The complete signal has an autocorrelative component.
- The discharge influences tidal low water and tidal high water: Primarily, the discharge dampens the tidal wave's impulse coming from the sea and thus the tidal range. Due to the increased discharge, the mean water is elevated.
- An increased mean water results in greater water depth, thus reducing energy dissipation and increasing the tidal range. The mean water thus is of an ambivalent nature: an increase from seawards results in a greater tidal range, while an increase caused by the discharge overall results in a decrease.
- The density of the water is not considered here. It is possible to calculate the change in the water level dh due to a local change in density over time ($dh = \frac{\rho_{t1}}{\rho_{t2}} \cdot h$); ρ_{t1} and ρ_{t2} are the water densities at the time $t1$ ($t2$ respectively) and the water depth h .

Two model functions can be set up based on these observations. The tidal characteristic number (*tcn*) and the mean water consist of the following:

$$tcn_{Gauge} = a \cdot tcn_{Heligoland} + b \cdot Discharge_{NeuDarchau}^n + c \cdot mean\ water_{Gauge} + offset \quad (3)$$

tcn: tidal characteristic number (tidal range, high water, low water)

$$MW_{Gauge}(t) = d \cdot MW_{Heligoland}(t + dt) + e \cdot Discharge_{NeuDarchau}^{n2}(t) + offsetmw \quad (4)$$

The lag (dt) of the mean water at Helgoland to the gauge is determined only once, via a cross correlation of the two time series. The first maximum determines the lag. No lag has been determined for the gauge of NeuDarchau, since only daily values were available.

5.2.1 Results

The findings of the above procedure are summarised to provide a result for the Elbe gauge of Hamburg-St. Pauli.

The calendar year 1997 is defined as the reference time range for which the parameters of the two model functions discussed above will be identified by means of a regression. Starting at Helgoland, the lag of the mean water is 331 minutes for the gauge of Hamburg-St. Pauli. This leads to the following values for the functions' parameters (see Tab. 1):

Table 1: Regression parameters for calendar year 1997; *: confidence interval; **: $n=n2=1$ for the gauge of Hamburg St. Pauli.

tidal range St. Pauli 1997	Value	CI* low (95 %)	CI* high (95 %)
a (influence of tidal range Helgoland)	0.737	0.715	0.760
b (influence of discharge NeuDarchau)	0.007	0.005	0.009
c (influence of mean water St. Pauli)	0.092	0.074	0.110
Offset	123.752	112.836	134.667
n^{**}	1		
mean water St. Pauli 1997	Value	CI* low (95 %)	CI* high (95 %)
d (influence of mean water Helgoland)	1.268	1.264	1.271
e (influence of discharge NeuDarchau)	0.033	0.033	0.033
Offsetmw	-111.983	-113.757	-110.209
$n2^{**}$	1		

The powers n and $n2$ are set to 1 in both model functions; first, because due to the small influence of the discharge on the St. Pauli gauge the algorithm does not converge and second, because the residual variance - as a measure of the quality - is almost the same. The correlation between the parameters is insignificant. The offset shows a higher correlation since all single components have an offset. However, a model function without an offset would also be possible, although it would provide a less satisfactory explanation of the measured signal.

Retrospectively, these functions are used to make *hindcast* calculations. Hindcast calculations imply that the entire system of the tidal Elbe is in a stable dynamic state and that the influences of mean water and discharge on the tidal range do not change over time. The difference between the measured values and the *hindcast* values yields the respective time series, adjusted for external influences (sea water and discharge), which is represented as the annual mean values of the tidal range (see Fig. 6) and mean water (see Fig. 7).

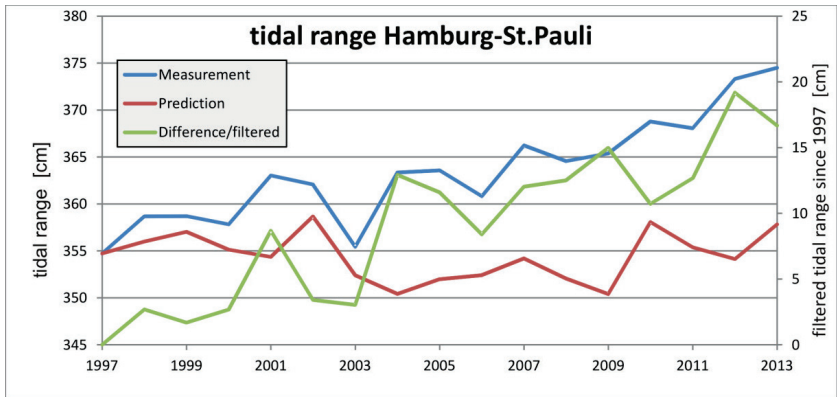


Figure 6: Mean annual tidal range at the gauge of Hamburg-St. Pauli based on measurements and forecasts as well as their difference, which represent the signal adjusted for external influences.

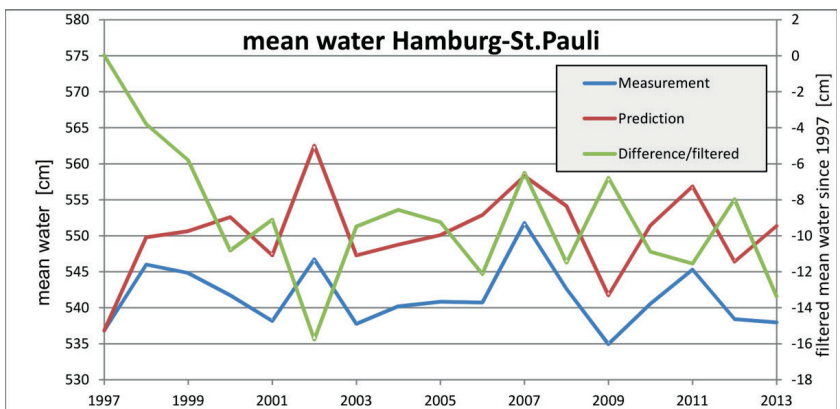


Figure 7: Mean annual mean water at the gauge of Hamburg-St. Pauli based on measurements and forecasts as well as their difference, which represent the signal adjusted for external influences.

5.2.2 Evaluation of the results

Two aspects are striking when evaluating the results (Fig. 6 and Fig. 7).

- Since 1997 at least, the tidal range in Hamburg-St. Pauli has been clearly increasing.
- In the years immediately following 1997 the mean water went down by around 10 cm and then stabilised.

Neither of these observations is entirely ascribable to external occurrences, but rather to inherent factors that triggered the changes. The Elbe estuary was affected by major changes during this period: not only was the fairway deepened from 13.5 to 14.4 m, significant morphological changes also took place in the Elbe delta, anthropogenic changes in the port of Hamburg and alterations in the lateral areas of the Elbe and the Nebenelbe which are in most cases associated with a decrease in volume.

NIEMEYER (2001) provides a theoretical discussion of the impacts of extension projects on the mean water. There is a close coincidence in time between the drawdown of the mean water and the fairway deepening; hence, a causal relationship is highly probable. The evolution of the tidal range presents a different picture, though, with a steady increase which is due to, firstly, the fairway deepening measures but also to the other influences mentioned before (anthropogenic and natural). This is where the regression method clearly reaches its limitations: although it indicates changes regarding a reference time range which are mainly adjusted for external influences, it is not capable of identifying the causes (anthropogenic or natural) of these changes.

Another shortcoming of the method relates to long-term trends since it implies stationarity. If it is applied to a system which is subject to trends, the method learns the conditions of the reference time range but not the trend. For an evaluation it is therefore important to know the overall history and its fundamental processes and trends. In the present case, the trend of an increasing tidal range at the gauge of Hamburg-St. Pauli has already been observed over a long period of time (see WSV & HPA (2011) or FICKERT and STROTMANN (2009)). Its causes are diverse and not all of them have been identified. They are not the subject of this paper.

To conclude it should be noted that the reliability of such methods is increased if the time series used cover longer periods. Thus, after filtering the residual natural variability which is still contained in the filtered time series can be detected.

5.3 Neural networks

The core of a neural network is a regression method. The network's topology determines the model function whose parameters are fitted (trained) using the data available. As with all regression methods there is a risk of overparameterisation if several input variables are highly correlated (multicollinearity). Since the input vector is often chosen randomly and thus cannot be reproduced, the learning algorithm used in neural networks can result in variations in the fitted parameters (weighting matrix) between trainings with the same data record. If the complexity of the model function becomes greater, the number of extrema in the solution space of an algorithm can increase. In combination with a randomly generated input vector for training reproducibility of the solution becomes a matter of chance.

A good understanding of the system helps to avoid using an overparameterised model along with all the deficiencies described above and to map the main processes in the network topology. To avoid multicollinearity, the correlations between the input variables have to be checked.

5.4 Other methods

Section 4.1.3 discusses the dilemma of Fourier and wavelet analyses: a very accurate frequency localisation requires long time series or, if a very high time resolution is used, this is only achieved at the expense of the desired high frequency resolution. There is an alternative, however - a relatively recent method called Hilbert Huang Transform (HHT) (see WIKIPEDIA FOR SOME EXAMPLES (2014)). This is a method that works well for signals from nonlinear and nonstationary systems. It consists of two major procedures:

the Empirical Mode Decomposition and the Hilbert Spectral Analysis. Its fundamental principle is that of instantaneous frequency (HUANG 2006). The output variables are the amplitude and frequency, both of which change over time. This method leaves behind it the familiar notion of the tide consisting of partial tides (which is in any case only a theory).

6 Conclusion

In view of the initial question this paper has discussed a small-scale example of a time series analysis of the water level in which a spectral method is combined with a simple statistical regression. The methods used must be assessed critically, in the light of their limitations, to ensure that the wrong conclusions are not drawn. In the example discussed here, the limitation is the trend: the regression method cannot account for trends because its basic assumption is stationarity.

The example does not mean that the method is restricted to the parameter water level because nearly all of the parameter time series concerning estuaries contain both a harmonic component due to the tide and a stochastic component related to meteorological influences. Which methods or combinations of methods are best suited for the time series analysis depends on the signal and the specific problem.

Using benchmarks helps to ensure that an appropriate analysis method is chosen - in this case, this would mean the use of completely artificial time series whose compositions are 100 percent known. Thus the plausibility of the conclusions and the limitations of a method can be easily verified.

If there is no certainty in this respect it is also possible to use more than one method, for example an analytical method combined with a numerical simulation model. The latter is used to identify the influence factors of individual components, for example the impact of natural dynamics on the tidal range at the gauge of Hamburg-St. Pauli.

Taking this generalised approach even further, considering the methods of mathematical modelling and signal analysis, it becomes obvious that, given the broadness of the topic, it is hardly possible for one single person to know about, let alone master, all these methods. Inter-institutional cooperation is therefore required in order to obtain information from the different methods and evaluate this information. Cooperation in research associations is the key to further developing the methods.

7 References

- BAW: Tidewasserstandsanalysen in Ästuaren am Beispiel der Unter- und Außenelbe. Hamburg, 2007.
- BAW: Hydraulic Engineering Methods. http://www.baw.de/methoden_en/index.php5/Hydraulic_Engineering_Methods, last visited: 27.03.2014.
- BERGH, J.; EKSTEDT, F. and LINDBERG, M.: Wavelets mit Anwendungen in Signal- und Bildbearbeitung. Springer-Verlag Berlin Heidelberg, Berlin, Heidelberg, Online-Ressource, 2007.
- BLATTER, C.: Wavelets. Eine Einführung; [für Mathematiker, Ingenieure und Informatiker]. Vieweg, Braunschweig, Wiesbaden, X, 178 p., 2003.

- BUTZ, T.: Fouriertransformation für Fussgänger. Teubner, Stuttgart, Leipzig, Wiesbaden, 183 p., 2003.
- CARTWRIGHT, D.E.: Tides. A scientific history. Cambridge University Press, Cambridge, New York, XII, 292 p., 2000.
- EUROPEAN UNION: Tide - Tidal River Development. http://www.tide-project.eu/index.php5?node_id=Reports-and-Publications;83&lang_id=1, last visited: 27.03.2014.
- FICKERT, M. and STROTMANN, T.: Zur Entwicklung der Tideverhältnisse in der Elbe und dem Einfluss steigender Meeresspiegel auf die Tidedynamik in Ästuaren. HTG-Kongress Lübeck, 2009.
- GÖNNERT, G.; ISERT, K.; GIESE, H. and PLÜB, A.: Charakterisierung der Tidekurve. Die Küste, 68, 2004.
- HARTUNG, J.; ELPELT, B. and KLÖSENER, K.-H.: Statistik. Lehr- und Handbuch der angewandten Statistik. Oldenbourg, München, Wien, XXVII, 975 S. p., 2005.
- HUANG, N.E. 2006: Compact Course in The Hilbert-Huang-Transformation (HHT) For Nonlinear And Non-Stationary Time Series Analysis. Braunschweig, 2006.
- KASTENS, M.: Tidewasserstandsanalyse in Ästuaren am Beispiel der Elbe. Die Küste, 72, 2007.
- KASTENS, M.: Analyses of time series and model hindcast of water levels after the last deepening of the Elbe estuary - a comparison. Poster Proceedings - ICCE 2008: 31st International Conference on Coastal Engineering, 31st August to 5th September 2008 Hamburg, Germany. Stolberg, 6-14, 2009.
- LIEBIG, W.: Schließen von Lücken in Pegelaufzeichnungen. Die Küste, 56, 1994.
- MALCHEREK, A.: Gezeiten und Wellen. Die Hydromechanik der Küstengewässer. Vieweg + Teubner, Wiesbaden, IX, 301 p., 2010.
- MILBRADT, P.: Analyse morphodynamischer Veränderungen auf der Basis zeitvarianter digitaler Bathymetrien. Die Küste, 78, 33-57, 2011.
- NIELSEN, P.: Coastal and estuarine processes. World Scientific, Singapore, 343 p., 2009.
- NIEMEYER, H.D.: Change of mean tidal peaks and range due to estuarine waterway deepening. Coastal Engineering Proceedings; No 26 (1998): Proceedings of 26th Conference on Coastal Engineering, Copenhagen, Denmark, 1998, 2001.
- OPPENHEIM, A.V.; SCHAFFER, R.W. and BUCK, J.R.: Zeitdiskrete Signalverarbeitung. Pearson Studium, München, Boston [u.a.], 1031 p., 2004.
- PRESS, W.H.: Numerical recipes. The art of scientific computing. Cambridge University Press, Cambridge, UK, New York, xxi, 1235 p., 2007.
- PUGH, D.: Changing sea levels. Effects of tides, weather, and climate. Cambridge University Press, Cambridge, U.K, New York, XIII, 265 p., 2004.
- SIEFERT, W.: Tiden und Sturmfluten in der Elbe und ihren Nebenflüssen. Die Entwicklung von 1950 bis 1997 und ihre Ursachen. Die Küste, 60, 1998.
- SIEFERT, W. and JENSEN, J.: Fahrrinnenvertiefung und Tidewasserstände in der Elbe. Hansa, Vol. 130, 10, 1993.
- WIKIPEDIA: Hilbert Huang Transform. http://en.wikipedia.org/wiki/Hilbert%E2%80%9393Huang_transform, last visited: 15.04.2014.
- WSV & HPA: Abschlussbericht der Beweissicherung zur Anpassung der Fahrrinne der Unter- und Außenelbe an die Containerschiffahrt. Hamburg, 2011.

Modelling Water Quality in the Elbe and its Estuary – Large Scale and Long Term Applications with Focus on the Oxygen Budget of the Estuary

Andreas Schöl, Birte Hein, Jens Wyrwa and Volker Kirchesh

Summary

The current status of numerical water quality modelling of the German part of the Elbe and its estuary (km 0 to 727) with the model QSim is presented and simulation results are compared with field data for validation. Based on a large scale 1d approach, a consistent input signal from the river (upper 585 km) is generated to investigate the context between phytoplankton development and oxygen deficits in the estuary with enhanced mean water depth (> 10 m). In the shallow and eutrophic river, phytoplankton biomass is produced up to a seasonal mean (May-October 2006) of nearly 150 µg chl a l⁻¹ causing oxygen supersaturation. In the freshwater part of the estuary, the algae biomass declines sharply and oxygen deficits occur. Our simulations demonstrate that net algae growth rates become negative due to light limitation, while high grazing losses by zooplankton (seasonal mean of 0.5 per day) causes a decline of the biomass. Due to the input of algal derived and easily degradable organic carbon imported from the river and organic carbon from algal die-off, the Elbe Estuary becomes heterotrophic and depleted of oxygen in summer.

Referring to the large scale 1d approach, we simulate and validate the long term development of the water temperature, phytoplankton, and oxygen of the Elbe Estuary for a 13-year period (1998-2010). Recent developmental steps towards more-dimensional water quality modelling with QSim by offline coupling with a hydrodynamic model are outlined. This approach is tested concerning the horizontal water temperature distribution of a side channel system of the estuary.

Keywords

water quality model, Elbe Estuary, water temperature, oxygen, phytoplankton

Zusammenfassung

Das eindimensionale Gewässergütemodell QSim wird für die deutsche Elbe einschließlich ihres Ästuars (km 0 bis 727) angewendet. Durch den Vergleich von Simulations- und Messergebnissen wird eine Validierung für das Modell gezeigt. Mit der Berechnung der Gewässergüte für den 585 km langen Flusslauf der Elbe wird ein konsistentes Eingangssignal für das Ästuar erzeugt, um damit den Sauerstoffhaushalt und die Entwicklung des Phytoplanktons im Bereich des Hamburger Hafens und der Seeschiffahrtsstraße mit seinen großen mittleren Wassertiefen (> 10 m) zu modellieren. Die Simulationen für das Jahr 2006 zeigen, dass in der Vegetationsperiode von Mai bis Oktober hohe Algenbiomassen von im Mittel etwa 150 µg chl a l⁻¹ im flachen und eutrophen Flussabschnitt der Elbe produziert werden. Diese hohe Primärproduktion führt auch zu deutlichen Sauerstoffübersättigungen auf der Fließstrecke. Im anschließenden limnischen Abschnitt des Elbe-Ästuars geben dann die Algengehalte deutlich zurück. Parallel

dazu treten Sauerstoffdefizite auf. Die Analyse der Modellergebnisse bezüglich des Rückgangs der Algen zeigt, dass das netto-Algenwachstum in den tiefen Abschnitten des Ästuars aufgrund der Lichtlimitierung negative Raten annimmt und gleichzeitig starke Verluste durch den Wegfraß durch das Zooplankton (Saisonmittel von 0.5 pro Tag) auftreten. Der Eintrag von lebenden Algen und leicht abbaubaren algenbürtigen Kohlenstoffverbindungen aus dem Fluss in das Ästuar führt im Sommer zu heterotrophen Bedingungen im Elbe-Ästuar und als Folge zu Sauerstoffdefiziten.

Mit dem großskaligen eindimensionalen Modellansatz wird zudem für einen 13-jährigen Zeitraum (1998-2010) die Wassertemperatur, das Phytoplankton und der Sauerstoff für den Flusslauf und das Ästuar simuliert und validiert. Darüber hinaus werden neue Entwicklungen vorgestellt, wie das Modell QSim mit mehrdimensionalen hydrodynamischen Modellen offline gekoppelt und betrieben werden kann. Für ein Testgebiet wird die horizontale Verteilung der Wassertemperatur in einem durch Nebenrinnen charakterisierten Abschnitt des Ästuars simuliert und mit Beobachtungswerten verglichen.

Schlagwörter

Gewässergütemodell, Elbe-Ästuar, Wassertemperatur, Sauerstoff, Phytoplankton

Contents

1	Introduction	204
2	The model QSim	206
	2.1 Concept of coupling QSim with hydrodynamic drivers	206
	2.2 Description of QSim modules	207
3	QSim application for the Elbe and its estuary	211
	3.1 Model area	211
	3.2 Boundary conditions	212
	3.3 Model calibration	213
4	Results	215
	4.1 Water levels in the estuary	215
	4.2 Longitudinal profiles of water quality parameters	216
	4.3 Validation of the long term simulation of water quality parameters	221
	4.4 Simulation of water temperature distribution in the Elbe Estuary with 2d QSim	225
5	Discussion	225
6	Conclusions and outlook	228
7	Acknowledgements	229
8	References	229

1 Introduction

Water quality conditions and management in estuaries have received increasing attention in recent years. One significant ecological issue in estuaries and adjacent coastal waters is

the appearance of low oxygen conditions (hypoxia) (RABALAIS et al. 2009, HOWARTH et al. 2011, ZHU et al. 2011).

It has been shown for many river systems that excessive nutrient loading in the catchment can foster phytoplankton blooms and eutrophication in the middle and lower part of rivers (SALMASO and BRAIONI 2008, PUSCH et al. 2009). The high organic matter load caused by phytoplankton leads to heterotrophic conditions in the estuaries of eutrophic rivers, mainly indicated by oxygen deficits (PAERL and PINCKNEY 1998, GARNIER et al. 2001). In well-mixed estuaries, the longitudinal location of low oxygen zones seems to be specific for each estuary. While in less eutrophied estuaries the oxygen minimum often occurs in the maximum turbidity zone, the oxygen minimum in more heavily loaded estuaries can be observed in the freshwater section (GARNIER et al. 2001). In addition to the amount of organic matter loading and the amount of freshwater (river discharge) entering the estuary, the bathymetry is an important factor influencing the oxygen concentration in the estuary.

In the freshwater zone of the Elbe Estuary, low oxygen conditions in summer regularly occurred during the last four decades. The phenomenon of hypoxia in the Elbe Estuary has been described by CASPERS (1984), ARGE ELBE (1984), FLÜGGE (1985) and more recently by BERGEMANN et al. (1996) and YASSERI (1999).

While most of the biogeochemical processes of oxygen depletion in estuaries are qualitatively well-known, a temporally and spatially detailed quantitative analysis is needed to fulfil requirements concerning management strategies, e.g. eutrophication control by nutrient reduction. Numerical modelling of surface water quality can be a useful tool to support these analyses and has been used extensively as a scientific and management tool to analyse and quantify oxygen deficits in estuaries (BILLEN et al. 2001, ZHENG et al. 2004).

This paper presents an approach of numerical modelling of water quality, particularly water temperature, algal as well as zooplankton development and oxygen conditions, in the German part of the Elbe and its estuary. To simulate water quality components, the physical transport and the biogeochemical processes have to be linked. Therefore, a hydrodynamic model is coupled with a water quality model simulating the biogeochemical processes. This general model coupling approach was realized in the Chesapeake Bay Model Package (CBMP) by CERCO and COLE (1993) and is nowadays realized in many "software families". Recently, a coupled hydrodynamic and biogeochemical model for the Schelde Estuary is applied by ARNDT et al. (2011) and GYPENS et al. (2013). Other developments are concepts of dynamic coupling of hydrodynamic models to biogeochemical moduls, such as Framework of Aquatic Biogeochemical Models (FABM) (BRUCE et al. 2013).

The model coupling approach can be applied for one or more dimensions to fulfil different resolutions in space, depending on the investigation objectives. In 1d model approaches, the systems are strongly simplified by considering a fully mixed water body and by neglecting lateral as well as vertical resolution. Nevertheless, these approaches are successfully used for large scales (where dominant longitudinal gradients exist) like catchments or large river sections, especially in the context of global change studies (BILLEN et al. 2001, DUCHARNE et al. 2007, QUIEL et al. 2011). In contrast, more-dimensional approaches are useful concerning the research on a smaller scale like harbour basins, distinct bays and also whole estuaries in which drying and flooding plays a major role.

2 The model QSim

The water quality model QSim simulates physical, chemical and biological processes in rivers (KIRCHESCH and SCHÖL 1999; SCHÖL et al. 2002, MATZINGER et al. 2013). QSim was established in the 1980s and has been expanded and improved since then (SCHÖL et al. 2006 a/b, BECKER et al. 2010, QUIEL et al. 2011).

QSim is a deterministic model with a modular structure, i.e. processes concerning the heat budget, nutrient as well as oxygen budget and plankton development are described as separate modules in the form of differential and algebraic equations without any stochastic effect.

2.1 Concept of coupling QSim with hydrodynamic drivers

A hydrodynamic model is needed for water quality simulation with QSim. Depending on the dimension of the hydrodynamic model, a 1d, 2d or 3d QSim simulation of water quality can be achieved. The 1d approach of QSim is coupled off-line with HYDRAX (OPPERMANN 1989). QSim and HYDRAX are integrated by the graphical user interface GERRIS (BFG 2013). The 2-dimensional approach of QSim has been recently coupled off-line with casu (WYRWA 2003) (Fig. 1). In this approach, the existing QSim code is embedded as FORTRAN-subroutines by implementation of shell-routines wrapping.

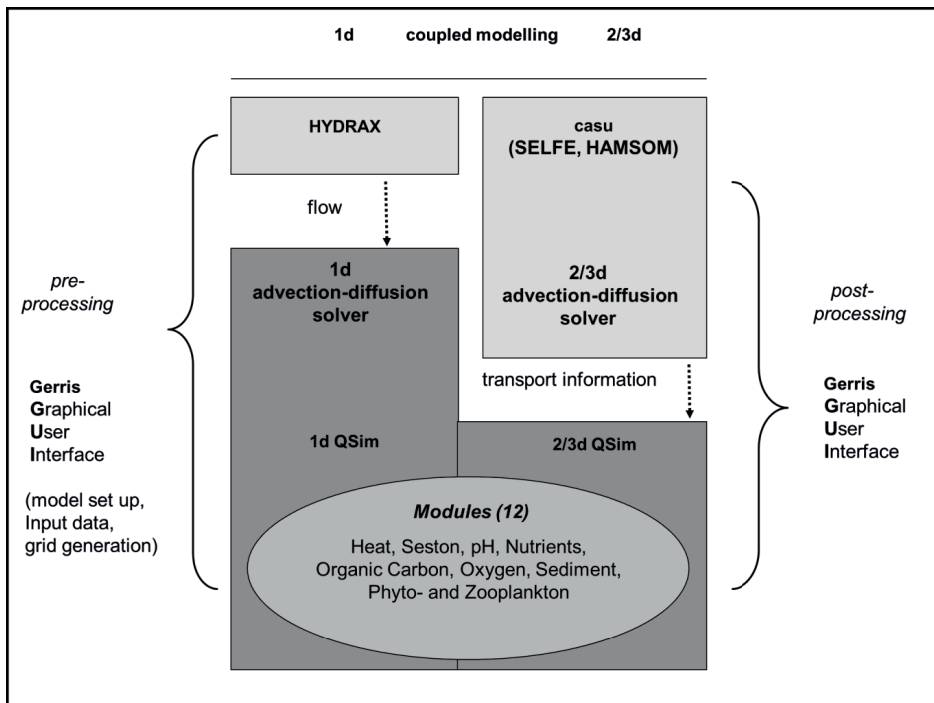


Figure 1: Concept of coupling between the water quality model (QSim) and hydrodynamic models (HYDRAX or casu).

1d QSim approach with HYDRAX

HYDRAX is a 1d hydrodynamic model to simulate unsteady flow in a network of water bodies (OPPERMANN 1989, 2010). In HYDRAX, the Saint Venant equations are solved numerically with the implicate difference scheme of Preismann (CUNGE et al. 1980). The non-linear system of equations is solved iteratively with two different Double Sweep methods for tree-based and network-based graphs (CUNGE et al. 1980, FRJASINOV 1970). The flow can be calculated either in a stationary or in a dynamic non-stationary way. HYDRAX calculates the hydraulic conditions (river discharge, water level, mean water depth, and flow velocity) along the river stretch using cross-sectional profiles, bed roughness and slope of the river stretch. At the upper boundary and the inflowing tributaries, measured river discharge is prescribed. At the lower boundary HYDRAX is forced by measured water levels. Data on the hydraulic conditions along the investigated water body are provided to QSim using the common grid structure.

Water quality input data are needed for the tributaries, for the upper and - in case of modelling an estuary with tidal changes of the flow direction – for the lower model boundary in order to indicate the starting conditions for model calculations. Generally, the biogeochemical processes in QSim are computed on an hourly basis. Due to stability reasons, sub-time steps are used to calculate the advection and diffusion of the 70 biological variables. For the case study Elbe, the second-order QUICKEST transport algorithm, which includes a limiter function, is used (LEONARD 1961).

2d QSim approach with casu

The 3d flow solver casu (WYRWA 2003), which is based on the numerical proposals of CASULLI and CHENG (1992), is used as a hydrodynamic driver. It solves the 3d shallow water equations. When discretised with only one depth layer, the computation is reduced to a 2d depth-averaged model. At downstream/seaward boundaries water levels are set, which is appropriate also for flow reversal in tidal motion. At upstream/landward boundaries model data from the 1d approach are used. Internally casu distributes both hydrodynamic conditions along the boundary faces. The water level is set constant along the downstream boundary line. The flow velocities at the boundaries are distributed assuming that each vertical would be a straight rough channel and all verticals have the same water level slope. Casu computes transient solutions. Stationary flow fields are obtained when the flow converges gradually to stationary boundary conditions. The 3d hydrodynamic driver casu in contrast to the 1d hydrodynamic model HYDRAX already includes an advection-diffusion (transport) solver which is needed for hydrodynamically active concentrations (salt, suspended sediment) and turbulence quantities. Casu uses ELM for advection and finite differences for diffusion (WYRWA 2003). The offline stored transport-matrices can be used directly by QSim by multiplication with the concentration fields (discretised as vectors).

2.2 Description of QSim modules

The model QSim comprises twelve modules that can be grouped into a heat module, which calculates the water temperature, seven biogeochemical modules for process description of the seston budget, pH-value, nutrients dynamics of nitrogen (N), phospho-

rous (P) and silicium (Si), organic carbon and oxygen content, three biological modules for phyto- and zooplankton and benthic filter feeders (not applied for the Elbe) and a sediment module which calculates early diagenesis of sediment dynamics including oxygen, carbon and nutrient fluxes. For all modules we hereby provide brief descriptions and references. Input variables and parametrisation of processes are given in Tab. 2 and 3.

Heat module

The basis for calculating the heat budget of a water body is the simplified heat balance equation. The water temperature is influenced by radiation (q_S), evaporation (q_V), convection (q_K), the temperature of the riverbed (q_{US}), the sediment-water heat exchange (q_U) and direct discharges (q_E), i.e. tributaries and thermal power stations, into the river. Input variables are measured data of global radiation, air temperature, relative humidity, cloudiness, and wind velocity (Tab. 2) at distinct sites of the model area. Further information of components and their parameterisation are given in IKSR (2013).

The heat balance equation can be written as:

$$\frac{\partial T_W}{\partial t} = \frac{q_S - q_V - q_K + q_{US} - q_U + q_E}{c_W * H * \rho_W} \quad (1)$$

T_W - water temperature [°C]

t - time [h]

q_S - heat flux from radiation [kJ*h⁻¹*m⁻²]

q_V - heat flux from evaporation [kJ*h⁻¹*m⁻²]

q_K - heat flux from convection [kJ*h⁻¹*m⁻²]

q_{US} - heat flux from radiation into the sediment [kJ*h⁻¹*m⁻²]

q_U - sediment - water heat exchange [kJ*h⁻¹*m⁻²]

q_E - heat flux from direct discharge [kJ*h⁻¹*m⁻²]

c_W - special heat capacity of water = 4.1868 10³ J*kg⁻¹*K⁻¹

H - average water depth of the cross section [m]

ρ_W - density of the water = 1,000 kg*m⁻³

However, this equation of the heat balance cannot be solved explicitly, as the different components are not independent of each other. Therefore, the equation is solved by iteration, taking into account that short time steps for iteration should be used in cases of low water depth in order to avoid large differences in water temperature during the iteration loops.

Biogeochemical modules

Nutrients (N, P, Si)

QSim calculates the important processes of the cycling of nutrients (KIRCHESCH and SCHÖL 1999). The nitrogen components are total nitrogen, ammonium, nitrite and nitrate. Main processes are assimilation by phytoplankton, ammonification by decay of organic matter, nitrification and denitrification. The growth of suspended nitrifiers (*Nitrosomonas* and *Nitrobacter*) is depending on water temperature, oxygen concentration and substrate concentration (ammonium or nitrite). The nitrification/denitrification process and the N-fluxes from/to the sediment are implemented in the sediment module. The balance of the particulate fraction of total phosphorus and the dissolved fraction of

ortho-phosphate is simulated. While ortho-phosphate is lost due to assimilation by algae, it is produced by respiration of algae, rotifers and benthic filter feeders (mussels) as well as by the decay of detritus. Faeces released by rotifers and benthic filter feeders are sources of ortho-phosphate after bacterial degradation. Dissolved silica is modelled, because it is a structural element of the cell wall of diatoms and can limit their growth. Besides the silica uptake by diatoms, a release of silica from the sediment during decay of diatoms is considered in the model.

Organic carbon

The hydrolysis of the biodegradable organic matter fractions to monomeric substances is calculated following the conceptual model of organic matter degradation by BILLEN (1991), who gave a general view of bacterial growth in aquatic systems. The organic matter is divided into five fractions, where the particulate refractory organic matter is a permanent sink and not linked to degradation processes by bacteria. The four other fractions are biodegradable, characterized by different hydrolysis rates. The biomass of each biological group that enters the organic matter fractions by mortality, excretion or in form of faeces is added equally to each of the five fractions. The substrate uptake rate of bacteria only depends on the available concentration of monomeric substances:

$$up_{Bac} = up_{Bac,max} * \frac{C_M}{C_M + K_{S,C_M}} * f_{Bac}(T) \quad (2)$$

- $up_{Bac,max}$ - maximal uptake rate of bacteria [d⁻¹]
- C_M - concentration of monomeric substances [mgC*l⁻¹]
- K_{S,C_M} - half saturation constant of bacteria for monomeric substances [mgC*l⁻¹]
- $f_{Bac}(T)$ - temperature dependence ratio [-]

In the QSim modelling approach, bacterial biomass is linked to total biodegradable carbon and to the degradability of the substrate. Both variables are derived from the ratio between carbon-based BOD₅ and chemical oxygen demand (COD). This approach enables to calculate the bacterial biomass from routine measurements, although the bacterial biomass itself was not measured (BERGFELD 2002).

Biological modules

Phytoplankton

In QSim, three major taxonomic phytoplankton groups with different physiological characteristics can be distinguished (Tab. 2). The algal biomass balance is:

$$\frac{dA}{dt} = (\mu - k_{resp} - k_{mort}) * A - A_{graz} - A_{sed} \quad (3)$$

- A - algal biomass [mg*l⁻¹]
- μ - actual growth rate [d⁻¹]
- k_{resp} - respiration rate [d⁻¹]
- k_{mort} - mortality rate [d⁻¹]
- A_{graz} - grazing losses [mg*l⁻¹*h⁻¹]
- A_{sed} - sedimentation losses [mg*l⁻¹*h⁻¹]
- t - time [h]

The effective limitation of phytoplankton growth by the three parameters temperature, light and nutrients is calculated by multiplying the production rate with the limitation factors of these parameters (SCHÖL et al. 2002; SCHÖL et al. 2006a).

$$\mu = P_{mean} * (Chla : C) * f_T * f_N * f_L \quad (4)$$

- P_{mean} - mean production rate in the vertical profile [mgC* mgChla⁻¹*h⁻¹]
- $Chla : C$ - chlorophyll-a/carbon ratio [mgChla*mgC⁻¹]
- f_T - effect of temperature on growth rate [-]
- f_N - effect of nutrients on growth rate [-]
- f_L - effect of light (photo-inhibition) on growth rate [-]

Nutrient limitation is defined by the most limiting nutrient.

$$f_N = \min \left(\left(N / (k_N + N) \right); \left(P / (k_P + P) \right); \left(Si / (k_{Si} + Si) \right) \right) \quad (5)$$

- $k_{N, P, Si}$ - half saturation constant of nutrient x [mg*l⁻¹]
- N - nitrogen concentration [mg*l⁻¹]
- P - phosphorus concentration [mg*l⁻¹]
- Si - silicate concentration [mg*l⁻¹]

Light limitation is calculated taking into account the quantum yield of phytoplankton during its transport through the vertical light gradient as well as the (light-dependent) chla/carbon ratio (OLLINGER 1999).

Zooplankton

Zooplankton is represented by rotifers as described in SCHÖL et al. (2002). In the Elbe, rotifers are the dominant group (HOLST 2006). Crustaceans become an important group in the estuary of the Elbe, but no separate modelling approach for this group is implemented in QSim.

$$\frac{dROT}{dt} = (\mu_{ROT} - resp_{b,ROT} - mort_{ROT}) * ROT \quad (6)$$

- ROT - biomass of rotifers [mgC*l⁻¹]
- μ_{ROT} - growth rate [d⁻¹]
- $resp_{b,ROT}$ - basic respiration rate [d⁻¹]
- $mort_{ROT}$ - mortality rate [d⁻¹]

Sediment module

The sediment module is designed after DI TORO (2001) as a two layer approach with a separate implementation for oxic and anoxic processes, respectively. Flux calculations take place at each time step to realize a dynamic pelagic-benthic coupling. Further details are described in BFG, 2013).

3 QSim application for the Elbe and its estuary

The description of the model area, boundary conditions, model calibration and parametrisation refer to the 1d QSim approach with HYDRAX. Model-specific options concerning the 2d approach (QSim coupled with casu) are mentioned.

3.1 Model area

The Elbe has a length of 1,094 km from its spring in the Giant Mountains (Czech Republic) to the North Sea (Germany). The main German tributaries are Schwarze Elster, Mulde, Saale and Havel.

The model area of the 1d approach starts about 367 km below the source of the Elbe at the border between the Czech Republic and Germany (Elbe-km 0) and reaches until the North Sea at Cuxhaven (Elbe-km 727). It comprises the stretch of the Elbe River up to the tidal weir of Geesthacht (km 0 to km 585) and the Elbe Estuary (km 585 to km 727) (Fig. 2). The estuary can be divided into a freshwater region (< 0.5 PSU), an oligohaline zone (0.5-5 PSU) and a mesohaline zone (5-18 PSU). These salinity limits are according to the “Venice System”. The zones have been determined based on a longitudinal salinity profile measured by the River Basin Community Elbe (FGG Elbe: <http://www.fgg-elbe.de/fgg-elbe.html>) on the 24/08/2006 at ebb tide. The mean discharge during the period 24/07/2006 to 24/08/2006 has been $413 \text{ m}^3\text{s}^{-1}$ at the station Neu Darchau (km 536).

The tributaries are considered as lateral boundaries. The river stretch is divided into 1622 segments. Generally, the spatial resolution of the river and the estuary is 500 m. The 1d approach is extended by the implementation of groyne fields influencing the main river by lateral transfers (SCHÖL et al. 2006a). The complete river stretch is modelled to get a consistent input data set for the water quality simulation of the estuary.

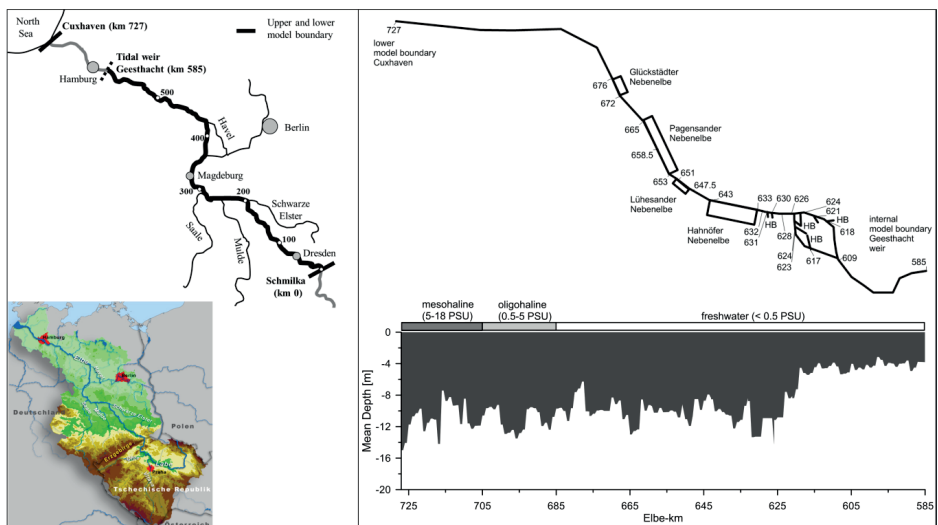


Figure 2: Entire model area (left) and 1d model structure of the Elbe Estuary with longitudinal profile of modelled mean water depth [m] (right) and salinity zonation. HB – Harbour Basin.

The 2d model approach covers only the Elbe Estuary. The irregular triangle mesh contains 42,442 nodes and 76,357 elements with a mean edge-length of 90 m ranging from 4.6 m to 440 m and a mean element size of 5,300 m² ranging from 18 m² to 120,000 m². For the 2d QSim approach, the biological and physical-chemical boundary conditions at the upstream inflow at Geesthacht (km 585) are taken from 1d model results. In Tab. 1, the hydrological properties of the 1d as well as the 2d approach are listed.

Table 1: Water volume [km³], water surface [km²] and mean depth [m] of the Elbe Estuary.

Model Elbe Estuary	Volume [km ³]	Water surface [km ²]	Mean Depth [m]
1d	2.3	245.9	8.2
2d	2.4	305	7.7

3.2 Boundary conditions

The 1d QSim application of the Elbe and its estuary uses a considerably set of input variables at all boundaries and for the atmospheric forcing (Tab. 2). For 2d QSim temperature simulations, the same meteorological forcing as in the 1d approach is applied, using the records from weather stations in Hamburg and Cuxhaven. Water temperatures at the upper boundary of the 2d approach at the weir of Geesthacht are based on the 1d model results.

Table 2: Input data needed for water quality modelling with QSim.

Morphological/ hydrological: Bathymetry (cross sections), discharge, water level
Meteorological: Global radiation, air temperature, cloud cover, relative humidity, wind velocity
Biological: Biological oxygen demand (carbon-derived, C-BOD and nitrification-derived, N-BOD), biomass of planktonic algae (chlorophyll a) and proportion of diatoms, green algae and cyanobacteria, zooplankton biomass, biomass of nitrifiers
Physical-chemical: Water temperature, oxygen, chemical oxygen demand, total nitrogen, nitrate, nitrite, ammonium, silicate, alkalinity, seston, total phosphor, ortho - phosphate, calcium, conductivity

Hydrology and water level

The upper model boundary at km 0 is forced with daily discharge data. For the four main tributaries (Schwarze Elster, Mulde, Saale, Havel) and six other large tributaries, daily discharge data are used, while for eight smaller tributaries only yearly mean discharge is considered. Depending on availability, daily or monthly data are applied for the sewage plants. The lower model boundary is forced with the water level of the gauging station Cuxhaven-Steubenhöft.

Meteorology

The following parameters have been provided as daily data by the German Weather Service for the years 1998-2010: daily sum of the global solar radiation (J*cm⁻²), minimum and maximum air temperature (°C), mean relative humidity (%), mean wind velocity (m*s⁻¹) and mean cloud cover. Along the river stretch the data of four stations (Dresden, Wittenberg, Magdeburg, Seehausen) and for the estuary of two stations (Hamburg and

Cuxhaven) are used. The solar radiation is not recorded at the station Magdeburg and Cuxhaven, and is therefore replaced by data of the nearby stations of Braunschweig respectively Hamburg.

Water quality parameters and phytoplankton biomass

Water quality parameters are provided by the River Basin Community Elbe (FGG Elbe) and by the Observational Network of Water Quality of Hamburg (Institute of Hygiene and Environment). The water quality data at Schmilka (km 3.9) and Cuxhaven (km 727) are used to force the model at the open boundaries. The data of the following stations are used for the main tributaries: Gorsdorf (Schwarze Elster), Dessau (Mulde), Rosenberg (Saale) and Toppel (Havel).

The main sewage plants situated in the river stretch of the Elbe (Dresden-Kaditz and Magdeburg-Gerwisch) as well as in the Elbe Estuary (Hamburg-Dradenau) are also implemented in the model.

3.3 Model calibration

Water level

The water level is calculated by the 1d hydrodynamic model HYDRAX. To characterise the flow, different zones can be differentiated (retention area, floodplain, main channel). For every zone, a different Manning roughness coefficient can be set.

For the Elbe a constant Manning coefficient is used for each zone (main channel $40 \text{ m}^{1/3}\cdot\text{s}^{-1}$, floodplain $12 \text{ m}^{1/3}\cdot\text{s}^{-1}$, retention area $0 \text{ m}^{1/3}\cdot\text{s}^{-1}$). For the Elbe Estuary, the roughness of the main channel is represented by a function of the roughness coefficient depending on the water level as shown in Fig. 3. For the floodplains of the estuary the same approach is applied using a factor of 0.3. The value for the retention area of the estuary is set to the same value like in the river stretch of the Elbe.

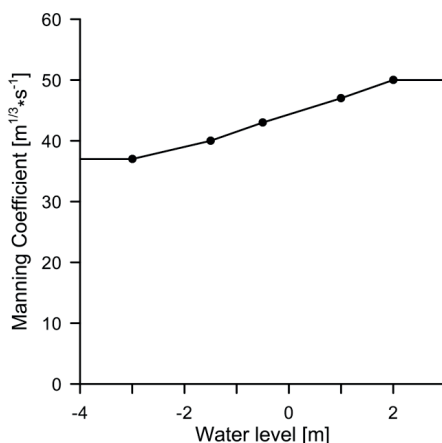


Figure 3: Manning roughness coefficient [$\text{m}^{1/3}\cdot\text{s}^{-1}$] used for the main channel of the Elbe Estuary.

Biological Parameters

The standard set of parameters which is either based on literature or on own experimental results was adjusted for the Elbe Estuary (Tab. 3). The light saturation for diatoms and green algae was increased, the maximum growth rate decreased. The adaptations were performed to reflect the specific species composition of the Elbe. The coefficient of absorption for yellow substances (humics) at 440 nm was increased by the factor 10 to parameterise the effect of high seston content of the Elbe Estuary.

Zooplankton abundances are not recorded in the regular monitoring programme of the Elbe. Therefore, abundances at the upper (km 0) and the lower (km 727) boundaries are estimated with the value of 25 Ind*1⁻¹. This low abundance is sufficient as an inoculum to enable the development of the zooplankton in dependency of the food supply by phytoplankton.

Table 3: List of parameters for green algae, diatoms, cyanobacteria, rotifers, nitrifiers and others in Qsim.

Parameter	Unit	Value
Green Algae / Diatoms / Cyanobacteria		
Chlorophyll/Biomass ratio	$\mu\text{gChla}*\text{mgBio}^{-1}$	21.5/21.5/21.5
Maximum growth rate	d^{-1}	1.6/ 1.3/ 1
Light saturation of the photosynthesis	$\mu\text{E}*m^{-2}*s^{-1}$	176/ 78/ 34
Half saturation constant Nitrogen (N)	$\text{mg}*\text{l}^{-1}$	0.048/ 0.018/ 0.02
Half saturation constant Phosphorus (P)	$\text{mg}*\text{l}^{-1}$	0.022/ 0.02/ 0.02
Half saturation constant Silicium (Si)	$\text{mg}*\text{l}^{-1}$	-/ 0.08/ -
Basic respiration	d^{-1}	0.085
Proportion of growth dependend respiration rate	-	0.2
C-BOD ₅ of phytoplankton		0.004/0.021/0.004
COD of phytoplankton		0.073/0.105/0.073
Maximum cell quota N	$\text{mg}*\text{mgBio}^{-1}$	0.049/ 0.1/ 0.085
Maximum cell quota P	$\text{mg}*\text{mgBio}^{-1}$	0.012/ 0.009/ 0.007
Maximum cell quota Si	$\text{mg}*\text{mgBio}^{-1}$	-/ 0.18/ -
Minimum cell quota N	$\text{mg}*\text{mgBio}^{-1}$	0.008/ 0.017/ 0.014
Minimum cell quota P	$\text{mg}*\text{mgBio}^{-1}$	0.0016/ 0.0011/ 0.0009
Minimum cell quota Si	$\text{mg}*\text{mgBio}^{-1}$	-/ 0.18/ -
Maximum uptake rate N	d^{-1}	0.09/ 0.31/ 0.31
Maximum uptake rate P	d^{-1}	0.69/ 0.62/ 0.62
Maximum uptake rate Si	d^{-1}	-/ 2.5/ -
Minimal O ₂ production	$\text{mg O}_2*\text{mgBio}^{-1}$	1.3
Maximal O ₂ production	$\text{mg O}_2*\text{mgBio}^{-1}$	1.8
Intensity of sedimentation	between 0 and 1	0.5/0.5/0
Temperature optimum	°C	33.5/20/26
Lethal temperature	°C	47/31/35
Rotifers		
Maximum ingestion rate	$\mu\text{gC}*\mu\text{gC}^{-2/3}*\text{d}^{-1}$	2.9
Half-saturation constant for C ingestion	$\text{mg}*\text{l}^{-1}$	0.43
Biomass (dry mass)	μg	0.3
Basic respiration	d^{-1}	0.12

Parameter	Unit	Value
Filterability of diatoms	0-1	0.6
Filterability of green algae	0-1	0.8
Filterability of cyanobacteria	0-1	0.1
Nitrifier		
Maximum growth rate Nitrosomonas	d ⁻¹	1.08
Half saturation constant Nitrosomonas	mg NH ₄ -N*l ⁻¹	0.48
Mortality rate Nitrosomonas	d ⁻¹	0.1
Maximum growth rate Nitrobacter	d ⁻¹	1.1
Half saturation constant Nitrobacter	mg NO ₂ -N*l ⁻¹	1.3
Mortality rate Nitrobacter	d ⁻¹	0.1
Other		
Maximum NH ₄ oxidation rate in sediments	m*d ⁻¹	0.25
Maximum denitrification rate in sediments	m*d ⁻¹	0.32
Hydrolysis rate for easily degradable particulate organic C-compounds	d ⁻¹	0.12
Hydrolysis rate for easily degradable dissolved organic C-compounds	d ⁻¹	18
Half saturation constant for hydrolysis of easily degradable dissolved organic C-compounds	mgC*l ⁻¹	0.25
Half saturation constant for hydrolysis of poorly degradable dissolved organic C-compounds	mgC*l ⁻¹	2.5
Half saturation constant for degradation of monomer C-compounds	mgC*l ⁻¹	0.1
Maximum uptake rate of monomer C-compounds of bacteria	d ⁻¹	24.7
Yield coefficient for bacteria biomass	-	0.25
Basic respiration heterotrophic bacteria	d ⁻¹	0.03
Absorption coefficient for yellow substances/humics at 440 nm	-	7.5

4 Results

4.1 Water levels in the estuary

For the station St. Pauli (km 623) measured and modelled water levels are compared for the 1d model HYDRAX and the 2d model casu (Fig. 4a and b). The hydrodynamic model HYDRAX simulates the point in time of high tide and low tide accurately. The amplitudes are also reproduced well. However, the values of the low tide are often underestimated. Based on hourly measured and simulated data for the period 25/09/2006 to 09/10/2006 the mean difference referring to the absolute values between measurements and simulations is 0.11 m.

Based on 15 min values simulated by the 2d approach with casu the mean difference for the period 03/07/2010 to 17/07/2010 is 0.10 m.

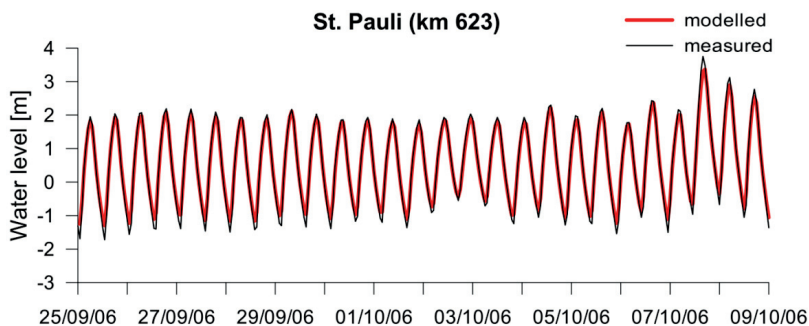


Figure 4a: Measured (black line) and modelled (red line) water levels [m] of the 1d model HY-DRAX at St. Pauli (km 623) for the period 25/09/2006 to 09/10/2006 (measured data: Hamburg Port Authority).

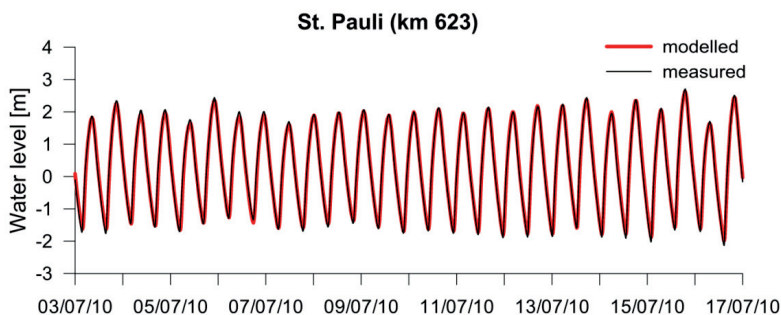


Figure 4b: Measured (black line) and modelled (red line) water levels [m] of the 2d model casu at St. Pauli (km 623) for the period 03/07/2010 to 17/07/2010 (measured data: Hamburg Port Authority).

4.2 Longitudinal profiles of water quality parameters

The 1d QSim simulations of the year 2006 are compared with measured data. Therefore, a seasonal mean from 01/05/2006 to 31/10/2006 as a representative value for the vegetation period is used. This period has beneficial conditions for algal growth due to sufficient global radiation, high water temperatures and low discharge conditions leading to water retention times in the river (km 0 to km 586) of more than 5 days.

For the considered period the position of the salinity threshold of 0.5 PSU was located at Brokdorf km 685 meaning that the freshwater region of the estuary comprised about 100 km until the tidal weir of Geesthacht (km 585) (Fig. 2).

Phytoplankton

The inoculum of algal biomass at the model boundary (km 0) is high with a mean value of $54 \mu\text{g chla} \cdot \text{l}^{-1}$. The longitudinal development of the phytoplankton is shown by the seasonal mean chla values and their standard deviations (Fig. 5). Both the modelled and the measured mean chla values increase along the river. The modelled values end up with a maximal mean of $143 \mu\text{g} \cdot \text{l}^{-1}$ at km 574 just some kilometres upstream the weir of Geesthacht (km 585), while the measured values reached $167 \mu\text{g} \cdot \text{l}^{-1}$ at km 598, just some

kilometres below the weir. Along the estuary, the algal biomass declines sharply. At km 660 near the seaward limit of the freshwater region a low mean value of $6 (\pm 9) \mu\text{g chl}a^*l^{-1}$ is calculated by the model. Measurements at that site have a seasonal mean of $12 (\pm 5) \mu\text{g chl}a^*l^{-1}$.

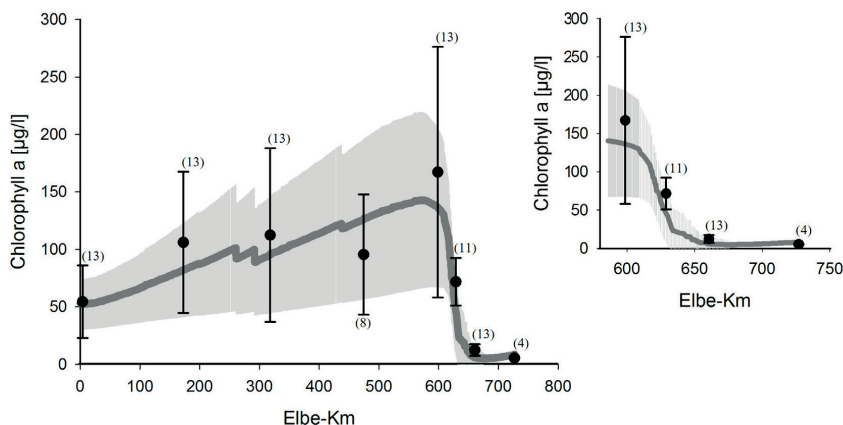


Figure 5: Longitudinal profile of measured (black dots) and modelled (dark grey line) seasonal means of chlorophyll a [μg^*l^{-1}] from Schmilka (km 0) to Cuxhaven (km 727) for May to October 2006. Number of measurements is given in brackets. Standard deviations of measurements reflected by bars and of modelled data ($n = 184$) by the light grey area.

Beside the coincident increase and decrease of the modelled and measured seasonal chla means, it is noteworthy that the standard deviations (σ) of model data and measurements have the same magnitude and longitudinal pattern. In the river, a wide range of chla concentrations are measured giving a high σ . This is mainly caused by changing discharge conditions, which cause different development times for algae in the river. This dependency is already indicated by the boundary values. The simulation reflects this pattern well. A correlation of the chla content in relation to the discharge conditions at km 586 shows a weak negative correlation with a $r^2 = 0.21$. In the estuary the seasonal variability of chla is only notable for the upper section, already at km 629 σ is lowered to $20 \mu\text{g chl}a^*l^{-1}$ with the measured mean of $71 \mu\text{g chl}a^*l^{-1}$. Concerning the modelling results the range of σ is $38 \mu\text{g chl}a^*l^{-1}$ related to a mean value of $45 \mu\text{g chl}a^*l^{-1}$. The σ -value is diminished even more at km 660 (values given above). At the estuarine sites the seasonal variability of the chla concentration becomes less influenced by river discharge, but, as shown by analysing the model results, increasingly influenced by zooplankton grazing.

Zooplankton

For the season in 2006 the simulations show a mean increase of zooplankton (represented by the rotifer *Brachionus sp.* in the QSim model approach) along the river stretch from estimated 25 Ind^*l^{-1} at the upper boundary at km 0 to 160 Ind^*l^{-1} at km 470 and 318 Ind^*l^{-1} at km 586 at the entrance to the estuary (data not shown). In the estuary, the development of zooplankton is strongly enhanced due to both optimal food supply and long residence times. In the area of the harbour the model results show a seasonal mean

of 1,482 Ind*1⁻¹ and a maximum abundance of up to 4,256 Ind*1⁻¹ (km 629). Further downstream the mean abundances decrease rapidly below 500 Ind*1⁻¹ at km 660.

There are only very few counted zooplankton data available, but in 2006 biweekly sampling at Cumlosen (km 470) by the Environmental Agency of Brandenburg and at Seemannshöft (km 629) by the Institute of Hygiene and Environment, Hamburg took place. Between 10 and 20 l water volume was filtered through a net of 55 µm meshes. The fixed samples were counted under an inverse microscope. Seasonal means of the year 2006 of the rotifer and crustacean zooplankton were 555 and 81 Ind*1⁻¹ at km 470 (n =13) as well as 822 and 221 Ind*1⁻¹ at km 629 (n =12).

Based on the modelled zooplankton abundances the grazing rates along the Elbe and in the estuary are calculated. Our 1d modelling approach identifies grazing as the dominant loss process for phytoplankton in the Elbe Estuary. Seasonal mean (May – October) grazing rates in the river at km 470 reach only 0.02 per day, but rise up to 0.5 per day with a maximum of 2.0 per day in the estuary at km 629.

BOD

Closely related to the algal development, the modelled seasonal mean C-BOD₅ increases along the river from 5.3 mg O₂*1⁻¹ at the start (model boundary) to a maximum of 7.0 mg O₂*1⁻¹ at km 577. In the estuary the mean values decrease from 5.5 mg O₂*1⁻¹ at km 629 down to values below 3 mg O₂*1⁻¹ at km 653 (Fig. 6). Because the C-BOD₅ is not part of the Elbe monitoring programme, the measured BOD₇ is applied for comparison. Because the incubation period differs by two days and the BOD includes the oxygen consumption by nitrification, the modelled C-BOD₅ value is multiplied the factor 1.5 to get the same range of values for both parameters. Due to methodologically caused high variation of the parameter and a low number of samples, the measured mean BOD₇ values do not show a clear trend in the river (range between 4.7 to 7.7 mg O₂*1⁻¹), but at the estuarine stations a clear decrease from 5.6 mg O₂*1⁻¹ at km 629 down to values not higher than 2 mg O₂*1⁻¹ is obvious.

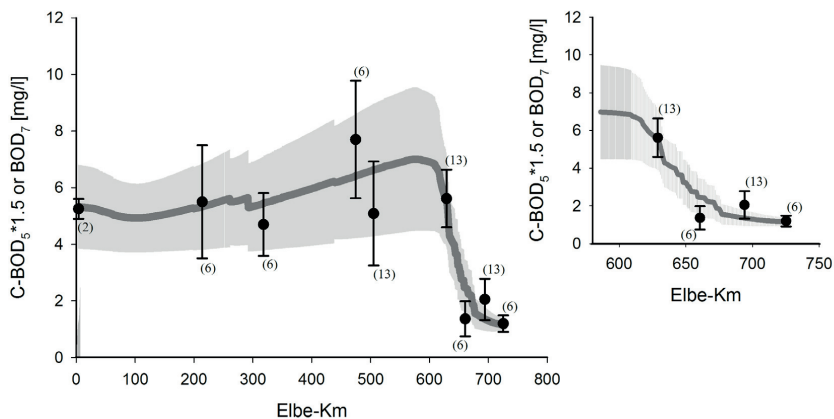


Figure 6: Longitudinal profile of seasonal means of measured BOD₅ [mg*1⁻¹] (black dots) and modelled C-BOD₇ [mg*1⁻¹] (dark grey line) from Schmilka (km 0) to Cuxhaven (km 727) for May to October 2006. Number of measurements is given in brackets. Standard deviations of measurements reflected by bars and of modelled data (n =184) by the light grey area.

Oxygen

The measured seasonal mean oxygen content is derived from continuous measurements by probes at the given monitoring sites (FGG Elbe: <http://www.fgg-elbe.de/fgg-elbe.html>). Along the river the measured mean values increase from 9.6 mg O₂*l⁻¹ at km 4 up to 12.6 mg O₂*l⁻¹ at km 474, while the maximum modelled value is reached at km 566 with a slightly lower maximum of 11.1 mg O₂*l⁻¹ (Fig. 7).

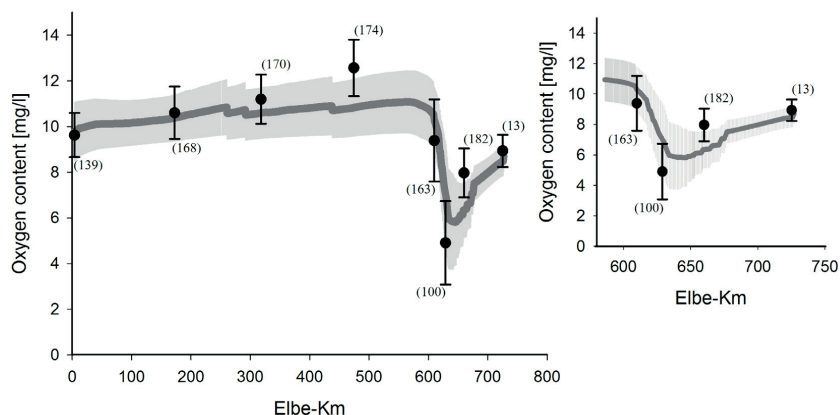


Figure 7: Longitudinal profile of measured (black dots) and modelled (dark grey line) oxygen content [mg*l⁻¹] from Schmilka (km 0) to Cuxhaven (km 727) for May to October 2006. Number of measurements is given in brackets. Standard deviations of measurements reflected by bars and of modelled data (n=184) by the light grey area.

Entering the estuary the oxygen content still remains high (measured: 9.4 mg O₂*l⁻¹; modelled: 10.4 mg O₂*l⁻¹) at km 609, the upper end of the Hamburg harbour. Further downstream a strong decrease of oxygen is measured and modelled, reaching an observed mean minimum at km 629 with 4.9 (± 1.83) mg O₂*l⁻¹ and a modelled mean minimum of 5.8 (± 1.90) mg O₂*l⁻¹ at km 644. At these both sites about 16 % of the measured and modelled values were below 3.1 mg O₂*l⁻¹ and below 3.9 mg O₂*l⁻¹, respectively. Further downstream at the seaward limit of the freshwater region at km 660, the oxygen content is elevated. The measurements show a mean value of 8.0 mg O₂*l⁻¹ and the model results a value of 6.4 mg O₂*l⁻¹, i.e. the increase of the oxygen concentration in the model simulation is less pronounced.

Considering the variability of the daily measured oxygen content, the highest σ with 1.8 mg O₂*l⁻¹ appears at km 609 as well as in the oxygen minimum zone of the estuary at km 629. Concerning the model results, a σ value of 1.8 mg O₂*l⁻¹ is calculated for the reach from km 619 to km 647.

Oxygen budget of the estuary

The simulated oxygen consumption as well as input rates show clear longitudinal differences (Tab. 4). In the upstream section of the estuary at km 609, higher utilisation rates (consumption -1.72 and input $1.04 \text{ mg O}_2 \cdot \text{l}^{-1} \cdot \text{d}^{-1}$) are calculated than at the more downstream sections. Additionally at both upstream sites (km 609 and km 629) the gap between consumption and input is large (the delta of the absolute values of the summed input as well as consumption rates is 0.68 and $0.66 \text{ mg O}_2 \cdot \text{l}^{-1} \cdot \text{d}^{-1}$, respectively), while at the furthest downstream section (km 660) a balanced oxygen budget is calculated.

Concerning the single processes a strong longitudinal decrease of algal related processes is obvious: production rates of $1.11 \text{ mg O}_2 \cdot \text{l}^{-1} \cdot \text{d}^{-1}$ fall down to $0.03 \text{ mg O}_2 \cdot \text{l}^{-1} \cdot \text{d}^{-1}$ and the absolute values of the respiration rates from 0.87 down to $0.04 \text{ mg O}_2 \cdot \text{l}^{-1} \cdot \text{d}^{-1}$. By this the phytoplankton oxygen balance concerning input versus respiration turns from a positive value (delta $0.24 \text{ mg O}_2 \cdot \text{l}^{-1} \cdot \text{d}^{-1}$ at km 609) into a negative one (delta $-0.07 \text{ mg O}_2 \cdot \text{l}^{-1} \cdot \text{d}^{-1}$ and $-0.01 \text{ mg O}_2 \cdot \text{l}^{-1} \cdot \text{d}^{-1}$ at km 629 and 660), i.e., the algae respire more oxygen than they produce. The overall decrease of the rates is simply explained by the decrease of algal biomass, while the change in ratio is mainly due to stronger light limitation in the deeper sections of the estuary.

Table 4: Oxygen budget in the freshwater region of the Elbe Estuary – seasonal (May – October 2006) mean rates [$\text{mg O}_2 \cdot \text{l}^{-1} \cdot \text{d}^{-1}$] and standard deviation (in brackets) of processes and the sum of consumption and input rates at three different sites (km 609, km 629, km 660).

Processes	Seasonal mean rate [$\text{mg O}_2 \cdot \text{l}^{-1} \cdot \text{d}^{-1}$]		
	km 609	km 629	km 660
Re-aeration	$-0.07 (\pm 0.15)$	$0.18 (\pm 0.14)$	$0.28 (\pm 0.09)$
O ₂ -production by algae	$1.11 (\pm 0.51)$	$0.19 (\pm 0.17)$	$0.03 (\pm 0.06)$
Σ Input	1.04	0.38	0.31
Respiration by algae	$-0.87 (\pm 0.40)$	$-0.26 (\pm 0.21)$	$-0.04 (\pm 0.05)$
Nitrification	$-0.02 (\pm 0.02)$	$-0.16 (\pm 0.15)$	$-0.10 (\pm 0.04)$
Heterotrophic consumption	$-0.26 (\pm 0.08)$	$-0.30 (\pm 0.13)$	$-0.12 (\pm 0.05)$
Respiration by zooplankton	$-0.07 (\pm 0.06)$	$-0.18 (\pm 0.17)$	$-0.04 (\pm 0.04)$
Sediment oxygen demand	$-0.49 (\pm 0.08)$	$-0.12 (\pm 0.01)$	$-0.02 (\pm 0.006)$
Σ Consumption	-1.72	-1.04	-0.31

The physical re-aeration rate is strongly driven by the existing oxygen saturation. Therefore due to a mean oversaturation during the season at km 609 an export of oxygen is calculated. Downstream the atmospheric oxygen input is higher at km 660 than at km 629, which might be due to a lower mean depth at this site of the estuary. Regarding the heterotrophic consumption of oxygen, it is evident that it is the most important consumption process at the sites further downstream (km 629 and km 660).

At km 629 all other rates (nitrification, sediment oxygen demand and respiration by zooplankton) have a significant proportion on the overall consumption of oxygen as well. At km 660, additionally to the heterotrophic consumption, only the nitrification is an im-

portant consumption process. Concerning the most upstream site at km 609, the sediment oxygen demand shows higher rates than the heterotrophic oxygen consumption. The comparable low mean water depth (3.6 m) at this site supports the impact of the sediment on the oxygen budget of the water column.

4.3 Validation of the long term simulation of water quality parameters

Water temperature

The long term series of the period 1998 to 2010 of modelled water temperature (daily means) is illustrated for three sites (km 609, 629, 660) along the estuary and compared to daily means of water temperature derived from continuous measuring stations at these sites (Fig. 8).

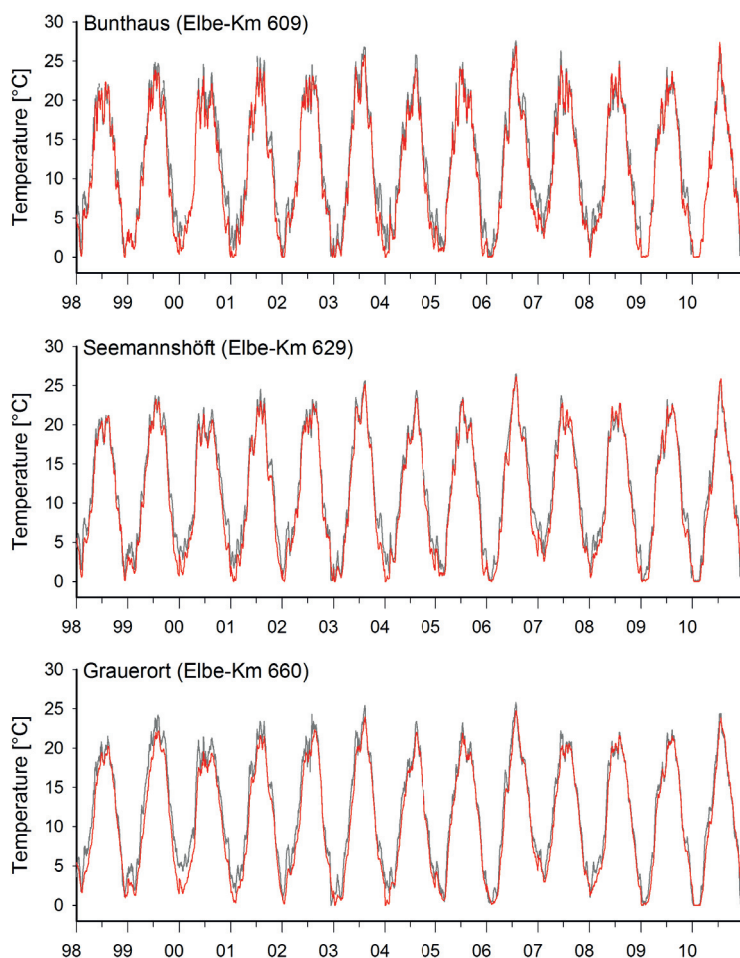


Figure 8: Measured (grey line) and modelled (red line) water temperature [°C] at Bunthaus (km 609), Seemannshöft (km 629) and Grauerort (km 660) for the years 1998-2010 (Measured data: Institute of Hygiene and Environment, Hamburg and NLWKN Stade).

The deviations are quantified by the calculation of the Nash-Sutcliffe Efficiency (NSE) (MORIASI et al. 2007). The NSE indicates the difference of a plot of measured and modelled data from a 1:1 plot. By using NSE it can be noticed that the modelled and measured values show a good agreement (the NSE based on daily data ranges between 0.960 and 0.967 at all sites) concerning the seasonal dynamics.

For the sites at km 609 and km 629 the compliance is weaker in winter (NSE: 0.888 and 0.944) than in summer, i.e., particularly during the vegetation period the modelled data fit the measured data well. The squared correlation coefficient (r^2) of measured and modelled values for all three sites range between $r^2 = 0.971$ and 0.976 . The corresponding slopes (s) of the linear correlation between $s = 0.931$ to 0.949 proof that the simulation slightly underestimates the water temperature. The seasonal differences between measured and modelled values can be explained by the lack of heat discharge from cooling plants, with the highest impact during winter time. Another reason for deviations between measurement and simulation is due to the 1d approach neglecting the effect of tidal flats on heat budget of the estuarine water body.

Chlorophyll

The algal biomass is continuously measured in the estuary at km 609 and km 629 by probes using the fluorescence-method. For comparison with the modelled chl_a values (Fig. 9), which are related to chl_a determined by German standard method using alcohol extraction and photometric measurement (see description of chl_a as a input parameter at the model boundaries), the fluorescence values are multiplied by factor 1.7.

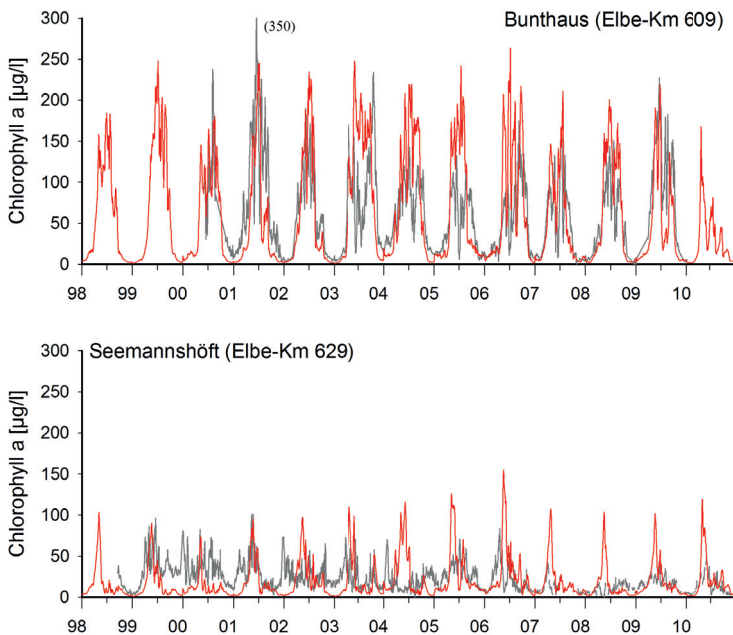


Figure 9: Measured (grey line) and modelled (red line) chlorophyll a [$\mu\text{g}\cdot\text{l}^{-1}$] at Bunthaus (km 609), Seemannshöft (km 629) and Grauerort (km 660) for the years 1998-2010 (Measured data: Institute of Hygiene and Environment, Hamburg).

For the period 2000 to 2009 the seasonal dynamics of chl_a at km 609 is adequately simulated for most of the years (NSE = 0.382), although for some distinct years, e.g. 2003 and 2006, an overestimation of chl_a by the simulation is visible. Using again the seasonal mean (May – October) for comparison a slightly higher mean of $108 (\pm 66) \mu\text{g chl}_a \cdot \text{l}^{-1}$ is calculated by the model in relation to the measured mean of $93 (\pm 51) \mu\text{g chl}_a \cdot \text{l}^{-1}$. Considering the modelled and measured values at km 629 for the period 1998 to 2010 seasonal differences are notably. In most of the years the simulated chl_a concentrations in spring and early summer overshoot the observations. Nevertheless, the seasonal mean of the simulated values ($28 \pm 27 \mu\text{g chl}_a \cdot \text{l}^{-1}$) is slightly lower than the measured one ($33 \pm 16 \mu\text{g chl}_a \cdot \text{l}^{-1}$). The seasonal differences are reflected in a low NSE of 0.007 for km 629.

Oxygen

For most of the sites along the estuary the modelled oxygen agrees well with the measurements (Fig. 10). The measured values are daily means calculated based on continuous measurements (each 5 min) with probes. The seasonal dynamics and especially the low oxygen contents in summer are well reproduced by the simulations. Concerning the whole period 1998 to 2010 the seasonal mean (May – October) of the oxygen content at km 609 is $9.6 \text{ mg O}_2 \cdot \text{l}^{-1}$ for the measurements and $10.3 \text{ mg O}_2 \cdot \text{l}^{-1}$ for the simulations, at km 629 5.7 and $6.9 \text{ mg O}_2 \cdot \text{l}^{-1}$, at km 635 6.4 and 6.2 , and at km 660 7.8 and $6.7 \text{ mg O}_2 \cdot \text{l}^{-1}$. The NSE reflects the good agreement between simulation and measurement for km 629 (NSE = 0.758), km 635 (NSE = 0.844) and km 660 (NSE = 0.725). However, the NSE for km 609 is lower (NSE = 0.284). These differences are confirmed by the squared correlation coefficient (r^2) of km 629 to 660, which range between $r^2 = 0.778$ and 0.857 , and a clearly lower r^2 of 0.296 at km 609. The corresponding slopes (s) show values above 1 for km 609 ($s = 1.016$) and km 629 ($s = 1.042$) meaning a slight overestimation of the modelled oxygen contents exists. At the more downstream stations the slopes fall below 1 (km 635 $s = 0.963$, km 660 $s = 0.936$) pointing to an underestimation of the simulated oxygen values.

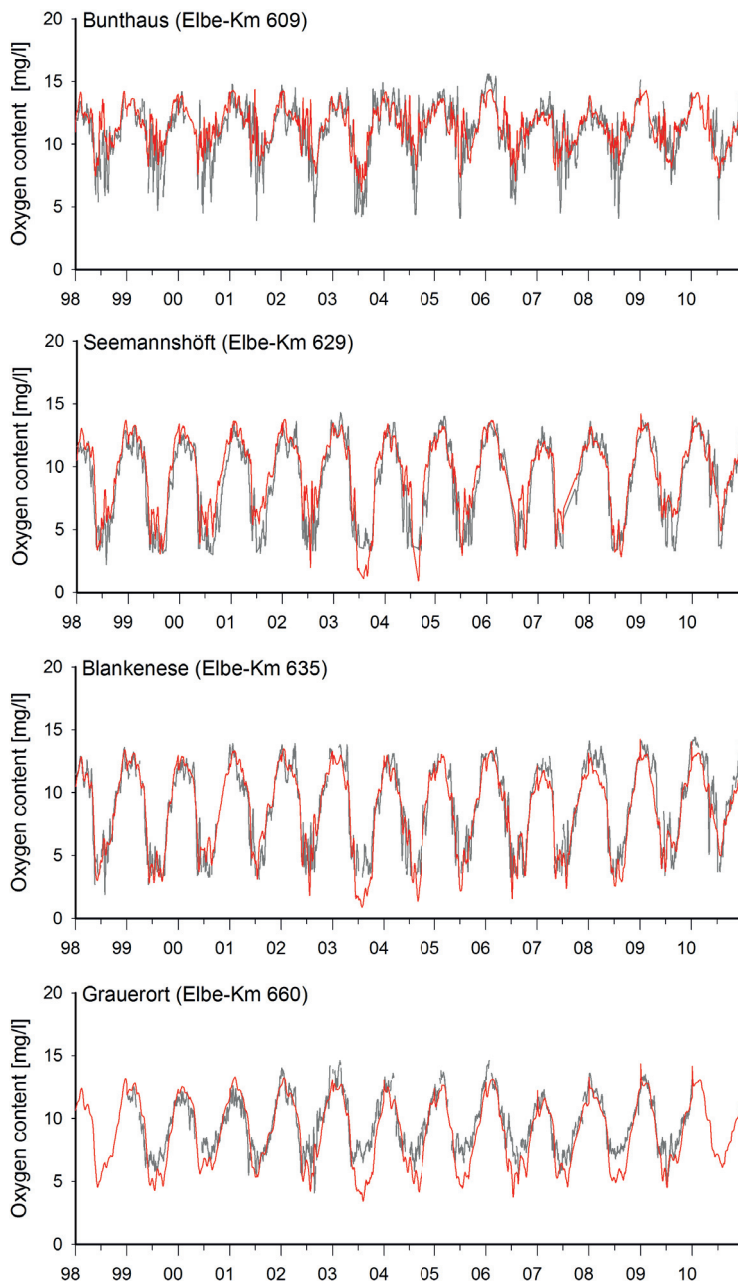


Figure 10: Measured (grey line) and modelled (red line) oxygen [$\text{mg}\cdot\text{l}^{-1}$] at Bunthaus (km 609), Seemannshöft (km 629), Blankenese (km 635) and Grauerort (km 660) for the years 1998-2010 (Measured data: Institute of Hygiene and Environment, Hamburg and NLWKN Stade).

4.4 Simulation of water temperature distribution in the Elbe Estuary with 2d QSim

The distribution of water temperature in the Elbe Estuary is simulated with a 2d approach of QSim coupled with the more-dimensional hydrodynamic model casu. The same meteorological forcing as in the 1d QSim model approach has been used. The upper model boundary is situated at the weir of Geesthacht (km 585) and is forced with the 1d model results for water temperature. For the 09/07/2010 the daily mean water temperature is higher in the side channel system and its tidal flats than in the main channel (Fig. 11). The measured and simulated daily means of water temperature in the main channel at buoy D1 (km 643) reached 23.62 and 23.35 °C and in the side channel at buoy HNE 24.41 and 24.09 °C, i.e. the difference between the main channel and the side channel is 0.79 and 0.74 °C respectively. The largest measured difference during the daily cycle in the main channel is 1.8 °C, while the simulated difference is lower with a value of 1.08 °C. Measured daily amplitude at buoy HNE is 3.4 °C and 1.7 °C for the simulation.

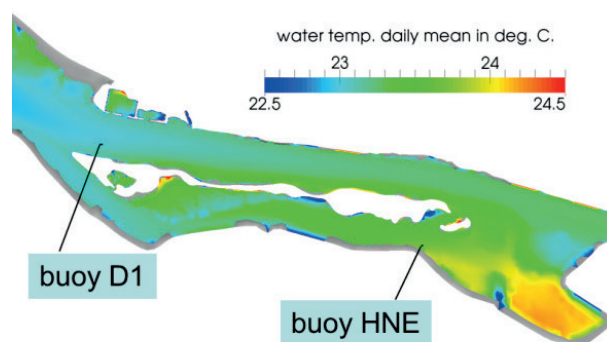


Figure 11: Distribution of daily mean water temperature [°C] on 09/07/2010 in the Elbe Estuary between km 636 and km 653 including the side channel Hahnöfer Nebenelbe and adjacent tidal flats.

Comparison of measurement and simulation of the water temperature for a ten day period from 03/07/2010 to 13/07/2010 shows that the overall level and range of temperature is sufficiently matched by the model results. Mean water temperature for measurements at buoy D1 is 23.41 °C and for simulations 23.06 °C, while at buoy HNE values of 24.41 and 24.03 °C were reached. Again the measured daily range of water temperature is higher than the simulated one. A mesh refinement is planned to reveal whether the transport modelling or the simulation of sediment heat balance is responsible for this effect.

5 Discussion

Water quality modelling is a very simplifying reproduction of the real world, mainly due to the necessary reduction of biological and functional diversity of ecosystems. For example, the phytoplankton community of the Elbe Estuary consists of more than 290 species (KOPPELMANN and KIES 1989 published in ARGE 1998), all with a species-specific

physiology. The water quality model QSim uses a common approach where only three functional algal groups (diatoms, green algae and cyanobacteria) with three sets of physiological parameters represent the whole community. Going deeper into detail, the model description of physiological processes is a simplification too, because separate processes often are combined or even neglected. Water flows (hydrodynamic) can be better reproduced in models, because water motion processes are more suitable for physical and mathematical descriptions.

A practical consequence of this difference in modelling simplification is the fact that many more calibration runs and re-runs of biogeochemical simulations are needed than for hydrodynamic simulations. This favours the approach of off-line coupling because of the advantage of saving hardware resources if only the biogeochemical simulations have to be run. By this approach, the computation of transport for a large number of variables, representing concentrations as well as process rates, for multiple long term water quality simulations becomes feasible.

We show the importance of large scale (catchment) water quality modelling for quantitative analysis of oxygen deficits in the freshwater region of the Elbe Estuary. Applying this approach, the importance of water residence times in each part of the system becomes obvious. There are comparably short retention times in the river (5-10 days), but elevated retention times in the tidally influenced estuary (weeks) depending on river discharges. Already in the freshwater region, including the deep section of Hamburg Harbour, retention times increase clearly. Water retention time changes are highly significantly at the scale of days, because this time scale is relevant for biological processes e.g. growth, decay or grazing (MONSEN et al. 2002).

A crucial point for modelling estuarine budgets and processes is the quality of the input signal from the river. The necessary data could be derived directly from measurements near the entrance of the river into the estuary, but seldom all of the needed parameters are measured in sufficient resolution, and therefore, no consistent set of parameters at the boundary is provided. Using input signals derived from measurements near the entrance of the estuary leads to another disadvantage concerning modelling that the modelled process rates of different modules are not immediately fully in agreement. To overcome these drawbacks we recommend a large scale approach and expanded the model area, including 585 km inland river stretch of the Elbe, although the focus remains on the oxygen budget of the estuary. Thereby, the modelling results in the estuary become less dependent on the boundary conditions and simulated model rates in the estuary become consistent.

In order to reflect biological seasonality, it is important to produce water quality simulations on a seasonal scale. For example, the yearly cycle of growth and decay of phytoplankton plays a major role to the oxygen budget of the estuary. Further on, even longer time spans are needed to evaluate the interannual variability of water quality for management purposes.

Based on the 1d approach, the requirements for long term modelling of water quality in the context of climate change research can be fulfilled. The results for the 13-year period (1998-2010) of the heat and the oxygen budget of the Elbe could be used as a reference period for studying impact of climatically changed air temperature or discharges. This approach is realized in the KLIWAS research program (BFG et al. 2014). The results show that in future scenarios the change of discharge conditions is the major influencing

factor on the algal development in the river section of the Elbe and on the resulting oxygen budget of its estuary (QUIEL et al. 2011, HEIN et al. 2014).

In the second section, we discuss the results concerning the modelling of phytoplankton and oxygen budget in the Elbe river/estuary system. The high importance of the river discharge and thereby riverine load of algal derived organic carbon is a very noticeable feature of the Elbe Estuary. This is less true for estuaries of rivers with a smaller catchment or in more arid areas of the world. These systems are more characterised by marine inflow or autochthonous primary production (COLE and PEIERLS 1992). In the case of the Elbe Estuary, the influence of the river load is restricted to the freshwater region, a very expanded zone in this estuary. Due to high importance of the riverine load, we simulate higher rates of microbial activity in the upper region of the estuary than more downstream sections of the Elbe Estuary. The longitudinal decrease of measured BOD₇-values in the estuary reflects the decline of microbial activity, with the lowest level of activity from the lower end of the freshwater zone until the mesohaline zone (km 660 and km 725), including the turbidity zone.

Our results confirm that only by a satisfying modelling of growth of phytoplankton in the eutrophic river section of the Elbe, the oxygen budget of the estuary can be analysed. In eutrophic rivers like the Elbe, phytoplankton is the main driver of organic carbon cycling and therefore providing carbon substrate for heterotrophic oxygen consumption by bacteria (THORP and DELONG, 2002). In addition, the phytoplankton directly produces or respire oxygen. In the freshwater region of the Elbe Estuary the direct impact of phytoplankton on the oxygen budget switches from a positive one (km 585 to km 609) – mean production is higher than respiration – to a negative one in the more downstream section of the estuary between km 609 and 629. Along this stretch, the water depth increases clearly and algae growth becomes light limited, while the respiration of the existing biomass is still high.

Looking at the fate of phytoplankton, a challenge for understanding and modelling is the disappearance of the algal biomass in the upper freshwater section of the Elbe Estuary. Physiological die-off, sedimentation or grazing are important internal and external loss processes, respectively (MORTAZAVI et al. 2000, HAGY III et al. 2005). The physiological die-off needed some time before algal biomasses disappeared, although a nutrient limitation may support the waning of the algae. In well mixed estuaries like the Elbe sedimentation needs areas of low flow velocities or a long lasting slack water period for an effective impact on the reduction of algal biomass. The influence of harbour basins in the Hamburg area may fulfil the above mentioned criteria and should be a subject for application of more dimensional modelling.

Our 1d modelling approach identifies grazing as the dominant loss process for phytoplankton in the Elbe Estuary. Seasonal mean high grazing rates of 0.5 per day mean that nearly 40 % of the standing stock of the phytoplankton is reduced per day. Calculated maximal grazing rates of 2.0 per day lead to a loss of 87 % and by that a nearly complete control of the algal biomass. In the Schelde estuary such high grazing pressure mainly by microzooplankton is described and community grazing rates of 0.41 to 1.83 per day were measured (LIONARD et al. 1997). The Elbe Estuary is a favourable habitat for estuarine copepods and for river borne rotifers, mainly due to the sufficient food supply. Already in the river, strong increases of zooplankton abundances were observed during longitudinal surveys from Schmilka to the weir of Geesthacht (HOLST 2006, HARDENBICKER

2014). The maximum reported abundances were reached at Geesthacht with up to 10,000 Ind* l^{-1} for the dominant zooplankton group of rotifers and up to 40 Ind* l^{-1} for crustaceans (HOLST 2006). Our modelling results for the year 2006 show a seasonal mean of 320 (+/- 190) rotifers of Ind* l^{-1} at the entrance to the estuary at km 586.

In the estuary, the zooplankton abundances reached a maximum of 4,250 Ind* l^{-1} at km 629 and a seasonal mean of 1,500 Ind* l^{-1} . The counted seasonal mean zooplankton (rotifers and crustaceans) abundances at that site were 1,050 Ind* l^{-1} . Comparable high abundances between 200 and 1800 Ind* l^{-1} were reported for the Schelde estuary (LIONARD et al. 1997). One explanation of the difference between modelled and observed abundances in the Elbe might be due to the fact that the zooplankton in the estuary is not longer represented by the rotifers as assumed in the QSim model approach, but copepods with higher biovolume and individual dry weight become the dominant group. Secondly, higher zooplankton abundances are simulated, because no external loss of zooplankton to a higher trophic level of the food web is taken into account. However, it is known that zooplankton is an important prey for fish larvae and juvenile fishes in estuaries (MEHNER and THIEL 1999) and abundances could be reduced clearly by feeding. Many further investigations and data are required to model and evaluate the role of zooplankton in the Elbe Estuary.

In addition to the longitudinal development of phytoplankton and oxygen, the lateral distribution of the oxygen concentrations is of scientific and management concerns. The importance of tidal flats, side channel systems or harbour basins as sinks or sources for oxygen are important issues which can only be studied in detail by applying a more dimensional model approach. As a first step we proof our coupling concept by simulating the heat budget of a side channel system, showing notable differences of water temperature between main channel and side channel. Higher water temperatures in the side channel are due to lower mean water depth and the warming effect by tidal flats.

6 Conclusions and outlook

The 1d QSim simulation approach confirms that the growth and decline of phytoplankton in the eutrophic Elbe and its estuary has to be simulated accurately to get a realistic picture of the oxygen budget of the estuary. In the eutrophic river phytoplankton biomass is produced up to a seasonal mean (May-October 2006) of nearly 150 $\mu\text{g chl}a \cdot l^{-1}$. In the freshwater region of the estuary algae growth becomes negative due to light limitation, leading to net oxygen consumption by algae due to respiration. Additionally, high grazing losses by zooplankton (seasonal mean of 0.5 per day) reduces algal biomass drastically. Algal derived organic carbon imported from the river and originated in the estuary during algal die-off provides the substrate for heterotrophic oxygen consumption by bacteria.

The large scale 1d QSim approach including a 585 km long river section provides a consistent set of water quality parameter as an input signal for modelling the oxygen budget of the Elbe Estuary. Furthermore, the ability of simulating large time periods which is a crucial need for climate change modelling of water temperature and oxygen has been proofed. In contrast, for detailed studies in the side channel systems of the Elbe Estuary with the tidal flats the higher resolution of the more dimensional model is shown to be essential. Such horizontal differences of water quality parameters mainly caused by

morphological structures as side channels or harbour basins are of ecological importance (improved oxygen conditions or feeding habitat for young fish) and should be subject of more dimensional modelling in estuaries. Even so more realistic modelling of water residence times in certain domains of the estuary based on more dimensional modelling is required.

7 Acknowledgements

We are grateful to Werner Blohm, Carsten Viergutz and Helmut Fischer for support and constructive remarks on the manuscript. The results shown here are based on the results of project 3.08 „Climate change related impacts on the oxygen budget of North Sea estuaries due to alterations of river discharge and nutrient and carbon load – potential adaptation strategies for sediment management“ of the research program KLIWAS financed by the Federal Ministry of Transport and Digital Infrastructure (BMVI).

8 References

- ARGE ELBE: Gewässerökologische Studie der Elbe. 98 pp., 1984.
- ARNDT, S.; LACROIX, G.; GYPENS, N.; REGNIER, P. and LANCELOT, C.: Nutrient dynamics and phytoplankton development along an estuary-coastal zone continuum: A model study. *Journal of Marine Systems*, Vol. 84, 3-4, 49-66, 2011.
- BECKER, A.; KIRCHESCH, V.; BAUMERT, H.Z.; FISCHER, H. and SCHÖL, A.: Modelling the effects of thermal stratification on the oxygen budget of an impounded river. *River Research and Applications*, Vol. 26, 5, 572-588, 2010.
- BERGEMANN, M.; BLÖCKER, G.; HARMS, H.; KERNER, M.; MEYER-NEHLS, R.; PETERSEN, W. and SCHRÖDER, F.: Der Sauerstoffhaushalt der Tideelbe. *Die Küste*, Vol. 58, 199-261, 1996.
- BERGFELD, T.: Dynamics of microbial food web components in three large rivers (Rhine, Mosel and Saar) with the main focus on heterotrophic nanoflagellates. Thesis. University Cologne, 126 pp., 2002.
- BFG: Das Gewässergütemodell QSim: Handbuch zur Benutzeroberfläche GERRIS. Report No. 1778, 99 pp., 2013.
- BFG; DWD; BSH and BAW: KLIWAS Auswirkungen des Klimawandels auf Wasserstraßen und Schifffahrt - Entwicklung von Anpassungsoptionen. Synthesebericht für Entscheidungsträger, KLIWAS-57/2014, 2014.
- BILLEN, G.: Protein degradation in aquatic environments. In: CHRÖST, R. (Ed.): *Microbial enzymes in aquatic environments*. Springer Verlag, New York, 122-142, 1991.
- BILLEN, G.; GARNIER, J.; FICHT, A. and CUN, C.: Modelling the Response of Water Quality in the Seine River Estuary to Human Activity in its Watershed Over the Last 50 Years. *Estuaries*, Vol. 24, 6B, 977-993, 2001.
- BRUCE, L.C.; COOK, P.L.M.; TEAKLE, I. and HIPSEY, M.R.: Controls on oxygen dynamics in a riverine salt-wedge estuary – a three-dimensional model of the Yarra River estuary, Australia. *Hydrol. Earth Syst. Sci. Discuss.*, Vol. 10, 9799-9845, 2013.
- CASPER, H.: Die Sauerstoffproduktion einer Bucht im Süßwasserbereich des Elbe-Ästuars. – Untersuchungen im „Mühlenberger Loch“ in Hamburg. *Archiv für Hydrobiologie, Suppl.-Bd. 62, 5, 509-542, 1984.*

- CASULLI, V. and CHENG, R.T.: Semi-implicit finite difference methods for three-dimensional shallow water flow, *International Journal for Numerical Methods in Fluids*, Vol. 15, 629-648, 1992.
- CUNGE, J.A.; HOLLY, F.M. and VERWEY, A.: *Practical Aspects of Computational River Hydraulics*. Pitman Advanced Publishing Program, London, 420 pp., 1980.
- CERCO, C.F. and COLE, T.: Three-dimensional eutrophication model of Chesapeake Bay. *Journal of Environmental Engineering*, Vol. 119, No. 6, 1006-1025, 1993.
- COLE, J.J. and PEIERLS, P.L.: Can phytoplankton maintain a positive carbon balance in a turbid, freshwater, tidal estuary? *Limnol. Oceanogr.*, 37, 1608-1617, 1992.
- DI TORO, D.M.: *Sediment flux modelling*. Vol. 116. Wiley, New York, 624 pp., 2001
- DUCHARNE, A.; BAUBION, C.; BEAUDOIN, N.; BENOIT, M.; BILLEN, G.; BRISSON, N.; GARNIER, J.; KIEKEN, H.; LEBONVALLET, S.; LEDOUX, E.; MARY, B.; MIGNOLET, C.; POUX, X.; SAUBOUA, E.; SCHOTT, C.; THÉRY, S. and VIENNOT, P.: Long term prospective of the Seine River system: Confronting climatic and direct anthropogenic changes. *Science of the Total Environment*, Vol. 375, 292-311, 2007.
- FLÜGGE, G.: *Gewässerökologische Überwachung der Elbe*. Abh. Naturw. Ver. Bremen, 40, 217-232, 1985.
- FRJASINOV, I.V.: Algoritm resenija raznostnyh zadac na grafah. *Zyurnal vycislitel'noj matematiki i matematiceskoj fiziki* 10, 1970.
- GARNIER, J.; SERVAIS, P.; BILLEN, G.; AKOPIAN, M. and BRION, N.: Lower Seine River and Estuary (France) Carbon and Oxygen Budgets During Low Flow. *Estuaries*, Vol. 24, 6B, 964-976, 2001.
- GYPENS, N.; DELHEZ, E.; VANHOUTTE-BRUNIER, A.; BURTON, S.; THIEU, V.; PASSY, P.; LIU, Y.; CALLENS, J.; ROUSSEAU, V. and LANCELOT, C.: Modelling phytoplankton succession and nutrient transfer along the Scheldt estuary (Belgium, The Netherlands). *Journal of Marine Systems*, Vol. 128, 89-105, 2013.
- HAGY III, J.D., BOYNTON, W.R. and JASINSKI, D.A.: Modelling phytoplankton deposition to Chesapeake Bay sediments during winter–spring: interannual variability in relation to river flow. *Estuarine, Coastal and Shelf Science*, Vol. 62, 25-40, 2005.
- HARDENBICKER, P.: *Phytoplankton dynamics in two large rivers: long-term trends, longitudinal dynamics and potential impacts of climate change*. Thesis, Technical University of Dresden, 119 pp., 2014.
- HEIN, B.; WYRWA, J.; VIERGUTZ, C. and SCHÖL, A.: Projektionen für den Sauerstoffhaushalt des Elbe-Ästuars – Folgen für die Sedimentbewirtschaftung und das ökologische Potenzial. *Schlussbericht KLIWAS-Projekt 3.08*. KLIWAS-42/2014, doi: 10.5675/Kliwas_42/2014_3.08, 2014.
- HOLST H.: Zooplankton im Pelagial des Hauptstroms. In: PUSCH, M. and FISCHER, H. (Eds.): *Stoffdynamik und Habitatstruktur in der Elbe – Konzepte für die nachhaltige Entwicklung einer Flusslandschaft*. Weißensee Verlag, Berlin, 56-64, 2006.
- HOWARTH, R.; CHAN, F.; CONLEY, D.J.; GARNIER J.; DONEY S.C.; MARINO, R. and BILLEN, G.: Coupled biogeochemical cycles: Eutrophication and hypoxia in temperate estuaries and coastal marine ecosystems. *Frontiers in Ecology and the Environment*, Vol. 9, 1, 18-26, doi: 10.1890/100008, 2011.
- IKSR: Estimation of the effects of climate change scenarios on future Rhine water temperature development – Extensive Version. *International Commission for the Protection of the Rhine*. Report, 214, 57 pp., 2013.

- KIRCHESCH, V. and SCHÖL, A.: Das Gewässergütemodell QSim - Ein Instrument zur Simulation und Prognose des Stoffhaushaltes und der Planktodynamik von Fließgewässern. *Hydrologie und Wasserbewirtschaftung*, Vol. 43, 302-309, 1999.
- LEONARD, B.P.: A stable and accurate convective modelling procedure based on quadratic upstream interpolation. *Computer Methods in Applied Mechanics and Engineering*, Vol. 19, 59-98, 1961.
- LIONARD, M.; AZEMAR, F.; BOULETREAU, S.; MUYLEAERT, K.; TACKX, M. and VYVERMAN, W.: Grazing by meso- and microzooplankton on phytoplankton in the upper reaches of the Schelde estuary (Belgium/The Netherlands). *Estuarine, Coastal and Shelf Science*, Vol. 64, 764-774, 2005.
- MATZINGER, A.; FISCHER, H. and SCHMID, M.: Modellierung von biogeochemischen Prozessen in Fließgewässern. *Handbuch Angewandte Limnologie*, 29, 5/12, 32 pp., 2012.
- MORIASI, D.N.; ARNOLD, J.G.; VAN LIEW, M.W.; BINGNER, R.L.; HARMEI, R.D. and VEITH, T.L.: Model evaluation guidelines for systematic quantification of accuracy in watershed simulations. *Transactions of the American Society of Agricultural and Biological Engineers*, Vol. 50, 885-900, 2007.
- MEHNER, T. and THIEL, R.: A review of predation impact by 0+ fish on zooplankton in fresh and brackish waters of the temperate northern hemisphere. *Environmental Biology of Fishes*, Vol. 6, 169-181, 1999.
- MONSEN, N.E.; CLOERN, J.E.; LUCAS, L.V. and MONISMITH, S.G.: A comment on the use of flushing time, residence time, and age as transport time scales. *Limnology and Oceanography*, Vol. 47, 5, 1545-1553, 2002.
- MORTAZAVI, B.; IVERSON, R.L.; LANDING, W.M.; LEWIS, F.G. and WENRUI, H.: Control of phytoplankton production and biomass in a river-dominated estuary: Apalachicola Bay, Florida, USA. *Mar. Ecol. Prog. Ser.*, Vol. 198, 19-31, 2000.
- OLLINGER, D.: Modellierung von Temperatur, Turbulenz und Algenwachstum mit einem gekoppelten physikalisch-biologischen Modell. Thesis, Universität Heidelberg, 1999.
- OPPERMANN, R.: Eindimensionale Simulation allmählich veränderlicher instationärer Fließvorgänge in Gewässernetzen. *Mitteilungen des Instituts für Wasserwirtschaft*, H. 50. VEB Verlag für Bauwesen, Berlin, 1989.
- OPPERMANN, R.: Das Programmsystem HYDRAX 5.0 – Mathematisches Modell und Datenschnittstellen. *Ingenieurbüro für Wasser und Umwelt Berlin*, 11 pp., 2010.
- PAERL, H. and PINCKNEY, J.: Ecosystem response to interannual and watershed organic matter loading: consequences for hypoxia in the eutrophying Neuse River Estuary, North Carolina, USA. *Marine Progress Series*, Vol. 146, 17-25, 1998.
- PUSCH, M.; ANDERSEN, H.E.; BÄTKE, J.; BEHRENDT, H.; FISCHER, H.; FRIBERG, N.; GANCARCZYK, A.; HOFFMANN, C.C.; HACHOL, J.; KRONVANG, B.; NOWACKI, F.; PEDERSON, M.L.; SANDIN, L.; SCHÖLL, F.; SCHOLTEN, M.; STENDERA, S.; SVENDSEN, L.M.; WNUK-GLAWDEL, E. and WOLTER, C.: Rivers of the Central European Highlands and Plains. In: TOCKNER, K.; ROBINSON, C.T. and UEHLINGER, U. (Eds.): *Rivers of Europe*. London, 525-576, 2009.
- QUIEL, K.; BECKER, A.; KIRCHESCH, V.; SCHÖL, A. and FISCHER, H.: Influence of global change on phytoplankton and nutrient cycling in the Elbe River. *Regional Environmental Change*, Vol. 11, 2, 405-421, 2011.
- RABALAIS, N.N.; EUGENE, R.; DIAZ, R.J. and JUSTIĆ, D.: Global change and eutrophication of coastal waters. *ICES Journal of Marine Science*, Vol. 66, 1528-1537, 2009.

- SALMASO, N. and BRAIONI, M.G.: Factors controlling the seasonal development and distribution of the phytoplankton community in the lowland course of a large river in Northern Italy (River Adige). *Aquatic Ecology*, Vol. 42, 533-545, 2008.
- SCHÖL, A; EIDNER, R.; BÖHME, M. and KIRCHESCH, V.: Integrierte Modellierung der Wasserbeschaffenheit mit QSim. In: PUSCH, M. and FISCHER, H. (Eds.): *Stoffdynamik und Habitatstruktur in der Elbe*, Bd. 5., Weißensee Verlag, Berlin, 233-242, 2006a.
- SCHÖL, A; EIDNER, R.; BÖHME, M. and KIRCHESCH, V.: Einfluss der Bühnenfelder auf die Wasserbeschaffenheit der Mittleren Elbe. In: PUSCH, M. and FISCHER, H. (Eds.): *Stoffdynamik und Habitatstruktur in der Elbe*, Bd. 5., Weißensee Verlag, Berlin, 243-263, 2006b.
- SCHÖL, A.; KIRCHESCH, V.; BERGFELD, T.; SCHÖLL, F.; BORCHERDING, J. and MÜLLER, D.: Modelling the chlorophyll *a* content of the River Rhine - Interrelation between riverine algal production and population biomass of grazers, rotifers and the zebra mussel, *Dreissena polymorpha*. *Internat. Rev. Hydrobiol.*, Vol. 87, 295-317, 2002.
- THORP, J.M. and DELONG, M.D.: Dominance of autochthonous autotrophic carbon in food webs of heterotrophic rivers. *Oikos*, Vol. 96, 3, 543-550, 2002.
- WYRWA, J.: Turbulenzmodellierung für stabil dichtegeschichtete Strömungen bei der Simulation des Transports von kohäsiven Sedimenten in Ästuaren. Thesis. TU Berlin, 2003.
- YASSERI, M.S.: Untersuchungen zum Einfluss von Sauerstoffmangelsituationen auf den mikrobiell-heterotrophen Stoffumsatz an Schwebstoffen in der Tideelbe. Adfontes-Verlag, Hamburg, 97 pp., 1999.
- ZHENG, L.; CHEN, C. and ZHANG, F.: Development of water quality model in the Satilla River Estuary, Georgia. *Ecological Modelling*, Vol. 178, 457-482, 2004.
- ZHU, Z.-Y.; ZHANG, J.; WU, Y.; ZHANG, Y.-Y.; LIN, J. and LIU, S.M.: Hypoxia of the Changjiang (Yangtze River) Estuary: Oxygen depletion and organic matter decomposition. *Marine Chemistry*, Vol. 125, 108-116, 2011.

Recent Advances in Wave Modelling for the North Sea and German Bight

Joanna Staneva, Arno Behrens and Nikolaus Groll

Summary

The ocean wave modelling has shown impressive developments, both on the theoretical aspects as in the quality of the results available to users. The state-of-the-art development of the WAM wave model for forecasts applications at operational services and for hindcasts and climate assessments for the North Sea and the German Bight is presented here. The ocean waves control the exchange of energy, momentum, heat, moisture, gas, etc. between the ocean and the atmosphere in the earth system. The impact of waves on currents and water levels in coastal areas is demonstrated. Therefore first steps towards a fully coupled atmosphere-wave-ocean model have been carried out. The synergy between wave observations and models for the North Sea and German Bight is increased on the road to improving the ocean state estimate and predictions in the coastal areas and generating up-to-date information, products and knowledge. Sea state reconstructions and climate scenarios computations with the WAM model have created a huge interest to use the data in industrial applications.

Keywords

wave modelling, coastal ocean forecasting, wave climate reconstructions, wave climate scenarios, wave-circulation interaction, North Sea, German Bight

Zusammenfassung

Die Modellierung der Wellen an der Meeresoberfläche ist durch beeindruckende Entwicklungen gekennzeichnet, sowohl vom theoretischen Aspekt her als auch in der Qualität der Resultate, die für die Nutzer zur Verfügung stehen. Der neueste Stand der Technik in der Entwicklung des spektralen Wellenmodells dritter Generation WAM, für Anwendungen in der Vorhersage der operationellen Dienste, für Hindcasts und für Bewertungen des Wellenklimas für die Nordsee und die Deutsche Bucht, wird hier vorgestellt. Die Wellen an der Meeresoberfläche kontrollieren den Austausch von Energie, Impuls, Wärme, Feuchte, Gas usw. zwischen dem Ozean und der Atmosphäre des Erdsystems. Der Einfluss der Wellen auf Strömungen und Wasserstand ist nachgewiesen. Daher sind erste Schritte in Richtung auf ein vollständig gekoppeltes Atmosphären-Wellen-Ozean-Modell unternommen worden. Die Synergie zwischen Wellen-Beobachtungen und Ergebnissen numerischer Modelle für die Nordsee und die Deutsche Bucht ist angestiegen im Zuge der Verbesserungen in der Abschätzung des Zustandes des Ozeans, der Vorhersagen in Küstengewässern und in der Gewinnung von aktuellen Informationen, Produkten und Kenntnissen. Berechnungen zu Rekonstruktionen des Meereszustandes und von Klimaszenarien mit dem WAM Modell haben zu einem großen Interesse geführt, die erzeugten Daten in industriellen Anwendungen zu nutzen.

Schlagwörter

Wellenmodellierung, Vorhersagen im Küstenbereich, Wellenklima-Rekonstruktionen, Wellenklima-Szenarien, Wellen-Zirkulation-Wechselwirkung, Nordsee, Deutsche Bucht

Contents

1	Introduction	234
2	Model Description WAM.....	235
3	Short-term pre-operational wave model for the North Sea and German Bight ...	236
4	Multi-decadal regional wave simulations.....	245
5	Wave-current interaction	250
6	Conclusions.....	251
7	References	252

1 Introduction

The ocean wave modelling has shown impressive developments during the last decades, both on the theoretical aspects as in the quality of the results available to users. The state-of-the-art Wave Model (WAM) for forecasts applications at operational services and for hindcasts and climate assessments is presented with focus on the new advances in the wave model development and applications in the Helmholtz-Zentrum Geesthacht (HZG) for the North Sea and German Bight regions.

During the last decade the north European coasts has been affected by severe storms which caused serious damages on the North Sea coastal areas. Additionally, human activities, e.g. offshore wind power plants (BERGENHAGEN et al 2010; BSH 2010), offshore oil industry, coastal recreations urges information about the sea state with a high detail (resolution) in the coastal environment. Predictions of extreme events like storm surges and flooding caused by storms are very important in order to avoid or at least minimize losses and human and material damages. Therefore, reliable wave forecasts and long term statistics of extreme wave conditions are needed for the coastal areas where various human activities are carried out, e.g. coastal securities, harbor activities, offshore wind energy, search and rescue, etc.

For the North Sea and German Bight regions the past and future wave conditions cannot be fully assessed from the analyses of observational data only, which, as it is well known, are sparse in both, time and space. Even more, statistics of long term changes in extreme wave conditions require long and homogenous wave data at high spatial and temporal resolution, which cannot be done based on the available observational records (WEISSE and GÜNTHER 2007). Numerical wave model systems have become the most common tool for producing high quality forecasts and long term hindcast wave data and to analyze trends and capability in severe extreme events (WEISSE and GÜNTHER 2007; GÜNTHER et al. 1998; WASA-Group 1998; GROLL et al. 2014). The climate change can influence the multidecadal wave conditions in the North Sea and thus may lead to the intensification of wave extremes in the future which will increase the risk in the coastal area. Potential changes in the wave climate in the North Sea under different climate sce-

narios are studied in GROLL et al. 2014, GRABEMANN and WEISSE (2008), DOBERNARD and ROED (2008). High-resolution small scale versions of WAM have been introduced by LUO and SCLAVO (1007) and MONBALIU et al. (2007). MOGHIMI et al (2005) applied the WAM and K-model for the North Sea and German Bight in order to study whether they were able to predict the near-shore wave conditions accurately. BEHRENS and GÜNTHER (2009) evaluated the capability of the wave model to predict extreme events as severe winter storms for the North Sea and Baltic Sea.

The ocean waves control the exchange of energy, momentum, heat, moisture, gas, etc. between the ocean and the atmosphere in the earth system. Understanding these processes is of utmost importance towards fully integrating of the atmosphere-wave-ocean models and their further coupling with biological, morphological, hydrographical systems. This topic reflects the increased interest in operational oceanography on order to reduce prediction errors of state estimates at coastal scales. The uncertainties in most of the presently used models result from the nonlinear feedback between strong tidal currents and wind-waves, which can no longer be ignored, in particular in the coastal zone where its role seems to be dominant. A nested modelling system is used in HZG to producing reliable now- and short-term forecasts of ocean state variables, including wind waves and hydrodynamics .Analysis of observations, as well as the results of numerical simulations are presented in STANEV et al. 2011.

The structure of the paper is as follows. The WAM is described in Section 2. Section 3 describes the short-term pre-operational wave model for the North Sea and German Bight. Results from the multi-decadal regional wave simulations are presented in Section 4. Section 5 covers ocean-current interactions followed finally by concluding remarks.

2 Model Description WAM

WAM is a third generation wave model which solves the wave transport equation explicitly without any presumptions on the shape of the wave spectrum. It represents the physics of the wave evolution in accordance with our knowledge today for the full set of degrees of freedom of a 2D wave spectrum. WAM computes the 2d wave variance spectrum through integration of the transport equation in spherical coordinates:

$$\frac{\partial F}{\partial t} + (\cos \phi)^{-1} \frac{\partial}{\partial \phi} (\dot{\phi} \cos \phi F) + \frac{\partial}{\partial \lambda} (\dot{\lambda} F) + \sigma \frac{\partial}{\partial \sigma} \left(\dot{\sigma} \frac{F}{\sigma} \right) + \frac{\partial}{\partial \theta} (\dot{\theta} F) = S \tag{1}$$

with

$F(\lambda, \phi, \sigma, \theta, t)$ wave energy density spectrum

(λ, ϕ) Longitude, Latitude

(σ, θ) intrinsic frequency, wave direction

$$\begin{aligned} \dot{\phi} &= (c_g \cos \theta + u_{North}) / R \\ \dot{\lambda} &= (c_g \sin \theta + u_{East}) / (R \cos \phi) \\ \dot{\theta} &= c_g \sin \theta \tan \phi / R + \dot{\theta}_D + \dot{\theta}_C \\ \dot{\sigma} &= \dot{\sigma}_C \end{aligned} \tag{2}$$

The source functions on the right of the transport equation comprise the contributions of wind input (S_{in}), nonlinear interaction (S_{nl}), dissipation (S_{dis}), bottom friction (S_{bf}) and wave breaking (S_{br}):

$$S = S_{in} + S_{nl} + S_{dis} + S_{bf} + S_{br} \quad (3)$$

The last release of the third generation wave model WAM Cycle 4.5.4 is an update of the WAM Cycle 4 wave model, which is described in KOMEN et al. (1994) and GÜNTHER et al. (1992). The basic physics and numerics are kept in the new release. The source function integration scheme made by HERSBACH and JANSSEN (1999), and the up-dates model (BIDLOT et al. 2005) are incorporated. Other main improvements introduced in WAM Cycle 4.5.4 are technical improvements, which take into account the new possibilities of Fortran 95 and the MPI (Message Passing Interface) for parallelization purposes. On request from the user community a number of additional options are added in the model. A big advantage of the new state-of-the-art version WAM Cycle 4.5.4 is its high-grade modular composition which allows an easy replacement of individual parts of the code.

3 Short-term pre-operational wave model for the North Sea and German Bight

Within the framework of COSYNA a pre-operational wave forecast system has successfully been implemented at HZG and is running continuously since December 2009. It provides 24 hour wave forecasts twice a day and makes the results available in the web under <http://www.coastlab.org>. The system includes a regional WAM model for the North Sea (spatial resolution: $\Delta\varphi * \Delta\lambda = 0.05^\circ * 0.08333^\circ \sim 5$ km) and a finer meshed local model for the German Bight ($\Delta\varphi * \Delta\lambda = 0.00928^\circ * 0.015534^\circ \sim 900$ m). The driving wind fields for both are provided by the German Met Service (DWD: Deutscher Wetterdienst), computed as U10-fields by the atmospheric model COSMO_EU. The model area of the COSMO_EU is shown in Fig. 1 (upper left). It provides forecast results for 78 hours with a spatial resolution of about 7 km.

The required boundary information used at the open boundaries of the North Sea model is derived from the regional wave model EWAM for Europe that is running twice a day in the operational wave forecast routine of the DWD. The depth distribution in the model grid for EWAM is given in Fig. 1 (upper right). The local model for the German Bight receives its boundary values from the North Sea wave model. The model grids and the depth distributions (Fig. 1, North Sea on the lower left and German Bight on the lower right side) for the two wave models correspond to those used in the setup for the GETM circulation model in order to simplify the coupling of both for the German Bight. The complete setup of the pre-operational COSYNA forecast system is concentrated in Fig. 1.

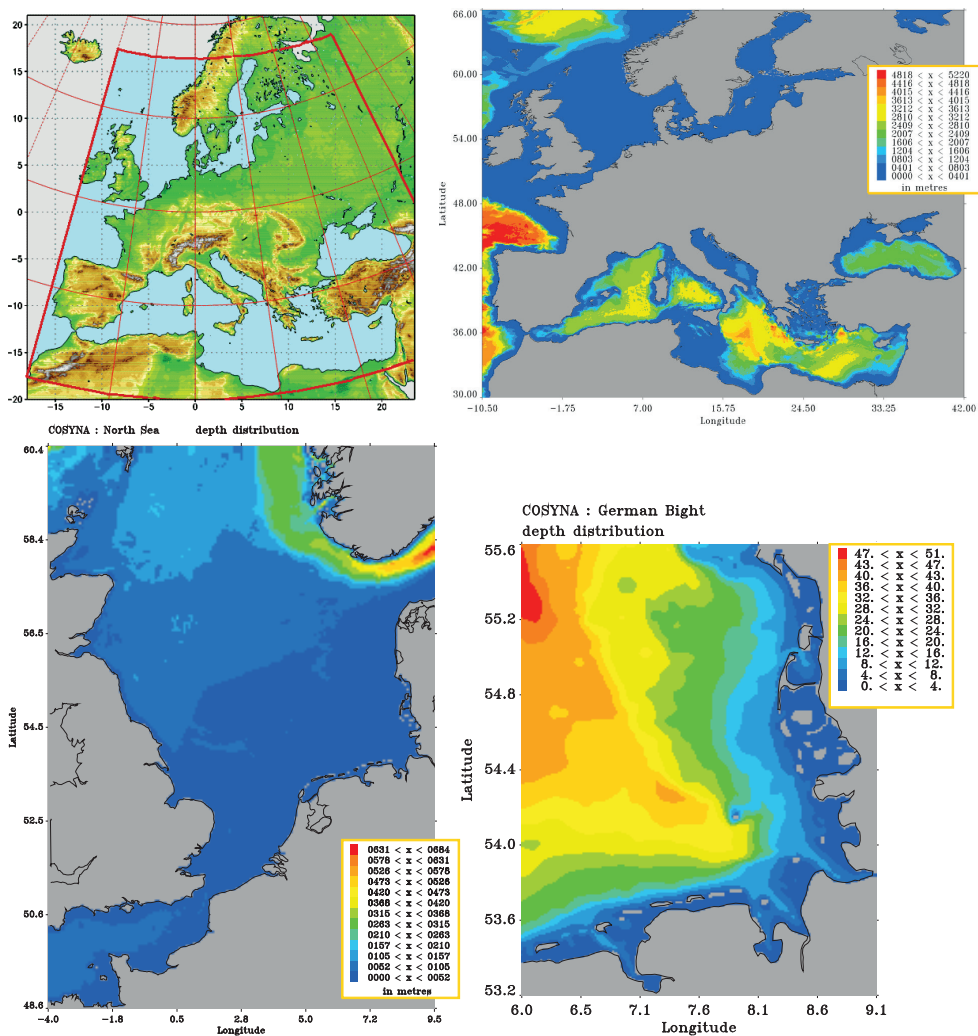


Figure 1: Setup of the pre-operational COSYNA wave forecast system for North Sea and German Bight. Driving wind fields are provided by the COSMO_EU model (upper left, the red line denotes the location of the EWAM in COSMO_EU), boundary values by the regional European wave model EWAM (upper right: EWAM depth distribution). Depth distribution of the model for the North Sea (lower left) and for the German Bight (lower right).

The wave models run in shallow water mode including depth refraction and wave breaking and calculate the two dimensional energy density spectrum at the active model grid points in the frequency-/direction space. The solution of the WAM transport equation is provided for 24 directional bands at 15° each with the first direction being 7.5° measured clockwise with respect to true north and 30 frequencies logarithmically spaced from 0.042 Hz to 0.66 Hz at intervals of $\Delta f/f = 0,1$.

Fig. 2 shows an example of the horizontal distribution of the significant wave height in the the North Sea and in the nest for the German Bight on the 15th of February 2012 at 06 UTC with significant wave heights up to 6.8 m.

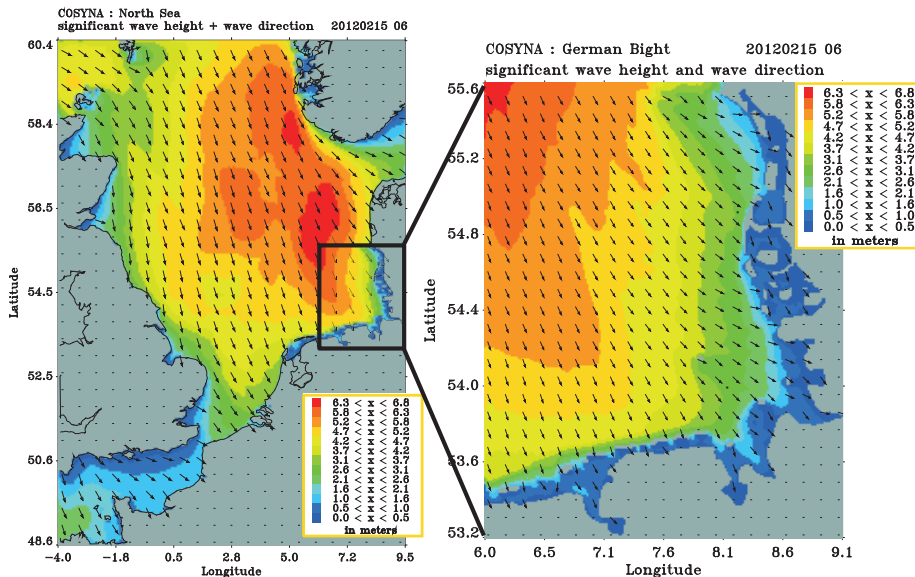


Figure 2: COSYNA wave forecast system for North Sea (left) and German Bight (right).

The results of both wave models include the full two dimensional spectral information and 29 integrated parameters which are included in Tab. 1. The latter are saved 3-hourly at each of the active model grid points and the spectral information is saved every 12 hours (restart file for the next forecast).

Table 1: Integrated parameters of the wave model output.

Parameter No.	Parameter	Dimension
1	Wind speed U10	m/s
2	Wind direction	Degree from North (towards)
3	Friction velocity	m/s
4	Drag coefficient	
5	Water depth	m
6	Current speed	m/s
7	Current direction	Degree from North (towards)
8	Dummy	
9	Significant wave height	m
10	Wave peak period	s
11	Wave mean period	s
12	Wave Tm1 period	s
13	Wave Tm2 period	s
14	Wave direction	Degree from North (towards)
15	Directional spread	Degree
16	Normalized wave stress	%

Parameter No.	Parameter	Dimension
17	Sea significant wave height	m
18	Sea peak period	s
19	Sea mean period	s
20	Sea Tm1 period	s
21	Sea Tm2 period	s
22	Sea direction	Degree from North (towards)
23	Sea directional spread	Degree
24	Dummy	
25	Swell significant wave height	m
26	Swell peak period	s
27	Swell mean period	s
28	Swell Tm1 period	s
29	Swell Tm2 period	s
30	Swell direction	Degree from North (towards)
31	Swell directional spread	Degree
32	Dummy	

The wave model results (integrated parameters) are validated against buoy data available in the area of the model grids. As a representative example the time series of the measured and computed significant wave heights H_s at two locations in the model grid for the North Sea for December 2010 is demonstrated at Fig. 3. The agreement between measured and modelled values is fairly well. Here we have to take into account that the measurements are compared with wave model forecasts: the first 12 hours of each forecast have been used, respectively. The measurements for validation of the North Sea model results are obtained from the GTS (Global Telecommunications System) net that provides continuously wind and wave data worldwide. The wave model simulations of the fine resolution German Bight set-up have been validated with measurements recorded by the buoys of the BSH (Bundesamt für Seeschifffahrt und Hydrographie, Hamburg) and by the buoys of the HZG. The main focus of attention in the COSYNA project is directed on the conditions in the German Bight, therefore the discussion of the comparisons between the wave model results with measurements will be more detailed for that area. Fig. 4 indicates the buoy locations in the German Bight where wave measurements are available.

As representative examples for the validation of the wave model results in the German Bight some comparisons with measurements will be discussed for October 2013. In the end of that month the severe storm Christian afflicted the coasts of Germany with high wind speeds above 30 m/s and significant wave heights of about 8 m. Time series of wind and wave heights at FINO station are given on Fig. 5. At 28th of October during storm Christian the wind speed increases rapidly to 30 m/s causing brake down of several buoys and making impossible to provide measurements for this extreme event.

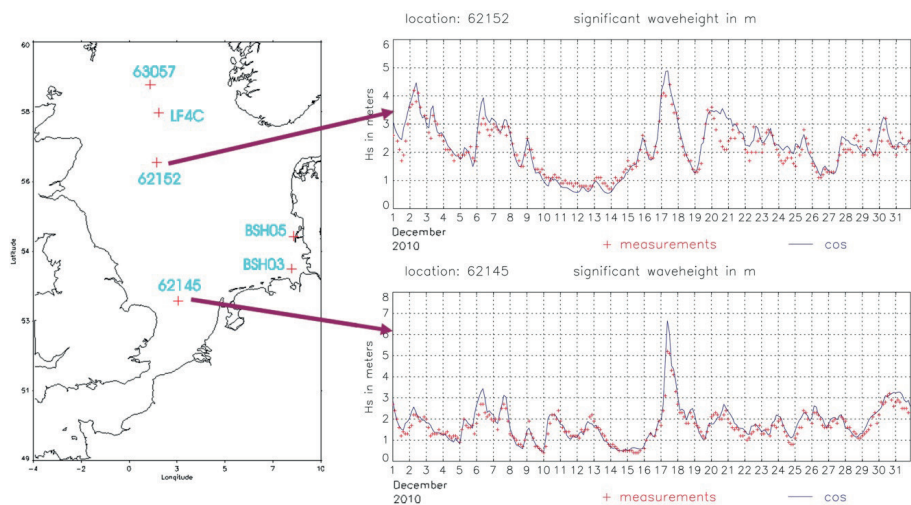


Figure 3: Time series of H_s for two locations in the North Sea model grid.

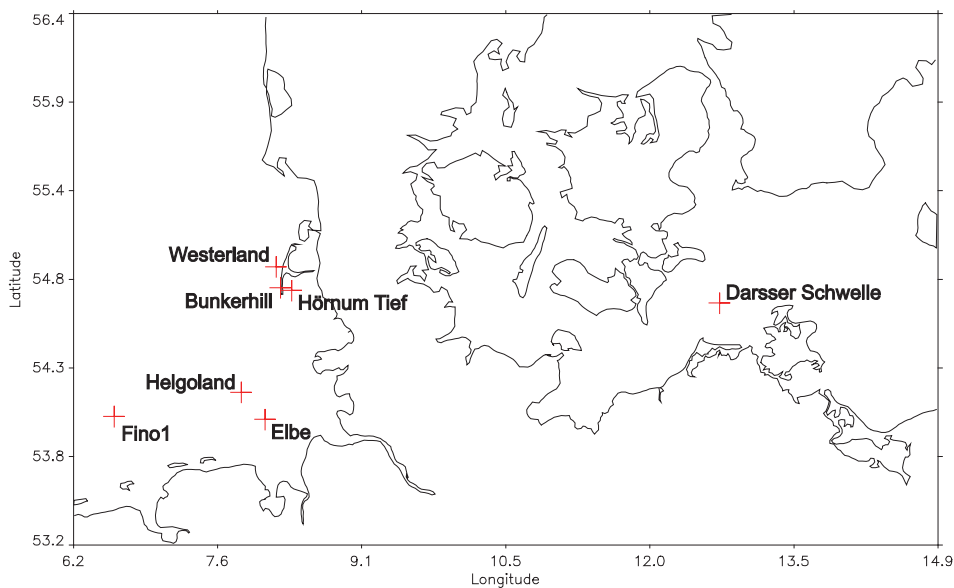


Figure 4: Buoy locations with measurements.

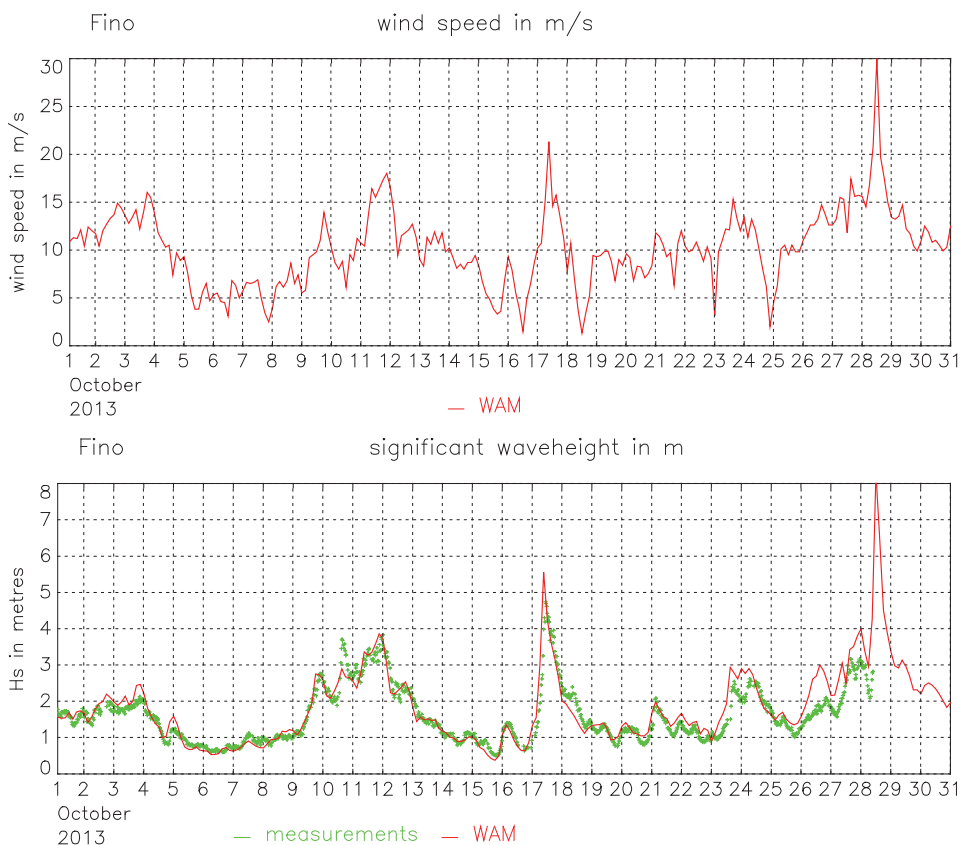


Figure 5: Time series of wind and wave heights at FINO station (storm Christian).

At Elbe and Helgoland stations (see Fig. 4 for their coordinates) the wave heights were lower than the ones at FINO station during Christian and they continuously recorded the wave parameters during the storm event. Fig. 6 includes the corresponding comparisons for significant wave heights, T_{m2}/T_z -periods and total wave directions at the location Elbe. The agreement between measured and modeled wave parameters is very good. The peak on the 28th of October (3 pm UTC) in H_s of about 6 m and in T_{m2} of about 8 s is well predicted by the wave model.

The same is valid for the comparisons done at Helgoland station despite the small underestimation at the peak by the model. The measured peak is higher here (7.7 m) compared with the Elbe station peak. The statistical analysis of the comparisons (see Tab. 2) supports the good quality of the pre-operational wave forecasts for the German Bight area.

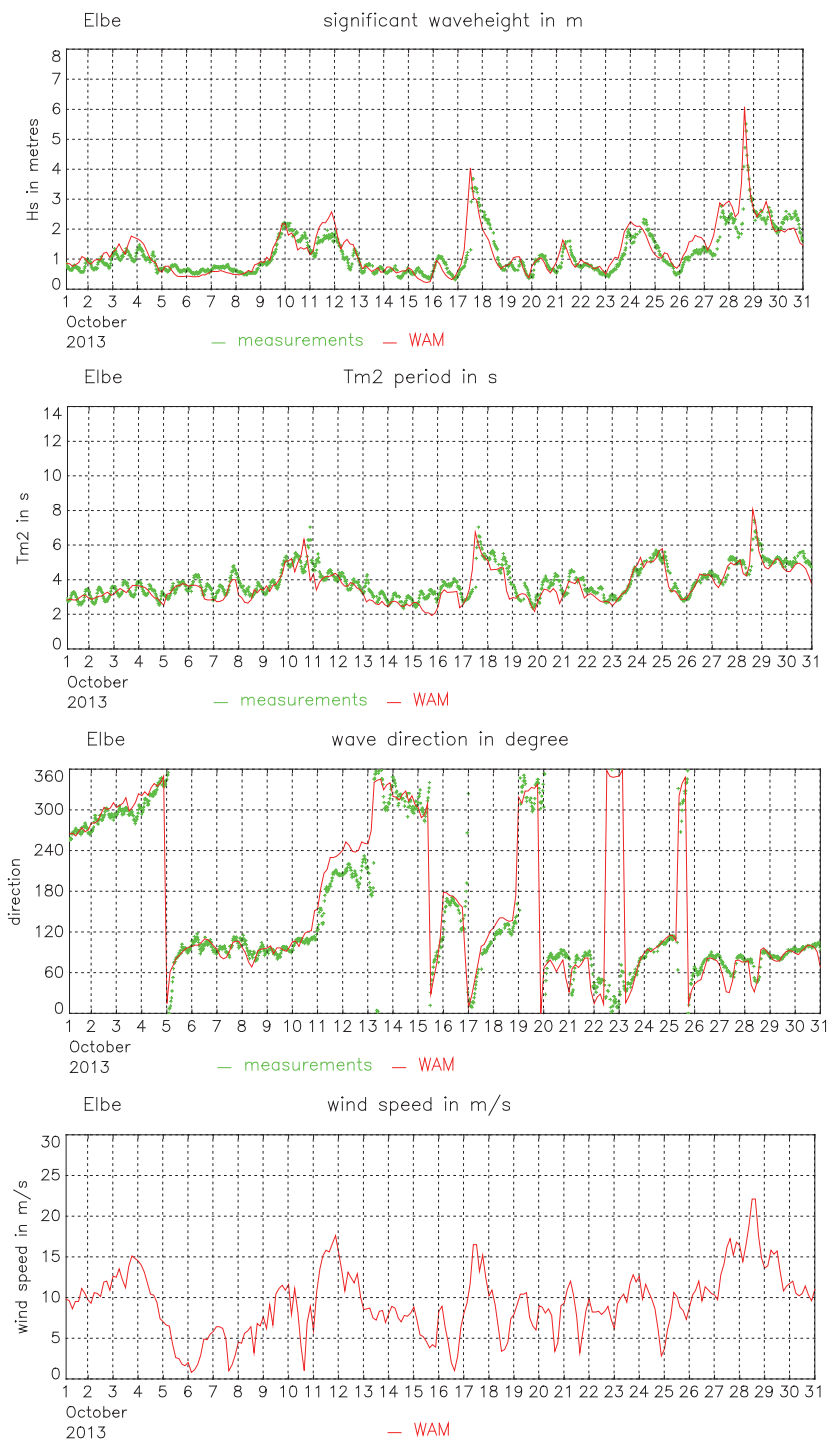


Figure 6: Time series of measured and computed wave parameters at the location Elbe.

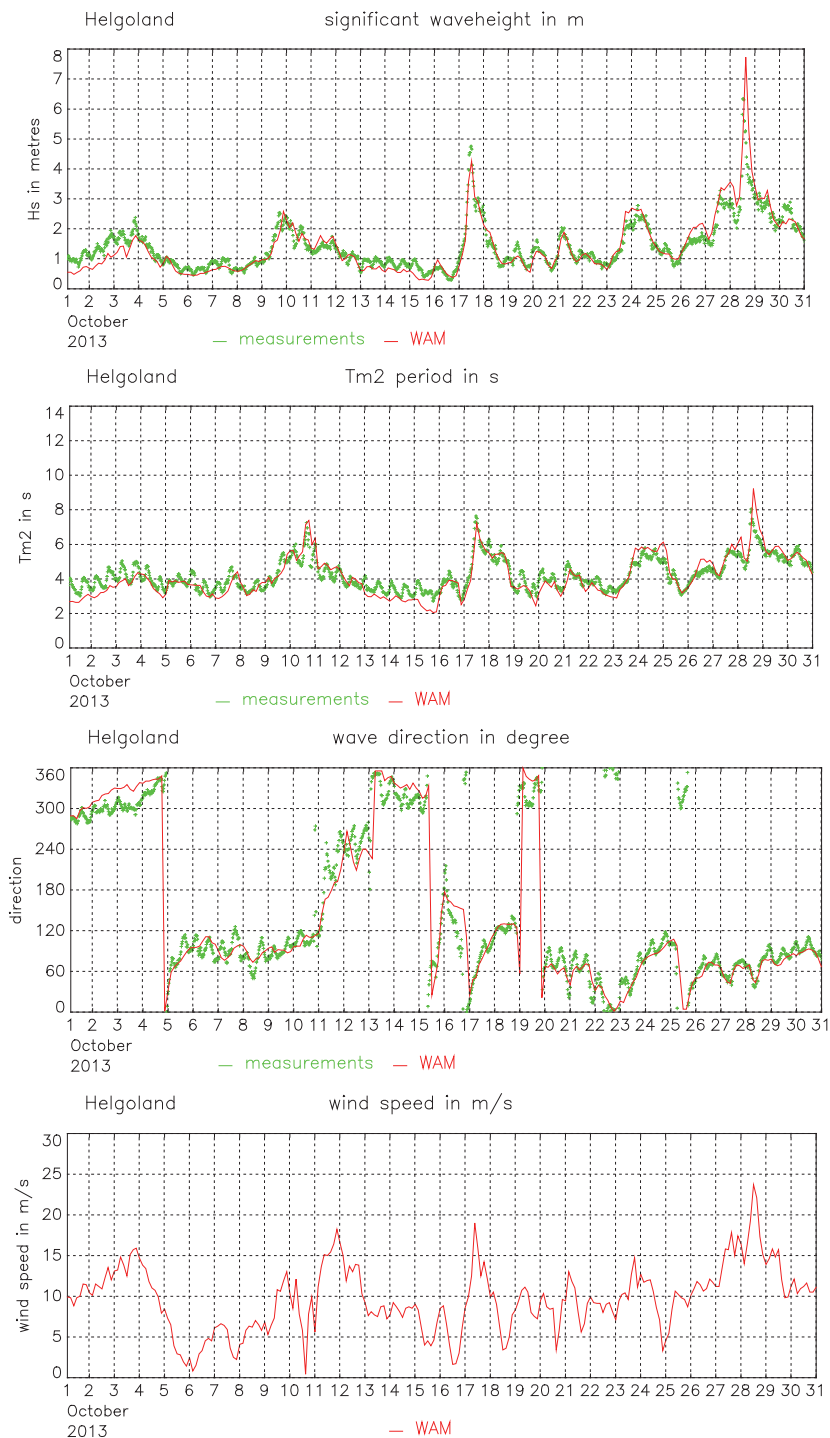


Figure 7: Time series of measured and computed wave parameters at the location Helgoland.

Table 2: H_s statistics for October 2013 at buoys located in the German Bight.

buoy	number of comparisons	mean of measurements	bias	root mean square error	skill	scatter index
H_s	-	(m)	(m)	(m)	-	(%)
Fino	218	1.59	0.11	0.33	0.86	19
Elbe	247	1.23	0.08	0.31	0.84	25
Westerland	247	1.17	0.14	0.28	0.88	21
Helgoland	247	1.45	-0.03	0.30	0.90	20
Tm_2/T_z		(s)	(s)	(s)		
Fino	218	4.53	-0.15	0.50	0.74	11
Elbe	247	3.92	-0.23	0.52	0.71	12
Westerland	247	4.07	-0.12	0.74	0.74	18
Helgoland	247	4.27	-0.11	0.52	0.80	12

skill : reduction of variance, scatter index : standard deviation*100/mean of the measurements

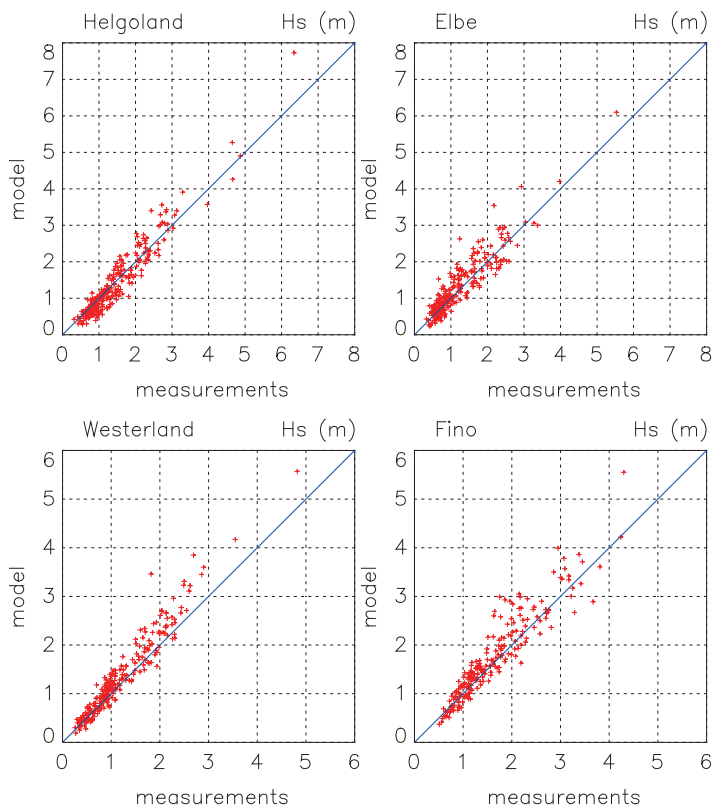


Figure 8: Scatterplots for measured and computed wave heights for October 2013.

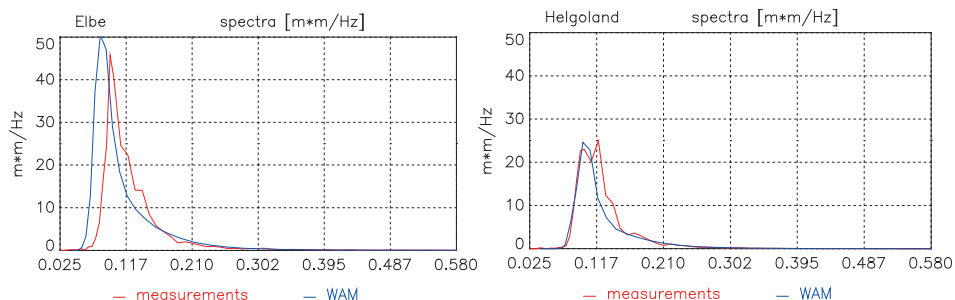


Figure 9: Comparison of measured and computed one-dimensional wave spectra at location Elbe (left) at the peak of storm Christian on 20131028 15:27 UTC (model results: 15:00 UTC) and at location Helgoland (right) at an intermediate peak on 20131017 11:46 UTC (model results: 12:00 UTC).

4 Multi-decadal regional wave simulations

Within coastDat (<http://www.coastdat.de/>) multi-decadal wave hindcasts and scenarios are provided as part of consistent meteo-marine reanalyses and scenarios. The objectives are to provide an assessment of ongoing and potential future changes in wave climate and to aid the development of adaptation options. Data from wave hindcasts are an essential part of the coastDat data base (WEISSE et al. 2009) that is used by more than 60 external partners from industry, administration and research. See Tab. 3 for which wave data is available within coastDat, the available wave parameters are given in Tab. 1.

Table 3: CoastDat wave datasets.

data set	time period	forcing	reference
Hindcast run-coastDat1	1958-2007	NCEP/NCAR Reanalyse	WEISSE and GÜNTHER (2007)
Hindcast run-coastDat2	1948-today	NCEP/NCAR Reanalyse	in progress
Scenario run-coastDat1	1961-1990/ 2071-2100	2x A2; 2x B2	GRABEMANN and WEISSE (2007)
Scenario run-coastDat2	1961-2100	4xA1B; 2x B1	GROLL et al. (2014); GRABEMANN et al. (2014)

The WAM model is used with nested grids for the North Sea for both hindcasts and future scenario simulations. The coarse grid covering the North East Atlantic takes into account for swell entering the North Sea, with about 50 km x 50 km spatial resolution. The fine grid simulations are using the spectral wave informations from the coarser model and has a resolution of about 5.5 km x 5.5 km. The hindcast simulations (WEISSE and GÜNTHER 2007) are driven by wind fields at 10 m height from the NCEP/NCAR global reanalyses regionalized by a regional climate model (FESER et al. 2005). The future scenario simulations are calculated by different combinations of GCMs, RCMs and emission scenarios (GRABEMANN and WEISSE 2008; GROLL et al. 2014 and GRABEMANN et al. 2014).

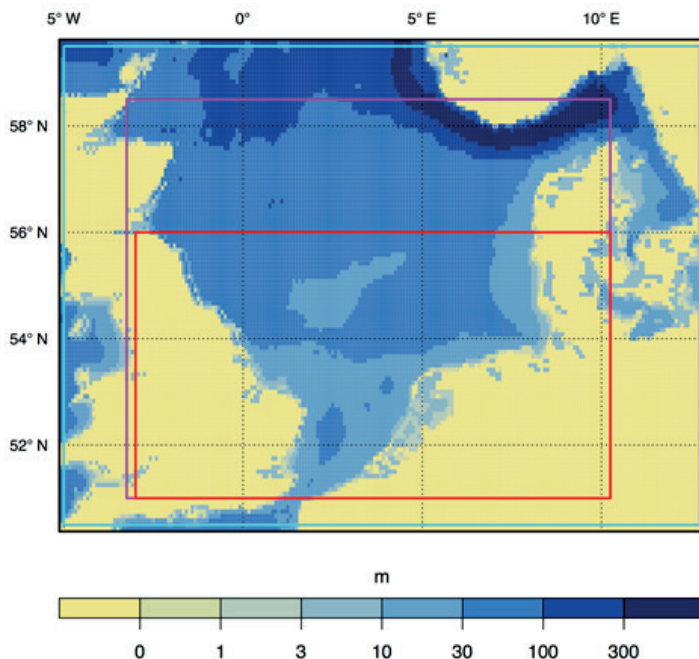


Figure 10: Simulated domains for the North Sea. Red box showing the domain in WEISSE and GÜNTHER (2007), the magenta box shows the domain for the climate change scenario simulations (GRABEMANN and WEISSE 2007; GROLL et al. 2014; GRABEMANN et al. 2014). The cyan box shows the new updated hindcast which is in progress and will be available soon.

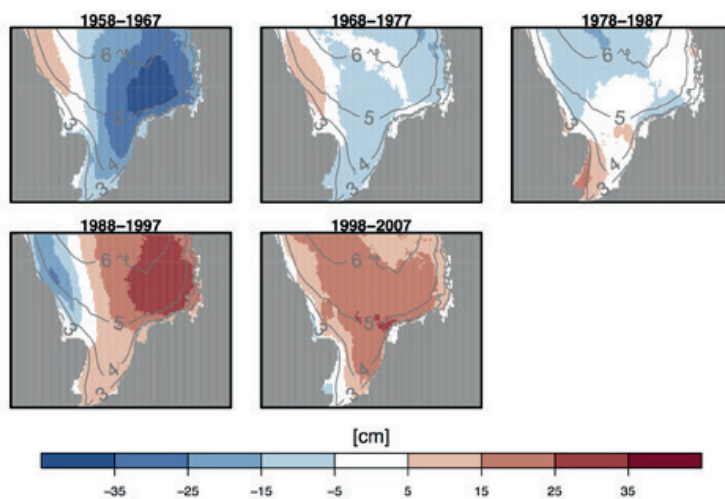


Figure 11: Difference of the 10-year-mean annual 99 %tile of significant wave height relative to the long-term-mean 1958-2007 (shown by contour lines) in the hindcast simulations (see WEISSE and GÜNTHER 2007).

To investigate long term changes of the waves parameters it is important to provide a database as much consistent as possible. This however is difficult to be done on the information based on observational data only. Using wave model simulations, one can minimize the effects of inhomogeneity caused by changes in instrumentation or measurement techniques.

Using WAM simulations Weisse and Günther (2007) studied the decadal variability of the wave parameters for the North Sea during the last decades. The differences of the ten-year-mean annual 99 percentile significant wave height of five periods relative to the long-term-mean 1958-2007 are demonstrated at Fig. 11. The results show an increase of the significant wave height towards the end of the 20th century, but also a weaker tendency to increase in the last ten years for the German Bight. In the newly available wave model hindcast, (work in progress), which will cover a longer period and the whole North Sea it will be possible to further investigate the wave climate variability in the North Sea region.

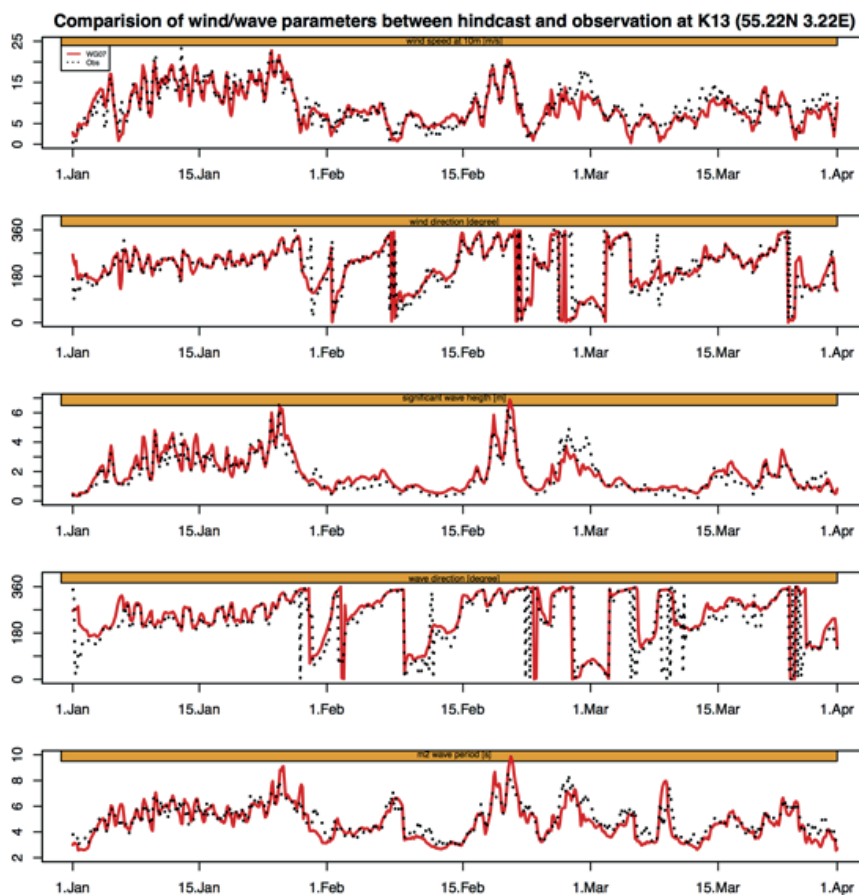


Figure 12. Time series of wind speed (m/s), wind directions (degrees, going to), significant wave height (m), wave direction (degrees, going to) and m2 (s) wave period at K13 for a 3-month period from 1 Jan 1993 to 31 Mar 1993. Observations (dotted black) and model results (red) (see WEISSE and GÜNTHER 2007).

Table 4: Set of ten climate change wave projections calculated within the framework of coastDat (see GRABEMANN et al. 2014).

acronym	time period	forced by RCM	forced by GCM	references
C20_1C A1B_1C B1_1C	1961-2000 2001-2100 2001-2100	COSMO-CLM ROCKEL et al. (2008)	ECAHM5/MPI-OM RÖCKNER et al. (2003) MARSLAND et al. (2003) with two initial conditions	GROLL et al. (2014) GRABEMANN et al. (2014)
C20_2C A1B_2C B1_2C	1961-2000 2001-2100 2001-2100			
C20_3R A1B_3R C20_3H A1B_3H	1961-2000 2001-2100 1961-2000 2001-2099	REMO JACOB et al. (2007) HIRHAM CHRISTENSEN et al. (2007)	ECAHM5/MPI-OM RÖCKNER et al. (2003) MARSLAND et al. (2003) with the third initial conditions	GRABEMANN et al. (2014)
C_E A2_E B2_E C_H A2_H B2_H	1961-1990 2071-2100 2071-2100 1961-1990 2071-2100 2071-2100	RCAO RUMMUKAINEN et al. (2001) RÄISÄNEN et al. (2004)	ECHAM4/OPYC3 RÖCKNER et al. (1999) HadAM3H GORDON et al. (2000)	GRABMANN and WEISSE (2007) GRABEMANN et al. (2014)

Validation of the hindcast simulations with wave observations at the platform K13 for a three month period in 1993 is demonstrated on Fig. 12. Beside some differences the hindcast simulations show a relatively good agreement with observations. A comparison of the 3-hourly significant wave height observations at the platform K13 and the results from the hindcast simulation or the period 1980-2000 is given in Fig. 13. For mean conditions a relatively good agreement can be found, whereas the higher waves show a small overestimation by the numerical simulations.

Within the framework of coastDat several wave studies with climate change scenarios have been compiled. GRABEMANN and WEISSE (2007) calculating time slice experiments for the period 2071 to 2100 and the reference period 1961-1990 with two emission scenarios (A2 and B2) and two different GCMs and one RCM. GROLL et al. (2014) were calculating transient simulations (1961-2100) with one GCM but with different initial conditions and two emission scenarios (A1B and B1) and with one RCM (CCLM). GRABEMANN et al. (2014) compared and discussed these eight wave experiment together with two wave simulations, using one GCM, one emission scenario (A1B) but different RCMs. See Tab. 4 for more details.

The difference of the 30-year-mean annual 99.9 percentile significant wave height between the period 2071-2100 and the corresponding reference climate 1961-1990 for these ten climate change simulations is shown in Fig. 14. Focusing at the German Bight all ten simulations show an increase towards the end of the 21th century, but the magnitude of the increase is much more uncertain and vary between almost zero and up to one meter. Also in other parts of the North Sea the spatial variability between the ten simulations is evident. Generally an increase in the eastern part of the North Sea can be found, whereas in the western parts the changes are less strong and even a decrease in

some of the simulations can be found. Analysis of the six transient simulations show also an strong multi-decadel variability throughout the whole simulation period and point to the internal climate variability of the climate system (GROLL et al. 2014 and GRABEMANN et al. 2014).

The data generated within the framework of coastDat delivers a long, consistent and homogenous as possible description of the North Sea wave climate, which is important to investigate and understand the climate variability in data sparse regions, like the North Sea. Wave data that are generated within these climate change and hindcast simulations are available to external clients and are used for a variety of offshore and coastal purposes. For instance during the planning and design phase of offshore wind farms wave data from the hindcast are used to calculate return values of extreme events and to estimate time windows for certain wave conditions that are necessary for construction and maintenance. The wave data is also used by ship yard companies to optimize the ship profiles. For details see WEISSE et al. (2009). Beside a regular update of the hindcast simulation, in the future, simulations with higher resolution, which is important for near-coastal applications are planned.

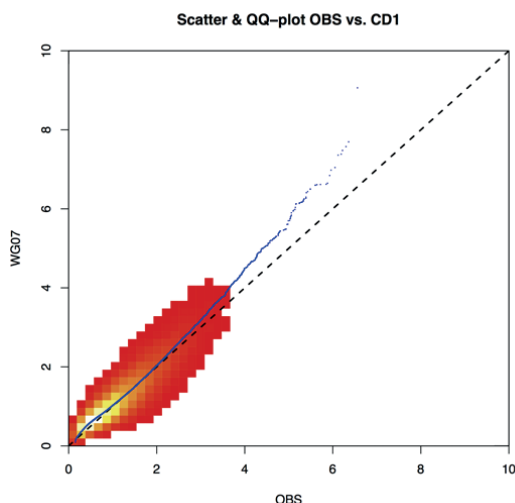


Figure 13: Scatter of 3 hourly significant wave height for the period 1980-2000 between observations at platform K13 and simulated data from the hindcast (WEISSE and GÜNTHER 2007). Blue dots showing the quantile-quantile plot for tenth percentiles wave height (0,0.1,0.2,.....99.8,99.9,100).

Not only wave climate simulations are part of the coastDat framework and are used by clients, but also other important marine climate variables, e.g. marine surface wind, water level, are considered, for more information see www.coastdat.de.

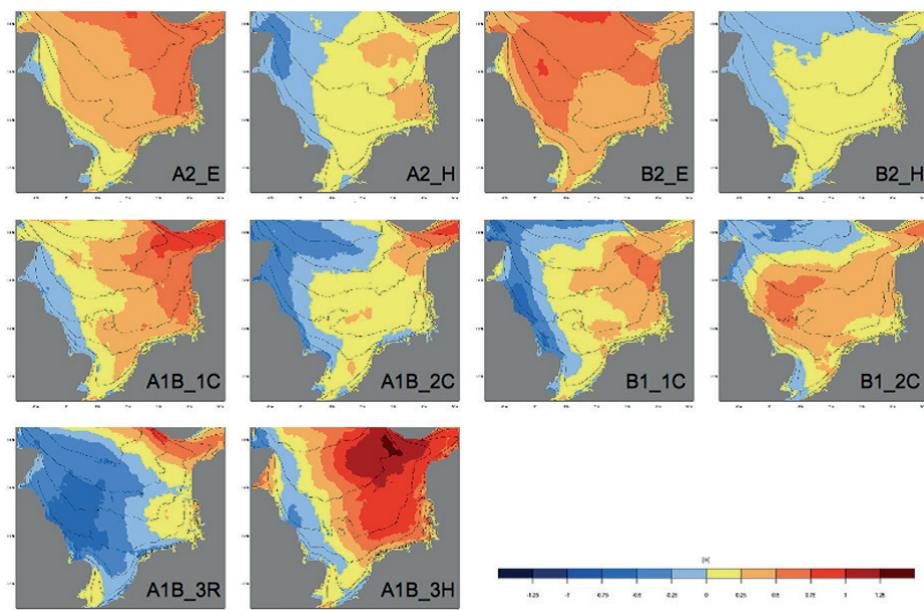


Figure 14: Differences of the 30-year mean of annual 99.9 percentile significant wave height in meters for the period 2071-2100 relative to 1961-1990 for each of the 10 projections. Black contour lines indicate the 30-year mean of annual 99.9 percentile significant wave height in meters for the corresponding reference period (see GRABEMANN et al. 2014).

5 Wave-current interaction

The role of the coupling of wave and circulation models on improving the ocean forecast is demonstrated for the German Bight region. The German Bight (southern North Sea) is characterized by wind-waves and strong tidal currents. As a result, processes like nonlinear feedback between currents and waves play an important role in this area. The coupling between the wave model (WAM) and hydrodynamical model (GETM, BURCHARD et al. 2002) improves the estimates of ocean state variables, especially in coastal areas like the Wadden Sea and estuaries (for more details about the model configuration see STANEVA et al. 2009). The coupling takes into consideration both: the effect of currents on waves and the effects of waves on upper ocean dynamics, in particular on mixing and drift currents. In WAM the depth and/or current fields can be non-stationary, grid points can fall dry and refraction due to spatially varying current and depth is accounted for in the quasi-stationary approach. GETM was modified to account for wave effects by introducing the depth dependent radiation stresses and Stokes drift. The terms were calculated from the integrated wave parameters according to MELLOR (2008). The gradient of the radiation stresses serves as an additional explicit wave forcing term in the momentum equations for the horizontal velocity components. The transfer of momentum by waves becomes important for the mean water level setup and for the alongshore currents generated by waves in the surf zone.

We demonstrate the role on coupling by analyzing the impact of waves on extreme events (storm on 06.12.2013, see Fig. 15). The radiation stress increases the average water levels, which is much pronounced in the coastal area. During normal conditions the differences of the sea level due to the coupling with wave model maximum 10-15 cm in the Elbe area. However, during the storm Xaver on 06.12.2013 (left), the differences of simulated sea level when considering waves are about 30-40 cm along the whole German coast. Therefore the uncertainties in most of the presently used models result from the nonlinear feedback between strong tidal currents and wind-waves, which can no longer be ignored in the operational oceanography, in particular in the coastal zone where its role seems to be dominant.

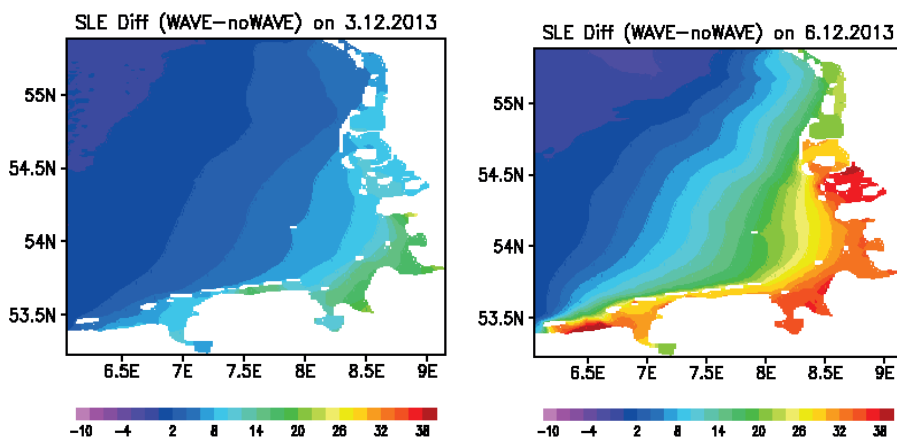


Figure 15: Sea surface elevation (SLE) difference between coupled wave-circulation model (WAM-GETM) and only circulation model (GETM) for the German Bight at 03.12.2013 (left) and during the storm Xaver on 06.12.2013.

6 Conclusions

Wave hindcasts and forecasts for the North Sea and German Bight are of great importance for the management of coastal zones, ship navigation, off-shore wind energy, naval operations etc. Storms and wind waves which they generate have direct impacts on the on the coastal and marine environment. The population living in the coastal areas is recently concerned with the impacts of erosion and flooding, and activities of what can be done to predict and further to minimize them. Important driving forces that cause serious damages on coastal environment are the wave conditions. Latter can be determined by using as a tool coastal numerical wave model systems. In this paper we summarized the recent advances in the field of wave modelling for the North Sea and German Bight regions. The state-of-the-art development of the WAM wave model for forecasts applications at operational services and for hindcasts and climate assessments for the North Sea and the German Bight in HZG is demonstrated. The synergy between observations and models for the North Sea and German Bight is increased on the road to improving the ocean state estimate and predictions in the coastal areas and generating up-to-date information, products and knowledge. The very good agreement between observations and model simulations is being demonstrated for both the long term wave

hindcasts and short term wave forecasts for the North Sea and German Bight area. It enables to provide reliable predictions as well as to analyze long term changes of wave conditions, including extreme events. The performance of the forecasting system is illustrated for the cases of several extreme events. Effects of ocean waves on coastal circulation are investigated during extreme events, as well. The improved skill resulting from the recent wave model developments, in particular during storms, justifies further enhancements of the both forecasts applications at operational services and long-term hindcasts and climate for the North Sea and the German Bight.

Short-term wave forecasts, sea state reconstructions and climate scenarios computations with the WAM model have created a huge interest to use the data in industrial applications. Within CoastDat multi-decadal wave hindcasts and scenarios are provided as part of consistent meteorological-marine reanalyses and scenarios aiming to provide an assessment of ongoing and potential future changes in wave climate and to aid the development of adaptation options. The pre-operational COSYNA wave forecast system for the North Sea and the German Bight provides wave forecasts twice a day delivering a number of wave parameters such as wave height, period and direction and is a very good example of how wave modelling products can support coastal management in the context of climate change and human activities. Data from wave forecasts and hindcasts form an essential part of the COSYNA and coastDat data base that are being actively used by partners from industry, administration and research

7 References

- BEHRENS, A. and GÜNTHER, H.: Operational wave prediction of extreme storms in Northern Europe, *Natural Hazards*, Volume 49, Issue 2 (2009), 387-399, doi: 10.1007/s11069-008-9298-3, 2009.
- BIDLOT, J.; JANSSEN, P. and ABDALLA, S.: A revised formulation for ocean wave dissipation in CY29R1. Memorandum Research Department of ECMWF, April 7, 2005 File: R60.9/JB/0516, 2005.
- BURCHARD, H. and BOLDING, K.: GETM - a General Estuarine Transport Model, No EUR 20253 EN, printed in Italy, European Commission, 2002.
- CHRISTENSEN, O.B.; DREWS, M.; CHRISTENSEN, J.H.; DETHLOFF, K.; KETELSEN, K.M.; HEBESTADT, I. and RINKE, A.: The HIRHAM Regional Climate Model Version 5 (beta). Technical Report 06-17, 22pp, Danish Meteorological Institute, 2007.
- GORDON, C.; COOPER, C.; SENIOR, C.A.; BANKS, H.; GREGORY, J.M.; JONES, T.C.; MITCHELL, J.F.B. and WOOD, R.A.: The simulation of SST, sea ice extents and ocean heat transports in a version of the Hadley Centre coupled model without flux adjustments. *Clim Dyn* 16, 147-166, 2000.
- GRABEMANN, I. and WEISSE, R.: Climate change impact on extreme wave conditions in the north sea: an ensemble study. *Ocean Dynamics* 58:199-212, doi: 10.1007/s10236-008-0141-x, 2008.
- GRABEMANN, I.; GROLL, N.; MÖLLER, J. and WEISSE, R.: Climate change impact on North Sea wave conditions: a consistent analysis of ten projections. Submitted to *Ocean Dynamics*, 2014.

- GROLL, N.; GRABEMANN, I. and GASLIKOVA, L.: North Sea wave conditions: an analysis of four transient future climate realizations. *Ocean Dynamics* 64, 1-12, doi: 10.1007/s10236-013-0666-5, 2014.
- GÜNTHER, H.; HASSELMANN, S. and JANSSEN, P.A.E.M.: The WAM Model Cycle 4.0. User Manual. Technical Report No. 4, Deutsches Klimarechenzentrum, Hamburg, Germany. 1992.
- HERSBACH, H. and JANSSEN, P.A.E.M.: Improvements of the short fetch behavior in the WAM model. *J. Atmos. Oceanic Techn.*, 16, 884-892, 1999.
- JACOB, D.; BÄHRING, L.; CHRISTENSEN, O.B.; CHRISTENSEN J.H.; CASTRO DE, M.; DÉQUÉ, M.N.; GIORGI, F.; HAGEMANN, S.; HIRSCHI, M.; JONES, R.; KJELLSTRÖM, R.; LENDERINK, G.; ROCKEL, B.; SÁNCHEZ, E.; SCHÄR, C.; SENEVIRATE, S.; SORNOT, S.; ULDEN VAN, A. and HURK VAN DEN, B.: An intercomparison of regional climate models for Europe: Design of the experiments and model performance. *Climatic Change* 81, Supplement 1:31-52, 2007.
- KOMEN, G. J.; CAVALERI, L.; DONELAN, M.; HASSELMANN, K.; HASSELMANN, S. and JANSSEN, P.A.E.M.: Dynamics and modelling of ocean waves. Cambridge University Press, Cambridge, UK, 1995.
- MARSLAND, S.; HAAK, H.; JUNGCLAUS J.; LATIF, M. and RÖSKE, F.: The Max-Planck-Institute global ocean/sea ice model with orthogonal curvilinear coordinates. *Ocean Modeling* 5, 91-127, 2003.
- MOGHIMI, S.; GAYER, G.; GÜNTHER, H. and SHAFIEEFAR, M.: Application of 3rd Generation shallow Water Wave Models in a Tidal Environment. *Ocean Dynamics*, 55, 10-27, 2005.
- MONBALIU, J.; PADILLA-HÉRNANDEZ, R.; HARGREAVES, J.C.; CARRETERO ALBIACH, J.C.; LUO, W.; SCLAVO, M. and GÜNTHER, H.: The spectral wave model WAM adapted for applications with high spatial resolution. *Elsevier Coastal Engineering* 41, 41-62, 2000.
- RÄISÄNEN, J.; HANSSON, U.; ULLERSTIG, A.; DÖSCHER, R.; GRAHAM, L.P.; JONES, C.; MEIER, H.E.M.; SAMUELSSON, P. and WILLÉN, U.: European climate in the late twenty-first century: regional simulations with two driving global models and two forcing scenarios. *Clim Dyn* 22:13-31, doi: 10.1007/s00382-003-0365-x, 2004.
- ROCKEL, B.; WILL, A. and HENSE, A. (eds): Special issue Regional climate modeling with COSMO-CLM (CCLM), vol 17. *Met.*, 2008.
- RÖCKNER, E.; BENGTTSSON, L.; FEICHTER, J.; LELIEVELD, J. and RODHE, H.: Transient climate change simulations with a coupled atmosphere-ocean GCM including the trophospheric sulfur cycle. *J Climate* 12, 3004-3032, 1999.
- RÖCKNER, E.; BÄUML, G.; BONAVENTURA, L.; BROKOPF, R.; ESCH, M.; GIORGETTA, M.; HAGEMANN; KIRCHNER, I.; KORNBLUEH, L.; MANZINI, E.; RHODIN, A.; SCHLESE, U.; SCHULZWEIDA, U. and TOMPKINS, A.: The atmospheric general circulation model echam5. part i: model description. *Mpi - rep 349*, Max Planck Institute for Meteorology, 2003.
- RUMMUKAINEN, M.; RÄISÄNEN, J.; BRINGFELT, B.; ULLERSTIG, A.; OMSTEDT, A.; WILLÉN, U.; HANSSON, U. and JONES, C.: A regional climate model for Northern Europe: model description and results from the downscaling of two GCM control simulations. *Clim Dyn* 17:339-359, 2004.

- STANEV, E.V.; SCHULZ-STELLENFLETH, J.; STANEVA, J.; GRAYEK, S.; SEEMANN, J. and PETERSEN, W.: Coastal observing and forecasting system for the German Bight – estimates of hydrophysical states, *Ocean Sci.*, 7, 569-583, 2011.
- STANEVA, J.; STANEV, E.; WOLFF, J.-O.; BADEWIEN, T.H.; REUTER, R.; FLEMMING, B.; BARTHOLOMAE, A. and BOLDING, K.: Hydrodynamics and sediment dynamics in the German Bight. A focus on observations and numerical modeling in the East Frisian Wadden Sea, *Cont. Shelf Res.*, 29, 302-319, 2009.
- WAMDI GROUP: The WAM Model – A Third Generation Ocean Wave Prediction Model. *Journal of Physical Oceanography*, 18, 1775-1810, 1988.
- WEISSE, R. and GÜNTHER, H.: Wave climate and long-term changes for the southern north sea obtained from a high-resolution hindcast 1958-2002. *Ocean Dynamics* 57, 161-172, doi: 10.1007/s10236-006-0094-x, 2007.
- WEISSE, R.; VON STORCH, H.; CALLIES, U.; CHRASTANSKY, A.; FESER, F.; GRABEMANN, I.; GÜNTHER, H.A.; PLÜSS, T.S.; TELLKAMP, J.; WINTERFELDT, J. and WOTH, K.: Regional meteorological-marine reanalysis and climate change projections. Results for northern Europe and potential for coastal and offshore applications. *Bulletin of the Amer Met Soc* 90(6):849–860, doi: 10.1175/2008BAMS2713.1, 2009.

An Operational Oil Drift Forecasting System for German Coastal Waters

Silvia Maßmann, Frank Janssen, Thorger Brüning, Eckhard Kleine, Hartmut Komo, Inge Menzenhauer-Schumacher and Stephan Dick

Summary

Today, the presented (oil-) drift and dispersion model is a well-established component of the German marine pollution response system. The oil drift model is part of a comprehensive operational ocean forecasting system applied at the Federal Maritime and Hydrographic Agency (BSH). Development of the oil drift model started already in the 1980's, but it was considerably advanced in several directions over the years. The latest development is the operationalization of the SeatrackWeb system at BSH.

A 3-dimensional regional ocean circulation model provides – in combination with numerical weather forecasts of the German Weather Service (DWD) – the forcing for the oil drift component. The region covered by the model system is the whole North and Baltic Sea with special focus on the German Bight and the western Baltic Sea. Based on the pre-calculated and archived forcing data the oil drift model can be run on demand at any time. The basic approach is a Lagrangian particle tracking method, i.e. the simulated oil spill is described by a large number of particles which carry characteristics of specific types of oil. By this approach not only the drift but also the so-called “weathering” of the oil can be calculated. All fundamental processes which alter the oil during the fate of an oil spill, e.g. spreading, dispersion, evaporation and emulsification, are included.

The particle tracking and oil weathering components, which are at the core of the model are connected to a modern, interactive, graphical user interface (GUI), which provides the user, e.g., with the possibility to directly start simulations from satellite detections of oil spills. The GUI gives access to several layers of useful information, e.g. ocean currents, wind direction, the location of oil platforms or shipping routes. Besides that, it visualizes ship signals from the Automatic Identification System (AIS), which are important means when it comes to the identification the potential source of an oil spill.

In this paper we first present the current BSH operational ocean forecasting system highlighting some recent developments. The core of the oil drift component will be described in some detail. The main part of the paper will show results of some real cases. Based on these results some scientific questions like, e.g., the influence of wave induced Stokes drift will be discussed.

Keywords

SeatrackWeb, oil spill, ocean forecast, operational ocean model, North Sea, Baltic

Zusammenfassung

Heute ist das hier dargestellte (Öl-) Drift- und Ausbreitungsmodell fester Bestandteil des deutschen Meeresverschmutzungsbekämpfungssystems. Das Öldriftmodell ist dabei Teil eines umfassenden operationellen Vorhersagesystems des Bundesamtes für Seeschifffahrt und Hydrographie (BSH). Die Entwicklung des Öldriftmodells begann bereits in den frühen 1980er Jahren, wurde aber über die Jahre in mehrere Richtungen wesentlich weiterentwickelt. Die jüngste Entwicklung ist die Operationalisierung von SeatrackWeb am BSH.

Ein 3-dimensionales regionales Ozeanmodell liefert – in Kombination mit der numerischen Wettervorhersage des Deutschen Wetterdienstes (DWD) – den Antrieb für die Öldriftkomponente. Die vom Modell abgedeckte Region ist die gesamte Nord- und Ostsee mit speziellem Fokus auf der Deutschen Bucht

und der westlichen Ostsee. Basierend auf den vorberechneten und archivierten Antriebsdaten, kann das Öldriftmodell nach Bedarf jederzeit gestartet werden. Der Modellansatz ist eine Lagrangesche Partikelverfolgungsmethode, d.h. das simulierte Öl wird beschrieben als große Anzahl von Partikeln, die die Eigenschaften des spezifischen Öltyps tragen. Mit dieser Methode wird nicht nur die Verlagerung, sondern auch die sogenannte „Verwitterung“ des Öls berechnet. Es werden dazu alle fundamentalen Prozesse, die das Öl während des Abbaus einer Ölverschmutzung verändern, d.h. Spreading, Dispersion, Verdunstung und Emulsifikation, simuliert.

Die Partikelverfolgungs- und Ölverwitterungskomponenten, die den Kern des Modells bilden, sind mit einer modernen, interaktiven, graphischen Anwenderoberfläche (GUI) verbunden, die dem Anwender z. B. die Möglichkeit gibt, Simulationen direkt von Satelliten-detektierten Ölflecken zu starten. Die GUI ermöglicht die Darstellung verschiedener Layer mit nützlichen Informationen wie z. B. Ozeanströmungen, Windrichtungen, die Lage von Ölplattformen und Schifffahrtsrouten. Daneben visualisiert sie die Schiffssignale des Automatischen Identifikationssystems (AIS), welche ein wichtiges Mittel zur Identifikation möglicher Quellen von Ölverschmutzungen sind.

In diesem Artikel präsentieren wir zuerst das derzeitige operationelle BSH-Meeresvorhersagesystem mit Schwerpunkt auf den jüngsten Entwicklungen. Der Kern der Driftmodellkomponente wird in einigem Detail beschrieben. Der Hauptteil des Artikels wird Ergebnisse von einigen realen Fällen zeigen. Basierend auf diesen Resultaten, werden einige wissenschaftliche Fragen wie z. B. des Einflusses der welleninduzierten Stokes Drifts diskutiert.

Schlagwörter

Seatrack Web, Ölverschmutzung, Meeresvorhersagen, operationelle Ozeanmodelle, Nordsee, Ostsee

Contents

1	Introduction	257
2	Model system	257
	2.1 Overview	258
	2.2 PADM.....	259
	2.3 Graphical User Interface.....	261
3	Results.....	262
	3.1 Ship average in Skagerrak area.....	262

3.2	Container drift in the German Bight.....	264
4	Concluding remarks and perspectives.....	269
5	Acknowledgement.....	270
6	References.....	270

1 Introduction

During and after the Deepwater Horizon oil spill caused by a drilling rig explosion in the Gulf of Mexico on 20 April 2010 oil spill models were intensively used to get an insight in pathways and fate of the enormous amounts of oil that have entered the ocean. Many countries around the world have built up an oil spill modelling capacity over the last decades which have been scrutinized in the light of this major accident at several places.

Oil spill models have become widely accepted and applied tools to assist the combatting of oil spills at sea. Several different drift models are operated by marine agencies, coastguards and institutions around the North and Baltic Sea. The Norwegian Meteorological Institute (met.no) develops OD3D and uses this as well as OSCAR in their forecasts. In Belgium the drift models FLOAT and OSERIT are developed and hosted by RBINS-MUMM and are used by the Belgian coastguard agency. In the UK CEFAS is responsible for doing the operational drift forecasts and they use their in-house developed CEFAS SPILL and commercial solutions like OILMAP or OSCAR. In the Netherlands RWS and Deltares use as well the commercial software OILMAP and also CHEMMAP. METEO-FRANCE is also able to do drift simulations in the North Sea with their drift model MOTHY, although this is not their main region of interest. Most of the models are very specialized towards simulation of oil at sea, whereas others are more generalized drift and dispersion models which can be applied to a wide range of applications like search-and-rescue at sea, the drift of all kinds of objects, including lost containers or buoys that have broken loose, and last but not least the fate of floating or submerged oil.

The Federal Maritime and Hydrographic Agency (BSH) has, among several other duties, the task to support the combatting of oil pollution in German territorial waters. This includes both, the support of the parties involved in oil combatting, e.g. the Central Command for Marine Emergencies, directly after an oil spill has happened as well as – at a later stage – the support of the prosecuting authorities in identifying the polluter in case of an illegal discharge. In order to fulfill this task BSH runs and maintains a comprehensive numerical model system. The system consists of several components. Two of them, namely the three-dimensional ocean circulation model BSHcmod and the drift and dispersion model SeatrackWeb are of special importance for the topic at hand and will be described in some detail below.

2 Model system

This section provides an overview of the applied model system. Some of the important features of the core part of the SeatrackWeb drift model – PADM – and of the graphical user interface (GUI) are summarized. The area, where users can perform drift simulations with the BSH setup of SeatrackWeb is presented here as well.

2.1 Overview

The numerical weather forecast models of the German Weather Service (DWD), COSMO-EU (LME) and GME, are at the top level of the applied model chain. LME and GME provide the needed atmospheric forcing for both ocean model components on a four-times-daily basis with a forecast lead time of up to 7 days. BSHcmod is run with a horizontal resolution of about 5 km for the whole North and Baltic Sea area and comes with a 2-way nested grid increasing the resolution to about 900 m in the German Bight and western Baltic Sea (DICK et al. 2001). A further refinement of grid resolution up to 90 m has recently been achieved for the sub-region of the Elbe estuary (MÜLLER-NAVARRA and BORK 2012). Besides the atmospheric forcing, the tidal water level at the open boundaries in the North Sea and freshwater inflow from the largest rivers are driving forces of the circulation model. At present BSHcmod provides a three day forecast of water level, current, temperature, salinity and ice coverage once a day in fully automatic fashion. The model output is archived with a time step of 15 minutes for water level and current and hourly for the other variables together with the atmospheric forcing. The model data archive provides the basis for all drift simulations and a range of further applications.

To forecast the drift of oil, objects and conservative substances a Lagrangian dispersion model is used. To date an in-house developed Lagrangian drift model, called BSHdmod.L (DICK and SOETJE 1990) is applied at BSH. BSHdmod.L uses the above mentioned archived BSHcmod model fields and wind forecasts of LME. It was one of the first Lagrangian dispersion models operationally predicting oil drift and fate in North and Baltic Sea and has been very successfully applied in the past e.g. during the Pallas wreck-age in 1998 or the Baltic Carrier collision in 2001. Later on the model code was shared with neighboring North and Baltic Sea countries like Denmark or Sweden, where it developed in parallel. The Swedish Meteorological and Hydrological Institute (SMHI) and the predecessor institution of the Forsvarets Center for Operativ Oceanografi (FCOO) used BSHdmod.L to upgrade the common HELCOM modelling and drift forecasting system for oils and chemicals called SeatrackWeb. They continuously developed the drift model core (called Particle Advection and Dispersion Model, PADM), enhanced it with a graphical user interface (GUI) and made it accessible via the internet (AMBJÖRN et al. 2011).

Several institutes run SeatrackWeb separately and in different versions. For example SMHI hosts the official HELCOM site (<https://stw-helcom.smhi.se/>) and extra production sites for special users in Swedish lakes and fjords (Vänern and Brodjorden) while FCOO hosts their own version for Danish users. BSH joined the SeatrackWeb developer group in 2006 and adapted SeatrackWeb for BSH special requirements for example the use of nested grids and an extended model area. Recently SeatrackWeb runs in operational mode using BSHcmod forcing. The BSH version of SeatrackWeb is available under <http://stw.bsh.de/seatrack>.

Mainly German authorities, including BSH itself, are the users of the BSH version of SeatrackWeb, so the target area of the model is the German Bight and the Western Baltic Sea with a 900 m resolution of the water current field (see blue area in Fig.1). Outside this area the currents have a resolution of about 5 km in the North-, Baltic Sea and in parts of the English Channel.

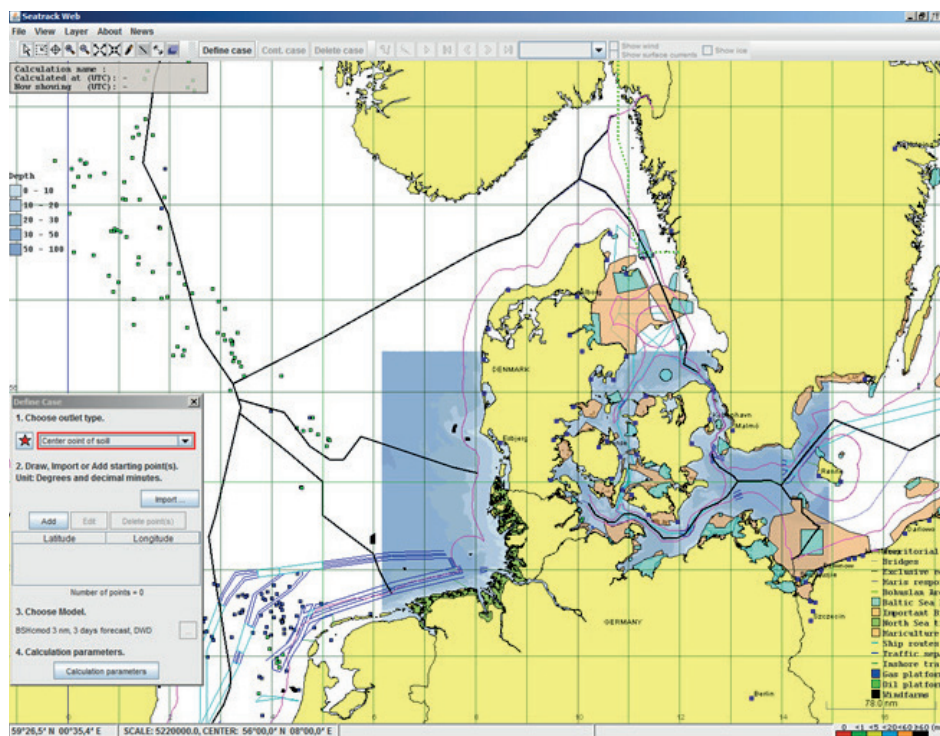


Figure 1: Maps and geographic information displayed in SeatrackWeb Java GUI. The blue area indicates depth values of the fine North and Baltic Sea grid of BSHcmod. Land as defined by the coastline is displayed in yellow.

2.2 PADM

PADM stands for Particle Advection and Dispersion Model and is the core of Seatrack-Web calculating the advection of a substance or object by representing it by a cloud of particles (with the so called Lagrangian method).

Each particle represents a certain amount of the simulated substance. The particles move individually in three dimensions not affecting the surrounding flow field. Except for the gravitational spreading algorithm the particles do not influence each other (no collisions, etc.). When particles hit a boundary, like a coastline, the bottom or the boundaries of the model domain, it sticks to, slips along or passes through this boundary. Oil, for example, sticks at the coastline and at the bottom, while objects slip along these boundaries.

Each particle holds a part of the total mass and additional properties like viscosity, density, height, etc. The particle properties change due to substance specific processes. If for example oil is at the surface it evaporates depending - amongst others - on temperature.

The particles are placed in a grid with rectangular, six-sided cells, where the x-direction runs from west to east (longitude), the y-direction from south to north (latitude) and the z-direction points upwards. At the boundaries of the cells the x-, y-, z-velocities

are given by the operational ocean model under consideration (e.g. BSHcmod), meaning that the particles move within the cell according to the given velocities resp. velocity gradients.

At the ocean surface the two-dimensional surface wind fields (e.g. LME) additionally move the particles, if desired. In each cell the bottom is flat and the location of the bottom depends on the bathymetry of the circulation model. For example a sloping bottom is represented by a staircase shape meaning the bottom consist of horizontal and vertical faces of the grid cells. In the horizontal the staircase shaped model coastline is replaced by a realistic coastline in order to have a more realistic representation.

Next to the purely advective displacement of the particles by a given wind and current field (as described above), horizontal as well as vertical spreading occurs as a result of water current or wind shear at various temporal and spatial scales (so called sub-grid processes). In SeatrackWeb the small-scale isotropic turbulent mixing is included by adding turbulent velocities depending on the turbulent kinetic energy and its dissipation rate randomly to the drift of the particles.

In case of an oil slick the density differences between water and oil and the viscous as well gravitational forces lead to horizontal surface spreading of oil at the interface between water and air. To compute this process slick heights computed from the Fay formulas (FAY 1971) give - by assuming cylindrical particles with individual particle volumes - particle radiuses. The spreading is then a result of an iterative procedure calculating non-overlapping discs.

The vertical dispersion of particles from the surface down into the water column depends on the kind of substance simulated. For dissolved substances the turbulent mixing is a major player, but for oil slicks breaking waves have to be included to simulate the breaking up of cohesive slicks and the dispersion of these droplets into the water column. For this purpose a dissipative energy due to breaking waves is computed from the significant wave height leading to a mass of oil to be dispersed for each droplet size. Then the new depth values are assigned randomly by adding extra negative vertical velocities to the movement of the particles.

Density differences between the particle and the surrounding water leads to sinking or rising. A formula primarily developed for oil (SOARES DOS SANTOS and DANIEL 2000) gives a buoyancy velocity depending on the reduced gravity, viscosity, diameter of the particle and a critical diameter. The critical diameter divides the particles into two regimes: the large, spherical-cap bubble and the small spherical droplet (Stokes's) regime. Other substances than oil also have a buoyancy velocity, which is simply the reduced gravity multiplied by an adjustable coefficient.

If the particles simulate the drift of oil, oil weathering processes like evaporation and emulsification influence its properties. Density depends on emulsification and evaporation. Each particle's viscosity changes due to temperature (the rate of evaporation) and the degree of emulsification. For details about the implementation of weathering processes we refer to AMBJÖRN et al. (2011) and the scientific documentation of SeatrackWeb (LIUNGMAN and MATTISSON 2011) accessible through <http://stw.bsh.de/seatrack> or <https://stw-helcom.smhi.se/>.

Stokes drift is a net drift caused by the orbital motion of deep-water waves, which is not exactly closed due to the decrease of orbital velocities with depth. In the considered hydrodynamic models this motion is neither resolved nor implicitly included in the

surface boundary conditions; therefore the Stokes drift velocities are calculated within SeatrackWeb. Stokes drift velocities are computed from the two-dimensional wave energy spectrum. The wave spectrum is not yet imported from an operational wave forecast model, but is instead based on the parameterized spectrum presented in DONELAN et al. (1985) for fetch-limited growth.

The appearance of sea ice is taken into account and influences almost all processes mentioned above. For instance the hydrodynamic model velocities are replaced by the ice drift velocity if ice concentrations are higher than 70 % and the particle is at the surface. Also the Stokes drift linearly decreases from 100 %, when the ice concentration is zero, to 0 %, when the ice concentration is 70 % or higher. Also the gravitational spreading of an oil slick linearly decreases to zero with increasing ice concentration (DICKINS 1992; VENKATESH et al. 1990). Oil dispersion by breaking waves from the surface down into the water column is also reduced for high ice concentrations higher than 30 %. Ice strongly damps the waves and limits the dispersion.

Although many processes are included, still a high level of uncertainty originates from the ocean and wind model applied. To mimic some of the uncertainty it is possible to add extra uncertainty spreading randomly, whose magnitude is a function of the wind forecast uncertainty, to the movement of particles at the surface.

2.3 Graphical User Interface

SeatrackWeb users typically configure drift simulations and display the results via the graphical user interface (GUI). SMHI develops and continuously updates, respectively renews the SeatrackWeb GUI. At present two versions of the GUI exist: one is a Java Client/Server application and the other one is a JavaScript web application tested in common internet browsers. The web application version is the latest one, but the Java Client version is still commonly used. At the BSH the current operational setup uses Java Client and therefore, only this version of the GUI will be presented.

Java Web Start starts the Java Client application on the user computer. Since the drift simulations itself are performed on the server site there are no specific requirements for the personal desktop computer performance. For more details about the SeatrackWebs Client/Server Java Application we refer to AMBJÖRN et al. (2011).

After successful login a coastline map opens and more layers with additional information may optionally be added. Fig. 1 shows the SeatrackWeb GUI of the BSH installation. For example, as it can be seen in Fig. 1, it is possible to display the location of oil and gas platforms, borders of the exclusive economic zone, marine traffic routes and biological sensitive areas. Furthermore, the bathymetric depths showing the resolution of the BSHcmod circulation model can be visualized. This information helps to identify how well ocean current fields are resolved in the drift simulation.

To set up a drift simulation the user has to provide some information guided by the GUI through different menus, e.g. kind of substance/object, kind of outlet (continuous, amount, rate, ...), position, start and end time of the simulation must be defined.

SeatrackWeb provides strong support for expert users, which can choose the forcing wind/current fields, give additional wind drag for floating objects, choose the kind of oil or add uncertainty due to wind.

In case of oil – depending on the availability of information on the kind of oil – SeatrackWeb gives the possibility to choose just an oil class (light, medium, heavy) or a specific oil (e.g. marine diesel, IFO 450, Bunker B, etc.). This choice has for example consequences on the rate of evaporation and emulsification.

Although the map is only 2-dimensional the drift simulation is 3-dimensional, meaning that it is possible to define an outlet in a certain depth and that the substance is dispersed in the water column if not prevented by buoyancy. The depth of a particle is color coded according to a legend shown in the lower right corner of the main window.

Further, the user has several options for analyzing the results. For example it is possible: to zoom in and out, add layers like for example traffic separation schemes, go forward and backward in time, show an animation, plot the trajectory of all particles or only of the barycenter of the particles, show wind and current data, and save map images. By saving the case the simulation result may be shared with other SeatrackWeb users or loaded in other systems through suitable interfaces. It is also possible to save tables and graphs showing the amount/percentage of oil at the surface, stranded, dispersed, emulsified, etc.

If the pollution source is unknown and a potential originator is searched for, AIS ship position can be loaded and displayed in combination with the drift simulation results. This helps to preselect ships to inspect. Displaying the EMSA provided oil spill detections in satellite images is also possible and helps finding possible polluters by backward simulations.

3 Results

In this section the performance of SeatrackWeb is demonstrated based on some real cases. First the results of an oil spill caused by the average of the cargo vessel “Full city” in the Skagerrak area in 2009 are shown. Then results of drifting objects, namely containers in the German Bight in 2012, are presented.

3.1 Ship average in Skagerrak area

On 30 July 2009 the cargo-vessel “Full City” anchored near the Norwegian coast in the Skagerrak area. During strong gale winds the anchor flukes broke off and the ship started to drift towards Sastein Island, where it ran aground by night losing about 300 tons of IF180 bunker oil (BROSTRÖM et al. 2011). Oil response action started next morning, but could not prevent a widespread pollution of the Norwegian coast causing ecological and economic damage. Drift models were used to predict the oil trajectory and a comparison of three model results – OD3D, SeatrackWeb and BSHdmod.L - was published by BROSTRÖM et al. (2011) afterwards. All models showed good agreement with observations. DAMSA used SeatrackWeb with HIROMB ocean model data and HIRLAM wind data. In this section the “Full City” case is considered again using SeatrackWeb with BSHcmod ocean model and GME+LME wind forcing data. The same forcing data was used by the drift model BSHdmod.L in the comparison in BROSTRÖM et al. (2011). Thus, differences in the oil spill trajectory are only due to the drift model.

In this paper SeatrackWeb uses the same initial setup as described in BROSTRÖM et al. (2011) including some additional uncertainty spreading due to wind as proposed in the

paper. Fig. 2 shows the oil distribution 6 h, 12 h, 24 h, 36 h, 48 h and 60 h after the initial release of oil. The particle distribution is almost equal to the BSHdmod.L results in BROSTRÖM et al. (2011), because the same forcing applies. The spreading is a bit stronger in SeatrackWeb, causing the oil spill to widen faster and more oil gets further southwestwards. Since SeatrackWeb uses a coastline instead of the model boundaries, it allows particles to strand on the coastline and the stair case shape of the model boundaries as seen in the BSHdmod.L results (see Fig. 9 in BROSTRÖM et al. (2011)), is not present any more.

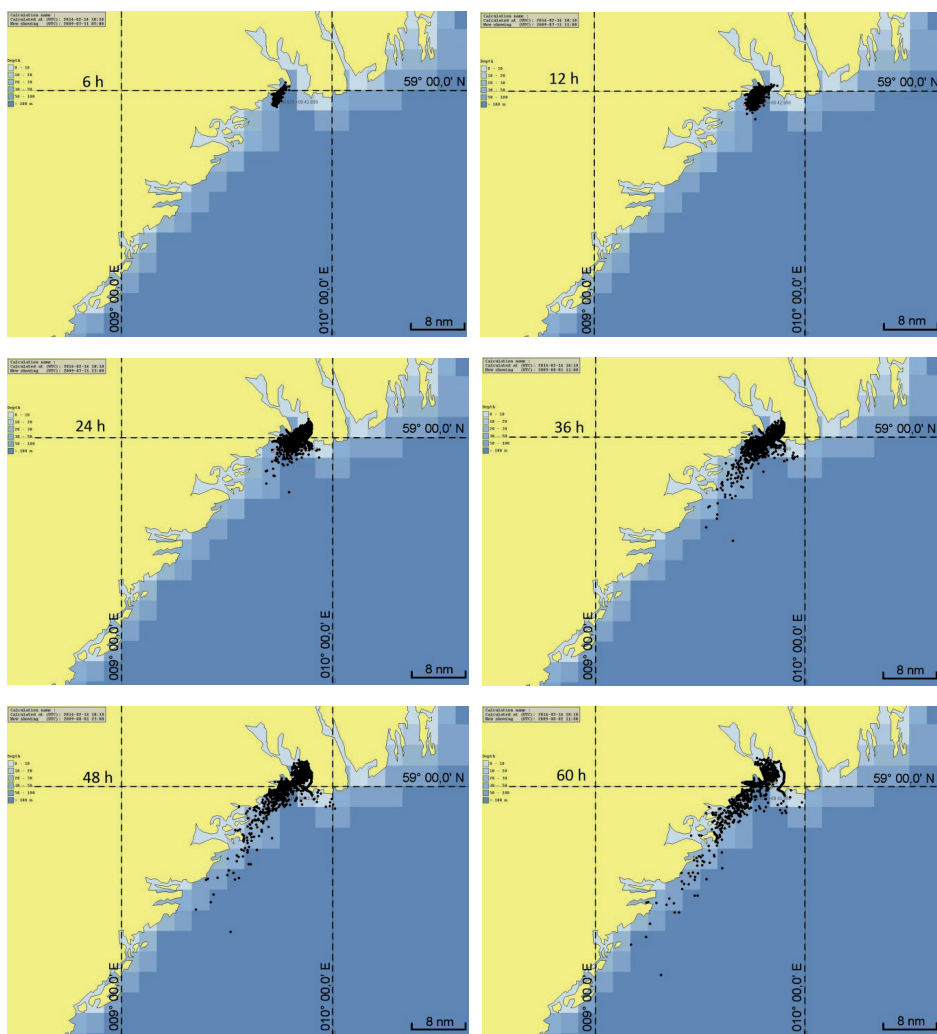


Figure 2: The Seatrack Web oil drift simulation results for the “Full City” case (6 h, 12 h, 24 h, 36 h, 48 h and 60 h after the initial release) using BSHmod and LME/GME forcing. Black dots represent oil positions, the blueish area shows the depth used in the BSHmod model (5 km resolution) and yellow is the land according to Seatrack Webs coastline.

The beaching of oil 72 h after the accident is shown in Fig. 3. Comparing it with the simulation results in BROSTRÖM et al. (2011) the extension of the oil beaching is approximately as far south as the OD3D results using 1.5 km resolution. One difference is that SeatrackWeb with BSHcmod forcing also has beaching of oil at Molen while OD3D does not predict this. Comparing our results with the SeatrackWeb results using HIRLAM/HIROMB forcing more oil is beached near the accident location and the oil does not travel that far south. The SetrackWeb simulations presented here and in BROSTRÖM et al. (2011) differ not only because of different forcing fields also because of additional uncertainty spreading.

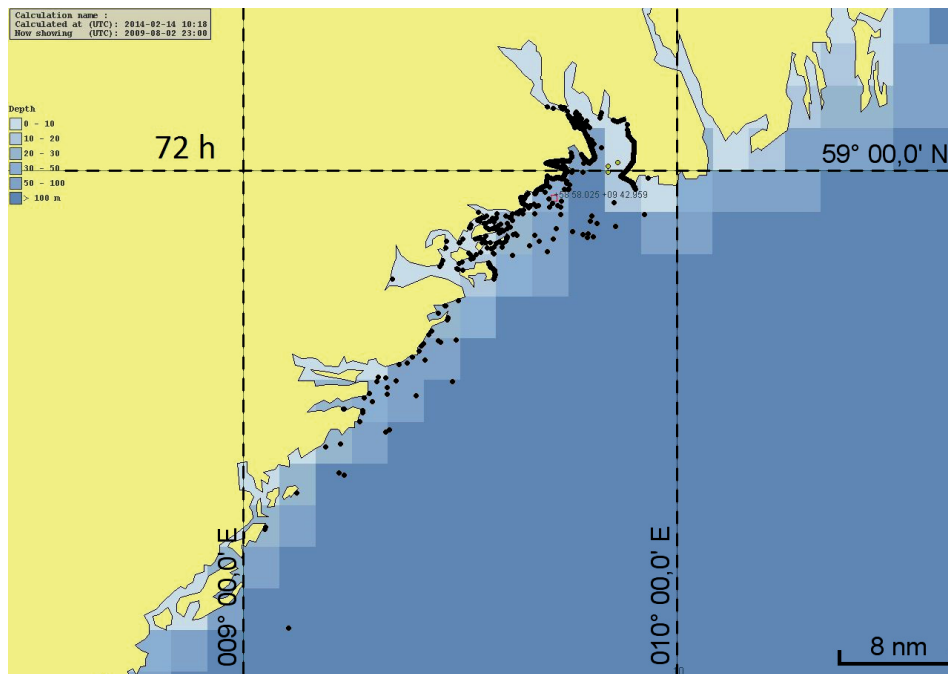


Figure 3: SeatrackWeb simulation results of the “Full City” case 72 h after the initial release using BSHcmod forcing.

3.2 Container drift in the German Bight

At 05:35 UTC on 06. January 2012 - just after a northwest gale causing a rough sea state and a storm surge - a cargo ship reported loss of ten 40-ft containers about 22 nm WNW of Helgoland near the German Bight Western Approach. Seven containers contained wood piles, two containers were empty reefer containers and one container included car spare parts. These containers were partly connected with twist locks, drifting in packages of two, three or four containers until most of them probably broke off distributing their content. Consequently, the pollution was more a danger for shipping than for wild life although there is always impact on ecology, tourism and economy in general by such accidents.

Container, container parts and wood piles were observed over ten days from ships and aircrafts. They were monitored by radar, accompanied by ship and - if possible - salvaged.

In the morning container and flotsam have been reported in a positions south-west of the accident location. This was about four hours after the average and pictures of some connected containers were made (see Fig. 4).



Figure 4: Container package observed at position 54° 18,06' N, 007° 13,30' E on 06.01.2012 at 09:36 UTC (the picture was kindly provided by the crew of the ETV Nordic).

The distance between some container packages was already more than $\frac{1}{2}$ nm. Whether the containers have been lost subsequently or whether processes like water turbulence or different flotage led to this separation is hard to tell. In the afternoon and evening of 06.01.2012 more observations have been made finding containers or remaining of containers respectively their content in direction WNW, SW and SE of the accident location. Since it is not possible to distinguish containers in these observations, it is not clear, whether the containers were observed several times or if each time different containers were found. Very valuable observations were made by the ship GS Neuwerk in the evening of 06.01.2012, when a container package was plotted by the ship radar for about 6 hours (see Tab. 1). Within this period we compare the drift simulations with these observations (see below).

About 33 h after the accident (afternoon 07.01.2012) an overflight sighted a container and a container package being about 8 nm apart. Probably the same objects were observed later SW-wards with a distance of about 13 nm apart from each other (SW-wards

and E-wards of Helgoland) in the afternoon of 08.01.2012 (about 58 h after the accident). Since we cannot verify that the objects were double sightings, we do not compare these observations with drift simulations. But this illustrates, that although the containers have been dropped off probably very close to each other (or even at the same position) at nearly the same time, the objects-over-board have already taken very different trajectories. The increasing distances between the containers observed 4 h, 33 h and 58 h after the accident (1/2 nm, 8 nm and 13 nm) illustrate the different behavior of drifting object depending on size, drowning, shape, etc.. Without knowing any of these properties the uncertainties of a drift simulation are very high. Additionally the turbulence and other processes of different scales in wind, waves and currents put a random forcing on the objects, which is not possible to predict deterministically.

Table 1: Observation of a container package made by GS Neuwerk 06.01.2012.

Time in UTC	Latitude	Longitude
17:18	54° 18.2' N	007° 11.6' E
17:30	54° 18.1' N	007° 11.9' E
17:45	54° 18.0' N	007° 12.4' E
18:00	54° 17.8' N	007° 12.9' E
18:15	54° 17.7' N	007° 13.4' E
18:30	54° 17.6' N	007° 13.9' E
18:45	54° 17.5' N	007° 14.4' E
19:00	54° 17.3' N	007° 14.9' E
19:30	54° 17.3' N	007° 15.5' E
19:45	54° 17.1' N	007° 16.4' E
20:00	54° 16.9' N	007° 16.9' E
20:15	54° 16.8' N	007° 17.4' E
20:30	54° 16.8' N	007° 17.9' E
20:45	54° 16.8' N	007° 18.3' E
21:00	54° 16.8' N	007° 18.6' E
23:30	54° 17.5' N	007° 21.4' E

Further the objects drifting characteristics may change over time. In the evening two connected containers, which were probably the ones reported east of Helgoland in the afternoon, were sighted by GS Neuwerk southwest of Helgoland. Again the positions were radar plotted, but in the morning of 09.01.2012 the containers broke off, and one deteriorated distributing wooden planks and a package of wood. Later the remaining blue container was salvaged. In the subsequent 6 days wood, wood packages and fragments of containers were found in the Elbe estuary and at the North Frisian coast near the Eider estuary.

We apply SeatrackWeb with BSHcmod/LME forcing simulating two connected containers drifting on 06. January 2012 between 17:18 UTC and 23:30 UTC and compare the results with observations (given in the Tab. 1). Fig. 5 shows the trajectory of the drift simulation in blue and of the observation in magenta. At the beginning the simulated trajectory follows nicely the observations, later the containers move more southwards than in the simulation. At the end of the simulation the distance between observed and

simulated position is about 1.2 nm. The mean minimal distance of the whole simulated trajectory to the observed trajectory is about 0.6 km and the mean error is about 0.7 km.

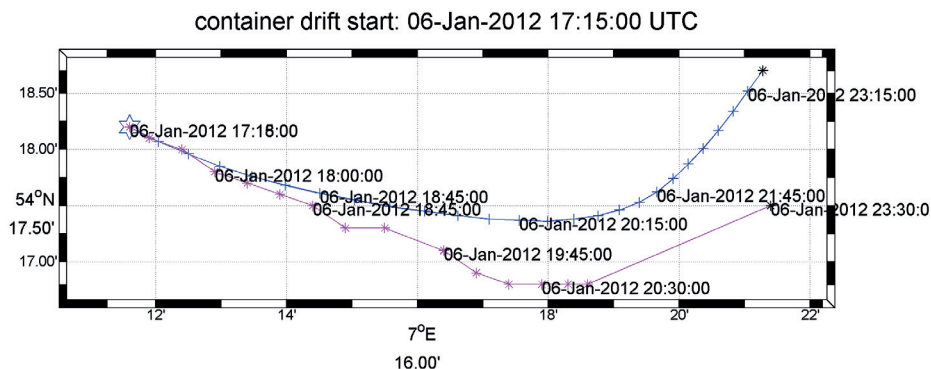


Figure 5: Seatrack web drift trajectory (blue) and observed trajectory (magenta) of two connected containers starting from a ship observed position (54° 18,2'N, 007° 11,6'E) at 06.01.2012 at 17:15 UTC ending at 06.01.2012 at 23:30 UTC (plot is made with Matlab). The star marks the starting point of the simulation. Seatrack Web uses a wind drag coefficient of 2.3 %.

To track possible error sources, we compare wind and wave measurements with the wind forcing used by the drift model. In Fig. 6 wind speed and direction at the simulated container position are plotted over time (the wind model data refers to 10 m height). The dots in magenta show the observed values at Fino1 station (measurements are in 33 m height). The observed wind speed is about 12 m/s increasing to 15 m/s and the wind model data is about 2-4 m/s lower than the observed one (increasing from 10 m/s to 13 m/s). Measured wind speed at Helgoland is generally a bit lower than the model wind, while TW Ems had a bit higher wind velocities. So overall the wind speed seems to match quite well.

The measured and modelled wind direction match quite as well (the measurements are systematically about 5° smaller than the wind direction used in the drift model) and show that the wind backed from WNW to WSW. The differences between observed and modelled values could be due to the height differences. Wind directions measured at TW Ems are almost equal to the ones at Fino1, while at Helgoland the wind direction is a bit more northerly and having more variations than the model wind. In general the wind forcing used in the drift simulation seems to be consistent with measurements, so errors in wind forcing seem not be the source of error for the drift simulation.

At Fino1 the measured significant wave height decreases from about 2.9 m to 2.6 m and the mean wave direction was from NNW until 22:15 UTC. At 23:15 UTC the wave direction reacts on the changing meteorological conditions and backs to WNW. At the wave rider station south of Helgoland the wave height was 1.7 m at the beginning and increased later to 1.9 m after 21:40 UTC. The wave direction was WNW backing to W at about 22:40 UTC. This turn in direction coincides in time with the wave direction changes at Fino1. These observations show spatial and temporal variability of the wind wave and swell.

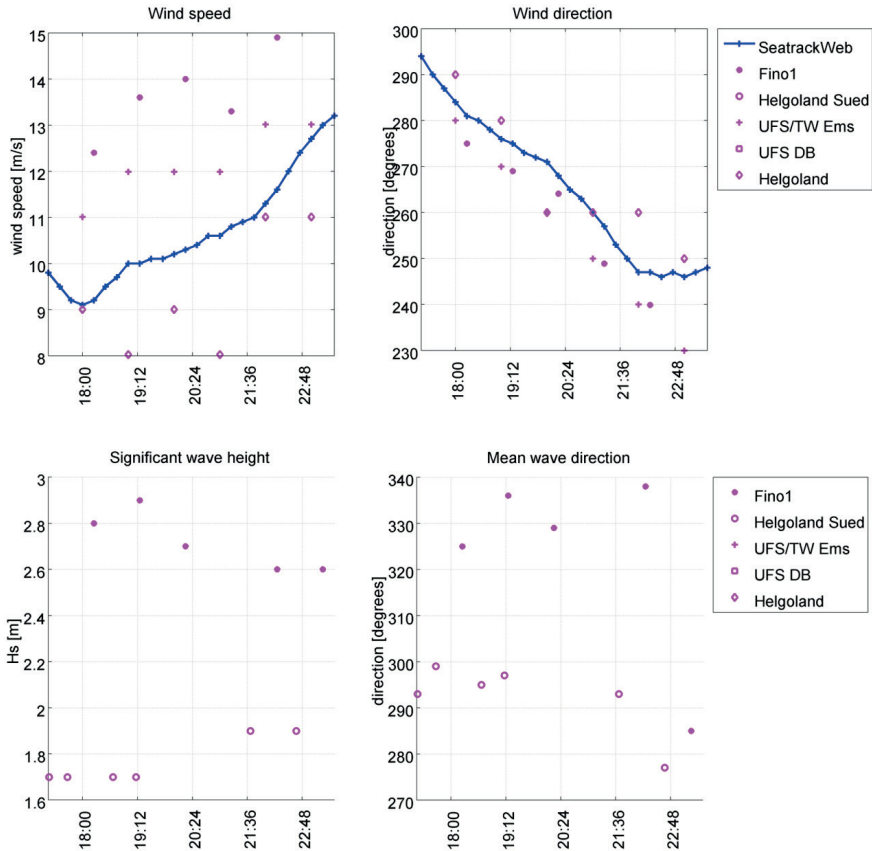


Figure 6: In blue wind speed and wind direction (in 10 m height) over time used by the drift model (GME+LME model data) at the simulated container positions. The dots in magenta show wind speed, wind direction, significant wave height and mean wave direction as measured at the station Fino1 (54° 0.86' N, 006° 35,03' E). The wind measurements of Fino1 are in 33 m height. The magenta circles show significant wave height and mean wave direction from the wave buoy at Helgoland Sued (54° 10.783' N, 007° 53,467' E). Wind speed and direction measurements at light vessel TW Ems (54° 10,0' N, 006° 20.8' E) in magenta crosses and at Helgoland in magenta diamonds.

SeatrackWeb uses parameterized Stokes drift from the model wind. This means that the displacement due to waves is computed from wind speed and direction. If the wind and wave direction match well (what is usually the case in fresh wind sea), the Stokes drift has the correct direction and size. In conditions when the wind and wave directions are different the parameterized Stokes drift cannot catch this change in direction. Probably this is the reason why the simulated container positions are more northwards than the observed ones.

4 Concluding remarks and perspectives

In this paper the application of the Lagrangian drift model SeatrackWeb to two real cases is presented. In the first case the drift of heavy oil in the Skagerrak released during the average of the “Full City” tanker in 2009 is simulated. The reported and simulated beachings are quite consistent. The other case dealt with the drift forecast of objects, namely containers. The results showed reasonably good agreement with observation considering the uncertainties of the weather model and the resolution of the ocean model. We identified that differences in swell and wind direction lead to errors in the drift forecast. Since the wave induced displacement is computed using the so called Stokes drift, which is parameterized by the wind, this component could be improved by directly using the Stokes drift from an operational wave model. The BSH has already access to wave model results of WAM (WAMDI 1988) run by the German Weather Service (DWD). In future the Stokes drift could be included in the wave model result files and SeatrackWeb could read in the Stokes drift velocities instead of computing it internally in the parametrized wave model of PADM. As a side effect the computing time of the drift simulation would also be reduced.

Concerning PADM the horizontal spreading of objects and oil is still an ongoing field of research. For example the influence of unresolved eddies, Langmuir circulations and gusts is an unsolved problem. These processes may increase the spreading. Also the thickening of oil in downwind direction and tar ball formation is not yet fully solved in SeatrackWeb.

Another factor for accurate results is the performance of meteorological and ocean models. BSHcmod runs only once a day due to limitations of computer resources, so the latest meteorological forcing is not used. In general the forecast quality of ocean models improves with the more recent wind forcing. The development of a modernized version of BSHcmod (so called HBM, see article in this journal) aims to have a faster model code suitable for modern, parallelized computer architectures. If the validation shows that the predicted currents are of the same or even better quality and HBM can run several times a day, the drift model forecasts will improve. Changing to HBM would only require small changes in the SeatrackWeb routines for reading and producing the setup and forcing files. Furthermore, HBM is already applied to the Elbe estuary. Including Elbe forcing as a further nesting level in SeatrackWeb will give finer resolved currents for the Elbe and would therefore increase the drift forecast quality in this region.

In case of oil spills the Central Command for Emergencies may choose for example dispersants and booms for oil combatting at sea. Applying dispersants changes the trajectory of the oil pollution, since the oil disperses in the water column having different currents and no direct wind drag. Any means of combatting oil will have to fulfill the condition that the intervention leads to less negative consequences than without. Where the oil or oil dispersant mixture will drift is very important information. To give predictions of the oil dispersant mixture is not yet possible in SeatrackWeb, but ongoing development together with Helmholtz-Zentrum Geesthacht (HZG).

Another important means for combatting oil at sea are booms. Booms keep oil in an area, prevent further spreading and facilitate oil recovery. SMHI currently sets a new version of the GUI in operation, where it is possible to simulate the application of booms. It is possible to estimate how much oil is trapped by each boom, which facilitates finding

their optimal position. BSH may update to this new version of the GUI, if the users of the BSH SeatrackWeb desire to use the new feature. Apart from new features the new GUI has the advantage that it does not need the Java Web Start, because it is simply web based meaning that only a web browser is needed, which makes it easier to use Seatrack-Web on mobile devices.

Also interfaces to AIS web services, CSN oil spill detections and to PADM are constantly updated to facilitate the exchange of input data and drift results for different applications. The AIS data covers mainly the Baltic Sea, since suitable data bases and interfaces to the North Sea data are still under development. Having AIS data of the North Sea would especially be important for prosecuting authorities to display AIS ship tracks and drift trajectories in a common window.

5 Acknowledgement

First of all we would like to thank the SeatrackWeb developer groups at SMHI and FCOO, where most of the mentioned Seatrack Web features have been developed over the past years. The observations and pictures of the container drift case were kindly provided by the Wasser- und Schifffahrtsamt Cuxhaven. Special thanks also go to the crew of the GS Neuwerk for plotting container positions. Last but not least we would like to thank the BSH sections M14, M23, M42 and Z32 for supplying wind/wave data and for the technical support.

6 References

- AMBJÖRN, C.; LIUNGMAN, O.; MATTSSON, J. and HAKANSSON, B.: Seatrack Web: The HELCOM Tool for Oil Spill Prediction and Identification of Illegal Polluters. In KOSTIANOY, A.G. and LAVROVA, O. Y. (Eds.): Oil Pollution in the Baltic Sea. Berlin Heidelberg, Springer-Verlag, 155-184, 2011.
- BROSTRÖM, G.; CARRASCO, A.; HOLE, L.R.; DICK, S.; JANSSEN, F.; MATTSSON, J. and BERGER, S.: Usefulness of high resolution coastal models for operational oil spill forecast: the "Full City" accident. *Ocean Sci.*, 7(6), 805-820, 2011.
- DICK, S.; KLEINE, E. and MÜLLER-NAVARRA, S.: The Operational Circulation Model of BSH (BSHcmod) - Model description and validation. *Berichte des Bundesamtes für Seeschifffahrt und Hydrographie*, 29, 2001.
- DICK, S. and SOETJE, K.C.: An operational oil dispersion model for the German Bight. *Deutsche Hydrographische Zeitschrift, Ergänzungsheft Reihe A*(16), 1990.
- DICKINS, D.F.: Behaviour of Spilled Oil at Sea (BOSS): Oil-in-ice Fate and Behaviour: DF Dickins Associates Ltd, Fleet Technology Limited, American Petroleum Institute, United States Minerals Management Service, Canada Conservation Protection, 1992.
- DONELAN, M.A.; HAMILTON, J. and HUI, W.H.: Directional spectra of wind generated waves. *Philosophical Transactions of the Royal Society of London, Series A*, 315, 509-562, 1985.
- FAY, J.A.: Physical processes in the spread of oil on a water surface, Paper presented at the Proc. of the Joint Conf. on Prevention and Control of Oil Spill, American Petroleum Institute, Washington, DC, 1971

- LIUNGMAN, O. and MATTSSON, J. (2011). Scientific Documentation of Seatrack Web: physical processes, algorithms and references. http://www.smhi.se/polopoly_fs/1.15600!Seatrack%20Web%20Scientific%20Documentation.pdf, last visited: 19.04.2014.
- MÜLLER-NAVARRA, S.H. and BORK, I.: Entwicklung eines operationellen Tideelbmodells auf der Basis des hydrodynamisch-numerischen Modellverfahrens BSHcmod für die Nord- und Ostsee (OPTTEL-A). Die Kueste, 79, 2012.
- SOARES DOS SANTOS, A. and DANIEL, P.: Oil spill modelling near the Portuguese coast. In RODRIGUEZ, G.R. and BREBBIA, C.A. (Eds.): Oil and hydrocarbon spills II. WIT Press, 11-18, 2000.
- VENKATESH, S.; EL-TAHAN, H.; COMFORT, G. and ABDELNOUR, R.: Modelling the behaviour of oil spills in ice-infested waters. Atmosphere Ocean, 26(3), 303-329, 1990.
- WAMDI: The WAM Model – A Third Generation Ocean Wave Prediction Model. Journal of Physical Oceanography, 18(12), 1775-1810, 1988.

Operational Ocean Forecasting for German Coastal Waters

Thorger Brüning, Frank Janssen, Eckhard Kleine, Hartmut Komo, Silvia Maßmann, Inge Menzenhauer-Schumacher, Simon Jandt and Stephan Dick

Summary

A numerical ocean forecasting system for the North and Baltic Seas has been applied at the Federal Maritime and Hydrographic Agency (BSH) since several decades. The model system is under permanent revision and the latest development – the implementation of the ocean circulation model BSH-HBM – is presented here. The circulation model is of particular importance because it provides the basic information for a couple of services at the German coast, like e.g. the sea level prediction and storm surge warning service, or oil spill forecasting and search-and-rescue applications.

An overview on the basic components of the model system will be given. The main part is the presentation of validation results and some applications of the new system which still is in the final calibration phase. An outlook on future developments both scientific and more technical, including completely new model components especially for data assimilation of ecosystem modelling completes the presentation.

Keywords

HBM, ocean forecast, operational ocean circulation model, North Sea, Baltic Sea

Zusammenfassung

Am Bundesamt für Seeschifffahrt und Hydrographie ist bereits seit einigen Jahrzehnten ein numerisches Ozeanvorhersagesystem für Nord- und Ostsee mit Fokus auf dem deutschen Küstenbereich in der operativen Anwendung. Alle Modellkomponenten befinden sich dabei in ständiger Weiterentwicklung. Hier wird die jüngste Modellentwicklung – die Einführung des Zirkulationsmodells BSH-HBM – beschrieben. Das Zirkulationsmodell ist eine wesentliche Informationsquelle für eine Reihe von Diensten an Deutschen Küsten (z.B. Wasserstandsvorhersage- und Sturmflutwarndienst, Öldriftvorhersage und Seenotrettung) und damit von zentraler Bedeutung in der Ozeanvorhersage.

Nach einem Überblick über das Modellsystem liegt der Schwerpunkt dieser Arbeit in der Darstellung der Modellergebnisse aus Validation und Anwendung des sich derzeit am Ende der Kalibrationsphase befindlichen Modells. Den Abschluss bildet ein Ausblick auf zukünftige Arbeiten sowohl in Bezug auf die inhaltliche als auch auf die technische Weiterentwicklung inklusive einiger neuer Modellkomponenten z.B. zur Ökosystemmodellierung und Datenassimilation.

Schlagwörter

HBM, Ozeanvorhersage, operationelles Ozeanzirkulationsmodell, Nordsee, Ostsee

Contents

1	Introduction	274
2	Model system	275
2.1	Equations.....	275
2.2	Setups / bathymetry	275
2.3	Forcing.....	277
2.4	Operational schedule / Computer facilities	277
2.5	Archive.....	277
3	Validation	278
3.1	Water level.....	278
3.1.1	North Sea	278
3.1.2	Baltic Sea.....	280
3.2	Currents	281
3.3	Water temperature	282
3.4	Salinity.....	283
3.5	Sea Ice	284
4	Results.....	284
4.1	Elbe flood in June 2013	284
4.2	Cyclone Xaver at 5th and 6th December 2013.....	285
5	Outlook.....	286
5.1	Operational schedule/Computer facilities.....	287
5.2	Data assimilation	287
5.3	High resolution estuary setups.....	287
5.4	Ecosystem modelling.....	288
5.5	Coupled models.....	288
5.6	Upgrade of computing facilities/massive parallelization	288
6	References	288

1 Introduction

The Federal Maritime and Hydrographic Agency (BSH) has a large need for ocean forecasting data to run its internal operational services, e.g. the sea level prediction and storm surge warning service and the ice service, and to support external customers like the national search-and-rescue centres, the Central Command for Maritime Emergencies or the German Navy. In order to fulfill all these operational obligations BSH runs and maintains a comprehensive numerical ocean forecasting system which is under permanent revision.

Operational modelling at BSH has already a considerable history starting at the predecessor institution DHI in the early 1980s and was in the beginning focused on the North Sea. Storm surge forecasting at the German Coast was – and still is – an important issue and thus was one of the applications that was tackled first. Later on the region of interest was extended to include the Baltic Sea which led to a fruitful cooperation in the Baltic

area. As part of this cooperation the model code developed at BSH – called BSHcmod – was spread in the Baltic Sea community. One branch (HIROMB) was installed and further developed at the Swedish Meteorological and Hydrological Institute (SMHI) and is until today the basis for the official HELCOM oil spill response system in the Baltic. Another branch started a few years later at Danish Meteorological Institute (DMI) where it founded the Danish storm surge warning system. All three model lines were actively developed over several years and somehow diverged over time. During recent years and with support of the MyOcean projects an effort was made to merge the three development lines into one. The outcome of this effort is the HIROMB-BOOS-Model (HBM) nowadays jointly developed by BSH, DMI, the Finnish Meteorological Institute (FMI) and the Marine Systems Institute at Tallinn University (MSI). At BSH the transition from the current operational model code BSHcmod towards HBM is not yet fully completed, so this publication, in which for the first time results from the future operational model HBM are presented, describes partly work in progress and mostly results from the ongoing calibration phase.

2 Model system

2.1 Equations

The equations of the physical kernel of HBM are mostly the same as those of BSHcmod which are described in DICK et al. 2001 and DICK et al. 2008. An important difference to the BSHcmod versions is the possibility to choose between dynamical vertical coordinates (KLEINE 2004) and z-coordinates with a free surface by a compiler flag. For operational use at BSH dynamical vertical coordinates are chosen.

Changes with the largest impact on the physical kernel (in comparison to the latest BSHcmod version 4) are the implementation of a new turbulence scheme – now a k-omega model is used, which is described in BERG 2012 – and the grid nesting. In HBM a fully dynamical two-way nesting is implemented. This means that the nested grid is a continuation of the grid into which it is nested. Therefore, areas which are covered by more than one grid within one setup are just calculated in one - the finest - grid. In all coarser grids the finer grid area is non-active. In the BSH NOKU-setup (see Fig. 2) this is realized in the inner German Bight and the Western Baltic, where only the so-called KU-grid (the fine grid) is active, whereas the corresponding points in so-called NO-grid (the coarse grid) are non-active (grey area in the NO-grid shown in Fig. 2). However, the products from NO-grid still cover the whole area. A more detailed description of the nesting equations and a very detailed description of the technical implementation with a focus on parallelization in HBM can be found in BERG and POULSEN 2012.

Furthermore some parameterizations were adjusted whereby especially the wind stress parameterization is noteworthy, because in contrast to BSHcmod-versions which use a linear approach, a quadratic approach for calculating the wind drag coefficient is chosen.

2.2 Setups / bathymetry

The BSH model system consists of four model grids which are calculated in three different setups. The first setup of the model chain is a 2D-model of the North East Atlantic

(NA, Fig. 1) with a horizontal resolution of about 10 km. Boundary values for the North- and Baltic Sea grid (NO, Fig. 2) are extracted from this setup. The North- and Baltic Sea grid has a horizontal resolution of about 5 km and 36 vertical layers at the maximum. Through the mentioned fully dynamical two-way nesting the finer coastal grid (KU, Fig. 3) with a horizontal resolution of about 900 m and a maximum of 24 vertical layers, which covers the inner German Bight and the Western Baltic, is integrated into the North- and Baltic Sea grid. Together these two grids form the second setup (this setup will be called NOKU henceforth) of the model chain. The third set up is formed by the Elbe grid (EL, Fig. 4), which was mainly developed in the OPTTEL-project (BORK and MÜLLER-NAVARRA 2011; MÜLLER-NAVARRA and BORK 2012). It has a horizontal resolution of 90 m and a maximum of 7 vertical layers. In contrast to the calculations within the OPTTEL-project which used a two-way nesting to the coastal grid, the Elbe-grid is calculated as a standalone setup in operational mode. The boundary values are provided by the NOKU setup.

The number of vertical layers in the three 3D-grids NO, KU and EL are a result of the same vertical partition. The upper 20 m are divided in ten layers of 2 m thickness. Between 20 m and 100 m water depth there are five layers of 3 m thickness and fourteen layers with a thickness of 5 m. In water depths below 100 m the resolution is relatively coarse with layer thicknesses up to 200 m.

The described setups are the 4th version, which has been developed and applied at BSH, so that the whole system of setups will be called V4 subsequently.

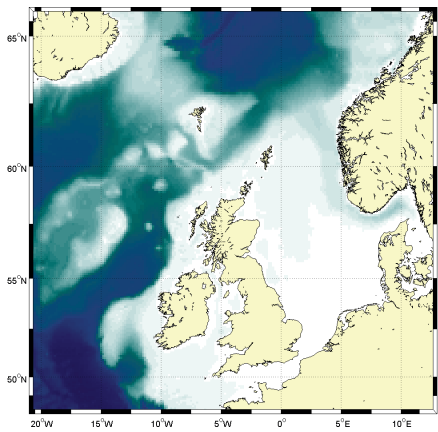


Figure 1: water depth of the NA-grid.

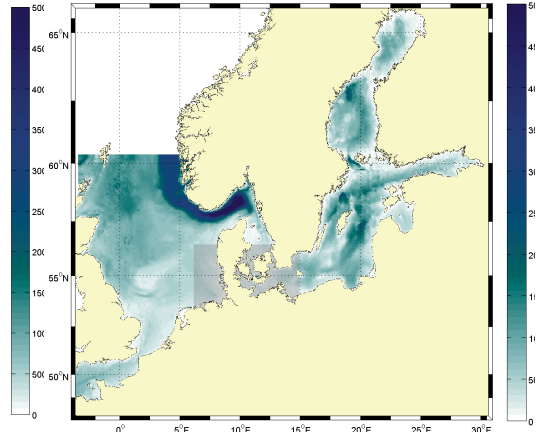


Figure 2: water depth of the NO-grid, during calculation the grey shaded area is non-active due to the nesting.

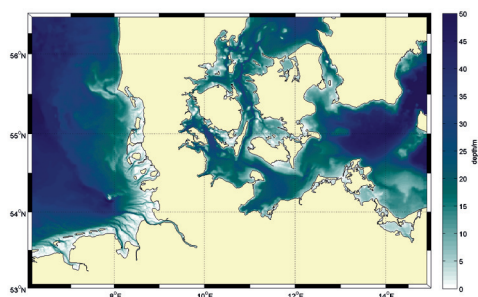


Figure 3: water depth of the KU-grid.

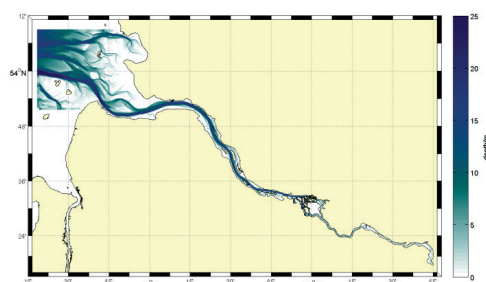


Figure 4: water depth of the EL-grid.

2.3 Forcing

Atmospheric forcing for all BSH model-setups is provided by the operational forecasts of the German Weather Service (DWD). The meteorological input parameters 10m-wind, air pressure, humidity, cloudiness and 2m-air temperature are received by BSH four times a day. Whereas the NA-setup needs forcing fields which are a combination of output from the global model GME (MAJEWSKI et al. 2012) with an effective horizontal resolution of 20 km and the European model COSMO-EU (SCHULZ and SCHÄTTLER 2011) with a horizontal resolution of currently 7 km, the NOKU- and the EL-setup are driven only by COSMO-EU data.

A radiation boundary condition is applied in the NA-setup, so that no external data for the open boundary is needed. At the open boundary of the NOKU-setup the sum of surge data from the NA-setup and tides based on 19 partial constituents are used. The EL-setup finally gets its open boundary data from the NOKU-setup.

Moreover eighty rivers are considered in the NOKU- and one (the Elbe) in the EL-setup. Whereas data of the German rivers is provided operational by the German Federal Institute of Hydrology (BfG), data for all Baltic rivers (except the Odra) is taken from the operational HBV model (BERGSTRÖM 1995) running at the SMHI. Because of a lack of data all the remaining rivers in the North Sea (mostly from the UK) are based on climatological data.

2.4 Operational schedule / Computer facilities

The described model system runs currently once per day on an IBM P7 755 server (4x8 core, 3.6 Ghz Power7 processors) with 16 openMP-threads and without MPI parallelisation. The HBM-code was compiled with the IBM-xlf-compiler. For illustrating results both MATLAB and GMT are used.

2.5 Archive

BSH maintains an extensive archive of model forecasts which includes data since 2000. All archived data are available free of charge. The longest consistent data set is the output

of the former V3-NOKU-setup calculated by the previous version of the BSHcmod model, which covers the 14 years from 2000 to 2013. The resolution of that setup was half of the resolution of the currently used V4 NOKU-setup. Data from the V4-NOKU-setup calculated by the BSHcmod V4 is archived from 2008 onwards.

Because both the NA- and the NOKU-setup of the described BSH-HBM model system are still in pre-operational mode, only results from the EL-setup calculated by HBM is archived at the moment. From this setup the output is available since April 2013.

3 Validation

A quantitative comparison of model results with different kinds of observations – often referred to as validation - is an important step in the operational model development cycle. Even though the model version presented here is still at a pre-operational stage and some calibration steps need further iteration, the results presented below already give an estimate of the lower limit of the quality of the upcoming operational model version.

The year 2008 was chosen as the main validation period because a comprehensive observational data set was already available for this year. A hindcast run initialized in November 2007 was carried out as basis for the validation. Some results of the validation of water level, currents, water temperature, salinity and sea ice will be presented in this section.

3.1 Water level

To analyse the simulated water levels it is sensible to split the analysis into two parts, respectively subsections: The first one on the North Sea, where tides are the main component of the local sea level elevation, so that the quality of the model output depends mainly on the quality of the simulated tides. Therefore both tides and total water levels were analysed in this subsection. The second subsection is focused on the Baltic Sea, where tides are virtually absent and only the total water levels are considered.

3.1.1 North Sea

As outlined in section 2.3 the tidal boundary conditions in the applied NOKU-setup are based on the 19 dominating tidal constituents. Moreover the validation period is only one year, so that a complete tidal analysis of the data is not feasible. Instead the analysis will be restricted to the two dominating semi-diurnal tidal constituents M2 and S2. A harmonic analysis of the modeled data yields the results given in Tab. 1 when compared with harmonic constants analysed from observations by the French Service Hydrographique et Océanographique de la Marine (SHOM 1982).

Table 1: Amplitude and phase calculated from BSH-HBM output as well as the error compared to data taken from SHOM (1982) for M2- and S2-tide at selected stations at the German coast.

Station	M2 amp [cm]	M2 amp err [cm]	M2 pha [deg]	M2 pha err [deg]	S2 amp [cm]	S2 amp err [cm]	S2 pha [deg]	S2 pha err [deg]
Borkum	107.6	2.8	278	8	28.1	1.0	338	5
Helgoland	113.2	4.6	312	0	30.8	1.9	13	-5
Cuxhaven	147.9	13.5	340	-4	37.1	2.7	46	-7
Buesum	154.7	-1.5	341	4	41.0	-1.1	47	0

The results in Tab. 1 show that both the amplitude as well as the phase of M2 and S2 is represented quite well by the model at the considered stations. Only the amplitude at Cuxhaven has a significant error in comparison with the SHOM data, but it should be kept in mind that there is also an uncertainty in the observed data. A recent analysis of a 19 year time series at tide gauge Cuxhaven by BSH (personal communication Patrick Goffinet) gave a M2 amplitude of 138 cm, which would reduce the model error to about 10 cm. Nevertheless the modeled M2 amplitude at Cuxhaven fails the BSH internal quality criteria at the moment and further calibration work is presently carried out.

When validating the water levels in the North Sea, the analysis is restricted to the peak values at high and low water because these are the values of highest interest. The exact timing of the peak values is not considered by this method.

Table 2: Bias and bias-corrected root mean square deviation from observations (RMSD) of total water level peaks during high and low water at selected stations at the German coast.

Station	Total water level			
	High water		Low water	
	Bias [cm]	RMSD [cm]	Bias [cm]	RMSD [cm]
Borkum	-3	11	10	14
Helgoland	3	14	10	11
Cuxhaven	19	18	5	14
Buesum	15	18	6	17

Whereas the bias' shown in Tab. 2 at the stations Borkum, Helgoland and Cuxhaven are mainly explainable by the error in tides, the bias in Buesum can partly be explained by the very difficult local topographic conditions around that station. The bias-corrected root mean square deviation from observations (RMSD) which is lower than 20 cm at all stations, is already sufficiently but there is of course potential for improvements in the future. The RMSD is, however, at the same level as it is in the current operational model BSHcmod.

For station Cuxhaven Fig. 5 shows the frequency distribution of high and low water level differences. If the bias is considered, the rate of events which are reproduced in a range of ± 10 cm is 39 % for high water and 49 % for low water. In a range of ± 20 cm it is 69 % for high and 85 % for low water. In the range of ± 30 cm more than 90 % of both high and low water events are reproduced.

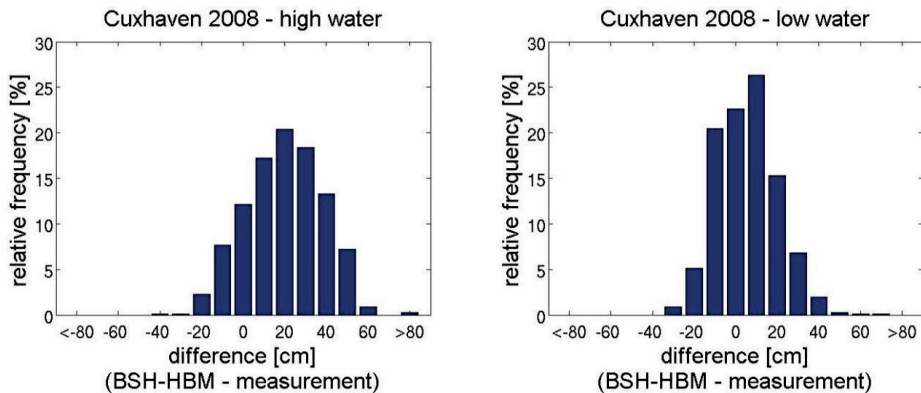


Figure 5: Frequency distribution of high (left) and low (right) water level differences at station Cuxhaven for the year 2008.

3.1.2 Baltic Sea

In the Baltic Sea, water level variations are caused mainly by wind effects and seiches, whereas the tidal signal is relatively small, so that water level predictions for the Baltic differ markedly from those for the North Sea. Therefore, the direct model-water level output is validated here. As it can be seen from the examples presented in Fig. 6, in which the results at station Warnemuende are shown, the model describes both the absolute water level elevation and the variability of it rather good.

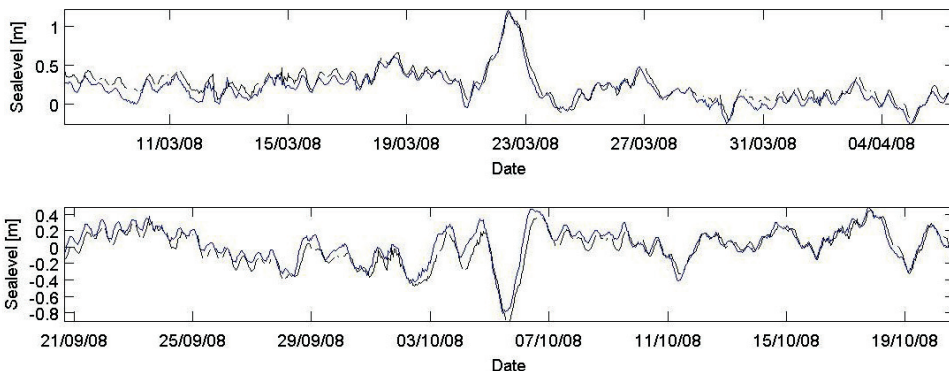


Figure 6: Water level time series during two storm events in 2008 at Warnemuende station. Observations are shown in black, BSH-HBM data in blue.

Tab. 3 indicates that the results at Warnemuende are representative for all German stations where correlations of about 90 % and RMSDs of about 10 cm are to be found. Moreover the simulated standard deviation equals nearly the observed one in all places.

Table 3: Overview of statistical metrics for water level elevation at German stations – N describes the total number of measurements, σ is the standard deviation from mean, RMSD is the bias-corrected root mean square deviation from measurements and r the correlation coefficient.

Station	Water level elevation						
	Observations			BSH-HBM			
	N	σ [m]	mean [m]	Bias [m]	σ [m]	RMSD [m]	r
Kiel-Holtenau	8158	0.25	0.05	0.07	0.28	0.12	0.90
Koserow	8301	0.21	0.10	0.18	0.23	0.10	0.90
Sassnitz	5792	0.21	0.13	0.15	0.22	0.10	0.89
Travemuende	8472	0.24	0.07	0.08	0.28	0.12	0.90
Warnemuende	7477	0.22	0.08	0.11	0.25	0.11	0.89

3.2 Currents

Due to the very high natural local variability of currents – caused e.g. by local topographic effects – on the one hand, and the model immanent spatial averaging on the other hand, it is always challenging to do direct model-observation comparisons. In addition to that, only a sparse set of measurements is available. For 2008 only data from a few stations in the Baltic can be used. A comparison between observed current speed and the current speed of the appropriate model cell shows for most part a good agreement, indicated by a modelled standard deviation that is in the same range than the observed one at all stations and a bias that is lower than 10 cm/s at most stations. As an example the time series for surface- and bottom current velocity at station Arkona is shown in Fig. 7.

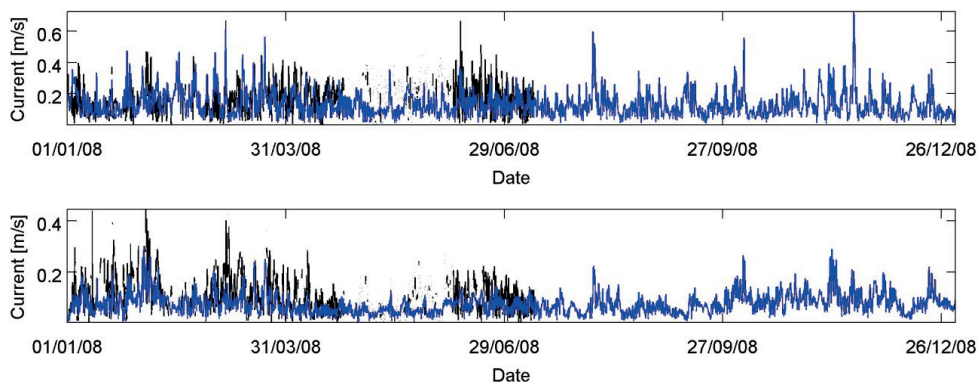


Figure 7: Current velocity time series at surface (above) and bottom (below) at Arkona station. Observations are shown in black, BSH-HBM data in blue.

3.3 Water temperature

With respect to water temperature, there is both a 'supercollated' L3 satellite product for validating the sea surface temperature (SST) and profile data in North and Baltic Sea available.

Regarding the SST, BSH-HBM shows a very accurate reproduction of the satellite data. Over the whole year 2008, the bias is almost in the whole NOKU-area less than 1°C and also the RMSD between BSH-HBM and satellite data is mostly less than 1°C (Fig. 8).

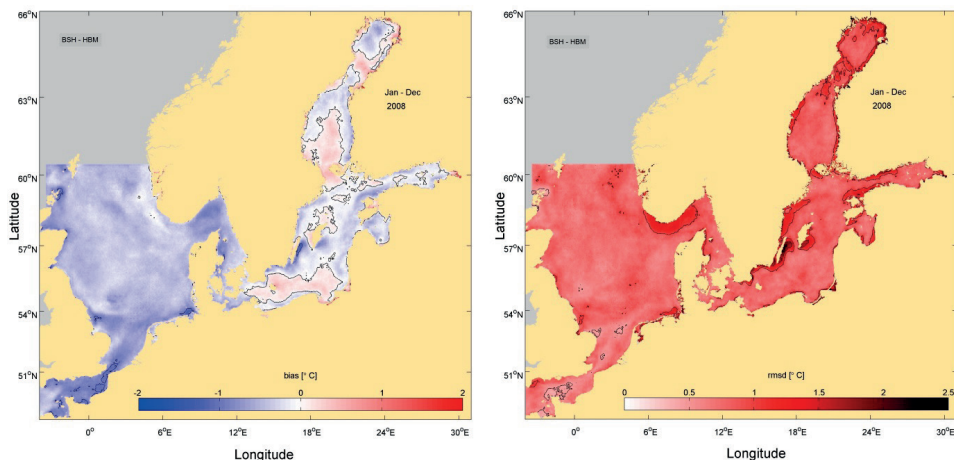


Figure 8: Bias (left) and RMSD (right) of BSH-HBM SST compared with 'supercollated' L3-satellite SST in 2008.

A more detailed analysis of modelled water temperature is possible at in-situ stations with larger water depth where sensors are available at different depth levels. Near-surface and near-bottom data have been taken into account at these stations.

The near-surface results confirm the results from the satellite based SST analysis. At the German stations the bias is less than 0.5°C , the RMSD is smaller than 0.7°C and the correlation is above 97 %.

At larger water depth, more pronounced deviations from observation are found. At large depth of more than 80 metres in the Baltic Sea the temperature is not well captured in the simulation. Due to the very long time scales of the deep water properties in the Baltic it is hard to say if there is really a severe model deficit e.g. due to a too coarse vertical resolution, or if most of the observed differences are due to the short one year validation-period which make the results prone to problems in the initialization and spin-up procedure.

Nevertheless, at German stations both in the North Sea and in the Baltic the correlation at bottom is mostly still more than 90 %, the RMSD is between 0.5° and 1.5°C and the bias is between 0.2° and 2°C . All in all there is a good overall agreement between HBM and the observed data at these stations as shown exemplarily in Fig. 9.

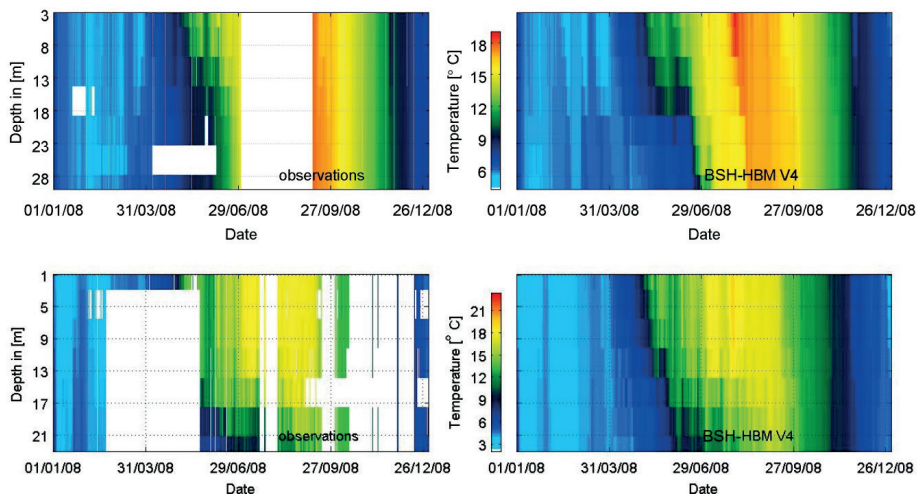


Figure 9: Temperature time-depth maps at station UFS Deutsche Bucht / North Sea (above) and at station Fehmarn Belt / Baltic Sea (below). In each case observation is shown on the left, BSH-HBM on the right.

3.4 Salinity

Unfortunately only few observations were available in the chosen calibration period, so only salinity at some Baltic stations has been analyzed. Generally the model captured the surface salinity quite well. Moreover, due to good initial conditions, the salinity below the halocline i.e. at depths greater than 60-80m, shows also a good agreement. At depths above the permanent halocline and below the surface like the bottom of all German Baltic stations measurements show generally stronger fluctuations than the model does and the bias and the RMSD are also relatively high. This is most probably owed to a combination of the complicated bathymetry of the Baltic Sea and the (probably too) coarse vertical resolution of the applied model setups. As an example Fig. 10 shows the salinity time series at station Fehmarn Belt.

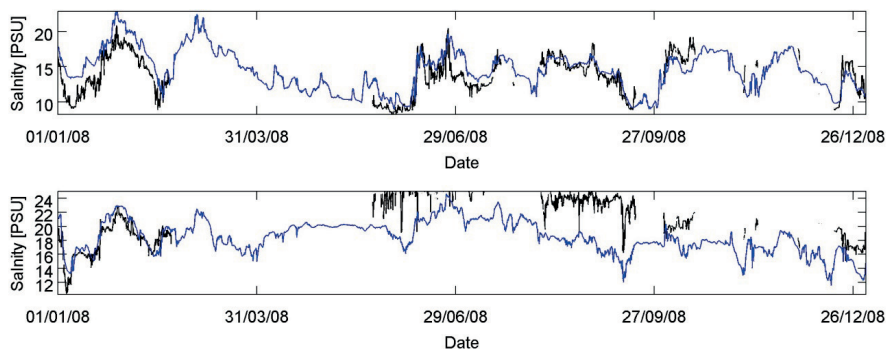


Figure 10: Salinity time series at surface (above) and bottom (below) at Fehmarn Belt station. Observations are shown in black, BSH-HBM data in blue.

In any case salinity is a parameter with a high potential for improvements in future model versions with higher (vertical) resolution and applied data assimilation.

3.5 Sea Ice

The winter of the year 2008 was relatively mild, so that only little sea ice was observed. Fig. 11 shows a comparison of computed and observed sea ice concentration on 01.03.2008 - the time with maximum sea ice extent in 2008. The sea ice extent and general distribution are quite similar. However, locally the concentrations differ significantly.

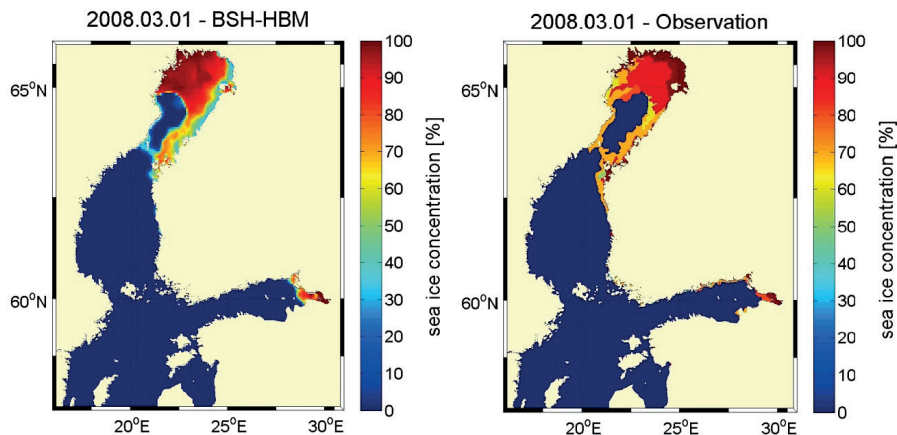


Figure 11: Comparison of predicted (left) and observed (right) sea ice concentration in the Baltic Sea on 1 March 2008.

4 Results

In this section some recent results will be presented which demonstrate that the new BSH-HBM model system could simulate special events of strong public interest. Two events which took place in 2013 are highlighted – on the one hand the “Elbe flood” in June and on the other hand the impact of cyclone “Xaver” from 5th to 7th December. During both events a strong increase in water levels had been experienced and as precise as possible forecasts were needed to minimize the consequences of these events for the affected population.

4.1 Elbe flood in June 2013

Heavy rainfall in south-east Middle Europe in May and June 2013 caused a flood at various rivers in that region. At the river Elbe water levels along the river were measured which were never observed before. Of course these enormous water masses caused also very high water levels in the tidal influenced part of the Elbe estuary between St.Pauli and the weir in Geesthacht which is influenced significantly by the river discharge anyway.

The forecast of the river discharge was characterized by high uncertainties and therefore a high variability from forecast to forecast. Indeed the best estimate forecast of BSH-

HBM works with discharge calculations from water level measurements in Neu Darchau which lies outside the EL-model region. Because the calculated river discharges of more than 4000 m³/s, which were nearly five times as high as the medium discharge, never occurred before, also these values were fraught with uncertainty.

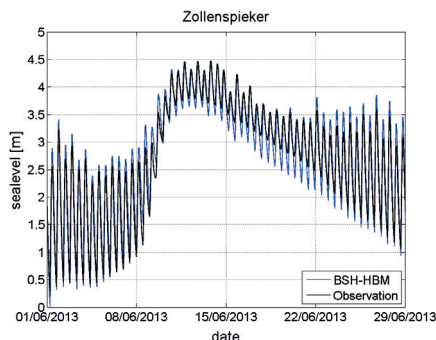


Figure 12: Water levels during Elbe flood at station Zollenspieker.

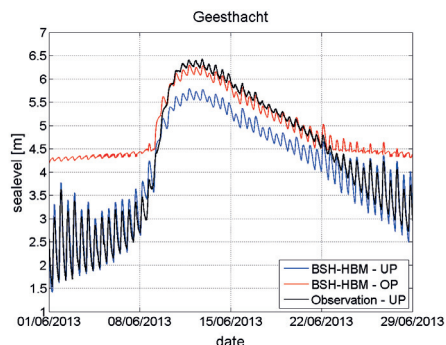


Figure 13: Water levels during Elbe flood at station Geesthacht-UP. Additionally model results at station Geesthacht-OP are shown.

In spite of these uncertainties BSH-HBM captured the Elbe flood very well at most stations between St.Pauli and Geesthacht like for example Zollenspieker (Fig. 12). Only directly below the weir in Geesthacht (“Unterpegel” - UP) the absolute peak was modelled about 0.5 m to low. However this could be explained with difficulties in modelling the weir itself, because during the flood the weir was completely opened and directly above the weir (“Oberpegel” – OP) the modelled water level matched very good to the observations (Fig. 13).

4.2 Cyclone Xaver at 5th and 6th December 2013

At 5th and 6th December 2013 the cyclone Xaver reached the inner German Bight with very high middle wind speeds between 45 and 55 knots (9-10 Beaufort) from north-westerly directions (Fig. 15). Because of these high middle winds and gales up to 12 Beaufort over almost the whole two days, up to four storm surges and up to two strong storm surges in a row could be observed at almost all German North Sea stations. The highest water level elevation during Xaver could be observed at station St.Pauli with a deviation of 3.98 m above the mean high water, which means a water level of 6.09 m above mean sea level – a very strong storm surge and the second highest observed value ever.

Even if the low waters were overestimated by BSH-HBM during Xaver, the model turned out to be a very useful tool for the scientists of the storm surge forecasting center because the storm surges were captured very well. At station Cuxhaven the errors of the maximum water levels during high waters were below 10 cm and at station St.Pauli they were below 25 cm (Fig. 14), which is a very good result taking the extraordinary high observed values into account.

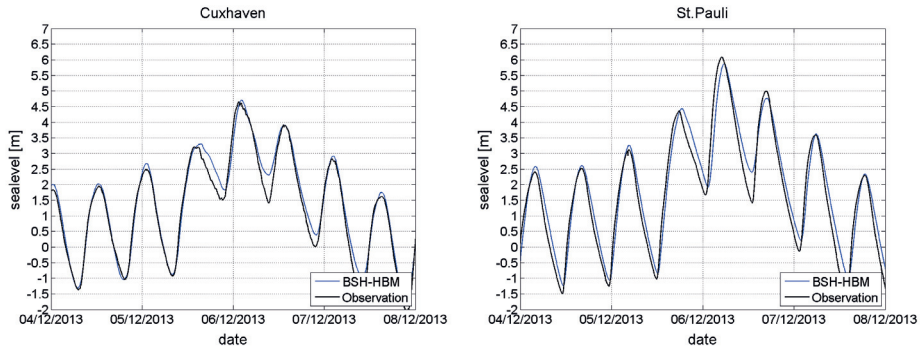


Figure 14: Water levels during Cyclone Xaver at stations Cuxhaven (left) and St.Pauli (right).

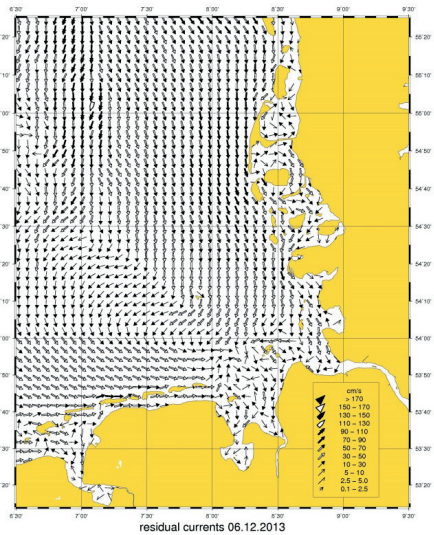
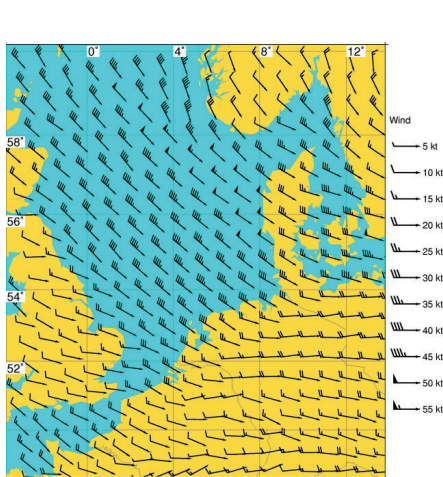


Figure 15: COSMO-EU middle 10m-wind at 6th December 2013 00 UTC.

Figure 16: BSH-HBM residual currents at surface in the German Bight at 6th December 2013.

Very impressive were also the modelled residual currents which were at surface between 30 and 90 cm/s in almost the whole German Bight (Fig. 16). Hence it was three times as high as compared to a situation with stable wind conditions of 4-5 Beaufort from one direction over a whole day.

5 Outlook

The model system in under permanent revision and steps to upgrade, adapt or extend the model system on the scientific as well the technical level are continuously taken according to the changing and typically growing customer demands. The main points of further development are listed below:

5.1 Operational schedule/Computer facilities

The latest hardware upgrade at BSH towards three IBM P7 755 servers (4x8 core, 3.6 Ghz Power7 processors) in combination with the strongly increased computing efficiency of the HBM code give a substantial speedup in the model runs compared to the former system. It is planned to use the free resources primarily for an improvement in operational schedule. The current status is that only the 2D storm surge model runs 4 times per day based on the latest meteorological forcing. The 3D circulation model is only run once a day. The final stage of the planned upgrade of the operational schedule will allow also for 4 runs per day with both the 3D NOKU and the 3D EL setup with a forecast lead time of at least 78 hours. As an intermediate step 2 runs per day are aimed at. Along with these changes goes an optimization of the data provision for internal and external customers, which will lead to a reduced delay between model run and data delivery as well as an increase in system robustness.

5.2 Data assimilation

All model runs carried out at BSH today are completely “free” model runs, i.e. there is no direct connection from model space to observational space, besides the indirect connection via the use of observational data in the boundary conditions. This lack of connection to observations has the strongest implication for physical processes in the ocean which are not directly connected to the atmospheric forcing like haline stratification. In order to overcome this limitation, data assimilation procedures have been developed over the last decades, first in meteorology and later on also in ocean modelling. BSH has started to build up a data assimilation capacity in close cooperation with the Alfred-Wegener-Institute (AWI). The first step was the implementation of a data assimilation scheme for sea surface temperature (SST) which resulted in a substantial error reduction in temperature (LOZA et al. 2012; LOZA et al. 2014). The assimilation of satellite born SST data was extended towards the use of temperature and salinity profiles (LOZA et al. 2013). In the next steps it is planned to include further sources of temperature and salinity data, i.e. from FerryBox lines, and extend the methods to handle also ocean currents, sea ice and water level. To make the data assimilation scheme - which is in a pre-operational stage at the moment - fully operational demands for a further upgrade of computational facilities at BSH mentioned above.

5.3 High resolution estuary setups

A very high spatial resolution is needed to attain accurate forecast of currents, water level and other parameters in complicated coastal areas like the German North Sea estuaries. A first step towards high resolution forecasts was made in the development of a setup with 90m horizontal grid spacing for the Elbe estuary in the OPTTEL project. The further development of the Elbe model became operational in the beginning of 2013. There are plans to extend the coverage of the high resolution setup towards the Jade/Weser and the Ems estuary with spatial resolution of at least 100m.

5.4 Ecosystem modelling

Several fields, among them the implementation of the European marine directives, e.g. the Water Framework Directive or the Marine Strategy Framework Directive, have an increasing demand for marine information which are not limited to the physical environment. In order to build up a capacity for providing biogeochemical information to a broad range of customers an ecosystem component is under development. Based on a coupling of HBM and the well-established ecosystem model ERGOM (NEUMANN 2000; MAAR et al. 2011) an operational setup for the North Sea and the Baltic Sea has been created which is in the calibration phase at the moment.

5.5 Coupled models

Another area of intensive development is the further integration of different model components into one coupled system.

Although the integration of ocean and ice has been established several years ago and runs fully operational at BSH there is still large room for improvements. Especially the simulation of ice rheology and related dynamics of sea ice is under further investigation.

Other areas of model coupling have already come a long way, too. The coupling of ocean currents and surface waves had entered a pre-operational stage already some years ago (MURAWSKI 2007) and is now reinvestigated based on the latest development of the single components (HBM for ocean circulation, WAM (KOMEN et al. 1994; KIESER et al. 2012) for surface waves). The next step in coupling, which has not been addressed at BSH so far, is the coupling of ocean and atmosphere where a coupled system based on COSMO (2013) and HBM is planned.

5.6 Upgrade of computing facilities/massive parallelization

Running an operational ocean forecasting system is a computationally expensive task. Steadily increasing user demands make a continuous upgrade of the computational facilities a necessity. In order to better support massive parallelization needed for future high resolution setups and especially the data assimilation the next computer generation at BSH will be a Linux cluster which will give a boost in scalability of the system and a strong reduction in computing costs.

6 References

- BERG, P.: Mixing in HBM. Scientific Report. Copenhagen, Danisch Meteorological Institute. 12-03, 2012.
- BERG, P. and POULSEN, J.W.: Implementation details for HBM. Technical Report Copenhagen, Danish Meteorological Institute. 12-11, 2012.
- BERGSTRÖM, S.: The HBV model. In: SINGH, V.P. (Ed.) Computer Models of Watershed Hydrology. Water Resources Publications, Highlands Ranch, CO., pp. 443-476, 1995.

- BORK, I. and MÜLLER-NAVARRA, S.H.: Entwicklung eines operationellen Tideelbmodells auf der Basis des hydrodynamisch-numerischen Modellverfahrens BSHcmod für die Nord- und Ostsee (OPTEL-A). Hamburg, Germany, Bundesamt für Seeschifffahrt und Hydrographie, 2011.
- CONSORTIUM FOR SMALL SCALE MODELING (COSMO): Core documentation of the COSMO-model.<http://www.cosmo-model.org/content/model/documentation/core/default.htm>, last visited: 11.10.2013
- DICK, S.; KLEINE, E. and JANSSEN, F.: A new operational circulation model for the North Sea and Baltic Sea using a novel vertical co-ordinate setup and first results. In: DALHIN, H.; BELL, M.J.; FLEMMING, N.C. and PETERSSON, S.E.: Coastal to Global Operational Oceanography: Achievements and Challenges. Proceedings of the Fifth International Conference on EuroGOOS, 20-22 May 2008, Exeter, UK: pp. 225-231, 2008.
- DICK, S.; KLEINE, E.; MÜLLER-NAVARRA, S.H.; KLEIN, H. and KOMO, H.: The operational circulation model of BSH (BSH cmod). Model description and validation, Berichte des Bundesamtes für Seeschifffahrt und Hydrographie 29/2001, Hamburg, Germany, Bundesamtes für Seeschifffahrt und Hydrographie, 2001.
- KIESER, J.; BRUNS, T.; LINDENTHAL, A.; BRÜNING, T.; JANSSEN, F.; BEHRENS, A.; LI, X.M.; LEHNER, S. and PLESKACHEVSKY, A.: First studies with the high-resolution coupled wave current model CWAM and other aspects of the project Sea State Monitor, presentation, <http://www.waveworkshop.org/13thWaves/index.htm>, Banff, 2012.
- KLEINE, E.: A class of hybrid vertical coordinates for ocean circulation modelling, Proceedings 6th HIROMB Scientific Workshop, St.Petersburg: 7-15, 2004.
- KOMEN, G.J.; CAVALERI, L.; DONELAN, M.; HASSELMANN, K.; HASSELMANN S. and JANSSEN, P.A.E.M.: Dynamics and Modelling of Ocean Waves, Cambridge University Press, Brest, 532 p., ISBN-13: 978-2-521-57781-6, 1994.
- LOZA, S.; SCHRÖTER, J.; DANIVLOV, S.; NERGER, L.; MAßMANN, S. and JANSSEN, F.: Assimilating NOAA SST data into the BSH operational circulation model for the North and Baltic Seas: Inference about the data. Journal of Marine Systems, 105-08, 152-162, doi: 10.1016/j.jmarsys.2012.07.008 , hdl:10013/epic.39926, 2012.
- LOZA, S.; DANIVLOV, S.; SCHRÖTER, J.; NERGER, L.; MAßMANN, S. and JANSSEN, F.: Assimilating NOAA's SST data and in situ T, S profiles into the BSH operational circulation model for the North and Baltic Seas. Poster, The Future of Operational Oceanography, Congress Center Hamburg, Hamburg, Germany, 8 October 2013 - 10 October 2013. hdl:10013/epic.42579, 2013.
- LOZA, S.; DANIVLOV, S.; SCHRÖTER, J.; JANJIC PFANDER, T.; NERGER, L. and JANSSEN, F.: Assimilating NOAA SST data into BSH operational circulation model for the North and Baltic Seas: Part 2. Sensitivity of the forecast's skill to the prior model error statistics, Journal of Marine Systems, 129, 259-270, doi: 10.1016/j.jmarsys.2013.06.011 , hdl:10013/epic.41927, 2014.
- MAAR, M., MÖLLER, E.F.; LARSEN, J.; MADSEN, K.S., WAN, Z.; SHE, J.; JONASSON, L. and NEUMANN, T.: Ecosystem modelling across a salinity gradient from the North Sea to the Baltic Sea. Ecological Modelling, 222, 1696–1711, 2011.

- MAJEWSKI, D.; FRANK, H.; LIERMANN, D. and RITTER, B.: Kurze Beschreibung des Globalmodells GME (20 km / L60) und seiner Datenbanken auf dem Datenserver des DWD. http://www.dwd.de/bvbw/generator/DWDWWW/Content/Forschung/FE1/Veroeffentlichungen/Download/GME_DBbeschr_1202,templateId=raw,property=publicationFile.pdf/GME_DBbeschr_1202.pdf, last visited: 01.02.2012.
- MÜLLER-NAVARRA, S.H. and BORK, I.: Entwicklung eines operationellen Tideelbmodells auf der Basis des hydrodynamisch-numerischen Modellverfahrens BSHmod für die Nord- und Ostsee (OPTEL-A), Die Küste (not published), 2012.
- MURAWSKI, J.: Die Wechselwirkung von Seegang und Strömung: Eine theoretische Grundlegung mit Modellanwendungen. dissertation. Universität Hamburg, GKSS 2007/12, 2007.
- NEUMANN, T.: Towards a 3D-ecosystem model of the Baltic Sea. Journal of Marine Systems, 25, 405–419, 2000.
- SERVICE HYDROGRAPHIQUE ET OCÉANOGRAPHIQUE DE LA MARINE (SHOM) (Ed.): Table des marées des grands ports du monde, Le Service, Brest, 186 p., ISBN-13: 978-2-110-80386-3, 1982.
- SCHULZ, J.P. and SCHÄTTLER, U.: Kurze Beschreibung des Lokal-Modells Europa COSMO-EU (LME) und seiner Datenbanken auf dem Datenserver des DWD. http://www.dwd.de/bvbw/generator/DWDWWW/Content/Forschung/FE1/Veroeffentlichungen/Download/LME_DBbeschr_1102,templateId=raw,property=publicationFile.pdf/LME_DBbeschr_1102.pdf, last visited: 01.02.2011.

Storm Surges in the Elbe, Jade-Weser and Ems Estuaries

Elisabeth Rudolph

Summary

Storm surges in the estuaries along the German Bight of Elbe, Jade-Weser and Ems may cause severe damages and endanger the life of the inhabitants of these coastal areas. The results of a sensitivity study are analysed in order to arrive at a better understanding of the importance of the processes modifying the height of a storm surge along an estuary. Hydrodynamic-numerical models can be used to carry out separate investigations on the impact of the wind over the estuary, the sea level rise at the mouth of the estuary and the fresh water discharge into the estuary. Wind, fresh water discharge and sea level rise are varied systematically, in line with today's knowledge, within the range of expected changes in future climates. The results of this sensitivity study show a bandwidth of possible changes in water levels during storm surge. This study enables vulnerabilities along the estuaries due to climate change to be identified and adaptation strategies to be developed.

Keywords

Storm surge, storm surge scenario, hydrodynamic numerical model, estuary, sensitivity study, wind, sea level rise, fresh water discharge

Zusammenfassung

Sturmfluten in den Ästuaren von Elbe, Jade-Weser und Ems können große Schäden verursachen und das Leben der Bewohner dieser Küstengebiete gefährden. Um ein besseres Verständnis für die Bedeutung der Prozesse zu bekommen, die die Höhe einer Sturmflut entlang des Ästuars beeinflussen, werden die Ergebnisse einer Sensitivitätsstudie analysiert. Durch den Einsatz hydrodynamischer numerischer Modelle der Ästuare können die Auswirkungen des Windes über dem Ästuar, eines Meeresspiegelanstieges in der Mündung des Ästuars und einer Zunahme des Oberwasserzuflusses in das Ästuar getrennt untersucht werden. Wind, Abfluss und Meeresspiegelanstieg werden auf der Grundlage des heutigen Wissens über die möglichen Auswirkungen des Klimawandels systematisch verändert. Die Ergebnisse der Sensitivitätsstudie geben einen Hinweis auf die mögliche Bandbreite der durch den Klimawandel hervorgerufenen Veränderungen der Sturmflutabschleppwasserstände, ermöglichen Vulnerabilitäten zu identifizieren und Anpassungsmaßnahmen zu entwickeln.

Schlagwörter

Sturmflut, Sturmflutszenario, hydrodynamisch numerisches Modell, Ästuar, Sensitivitätsstudie, Wind, Meeresspiegelanstieg, Oberwasserzufluss

Contents

1	Introduction	292
2	Numerical modelling of storm surges	293
3	Sensitivity study	293
4	Results	294
4.1	Sea level rise	294
4.2	Local wind over the estuaries	296
4.3	Fresh water discharge	296
5	Conclusions	298
6	Acknowledgement	299
7	References	299

1 Introduction

Numerical models of estuaries have been used for different purposes. OPTTEL showed that hydrodynamic-numerical models of the Elbe estuary can be used to produce a reliable forecast of water level, current velocity and salinity under ordinary and under storm surge conditions (BORK and MÜLLER-NAVARRA 2012; KREMP et al. 2012). In MUSE numerical models were used amongst others to hindcast historical storm surges in order to investigate what a historic storm surge would look like in today's topography (MÜLLER-NAVARRA et al. 2006). Hydrodynamic numerical models of estuaries can be useful in investigating the importance of the processes causing or modifying storm surges in estuaries.

Autumn and winter storms over the North Sea may cause storm surges in the estuaries in the German Bight of Elbe, Jade-Weser and Ems. Storm surges in these estuaries are not only influenced by the tidal dynamics and the wind set up in the German Bight, but also by processes in the actual estuaries, which reach up to 100 km into the North German Plain. Local wind effects over the estuaries, the bathymetry i.e. the flood plains connected to the estuary or the fresh water discharge into the estuary also influence water levels during storm surge.

Climate change may alter the bandwidth of values of these parameters. A sensitivity study is performed to investigate the influence of wind, fresh water discharge und sea level rise on the highest water levels during storm surge. Numerical models of the Elbe, Jade-Weser and Ems estuaries enable the impact of each process to be investigated separately. Wind, fresh water discharge and sea level rise are varied systematically in line with today's knowledge of expected changes in future climates.

The Elbe, Jade-Weser and Ems estuaries host the waterways to the ports of Hamburg (Elbe), Bremerhaven (Weser), Bremen (Weser) or Emden (Ems). As storm surges may cause severe damages along an estuary and endanger the life of the inhabitants of coastal areas, it is important to understand the processes that modify a storm surge along an estuary. This understanding can help in the development of adaptation measures to improve e.g. shore protection along the estuaries today and in times of climate change (SCHULTE-RENTROP and RUDOLPH 2012; SEIFFERT and HESSER 2014).

2 Numerical modelling of storm surges

The hydrodynamic numerical model UnTRIM (CASULLI and LANG 2004; CASULLI and WALTERS 2000) is used for the investigation presented here. UnTRIM is a 3-dimensional finite difference model. It solves the shallow water equations and the transport equations of salt on an unstructured orthogonal grid. UnTRIM is an adequate tool for applications in geometrical complex estuaries with large periodically wetting and drying tidal flats.

The models of the estuaries use bathymetries measured in 2003 (Elbe and Jade-Weser) and 2006 (Ems). The model domain covers the area of the estuary influenced by storm surges. During storm surges the weirs at Geesthacht (Elbe), Hemelingen (Weser) and Herbrum (Ems) are lowered. This means that the influence of the storm surge is also apparent in the riverine part of the Elbe, Weser and Ems. Fig. 1 shows a schematic map of the area. For the study presented here it is assumed that the storm surge barrier in the Ems at Gandersum is not in use (results of simulations with an operated barrier are shown in SEIFFERT and HESSER (2014)).

The model is forced at the boundaries with fresh water discharge at the upstream end of the estuary, with water level and salinity at the seaward open boundary and with wind over the estuary during the periods of interest. For the reference scenario (“today”) the wind fields are provided by the German Meteorological Agency (DWD), the water level at the boundary to the North Sea is generated from measurements and the measured fresh water discharge is used. The models of the estuaries will provide time series of e.g. water levels and current velocities at each grid point. For each estuary an individually calibrated model is used.

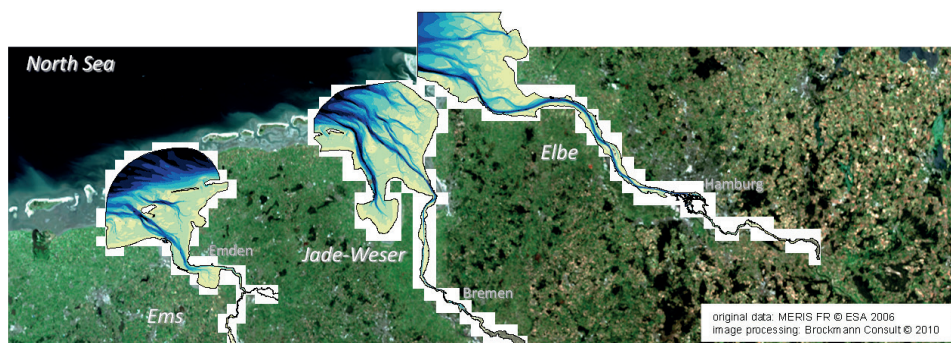


Figure 1: Schematic picture of the modelled area of the estuaries of Ems, Jade-Weser and Elbe in the German Bight. The distance from Cuxhaven at the mouth of the Elbe to Hamburg is about 100 km.

3 Sensitivity study

The height of a storm surge in an estuary is determined by the water level at the estuaries' boundary to the North Sea, the river run off into the estuary and the wind field over the estuary. A sensitivity study is used to investigate scenarios that highlight central elements of a possible future. Numerical models of the estuaries can be used to investigate the identical scenarios in all three estuaries. Common and different reactions to changes in the driving forces of storm surges in estuaries can be identified.

The scenarios are built on the basis of high historical storm surges: the storm surge of 3. January 1976 (SF76) in the Elbe and the Weser and the storm surge of 1. November 2006 (SF06) in the Ems estuary. The implied assumption here is that the basic storm characteristics over the German Bight will not change in response to climate change and that storm surges that occurred in the past are therefore just as likely to occur under future climate conditions. The sensitivity study investigates the influence of

- sea-level changes in the North Sea,
- increased fresh water discharge into the estuaries and
- increased local wind speed over the estuary

on the highest water level HW along the estuaries during storm surge. The parameters mentioned are varied systematically according to the knowledge of expected changes in a future climate (BECKER 2012; HEINRICH et al. 2012; HORSTEN et al. 2012). The reference storm surge scenario uses the measured development of the water level at the boundary to the North Sea, the measured wind speed over the estuary and the measured fresh water discharge.

The sea level changes are added to the boundary values at the estuaries boundary to the North Sea. Three different sea level rise scenarios - all three of which can be found in the literature (GÖNNERT et al. 2009) - are investigated: 25 cm, 80 cm and 115 cm. In order to investigate the influence of the local wind speed over the estuaries the wind speed is increased by 10 %.

Table 1: Measured fresh water discharges at Neu Darchau (Elbe), Intschede (Weser) and Versen (Ems) during historic storm surges and characteristic discharges (HPA HAMBURG PORT AUTHORITY 2012; NLWKN NIEDERSÄCHSISCHER LANDESBETRIEB FÜR WASSERWIRTSCHAFT, KÜSTEN- UND NATURSCHUTZ 2013).

	Elbe [m^3/s]	Weser [m^3/s]	Ems [m^3/s]
3 January 1976	500	250	114
1 November 2006	299	147	33
MQ (mean discharge)	709	326	80
HHQ (highest discharge observed)	3620	3500	1200
Q _{design storm surge}	2200	2000	700

The fresh water discharge Q is provided for the numerical model at the upper end of the estuaries. The storm surge scenarios are modelled with the measured discharge as well as with three increased discharges, 2000 m^3/s , 3000 m^3/s and 4000 m^3/s for the Elbe and Weser, 350 m^3/s , 700 m^3/s and 1200 m^3/s for the Ems. For comparative purposes Tab. 1 shows characteristic measured discharge values.

4 Results

4.1 Sea level rise

Fig. 2 shows time series of the water level at Hamburg (Elbe-km 623N), Bremen (Weser-km 0) and Emden (Ems-km 40) for today's sea level and for a sea level rise of 25 cm, 80 cm and 115 cm at the mouth of the estuaries. The sea level rise increases the high and low water levels during the tides before the storm surge as well as on the day of

the storm surge. The highest water level during storm surge is higher and high water time occurs several minutes earlier due to a sea level rise. High water levels, e.g. water levels higher than NHN + 3.00 m last up to several hours longer due to a sea level rise.

The highest water level during the storm surge period (HW) is analysed for all scenarios on a profile along the estuaries from the mouth of the estuary to Bleckede (Elbe), Intschede (Weser) and Bollingerfähr (Ems). Fig. 3 shows the highest water levels during storm surge (HW) for the reference scenario and the three sea level rise scenarios investigated.

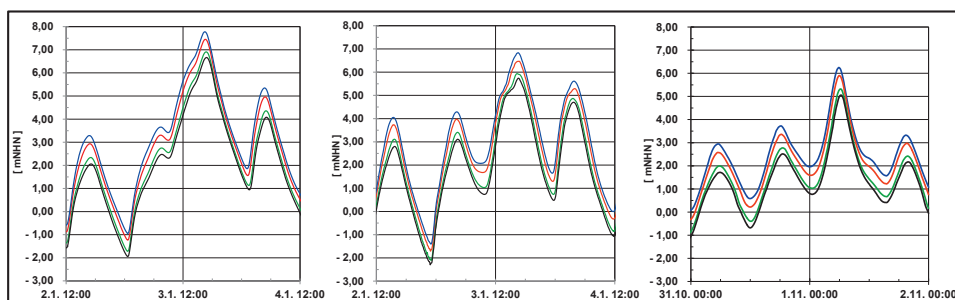


Figure 2: Sensitivity study sea level rise: time series of the water level at Hamburg (Elbe-km 623N, SF76, left), Bremen (Weser-km 0, SF76, center) and Emden (Ems-km 40, SF06, right). The reference scenario is indicated in black. The amount of sea level rise at the mouth of the estuary of 25 cm is indicated in green, 80 cm in red and 115 cm in blue.

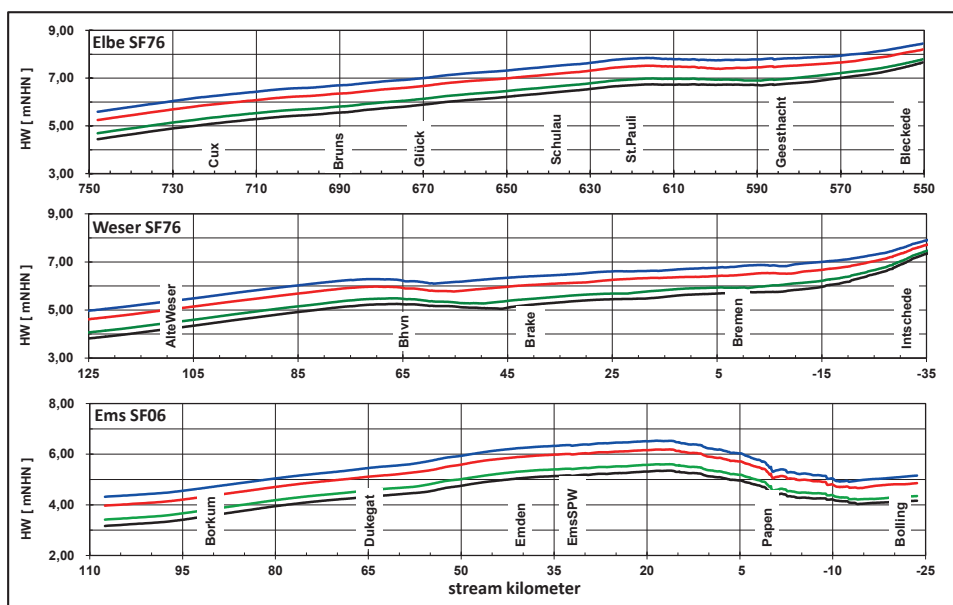


Figure 3: Sensitivity study sea level rise: Highest water level during storm surge HW along the estuaries of Elbe (top), Weser (middle) and Ems (bottom). The amount of sea level rise at the mouth of the estuary of 25 cm is indicated in green, 80 cm in red and 115 cm in blue.

A sea level rise at the mouth of the estuary raises the highest water levels during storm surge along the whole profile, which includes the whole area that is already being affected by storm surges today.

4.2 Local wind over the estuaries

A second sensitivity study investigates the influence of the local wind over the estuary during storm surges. For the purposes of this artificial sensitivity study it is assumed that the wind speed increases by 10 % over the estuaries during the period investigated. During the reference storm surge scenario SF76 wind speeds over the Elbe reach 29 m/s in the area of the mouth and 20 m/s in the area of Hamburg. Over the Weser wind speeds reach 25 m/s in the mouth area during reference scenario SF76 and 22 m/s in the area of Bremen. During the reference storm surge scenario SF06 the wind speeds over the Ems reach 25 m/s in the mouth area and 16 m/s in the area of Emden. Only low winds are observed over the three estuaries on the day prior to the reference storm surge scenarios.

Fig. 4 shows the influence of local wind on water levels during storm surge for today's mean sea level and for a sea level rise of 80 cm. As expected, increased wind speed has no influence on the water levels on the day before the storm surge, that is during periods with low wind speeds. On the day of the storm surge an increase in wind speed of 10 % causes an increase in water level of up to 30 cm for the scenario with today's mean sea level as well as for the scenario with a sea level rise of 80 cm.

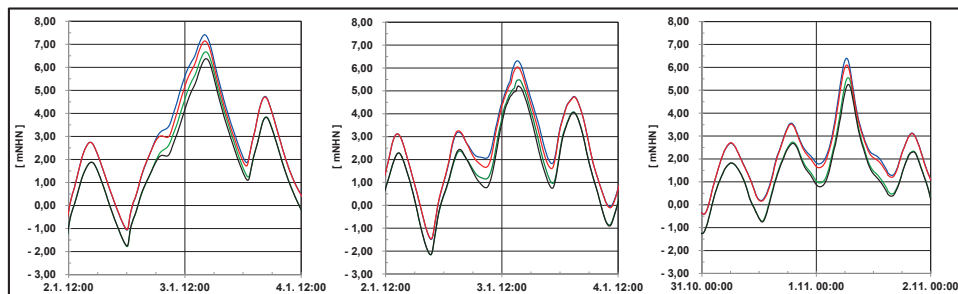


Figure 4: Sensitivity study wind and sensitivity study wind and sea level rise: time series of the water level at Schulau (Elbe-km 640, SF76, left), Brake (Weser-km 40, SF76, center) and Terborg (Ems-km 25, SF06, right). Black: today's sea level, green: today's sea level and increase of local wind speed by 10 %, red: sea level rise of 80 cm, blue: sea level rise of 80 cm and increase of local wind speed by 10 %.

4.3 Fresh water discharge

The influence of the fresh water discharge on the highest water levels during storm surge in the Elbe estuary is described e.g. in LÄNDER-ARBEITSGRUPPE (1988). Measurements were analysed and the amount of increase in water level per 1000 m³/s of fresh water discharge for several places of interest was derived. A numerical model can be used to investigate a broader range of combinations of fresh water discharge and storm surge.

Fig. 5 shows how increased fresh water discharge (3000 m³/s in the Elbe and Weser, 700 m³/s in the Ems) influences water levels during storm surge for today's mean sea

level and for a sea level rise of 80 cm at the mouth of the estuaries for Hamburg (Elbe-623N), a central location in the Elbe estuary, for Bremen (Weser-km 0) in the upper part of the Weser estuary and for Emden (Ems-km 40) in a wide area of the Ems estuary.

An increase in fresh water discharge increases the high and low water levels on the day before the storm surge and reduces the tidal range, especially in the central and upper part of the estuaries today and in the scenario with additional sea level rise. The influence of the increased discharge on the highest water level during storm surge also depends on the location in the estuary. The highest water level in Bremen is increased by several decimetres during storm surge as a result of increased fresh water discharge, whereas in Emden only a very small increase can be found.

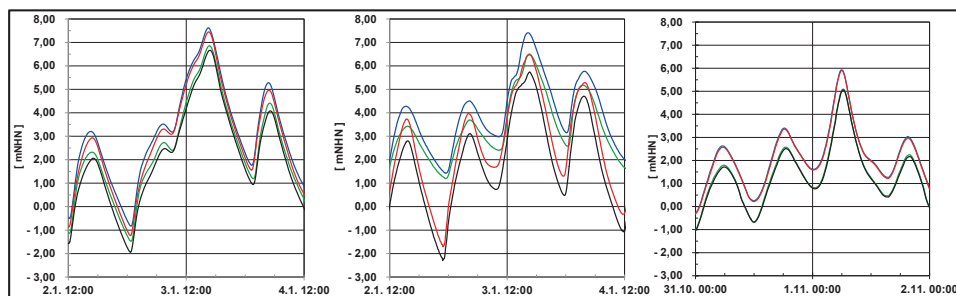


Figure 5: Sensitivity study fresh water discharge and sensitivity study fresh water discharge and sea level rise: time series of the water level at Hamburg (Elbe-km 623N, SF76, left), Bremen (Weser-km 0, SF76, center) and Emden (Ems-km 40, SF06, right). Black: today's sea level, green: today's sea level and discharge $3000 \text{ m}^3/\text{s}$ for Elbe and Weser and $700 \text{ m}^3/\text{s}$ for Ems, red: sea level rise of 80 cm, blue: sea level rise of 80 cm and discharge $3000 \text{ m}^3/\text{s}$ for Elbe and Weser and $700 \text{ m}^3/\text{s}$ for Ems.

The highest water level during the storm surge period (HW) is analysed for all fresh water discharge scenarios and combined fresh water discharge with sea level rise scenarios on a profile along the estuaries from the mouth of the estuary up to Bleckede (Elbe), Intschede (Weser) and Bollingerfähr (Ems). Fig. 6 shows the highest water levels during storm surge for the scenarios mentioned.

It shows that in the mouth of three estuaries investigated, the highest water level during storm surge HW is mainly modified by a sea level rise. HW increases here to an extent approximately equal to the rise in sea level. In these wide parts of the estuaries, with flood and ebb volumes which are much larger than the fresh water discharge, an increase in discharge has no significant influence on the water level. In the upper, narrow parts of the estuaries the highest water level during storm surge is modified by the fresh water discharge. Towards the riverine part upstream of the estuary the fresh water discharge is the single parameter determining the water level. In the central part of the three estuaries investigated the highest water level during storm surge is modified both by sea level rise and changes in fresh water discharge.

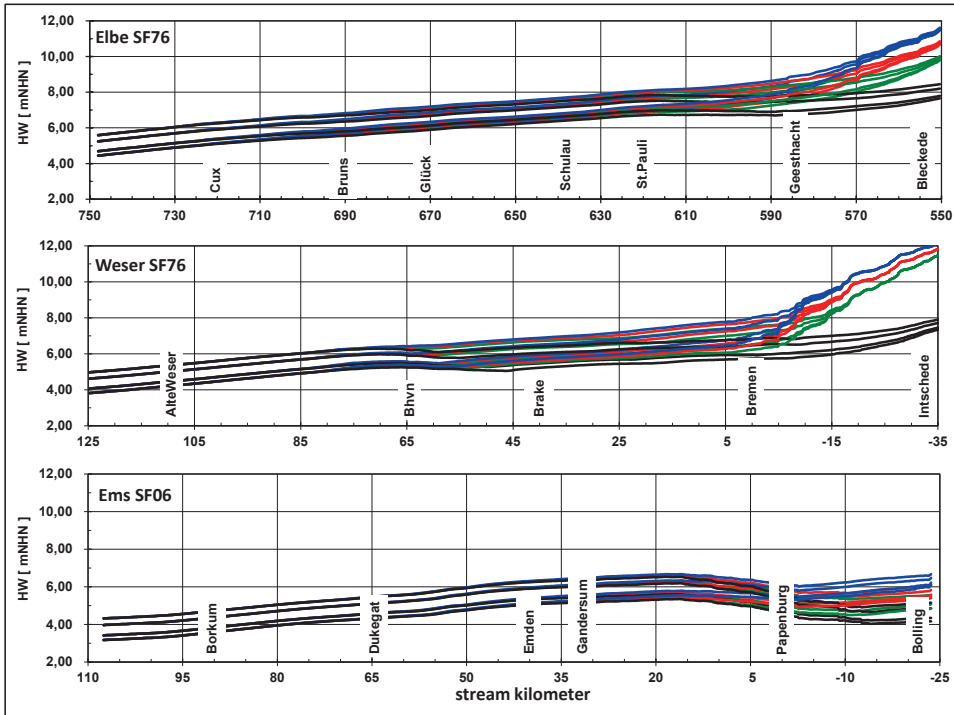


Figure 6: Sensitivity study fresh water discharge in combination with sea level rise: Highest water level during storm surge HW along the estuaries of Elbe (top), Weser (middle) and Ems (bottom) for a sea level rise at the mouth of the estuaries of 25 cm, 80 cm and 115 cm. The colours indicate the amount of fresh water discharge. Black Elbe 500 m³/s, Weser 250 m³/s, Ems 32 m³/s, green: Elbe and Weser 2000 m³/s and Ems 350 m³/s, red: Elbe and Weser 3000 m³/s and Ems 700 m³/s, blue: Elbe and Weser 4000 m³/s and Ems 1200 m³/s.

5 Conclusions

In order to develop a strategy for adaptation to climate change for the German estuaries it is important to understand today's situation and to analyse what developments climate change will bring about in the future. The impact of climate change on storm surges in the German estuaries of the Elbe, Jade-Weser and Ems is investigated using a sensitivity study. The study analyses the influence of sea level rise at the mouth of the estuary, wind over the estuary and fresh water discharge. Hydrodynamic numerical models of the Elbe, Jade-Weser and Ems estuaries can be used to investigate the impact of each process separately. Wind, fresh water discharge and sea level rise are varied systematically in line with today's knowledge of expected changes in future climates. The three estuaries examined show the same response to the scenarios investigated. The results of the study are summed up in Tab. 2.

In the mouth of the estuaries, the highest water level during storm surge is determined by conditions in the North Sea, i.e. storm surge and sea level rise (slr). In the central and landward reaches, the highest water level during storm surge is determined both by conditions in the North Sea and inland (fresh water discharge Q). An increase in local wind

over the estuary influences the highest water levels during storm surge along the whole estuary.

All the scenarios considered result in a rise in the highest water level during storm surge, earlier occurrence of the highest water level during storm surge and in a longer duration of high water levels.

Table 2: Changes in the highest water levels during storm surge in the estuaries of Elbe, Weser and Ems for the scenarios investigated in the sensitivity study.

	mouth of the estuary	central estuary	upper estuary
sea level rise slr	+ slr	+slr \pm 10 cm	+ slr \pm 10 cm
fresh water discharge	\pm 1 cm	5 cm to 30 cm	10 cm to 100 cm
combination Q & slr	+ slr	\leq (slr + Q)	\leq (slr + Q)
local wind	up to 10 cm	up to 30 cm	up to 30 cm
combination wind & slr	\sim (slr + wind)	\sim (slr + wind)	\sim (slr + wind)

The results of this sensitivity study are used by SEIFFERT and HESSER (2014) to investigate climate change impacts and to develop adaptation strategies in German estuaries.

6 Acknowledgement

This work has been carried out within the research programmes KLIWAS 'Impact of climate change on waterways and navigation' and KLIMZUG-Nord 'Regional strategies concerning climate changes in the metropolitan area of Hamburg'. KLIWAS is financed by the German Federal Ministry of Transport, Building and Urban Development; KLIMZUG-Nord is supported by the German Federal Ministry of Education and Research (01LR0805A), the city of Hamburg and the metropolitan area of Hamburg. Thanks to all coworkers in the KLIWAS/KLIMZUG-Nord team at the Federal Waterways Engineering and Research Institute in Hamburg for their support and for carrying out some of the numerical simulations. Special thanks go to Annette Büscher, Anika Johansen, Annkathrin Rinnus, Rita Seiffert and Norbert Winkel.

7 References

- BECKER, P.: Climate and Climate Impact Research in Germany – Where Do We Stand Today? In: FEDERAL MINISTRY OF TRANSPORT, BUILDING AND URBAN DEVELOPMENT (ed.): KLIWAS - impacts of climate change on waterways and navigation in Germany. 17-19, 2012.
- BORK, I. and MÜLLER-NAVARRA, S.: OPTTEL-A - Entwicklung eines operationellen Tideelbmodells auf der Basis des hydrodynamisch-numerischen Modellverfahrens BSHmod für die Nord- und Ostsee. Die Küste, 79, 2012.
- CASULLI, V. and LANG, G.: Mathematical Model UnTRIM - Validation Document. Bundesanstalt für Wasserbau (Hamburg), 2004.
- CASULLI, V. and WALTERS, R.A.: An unstructured grid, three-dimensional model based on the shallow water equations. In: International Journal for numerical methods in fluids, 32, 331-348, 2000.

- GÖNNERT, G.; JENSEN, J.; STORCH, H. VON; THUMM, S.; WAHL, T. and WEISSE, R.: Der Meeresspiegelanstieg - Ursachen, Tendenzen und Risikobewertung. *Die Küste*, 76, 225-256, 2009.
- HEINRICH, H.; MIKOLAJEWICZ, U.; MEYER-REIMER, E.; SEIN, D.; KLEIN, B.; GANSKE, A. and BÜLOW, K.: Impacts of Climate Change on Waterways in Estuaries, on Coasts and in the Sea. In: Federal Ministry of Transport, Building and Urban Development (ed.): *KLIWAS - impacts of climate change on waterways and navigation in Germany*. 121-123, 2012.
- HORSTEN, T.; KRAHE, P.; NILSON, E.; BELZ, J.U. and EBNER VON ESCHENBACH, A.: Impacts of Climate Change on the Elbe. In: FEDERAL MINISTRY OF TRANSPORT, BUILDING AND URBAN DEVELOPMENT (ed.): *KLIWAS - impacts of climate change on waterways and navigation in Germany*. 89-93, 2012.
- HPA HAMBURG PORT AUTHORITY (ed.): *Deutsches Gewässerkundliches Jahrbuch - Elbegebiet, Teil III 2008. Untere Elbe ab der Havelmündung*. 178 p., 2012.
- KREMP, C.; RUDOLPH, E. and SEHILI, A.: OPTEL-C: Entwicklung eines operationellen Tidemodells der Elbe sowie einer Modellkopplung mit dem BSH-Vorhersagemodell der Nordsee. *Die Küste*, 79, 2012.
- LÄNDER-ARBEITSGRUPPE: Bemessungswasserstände entlang der Elbe. *Die Küste*, 47, 31-50, 1988.
- MÜLLER-NAVARRA, S.; BORK, I.; JENSEN, J.; KOZIAR, C.; MUDERSBACH, C.; MÜLLER, A. and RUDOLPH, E.: Modellstudien zur Sturmflut und zum Hamburg-Orkan 1962. In: *HANSA International Maritime Journal*, Vol. 143, 12, 72-88, 2006.
- NLWKN NIEDERSÄCHSISCHER LANDESBETRIEB FÜR WASSERWIRTSCHAFT, KÜSTEN- UND NATURSCHUTZ (ed.): *Deutsches Gewässerkundliches Jahrbuch - Weser-Emsgebiet 2010*. 301 p., 2013.
- SCHULTE-RENTROP, A. and RUDOLPH, E.: A Sensitivity Study of Storm Surges Under the Conditions of Climate Change in the Elbe Estuary. In: FILHO, W.L. (ed.): *Climate Change and Disaster Risk Management*. Berlin, 295-309, doi: 10.1007/978-3-642-31110-9_18, 2012.
- SEIFFERT, R. and HESSER, F.: Investigating climate change impacts and adaptation strategies in German estuaries. *Die Küste*, 81, 2014.

Optimization of Empirical Storm Surge Forecast – Modelling of High Resolution Wind Fields

Jana Kristandt, Benedict Brecht, Helmut Frank and Heiko Knaack

Summary

Aim of this study is to improve the empirical storm surge forecast for the coast of Lower Saxony using modelled high resolution wind fields over the North Sea. The hindcast of historic storms is done by Deutscher Wetterdienst (German Weather Service, DWD) using their operational model chain (GME, COSMO-EU, COSMO-DE). COSMO was run in forecast and in nudging mode. The NLWKN-Coastal Research Station used the modelled wind fields to optimize the empirical storm surge forecast with a variety of empirical and neural network approaches.

Keywords

storm surges, storm surge forecast, artificial neural networks, empirical modelling, weather forecast models (GME, COSMO), wind simulation, North Sea

Zusammenfassung

Ziel der Untersuchung war eine Verbesserung der empirischen Sturmflutvorhersage für die Niedersächsische Küste auf Basis hochauflösender Windfelder über der Nordsee. Dazu wurden historische Stürme vom Deutschen Wetterdienst (DWD) mithilfe der operationellen Modellkette (GME, COSMO-EU, COSMO-DE) nachgerechnet. Die COSMO-Läufe wurden mit und ohne „Nudging“ modelliert. Die Forschungsstelle Küste des Niedersächsischen Landesbetriebs für Wasserwirtschaft, Küsten- und Naturschutz (NLWKN) nutzte diese Winddaten um ihre Sturmflutvorhersage durch verschiedene empirische Ansätze und künstliche Neuronale Netzwerke zu verbessern.

Schlagwörter

Sturmfluten, Sturmflutvorhersage, künstliche neuronale Netze, empirische Modellierung, Wettervorhersagemodelle (GME, COSMO), Windmodellierung, Nordsee

Contents

1	Introduction	302
2	High resolution modelling of wind fields.....	303
2.1	Model chain.....	303
2.2	Nudging runs.....	304
2.2.1	Availability of nudging data	305
2.3	Results	306

2.3.1	Verification.....	306
2.3.2	Storm tracks.....	308
3	Empirical storm surge forecast.....	309
3.1	Procedure and data base.....	310
3.1.1	Data availability.....	310
3.1.2	Data preprocessing.....	310
3.2	Trigonometric approach.....	311
3.2.1	Analysis of further parameter.....	312
3.3	Neural network approach.....	313
3.4	First Test: Storm surge of 6 th December 2013 (“Xaver”).....	314
4	Conclusion and Outlook.....	315
5	References.....	316

1 Introduction

Storm surges are a severe risk for the low-lying coasts of the North Sea. Storm surges are induced by cyclones crossing Northern Europe from west to east. Strong westerly to northwesterly wind fields on the back side of the low pressure area can drive water masses into the German Bight and force the water level to increase by several meters along the coasts of the Netherlands, Germany and Denmark. If favorable meteorological conditions coincide with astronomical high tide, a storm surge is approaching the coast with the potential of heavy damages and risk of life (e.g. SCHMITZ 1978a; JENSEN and MÜLLER-NAVARRA 2008).

Over the last decades, different approaches were developed to forecast storm surges ranging from simple to elaborated empirical relations (e.g. ANNUTSCH 1978; MÜLLER-NAVARRA and GIESE 1997) or numerical hydrodynamic models (e.g. SCHMITZ 1978b; PHILIPPART and GEBRAAD 1997; DICK et al. 2001; MÜLLER-NAVARRA et al. 2003). A considerably large progress was enabled due to the enormous improvement of weather forecasting by numerical weather prediction from global scales to limited area models with high resolution. For many years the Deutscher Wetterdienst (DWD, German Weather Service) operates a chain of numerical weather forecasting models, which are continuously improved. The numerical weather prediction at the DWD started in 1968 with the BKL model (baroclinic model without moisture), followed in 1978 by the BKF model (baroclinic moisture model, 254 km mesh size; promet 2/3 1978). It was replaced in 1991 by the global model GM with 190 km mesh size and a limited-area model EM with 50 km mesh size. These were in turn replaced in 1999 by the GME (MAJEWSKI et al. 2002) with at that time 60 km mesh width and the regional model LM (now COSMO-EU) with 7 km mesh size. Now the model chain of the DWD ranges from the global model GME (20 km mesh size) via the limited area-model COSMO-EU with 7 km mesh size down to COSMO-DE (operationally since 2007) with 2.8 km mesh width. In 2014 the new global model ICON shall become operational with a mesh width of 13 km. The DWD provides the German coastal authorities with the necessary meteorological data.

In the 1990th the antecessor of the Lower Saxony Water Management, Coastal Defense and Nature Conservation Agency (NLWKN) established a regional storm surge

forecasting service for the coast of Lower Saxony. It uses an empirical approach based on predicted wind speed and direction in the southern part of the North Sea. Confronted with a lack of high resolution meteorological data over the North Sea during storm surge events, DWD and the Coastal Research Station of NLWKN started a project in 2011, to hindcast 39 historical storm surge events at the North Sea coast from 1962 till 2011 (see Tab. 1).

2 High resolution modelling of wind fields

2.1 Model chain

High resolution wind fields are necessary to predict the occurrence of storm flood events and their magnitude. Therefore DWD produced wind fields of 39 historical storm flood events (see Tab. 1) using its global model GME (MAJEWSKI 2002) and the limited-area non-hydrostatic model COSMO (COSMO model documentation 2014), which is run in the two versions COSMO-eu and COSMO-de. GME is a hydrostatic model operating on an icosahedral grid.

Table 1: Date and wind surge [cm] at Norderney of the modelled storm events.

no.	date	surge	no.	date	surge	no.	date	surge
1	16.02.1962	297	14	14.02.1989	159	27	05.02.1999	220
2	30.11.1966	206	15	25.01.1990	182	28	03.12.1999	201
3	23.02.1967	228	16	26.02.1990	250	29	30.01.2000	223
4	01.03.1967	206	17	20.08.1990	117	30	28.10.2002	146
5	19.11.1973	255	18	20.12.1991	197	31	01.11.2006	255
6	06.12.1973	241	19	22.01.1993	213	32	12.01.2007	199
7	14.12.1973	235	20	09.12.1993	147	33	18.01.2007	129
8	03.01.1976	275	21	20.12.1993	192	34	18.03.2007	216
9	21.01.1976	275	22	28.01.1994	247	35	09.11.2007	255
10	31.12.1977	248	23	13.03.1994	171	36	25.11.2007	147
11	24.11.1981	237	24	01.01.1995	201	37	13.03.2008	133
12	02.02.1983	223	25	10.01.1995	228	38	12.11.2010	155
13	05.12.1988	159	26	29.10.1996	165	39	04.02.2011	133

For these simulations GME has a mesh width of 30 km and 60 vertical layers. Operationally, GME runs on a 20 km grid. Here, GME is initialized four times a day (00, 06, 12, and 18 UTC) from reanalysis data of ECMWF. For storms before 1979 we use ERA-40 (UPPALA et al. 2005) which uses a 3-dimensional variational assimilation on a 125 km grid. In and after 1979 the ERAInterim analysis (DEE et al. 2011) is used. It employs a 12-hourly 4-dimensional variational assimilation scheme on a horizontal grid of about 80 km mesh width. GME provides initial and boundary data for COSMO-eu with a mesh width of 7 km and 40 vertical layers. COSMO-eu in turn drives COSMO-de which has a mesh width of 2.2 km and 65 vertical layers. At this resolution deep convection can be explicitly resolved (BALDAUF et al. 2011).

Therefore, only shallow convection is parameterized in COSMO-de. Compared to the operational COSMO-EU at the DWD the domain of COSMO-eu is smaller in the south and the east (see Fig. 1) as these regions are not important for storm surge predictions at

the North Sea coast. The domain of COSMO-de is increased in the north, west and south compared to the operational COSMO-DE (see Fig. 1). The vertical resolution is increased from operationally 50 to 65 layers. COSMO-de serves as test bed for a possible new operational setup of COSMO-DE.

At first all storms were simulated in pure forecast mode. I.e. one storm was simulated as a series of short range forecasts which started from new reanalysis data. During the first few hours of a forecast the models must adapt to the interpolated analysis. Therefore, these forecast hours are discarded.

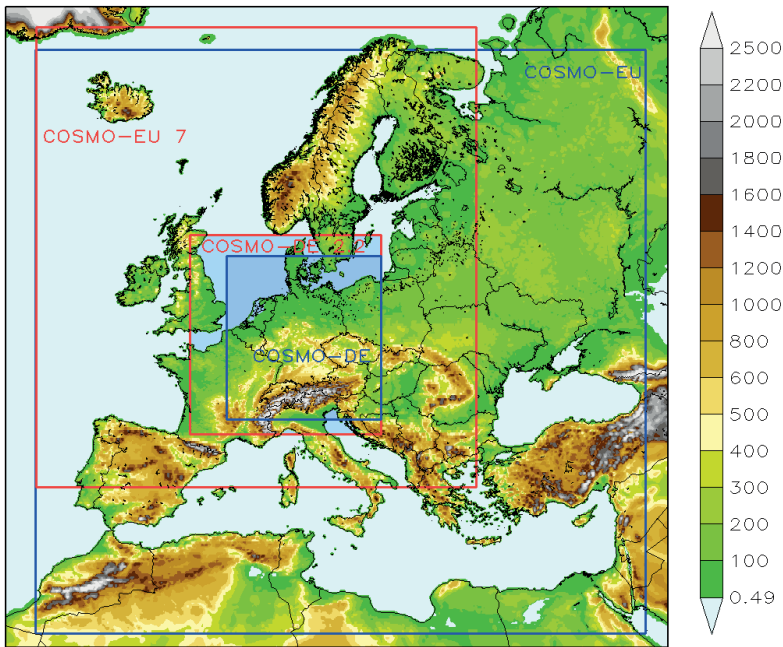


Figure 1: Domains of COSMO: The red lines show the domains of the 7 km COSMO-eu and 2.2 km COSMO-de. The blue lines show the domains of the operational versions COSMO-EU and COSMO-DE.

2.2 Nudging runs

To get the best possible analysis at high resolution the simulations with COSMO were additionally done with the Newtonian relaxation or nudging technique (STAUFFER et al. 1990) to obtain one continuous analysis without jumps. With this method the prognostic variables of the model are relaxed towards prescribed values within a timeframe (SCHRAFF 1997). In this case the prescribed values are direct observations, which is advantageous for synoptic observations (STAUFFER and SEAMAN 1994). The relaxation against the observations is done via additional terms in the prognostic equations. In practical applications, the nudging term should and usually do remain smaller than the largest term of the dynamics. This situation is related to the basic idea of the method that the model fields are to be relaxed towards the observed values without significantly disturbing the dynamic balance of the model (SCHRAFF and HESS 2002).

If available, the following observations are used: Radiosondes provide both the upper air and the surface horizontal wind, temperature and humidity as well as the pressure on the lowest model level. Aircraft measurements supply horizontal wind and temperature. Data from wind profilers yield the upper-air wind, and near surface observations give station pressure, 10 m wind, and 2 m humidity. 10 m winds are only used for stations below 100 m above sea level to select only stations in flat terrain. The 2 m temperature is not assimilated, due to the potential disadvantage to the stability of the planetary boundary layer (STAUFFER et al. 1991). A more detailed description of the nudging in COSMO is given by SCHRAFF and HESS (2002).

2.2.1 Availability of nudging data

The data availability increases from older to newer storms. The total available observations per 6 hours for the COSMO-eu area are 2000-3000 Synop land and ship (relation 10:1) observations for events from 1966-1976. It increased in 1977 to approximately 5000 per 6 h mainly due to an increased frequency of Synop measurements (to 3 hourly or hourly observations), and to the first use of drifting buoys and aircraft observations. Then, it slowly increased to 15000 observations in the year 2000. Wind profiler data is available since 2000, and radiosonde measurements since 1991. Since 2006 over 40000 observations in 6 hours are available. As an example Fig. 2 shows the coverage of available Synop land and ship data on 29th October 2006 during storm “Britta”.

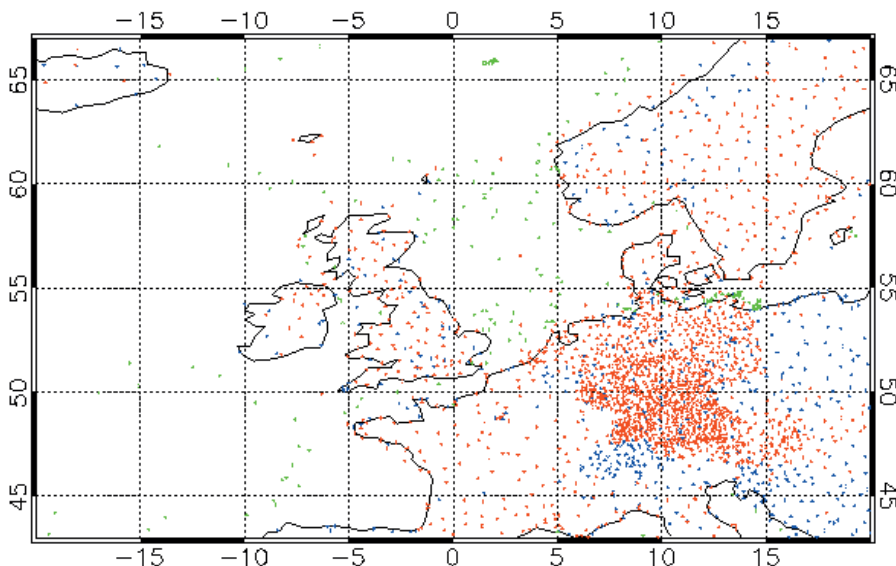


Figure 2: Data coverage of Synop land and ship data on 29th October 2006. The blue dots show the manned land stations, the red dots the automatic land stations and the green dots the ships.

The used data is less than the available data owing to the quality control, the availability of meta information like station height, or differences between real station height and model orography. Approximately 40 % to 90 % of the available data is used for the nudging.

For the storms from 1966-1976 only 40 %-50 % of the data are used by the model, mostly due to missing station altitudes of Synop land stations. From 1977-2000 80 %-90 % of the measurements are accepted. For later runs this ratio decreases again to 60 %-65 %.

2.3 Results

We present results for storm “Britta” in October 2006. This storm originated over Newfoundland. It travelled eastward crossing the Shetlands to the West coast of Norway. There “Britta” changed direction and moved southeastward over the Skagerrak. The water was pushed for many hours, first by northwesterly winds, and later by north northwesterly winds into the German Bight, see Fig. 3, which resulted in the high water level. As is typical for northern hemisphere mid-latitude storms the strongest winds of “Britta” occurred on the southwest side of the low pressure center behind the cold front.

2.3.1 Verification

The COSMO model data was verified with observations of up to 24 Synop stations at or near the North Sea coast of Denmark, Germany and the Netherlands, plus some stations in the North Sea (platforms, fire ships). However, not all stations were available for all storms. The verification was made for sea level pressure, pmsl, wind speed at 10 m, v_{10m} , and wind direction at 10 m, dd_{10m} . We calculated the bias of the model (model-obs), and the RMSE of the model values vs. the observation values. Here, we show the results of storm “Britta” in October 2006. The results of the other storms are qualitatively similar. For “Britta” observations from 18 stations were available for verification.

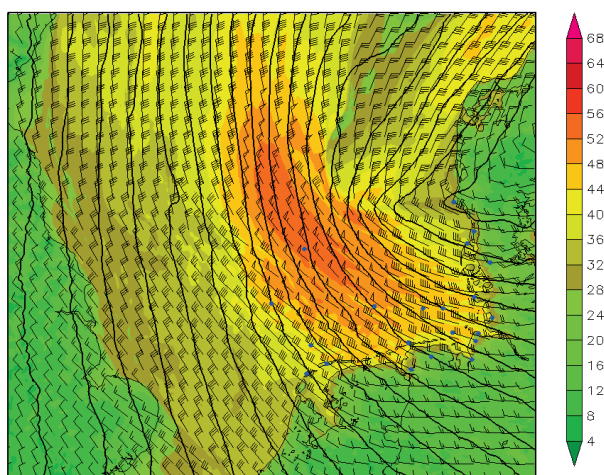


Figure 3: Wind field over the North Sea of storm “Britta” at the 29th October 2006, 1 UTC, 3 hours before the water reached the highest level at Norderney. Results from the COSMO-de nudging run are shown. The wind 10 m above ground is given in knots. Contour lines show pmsl in 2 hPa intervals. The blue dots indicate the locations of the stations which were used for verification.

For the verification we can compare both COSMO models, and nudging runs with forecast runs (see Fig. 3). For COSMO-eu the RMSE and biases for all 3 variables, v_{10m} , dd_{10m} , and $pmsl$, are less for the nudging analysis than for the forecast runs. The biases are 1.0 m/s compared to 1.2 m/s, 4° vs. 11° , and 0.1 hPa vs. 0.35 hPa (see Fig. 4 at the left). The RMSE values are 2.1 m/s vs. 2.3 m/s, 20° vs. 28° , and 0.6 hPa vs. 0.7 hPa (see Fig. 5 at the left). For this storm the results of the nudging runs were better than the forecast runs for all variables.

COSMO-de showed qualitatively similar behavior for the RMSE and the bias. The RMSE of the nudging runs versus the normal forecast runs were 1.9 m/s vs. 2 m/s, 19° vs. 25° , and 0.6 hPa vs. 0.7 hPa for $pmsl$ (see Fig. 5 at the right). Hence, the nudging runs were slightly better than the runs without nudging. The biases are 0.1 m/s compared to -0.3 m/s, 2.5° vs. 7° , and 0.01 hPa vs. 0.25 hPa (see Fig. 4 at the right). The sign of the 10 m wind speed bias of the normal forecast run changed compared to COSMO-eu. However, the nudging runs showed better results than the forecast runs.

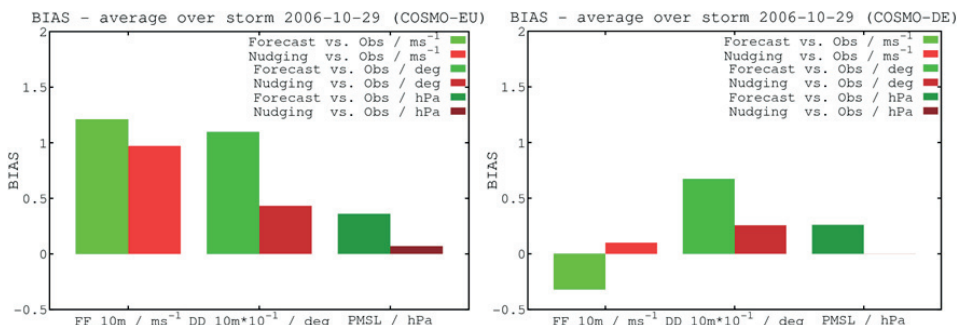


Figure 4: The biases of storm “Britta” for the three variables v_{10m} , dd_{10m} and $pmsl$ for COSMO-eu (left) and COSMO-de (right) and both for nudging runs (red) and runs without nudging (green).

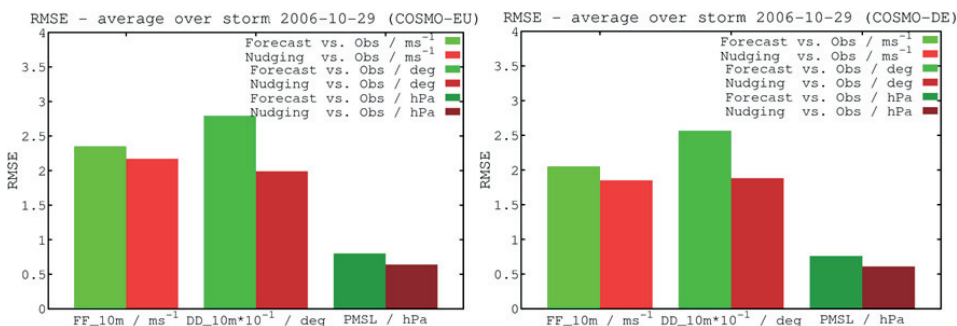


Figure 5: The RMSEs of storm “Britta” for the three variables v_{10m} , dd_{10m} and $pmsl$ for COSMO-eu (left) and COSMO-de (right) and both for nudging runs (red) and runs without nudging (green).

In general we saw that the largest improvement by the nudging results for the variable $pmsl$. For every time series of the nudging runs of any station the RMSE and biases of $pmsl$ were better than those of the normal forecast runs. For wind speed and direction

the forecast without nudging was better for a few stations compared to the nudging runs, but not averaged over all stations.

Comparing COSMO-eu and COSMO-de we obtained the following results. The RMSE values of COSMO-de are only minimally better than those of COSMO-eu. Also, the biases of COSMO-de are smaller. The 10 m wind speed bias of COSMO-de is much smaller than that of COSMO-eu. Where does this big difference of the wind speed bias come from? By calculating the mean wind speed difference of COSMO-eu and COSMO-de we saw the main difference over plain land outside the Alps which is the result of different roughness length, z_0 . The differences in z_0 come from the usage of different land use classifications. For COSMO-eu z_0 was derived from the GLC2000 data set (BARTHOLOMÉ and BELWARD 2005), whereas for COSMO-de the newer GlobCover data set (ARINO et al. 2008) has been employed. Outside the Alps z_0 is higher in the data derived from GlobCover which yields lower near surface winds which are in better agreement with the observations. In the Alps z_0 for COSMO-eu contains an additional contribution from the orographic variability. We ran COSMO-eu with z_0 derived from GlobCover for three storms (“Tilo” 2007, “Kyrill” 2007, and “Britta” 2006). The wind speed bias of COSMO-eu decreased by 0.2 m/s averaged over all stations, 0.1 m/s for sea stations and 0.35 m/s for land stations which is an improvement for the storm. Hence, GlobCover yields better roughness values for COSMO-eu than GLC2000.

2.3.2 Storm tracks

An interesting information for studies on storm surges is the path of the storms. Therefore we plotted storm tracks for the events, which led to an accumulation of water of more than 2 m at the gauge Norderney (23 events). A storm track is defined here as the path of the pressure minimum in time. The tracks of the storms with the eight highest water levels at Norderney are shown in Fig. 6. The highest water level for almost all stations at the German North Sea coast occurred during the severe storm “Capella” in 1976, but for gauge Norderney it was the storm flood in 1962.

According to PETERSEN and ROHDE (1991) we can distinguish three classes of storm paths.

The Scandinavia type crosses longitude 8° E between 60° N and 65° N. The low pressure systems of this type originate between Greenland and Iceland and travel slowly southeastwards. Despite lower wind speed than the other two types, the German Bight is filled with a lot of water, because of the long residence time. One example for this storm type is the flood on February 1962. Of the 23 highest water levels we found six of the Scandinavia type.

The Skagerrak type is characterized by very high water levels which affects mostly the whole North Sea. It is the most frequented type and crosses 8° E between the 57° N and 60° N. We found 12 out of 23 events of this type.

Storms of the Jutland type mostly develop at the North American coast (Newfoundland) and move rapidly eastwards over the British Isles to cross the 8° E between 55° N and 57° N. They are of short duration, but very strong storms with a wind direction first from southwest, later turning to northwest. They mostly affect the west coast of Schleswig-Holstein and the estuary of the Elbe. The storm “Capella” in 1976, for example, was of this type. Out of 23 storms we found 4 of this type.

One storm of the 23 highest events did not cross the longitude 8° E and remained nearly stationary in the North Atlantic east of Iceland (in February 1967, no. 4 in Tab. 1).

If we look at the genesis of the storms and their tracks until they hit the North Sea coast some storms are a combination of different types (GÖNNERT et al. 2001). For example, Fig. 6 shows the storm in December 1977, which developed between Iceland and Greenland like a Scandinavia type, but moved southward to cross 8° E as a Skagerrak type.

3 Empirical storm surge forecast

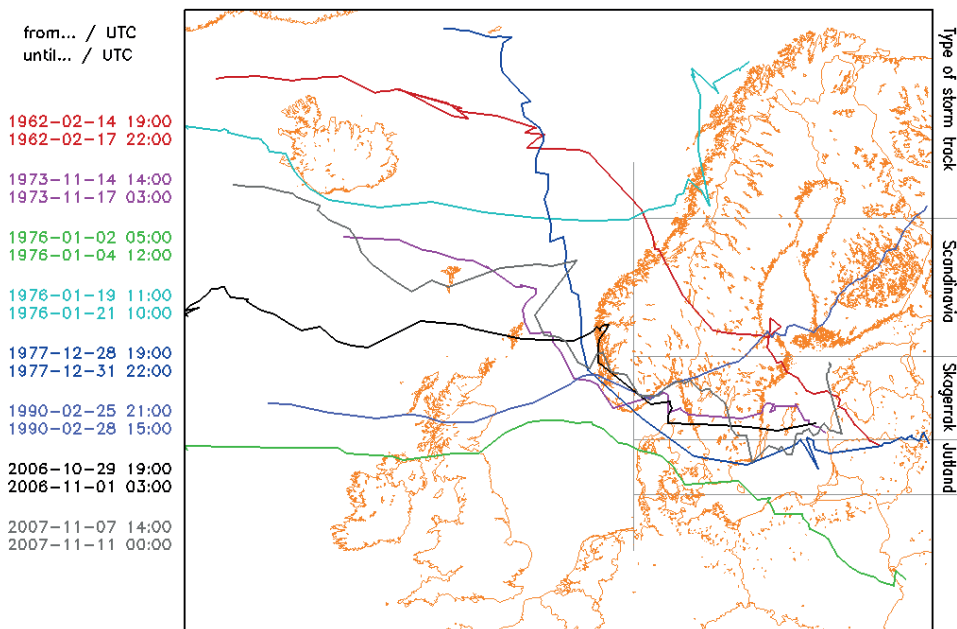


Figure 6: Tracks of the eight storms, which caused the highest accumulation of water at the gauge Norderney from 1962 till 2011. On the right side the storm flood types according to PETERSEN and ROHDE (1991) are shown.

The storm surge forecasting service of the NLWKN provides a 5day-forecast of the set-up at tidal high water -based on the weather forecasts of the DWD- for the gauges Norderney (representing the East-Frisian Islands), Emden (Ems-Estuary), Benseniel (East-Frisian Coast), Bremerhaven (Weser-Estuary) and Cuxhaven (Elbe-Estuary). The service was founded as an internal service for work scheduling of coastal protection and construction works. The information is also made available to the public via internet.

Based on the hindcasted wind fields an improvement of the storm surge forecast and an intense regionalization of the service were aimed for (the latter is not subject of this report).

3.1 Procedure and data base

3.1.1 Data availability

The DWD hindcasted 39 time series of 4 to 11 days, including 42 storm surges. The time series start 2 to 3 days before the actual storm surge and end roughly one day after. If two storm surges follow each other closely, the events are packed. Altogether the modelled wind data covers 335 high tides. Roughly one fifth of that are minor storm surges, 7 % are severe and less than 1 % are extreme storm surges. This data was used as input for the calculation of empiric formulas, neural networks and numerical modelling to conduct a variety of studies. A database with measured and astronomical water levels for numerous gauges along the Dutch and East-Frisian Coast was assembled as target and validation data. Due to limited time series in combination with large gaps in measured water level, especially during storm events, this project focused on the gauges of Norderney, Cuxhaven and Emden, where the most complete time series are available.

One limitation of this study is the unequal distribution of wind data (Fig. 1). Due to the focus on storm surges, all the modelled storms have main wind directions between west and northwest and -of course- high wind velocities. This means that the developed formulas are not meant to forecast low water situations with e.g. offshore winds. Even “normal” situations with low velocities must be regarded with caution.

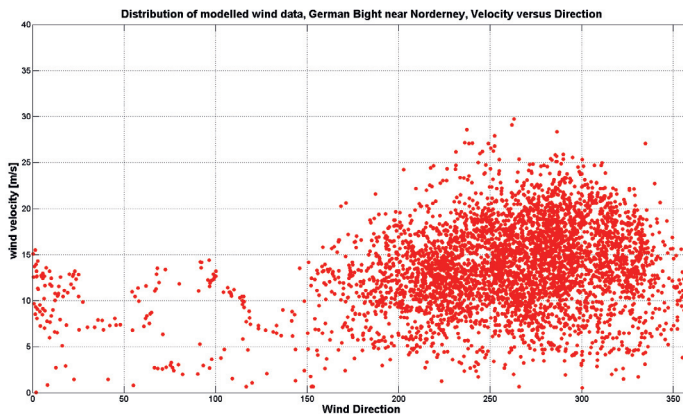


Figure 7: Distribution of wind direction versus velocity in the model output on sea near Norderney.

3.1.2 Data preprocessing

The previous used empiric relations between wind and surge were obtained from wind measurements. Data gaps and limited spatial distribution of measuring stations, especially over the open North Sea were a main limiting factor. Now in contrast, using spatial and temporal high-resolution modelled data, it was necessary to limit the number of wind data points to be used for analysis to keep the calculations practical and to not overfit the equations.

The modelled data was reduced to a grid with a cell distance of 1° (Fig. 8, left). Analysis with a stepwise-regression showed that the dominant influence of the wind on the water level along the Lower-Saxony Coast is localized in the German Bight, the entrance of the North Sea and the southwestern part in front of the coast of Norfolk. As not the exact position of the Wind input point is of importance, but the overall wind situation in the respective area, a spatial mean of up to 4 points (Fig. 8, left) was chosen to get rid of minor local and short-term effects. For the same reason, a temporal mean of three hours is used.

Within the German Bight eight positions were chosen to include the influence of the local wind directly in front of the coast (Fig. 8, right). The wind at these positions is already used in the presently used forecast formulas.

Analysis of the delay between wind occurrence and corresponding surge obtained a mean time lag of about 1h per 75 km. This fits well with the equation for velocity of shallow waves: $c = \sqrt{g \cdot d}$, ($g = 9.81 m/s^2$, $d =$ water depth). A depth of 100 m (mean depth of the North Sea) leads to a speed of roughly 100 km/h, a depth of 30 m as in the southern part of the North Sea to a speed of about 60 km/h.

For the derivation of new formulas, the data of the hind casted storm surges were split into two evenly distributed but independent. The validation data set consists of roughly 28 % of the data. The remaining was used for the setup of formulas and neural networks.

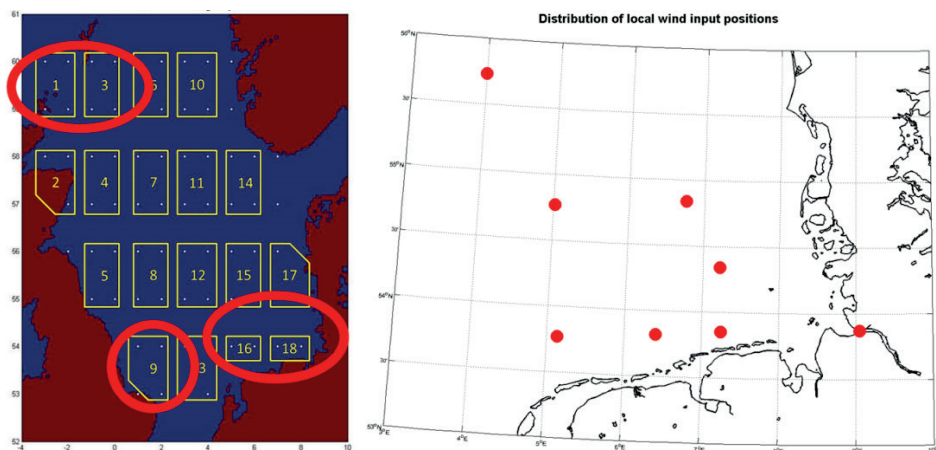


Figure 8: Reduction and choice of wind data points (left), position of local wind output (right).

3.2 Trigonometric approach

Based on the formula of ANNUTSCH (1978) a simple trigonometric approach was used to develop a new formula, taking into consideration not only the local but as well the wind on more distant parts of the North Sea:

$$\begin{aligned}
 Setup = a_0 + \sum_w a_{w1} * WS^2 * \sin(WD) + a_{w2} * WS^2 * \cos(WD) + a_{w3} * WS^3 * \\
 \sin(WD) + a_{w4} * WS^3 * \cos(WD) + \sum_{param} a_{param} * Value
 \end{aligned}
 \tag{1}$$

(with w number of the corresponding positions, WS windspeed, WD wind direction; $param$ are further parameters like air pressure (see below)). This approach works for exposed gauges directly at the open coast only. For estuary gauges it is necessary to implement a preceding gauge at the open coast near the estuary, from which the water level in consideration of the local wind is passed on to the destination gauge. This paper focuses on the forecast of the exposed gauge of Norderney.

In a first step of the study, the best wind input quantities concerning position, spatial and temporal interpolation and delay (see section 3.1.2) were identified. Secondly, the influence of further parameters like air pressure, changes in air pressure, astronomic set up and mean tidal water level on the setup was analyzed.

External waves were neglected due to existing studies (i.e. GÖNNERT 2003) and the impracticability for routine use due to the short timeframe.

3.2.1 Analysis of further parameter

Implementing the difference of air pressure to standard pressure of 1013hPa and the 3hourly-change in air pressure increases the quality of the forecast. SCHMITZ (1978b) has already pointed to the impact of air pressure and gradient. In the new approach it was realized by including the corresponding values from a point 70 km north of Norderney as representative for the German Bight.

The influence of astronomic offset was difficult to obtain due to a lack of data for the older storm surges. Own calculation of astronomical tides did not achieve the accuracy needed for the investigations. Some tests with limited data have shown that the implementation of astronomical residuals increase the quality of the model for set-ups in the “normal” range, when the astronomic residuals are in the same order than the wind set-up, whereas the general quality of the formula decreases within this tests due to the reduction of data amount. As the focus of this study is on the forecast of storm surges, the influence of astronomic residuals is neglected in the moment but is subject of the still running investigations.

As the tidal rise is in the order of a severe to extreme storm surge, the position of the mean tidal curve (i.e. high or low water) is of high importance for the calculation of storm surges (GÖNNERT 2003). Accordingly, the implementation of the mean tidal curve as time series on the approach shows a significant improvement for the forecast.

Altogether, the regression between measurements and the output of the described trigonometric approach shows a root mean squared error (“RMSE”) of about 31 cm (Fig. 9).

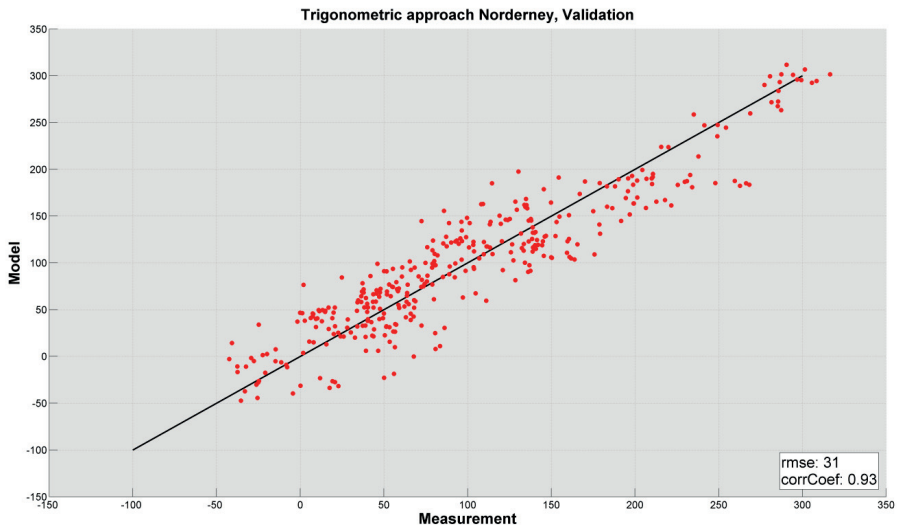


Figure 9: Validation of trigonometric approach for Norderney, measurement (x-axis) versus model (y-axis).

This sounds much, but taking into consideration the wide span of water set up between - 50 and plus 300 cm, the neglecting of astronomical residuals – especially for low surge events- as well as the uncertainties in the modelled meteorological data together with the general difficulties in forecasting storm events the results seems good. The formulas are tested now in the operational forecast and have passed satisfyingly a first test during storm “Xaver” (section 3.4).

3.3 Neural network approach

Beside the trigonometric approach, the application of a neural network was tested. Due to the requirement of the NLWKN a network only using meteorological parameter and mean tidal cycles – as in the trigonometric approach – was favored to get a forecast of at least one day. Considering preceding (measured or modelled) water levels denote a much shorter forecasting interval.

As network structure a feed-forward net with 2 layers and 10 neurons in the hidden layer was chosen as the best fitting one (Fig. 10). The input is arbitrary expendable; the output is the setup of water level.

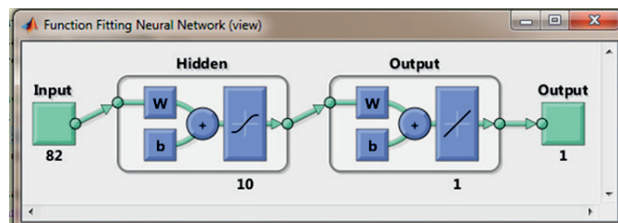


Figure 10: Schematic view of Neural Network.

As input the same data set as for the trigonometric approach was used for the neural network. The “RMSE” for Norderney is 25 cm (Fig. 11), meaning an even better result than for the trigonometric approach.

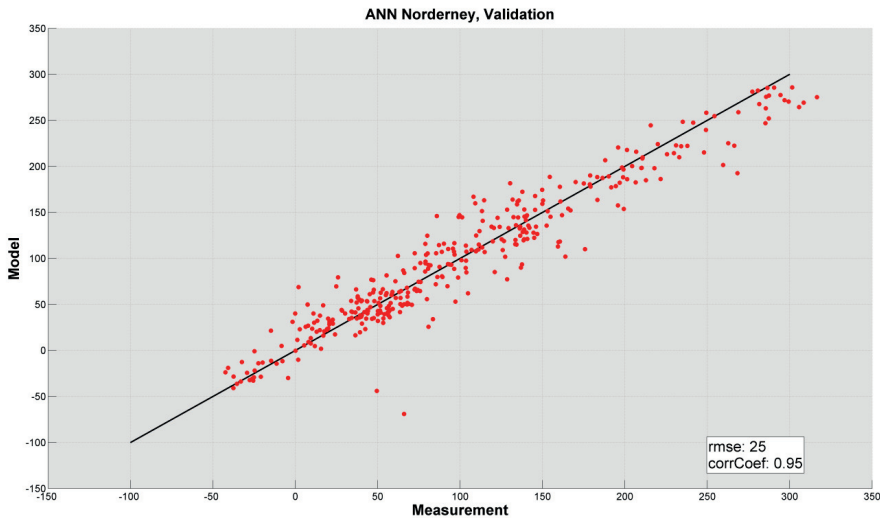


Figure 11: Validation of neural network for Norderney, measurement (x-axis) versus model (y-axis).

But it appears that the results must be regarded with caution, as the adding of only a few more wind datasets or other parameters leads to an evident overfitting of the model. Now working parallel to the daily forecast it must be checked if this tool is applicable for operational use. The test during storm Xaver at least was promising (see section 3.4).

3.4 First Test: Storm surge of 6th December 2013 (“Xaver”)

Both models, the trigonometric approach and the neural network, are used parallel to the operational forecast since November 2013. At the beginning of December, the cyclone “Xaver” led to a chain of storm surges of which the one of December 6th, early morning, was one of the highest storm surges at the Coast of Lower Saxony of the last hundred years. At the gauge of Norderney the storm surge with a height of 2.83 m above the mean high water level was only exceeded by the one of February 1962.

During this event, the new approaches proved to be valuable instruments for the storm surge forecast service of the NLWKN.

Exemplarily, the forecast results at the morning of 5th of December are shown in Fig. 12. The forecast based on the predicted wind and air pressure data provided by the DWD, using the COSMO-EU-Modell, run 12/5., 00:00UTC. The results of the present formula are plotted in dark blue, the trigonometric approach in green, the ANN-results in red and the measurements in black.

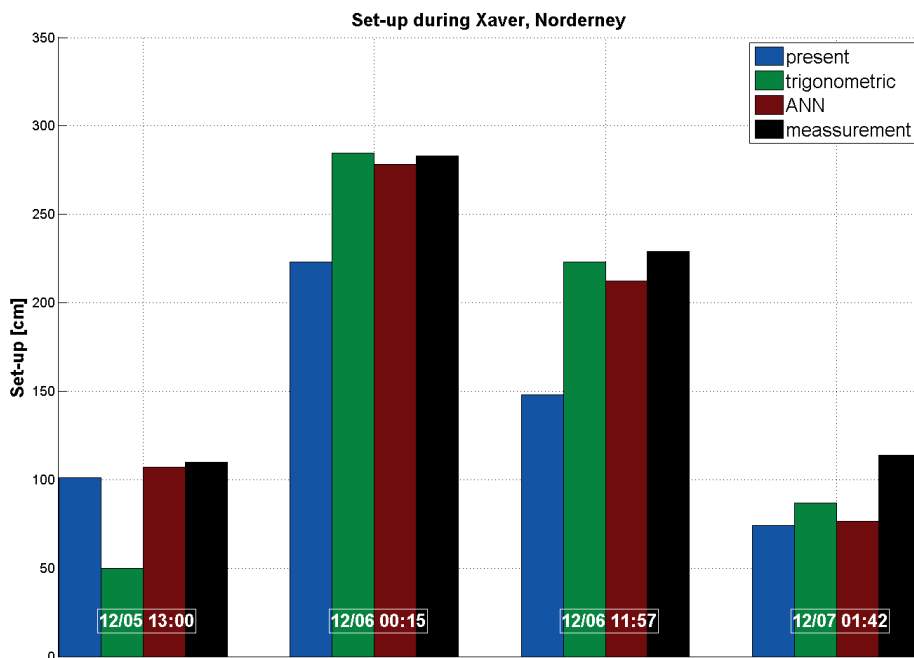


Figure 12: Modeled and measured surges during storm Xaver at Norderney, December 5-7, 2013, comparison of different forecast-models.

Both trigonometric and neural network approach forecasted the two main surges with very satisfying results with a deviation at Norderney less than 20 cm. The results of the new models are significantly better than the results of the present formula. The first surge as well was predicted quite well except the forecast of the trigonometric model for Norderney. The reason for the failing at this point is not clear to us. Deviations between prediction and measurement for the last surge on 12/7 are higher, but it has to bear in mind that there are more than 48 hours between the wind forecast and the resulting storm.

4 Conclusion and Outlook

Storm surges at the coast of Lower-Saxony are driven mainly by the local wind in the German Bight. Furthermore, the wind at the entrance of the North Sea and in the South-Eastern part next to the Norfolk Coast is of importance for empirical storm surge forecast.

To make available a data set with high resolution wind fields and other meteorological variables DWD simulated a set of 39 historical storm events from 1962 till 2011 in the project ‘‘OptempS-MohoWif’’. The high resolution meteorological data for the North Sea is of great importance for the improvement of empirical storm surge forecasting and other questions about coastal development and protection.

The wind data was calculated with two versions of the limited area model COSMO of DWD. COSMO-eu provided data for the whole North Sea including the entrance of the North Sea bordering to the North Atlantic and the South-Eastern part with the English

Channel. For the German Bight additional data was provided by COSMO-de on a 2.2 km grid. Both models were run in nudging and normal forecast mode. I.e. we have a mini ensemble with 4 members for each storm event. Thereby DWD tested the 2.2 km horizontal grid resolution and 65 vertical layers for COSMO-de, which might become a new operationally setup of COSMO-DE. As expected we got better results for the nudging runs than for the normal forecasts. Comparing COSMO-de and COSMO-eu we see minimally lower values of RMSE of wind and sea level pressure for COSMO-de. The biases for pmsl differ marginally at very low values, but for the 10 m wind they differ significantly. It was shown, that using GlobeCover land use data instead of GLC2000 data could give better results for the wind speed biases for COSMO-eu. Further tests will be made testing a wind speed dependent Charnock constant to calculate the sea surface roughness length.

The newly determined empirical relation between wind, pressure and the surge at the coast of Lower Saxony seems to be a promising approach for the optimization of storm surge forecasting in that region. Its capability was shown at a first test in December 2013 during the severe storm surge "Xaver". On the other hand the test operation in winter 2013/2014 shows the limitation of the forecasting for less intense wind setup, induced by wind directions other than West to Northwest. This concerns especially the chosen approach with artificial neuronal networks. This limitation clearly relies on the focus of the training data set on storm surges with wind directions in the mentioned sector.

The new storm surge forecasting approach at the NLWKN has to be further tested and successive adjustments have to be made to new meteorological data which will be provided by the operational weather forecasting models of the DWD.

5 References

- ANNUTSCH, R.: Über das empirisch-statistische Sturmflutvorhersageverfahren des Deutschen Hydrographischen Instituts. *Promet*, 8 H. 4, 9-12, 1978.
- ARINO, O.; BICHERON, P.; ACHARD, F.; LATHAM, J.; WITT, R. and WEBER, J.-L.: GlobCover the most detailed portrait of Earth. *ESA Bulletin*, 136, 25-31, 2008.
- BALDAUF, M.; SEIFERT, A.; FÖRSTNER, J.; MAJESWKI, D.; RASCHENDORFER, M. and REINHARDT, T.: Operational Convective-Scale Numerical Weather Prediction with the COSMO model: Description and Sensitivities. *Mon. Wea. Rev.*, 139, 3887-3905, 2011.
- BARTHOLOMÉ, E. and BELWARD, A.S.: GLC2000: a new approach to global land cover mapping from Earth observation data. *Int. J. Remote Sens.*, Vol. 26, No. 9, 1959-1977, 2005.
- CONSORTIUM FOR SMALL-SCALE MODELLING: COSMO model documentation: <http://www.cosmo-model.org>, last visited: 07.01.2014.
- DEE, D.P.; UPPALA, S.M.; SIMMONS, A.J.; BERRISFORD, P.; POLI, P.; KOBAYASHI, S.; ANDRAE, U.; BALMASEDA, M.A.; BALSAMO, G.; BAUER, P.; BECHTOLD, P.; BELJAARS, A.C.M.; VAN DE BERG, L.; BIDLOT, J.; BORGMANN, N.; DELSOL, C.; DRAGANI, R.; FUENTES, M.; GEER, A.J.; HAIMBERGER, L.; HEALY, S.B.; HERSBACH, H.; HÓLM, E.V.; ISAKSEN, I.; KÁLLBERG, P.; KÖHLER, M.; MATRICARDI, M.; McNALLY, A.P.; MONGE-SANZ, B.M.; MORCRETTE, J.-J.; PARK, B.-K.; PEUBEY, C.; DE ROSNAY, P.; TAVOLATO, C.; THÉPAUT, J.-N. and VITART, F.:

- The ERA-Interim reanalysis: configuration and performance of the data assimilation system. *Q. J. R. Meteorol. Soc.*, Vol. 137: 553-597, 2011.
- DEUTSCHER WETTERDIENST: Das barokline Model BKF. *Promet* 2/3 1978, p. 48, 1978
- DICK, S.; KLEINE, E.; MÜLLER-NAVARRA, S.H.; KLEIN, H. and KOMO, H.: The operational Circulation Model of BSH (BSHcmod) – Model Description and Validation. *Ber. d. Bundesamtes für Seeschifffahrt und Hydrographie*, Nr. 29, 49p, 2001.
- FRANK, H. and MAJEWSKI, D.: Hindcasts of historic storms with the DWD models GME, LMQ and LMK using ERA-40 reanalyses. *ECMWF Newsletter*, Vol. 109, 16-21, 2006.
- GÖNNERT, G.: Sturmfluten und Windstau in der Deutschen Bucht. Charakter, Veränderungen und Maximalwerte im 20. Jahrhundert. *Die Küste* 67: 185-365, 2003.
- GÖNNERT, G.; DUBE, S.K.; MURTY, T. and SIEFERT, T.: Global Storm Surges: Theory, Observations and Applications - Preface and Contents. *Die Küste* 63, Global Storm Surges, 2001.
- JENSEN, J. and MÜLLER-NAVARRA, S.H.: Storm Surges on the German Coast. *Die Küste* 74, 92-124, 2008.
- MAJEWSKI, D.; LIERMANN, D.; PROHL, D.; RITTER, B.; BUCHHOLD, B.; HANISCH, T.; PAUL, G.; WERGEN, W. and BAUMGARDNER, J.: The Operational Global Icosahedral-Hexagonal Gridpoint Model GME: Description and High-Resolution Tests. *Mon. Wea. Rev.* 130, 319-338, 2002.
- MÜLLER-NAVARRA, S.H. and GIESE, H.: Empirische Windstauformeln für die Deutsche Bucht. *Deutsche IDNDR-Reihe* 7, 37-41, 1997.
- MÜLLER-NAVARRA, S.H.; LANGE, W.; DICK, S. and SOETJE, K.C.: Über die Verfahren der Wasserstands- und sturmflutvorhersage: Hydrodynamisch-numerische Modelle der Nord- und Ostsee und ein empirisch-statistisches Verfahren für die Deutsche Bucht. *Promet* 29, 117-124, 2003.
- PETERSEN, M. and ROHDE, H.: Sturmflut: Die großen Fluten an den Küsten Schleswig-Holsteins und in der Elbe. Neumünster, 1991.
- PHILIPPART, M.E and GEBRAAD, A.: A new storm surge forecasting system. In: STEL, J.H. et al. (Ed.). *Operational oceanography: the challenge for European co-operation: Proceedings of the First International Conference on EuroGOOS 7-11 October 1996, The Hague, The Netherlands*. Elsevier Oceanography Series, 62, 487-495, 1997.
- SCHRAFF, C.H.: Mesoscale Data Assimilation and Prediction of Low Stratus in the Alpine Region. *Meteorol. Atmos. Phys.* 64, 21 50, 1997.
- SCHRAFF, C. and HESS, R.: Datenassimilation für das LM. *Promet*, Jahrgang 27, Nr. 3/4, 156-164, 2002
- SCHMITZ, H.P.: Sturmfluterzeugende Vorgänge in der Nordsee. *Promet* 4, 2-5, 1978a
- SCHMITZ, H.P.: Vorhersageverfahren und ihre Probleme. *Promet* 4, 9-12, 1978b.
- STAUFFER, D.R. and SEAMAN, N.L.: Use of Four-Dimensional Data Assimilation in a Limited-Area Mesoscale Model Part I: Experiments with synoptic scale data. *Mon. Wea. Rev.* 118, 1250-1277, 1990.
- STAUFFER, D.R. and SEAMAN, N.L.: Multiscale four-dimensional data assimilation. *J. Appl. Meteorol.* 33, 416-434, 1994.

- STAUFFER, D.R.; SEAMAN, N.L. and BINKOWSKI, F.S.: Use of Four-Dimensional Data Assimilation in a Limited-Area Mesoscale Model Part II: Effects of Data Assimilation within the Planetary Boundary Layer. *Mon. Wea. Rev.* 119, 734-754, 1991.
- UPPALA, S.M.; KÁLLBERG, P.; SIMMONS, A.; ANDRAE, U.; DA COSTA BECHTOLD, V.; FIORINO, M.; GIBSON, J.; HASELER, J.; HERNANDEZ, A.; KELLY, G.; LI, X.; ONOGI, K.; SAARINEN, S.; SOKKA, N.; ALLAN, R.; ANDERSSON, E.; ARPE, K.; BALMASEDA, M.; BELJAARS, A.; VAN DE BERG, L.; BIDLOT, J.; BORMANN, N.; CAIRES, S.; CHEVALLIER, F.; DETHOF, A.; DRAGOSAVAC, M.; FISHER, M.; FUENTES, M.; HAGEMANN, S.; HÓLM, E.; HOSKINS, B.; ISARXSEN, L.; JANNSEN, P.; JENNE, R.; MCNALLY, A.; MAHFOUF, J.-F.; MORCRETE, J.-J.; RAYNER, N.; SAUNDERS, R.; SIMON, P.; STERL, A.; TRENTBETH, K.; UNTCH, A.; VASILJEVIC, D.; VITERBO, P. and WOOLLEN, J.: The ERA-40 re-analysis. *Q. J. R. Meteorol. Soc.*, Vol. 131, 2961-3012, 2005.

Extreme Storm Surge Prediction Using Hydrodynamic Modelling and Artificial Neural Networks

Mohamed Tayel and Hocine Oumeraci

Summary

On coastlines with shallow shelf areas (e.g. North Sea), a combination of high tides, storm surges, wind waves and mutual interactions generally represent the major sources of coastal flood risks: The contribution of the mutual interactions between the various components still remains the most unknown, despite the now routine linking of tidal and surge components in the current operational hydrodynamic storm-tide models. In fact, a proper physically-based coupling of all constituents will probably take decades to be implemented in the current operational models due to the highly complex and stochastic nature of the entire storm-tide system. Meanwhile, rather a more pragmatic data-driven approach is required to assess the contributions of these non-linear interactions to the resulting extreme storm-tide. Such a pragmatic approach is proposed, which is based on two types of artificial neural networks (ANNs) models called NARX (Nonlinear AutoRegressive eXogenous inputs): (i) NARX neural network model to predict the extreme storm-tide (Type-A), (ii) NARX neural network model to nonlinearly correct the numerical storm-tide results from TELEMAC2D and TOMAWAC (Type-B). Ensembles methods are then used to reduce variance and minimize error especially in extreme storm-tide events. The approach was applied for two pilot sites in the North Sea (Cuxhaven and Sylt). The results show that the ensemble models are able to extract the contribution of the nonlinear interaction between the different extreme storm-tide components at both sites by subtracting the results of the hydrodynamic models (linear superposition of storm-tide constituents) from the ensemble results. In most extreme storm-tide events considered in this study, the contribution of the nonlinear interaction resulted in the reduction of the extreme water levels when compared with the linear superposition of extreme storm-tide components. However, under certain conditions, the nonlinear interactions might result in higher storm-tides than the linear superposition (e.g. storm of January 2000 at Cuxhaven and Sylt).

Keywords

extreme storm-tide, North Sea, storm surge constituents, non-linear interactions, artificial neural network (ANN), hydrodynamic modelling, hybrid modelling

Zusammenfassung

Bei Küsten mit flachen Schelfgebieten wie die Nordsee, stellen extreme Sturmflut-Wasserstände aus Windstau und Gezeiten, Windwellen und deren Wechselwirkungen in der Regel die Hauptquelle von Hochwasserrisiken im Küstenbereich. Der relative Beitrag dieser Wechselwirkungen zwischen den Sturm-

flut-Komponenten zum resultierenden Extremwasserstand ist immer noch weitestgehend unbekannt – trotz der mittlerweile routinemäßigen Kopplung der Komponenten aus Windstau und Gezeiten in den derzeitigen operationellen hydrodynamischen numerischen Modellen (HNM). Aufgrund der hochkomplexen und stochastischen Natur der gesamten Sturmflut, wird die Implementierung einer weitgehend physikalisch-basierten Kopplung aller Sturmflut-Komponenten wahrscheinlich in die operationellen HNM noch Jahrzehnte Forschung benötigen. Mittlerweile wird eher ein pragmatischer datenbasierter hybrider Ansatz benötigt, um die nicht-linearen Wechselwirkungen zwischen allen Komponenten der resultierenden extremen Sturmflut-Wasserstände zu ermitteln. Solch ein pragmatischer Ansatz wird hier vorgeschlagen, der auf zwei Arten von KNN-Modellen (Künstliche Neuronale Netze) bezeichnet als NARX (Nicht-lineare AutoRegressive exogene Eingänge) basiert: (i) NARX neuronale Netzwerkmodell für extreme Sturmflutvorhersagen (Type-A), (ii) NARX neuronale Netzwerkmodell für die Korrektur der in HNM wie TELEMAC2D und TOMAWAC ermittelten nichtlinearen Effekte (Type-B). Besonders bei extremen Sturmflutereignissen, werden Methoden der Ensemble-Modellierung verwendet, um die Varianz zu reduzieren und Fehler zu minimieren. Der vorgeschlagene hybride Ansatz wurde beispielhaft für zwei Pilot-Standorte an der deutschen Nordseeküste (Cuxhaven und Sylt) implementiert. Die Ergebnisse an beiden Standorten zeigen, dass der hybride Ansatz in der Lage ist, die Beiträge der nichtlinearen Wechselwirkungen zwischen allen Sturmflut-Komponenten durch Subtraktion der Ergebnisse der hydrodynamischen Modelle (lineare Überlagerung aller Sturmflut-Komponenten) von den Ergebnissen der Ensemble-Modelle zu extrahieren. Für die extremsten Sturmflutereignisse im Zeitraum 1991–2007, die in dieser Studie berücksichtigt wurden, führte der Beitrag der nichtlinearen Wechselwirkung im Vergleich mit der linearen Überlagerung von extremen Sturmflut-Komponenten in der Regel zur Reduzierung der resultierenden Wasserstände. Jedoch zeigten die Ergebnisse, dass unter bestimmten Bedingungen die nichtlinearen Wechselwirkungen auch zu höheren Sturmflut-Wasserständen als die lineare Überlagerung führen können (z. B. Sturm vom Januar 2000 bei Cuxhaven und Sylt).

Schlagwörter

Extreme Sturmfluten, Nordsee, Sturmflutkomponenten, nicht-lineare Effekte, künstliche neuronale Netze (KNN), hydrodynamische numerische Modelle (HNM), hybride Modellierung

Contents

1	Introduction	321
2	Development of the NARX models for extreme storm surge prediction at Cuxhaven and Sylt.....	322
2.1	Input variables selection and preparation for the developed NARX models	323
2.2	NARX models for Cuxhaven and Sylt using ensemble methods.....	323
3	Evaluation of the effect of nonlinear interactions between extreme storm-tide constituents	327
3.1	Overall approach.....	330
3.2	Extraction of the nonlinear interaction approximated by the numerical model in the η_{su-t} TEL results (steps 1 to 5 in Fig. 5)	331
3.3	Extraction of the complementary terms for the nonlinear interaction using the predicted η_{EFN} results (steps 6 to 8 in Fig. 5)	333

3.4	Nonlinear interaction between all storm-tide components (step 9 in Figure 5).....	336
4	Concluding remarks	340
5	Acknowledgement.....	341
6	References.....	341

1 Introduction

It is uncertain whether nature has yet had enough time to “implement” all the physically possible worst combinations of all constituents for the generation of the most extreme storm-tide (“perfect storm-tide”). In fact, extreme storm-tide events depends on many factors that can be classified into three categories as depicted in Fig. 1 (a) Meteorological factors with non-stationary and stochastic characteristics such as wind speed and direction, storm characteristics and its track, sea level pressure, and rivers discharge. (b) Deterministic factors like astronomical tides and tidal resonance, which may greatly affect the tidal ranges in a shelf sea like the North Sea and depends on geometry, friction and rotation. (c) Local factors in a shallow water region, such as local bathymetry changes, roughness of the continental shelf and shoreline geometry. In the North Sea, the external surges that are generated outside and then propagate to the interested area contribute also nonlinearly to the resulting extreme storm-tide level.

The greatest difficulties towards the determination of the physically possible “perfect storm-tide” essentially arise from the fact that the nonlinear interactions between the various constituents are still unknown. Despite the now routine approaches of linking the tide and surge components in present operational storm-tide models and the substantial progress in recent research of air-sea interactions, a proper process-based coupling of all constituents will certainly take decades to be implemented in the current numerical models.

So the main objective of this study is the development of a new hybrid modelling approach which has been performed in collaboration with the joint XTREM-Risk project (OUMERACI et al. 2009) in which considerable data for Sylt and Cuxhaven have been collected, generated and analyzed (GOENNERT and GERKENSMEIER 2012) and (WAHL et al. 2012). The new approach combines NARX models with the hydrodynamic numerical model TELEMAC2D (HERVOUET and VAN HAREN 1994; HERVOUET 2007) and wave field model TOMAWAC (BENOIT 2003; BENOIT et al. 2001)), that can be applied to coastal areas and estuaries as an “operational”, low cost modelling tool in order (i) to account for the high nonlinearity of the processes at the two sites exemplarily considered in this study (Sylt island and Cuxhaven) in the North Sea, Germany and (ii) to fill the gaps in long-term data series by using sequential time series predictions at the given sites.

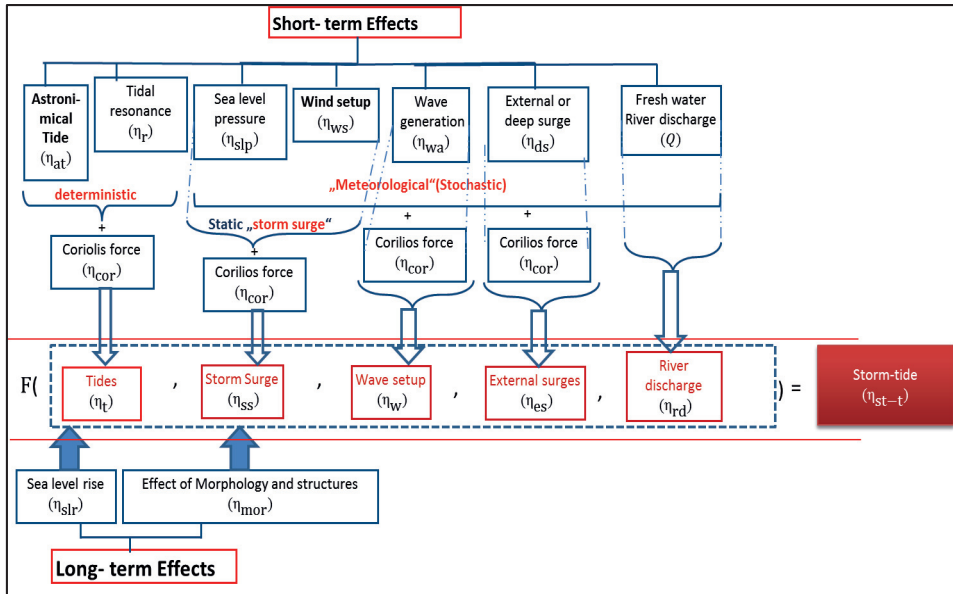


Figure 1: Main components contributing nonlinearly to the generation of extreme water levels and used terminology (modified from OUMERACI (2009)).

2 Development of the NARX models for extreme storm surge prediction at Cuxhaven and Sylt

Using the hourly meteorological forcing between 1970 and 2007 generated by the Regional Climate Model (RCM) SN-REMO (VON STORCH et al. 2000), along with the observed water level data from 1997 to 2007 for Cuxhaven and from 1999 to 2007 for Sylt, two types of ANNs models called NARX (Nonlinear AutoRegressive eXogenous inputs) were developed: (i) NARX neural network model to predict the extreme storm-tide (Type-A), (ii) NARX neural network model to nonlinearly correct the numerical storm-tide results from TELEMAC2D (Type-B).

The construction of each NARX model type is performed in two phases (see Tab. 1), due to the large number of neural architectural parameters (e.g. the number of hidden layers and number of hidden neurons in each layer) that can be modified. The first phase deals with the determination of the optimum number of input variables time series lags that should be included as input, also the optimum architectural parameters and best training algorithm using STATISTICA Automated Neural Networks (SANN). In the second phase, the final NARX model type is developed using Matlab neural networks toolbox for further structural parameters configuration and modifications that are based on the optimum structure obtained by SANN.

The use of ensembles methods can significantly reduce variance and minimize error especially in extreme storm-tide events. The ensemble forecasting method averages results from the best NARX models. Several different ensemble fitting neural network (EFN) models are developed and tested, varying the architectural parameters used for each ensemble.

Finally, the two types of NARX models and their ensemble prediction results are validated in terms of correlation coefficient (r), root mean square of error (RMSE) and standard deviation (σ) using observed water level data, in order to determine the models with the best prediction performance for water levels at the two locations between 1991 and 2007 (TAYEL and OUMERACI 2014; TAYEL 2015).

2.1 Input variables selection and preparation for the developed NARX models

Extreme water levels at an open coast may consist of the following six components: wind setup due to wind shear at the water surface; wave setup caused by wind-induced waves transferring momentum to the water column; pressure setup due to the atmospheric pressure decrease over the spatial extent of the storm system; Coriolis forced setup or setdown due to the effects of the rotation of the earth acting on the wind driven alongshore current at the coast; seiche due to resonance effects initiated by moving wind system, and an astronomical tide component.

The ANN models in the learning phase capture the nonlinear nature between extreme water level components using a moderate time span (approximately 5 years) of the observed water levels at Cuxhaven and Sylt. A subset of the observed water level data at Cuxhaven and Sylt for learning and validating the models should be selected such that it does not contain gaps and/or a substantial amount of improbable observed values. This criterion is fulfilled for Cuxhaven data between 1998 and 2007, while for Sylt between 2000 and 2007. The observed water level data for each year of the above selected periods are recorded with time interval between 10 minutes and 1 hour, which are temporally interpolated in order to be synchronized with the available meteorological data every hour (TAYEL and OUMERACI 2012).

Tab. 2 shows the input and output data for the two developed NARX models at Cuxhaven and Sylt. The input deck of the two NARX models types consists of the astronomical tidal forecasts, significant wave height produced by TOMAWAC numerical wave model, the two wind speeds components in east-west direction (wind U component or zonal component) and in south-north direction (wind V component or meridional component), external surge from Wick station, and sea level pressure for Cuxhaven and Sylt in addition to the Elbe river discharge (in case of Cuxhaven only).

2.2 NARX models for Cuxhaven and Sylt using ensemble methods

The input deck of the ensemble fitting neural network (EFN) models (Fig. 2) consists essentially of four different storm-tide prediction results from the best three NARX Type-A models and the best NARX Type-B model. In addition, the input deck contains the time lagged meteorological forces (sea level pressure, zonal and meridional wind speed components) for Cuxhaven or Sylt. The output of the EFN models is the difference between the observed storm-tide (η_{OB}) and the predicted storm-tide by NARX Type-B (η_B) either at Cuxhaven or Sylt. So, the developed EFN networks are trained in a way that makes the developed EFN models learn more nonlinear interaction terms “if possible” without changing the long term time series prediction performance gained from the results of both NARX Types A and B.

Table 1: Development phases 1 and 2 for NARX models Type A and Type B at Cuxhaven and Sylt.

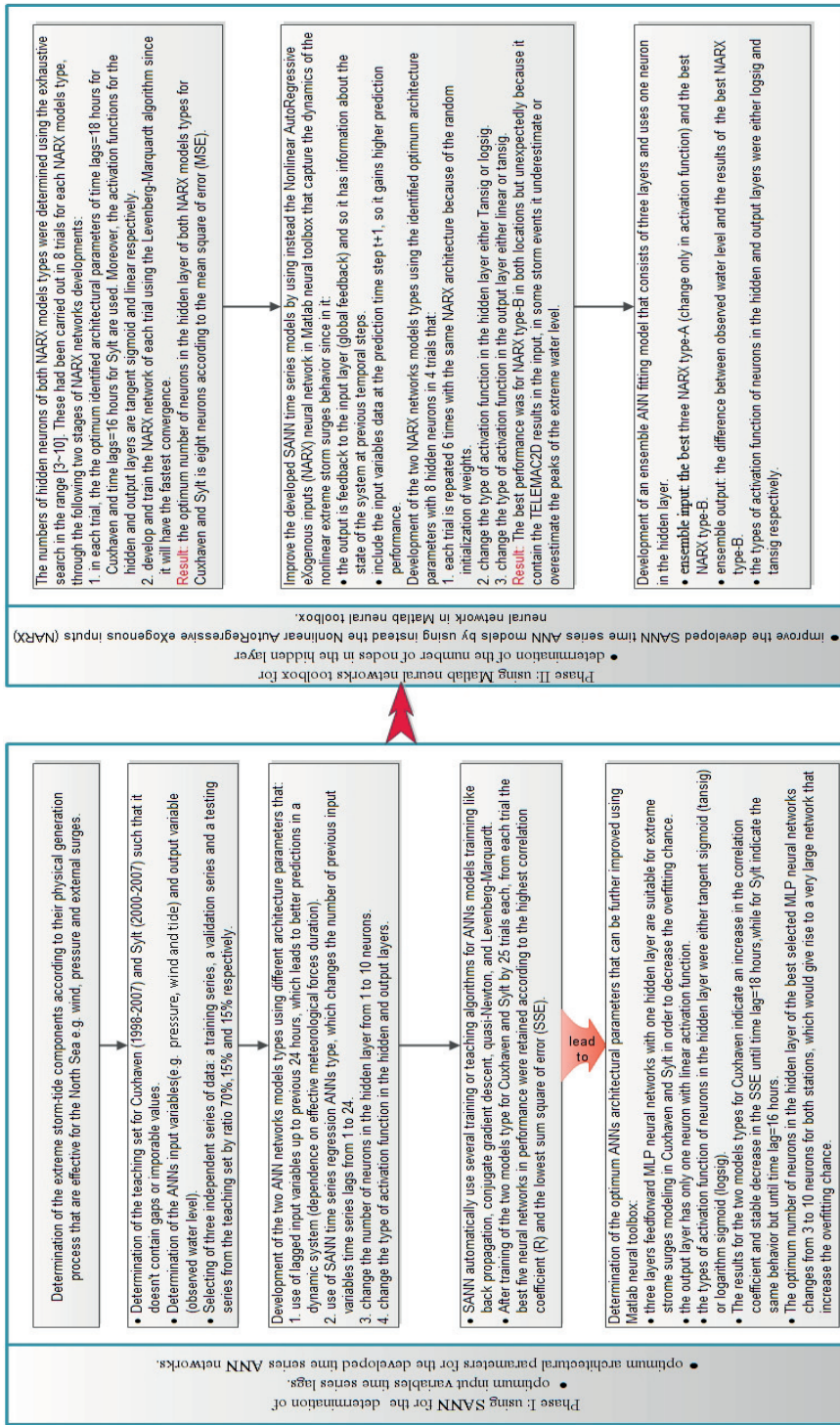


Table 2: Input and output for the developed NARX models Type A and Type B at Cuxhaven and Sylt.

Description	Cuxhaven (Type-A and Type-B)	Sylt (Type-A and Type-B)
Input	<ul style="list-style-type: none"> • Time series of wind U component. • Time series of wind V component. • Time series of sea level pressure. • Time series of observed water level. • Time series of Elbe River discharge. • Time series of external surge at Wick. • Astronomical tidal prediction time series. • TOMAWAC Significant wave height (Hs) results time series. • TELEMAC2D surge-tide results time series (for Type-B only). 	<ul style="list-style-type: none"> • Time series of wind U component. • Time series of wind V component. • Time series of sea level pressure. • Time series of observed water level. • Time series of external surge at Wick. • Astronomical tidal prediction time series. • TOMAWAC Significant wave height (Hs) results time series. • TELEMAC2D surge-tide results time series (for Type-B only).
output	Time series prediction of extreme water level every hour	Time series prediction of extreme water level every hour
Training period	1998 to 2005	2000 to 2005
Prediction period	1991 to 2007	1991 to 2007

The optimum architectural parameters (Fig. 2) are: one neuron in the hidden and output layers with the time lags of meteorological input variables $d_u=18$ hours for Cuxhaven and $d_u=16$ hours for Sylt. Only the activation function type is changed for the hidden and output layers. The transfer functions tansig or logsig are possible in the hidden layer, while for the output layer tansig , logsig and linear functions are more appropriate candidates. The development of EFN models has been implemented in six trials using the built-in matlab Levenberg-Marquardt algorithm. In each trial, the activation function type is changed either for the hidden or output layers.

Using the observed water level during storms from 1998 to 2007 for Cuxhaven and from 2000 to 2007 for Sylt, the EFN model prediction results (η_{EFN}) were “validated” in terms of correlation coefficient (r), RMSE and σ . The results show that the logsig and tansig activation functions in the hidden and output layers respectively give the best performance (lowest RMSE and highest correlation) for Cuxhaven and Sylt. For the EFN models in Cuxhaven, the lowest RMSE is 0.148 m with a correlation of 0.99. The best EFN model for Sylt has an RMSE of 0.124 m and a correlation of 0.98.

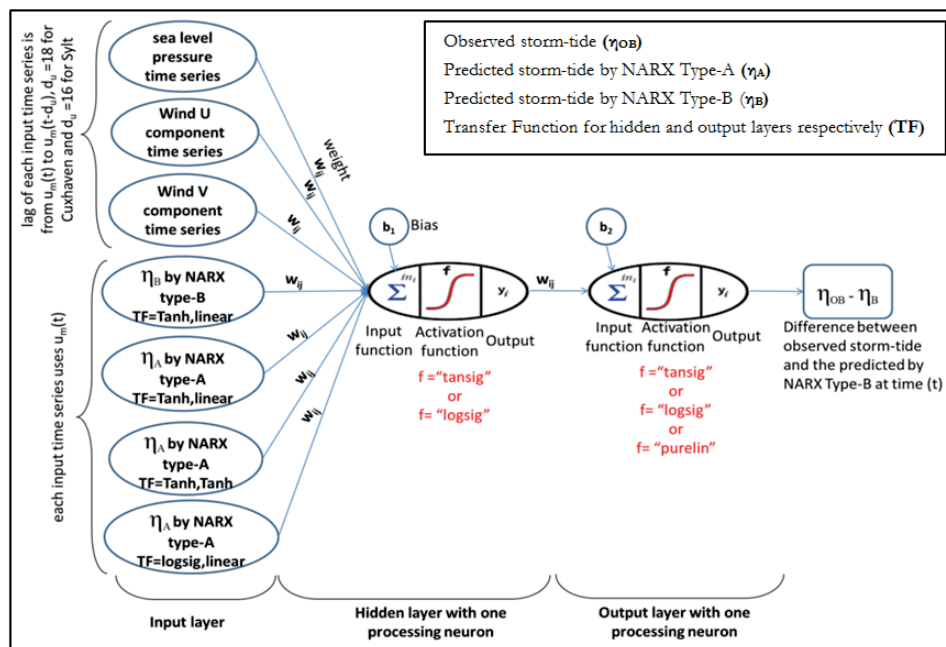


Figure 2: Input and output variables of the Ensemble Fitting Network (EFN) for Cuxhaven and Sylt with one neuron in the hidden and output layers.

The validation results of best η_{EFN} are close in value to its counterparts from the best NARX Type-B results at both sites Cuxhaven and Sylt. So, the long term prediction performance gained with the results of NARX model Type-B is inherited inside the η_{EFN} as shown in Fig. 3. During the storm of January 2000 at Sylt and in December 1999 at Cuxhaven (Fig. 3), the height and occurrence time of η_{EFN} highest peak are approximately the same as those of the actually observed water level η_{OB} .

The inter-comparison of the actually observed water level (η_{OB}), the numerically predicted water level ($\eta_{su-t TEL}$) and the ensemble results (η_{EFN}) is graphically summarized by meaningfully making use of the Taylor diagram approach (TAYLOR 2001) as shown in Fig. 4. The η_{OB} data from 1998 to 2007 for Cuxhaven and from 2000 to 2007 for Sylt are used for this comparison. The position of each label on the Taylor diagram is determined by the values of the correlation coefficient (r), root mean square of error (RMSE) and standard deviation (σ). In the Taylor diagrams, these statistical parameters are normalized by dividing both the RMSE and the σ of the compared results by the standard deviation of the observations ($\sigma_{observed}$). The key issue in the Taylor diagram approach (TAYLOR 2001) is to recognize the relationship between the four statistical parameters of interest (here RMSE, σ_{result} , $\sigma_{observed}$ and r):

$$(\text{RMSE})^2 = (\sigma_{\text{result}})^2 + (\sigma_{\text{observed}})^2 + 2 * \sigma_{\text{result}} * \sigma_{\text{observed}} * r \quad (1)$$

The η_{EFN} results have a correlation of 0.99, 0.98 and a normalized RMSE of 0.13 m, 0.17m at Cuxhaven and Sylt, respectively. Moreover, the EFN models perform better during the individual extreme storm events than NARX model Type B as depicted in

Fig. 3 during the storms of December 1999 at Cuxhaven and January 2000 at Sylt. The ensemble models (η_{EFN}) predict correctly the occurrence time of the η_{OB} highest peak during the storm of December 1999 at Cuxhaven, while the occurrence time of η_B highest peak predicted by NARX model type B is delayed by one hour. Moreover, the η_{EFN} highest peak resulting from the ensemble model reaches 3.84 m, which is better predicted than by NARX model type B with η_B peak of only 1.9 m. However, there is still a difference of 0.66 m between η_{EFN} and η_{OB} during the storm of December 1999 (called Anatol) at Cuxhaven, which is mainly due to the overestimation of the predicted sea level pressure by the climate model SN-REMO as compared to the observed pressure. The observed core pressure of Anatol on 3rd of December is 953 hPa (Nilsson et al. 2005), while the predicted by SN-REMO reaches 986 hPa. It decreases the water level by one centimeter for each hPa increase in pressure, which reaches 33 cm. Moreover, this increase in sea level pressure results in a reduction of predicted wind speed than the observed during the storm, which reaches up to 5 m/s (Nilsson et al. 2005) and decrease further the predicted water level. Hence, this leads to the shift down of η_{EFN} curve even at the trough, which occurs before the highest peak (see Fig. 3 (a)). During the storm of January 2000 at Sylt, the η_{EFN} highest peak is exactly the same as the η_{OB} highest peak with 3.02 m, while the η_B maximum highest peak predicted by NARX model type B is overestimated.

3 Evaluation of the effect of nonlinear interactions between extreme storm-tide constituents

The used hydrodynamic model “TELEMAC2D” (version 6.2 in parallel processing mode) solves the non-conservative form of the shallow water equations, written with h (depth) and u, v (flow velocity components) as the unknowns (HERVOUET 2007). It considers the propagation of long waves such as surge and tide, including the non-linear interaction between them. The numerical solution of these equations is based upon the fractional step method with two steps: (i) Advection and (ii) Propagation, diffusion and source terms (representing the wind, Coriolis force, bottom friction, a source or sink of momentum within the domain). The method of characteristics has been applied to solve the advection of velocities u and v . The propagation, diffusion and source terms are solved by the finite element method, where an implicit time discretization allows the elimination of the non-linearity in the equations. In that case, the nonlinear terms are approximated linearly in time. Variation in the formulations and space discretization transform the continuous equations into a linear discrete system, which is solved using an iterative procedure based on the conjugate gradient method (HERVOUET and VAN HAREN 1994). This treatment of the nonlinear terms can lead to either underestimated or overestimated water level peaks during extreme storms and to incorrect prediction of their occurrence times.

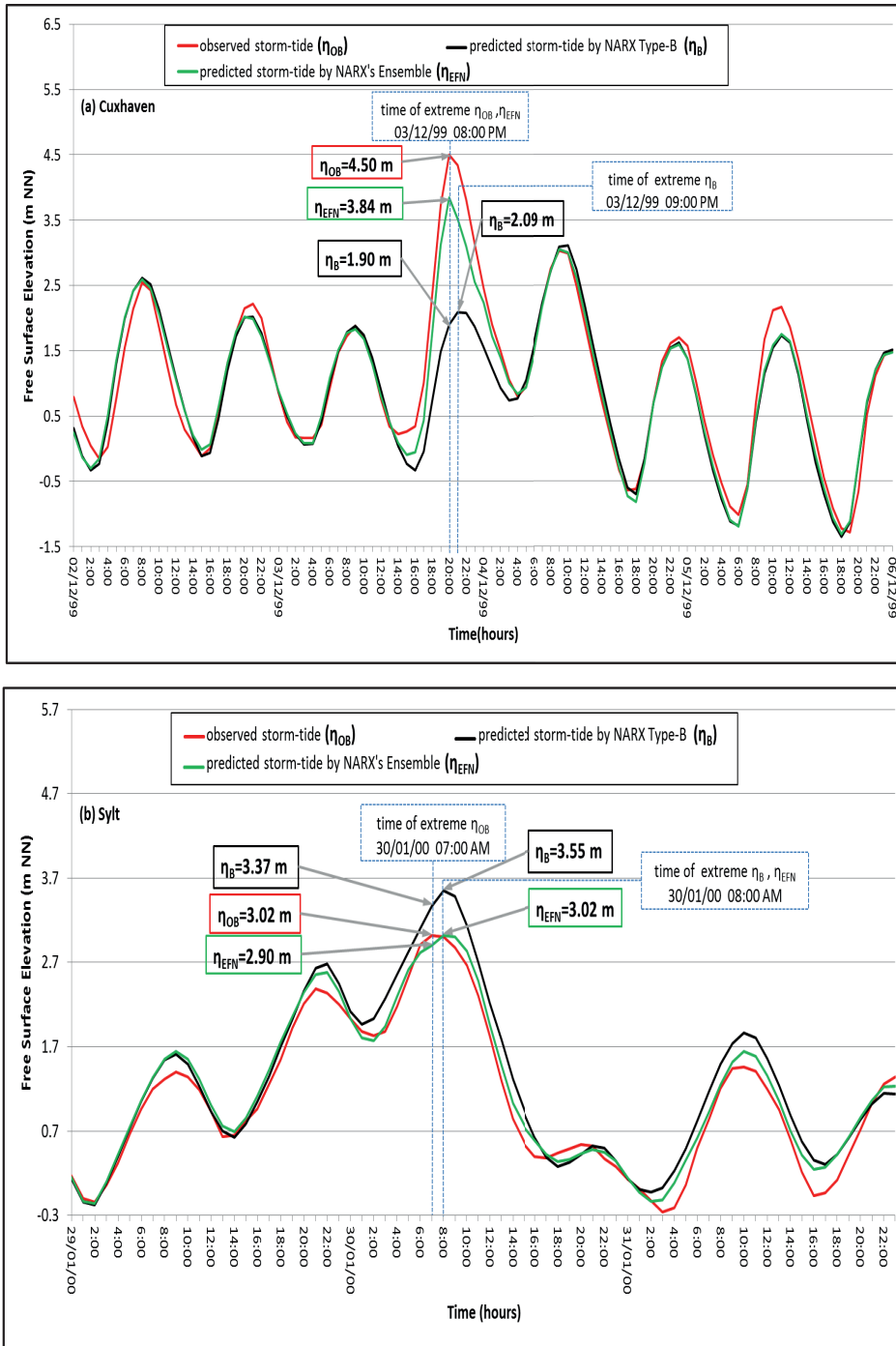


Figure 3: Results of NARX ensemble models and NARX Type-B models at Cuxhaven during the storm of December 1999 (a) and at Sylt during the storms of January 2000 (b).

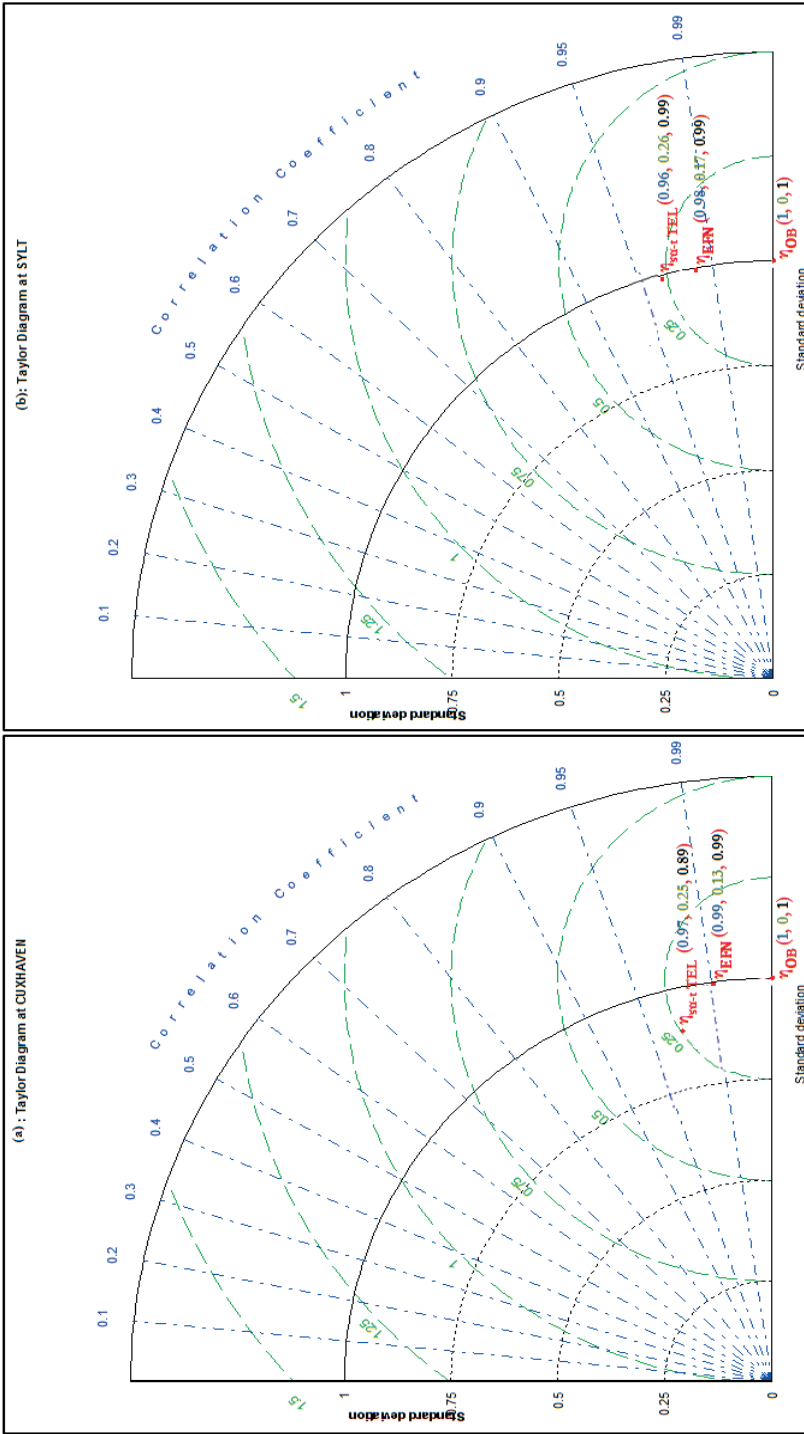


Figure 4: TAYLOR diagrams of the observed storm-tide (η_{OB}), the predicted surge-tide (η_{TEL}) by TELEMAC2D and the predicted storm-tide (η_{FEN}) by NARX Ensemble models at Cuxhaven (a) and Sylt (b) based on the correlation coefficient (\hat{r}), normalized root mean square error (RMSE) and normalized standard deviation ($\hat{\sigma}$).

3.1 Overall approach

A proper prediction based on the complete understanding of the processes underlying the nonlinear interactions may require several decades to be implemented in the current operational hydrodynamic models. Therefore, the data-driven modeling using ANN methodology is used for complementing the nonlinear interaction terms by learning from the observed water levels. Through a combined use of the developed NARX ensemble and a state of the art hydrodynamic model such as “TELEMAC2D”, it is possible to extract the nonlinear interaction between the different extreme surge components as summarized in the following nine steps (Fig. 5):

1. Prescribe the forcing responsible for the generation of all extreme storm-tide components to the North Sea mesh in TELEMAC2D (Fig. 6) as “inputs” along with their boundary conditions (e.g. sea level pressure, meridional and zonal wind speed components represent the forcing factors for storm surge component).
2. Evaluate each component of the extreme storm-tide η_{st-t} (as defined in Fig. 1) independently using the North Sea mesh in TELEMAC2D (Fig. 6). So, the boundary conditions of each component are prescribed separately for the North Sea model area.
3. The components obtained from step 2 are linearly superposed in order to predict the linear surge-tide for Cuxhaven or Sylt (η_L); i.e. the nonlinear interaction between the components is not considered. The linear surge-tide does not include the wave setup effect (η_w), since it has almost no contribution to the observed storm-tide at Cuxhaven and Sylt.
4. Drive the North Sea mesh in TELEMAC2D using the boundary conditions of all components, which are prescribed simultaneously in order to predict the surge-tide ($\eta_{st-t TEL}$).
5. Calculate the difference between $\eta_{st-t TEL}$ predicted in step 4 and η_L predicted in step 3 in order to extract the nonlinear interaction between the components as approximated in TELEMAC2D (η_{NLT}).
6. Calculate the difference between the observed storm-tide (η_{OB}) and the approximated surge-tide by TELEMAC2D ($\eta_{st-t TEL}$), which are assumed to represent the complementary nonlinear interaction (η_{NLE}): so $\eta_{NLE} = \eta_{OB} - \eta_{st-t TEL}$.
7. Train and develop the NARX ensemble models using the η_{NLE} calculated in step 6, which is not considered by TELEMAC2D.
8. Predict the complementary nonlinear interaction η_{NLE} using the developed NARX ensemble models for Cuxhaven and Sylt from 1991 to 2007.
9. Linearly add the approximated nonlinear interaction η_{NLT} by TELEMAC2D of step 5 and its complementary η_{NLE} by NARX ensemble models of step 8 in order to get the total nonlinear interaction (η_{NL}): $\eta_{NL} = \eta_{NLT} + \eta_{NLE}$.

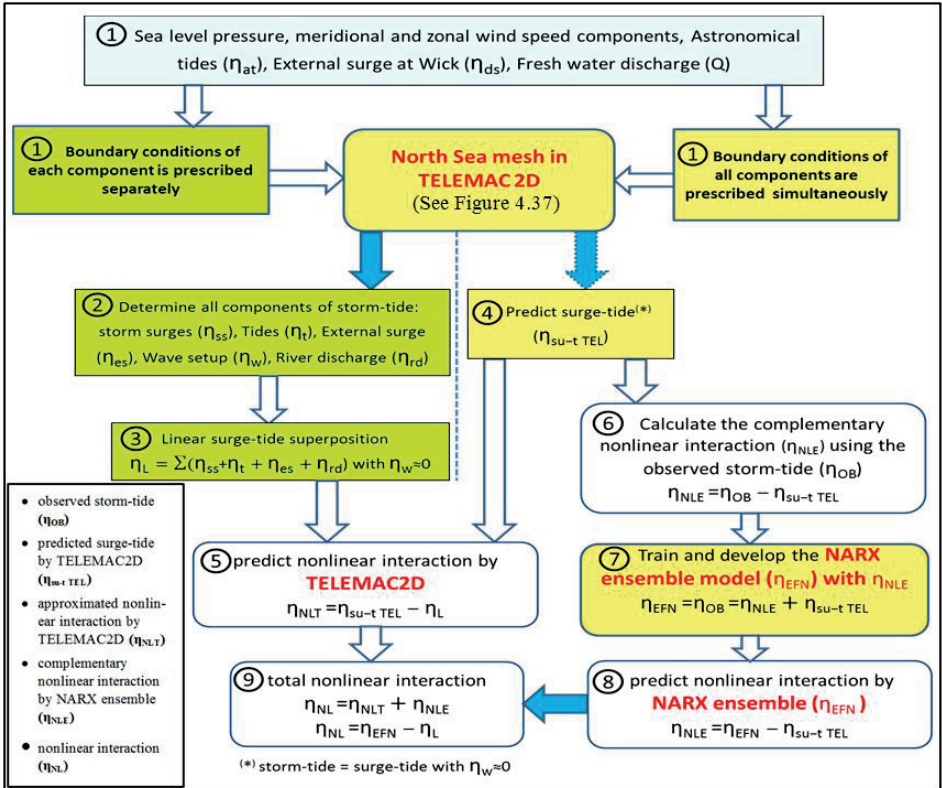


Figure 5: Extraction of the component η_{NL} resulting from the nonlinear interactions between the different extreme surge components for Cuxhaven and Sylt.

3.2 Extraction of the nonlinear interaction approximated by the numerical model in the $\eta_{su-t TEL}$ results (steps 1 to 5 in Fig. 5)

Procedure

For the extraction of the approximated nonlinear interaction effect (η_{NLT}) considered in the predicted surge-tide by TELEMAC2D ($\eta_{su-t TEL}$), the linear superposition of the extreme surge-tide components (η_L) should be subtracted from the $\eta_{su-t TEL}$: $\eta_{NLT} = \eta_{su-t TEL} - \eta_L$. The η_L consists of the linear addition of tide (η_t), storm surge (η_{ss}), external surge (η_{es}) and rivers discharge (η_{rd}) effects, which are simulated independently from each other by TELEMAC2D over the North Sea area (Fig. 6). The effect of wave setup (η_w) on the extreme storm-tide depends on the location of the selected site (inside or outside the surf zone). Both sites are outside of the surf zone and the effect of wave setup on the η_L and $\eta_{su-t TEL}$ can thus be neglected.

For the surge-tide $\eta_{su-t TEL}$ simulations by TELEMAC2D, the boundary conditions of the North Sea hydrodynamic model are prescribed using all of the extreme storm surges components between 1991 and 2007 (TAYEL and OUMERACI 2012). These boundary

conditions are shown in Fig. 6, on the northern open sea boundary (Northern border: Scotland-Norway), the tidal water level on each node and the external surge either from Wick or Lerwick stations are linearly added. On the western boundary (West border: France-England) only the tidal water level is prescribed at each node. So, the influence of the shallow water can be taken into account when the tidal wave plus external surge propagate from the open boundary up to the German coast. On the southern onshore edge of the estuaries the fresh water discharge of the adjacent rivers / estuaries are prescribed at each river section.

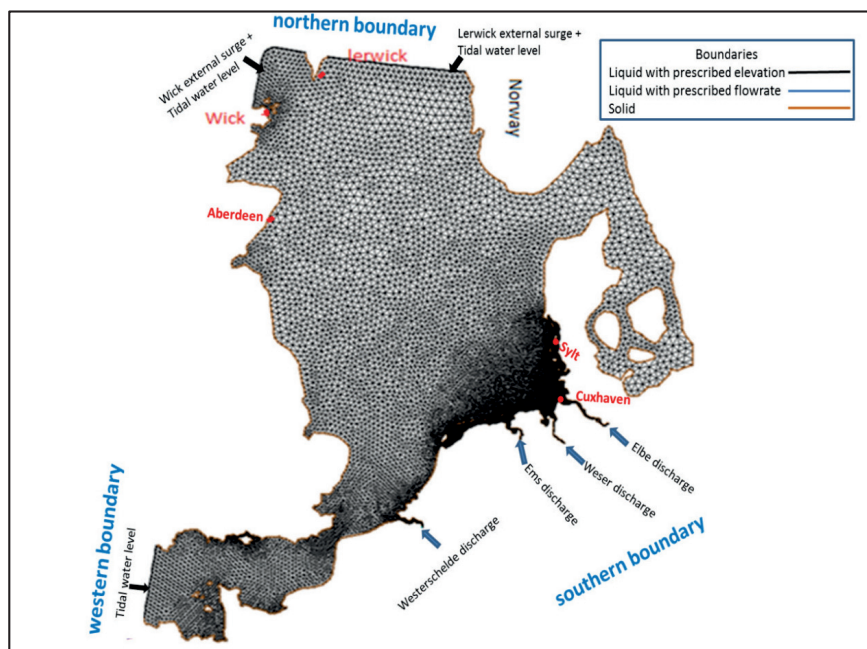


Figure 6: Boundary conditions of the North Sea mesh inside TELEMAC2D with the prescribed water elevation at open-sea and flow rate of southern fresh water discharge.

In the linear superposition surge-tide η_L simulations, the boundary conditions for each component are prescribed separately in order to evaluate its effect during storms. For example, only the tidal water level on each node of the Northern and West borders are prescribed for evaluating the tidal effect, while the meteorological forces only drive the model for evaluating the storm surge effect without prescribing any of the open-sea or river discharge boundary conditions.

Results

During the storms of January 2000, November 2006 and November 2007, the temporal variations of the predicted linear superposition η_L with the contribution of each component at Cuxhaven and Sylt are predicted. At the times of the observed extreme water level η_{OB} ($(\eta_{OB})_{max}$) during these three storms, the highest η_L peaks at Cuxhaven reach 3.22 m, 3.17 m and 3.31 m for the storms in January 2000, November 2006 and Novem-

ber 2007, respectively, which are higher than their counterparts at Sylt of 2.52 m, 1.96 m and 2.44 m, respectively. Since the contribution of storm surge (η_{ss}) and tide (η_t) at Sylt are lower than those at Cuxhaven due to the difference in geographical locations of the two sites. The storm surge, tide and external surge components have the largest contribution to the η_L at both sites, while the effect of rivers discharge and wave setup are almost negligible. Fig. 7 shows the contribution of each extreme storm-tide component during the storm of January 2000 at Cuxhaven and Sylt. The highest contribution is from storm surge effect with maximum of 3.00 m and 2.28 m at Cuxhaven and Sylt, respectively. The tide effect is less than the storm surge at the time of $(\eta_{OB})_{\max}$ in both sites; it reaches 1.00 m and 0.56 m at Cuxhaven and Sylt, respectively. Only during the storm of January 2000, the external surge has positive effect on η_L in Cuxhaven and Sylt at the times of $(\eta_{OB})_{\max}$ by 0.34 m and 0.26 m, respectively. In contrast during the storms of November 2006 and 2007 in both sites, the external surge has negative effect on η_L ranging from -0.05 m to -0.13 m at the times of $(\eta_{OB})_{\max}$.

For Cuxhaven and Sylt during the storms of January 2000, November 2006 and November 2007, the heights of η_L peaks overestimate always the $\eta_{st-t TEL}$ peaks that include the nonlinear interaction η_{NLT} approximated by the numerical model TELEMAC2D. At the times of $(\eta_{OB})_{\max}$ during these three storms, the predicted $\eta_{st-t TEL}$ reach 3.04 m, 2.97 m and 3.19 m respectively at Cuxhaven, which are lower than the predicted η_L of 3.22 m, 3.17 m and 3.31 m, respectively for the storms in January 2000, November 2006 and November 2007.

Fig. 8 shows the temporal variations of the predicted linear superposition η_L and surge-tide $\eta_{st-t TEL}$ by TELEMAC2D in addition to the approximated nonlinear interaction (η_{NLT}) at Cuxhaven and Sylt during the storm of January 2000. The extreme linearly predicted water level η_L ($(\eta_L)_{\max}$) and the extreme predicted surge-tide $\eta_{st-t TEL}$ ($(\eta_{st-t TEL})_{\max}$) at Cuxhaven reach 3.37 m and 3.24 m respectively, while they were 3.28 m and 3.04 m at Sylt respectively. At both sites, the occurrence times of $(\eta_L)_{\max}$ and $(\eta_{st-t TEL})_{\max}$ during this storm are exactly the same. Moreover, the $(\eta_{st-t TEL})_{\max}$ at Sylt during the storms of January 2000 and November 2006 occur before the $(\eta_{OB})_{\max}$ by 9 hours. Since the highest storm surge peak at Sylt during these storms are synchronized approximately with high tide (see Fig. 7(b)). Moreover, the maximum positive external surge of 0.5m (Fig. 7(b)) at Sylt occurred at the time of storm surge peak during the storm of January 2000.

3.3 Extraction of the complementary terms for the nonlinear interaction using the predicted η_{EFN} results (steps 6 to 8 in Fig. 5)

Procedure

The predicted storm-tide by NARX ensemble (η_{EFN}) includes the complementary terms (η_{NLE}) for the approximated nonlinear interaction by TELEMAC2D (η_{NLT}). The complementary terms (η_{NLE}) are basically the linear addition of

- (i). Difference between the predicted storm-tide by NARX Type-B model (η_B) and the predicted surge-tide by TELEMAC2D ($\eta_{st-t TEL}$).

- (ii). Difference between the predicted storm-tide by NARX ensemble (η_{EFN}) and the predicted storm-tide by NARX Type-B model (η_B).

So, the predicted η_{NLE} is obtained by direct subtraction of the predicted $\eta_{sm-t TEL}$ from η_{EFN} (i.e. $\eta_{NLE} = \eta_{EFN} - \eta_{sm-t TEL}$). Since the developed NARX ensemble is trained based on the observed water level (η_{OB}), so the predicted storm-tide by η_{EFN} and η_{OB} are considered as equivalent (see step 7 in Fig. 5).

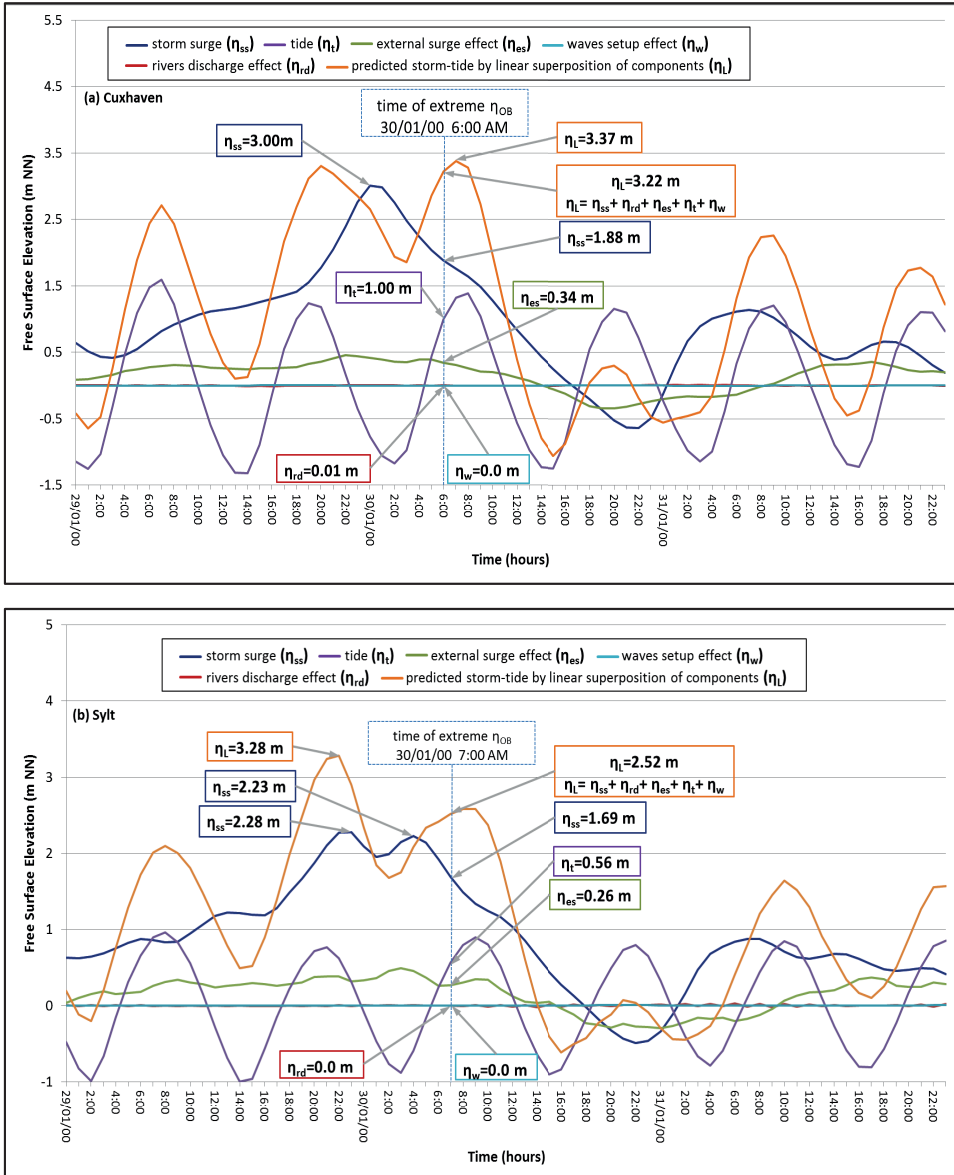


Figure 7: Storm-tide prediction by linear superposition η_L and contribution of each extreme storm-tide component during the storm of January 2000 at Cuxhaven (a) and Sylt (b).

Results

The temporal variations of η_{EFN} with the complementary terms (η_{NLE}) at Cuxhaven and Sylt are predicted for the storms of January 2000, November 2006 and November 2007. The η_{EFN} peaks, which occur directly before the times of $(\eta_{OB})_{\max}$ at both sites, are always overestimated by the predicted $\eta_{sw-l TEL}$ peaks and η_L peaks. This is due to the strong reduction of η_{EFN} peaks by η_{NLE} and η_{NLT} . At Cuxhaven during these three storms, the effect of η_{NLE} causes a reduction of the η_L peaks, which occurs directly before the times of $(\eta_{OB})_{\max}$, by -0.12 m, -0.36 m and -0.14 m in addition to the reduction of η_{NLT} by -0.34 m, -0.18 m and -0.34 m respectively for the storms of January 2000, November 2006 and November 2007. In contrast, at the times of $(\eta_{OB})_{\max}$ in Cuxhaven and Sylt, The η_{NLE} results in the overestimation or underestimation of the η_{EFN} peaks when compared with the $\eta_{sw-l TEL}$ and η_L peaks according to the following two conditions:

- (i). If the η_L and $\eta_{sw-l TEL}$ peaks, which occur directly before the time of extreme η_{EFN} ($(\eta_{EFN})_{\max}$), are < 3.00 m and < 2.50 m respectively, then their following peaks would overestimate the peak of η_{EFN} at the time of $(\eta_{EFN})_{\max}$. Since the peaks of η_{EFN} , η_L and $\eta_{sw-l TEL}$, which occur before the times of peak $(\eta_{EFN})_{\max}$, do not increase the mean water level (MWL) during the storm significantly. Therefore, the following peaks of η_{EFN} , η_L and $\eta_{sw-l TEL}$ will propagate under a pronounced shoaling effect that increase their heights simultaneously. For example, the η_{NLE} decreases $(\eta_{sw-l TEL})_{\max}$ by -0.08 m and -0.11 m respectively during the storms of November 2006 (see Fig. 8(d)) and November 2007 at Sylt. Moreover, the η_{NLT} causes a decrease of $(\eta_L)_{\max}$ by -0.04 m and -0.14 m respectively, which is added to the η_{NLE} decrease and support it.
- (ii). If the η_L and $\eta_{sw-l TEL}$ peaks, which occur directly before the time of $(\eta_{EFN})_{\max}$, are ≥ 3.00 m and ≥ 2.50 m respectively, then their following peaks would underestimate the peak of η_{EFN} at the time of $(\eta_{EFN})_{\max}$. Since only the peaks of η_L and $\eta_{sw-l TEL}$, which occur before the times of $(\eta_{EFN})_{\max}$, increase the MWL during the storm to a limit by which their following peaks will propagate under no shoaling effect. Therefore, the following peaks of η_L and $\eta_{sw-l TEL}$ will propagate in deeper water with less pronounced shoaling, which decrease their heights simultaneously. In contrast, the peak of η_{EFN} propagates under strong shoaling effect that increases its height, as their counterparts in condition (i). For example, during the storms of January 2000 (Fig. 8(a)), November 2006 (Fig. 8(c)) and November 2007 at Cuxhaven, the η_{NLE} increases $(\eta_{sw-l TEL})_{\max}$ by 0.53 m, 0.21 m and 0.29 m respectively. However, the η_{NLT} decreases $(\eta_L)_{\max}$ by -0.14 m, -0.20 m and -0.12 m respectively for the storms of January 2000, November 2006 and November 2007.

During these three storms, the times of $(\eta_L)_{\max}$ and $(\eta_{sw-l TEL})_{\max}$ are shifted with the same amount of time from the time of $(\eta_{OB})_{\max}$ at both site. Therefore, only the complementary nonlinear terms η_{NLE} can be considered as the main factor to shift the times of $(\eta_{EFN})_{\max}$. During the storm of November 2006 at Sylt (see Fig. 8(d)), the times of η_L and $\eta_{sw-l TEL}$ peaks occurred two hours before the time of $(\eta_{OB})_{\max}$ and $(\eta_{EFN})_{\max}$.

3.4 Nonlinear interaction between all storm-tide components (step 9 in Figure 5)

Procedure

Since the predicted storm-tide by η_{EFN} and η_{OB} are considered as equivalent (see step 7 in Fig. 5), the nonlinear interaction between all storm-tide components at Cuxhaven and Sylt (η_{NL}) is the difference between the predicted storm-tide by NARX ensemble (η_{EFN}) and the linear storm-tide (η_L): ($\eta_{NL} = \eta_{EFN} - \eta_L$). So, the η_{NL} obtained in step 9 in Fig. 5 can be considered as equivalent to the linear superposition of the nonlinear interaction η_{NLT} approximated in step 5 by TELEMAC2D and the complementary nonlinear terms η_{NLE} predicted by NARX ensemble (EFN) trained in step 7 by the results of step 6: $\eta_{NL} = \eta_{NLT} + \eta_{NLE}$.

Results

At Cuxhaven during the storms of January 2000, November 2006 and November 2007, the inclusion of the total nonlinear interaction η_{NL} in the predicted η_{EFN} leads to overestimate the result $(\eta_L)_{\max}$ obtained from linear superposition in Step 3 by 0.39 m, 0.01 m and 0.17 m respectively. Moreover, the time of arrival for $(\eta_{EFN})_{\max}$ during the storm of November 2006 at Cuxhaven is delayed by one hour (Fig. 8(c)). Since the increase effect by η_{NLE} , which is mainly from the storm-tide wave shoaling, results in the slowing down and increasing height of $(\eta_{EFN})_{\max}$. In contrast, at Sylt during the storms of November 2006 (Fig. 8(d)) and November 2007, the inclusion of the η_{NL} in the predicted η_{EFN} leads to underestimate the $(\eta_L)_{\max}$ by -0.12 m and -0.25 m respectively, since the reduction induced by η_{NLE} is supported by the reduction of η_{NLT} .

The proposed hybrid approach is applied in Fig. 9 to analyze comparatively the extreme effect of nonlinear interaction by all extreme storm-tide components during the period between 1991 and 2007. The results in Fig. 9 a and b for Cuxhaven and Sylt, respectively, are summarized in the following three stages:

Stage 1- Predict the highest possible storm-tide from 1991 to 2007 ($(\eta_{EFN})_{\max}$) (steps 1 to 9 in Fig. 5), which occurs at time t_{\max} , using the developed NARX ensemble model. This also includes the nonlinear interaction component η_{NL} at time t_{\max} (step 9 Fig. 5).

Stage 2- Evaluate the effect of each extreme storm-tide component depicted in Fig. 1 and their nonlinear interaction on $(\eta_{EFN})_{\max}$ at time t_{\max} as follows:

- 2.1. Using TELEMAC2D (steps 1 and 2 in Fig. 5), predict each storm-tide component independently at time t_{\max} (occurrence time of the peak $(\eta_{EFN})_{\max}$ predicted in Stage 1).
- 2.2. Apply the proposed hybrid approach in Fig. 5 to evaluate the effect of nonlinear interaction (η_{NL}) between the components predicted in sub-stage 2.1 at time t_{\max} (steps 3 to 9 in Fig. 5).

Stage 3- Evaluate the highest physical limit of storm-tide from 1991 to 2007 as follows:

- 3.1. Evaluate each storm-tide component independently, which occurred over the entire period from 1991 to 2007 using TELEMAC2D (steps 1 and 2 in Fig. 5). The coupling between TELEMAC2D and TOMAWAC is used to predict the wave setup component for years 2000, 2006 and 2007 only.
- 3.2. Apply the proposed hybrid approach in Fig. 5 to predict the nonlinear interaction (η_{NL}) between the components obtained from sub-stage 3.1, which occurred over the entire period from 1991 to 2007.
- 3.3. Extract the highest peak of each storm-tide component evaluated in sub-stage 3.1 and the highest peak of their nonlinear interaction ($(\eta_{NL})_{\max}$) predicted in sub-stage 3.2, independently of their occurrence in time over the entire period 1991-2007; i.e. the extracted peaks do not necessarily occur at the same time.
- 3.4. Superpose linearly the extracted highest peaks from sub-stage 3.3 ($(\eta_{all})_{\max}$) which might be considered to represent the highest physical limit of extreme storm-tide over the entire considered time period, though it is very improbable that the peaks of superposed storm-tide constituents will occur at the same times.

The linear superposition ($(\eta_{all})_{\max}$) is always higher than the highest possible storm-tide ($(\eta_{EFN})_{\max}$) (see Fig. 9) at both sites over the entire time period 1991-2007. Since the maximum of each component and nonlinear interaction occur independently at different times. The $(\eta_{all})_{\max}$ and $(\eta_{EFN})_{\max}$ at Cuxhaven, which are respectively 7.21 m and 4.00 m, are higher than their respective counterparts at Sylt of 5.66 m and 3.2 m. However, the percentages of $(\eta_{NL})_{\max}$ and external surges maximum ($(\eta_{es})_{\max}$) at Cuxhaven, which are respectively 21 % and 9.5 %, are lower than their respective counterparts at Sylt of 25.80 % and 10.97 %. Since the storm surges and tide at Cuxhaven are higher than their counterparts at Sylt, which leads to deeper water depth at Cuxhaven with less pronounced shoaling effect. Furthermore, the effect of nonlinear interaction η_{NL} on $(\eta_{EFN})_{\max}$ at Cuxhaven results in a reduction of water level by 4 %. In contrast, the η_{NL} at Sylt results in increase of water level by 18.6 %.

Fig. 9 shows that the relative contribution of wave setup ($(\eta_w)_{\max}$) is negligibly small with maximum values up to 1.2 % at both pilot sites. Moreover, the contribution of river discharge maximum ($(\eta_{rd})_{\max}$) at Sylt and Cuxhaven is not more than 1 % and also without any noticeable effect.

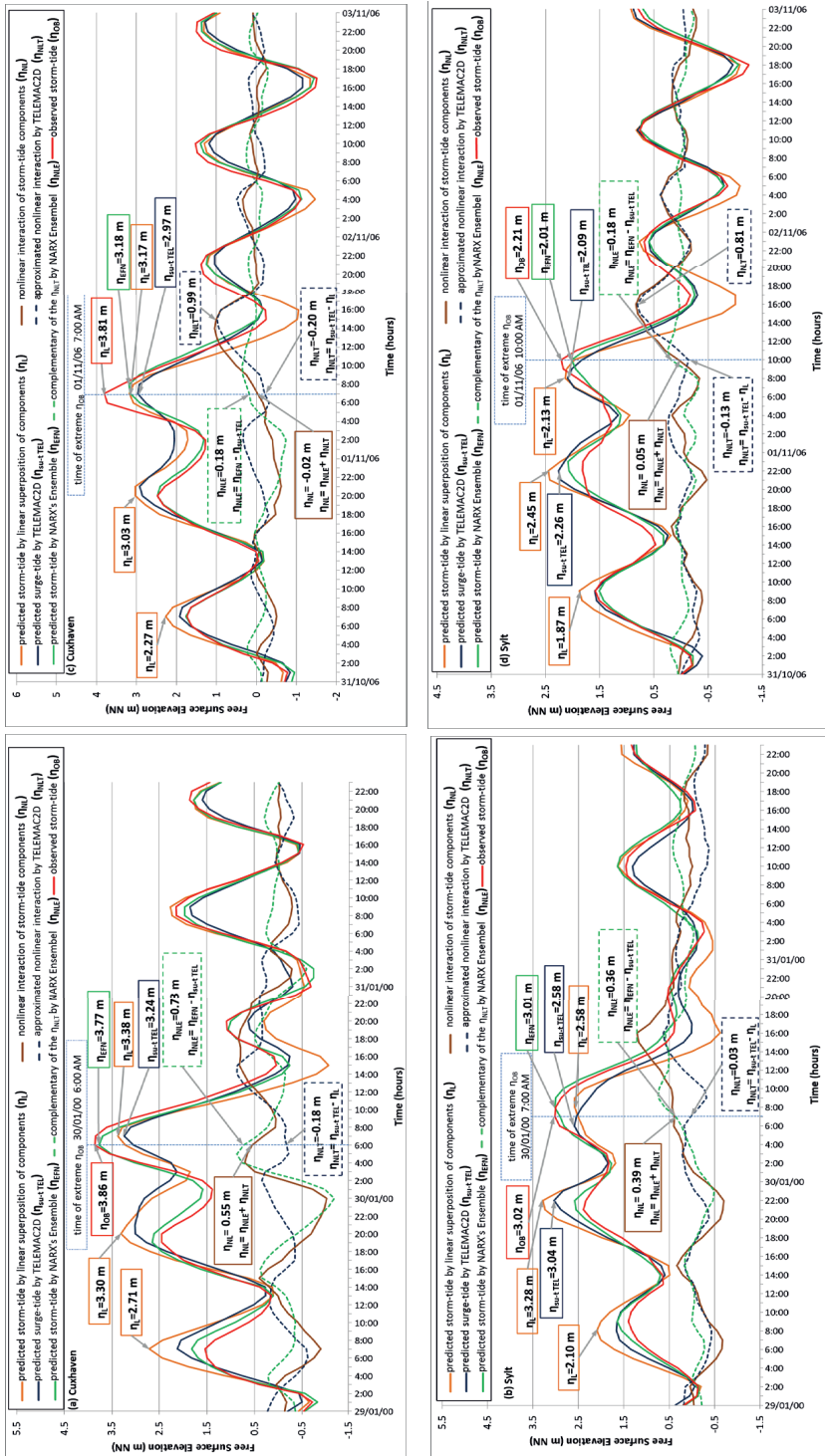


Figure 8: Storm-tide prediction by linear superposition η_{L} , TELEMAC2D $\eta_{TELMAC2D}$, and NARX ensemble η_{NARX} with the effect of nonlinear interaction η_{NL} between extreme storm-tide components during the storm of January 2000 and November 2006 at Cuxhaven (a and c respectively) and Sylt (b and d respectively).

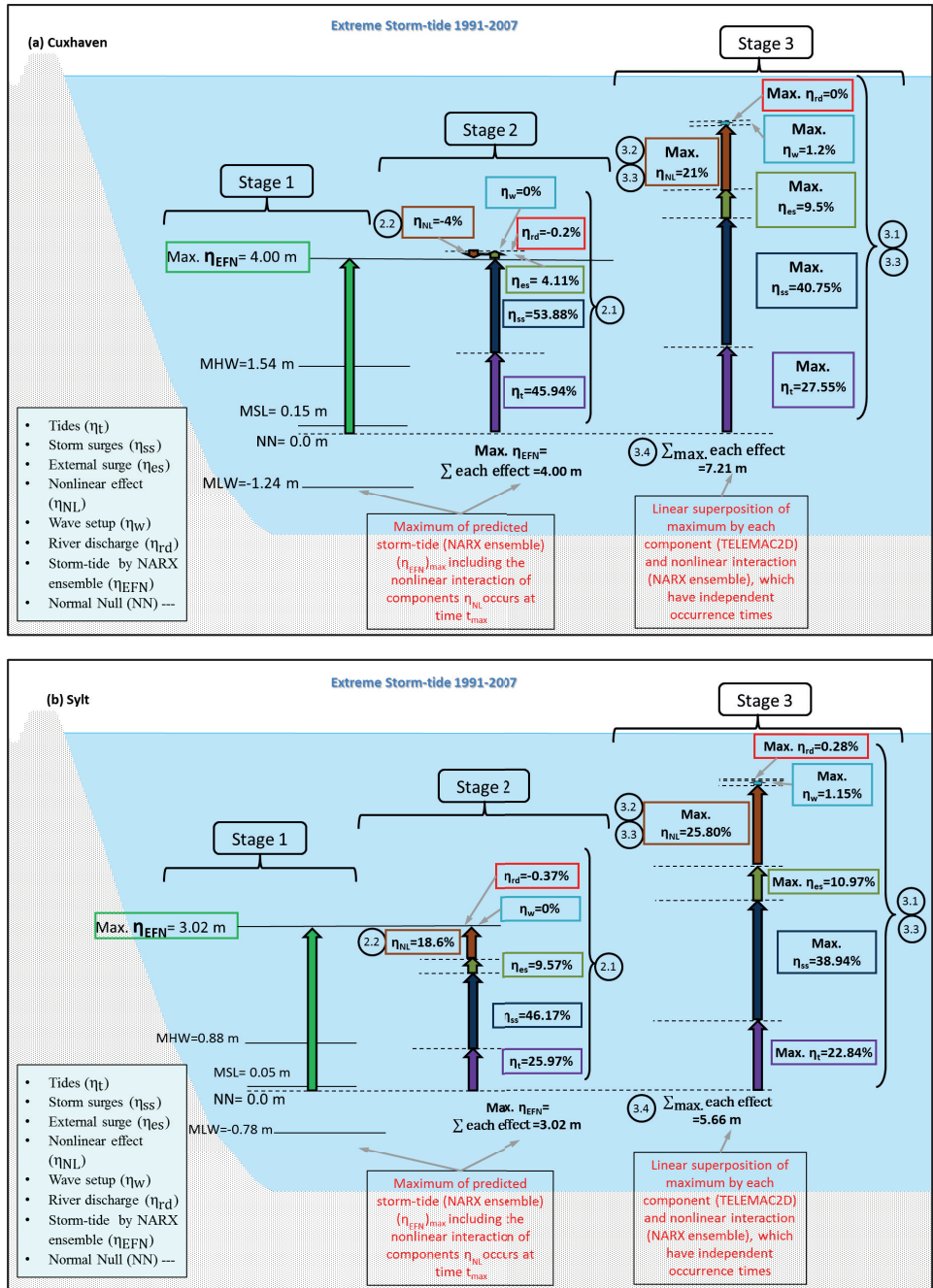


Figure 9: Maximum combination of the constituents in Fig. 1 along with the nonlinear interaction between them (η_{NL}) and the predicted storm-tide by NARX ensemble (η_{EFN}) at Cuxhaven (a) and Sylt (b) during the period from 1991 to 2007.

4 Concluding remarks

Combining the strengths of ANN methodology with those of numerical modelling (TELEMAC2D and TOMAWAC) provides a powerful and computationally efficient operational model system for storm-tide prediction as exemplarily shown in Cuxhaven and Sylt. It can also be applied for reconstructing the missing data using sequential time series predictions by NARX ensemble, which reduces the amount of training data (usually five years show very good performance). Another advantage of the hybrid model system is its capability to account for nonlinear interaction between the extreme storm-tide constituents, so the substantial errors in both magnitude and timing of the results predicted by numerical modelling can be corrected. Two types of NARX models and their ensemble were developed and validated using the observed water level between 1999 and 2007 at Cuxhaven and Sylt. For Cuxhaven's NARX ensemble model, the lowest RMSE is 0.148 m with a correlation of 0.99. The NARX ensemble model in Sylt has an RMSE of 0.123 m and a correlation of 0.98.

The account for nonlinear interaction by NARX ensemble models may result either in the reduction or increase of the highest water level during storms when compared with the linear superposition of extreme storm-tide components according to the following two situations at both locations (Cuxhaven and Sylt):

- (i). If the η_L peak resulting from linear superposition, which occurs directly before the time of $(\eta_{EFN})_{\max}$ resulting from the NARX ensemble model, is less than 3 m, then its following peak would overestimate the peak of η_{EFN} at the time of $(\eta_{EFN})_{\max}$. Since the peaks of η_{EFN} and η_L , which occur before the time of $(\eta_{EFN})_{\max}$, do not increase significantly the mean water level (MWL) during the storm. Therefore, the following peaks of η_{EFN} and η_L will propagate under more pronounced shoaling effect that increases their heights simultaneously.
- (ii). If the η_L peak, which occurs directly before the time of $(\eta_{EFN})_{\max}$, is larger than 3.00 m, then its following peak would underestimate the peak of η_{EFN} at the time of $(\eta_{EFN})_{\max}$. Since only the peak of η_L , which occurs before the time of $(\eta_{EFN})_{\max}$, increases the MWL during the storm to a limit by which its following peak will propagate under less pronounced shoaling effect.

The highest peak of each constituents predicted series by TELEMAC2D and the nonlinear interaction (η_{NL}) predicted by the NARX ensemble over the entire time period 1991-2007 at Cuxhaven and Sylt are added together linearly ($(\eta_{all})_{\max}$). The result is assumed to represent the highest physical limit of extreme storm-tide over the entire considered time period, though it is very improbable that the peaks of superposed storm-tide constituents will occur at the same times. The peak obtained through linear superposition ($(\eta_{all})_{\max}$) at Cuxhaven, which reaches 7.21 m, is higher than its counterpart at Sylt of 5.66 m. The maximum effect of the nonlinear interaction (η_{NL})_{max} at Cuxhaven, which reaches 21 %, is lower than its counterpart of 25.80 % at Sylt. Since the storm surges and tide at Cuxhaven are higher than their counterparts at Sylt, thus resulting in higher water level with less pronounced shoaling effect.

The still ongoing PhD work is now focusing on the determination of the worst extreme water levels, which are physically possible in the 21st century under the projected climatic change for the North Sea area. Moreover, since long-term water level observations at Sylt may be not available in the past, it is valuable and cost effective for a coastal engineering study to establish the nonlinear relationship in order to predict the water levels at Sylt using the available water levels at Cuxhaven.

5 Acknowledgement

Financial support provided for the first author by German Academic Exchange Service (DAAD) for pursuing the doctoral studies in the frame of the GERLS 2009/2010 programme (German Egyptian Research Long-term Scholarship) is gratefully acknowledged. Furthermore, the Federal Ministry for Education and Research (BMBF) is acknowledged for funding the project XtremRisK (grant number 03F0483A) led by the co-author. Thanks to Prof. Jensen from Research Institute for Water and Environment-University of Siegen, Dr. Gönnert from Agency of Roads, Bridges and Waters, Dr. Plüß from the Federal Waterways Engineering and Research Institute (BAW) and Dr. Weisse/Dr. Meyer from Helmholtz-Zentrum Geesthacht (HZG) in Hamburg for sharing their data and all their support, especially at the beginning of the PhD study.

6 References

- BENOIT, M.: Logiciel TOMAWAC de modélisation des états de mer en éléments finis. Notice de la version 5.2, Rapport HP-75/02/065/A, EDF-LNHE., 2003.
- BENOIT, M.; MARCOS, F. and BECQ, F.: development of a third generation shallow-water wave model with unstructured spatial meshing, *Coast. Eng. Proc.*, 1(25), doi:10.9753/icce.v25., 2001.
- GOENNERT, G. and GERKENSMEIER, B.: a new method of approaching extreme storm events for design level or risk analysis, *Coast. Eng. Proc.*, 1(33), management. 2, 2012.
- HERVOUET, J.-M.: *Hydrodynamics of Free Surface Flows: Modelling with the Finite Element Method*, John Wiley & Sons., 2007.
- HERVOUET, J.-M. and VAN HAREN, E.: *TELEMAC-2D Principle Note*. Electricité de France, Technical Report., 1994.
- NILSSON, C.; BÄRRING, L. and GOYETTE, S.: Relating Forest Damage Data to the Wind Field from High Resolution RCM Simulations: Case study of Anatol Passing Sweden in December 1999, in *Geophysical Research Abstracts*, vol. 7, p. 09883., 2005.
- OUMERACI, H.: *Storm Surge and design water levels (lecture notes in German)*, 2009.
- OUMERACI, H.; JENSEN, J.; GÖNNERT, G.; PASCHE, E.; KORTENHAUS, A.; NAULIN, M.; WAHL, T.; THUMM, S.; UJEYL, G. and GERSHOVICH, I.: Flood risk analysis for a megacity: The German XtremRisK project, in *Proc. Conference on Road Map towards a Flood Resilient Urban Environment*, p. 8., 2009.
- VON STORCH, H.; LANGENBERG, H. and FESER, F.: A spectral nudging technique for dynamical downscaling purposes. *Mon. Weather Rev.*, 128(10), 2000.
- TAYEL, M.: *Combined Neural Network and Numerical Model for Extreme Storm Surges*, PhD thesis TU-Braunschweig, Germany, 2015 (in preparation).

- TAYEL, M. and OUMERACI, H.: Meteorological data preparation from 1970 to 2007 and configuration of the North Sea TELEMAC2D model. Leichtweiß Inst. Hydraul. Eng. Water Resources Braunschweig. Germany, Internal report (Nr. 3), 90, 2012.
- TAYEL, M. and OUMERACI, H.: A hybrid approach using hydrodynamic modelling and artificial neural networks for extreme storm surge prediction, Submitt. J. Coast. Eng. Jpn., (XtremRisK Special Issue), 32, 2014.
- TAYLOR, K.E.: Summarizing multiple aspects of model performance in a single diagram, J. Geophys. Res., 106(D7), 7183–7192, doi:10.1029/2000JD900719, 2001.
- WAHL, T.; MUDERSBACH, C. and JENSEN, J.: Statistical assessment of storm surge scenarios within integrated risk analyses4results of the XtremRisK project, Compr. Flood Risk Manag. Res. Policy Pract., 22, 2012.

Hydrodynamic Numerical Models Suitable for Application to the German Fairways and Ports at the Baltic Sea Coast

Guntram Seiß

Summary

Since the early 1990s there has been a growing demand for fairways to the ports along the German Baltic Sea coast to be adapted for modern types of vessels. Practical planning by fairway management authorities is also influenced by a growing and broadly shared understanding of climate change.

This has resulted in new assessment requirements during planning processes and the consultations of the Federal fairway management authorities. It was necessary to adapt modelling tools to fit them to deal with issues concerning the Baltic Sea coast. The highly baroclinic nature of the system required inclusion of thermic processes. Long-term modelling requires faster models and the limited staff of the institute required a flexible, efficient modelling toolbox.

In parallel to the development of a modelling framework for the Baltic Sea coast, issues relating to the entrance of the Peenestrom, the ports of Wismar and Rostock and the Schlei estuary also needed to be addressed. Further insights on the reaction of inner coastal waters to changes in sea level were also tackled in the context of the KLIWAS project. Some of these project highlights are presented here.

Keywords

Baltic Sea, port entry, toolbox, numerical models, climate change, fairway, adaption

Zusammenfassung

Seit den frühen 1990er-Jahren besteht ein wachsender Bedarf der Anpassung der Häfen der Deutschen Ostseeküste an moderne Schiffstypen. Die neuen Erkenntnisse der Gesellschaft über den Klimawandel beeinflussen ebenfalls die praktische Planung der Wasserstraßenverwaltung.

Diese Entwicklungen führten zu neuen Anforderungen in der Begutachtung während der Planungsprozesse und der Beratung der Wasserstraßenbehörden des Bundes. Die Werkzeuge zur Modellierung mussten angepasst werden, um die Fragen betreffend die Ostseeküste abdecken zu können. Die stark barokline Natur des Systems machte es erforderlich, thermische Prozesse zu berücksichtigen. Modellierung über lange Zeiträume erfordert schnellere Modelle und die begrenzte Zahl der Mitarbeiter einen flexiblen, effizienten Modellbaukasten.

Parallel zur Entwicklung des Baukastens für die Ostseeküste mussten Fragen an den Zufahrten zum Peenestrom, der Schlei und der Häfen von Wismar und Rostock beantwortet werden. Innerhalb des Projektes KLIWAS wurden weitere Erkenntnisse zur Reaktion der inneren Küstengewässer auf einen Anstieg des Meeresspiegels erarbeitet. Von diesen Projekten werden hier Schlaglichter präsentiert.

Schlagwörter

Ostsee, Hafenzufahrt, Werkzeugkasten, numerische Modelle, Klimawandel, Fahrwasser, Anpassung

Contents

1	Introduction.....	344
2	Challenges.....	344
3	Model description	345
4	History of the Baltic Sea modelling kit.....	349
5	Further applications.....	350
6	Conclusion.....	350
7	References	352

1 Introduction

Since the early 1990s there has been increasing demand for the modernisation and adaption of the waterway infrastructure of the new federal states of Germany in the eastern part of the country which joined the Federal Republic of Germany following reunion with the territories of the former German Democratic Republic. The depth of fairways has required alteration as the size of vessels built in the shipyards of Wolgast and Wismar has grown. The draft and width of ship units which will enter the ports of Rostock and Wismar in the future will also require further adaption of fairways.

The inner coastal waters are valuable natural habitats and recreational regions. The increasing availability of public information has sharpened the general public's awareness of environmental issues. Conflicts between growing volumes of commercial traffic and other competing interests are consequently becoming more and more apparent and need to be solved in a constructive manner in the planning phase.

The need to find acceptable solutions to environmental conflicts results in new assessment requirements and consequently the decision to develop a modelling framework for the Baltic Sea with a focus on the German coast.

2 Challenges

The fairways planning process needs to address several types of issues. The most important of these with regard to the Baltic Sea coast are:

- Changes in local mean sea level and its variability
- Changes in local salinity and temperature
- Spreading of dumped substances
- Changes in wave characteristics and wave induced stresses

Even if there is not always a benefit in precisely reproducing the physical system in order to answer the issues which arise during an approval procedure, any opponents of a traffic measure will negate the credibility of model results if the accuracy of the modelling systems used clearly fail to provide a natural view of their area of interest.

High modelling standards for the approval of traffic planning in Germany include the following topics:

- Small-scale bathymetric structures, such as fairways or islands, must be geometrically approximated sufficiently well enough in the area of interest.
- The seaward open model boundary should be kept as far away as possible to avoid the influence of model reactions on bathymetry changes reaching that boundary.
- The dynamics driven by temperature, salinity and sediments must be included.

The dynamics of the Baltic Sea are characterised by long-term circulation, driven by wind and density changes. A permanent halocline is present in the deeper basins of the Baltic. Singular events, such as storm surges and salt water inflows from the North Sea, are added to this basic state. In the winter, cooling causes strong convection and leads to a partial ice cover. In the summer, heating leads to a sharp thermocline. All these processes have a strong influence on spatial and time resolution and model calibration.

3 Model description

In order to fulfil all the requirements required for the approval processes we chose to develop a modelling framework for the Baltic Sea (SEIB 2012, RAHLF and SEIB 2012). The framework is a modular system containing the following components, which are independently variable:

- Numerical solver software
- Pre-processing tools
- Post-processing and presentation tools
- Model grids
- High resolution digital bathymetry models
- Boundary forcing data
- Calibration data

Only the model grids and boundary forcing data depend on the numerical solver software used. Basic datasets, such as digital bathymetries, gauge data for validation or geographic information used to illustrate result pictures, are provided in a central place. These datasets can be used by any model. Pre- and post- processing software tools are provided by the BAW modelling group (BAW 1996-2014).

The model grids are derived from a basic grid which covers the whole Baltic Sea with an open boundary at the Skagerrak. Spatial resolution becomes more detailed from the inner Baltic Sea to the coastline. For the regions of interest, the basic grid is substituted with an inlay grid which is suitable for resolving the details of the bathymetry subject for a specific issue (Fig. 1). High resolution inlay grids are part of the framework database and currently exist for the Warnow mouth, the Kiel Fjord and the Schlei Fjord. They can also be run as standalone models with a limited area of application, e.g. fast prediction of accurate water levels or currents.

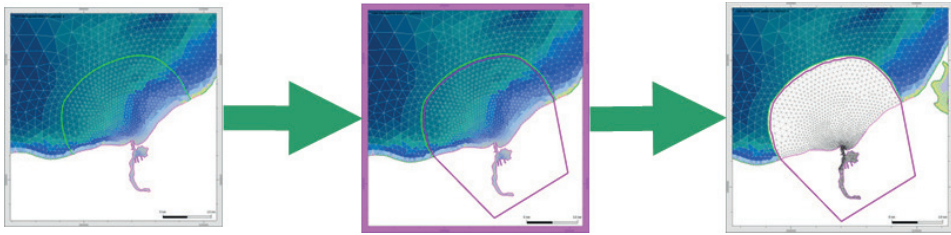


Figure 1: Principle of generation of a regionally refined grid by substitution of an area by an inlay grid.

In our institute we usually apply the UNTRIM model code as the numerical solver of the hydrodynamic equations (CASULLI und WALTERS 2000) (CASULLI und ZANOLLI 2002).

Atmospheric boundary data were originally provided by the German Weather Forecast system and were pre-processed to fit the input format of the modelling software. Data from 01/2005 to 11/2012 are currently available for use. In this case, the model software must be adapted to the common data format NetCDF (UNIDATA PROGRAM CENTER).

Gauge data from Smögen, a village approximately 120 km north to northwest of Gothenburg, can be used for steering of the sea level at the open boundary if a time shift of 30 minutes is applied to the time series (Fig. 2).

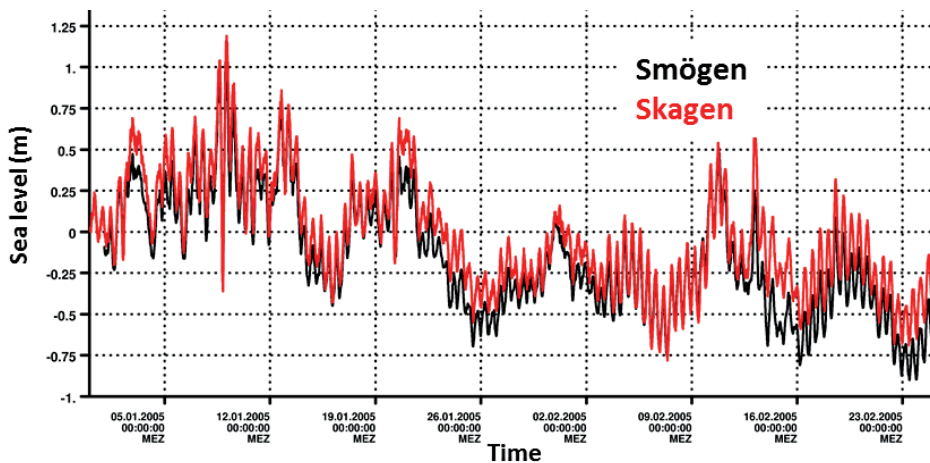


Figure 2: Typical time series at the open boundary.

This approximation is good enough to reproduce the tidal signal and the long-term development of the mean sea level in the interior. These data are available for the period 2001 to 2012. Precompiled boundary data are already available for several years. The boundary conditions can be reconstructed for previous years using the long-term signal of the gauge of Gothenburg and the tidal harmonics of Smögen or by using the gauge of Skagen directly. Several software tools are available to support the generation of realistic boundary time series (BAW 1996-2014).

The current version of the UNTRIM simulation software still uses proprietary data formats of BAW to import boundary conditions. Support of the internationally

distributed NetCDF (UNIDATA PROGRAM CENTER) data format is in progress and will represent a huge technical step forward in the use of existing datasets provided by other institutions.

The model state can be initialised using the dataset of (JANSSEN et al. 1999). However, some programming effort will still be required in order to use these NetCDF data (UNIDATA PROGRAM CENTER) in the model software UNTRIM as they are provided.

Models are validated by comparing measured water levels at several gauges with the time series simulated by the model. Some data sources are available for gauge data via the internet for the Baltic Sea. Additionally, the database of the German Waterway Management Authorities provides high resolution time series of all their supported gauges from 1989 to the present. Fig. 3 shows a typical example of such a gauge station. Historical measurements from paper archives are now being continuously digitized and integrated into this database resource. A standard procedure is applied to recompile in the BAW all the data provided from different sources. This guarantees comparable quality and provides a data format which is readable by post-processing tools.



Figure 3: Modern gauge equipment, which is indicated by the smallness of the gauge house, at “Wismar Baumhaus” provides high resolution time series of water levels (photo: Seiß, 2009).

A typical validation step is to visually compare the simulated curve with the one provided by the gauge at the same location. Differences are calculated to estimate the maximum range of error in instantaneous water levels. Deviations may result from an energy distribution in the model domain which deviates from reality and which is indicated by the amplitudes of the extreme events. Phase shifts indicate that the spectra of the model

differ from nature. Different mean sea levels are not normally so important for validation. They often indicate systematic deviation of the reference level of the seaward boundary condition, and a constant correction is therefore applied.

Fig. 4 shows the measured and the simulated time series at the Schleswig gauge lying at the end of the Fjord for an extreme low water situation. In this simulation the high resolution Schlei Fjord grid is used, driven by the local wind derived from Schleswig weather station. The water level at the open boundary was steered with the gauge Schlei-münde.

The comparison clearly shows that, because the boundary values and bathymetry are represented well enough, the model is able to reproduce the hydrodynamics inside this very complex geometry. In this case in particular there was no need to adapt parameters to achieve this high-quality result. All the physical forces (advection, pressure, dissipation, external forces) appear to be of the right order inside the model. The result suggests that it may always be possible to obtain a good representation of hydrodynamics with a numerical model if the relevant processes are resolved in the time-space domain.

Even the two extreme low water level events are reproduced. These events depend critically on the quality of the local wind field, which could be represented by using the wind speed of the meteorological station Schleswig multiplied by a suitable factor. The factor is needed to emphasise the fact that the wind speed is higher over the water surface due to reduced friction.

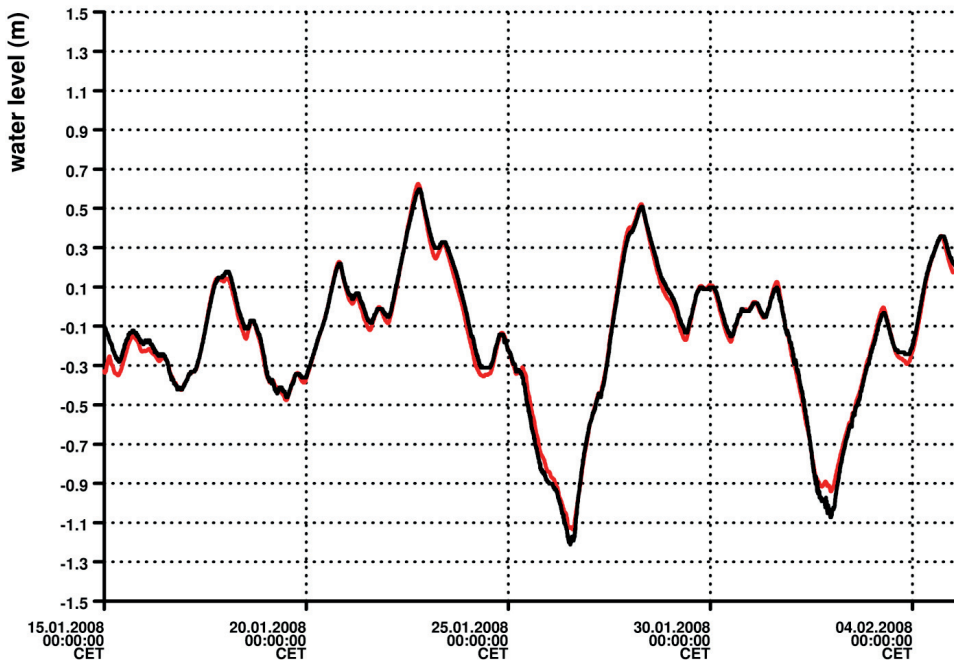


Figure 4: comparison of simulated water level (red curve) with gauge values (black curve) at Schleswig.

4 History of the Baltic Sea modelling kit

The first projects were performed with a model grid with open boundaries at Fehmarn, Bornholm and to the south of the Sound (BAW 2009/2010). This approach was good enough to deal with the issues arising within the project context, but failed to represent absolute salinity in a realistic manner as the errors in boundary conditions could be rather large on the open boundaries which intersect a zone of a relatively large salinity gradient. Providing sufficient data for salinity became a considerable issue.

These experiences resulted in the decision to develop a grid covering the whole Baltic Sea. Only one open boundary at Skagen made it easier to provide sufficient boundary values for water level, salinity and temperature.

The first modular grid was built for a consultation project on the region of the Warnow mouth (BAW 2011). Example results from this study are shown in Fig. 5. The picture shows the change in the variability of the parameter salinity due to a dredging measure. The analysis is based on a period of four weeks with extreme events of high and low water levels. The colours can be interpreted as follows:

- The blue colours in the northern part indicate a damping of salinity variability because the zone of the highest salinity variability has been shifted to the south.
- The red colours indicate the increase of variability in the southern part, which is increasingly influenced by the sea and the advective transport of seawater.

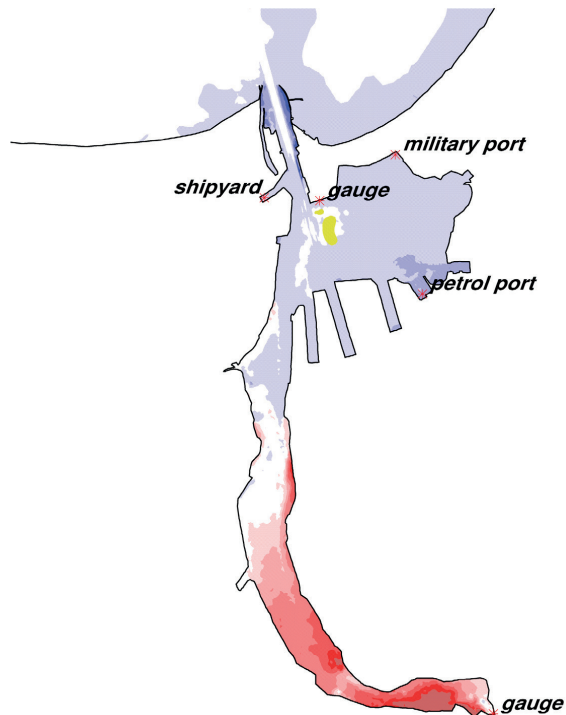


Figure 5: Change in the variability of salinity in the region of the Warnow mouth due to a deepening of the fairway.

This example indicated that the concept of using a complete Baltic Sea model with refinement only in the region of interest works quite well.

However, one important process - temperature driven dynamics – was still missing. Forcing by space-dependent surface air temperature was realised in subsequent years. The data pool was reorganised and completed. New strategies have been developed to create sufficient boundary values for water level even if the gauges Skagen and Smögen are not available by using spectral information of tides and long term signals of other nearby gauges.

5 Further applications

A study of tracer spreading has been undertaken in the Schlei Fjord. This study was performed with a high resolution inlay model which was run as a standalone model with boundary values created from the basic Baltic Sea model. The configuration in the inner part is shown in Fig. 6. A tracer source near Schleswig simulates the inflow of polluted water.

To evaluate the typical time scales until the Fjord has been adapted to a dynamic steady state, the tracer concentration of a single point in the inner fjord was fit to an exponential function. This procedure is illustrated by Fig. 7 for a position in the inner Schlei Fjord. The average time series of tracer concentration clearly shows exponential characteristics. The derived typical exponential time scale of the red curve fit is about 142 days within which the concentration reaches 90% of the equilibrium state value.

The Schlei Fjord model was also used in KLIWAS as part of a sensitivity study dealing with the influence of a rising sea level on the variability of short-term water level changes due to meteorological events. This study compared the results generated by a low resolution inlay model with the results provided by the high resolution version. The signal characteristic in the change of water level variability is the same in both models. But the finer resolution model shows less pronounced changes in sea level variation compared with the coarse resolution model. The step from qualitative answers to quantitative values is determined by the sufficient time-space resolution of the model used, as is also shown in the validation example.

6 Conclusion

The concept of a Baltic Sea model construction kit appears to fulfil the needs of the BAW in modelling coastal processes for the practical purpose of supporting the management of German fairways. A wide range of practical applications shows the flexibility and strength of the concept of a modular modelling framework. The quality of the results depends mainly on the quality of the input data used by the simulation software. Real events can be reproduced to a high standard, if the grid resolution is appropriate.

Efforts should be made to press ahead with the use of common data format standards within the modelling software to provide easier and more cost-effective access to the third-party proofed datasets which are already available.

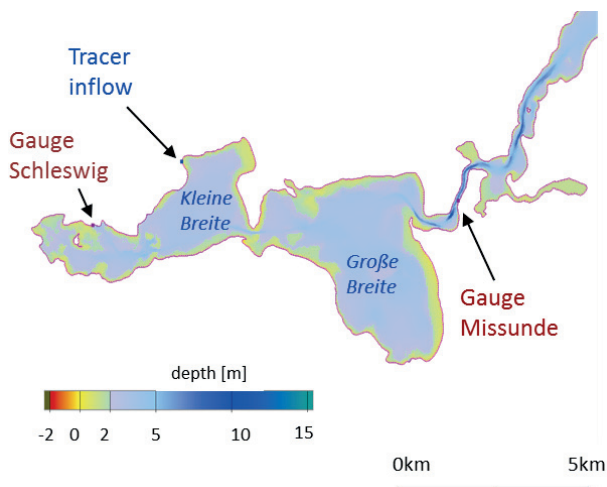


Figure 6: Model bathymetry of the inner Schlei Fjord with inflow position and gauge positions.

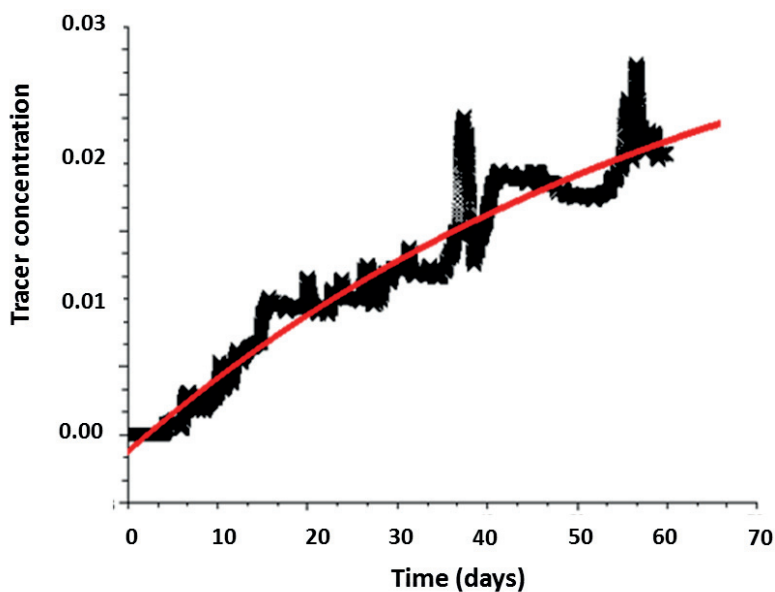


Figure 7: Evaluation of tracer concentration at a station in the inner Schlei Fjord due to entrainment. The markers show the modelled values, the straight line the exponential fitting curve.

Several physical aspects will still need to be improved or integrated into the software part of the Baltic Sea modelling kit in the future, but the high quality data part is now ready for use. The next steps in software improvement could be to include a simple ice model and eventually test other modelling software products which use unstructured grids.

7 References

- BAW: Program Descriptions. Bundesanstalt für Wasserbau, http://www.baw.de/methoden_en/index.php5/Program_Descriptions, last visited: 01.04.2014.
- BAW: Fahrrinnenanpassung, Anpassung der inneren Hafengewässer und Hafenausbau Wismar. Hydrodynamik. Bundesanstalt für Wasserbau, Hamburg, 2009/2010.
- BAW: Machbarkeitsstudie zum Ausbau des Seekanals Rostock auf eine Tiefe von 16,60 m unter NHN. Hydrodynamik. Bundesanstalt für Wasserbau, Hamburg, 2011.
- CASULLI, V. and WALTERS, R.A.: An unstructured grid, three-dimensional model based on the shallow water equations. In: *International Journal for Numerical Methods in Fluids*, Vol. 32, 3, 331-348, 2000.
- CASULLI, V. and ZANOLLI, P.: Semi-implicit numerical modelling of nonhydrostatic free-surface flows for environmental problems. In: *Mathematical and Computer Modelling*, Vol. 36, 9-10, 1131-1149, doi: 10.1016/S0895-7177(02)00264-9, 2002.
- JANSSEN, F.; SCHRUM, C. and BACKHAUS, J.O.: A climatological data set of temperature and salinity for the Baltic Sea and the North Sea. *Bundesamt für Seeschifffahrt und Hydrographie*, Hamburg, 245 p., 1999.
- RAHLF, H. and SEIB, G.: Aktuelles HN-Modell der Ostsee. Grundlage für Untersuchungen in den Ostseehafenzufahrten. In: *BAW aktuell*, 2, 14, 2012.
- SEIB, G.: Das Ostseemodell der Bundesanstalt für Wasserbau. Technische Dokumentation. Bundesanstalt für Wasserbau Dienststelle Hamburg, 2012.
- UNIDATA PROGRAM CENTER (ed.): Network Common Data Form (NetCDF). overview website. <http://www.unidata.ucar.edu/software/netcdf/>, last visited: 01.04.2014.

Evaluation of Changes in the Tidal Regime of the Ems-Dollard and Lower Weser Estuaries by Mathematical Modelling

Gerald Herrling, Johanna Elsebach and Anne Ritzmann

Summary

Investigations for the Ems-Dollard and the Lower Weser estuaries have been done to compare the hydrodynamic regimes for historical and recent states. The research incorporates the identification of long-term spatial developments on the basis of historical and recent bathymetrical data and the application of process-based numerical modelling in order to hindcast the hydrodynamic regime. For the Ems-Dollard estuary the bathymetrical state of 1937 was reconstructed. This reference state represents the estuary prior to the main anthropogenic impacts of channel streamlining and deepening. A model bathymetry of the year 2005 was applied for comparison. For the Lower Weser estuary a historical state of 1887 was reconstructed and compared to the situation of the year 2000. Here, 1887 represents the situation prior to the “Weser correction” by Ludwig Franzius. Model results enable the comparison of hydrodynamic parameters and thus allow the quantification of changes in water levels, current velocities, tidal volumes, tidal discharges and the duration of tidal phases.

In the Lower Ems, the comparison of hydrodynamic parameters is assessed in the time domain at one specific location during one tidal cycle and for time-averaged values at a longitudinal section. Tidal discharges, volumes and current velocities have significantly increased between 1937 and 2005, whereas the duration of the tidal phases has remained almost constant in time for at least the section between Leerort and Pogum. For the aforementioned longitudinal section, the difference between mean flood and mean ebb discharges has increased from 1937 until now. In the outer Ems, a spatial comparison of tidal current velocities shows the differences in flow pattern and magnitudes. Comparing the present to the historical model state, tidal current velocities have slightly increased and the current patterns are more concentrated on the deepened tidal inlet and channels. The diversification of current magnitudes on a spatial scale has been significantly reduced with respect to 1937. Shallow water areas with reduced current velocities have almost disappeared in the tidal inlet.

The Ems-Dollard estuary and particularly the Lower Ems experienced a dramatic change of its tidal regime due to human interferences. The estuarine deepening and streamlining upstream of the Dollard Bay created long-term morphodynamical processes being still of importance. In the last centuries, natural and anthropogenic interferences in the Dollard Bay resulted in a strong reduction of tidal prism being responsible for changes to the tidal regime in the outer Ems-Dollard estuary.

For the Lower Weser estuary, the evaluation of hydrodynamic parameters along a longitudinal section between Bremen and Bremerhaven reveals a significant increase in mean tidal discharges and mean tidal volumes since 1887. Due to the shift of the natural flood current limit from Vegesack to Bremen, the duration of tidal phases nowadays feature a

steep gradient in exactly this area, which means a sudden decrease in ebb duration and thus increase in flood duration. The spatial distribution of depth-averaged current velocities for the model states of 1887 and 2000 shows the enormous effect of streamlining the waterway and cutting-off of secondary channels since 1888. The strong anthropogenic impacts changed shallow water areas and secondary channels of relatively low current conditions into one straightened waterway characterized by high current magnitudes.

Keywords

Ems-Dollard-estuary, HARBASINS, Weser correction, waterway streamlining and deepening, Delft3D, process-based model, estuarine hydrodynamics, regime shift, comparison historical and present state

Zusammenfassung

In den Ästuaren von Ems-Dollart und Unterweser wurden Untersuchungen zum Vergleich der historischen und aktuellen Zustände des hydrodynamischen Regimes durchgeführt. Auf der Basis historischer und aktueller Topographien wurden für beide Ästuarer numerische Modelle erstellt, um die räumliche und zeitliche hydrodynamische Entwicklung auszuwerten. Für das Ems-Dollart-Ästuar dient dafür als Referenzzustand das Jahr 1937, welches den Zustand vor den umfassenden anthropogenen Eingriffen wie Begradigung und Vertiefung darstellt. Den Vergleich mit dem aktuellen Zustand ermöglicht eine Modelltopographie des Jahres 2005. Der natürliche, historische Zustand der Unterweser wurde aus Topographiedaten des Jahres 1887 rekonstruiert, unmittelbar vor der Weserkorrektur nach Ludwig Franzius. Topographische Daten von 2000 repräsentieren den aktuellen Zustand. Die Modellergebnisse ermöglichen einen Vergleich hydrodynamischer Parameter und somit die Quantifizierung der Veränderungen von Wasserständen, Strömungsgeschwindigkeiten, Tidevolumen, Tidedurchfluss und Dauer der Tidephasen.

An der Unterems wurden hydrodynamische Parameter als Zeitreihen an einer Position für einen Tidezyklus ausgewertet und als zeitlich gemittelte Werte längs des Fahrwassers. Tidedurchfluss, Tidevolumen und Strömungsgeschwindigkeiten sind im Zeitraum 1937 bis 2005 signifikant angestiegen, während die Dauer der Tidephasen zumindest im Abschnitt zwischen Leerort und Pogum annähernd gleich geblieben ist. In Längsrichtung betrachtet hat die Differenz zwischen mittlerem Flut- und Ebbdurchfluss seit 1937 zugenommen. Für die Außenems zeigt ein räumlicher Vergleich der Tideströmungsgeschwindigkeiten die Unterschiede von Strömungsmuster und -intensität. Die Strömungsgeschwindigkeiten haben seit 1937 leicht zugenommen bei einer Konzentration auf die vertiefte Flussmündung und die tiefen Rinnen. Die räumliche Diversität der Strömungsgeschwindigkeiten und strömungsberuhigte Flachwasserbereiche im Mündungsbereich sind seit 1937 signifikant vermindert.

Für das Ems-Dollart-Ästuar und insbesondere die Unterems ist eine dramatische Veränderung des Tideregimes aufgrund anthropogener Faktoren festzustellen. Die Vertiefung und Begradigung des Ästuars stromauf des Dollarts hat langfristige morphodynamische Prozesse geschaffen, die noch immer von Bedeutung sind. Die natürlichen und anthropogenen Eingriffe der letzten Jahrhunderte im Dollart führten zu einer starken Reduzierung des Tideprismas, das für die Veränderungen des Tideregimes im äußeren Ems-Dollart-Ästuar verantwortlich ist.

Für das Weserästuar verdeutlicht die Auswertung hydrodynamischer Parameter in Längsrichtung zwischen Bremen und Bremerhaven einen signifikanten Anstieg des mittleren Tidedurchflusses und des mittleren Tidevolumens seit 1887. Aufgrund der Verlagerung der natürlichen Flutstromgrenze von

Veegesack nach Bremen zeigen die Tidephasendauern in diesem Bereich heutzutage einen steilen Gradienten, was eine plötzliche Verkürzung der Ebbdauer bzw. Verlängerung der Flutdauer bedeutet. Die Veränderung der Strömungsgeschwindigkeiten zwischen beiden Modellzuständen 1887 und 2000 zeigt die massiven Auswirkungen von Flussbegradigung und Abtrennung von Nebenarmen. Der starke anthropogene Einfluss hat Flachwasserbereiche und Rinnen mit geringer Strömung in ein begradigtes Fahrwasser mit hohen Strömungsgeschwindigkeiten verwandelt.

Schlagwörter

Ems-Dollart-Ästuar, HARBASINS, Korrektion Unterweser, Flussbegradigung und Fahrwasservertiefung, Delft3D, prozessbasiertes Modell, Ästuardynamik, Nachhersage (bindcast), Regime Veränderung, Vergleich historischer und aktueller Zustand

Contents

1	Introduction	355
2	Methodology and Data	356
3	Results	358
3.1	Results at one specific location in the Lower Ems	358
3.2	Results along a longitudinal section in the Lower Ems	359
3.3	Spatial results in the Outer Ems	363
3.4	Results along a longitudinal section in the Lower Weser estuary	365
3.5	Spatial results for the Lower Weser estuary	367
4	References	368

1 Introduction

In the course of the last centuries, many European estuaries and coastal waters experienced significant changes in their littoral environment not only due to natural processes but more and more due to human interference. Major anthropogenic pressures in estuaries and their habitats have been: land reclamation by establishing dykes on supratidal marshes and foreland, harbor extensions, implementation of groins and training walls, deepening and streamlining of waterways. These anthropogenic impacts change primarily both hydrodynamics and topography of estuaries.

In the framework of the European Interreg IIIb project HARBASINS (“Harmonised River Basins Strategies North Sea”) the aim of the workpackage “Hydro- and Morphological Pressures and Impacts” was to generate process-based knowledge on these effects by high-resolution mathematical modelling. For this purpose, investigations have been carried out for the Ems-Dollard and Lower Weser estuaries. Objective was to compare the hydrodynamic regimes for recent and historical states and assess their long-term spatial developments. This paper is meant as a review on the formerly achieved research results (HERRLING and NIEMEYER 2007a, b, c; HERRLING and NIEMEYER 2008a, b, c; HERRLING and ELSEBACH 2008).

The study areas are located at the southern North Sea coast (Fig. 1) and marked by characteristic geomorphological features for this type of coastline: deep tidal channels and inlets, intertidal flats and the inner estuarine environment. The investigated estuaries are considered to be mesotidal with increasing tidal ranges further upstream. Their tidal limit is set by artificial tidal barriers located at 50 km and 70 km upstream of the estuarine mouth for the Ems-Dollard and the Lower Weser estuary, respectively.

Both estuaries have long histories of considerable anthropogenic interferences. The Dollard Bay already was marked by dyking and land reclamations in the period between the 17th and the 20th century (HERRLING and NIEMEYER 2007a). By the end of the 19th century groins, harbors and navigation measures were built in the Lower Ems and the Emden fairway. Since the 1950s, maintenance dredging of the navigational channel became common practice in the Lower Ems. In the Lower Weser estuary, streamlining the waterway and cutting-off of secondary channels from 1888 until 1895 were the strongest human impacts, nowadays known as “Weser correction”, planned by Ludwig Franzius. Another significant anthropogenic intervention was the waterway deepening of 9 meters below the “nautical chart datum” (SKN) just after 1972.

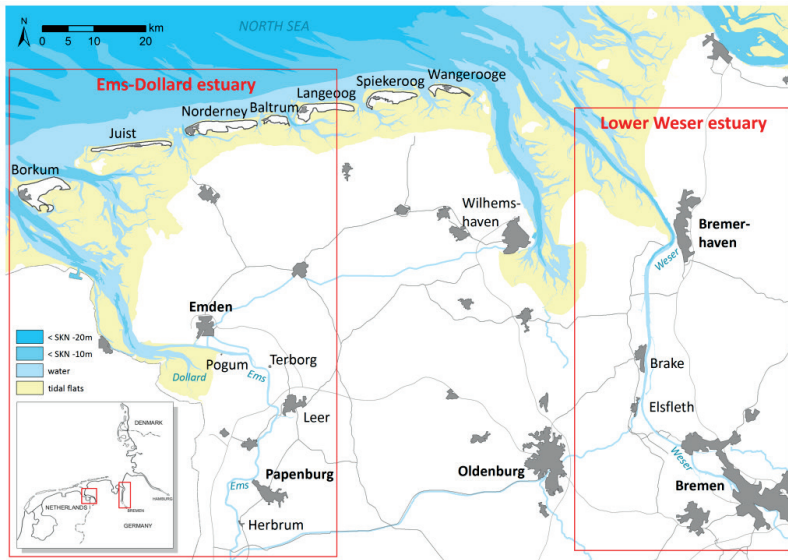


Figure 1: Areas of investigation: Ems-Dollard estuary and Lower Weser estuary.

2 Methodology and Data

To identify significant changes in the tidal regime due to human impacts, it seems reasonable to compare prevailing hydrodynamic parameters to those of historical states. But continuous current measurements of historical states hardly exist or are temporally and spatially limited in most cases. Alternatively mathematical hydrodynamic modelling can compensate this lack of data if for a chosen reference status sufficient bathymetrical data is available. The historical model configuration is applied for hydrodynamic hindcasting, i.e. the reproduction of the hydrodynamic regime prior to the main human impacts like

streamlining and deepening of the waterways. Aim is the comparison of hindcasted hydrodynamic parameters like current velocities and tidal volumes with the output of a current model state incorporating data of recent bathymetric surveys. Hydrodynamic models of the Ems-Dollard and the Lower Weser estuary were established by applying the vertically averaged version of the modelling system Delft3D (DELTA RES 2006). The resolution of the numerical, curvilinear grids is in the order of 800 meters at the seaward boundaries and reaches up to 15 meters at the upstream river sections.

Historical marine charts and maps due to topographic surveys have been required from authorities and local waterway agencies. Marine charts of the years 1923, 1926, 1941 and 1952 are used to reconstruct the historical model bathymetry in the outer Ems-Dollard estuary and the Dollard Bay. At the riverine section of the Lower Ems cross-sectional survey data at a distance of about 300 to 400 meters is available for the years 1927 and 1933. The area in between the cross-sections is reconstructed by interpolating linearly along the flow-directed lines of the numerical grid. The data is found to be adequate to model the hydrodynamic state prior to the main human impacts. In the following, the historical configuration of the Ems-Dollard model is referred to the year 1937, since the oldest available water level observations being necessary for the model calibration go back to 1937. Recent data of bathymetric surveys based on echo-sounding (2004) and high-resolution airborne laser-scanning (2005) is used for the present model bathymetry.

For the Lower Weser bathymetrical data gathered from historical maps of the year 1887 represent the state prior to the correction of 1888. Data for the present state is based on airborne laser-scanning and echo-sounding surveys carried out between 1996 and 2000. Two digital elevation models have been created using GIS techniques. They were used as input for the model configurations of 1887 and 2000, covering the area of the Lower Weser from Bremerhaven (km 65) to Bremen (km 0).

The open model boundary conditions are selected in a manner to generate mean hydrodynamic flow conditions allowing the comparison of the computed tidal regimes of both mentioned model states. It is aimed to reproduce an average tide, a tide with mean high water level (MHWL) and mean low water level (MLWL), which is in tune with mean water level observations of the historical and the present state, respectively. The sea boundary conditions are generated by a nesting procedure with the overall German Bight Model (VERBOOM et al. 1992), except for the historical configuration of the Lower Weser model. Here, the record of a mean tide of 1887 (FRANZIUS 1888) was adapted and implemented at the sea boundary being located close to Bremerhaven at the mouth of the estuary. The selected type of boundary conditions only represents the astronomical tide without any meteorological effects. Apart from the generation of a mean tide at the sea boundary, the run-off at the upstream riverine boundary is set in order to match long-year mean discharges. The freshwater discharge has been assumed to be identical for the present and the historical model states, thus 82 m³/s and 327 m³/s for the Ems and Weser, respectively. The historical and current models of the Ems-Dollard and the Lower Weser estuary are calibrated by fine-tuning numerical and physical parameters, e.g. the bottom roughness. The quality of the models is verified by means of computed and observed water level comparison at gauge locations along the estuaries.

3 Results

The model results for the Ems-Dollard estuary with configurations of 1937 and 2005 enable a quantitative comparison of the hydrodynamic regimes. In the Lower Ems, the comparison of hydrodynamic parameters is assessed at one specific location and at a longitudinal section from the tidal barrier at Herbrum to the Dollard Bay. In the Outer Ems, a spatial comparison of current velocities shows the differences in flow regime. For the Lower Weser, hydrodynamic parameters are evaluated for the section between the tidal weir in Bremen and downstream as far as Bremerhaven. An example of significant changes in the hydraulic regime is given for a certain stretch between Brake and Elsfleth.

3.1 Results at one specific location in the Lower Ems

Modeled tidal discharges and volumes are monitored through cross-sections along the mentioned stretch at the distance of one kilometer each. Computed hydrodynamic parameters are evaluated exemplarily at kilometer 35 in the Lower Ems for the period of one tidal cycle, representing mean tidal conditions for 1937 and 2005. This comparison reveals the changes of the tidal regime in time. The observation point is located about 5 kilometers upstream of Terborg at a straight stretch in order to avoid fluctuations in current velocities due to secondary flows or sudden channel constrictions. Time series of water levels referenced to German datum [mNN], i.e. approx. mean sea level, and current velocities [m/s] are compared for mean flow conditions between 1937 and 2005 (Fig. 2).

Generally, the tidal range and the current velocities of the model state of 2005 have increased with respect to the situation in 1937. Nowadays, the tidal curve is significantly broader at high tide with a steepened flood and ebb phase section. Flood current velocities have significantly increased for the first part of the flood phase. At the given cross-section and generally in the Lower Ems, the overall tendency is towards a flood-dominated tidal flow.

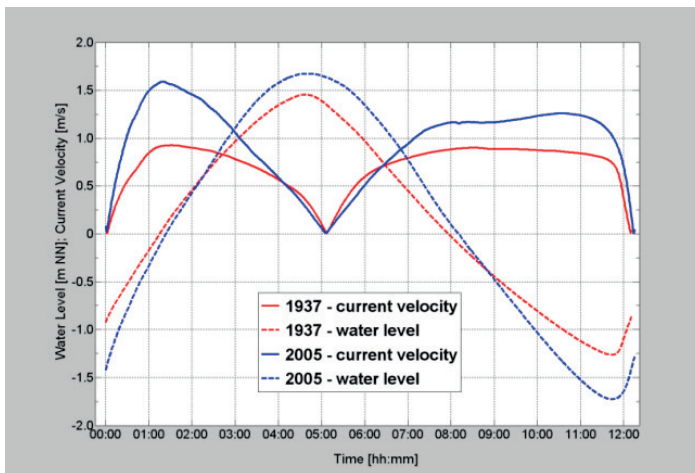


Figure 2: Modelled mean tidal water level and mean current velocity in the cross-section at kilometer 35 downstream of the tidal barrier at Herbrum in the Lower Ems.

The time series of the momentary tidal discharges and related hydrodynamic parameters are computed for 1937 and 2005 due to the cross-sectional flow at kilometer 35 for one mean tidal cycle (Fig. 3). Mean tidal fluxes and mean tidal volumes have increased from 1937 to 2005, whereas the mean tidal phases have remained almost constant in time for ebb and flood tides. The mean tidal flux computed as the arithmetical average over one tidal phase increased from 811 to 1394 m³/s (72 %) for flood tide and from 717 to 1114 m³/s (55 %) for ebb tide. The mean flood tidal volume V_f increased by about 73 % from 14.8 to 25.6 Mill. m³, whereas the mean ebb tidal volume V_e increased by approximately 55 % from 18.4 to 28.5 Mill. m³.

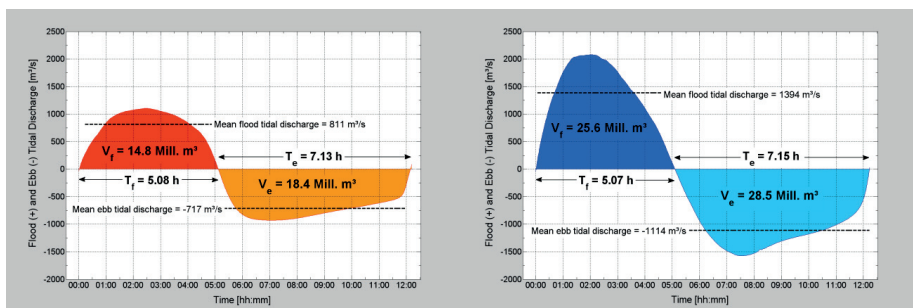


Figure 3: Mean tidal flux, mean tidal volume V and mean tidal period T in the cross-section at kilometer 35 downstream of the tidal barrier in the Lower Ems for the model state of 1937 (left) and 2005 (right).

3.2 Results along a longitudinal section in the Lower Ems

Computed results for the states of 1937 and 2005 at the longitudinal section from the tidal barrier at Herbrum downstream to the Dollard Bay highlight differences in hydrodynamic parameters such as mean water levels, mean and maximum tidal discharges, mean tidal volumes, mean tidal current phases as well as means and maximum current velocities.

Modelled tidal discharges and volumes are monitored through cross-sections along the mentioned stretch at the distance of one kilometer each. Water levels and depth averaged current velocities are computed at observation points every kilometer along the centerline of the waterway, thus at about the deepest part of each previously mentioned cross-section. Tidal discharges and volumes can only be properly determined as far downstream as Pogum. Further downstream, where the Lower Ems discharges in the Dollard Bay, it is not evident to set the width of the cross-section, because water masses are flooding sideways over the Geise training wall into the Emders fairway and vice-versa. This almost circular flow pattern is different from the directed flow in a channel and thus not comparable with the parameters evaluated in the Lower Ems. There is a significant increase of the tidal discharges and the tidal volumes at Leerort, which can be assigned to the freshwater discharge contributed by the Leda tributary.

Mean water levels

Observed and computed mean water levels (MHWL and MLWL) are compared at the longitudinal section from the tidal barrier at Herbrum to the location Knock at about

67 kilometers downstream (Fig. 4). MHWL and MLWL for the state of 1937 (red) are plotted against those of 2005 (blue). Computed values are due to the simulation of one representative mean tide for 1937 and 2005. Observations are based on 5-year-period time series: for 1933 to 1937 and 2001 to 2005, with an exception of the historical observations at Herbrum being available only for the period from 1936 until 1940. The differences between the modeled and the observed values are in the order of 5 to 10 centimeters. Thus, the amplitude of the tidal wave propagating upstream is reproduced satisfactorily for both model states.

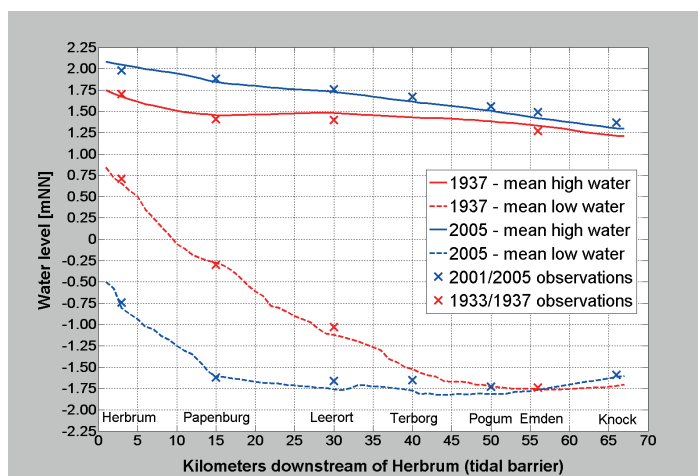


Figure 4: Modeled and observed MHWL and MLWL along a longitudinal section between Herbrum and Knock for the model states of 1937 and 2005.

At Emden, the observed MLWLs, both for the present and the historical situation, are exactly at the level of -1.74 mNNG (the red cross is exactly on top of the blue cross). There is evidence to suggest that Emden is the location where the decrease of the MLWL, as the effect of the waterway deepening and streamlining, is leveled out against the increase of the MLWL due to the secular sea level rise. This implication is very well reproduced by the models; the MLWL lines of both model states intersect at Emden.

Mean and maximum tidal discharges

The tidal discharge is determined as the momentary flow [m^3/s] recorded with an interval of one minute through cross-sections at every kilometer at the section between Herbrum and Pogum. The mean tidal discharge is the arithmetical average of the recorded momentary flows over the period between two subsequent slack-tides, for ebb- and flood-directed currents, respectively (Fig. 5a).

The maximum tidal discharge is evaluated at the peak flow for ebb and flood current phases (Fig. 5b). Both, ebb and flood tidal discharges have significantly increased since 1937 for the whole section. Although the freshwater discharge counteracts the tidal flow during flood tide, the mean tidal flood discharge is higher than the mean tidal ebb discharge in the section between Leerort and Pogum for the historical state and between kilometer 17 and Pogum for the state of 2005. In this context one has to bear in mind

that the flood current phase is significantly shorter than the ebb current phase and thus the equilibrium of the estuarine in- and outflow is maintained.

Considering the section between Leerort and Pogum, the net difference between mean ebb and mean flood discharge is in the order of $100 \text{ m}^3/\text{s}$ for the state of 1937 compared to $300 \text{ m}^3/\text{s}$ for the year 2005, whereas the duration of the tidal phases did not change significantly between both model states. This circumstance is to be regarded as an evidence for the increase of the tidal asymmetry with respect to the state of 1937.

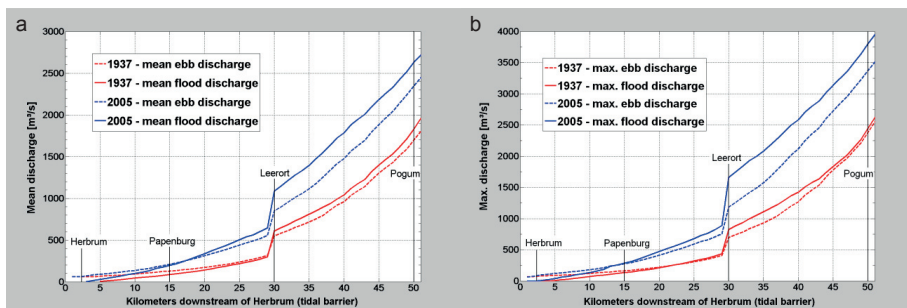


Figure 5: Comparison of mean (a) and maximum (b) tidal discharges in the Lower Ems between the model states of 1937 and 2005 for flood and ebb tide.

Mean tidal volume

The freshwater discharge and hence the difference between mean ebb and flood tidal volume is identical for both model states (Fig. 6a). Generally, the mean tidal volume computed for today's mean hydrodynamic conditions is significantly higher compared to the equivalent of 1937 as a result of the anthropogenic streamlining and deepening of the channel-cross-sections leading to a smaller hydraulic resistance.

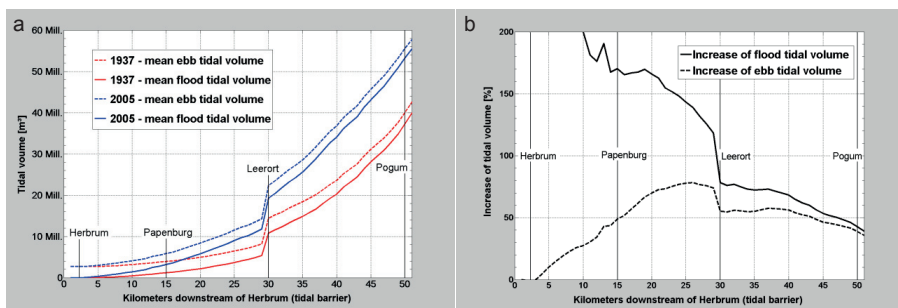


Figure 6: Comparison of mean tidal volumes at a longitudinal section in the Lower Ems for the model states of 1937 and 2005 (a); relative increase [%] in mean flood and ebb tidal volume between 1937 and 2005 in relation to the mean tidal volume of 1937 (b).

The percentage increase of the mean tidal volume is expressed relative to the mean tidal volume of 1937 (Fig. 6b). The relative increase ranges from 100 percent at Papenburg to up to 600 percent at Herbrum. In 1937, the hydraulic resistance of the channel bed was higher than today preventing the tidal wave to propagate as far in the upper estuary as today. As a consequence the tidal range used to be much smaller in the upper section explaining the relative very high increase in tidal volume. Further downstream the relative

increase in flood tidal volume since 1937 is in the order of 70 % at Leerort decreasing gradually to about 40 % at Pogum. The relative increase in the mean ebb tidal volume with about 75 % is highest in the section between Papenburg and Leerort. At Pogum the increase is almost 40 %, thus similar to the increase in mean flood tidal volume.

Mean tidal current phase

The mean tidal current phases are determined as the duration [h] between two slack-tides for ebb and flood tide, respectively (Fig.7). The mean flood current phase is generally shorter than the mean ebb current phase with decreasing trend towards the upper part of the estuary. At the tidal limit close to Herbrum, the duration of the flood current phase is zero, whereas the duration of the ebb current phase is about 12.4 hours – one complete tidal cycle. In the section between Herbrum and Leerort, the duration of the mean flood current phase is significantly longer for the present situation compared to 1937 (e.g. about 45 min at Papenburg). As the duration of one complete tide is fixed to 12.4 hours, consequently the mean ebb current phase has to be shorter by the same extent nowadays. Downstream of Leerort almost no differences occur in the duration of the mean current phases between the present and the historical state.

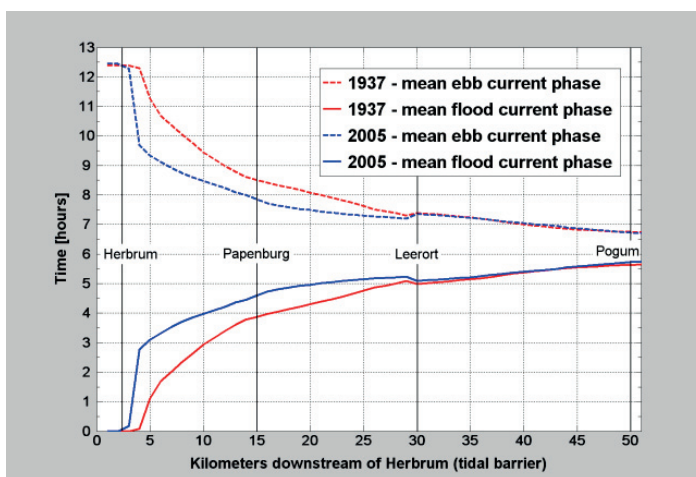


Figure 7: Comparison of mean tidal current phases in the Lower Ems between the model states of 1937 and 2005 for flood and ebb tide.

Mean and maximum current velocities

The mean and maximum current velocities are determined for mean hydrodynamic flow conditions at the longitudinal section between Herbrum and Knock (Fig. 8). The current velocities are monitored every kilometer at about the deepest part of the waterway's cross-section. High fluctuations in magnitudes between subsequent monitoring points are due to changes in bottom depth, sudden flow constrictions or the effect of secondary flows in river bends. Hereafter it is focused to point out a qualitative trend in the relation between current velocities. The determination of the current velocities at the middle of the waterway is considered to be a relevant parameter to evaluate the qualitative sediment load, because high shear stresses in the middle of the cross-section initialize the sediment transport.

Generally, mean and maximum current velocities are higher for the present than for the historical model state during both ebb and flood phases. Upstream of Leerort (km 30), the difference of current velocities between ebb and flood on the one hand and between the model state of 1937 and 2005 on the other tend to increase. Considering the present model state at the stretch between kilometer 25 and 40, the maximum current velocities are significantly higher for flood tide compared to ebb tide. The maximum current velocities as regards the historical state for the same section are similar for ebb and flood tide. Downstream of Terborg (km 40), the mean current velocities are higher for ebb than flood tide, whereas the maximum current velocities of ebb and flood tide are generally more in agreement for both model states.

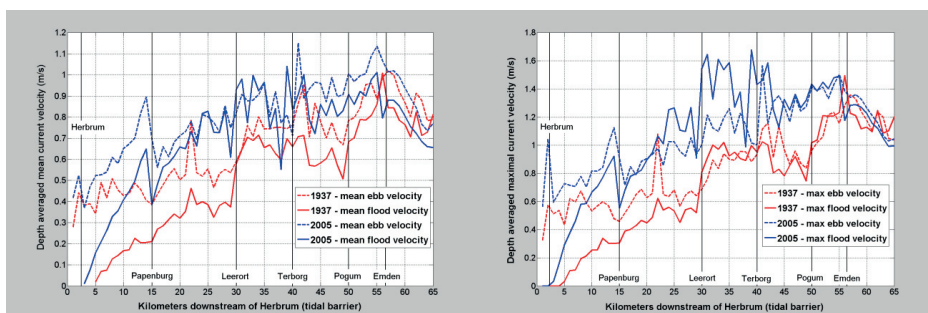


Figure 8: Comparison of mean (a) and maximum (b) current velocities in the Lower Ems between the model states of 1937 and 2005 for flood and ebb tide.

3.3 Spatial results in the Outer Ems

The application of mathematical models does not only allow the evaluation of hydrodynamic parameters in predefined points or cross-sections, but also at a spatially broader scope. The migration of tidal channels and tide dominated current pattern can be highlighted.

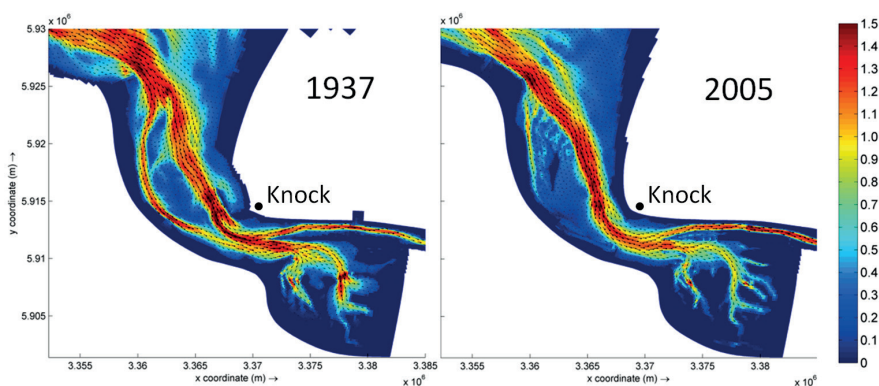


Figure 9: Comparison of maximum flood current velocities [m/s] in the transitional waters with respect to the location Knock for the model states of 1937 (a) and 2005 (b).

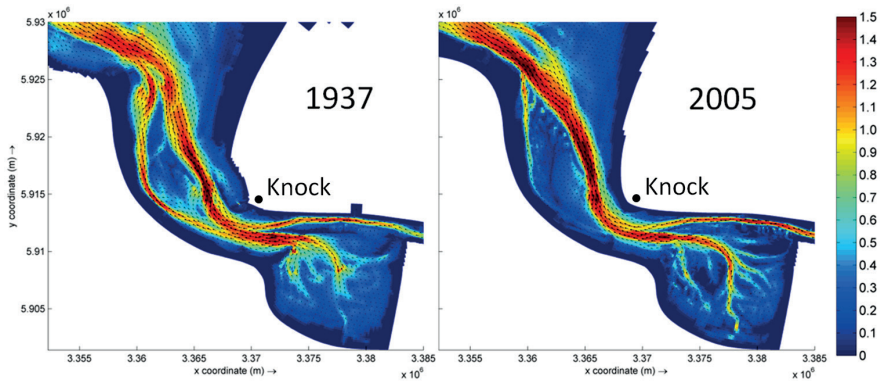


Figure 10: Comparison of maximum ebb current velocities [m/s] in the transitional waters with respect to the location Knock for the model states of 1937 (a) and 2005 (b).

In the area of the transitional waters of the Ems-Dollard estuary, the maximum flood and ebb current velocities are determined for the instant of time when flood and ebb peak velocities are reached at the location Knock (Fig. 9 and 10). At the tidal inlet and in the seaward area, as regards the state of 1937, the current pattern is broadly extended with spatially varying current magnitudes, whereas the current pattern is significantly concentrated on the deepened waterway for the state of 2005. For the state of 1937, a significant part of the tidal volume is exchanged through the Bocht van Watum which is the smaller tidal channel to the West in the estuarine inlet. Nowadays, this tidal channel is almost silted-up and the tidal currents concentrate on the main inlet and thus have increased in magnitude.

In the Lower Ems, the maximum flood current velocities are highest at the stretch between Terborg and Oldersum (Fig. 11). A general increase of maximum flood current velocities can be determined from 1937 to 2005, especially in the river bends. For the historical state, secondary channels exist in the straight sections upstream of Terborg and downstream of Oldersum, whereas the tidal currents in 2005 are focused on one single channel.

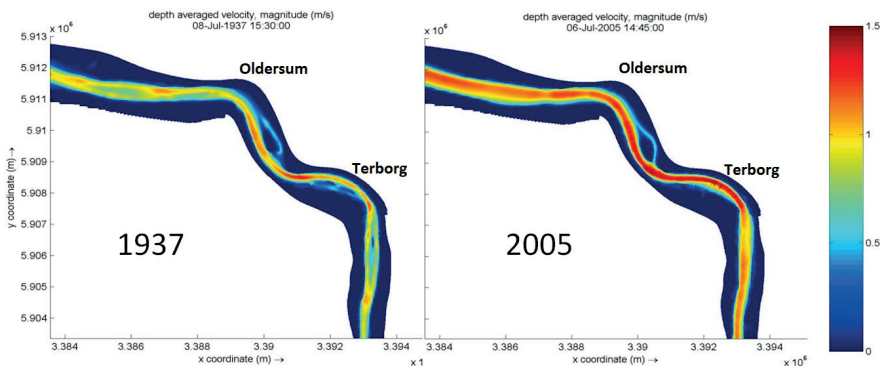


Figure 11: Comparison of maximum flood current velocities [m/s] in the Lower Ems at the section between Terborg and Oldersum for the model states of 1937 (a) and 2005 (b).

3.4 Results along a longitudinal section in the Lower Weser estuary

Results for the model states of 1887 and 2000 at the longitudinal section beginning at the artificial weir in Bremen downstream to Bremerhaven highlight differences in hydrodynamic parameters such as mean tidal discharges, mean tidal volumes and mean tidal current phases.

Mean tidal discharge

The mean tidal discharge in the section between Bremen and Bremerhaven is evaluated for mean ebb and mean flood current phases (Fig. 12). Both, ebb and flood tidal discharges have significantly increased since 1887 for the whole section. Considering the present state, the zone between Bremerhaven and Vegesack shows almost no difference in mean ebb and mean flood tidal discharges, whereas upstream, the river is determined by higher mean ebb than mean flood discharges due to the counteracting of river and tidal flow and smoothing of the river bed due to anthropogenic changes (LECHER et al. 2001). In 1887, the mean flood discharge was higher downstream of Elsfleth compared to a contrary pattern for the upstream section up to the natural flood current limit at Vegesack.

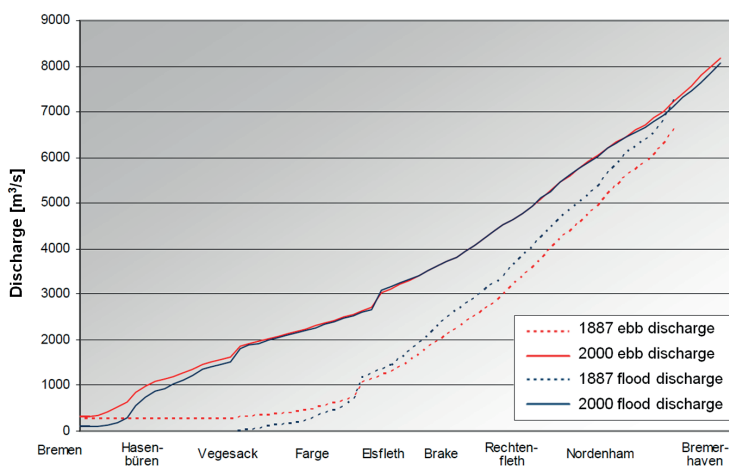


Figure 12: Mean ebb and mean flood tidal discharges of the Lower Weser estuary for the model states of 1887 and 2000.

Mean tidal volume

The freshwater discharge and hence the difference between mean ebb and mean flood tidal volume is assumed to be identical for both model states. The mean tidal volume for the current state is significantly higher compared to the computed equivalent of 1887 (Fig. 13), presumed to be a result of the Weser corrections. The present mean tidal volume shows a linear trend for the whole section, whereas the 1887 state shows two certain trends: a steep increase for the section Elsfleth to Bremerhaven and an almost constant mean tidal volume for the upstream stretch, associated to the former natural flood current limit at Vegesack up to the tidal limit at Bremen (ZANKE 2002).

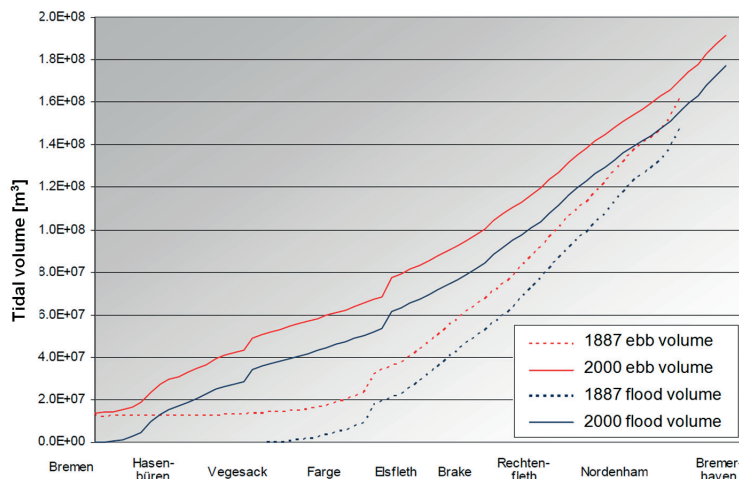


Figure 13: Tidal volume along a longitudinal section in the Lower Weser estuary for the model states of 1887 and 2000.

Mean tidal current phase

Concerning both model states, the mean flood current phase is generally shorter than the mean ebb current phase with a decreasing trend towards the downstream section. Along the whole section the duration of the mean flood current phase is significantly longer for the present situation compared to 1887, consequently the mean ebb current phase is shorter by the same extent. At the tidal weir in Bremen, the duration of the flood current phase is almost zero, whereas the duration of the ebb current phase is about 12.4 hours – one complete tidal cycle (Fig. 14). The steep decrease in ebb duration between Bremen and location Hasenbüren (and hence the increased flood duration) is attributed to the reflection at the artificial weir as well as the changed roughness of the river bed due to the Weser corrections. The historical state shows a smooth continuous decline in downstream direction of the former natural flood flow current limit at Vegesack. Concerning the present state, the difference between ebb and flood tide is decreasing very quickly for the short section Bremen to Hasenbüren followed by almost constant phase lengths downstream.

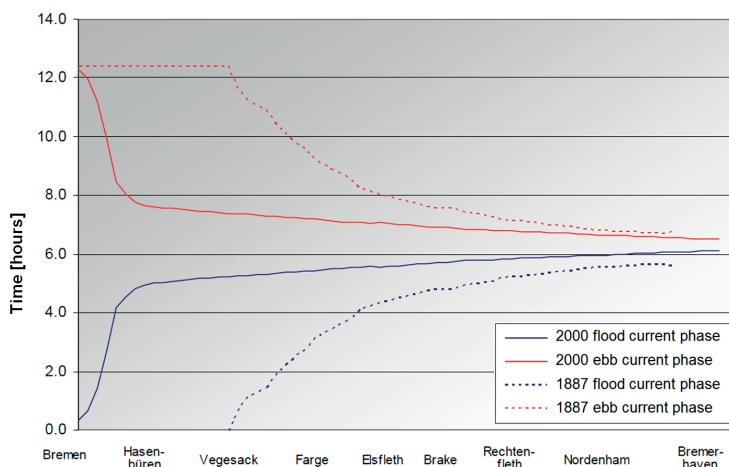


Figure 14: Mean tidal current phases in the Lower Weser estuary for the model states of 1887 and 2000.

3.5 Spatial results for the Lower Weser estuary

Another example of significant changes in the hydraulic regime is given for the Lower Weser estuary in the area of Brake (Fig. 15). The state of 1887 is considered as the natural reference state prior to the correction, starting in 1888. The current state is represented by the year 2000.

The spatial distribution of depth-averaged current velocities for the model states of 1887 and 2000 shows the enormous effect of streamlining the waterway and cutting-off of secondary channels. The strong anthropogenic impacts have changed shallow water areas and secondary channels of relatively low current conditions into one straightened waterway characterized by high current magnitudes. Maximum flood current velocities increased from about 0.7 m/s to 0.9 m/s (approximately 30 %) in the primary channel near Brake. In addition, the spatial variation of current magnitudes over the river width has disappeared due to the channel deepening and fixation.

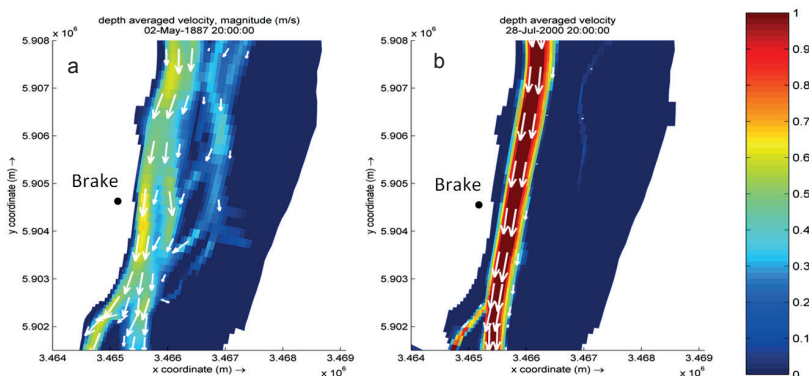


Figure 15: Comparison of maximum flood current velocities [m/s] in the Lower Weser in the area of Brake for the model states of 1887 (a) and 2000 (b).

4 References

- DELTAWARE: User Manual Delft3D-Flow. Delft, 2006.
- FRANZIUS, L.: Die Korrektio n der Unterweser. Bremen, 1888 reprint in: Die Küste, 51, 1991.
- HERRLING, G. and ELSEBACH, J.: Assessment criteria for the Identification of human impacts on water bodies by morphodynamic investigations. Proceedings of the 31st ICCE, Vol. 5: 4620-4632, 2008.
- HERRLING, G. and NIEMEYER, H.D.: Long-term Spatial Development of Habitats in the Ems-Dollard estuary, report of the European project HARBASINS, www.nlwkn.niedersachsen.de/wasserwirtschaft/nordseekueste/FSK/kuesteningenieurwesen/2007a
- HERRLING, G. and NIEMEYER, H.D.: Set-up of a hydrodynamic model for the Ems-Dollard estuary, report of the European project HARBASINS, www.nlwkn.niedersachsen.de/wasserwirtschaft/nordseekueste/FSK/kuesteningenieurwesen/2007b
- HERRLING, G. and NIEMEYER, H.D.: Reconstruction of the historical tidal regime of the Ems-Dollard estuary prior to significant human changes by applying mathematical modeling, report of the European project HARBASINS, www.nlwkn.niedersachsen.de/wasserwirtschaft/nordseekueste/FSK/kuesteningenieurwesen/2007c
- HERRLING, G. and NIEMEYER, H.D.: Comparison of the hydrodynamic regime of 1937 and 2005 in the Ems-Dollard estuary by applying mathematical modeling, report of the European project HARBASINS, www.nlwkn.niedersachsen.de/wasserwirtschaft/nordseekueste/FSK/kuesteningenieurwesen/2008a
- HERRLING, G. and NIEMEYER, H.D.: Set-up of a Morphodynamic Model for the Ems-Dollard estuary, report of the European project HARBASINS, www.nlwkn.niedersachsen.de/wasserwirtschaft/nordseekueste/FSK/kuesteningenieurwesen/2008b
- HERRLING, G. and NIEMEYER, H.D.: Identification of the spatial effect of solid structures on the hydro- and morphodynamics in the Ems-Dollard estuary, report of the European project HARBASINS, www.nlwkn.niedersachsen.de/wasserwirtschaft/nordseekueste/FSK/kuesteningenieurwesen/2008c
- LECHER, K.; LÜHR, H.P. and ZANKE, U.C.E.: Taschenbuch der Wasserwirtschaft. Berlin, 2001.
- VERBOOM, G.K.; DE RONDE, J.G. and VAN DIJK, R.P.: A Fine Grid Tidal Flow and Storm Surge Model of the North Sea. Parey Verlag, Cont. Shelf Res., Vol. 12, 213-233, 1992.
- ZANKE, U.C.E.: Hydromechanik der Gerinne und Küstengewässer. Berlin, 2002.

Modelling Large Scale Sediment Transport in the German Bight (North Sea)

Manfred Zeiler, Peter Milbradt, Andreas Pliß and Jennifer Valerius

Summary

The main objective of the multidisciplinary research project “AufMod” (2009-2012) was the development of model-based tools for analyzing long-term sediment transport and morphodynamic (MD) processes in the German Bight. AufMod aimed at bringing together marine geoscientists and coastal engineers to build up consistent bathymetric and sedimentological databases and to compare different numerical models using the same data input and model grid with respect to uncertainties in their results.

AufMod provides a suite of consistent annual bathymetries as well as initial sediment parameters which can be used by numerical MD models for further analyses. Different patchy datasets from bathymetric survey campaigns since 1948 have been compiled and have undergone a sophisticated postprocessing procedure to overcome inconsistencies arising from the use of different echosounding techniques, vessels, tidal correction and so on. For the first time, data on grain size distribution have been composed for the entire North Sea including the German Bight in order to analyze geomorphological processes and to calculate sediment input parameters for morphodynamic modelling. By establishing a so-called “Functional Seabed-Model” consistent annual bathymetries and initial sediment distribution and composition (grain size distribution) have been made available together with their spatial and temporal uncertainties.

The morphodynamic numerical model simulations cover a time span from 1996 to 2008. They are based on natural processes and take account of the whole variability of tides, external surge, river run-off, wind and waves. “AufMod” provides a suite of consistent annual bathymetries as well as initial sediment parameters which can be used by numerical MD models for further analyses. By using the same model grids the strength and weakness of the different numeric models can be evaluated and their uncertainties can be assessed. The morphodynamic model results provide a first comprehensive impression of the resulting sediment transport pathways in the German Bight.

Further model runs have focused on the sensitivity of sediment transport and the morphological response due to wind forcing, mean sea level rise and variation in porosity.

Keywords

North Sea, German Bight, sediment mixture, sediment distribution, porosity, bathymetry, sediment transport, morphodynamic, numerical modelling, mean sea level rise

Zusammenfassung

Der Aufbau von integrierten Modellsystemen (AufMod) zur Analyse der langfristigen Morphodynamik in der Deutschen Bucht war Ziel des KFKI-Verbundforschungsvorhabens (Laufzeit: 2009-2012). Aus-

löser hierfür war eine im Jahr 2008 durchgeführte Ausschreibung des KFKI mit einer detaillierten Anforderungsliste.

Im Projekt wurde sehr frühzeitig die Entscheidung getroffen, ein umfassendes softwaregestütztes Bodenmodell zu generieren, das die Daten zur Bathymetrie und Sedimentbeschaffenheit gemeinsam verwaltet und funktional, d. h. nach spezifischen Vorgaben, verarbeiten und dem Anwender anforderungsgerecht zur Verfügung stellen kann (Funktionales Bodenmodell).

Die Betrachtung der Sedimentprozesse in der Deutschen Bucht kann nicht ohne die Berücksichtigung der Prozesse in der gesamten Nordsee erfolgen. Deshalb wurden auch umfangreiche Daten der Anrainerstaaten akquiriert und in das Funktionale Bodenmodell übernommen. Die großräumigen und langfristigen Sedimentbewegungen sind auch von lokalen, teilweise zeitlich beschränkten Prozessen beeinflusst. Deshalb fokussierte sich das Funktionale Bodenmodell auf bestimmte Gebiete: den Schelf bzw. das Küstenvorfeld, den Vorstrandbereich, die Bereiche von Inseln und im Wattenmeer.

Im Rahmen der Anwendung deterministischer Prozessmodelle wurde ein konsequenter Multi-Modell-Ansatz mit Simulationsmodellen unterschiedlicher Prozessauflösung verwendet, um die Streubreite der Ergebnisse abschätzen zu können. Für die Modelle, welche auf unstrukturierten Modellverfahren basieren, wurden überwiegend identische Gitternetze und Randwerte verwendet. Soweit möglich, wurde auch ein einheitliches Post-Processing durchgeführt, um den Vergleich der Modellergebnisse mit einheitlichen Methoden zu gewährleisten.

Abschließend wurde eine gemeinsame Synthese erarbeitet, die alle relevanten Ergebnisse der Teilprojekte einbezieht und eine übergreifende, gemeinsame Bewertung zur Beantwortung der in der KFKI-Ausschreibung formulierten Ziele erstellt.

Schlagwörter

Nordsee, Deutsche Bucht, Sedimentverteilung, Sedimentzusammensetzung, Porosität, Bathymetrie, Topographie, Sedimenttransport, Morphodynamik, Numerische Modellierung, Meeresspiegelanstieg

Contents

1	Introduction	371
2	Study site.....	372
3	Data base	373
3.1	Sediment data.....	373
3.2	Bathymetric data.....	375
3.3	Hydrodynamic and meteorological data.....	377
4	Functional seabed model	378
5	Numeric modelling toolbox	383
5.1	Model domain (grid)	383
5.2	Boundary conditions	384
5.3	Model calibration and validation	384
5.4	Sensitivity studies	385
6	Sediment transport in the German Bight.....	386
6.1	Sediment transport paths.....	386

6.2	Sediment balance	388
7	Conclusion	389
8	References	390

1 Introduction

A better understanding of the morphodynamic processes along the German North Sea coast is crucial for coastal defense, cost-effective maintenance of shipping lanes and planning of coastal infrastructure (e.g. submarine cables) as well as, more recently, environmental assessment in the context of implementing EU directives. The German Coastal Engineering Research Council (KFKI) consequently published a call for proposals in 2008 focusing on enhanced numeric modelling of relevant large-scale and long-term sediment transport pathways, including their directions and mass budgets. The AufMod R&D project was conducted by a multi-disciplinary research group under the leadership of the Federal Waterways Engineering and Research Institute (BAW) from 2009 until 2012. Its purpose was to develop an integrated model system for analyzing the long-term morphodynamics in the German Bight (North Sea).

The multidisciplinary research project AufMod (German acronym for “Model-based analysis of long-term morphodynamic processes in the German Bight”) was funded by the Federal Ministry of Education and Research (BMBF) to investigate long-term sediment transport and morphodynamic processes. The project focuses on the German Bight, located in the southeastern part of the North Sea. AufMod takes a combined data-based and process-based modelling approach to investigate long-term sediment transport.

The research group comprised the Federal Waterways Engineering and Research Institute (BAW), the Federal Maritime and Hydrographic Agency (BSH), the Christian-Albrechts-University of Kiel, the University of Bremen, the University of the Federal Armed Forces Munich, Senckenberg Institute Wilhelmshaven and smile consult GmbH, Hannover.

The principal goals of AufMod were

- to establish to the greatest extent possible a consistent and plausible database with respect to bathymetries and physical sediment properties and to provide these for third parties beyond the lifetime of the project;
- to build up and develop a morphodynamic modelling toolbox including tides, waves, and wind-induced currents;
- to analyze different scenarios of sea level rise with respect to climate change; and
- to share the treated data for online publishing in cooperation with the R&D-project Marine Infrastructure in Germany (MDI-DE) in an information model.

One main scientific objective of AufMod is to identify processes and effects which are relevant to long-term sediment transport and the morphodynamic reaction of the sea bed. The concept of the AufMod project implied the observation of the compartments air, water, and seabed (e.g., meteorological, hydrodynamic and sediment data), the analysis of morpho- and sediment dynamic processes using data-based and process-based models and the allocation of the results (products) via an integrated spatial data infrastructure (Fig. 1).

The “Functional Seabed Model” FSM was initially set up to build a consistent bathymetric and sediment database, to test the suite of numeric morphodynamic models which are used in AufMod, including aspects of validation, and to facilitate critical discussion of first results, namely sediment transport pathways in the German Bight from different model runs. AufMod takes a combined data-based and process-based modelling approach to the investigation of long-term sediment transport.

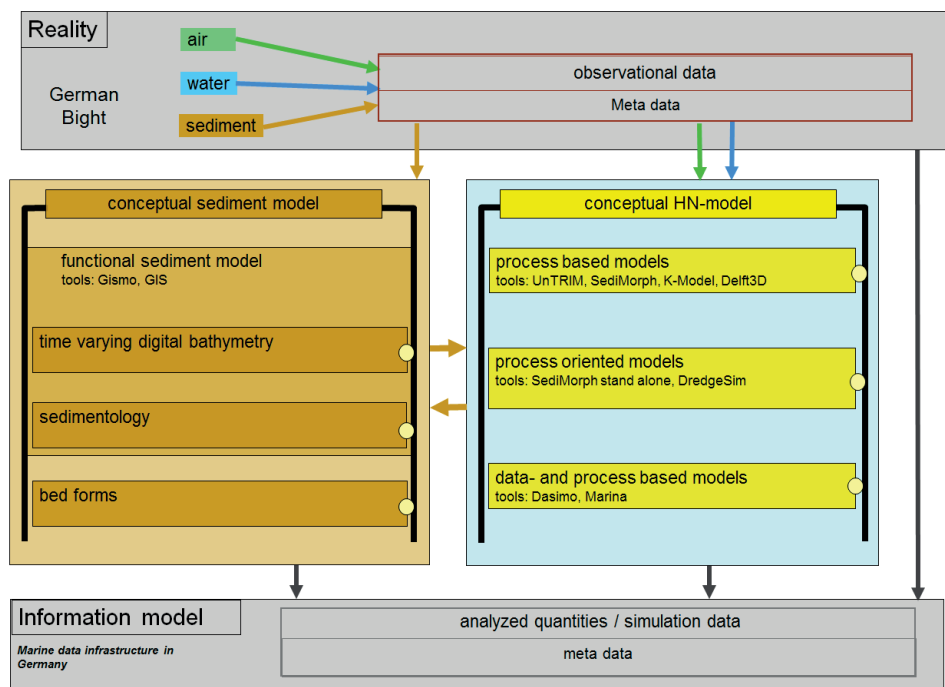


Figure 1: Conceptual model of AufMod.

2 Study site

The project focuses on the German Bight, which is located in the southeastern part of the North Sea where semidiurnal tides enter from the west (The Netherlands) and propagate counter clockwise along the coastline of the German Bight towards the Danish waters under the influence of Coriolis accelerations. The tidal range varies from app. 1.5 m (Islands Borkum and Sylt) to app. 3.5 m (in the Elbe river mouth).

The seabed is dominated by different sand deposits which are prone to sedimentation and erosion under the recent hydrodynamic regime. Coarser sediments occur in the tidal channels, where current speed reaches up to 1.5 m s^{-1} . Coarse sands and gravels also occur in some parts of the shelf, where they represent relict sediments of the Saalian glaciation and/or fluvio-glacial sediments from the Weichselian.

3 Data base

The database for all investigations can be characterized using the data from the seabed which is needed to describe physical sediment properties (e.g., grain size distribution, porosity, ...), bathymetry over several years and bed forms. Different datasets were therefore compiled and assessed in AufMod:

1. sedimentological data,
2. bathymetry data,
3. hydrodynamic and meteorological data and
4. model results after model set-up, running and interpolation as well as interpretation.

3.1 Sediment data

The following parameters were relevant for morphodynamic modelling:

1. grain size analyses of surface sediments,
2. porosity,
3. thickness of the mobile sand layer and
4. content of organic matter in muddy sediments.

Table 1: Sources of sedimentological datasets.

Data	Source	#	Spatial Extent	Temporal Extent
MUDAB - grain size distributions	BSH	25.309	North Sea	1924-2008
WADABA - grain size distributions	Helmholtzzentrum Geesthacht	1.449	German Wadden sea	1987-2003
Grain size distributions Spiekeroog	Research institute Senckenberg am Meer, Wilhelmshaven	941	Shore face Spiekeroog	1986-1989, 2005
Grain size distributions Great Britain	British Geological Survey (BGS), Nottingham, Great Britain	15.946	North Sea sector Great Britain	
Grain size distributions Netherlands	Geological Survey of the Netherlands (TNO), Utrecht, The Netherlands	6.619	North Sea sector Netherlands	1969-2006
Grain size distributions Norway	Norges geologiske undersøkelse (NGU), Trondheim, Norway	129	Skagerrak	1992-1994
Interpolated medians of grain size distributions Belgium	Royal Belgian Institute of Natural Sciences, Brussels, Belgium	250m-Grid	North Sea sector Belgium	
Grain size distributions Belgium	Royal Belgian Institute of Natural Sciences, Brussels, Belgium	3.468	North Sea sector Belgium	1984-2009
Grain size distributions Denmark	GEUS, Copenhagen, Denmark	215	North Sea	2000-2008
Grain size distributions Denmark	Danish Coastal Authority, Ministry of Transport and Energy, Denmark	215	North Sea sector Denmark	2010
GPDN - grain size distributions	Geopotential Deutsche Nordsee (BSH, BGR, LBEG), Germany	1.363	North Sea sector Germany	2008-2011
SedDB (Küste) – grain size distributions	BfG, Koblenz, Germany	4.949	Elbe-, Jade-, Weser-, Ems-estuary	1982-2009
Grain size distributions Sedimentatlas Waddenzee	Waterdienst (Rikswaterstaat, Ministerie van Infrastructuur en Milieu), Lelystad, Netherlands	7.502	Wadden sea of the Netherlands	1989-1997
Grain size distributions Offshore Windfarms licensing procedures	BSH (confidential), Germany	4.383	North Sea sector Deutschland	2000-2008
FeDaBa - grain size distributions	BfG, Koblenz, Germany	3.163	Elbe-, Jade-, Weser-, Ems-estuary	1980-2012
GROBEKART - grain size distributions	AWI, Germany	4.373	Shelf of Schleswig-Holstein	2004-2011

The grain size analyses cover the German Bight in a quite high spatial resolution of one half to one nautical mile. In contrast to the bathymetric database, hardly any time series

are available (Tab. 1). The grab samples were collected over a time span of app. 90 years; most of them between 1960 und 1970. Fig. 2 depicts the sample locations together with the individual data sources. Grain size data were made available for the whole North Sea area. The particle size distributions are stored as a sum curve in a logarithmic scale, according to their resolution. The individual grain size fractions of the cumulative particle distribution are interpolated using linear or constrained cubic spline interpolation (KRUGER 2004).

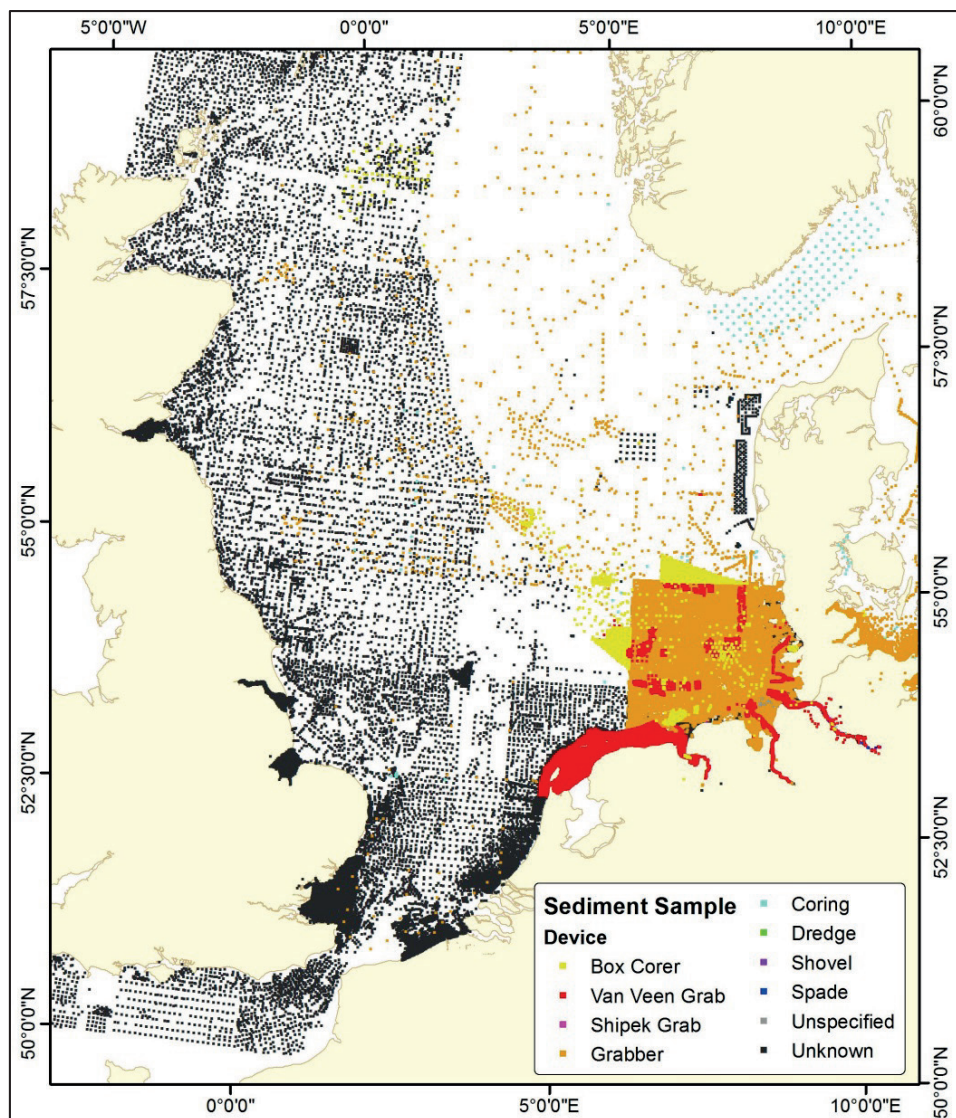


Figure 2: Locations of grain size data in the North Sea.

Hardly any porosity data is available for the German North Sea, especially for sandy sediments. Porosity of marine sands in the tidal flats of the inner German Bight ranges by about 40 % (FÜCHTBAUER and REINECK 1963). Porosity measurements were carried out for fine-grained sediments in the Elbe-Weser estuary during the AufMod project.

Fig. 3 illustrates data points on the thickness of the mobile sand cover, which is used as a proxy for the available sediment budget. These data result from previous R&D projects and geological mapping programs.

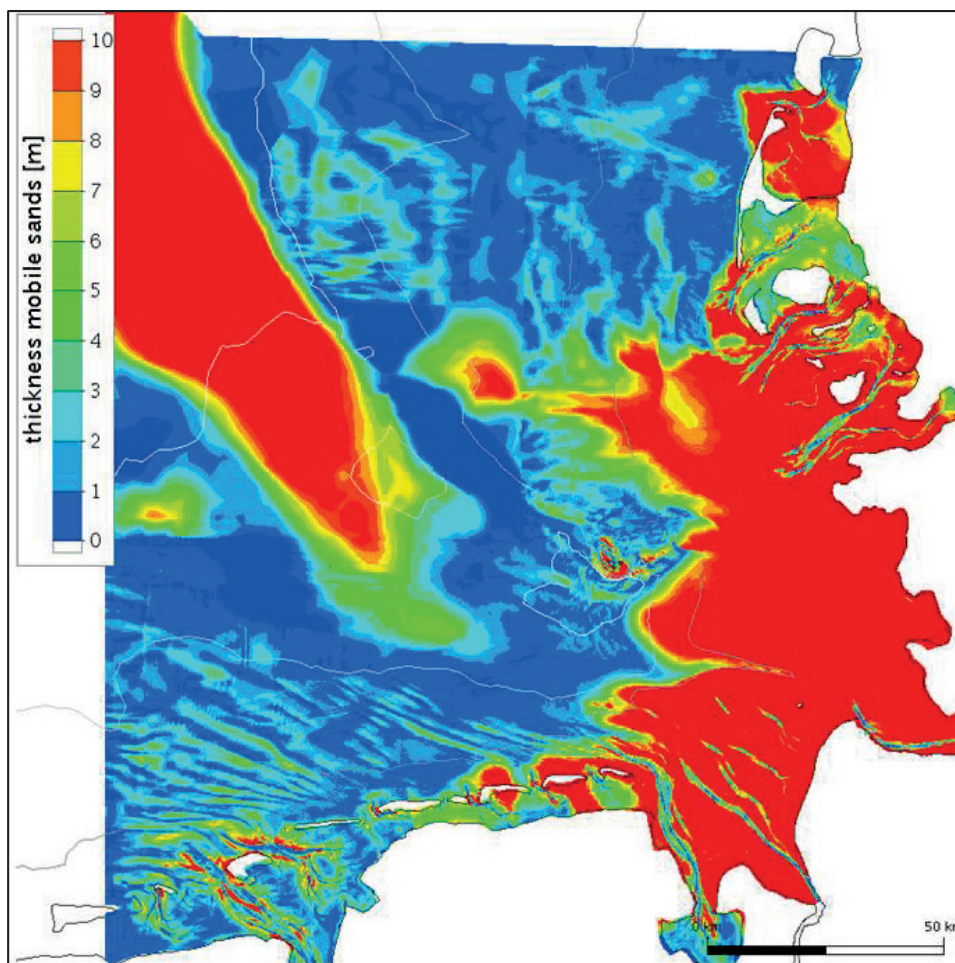


Figure 3: Thickness of the uppermost sediments (mobile sand cover and Holocene sediments) in the German Bight.

3.2 Bathymetric data

To describe the changes of the bathymetry we considered the digital terrain model as a continuous function $z(x,y,t)$ in space and time. This digital bathymetric model in space and time is represented by discrete survey points and associated interpretation methods.

The first step was to compile bathymetric data from the different data sources (Tab. 2). Fig. 4 illustrates the spatial and temporal distribution of the different bathymetric surveys which have been subject to the quality assessment of the hydrographic survey requirements; most of them have been performed in the Elbe, Weser and Ems estuaries and, subsequently, within the shallow waters down to 20 m of water depths in different time intervals.

In the next step the bathymetric database was enhanced with relevant metadata in order to describe the survey data in a comprehensive manner. The spatial confidence region, the temporal confidence interval, the accuracy of measurement and the recommended interpolation method are specified in the metadata for each data set, for example.

In total, 1.7 billion data from more than 16,000 bathymetric surveys have been compiled in this way covering a time span from 1948 to 2012.

Table 2: Suppliers of bathymetric data.

Source	Spatial Extent	Temporal Extent
BSH	German North Sea	1983-2012
BSH	Digitized operating sheets of hydrographic surveys for different subareas of the German North Sea	1974-1979
KFKI-Project 03KIS308	Digitized operating sheets of hydrographic surveys for different subareas of the German North Sea	1948-1982
WSA Bremen	Weser	2008-2009
WSA Bremerhaven	Weser estuary, Jade Bight	1996-2009
WSA Cuxhaven	Elbe estuary up to the north west of Helgoland	1990-2012
WSA Emden	Ems estuary	1990-2011
WSA Tönning	Channels of the North Frisian Wadden Sea	1990-2010
WSA Wilhelmshaven	Shipping channel of the Jade, area around Spiekeroog and Wangerooge	1996-2012
NJWKN	Northern beach area of Juist and Langeoog	1983-2007
LKN-SH	Base map of the Wadden Sea	1935-2012
Landesvermessungsamt Schleswig-Holstein	ALS - data for the Wadden Sea (Schleswig-Holstein)	2005/06
British Oceanographic Data Centre	Digital Elevation Models of the North Sea	1998, 2008
Danish Hydraulic Institute	Digital Elevation Models of the North Sea	2003, 2009
Kystdirektoratet/The Danish Coastal Authority	Danish Wadden Sea, Blavandshuk to Hindenburgdamm	2008
Senckenberg am Meer, Wilhelmshaven	Shore face of Spiekeroog	2003, 2007
JadeWeserPort Logistics Zone GmbH & Co.KG	Jade	2010

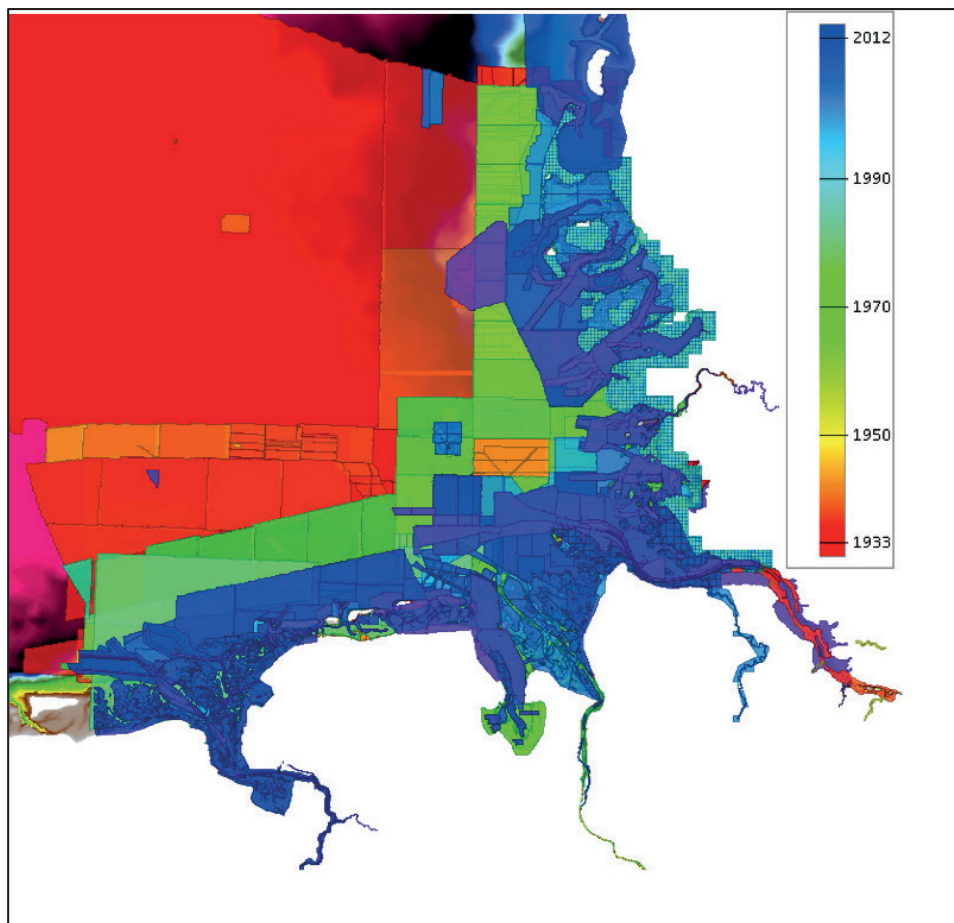


Figure 4: Spatial and temporal extent of bathymetric surveys in the German Bight (North Sea) used for morphodynamic analyses.

3.3 Hydrodynamic and meteorological data

Meteorology and hydrodynamics are the driving forces of the morphodynamic in the German Bight. Hydrodynamic and morphodynamic models as well as morphodynamic analysis require information about the time varying water levels along the open (seaward) boundary, river discharge quantities and wind velocities in time and space in addition to bathymetry and sediment data:

- Water levels: The tidal signal was derived from the global tide model FES2004.
- Run off from measurements in the German Bight and long-time means for the other river discharges from analysis.
- Wind fields are taken from forecast weather model runs by the German Weather Forecast Service (DWD).

4 Functional seabed model

The term “Functional Seabed Model (FSM)” is introduced to describe a database for morphodynamic analyzes which include data-based models of annual bathymetries and sediment properties for any location and time within the study site. Moreover, the FSM also depicts the temporal evolution of the seabed. The two-dimensional models of the annual bathymetries and sediment properties were generated by appropriate interpolation and approximation methods (MILBRADT 2011).

At present, the FSM provides information on:

- topography (bathymetry),
- thickness of the mobile sediment layer,
- porosity,
- grain size distribution,
- organic matter content,
- resistance of consolidated sediments and
- bedforms.

Firstly, the Functional Seabed Model consists of a time-invariant model (so-called “background layer”) which comes into operation for interpolation or approximation when survey data are missing for a specific site. The topographic background layer includes the model grid of BAW for the North Sea and summarizes bathymetric data up to 1989. The background layer of the sediment thickness dates back to 1985 and has been estimated, via the depth of erosion between the years 1985 and 2009, to be at least 1 m. Porosity was set to 25 %, organic matter to 5 %. The FSM suggests that consolidated sediment underlies the mobile sand cover which itself cannot be mobilized.

Cumulative grain size distributions are typically used in the FSM. A representative distribution of d50 (median) based on the combination of grain size data from BSH and model runs was modelled for the background layer. This resulted in a consistent d50 layer, especially in the estuaries and in the tidal flats for which grab samples are not available in a sufficient spatial resolution.

Secondly, the FSM embodies a time-variant module which was developed using a multi database system. It produces annual digital terrain models (Fig. 5) to provide the user with quasi-synoptic topographies from the coastline down to a water depth of app. 20 m. Moreover, each annual bathymetry is linked with layers for spatial uncertainty, e.g. spatial confidence (Fig. 6) and minimum distance with respect to the dataset in time.

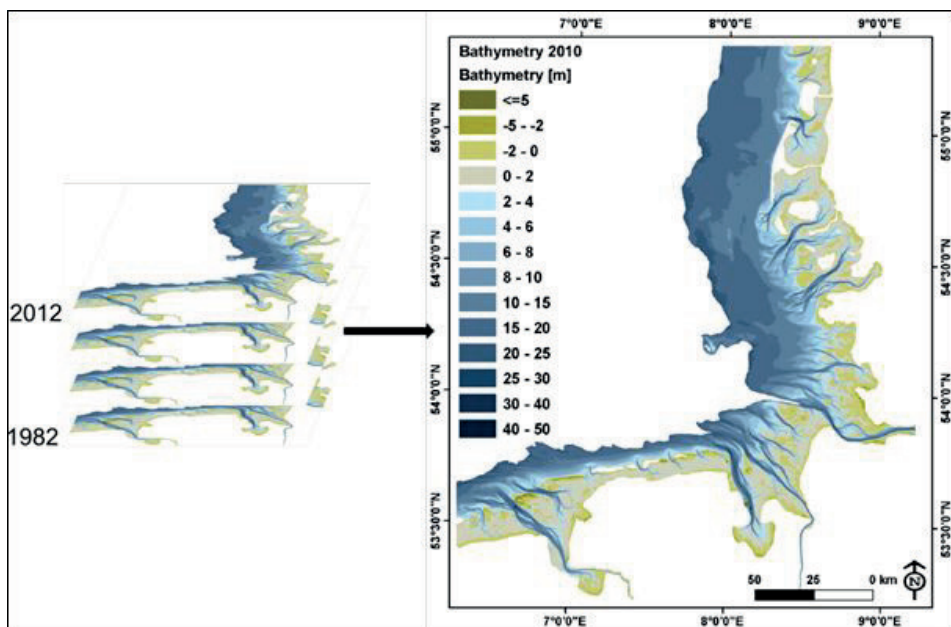


Figure 5: Example for an annual bathymetry (digital terrain model) and layers for spatial and temporal uncertainty.

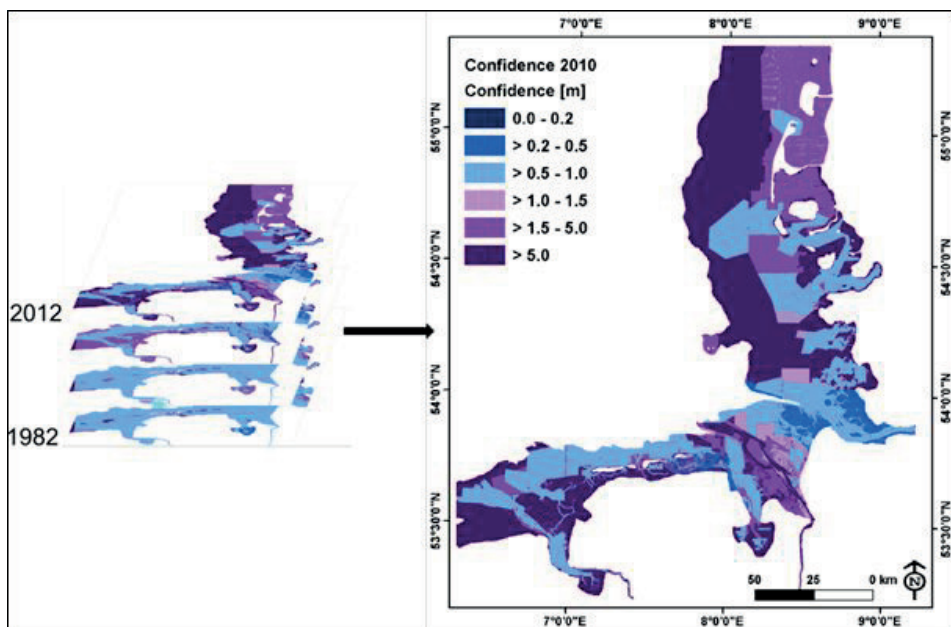


Figure 6: Spatial confidence for annual bathymetry shown in Fig. 5.

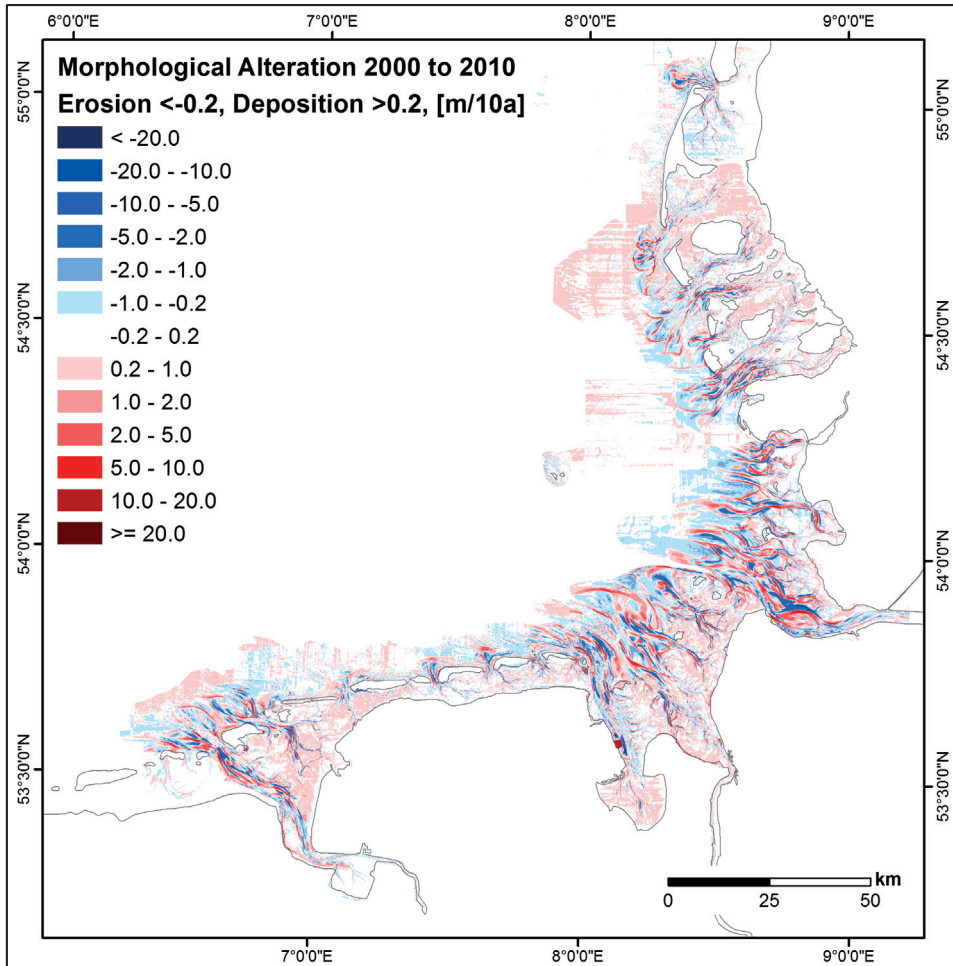


Figure 7: Example for morphologic alteration based on annual bathymetries.

The annual topographies are the prerequisite for modelling further datasets on the temporal evolution of the seabed:

- morphologic alteration (Fig. 7), e.g. topographic differences for 1, 5, 10, 30 years,
- morphologic space (Fig. 8), e.g. difference of the historically highest and lowest water depth at each location over distinct time intervals (5, 10, 30 years) and
- morphologic drive (Fig. 9), e.g. difference of maximum and minimum annual depth change for distinct time intervals (5, 10, 30 years).

The distribution of statistical parameters, derived from the cumulative grain size distribution, was modelled for sediment properties, e.g. median (Fig. 11) or sorting (Fig. 10) as well as different grain size classes. These parameters are helpful in at least analyzing sediment dynamics on the shelf beyond 20 m of water depth, where bathymetric time series are scarce and even morphological changes are with the range of uncertainty of the survey data.

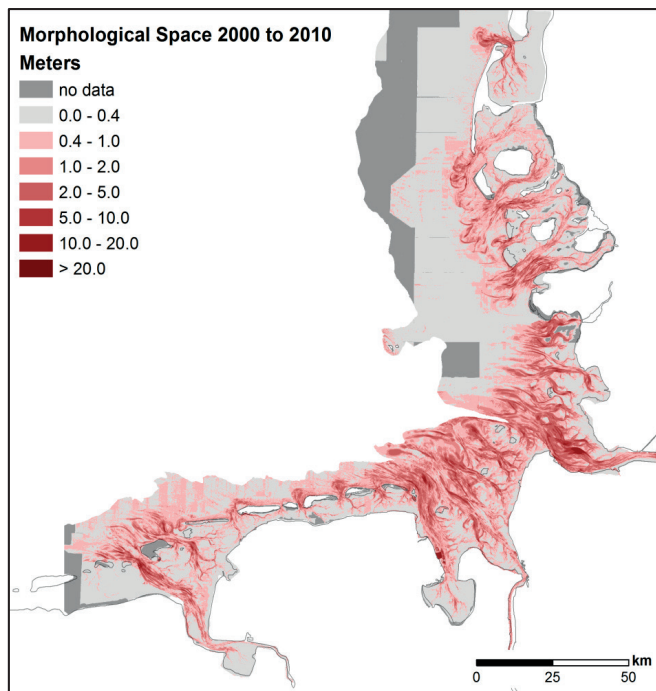


Figure 8: Example for morphologic space based on annual bathymetries.

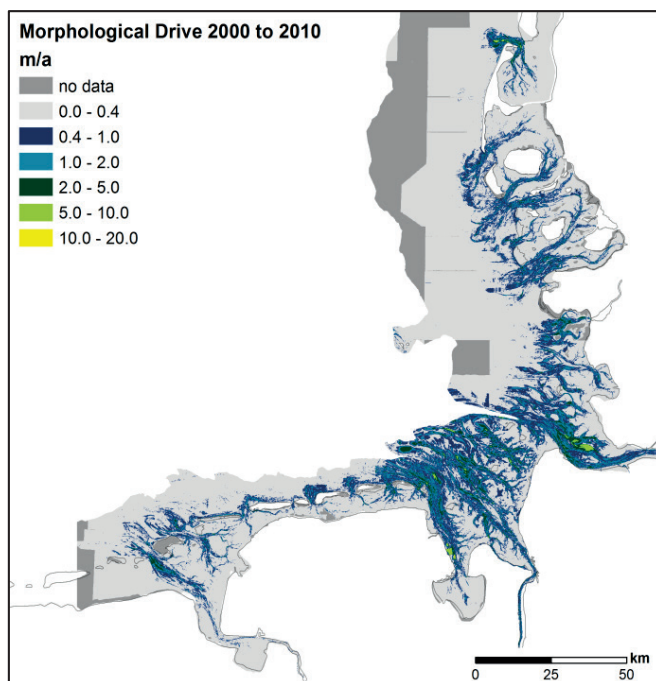


Figure 9: Example for morphologic drive based on annual bathymetries.

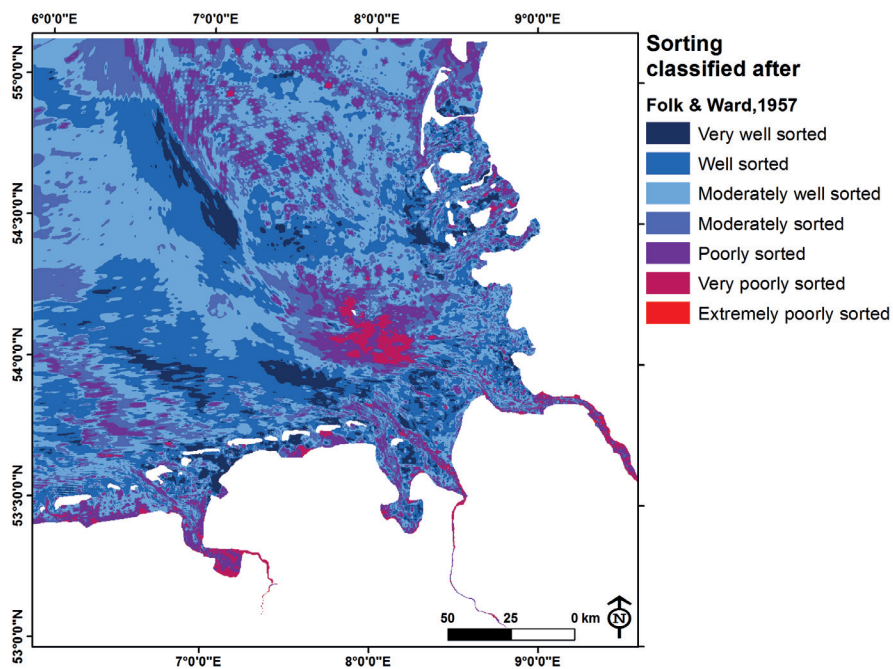


Figure 10: Sorting of surface sediments in the German Bight (North Sea).

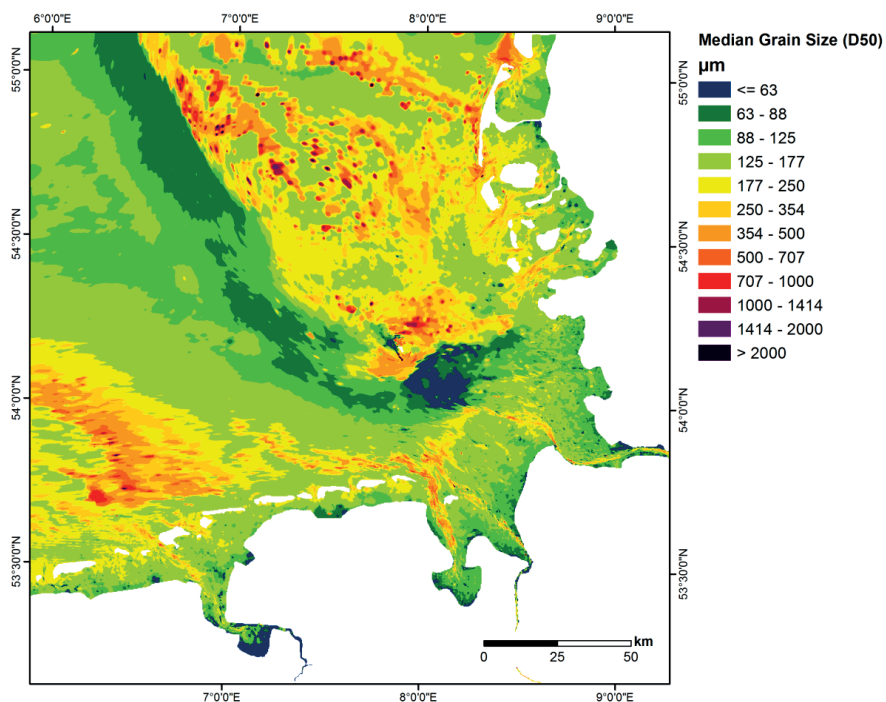


Figure 11: Median grain size (D50) of surface sediments in the German Bight (North Sea).

5 Numeric modelling toolbox

Numerical simulation models have been established in recent decades as a prognostic engineering tool for the evaluation of large-scale sediment transport conditions in the German Bight, with a focus on the effects of:

- pending climate change,
- offshore renewable energy systems and their connection to the mainland and, last but not least,
- the safety and efficiency of navigation

It is important to bear in mind that the operation of morphodynamic simulation models is still subject to considerable uncertainty and that development work is still ongoing on both models and field measurement methods.

In the context of using deterministic numerical models within AufMod a consistent multi-model approach was established as a numerical toolbox (Tab. 3). These models apply different process resolutions in order to estimate the spread of the results. All models were set up to cover the entire North Sea, including a finer grid resolution for the German Bight. Sediment transport due to tidal currents, wind-driven circulation and waves were taken into account.

Table 3: Modelling systems used in AufMod.

Time scale	Hydrodynamics	Waves	Morphodynamics
Short-term Day – 12 month	MARINA	MARINA	MARINA
Medium-term 1 – 10 years	UnTRIM DELFT3D-FLOW	UnK SWAN	SediMorph DELFT3D-MOR
Medium-term 1 – 10 years Long-term 10 – 100 years	TELEMAC	TOMAWAC	SISYPHE

5.1 Model domain (grid)

The numerical toolbox encompassed the hydrodynamic and sediment transport modelling systems applying one domain (grid): UnTRIM2007 (CASULLI and ZANOLLI 2002), TELEMAC (HERVOUET 2000) and MARINA (MILBRADT, smile consult) (Fig. 12 left) and a two model domain concept operated by DELFT3D (LESSER et al. 2004; Fig. 12, right). In order to represent well determined meteorological and tidal conditions, all models were forced with the same boundary conditions for water level, river discharges and wind.

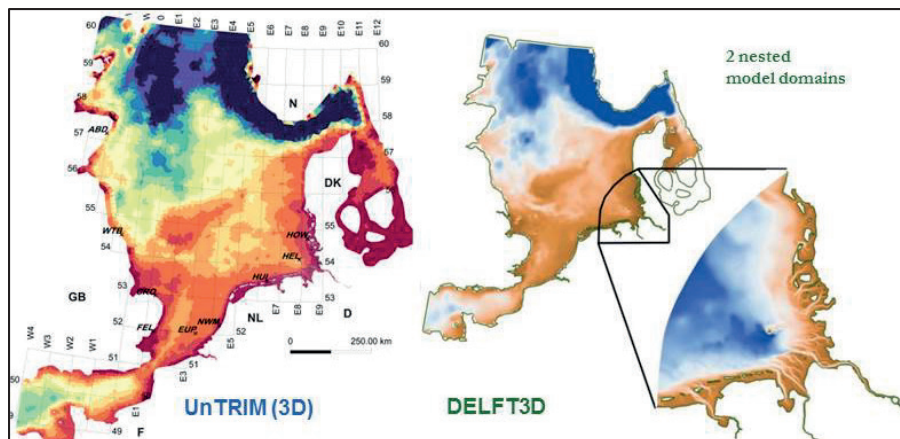


Figure 12: Model domain of the North Sea: UnTRIM, TELEMAC and MARINA (left) and a nested model of the North Sea and German Bight for DELFT3D (right).

5.2 Boundary conditions

The boundary conditions applied for all model runs are the same for all model systems in AufMod. An overview for this is given in Fig. 13.

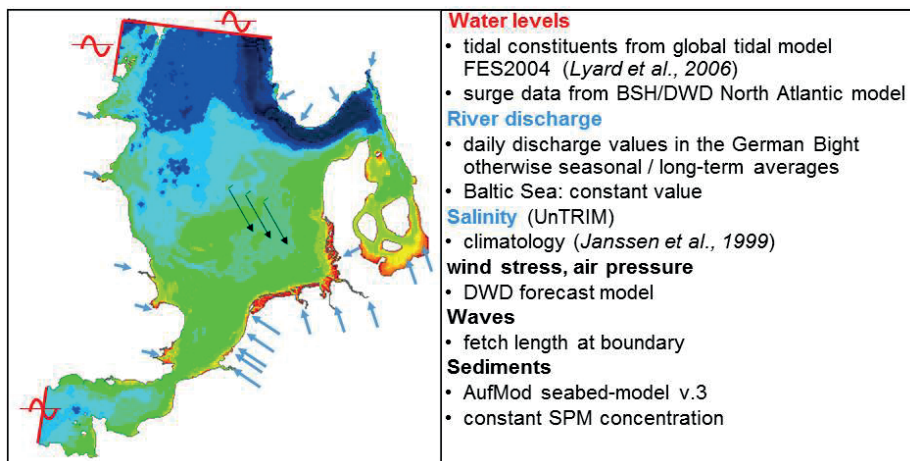


Figure 13: Boundary conditions for all model runs used in AufMod.

5.3 Model calibration and validation

The process of calibration and subsequent validation of morphodynamic simulation models has been operated in several steps.

An analysis of the uncertainties of the measured basis data was developed before initiating a basic model calibration. This was also the case for the measured data used for validation purposes. The inaccuracy of data throughout the whole data flow (measurements

and modelling) provided the range and variation of the model parameterization for the model calibration. The model results must fall within the scope of uncertainty in the destination parameters of the calibration and validation.

The plausibility of the morphodynamic model components was checked using regular measurements of the seabed in connection with adequate spatial and temporal interpolation methods. Besides volumetric analysis of seabed evolution, bed forms and changes in the sediment mixture are also relevant.

An example of the validation of hydrodynamic model components is the documented comparison of measurements with simulation results for waves and water levels (M2-components). Given that there was a large number of a different model results available, only two comparisons were documented for waves and water level (harmonic analysis: M2-tide), see Fig. 14.

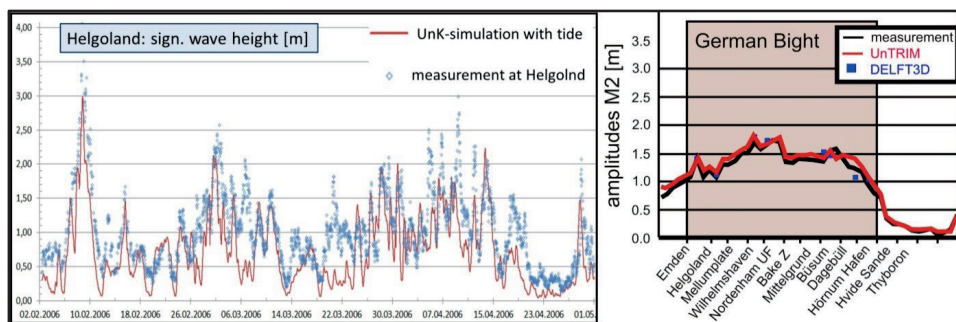


Figure 14: Comparison measurements / calculation (left: waves / right: water level).

Sediment transport cannot be acceptably validated simply by comparing measured data at certain locations. The measurement methods and uncertainties concerning the interpretation of the data, as well as the scarce availability of spatiotemporal data, cannot be directly compared with the model results themselves.

To ensure the plausibility of the morphodynamic model constituents three main parameters are taken into account:

1. morphologic space,
2. volumetric changes of the bathymetry and
3. histograms of sediment volume / mass transport.

5.4 Sensitivity studies

Miscellaneous sensitivity studies were set up to investigate the influence of sediment transport and morphodynamic relating to the

- influence of wind / wave action (KÖSTERS and WINTER 2014),
- porosity (PLÜB and KÖSTERS 2014),
- sediment mixture (VALERIUS, KÖSTERS and ZEILER 2014),
- long term simulations (PUTZAR and MALCHEREK 2012; PUTZAR and MALCHEREK 2014; MILBRADT 2011), and
- mean sea level rise (PLÜB and Kösters 2014).

6 Sediment transport in the German Bight

The sediment transport quantities are charged from different sources. Beneath the estuary discharges into the German Bight the exchange with adjacent regions of the North Sea are considerable. Several studies have been performed in the past to estimate wide area sediment transport within the North Sea and the German Bight. Fig. 15 shows the basic results.

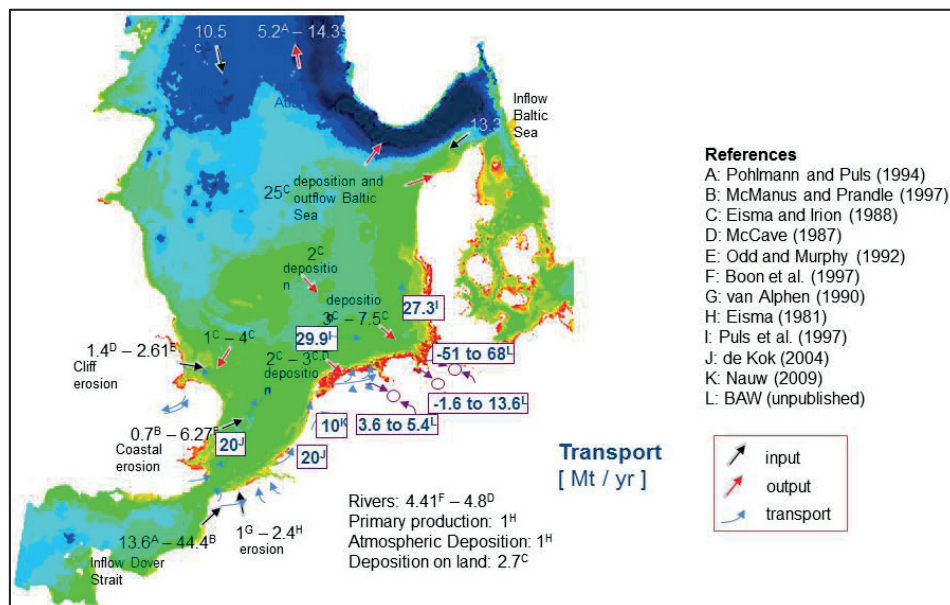


Figure 15: Estimation of sediment transport budgets in the literature.

6.1 Sediment transport paths

Identifying sediment transport paths in the German Bight was one of the main targets in AufMod. The sediment transport paths were calculated from the vectors of the resulting total transport (suspended and bed-load sediment transport) for the year 2006, including the wave effect. Fig. 16 shows the sediment transport paths in the southern North Sea calculated by TELEMAC (A), MARINA (B) and UnTRIM (C), as well as the mean value resulting from these different simulation runs (D).

The basic trend of the movement of sediment from west to east seaward of the West- and East Frisian coast is shown. Mixed inconsistent transports predominate within the inner German Bight (Jade, Weser, Elbe estuary up to approximately Helgoland). On the western part of the North Frisian coast the vectors deviate widely seaward in a northerly direction. A left-turning circulation arises in the area between Wash and Doggerbank.

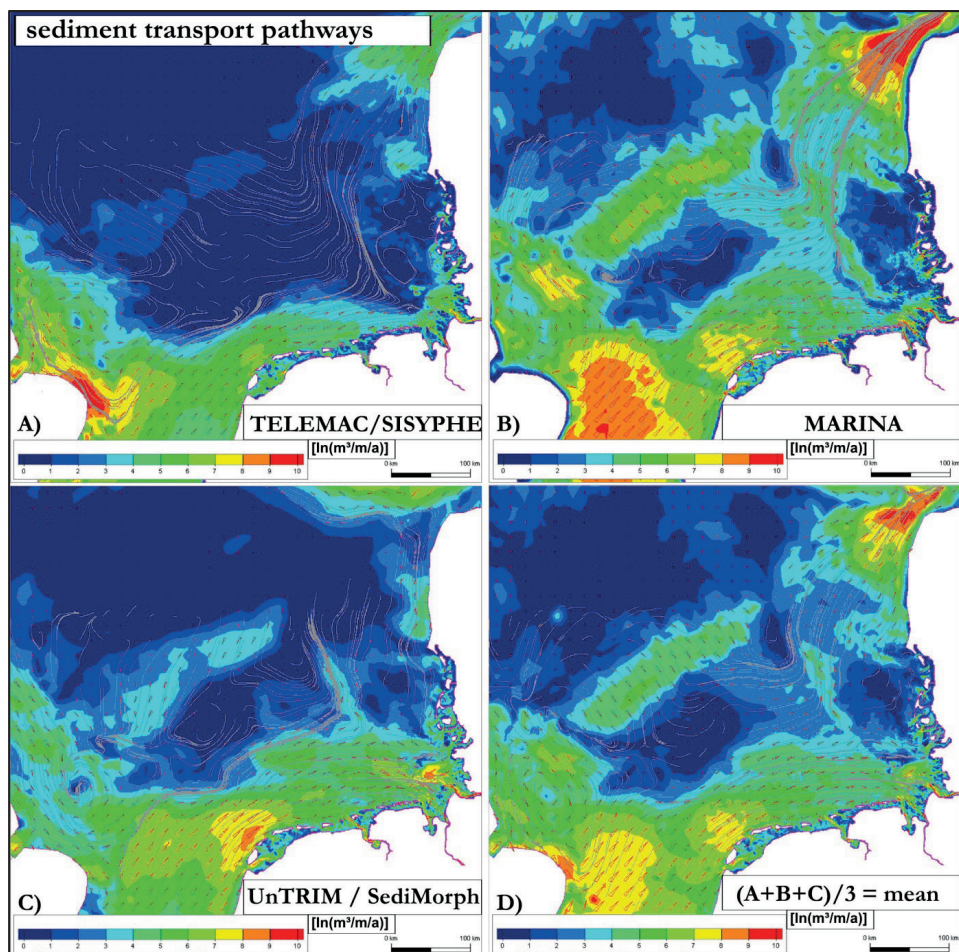


Figure 16: Sediment transport pathways from different model systems and mean value of them.

The shape and position of the sediment transport pathways proved relatively stable over the various years of simulation. The deficiency of sediment in the region of the North Frisian Islands (northern part of the German Bight) is especially apparent in all model results.

The variability of the sediment transport pathways is considerably higher in the outlet regions of the German estuaries owing to the complex bathymetric situation and the river run off which has a marked influence on sediment transport. Fig. 17 documents the mean sediment transport pathways for the mouth of the Elbe estuary for the year 2000 (top panel) and for 2010 (lower panel).

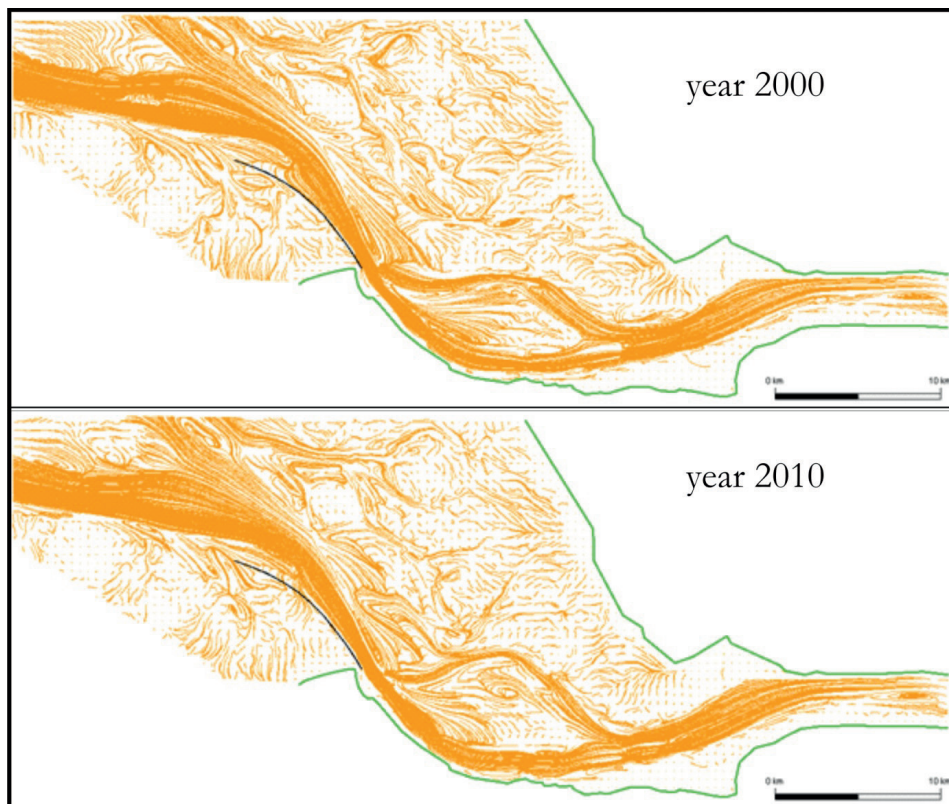


Figure 17: Characteristic sediment transport pathways in the mouth of the Elbe estuary for the year 2000 and 2010.

6.2 Sediment balance

The net sediment transport quantity entering and leaving the German Bight was estimated by defining analysis profiles to integrate the sediment mass over one year as a balance.

Fig. 18 shows these results for three different model investigations: Un-TRIM (red: 1996-2007), TELEMAC (green: 1998 and 2006) and MARINA (light blue: 2006). Compared with the duration [d] of high wind (> 18 m/s) at Helgoland, there is a remarkably clear correlation between transport and wind.

The export of sediment mass from the German Bight is one order of magnitude smaller than the input. No results for the exchange with the estuaries are available due to the relatively coarse spatial grid resolution of the numeric models. These exchange quantities are consequently not well incorporated to the mass balance.

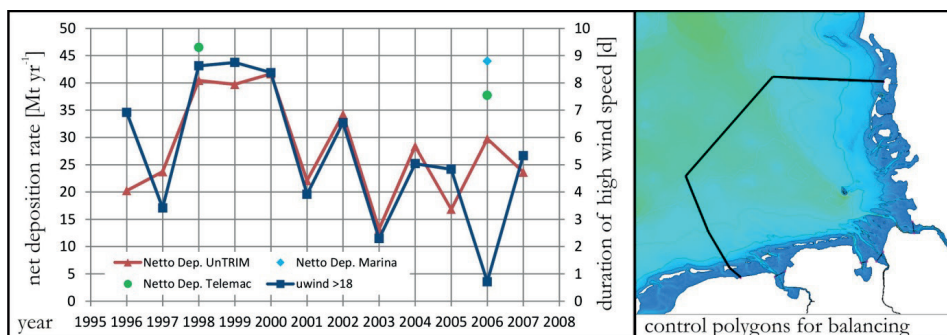


Figure 19: Net sediment deposition integrated over the boundary of the German Bight derived from UnTRIM (red), TELEMAC (green) and MARINA (light blue) and duration of high wind (> 18 m/s) at Helgoland – control sections for balancing are marked in the right panel.

The highest net deposition quantity of the investigated yearly simulations is 42 Mtyr⁻¹. This amount is only reproduced in other years to a 1/2 or 1/3 amount. The comparison of the different model results shows e.g. for the year 1998 a relatively good agreement (40.5 - 46.5 Mtyr⁻¹). In 2006 the difference is distinct (30 Mt/a - 44 Mtyr⁻¹).

The comparison with the duration of high wind speed shows a predominantly large correlation with the net deposition quantity. This suggests that meteorological forcing has a strong effect in relation to the magnitude and direction of the residual velocities / transport in the German Bight.

The depth variable distribution of the net transport mass is of special interest. Detailed analyses show that a predominant portion is transported in a depth range of between 10 - 20 m. The transport rates behind the East Frisian Islands, on the wadden area towards the coast, are noticeably smaller.

7 Conclusion

There are many reasons why the assessment of morphological conditions in the German Bight is associated with great uncertainties. The measuring techniques and field data in themselves fail to provide a reasonably sufficient level of accuracy. Of course, all models are based on numerous simplifications, and simulation models as such are also restricted due to the numerical approximation of physics and the limitations (construction, evolution ...) of computer systems.

It will only be possible to obtain greater confidence concerning the reproduction, analysis and prediction of sediment transport and morphodynamics in the German Bight within a multidisciplinary approach. This integrated concept provides a broad consistent dataset for future analyses and numeric modelling of morphodynamic processes in the German Bight.

Uncertainty can be reduced by adopting a multi-model approach to data and process based simulation models. The application of different spatial and temporal model improvements, as well as miscellaneous physical approximations in different modelling systems, will also improve the accuracy of the overall findings.

The process-based modelling approach enables large area circulation and sediment transport processes in the entire German Bight to be simulated and analyzed. This is

essential in order to stipulate seaward boundary conditions when setting up estuary modelling. Model simulation results show a high level of local variability of magnitude and direction in overall cyclonic coastal sediment transport in the German Bight. Furthermore, the model results suggest an equivalent effect of the tidal-driven sediment transport in contrast to the overall transport based on tides, winds and waves.

It is not possible at present to provide reliable validation of the transported sediment mass on the basis of the available measurement data. A quantitative analogy with geological analysis confirms the overall role of the German Bight as a net deposition area of sediment. The models used predict a net deposition rate of between 13 and over 46 Mtyr⁻¹. To date this balance does not show the interaction between the coastal and estuarine transport process very well.

The sediment deposition rate is closely linked with current variable meteorological forcing. Future research should consider the influence of dredging and dumping activities in the outer estuaries which are crucial for the net deposition rate.

The morphodynamic studies of AufMod also show large variation between the various simulation results. Evaluation of the AufMod project is limited, however, by the uncertainty in the measurement data in space and time. Further development of morphodynamic modelling, especially for the effects of interactions between the coast and estuaries, presents an ongoing challenge for future research projects.

An elaborated final report, which includes all the results from the various institutions, is also available (HEYER and SCHROTTKE, 2013).

8 References

- BOON, J., VAN DER KAAIJ, T., VOS, R.J., GERRITSEN, H.: Modelling of suspended particulate matter (SPM) in the North Sea. Model set-up and first sensitivity analysis. Delft Hydraulics Research Report, Z2025, 1997.
- CASULLI, V. and ZANOLLI, P.: Semi-Implicit Numerical Modelling of Non-Hydrostatic Free-surface Flows for Environmental Problems. *Mathematical and Computer Modelling*, 36, 1131–1149, 2002.
- DE KOK, J.M.: Slibtransport langs de Nederlandse kust. Bronnen, fluxen en concentraties. RIKZ/OS/2004.148w, 2004.
- EISMA, D.: Supply and deposition of suspended matter in the North Sea. In: Nio, S.D., Schüttenhelm, R.T.E., Van Weering, T.C.E. (Eds.), *Holocene Marine Sedimentation in North Sea Basin*. Spec. Publ. Int. Assoc. Sedimentol. 5, 415-428, 1981.
- EISMA, D. and IRION, G.: Suspended matter and sediment transport. In *Pollution of the North Sea -An Assessment*, eds. W. Salomons, B.L. Bayne, E.K. Duursma and U. Förstner, Springer, 20-35, 1988.
- HERVOUET, J.M. and BATES, P.: The TELEMAC Modelling System. *Special Issue of Hydrological Processes* 14, 2000.
- HEYER, H. and SCHROTTKE, K.: Aufbau von integrierten Modellsystemen zur Analyse der langfristigen Morphodynamik in der Deutschen Bucht – AufMod <http://edok01.tib.uni-hannover.de/edoks/e01fb14/780783271.pdf>, doi: 10.2314/GBV:780783271, 2013.

- KÖSTERS, F. and WINTER, C.: Exploring German Bight coastal morphodynamics based on modelled bed shear stress. *Geo-Marine Letters*, 34, 21-36, doi: 10.1007/s00367-013-0346-y, 2014.
- KRUGER, C.J.C.: Constrained Cubic Spline Interpolation for Chemical Engineering Applications. (<http://www.korf.co.uk/spline.pdf>), 2004.
- LESSER, G. R.; ROELVINK, J. A.; van KESTER, J. A. T. M. and STELLING, G. S.: Development and validation of a three-dimensional morphological model. *Coastal Engineering*, 51, 883-915, 2004.
- MCCAIVE, I.N.: Fine sediment sources and sinks around the East Anglian Coast (UK). *Journal of the Geol. Soc. London*, 144, 149-152, 1987.
- MILBRADT, P.: Sedimenttransport und Morphodynamik in der Deutschen Bucht. *Die Küste*, 78, 33-58, ISSN 0452-7739, 2011.
- MILBRADT, P.; KÖSTERS, F.; PUTZAR, B. and PLUESS, A.: Analyse morphodynamischer Veränderungen auf der Basis zeitvarianter digitaler Bathymetriem. *Die Küste*, 80, 2014.
- MCMANUS, J.P., PRANDLE, D.: Development of a model to reproduce observed suspended sediment distributions in the southern North Sea using Principal Component Analysis and Multiple Linear Regression. *Continental Shelf Research*, 17 (7), 761-778, 1997.
- NAUW, J.J. and RIDDERINKHOF, H.: Slibtransport door het Marsdiep op basis van veerbootmetingen (Ferry based observations of the total suspended matter transport in the Marsdiep inlet), project nr. RKW-1700, NIOZ report 2009-7, 2009.
- NAUW, J.J., GERKEMA, T., WIELSMA, E., VAN DER VEGT, M., BRINKMAN, B. and RUARDIJ, P.: Comparison between ADCP data and GOTM in the North Sea within "Wadden Sea ecosystem data assimilation and integrated modeling", ZKO symposium (Texel, 2009-03-09), 2009.
- ODD, N.V. and MURPHY, D.: Particulate pollutants in the North Sea. Calibration of a 20 km gridded 3D model simulating a representative annual cycle of mud transport. H. R. Wallingford, Report SR 292, 15 pp., 1992.
- PLUESS, A.: Das Nordseemodell der Bundesanstalt für Wasserbau, Dienststelle Hamburg *Die Küste*, 67, 83-128, ISBN 3-8042-1058-9, 2003.
- PLUESS, A. and KÖSTERS, F.: Morphodynamic modelling for the entire German Bight: an initial study on model sensitivity and uncertainty. *Advances in Geoscience*, 39, <http://edok01.tib.uni-hannover.de/edoks/e01fb14/780783271.pdf>, doi: 10.5194/adgeo-39-61-2014, 61-68, 2014.
- POHLMANN, T. and PULS, W.: Currents and transport in water. In: SÜNDERMANN, J. (ed.) *Circulation and contaminant fluxes in the North Sea*. Springer-Verlag Berlin Heidelberg New York, 345-402, 1994.
- PULS, W.; HEINRICH, H. and MAYER, B.: Suspended Particulate Matter Budget for the German Bight, *Marine Pollution Bulletin*, 34, 6, 398-409, PII: s0025-326X(96)00161-0, 1997.
- PUTZAR, B. and MALCHEREK, A.: Development of a Long Term Morphodynamic Model of the German Bight. In: BOURBAN, S.; DURAND, N. und HERVOUET, J.-M. (Hrsg.): *XIXth TELEMAC-MASCARET Users Conference*, 2012.
- PUTZAR, B. and MALCHEREK, A.: Entwicklung und Anwendung eines Langfrist-Morphodynamikmodells für die Deutsche Bucht. *Die Küste*, 80, 2014.

- RICKLEFS, K. and ASP, N.: Geology und Morphodynamics of a Tidal Flat Area along the German North Sea Coast. *Die Küste*, 69, 93-127, 2005.
- SCHROTTKE, K. and ABEGG, F.: Near-Bed Suspended Sediment Dynamics in a Tidal Channel of the German Wadden Sea. *Die Küste*, 69, 353-368, 2005.
- VALERIUS, J.; KÖSTERS, F. and ZEILER, M.: Erfassung von Sandverteilungsmuster zur großräumigen Analyse der Sedimentdynamik auf dem Schelf der Deutschen Bucht. *Die Küste*, 80, 2014.
- VAN ALPHEN, J.S.L.J.: A mud balance for Belgian-Dutch coastal waters between 1969 and 1986. *Netherlands Journal of Sea Research*, 25 (1/2), 19-30, 1990.
- ZEILER, M.; SCHULZ-OHLBERG, J. and FIGGE, K.: Mobile sand deposits and shoreface sediment dynamics in the inner German Bight (North Sea). *Marine Geology*, 170, 363-380, 2000.
- ZEILER, M.; SCHWARZER, K. and RICKLEFS, K.: Seabed Morphology and Sediment Dynamics. *Die Küste*, 74, 31-44, 2008.
- WINTER, C.: Macro scale morphodynamics of the German North Sea Coast. *Journal of Coastal Research*, 64, 706-710, 2011.

On SPM Dynamics in the Turbidity Maximum Zone of the Weser Estuary

Frank Kösters, Iris Grabemann and Reiner Schubert

Summary

The estuarine turbidity maximum zone (ETM) of high suspended sediment concentration is highly variable on different time scales. As the ETM is closely linked to river siltation problems, an improved understanding can help to optimise sediment management within the estuary. Variability on intratidal, spring-neap and river discharge-related (seasonal) time scales is reviewed based on data from older measurements and recent monitoring and compared with modelling results. Previous results describing intratidal dynamics as a cyclic process of advection, deposition and resuspension are corroborated. Strong coupling is evident between the ETM and the mixing zone, not only on the intratidal movement but also as a shift of both in reaction to changes in river discharge. Spring-neap variations are mainly evident as changes in suspended sediment concentration and small changes in the ETM extension.

Keywords

suspended sediment transport, Weser estuary, estuarine turbidity maximum, mixing zone

Zusammenfassung

In der Trübungszone eines Ästuars schwanken die hohen Schwebstoffkonzentrationen auf unterschiedlichen Zeitskalen. Da mit der hohen Schwebstoffkonzentration auch hohe Sedimentationsraten und eine Verschlickung von Hafenanlagen verbunden sein können, ist ein umfassendes Systemverständnis zur Optimierung des Sedimentmanagements notwendig. Auf der Basis von zurückliegenden Messkampagnen und Daten aus Dauermessungen wird die Variabilität der Trübungszone auf intratidalen Zeitskalen, dem Spring-Nipp-Zyklus und verbunden mit Änderungen des Oberwasserabflusses (saisonale Zeitskala) untersucht und mit Modellergebnissen verglichen. Vorhergehende Ergebnisse, die die intratidale Variabilität als zyklischen Prozess aus Advektion suspendierten Materials, Deposition und Resuspension beschreiben, werden auf Basis der aktuellen Ergebnisse bestätigt. Eine starke Kopplung von Brackwasserzone und Trübungszone ist nicht nur auf der intratidalen Zeitskala sichtbar, sondern auch auf längeren Zeitskalen als Reaktion auf geänderte Oberwasserabflüsse. Der Spring-Nipp-Zyklus zeigt sich in den Schwebstoffkonzentrationen, die bei Springtide deutlich größer sind als bei Nipptide, und geringfügig in der Ausdehnung der Trübungszone.

Schlagwörter

Schwebstofftransport, Weserästuar, Trübungszone, Brackwasserzone

Contents

1	Introduction	394
2	Regional setting	395
3	Materials and methods	397
3.1	Measurements	397
3.2	Numerical modelling system	398
4	Results and discussion	398
4.1	Intratidal variability	399
4.2	Spring-neap variability	401
4.3	River discharge-related variability	403
5	Summary and conclusions	405
6	Acknowledgements	406
7	References	406

1 Introduction

In estuaries like the Weser estuary (Germany), large amounts of sediment are resuspended, transported and partly deposited during every tidal cycle frequently resulting in the development of regions of relatively high suspended particulate matter (SPM) concentration. These estuarine turbidity maximum (ETM) zones are often associated with high siltation rates. As an example, DE NIJS et al. (2009) have shown for the port of Rotterdam that tidal variations in the ETM location are the dominant mechanisms in harbour siltation. In the Weser estuary, SCHROTTKE et al. (2006) found fluid mud formation in the ETM region potentially affecting the nautical depth in the navigational channel. The ETM region of a river may therefore require a high level of dredging of muddy sediments, as shown e.g. in LANGE et al. (2008) for the Weser estuary.

Discussion of the dynamics of the ETM have to distinguish between different processes and time scales. ETM formation processes on seasonal to multi-annual time scales result in the accumulation of mud deposits while sub-tidal to tidal time scales describe the dynamics of the ETM once local sediment sources are present. The generation and maintenance of the ETM are related to different mechanisms which vary in their impact on particular estuaries as well as in different environmental conditions (e.g. high or low river discharge) in a specific estuary. "These processes include the residual "estuarine gravitational circulation" due to the near bottom inflow of salty water (e.g. FESTA and HANSEN 1978) and the net upstream transport of sediments resulting from higher flood peak velocities than ebb peak velocities ("tidal pumping", e.g. OFFICER 1981) and due to changes in vertical mixing efficiency during times of stratification ("tidal mixing asymmetry", e.g. JAY and MUSIAK 1994). In some estuaries a second ETM can develop further upstream of the mixing zone (e.g. in the Ems estuary, TALKE et al. 2009). A general overview of the relevant processes is given in e.g. DYER (1997).

For the Weser estuary, the importance of local sediment sources and their resuspension within the tidal cycle has already been pointed out by WELLERSHAUS (1982) and the intratidal displacement of material has been described in detail by RIETHMÜLLER et al.

(1988) and GRABEMANN and KRAUSE (1989) based on measurements and corroborated by LANG et al. (1989) and LANG (1990) using a numerical model. On longer time scales, the position of the ETM in the Weser estuary varies together with the mixing zone forced by changes in river discharge (GRABEMANN and KRAUSE 1989, GRABEMANN and KRAUSE 2001). Although river discharge-related changes have been observed, to date they have not been reproduced in numerical models for the Weser estuary.

The ETM dynamics of the Weser estuary on different time scales are reviewed in the following based on previous research, analysis of new measurements and on numerical modelling results. The main focus is on intratidal SPM displacement, spring-neap variability and on river discharge-related changes in the position of the ETM. This study corroborates previous results which were based only on measurements with process studies illustrating ETM variability on different time scales.

2 Regional setting

The Weser estuary (Fig. 1), which is located in the southeastern North Sea, is a generally well-mixed meso- to macrotidal estuary. The upper reach of the Weser estuary (km 0-65) from Bremen to Bremerhaven has a channel-like character and has been repeatedly deepened in the past to its present minimum depth of about 9 m below German nautical chart datum (SKN -9 m) in the navigation channel (see review by LANGE et al. 2008). The outer Weser estuary (km 65-120) is funnel-shaped and characterised by two main tidal channels, extensive tidal flats and numerous smaller tidal channels and creeks. The western channel has been permanently stabilised for navigation by the construction of training works and groynes and is kept at a minimum depth of about SKN -14 m. Outside of this artificially stabilised area strong morphological changes can be observed (e.g. DIECKMANN 1989).

Surface sediments in the navigational channel are sand dominated. In the outer Weser estuary the river bed consists mainly of fine to medium sands, in the lower estuary of medium to coarse sands. A noticeable exception is the region between km 55 and km 66 which is dominated by mud (median grain size $<63 \mu\text{m}$) consisting of silt and clay with variable amounts of organic matter. This transect is part of the region from about km 45 to about km 70 in which the ETM typically occurs. The composition of sediments varies temporally in the mud stretch. On tidal time scales patches of fluid mud can form (SCHROTTKE et al. 2006) and on longer time scales the silt content can vary; i.e. after times of high river discharge the silt fraction is reduced.

The long-term mean (average for the years 1970 to 2010) discharge (MQ) is $325 \text{ m}^3/\text{s}$; the long-term mean of the annual minimum (MLQ) and maximum discharges (MHQ) are $117 \text{ m}^3/\text{s}$ and $1220 \text{ m}^3/\text{s}$, respectively, measured at the gauge station Intschede 32.5 km upstream of the tidal weir (DEUTSCHES GEWÄSSERKUNDLICHES JAHRBUCH 2013). An analysis of daily discharge values for 1955-2012 shows that the most frequent discharge is about $150 \text{ m}^3/\text{s}$; 50 % and 75 % of the time the discharge is between $100 \text{ m}^3/\text{s}$ and $250 \text{ m}^3/\text{s}$ and between $100 \text{ m}^3/\text{s}$ and $400 \text{ m}^3/\text{s}$, respectively.

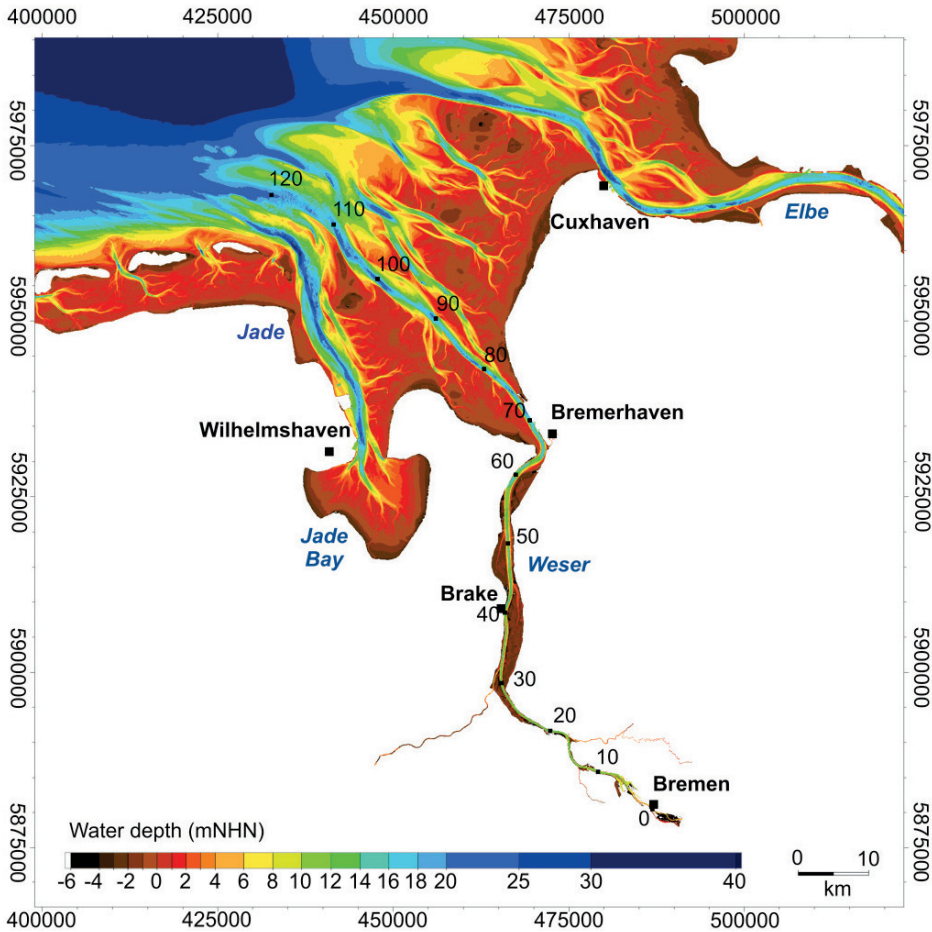


Figure 1: Morphology of the Weser estuary. Numbers along the main shipping channel denote the distance from the Wilhelm-Kaisen-Bridge (“Große Weserbrücke”) about 5 km downstream of the weir in Bremen.

The long-term mean SPM concentration of the river water for the years 1970 to 2010 is 38 g/m^3 (DEUTSCHES GEWÄSSERKUNDLICHES JAHRBUCH 2013). Thus, the long-term mean fluvial input of suspended sediment into the estuary is about 450 tons per half tide. On an annual time scale it varies strongly. The amount of suspended sediments entering the estuary from the adjacent sea is unknown, but upstream movement of marine material across the freshwater-saltwater interface (FSI) has been detected (e.g. IRION et al. 1987). Within the ETM, the SPM concentration increases with depth for most of the tidal cycle (e.g. RIETHMÜLLER et al. 1988, Figs. 3 and 4; see also Fig. 2 in this section). The SPM concentration can exceed 1000 g/m^3 near the bottom. Outside of the ETM region, the SPM concentration is generally less than 50 g/m^3 .

Generally, the ETM is associated with the low-salinity region of the mixing zone. The location of the upstream limit of the mixing zone defined by the tidally averaged freshwater-saltwater interface (FSI), in the Weser commonly defined based on the 2 PSU

isohaline, depends on the river discharge. During times of low river discharge the location of the FSI can occur about 15 km further upstream than in times of MQ (SEIFFERT et al. 2012). For a typical summer situation after several weeks of low river discharge, a snapshot of measured sediment concentrations during flood tide shows the ETM between km 45 and km 65 (Fig. 2).

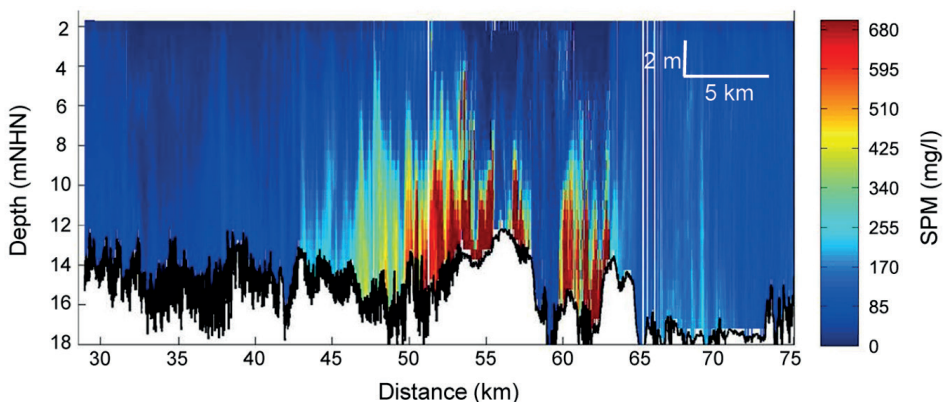


Figure 2: Along-stream transect of SPM concentration in June 2009 during a cruise from Bremerhaven to Bremen at flood tide (AquaVision BV 2009). Note that the measurements were not taken at the same tidal phase.

The locations of the mixing zone and the ETM are also influenced by mean sea-level. In a climate change sensitivity study HOLZWARTH et al. (2011) found an upstream shift of the mixing zone of more than 3 km for an increase of 80 cm in mean sea level and a related upstream shift of the ETM by the same order of magnitude.

3 Materials and methods

3.1 Measurements

The German Waterways and Shipping Administration of the Federal Government (WSA Bremerhaven) is conducting long-term near-surface time series measurements of turbidity which started in 2002 with one station. Since 2011, nine stations have been in operation. Furthermore, in the late 1990s, in 2002 and 2003, time series measurements of turbidity together with salinity and current velocity were undertaken simultaneously in two to three water depths at three to six locations along the estuary over a period of a few weeks with low, mean and high river discharge. For each station, the mean, the 5 % and 95 % percentile turbidity were calculated for chosen river discharge intervals. Based on these station data along the estuary longitudinal transects were derived and subsequently normalized by mean discharge conditions. The extensions of the ETM were estimated from these transects using a threshold normalized turbidity of 0.6. The data analysis was divided into near-surface measurements (for the years 2008-2012 at 8-9 stations, MES_Surf in Fig. 7) and near-bottom measurements (for the years before 2003, MES_Depth in Fig. 7).

3.2 Numerical modelling system

The transport of suspended sediments in the Weser estuary was simulated with the coupled modelling system UnTRIM-SediMorph. The hydrodynamic model UnTRIM (CASULLI and ZANOLLI 2005) uses a finite volume-finite difference method which solves the momentum and transport equations on a horizontally unstructured grid. It was set-up three-dimensionally with a median spatial resolution increasing from about 180 m in the outer estuary to 60 m in the inner parts and a vertically constant resolution of 1 m.

The hydrodynamic model is coupled to the sediment transport module SediMorph, which has been developed at BAW (BAW 2005). Sediment transport is treated for individual size fractions with a given mode of transport either as suspended load or bed load. In this study, suspended sediments are modelled using three different size classes (fine, medium and coarse silt); bed load transport is split into four fractions (fine, medium and coarse sand and gravel). The size of these fractions was chosen according to the Udden-Wentworth scale. Density and porosity are taken to be constant at $2,650 \text{ kg/m}^3$ and 40 %, respectively. Sediments with a diameter larger than gravel, e.g. boulders, are included as gravel and sediments finer than fine silt are included as fine silt. Based on the spatially variable sediment distribution, characteristic values such as the mean grain size are calculated to derive a sediment grain-related roughness. Account is also taken of the form roughness of small scale bed features. SediMorph calculates sediment deposition-erosion and bedload transport based on the bed shear stress obtained from near bed velocity and roughness. Changes in bottom evolution are not taken into account.

The model topography represents the year 2002 in order to be compatible with available measurements to force the model. As the lower Weser estuary is maintained at a given minimum depth and laterally fixed, the changes compared to 2014 are small. However, no account is taken of morphological changes in the outer estuary. The observed composition of sediments at the bed is represented by the seven different sediment fractions described above.

The model is set-up as a process study but realistic forcing is applied. Wind stress at the surface was obtained from the operational German National Meteorological Service (DWD) weather forecast model (COSMO/LM, e.g. DOMS et al. 2002). At the lateral open sea boundaries, water levels from a BAW measurement campaign in 2002 are prescribed. River discharge was included based on daily averages of measurements at the Intschede station about 30.5 km upstream of the tidal barrier (data provided by the Federal Waterways and Shipping Administration). While the model does include salt transport, it does not take heat transport into account. A model validation (BAW 2009) has been successfully performed. The representation of water levels is close to observed values, the mean error of water level amplitude and phase at the individual gauge stations in the Weser estuary is between -15 cm and +12 cm and -23 minutes and +5 minutes respectively.

4 Results and discussion

In the following, SPM dynamics on intratidal, spring-neap and seasonal (changes in river discharge) time scales based on recent measurements and results from numerical simulations are presented and compared with published findings.

4.1 Intratidal variability

On the shortest time scale considered here, suspended sediments are transported within the tidal cycle. On this intratidal time scale, strong variability of SPM is due to the deposition of material over slack waters, subsequent resuspension and depletion of temporarily-formed and spatially-limited deposits during the following ebb or flood, and subsequent transport by tidal currents. This periodic deposition of suspended sediments has been shown in great detail by RIETHMÜLLER et al. (1988) for low river discharge in a specific region of the Weser estuary. GRABEMANN and KRAUSE (1989) have found that this cyclic behaviour is typical for other river discharge conditions also. This cyclic behaviour is also reproduced in the numerical simulations and illustrated for two tidal cycles in Fig. 3. For the chosen river discharge of about 300 m³/s, the simulated ETM is centred around km 64.

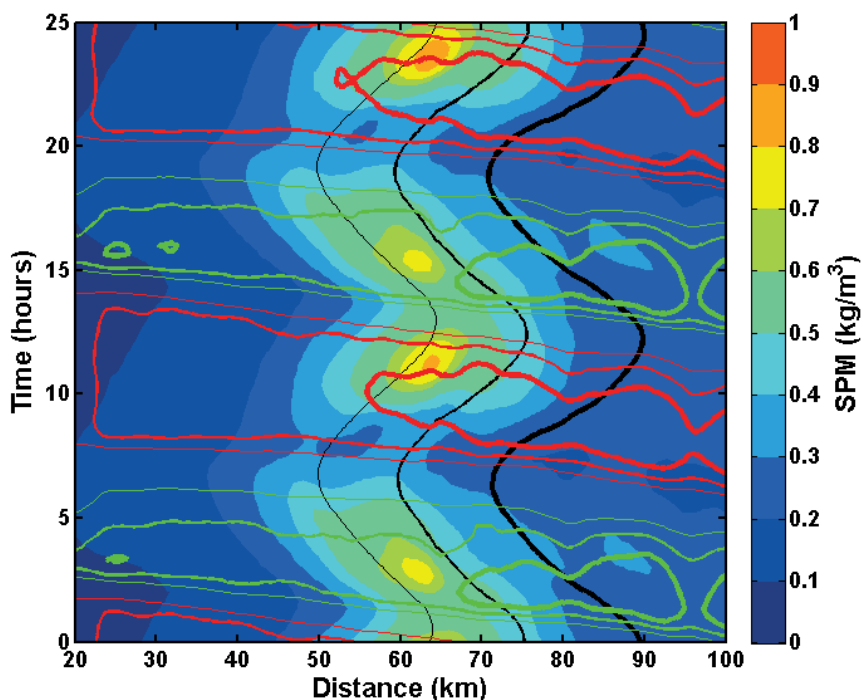


Figure 3: Spatial and temporal distribution of SPM concentrations (colour scale), salinity and current velocities (isolines) based on model results. Salinities of 2, 10 and 20 are shown as black isolines, where higher salinities are represented by thicker lines. Flood and ebb current velocities are shown as green and red isolines, respectively. An increase in line thickness represents an increase of current velocity (0.5 m/s, 0.75 m/s and 1.0 m/s, respectively).

The simulations confirm that the region with increased SPM concentrations moves with the low salinity region of the mixing zone (Fig. 3). High SPM concentrations are commonly located between the 2 and 10 PSU isohalines. The coupling of mixing zone and ETM is consistent with conceptual mechanisms proposed to explain the ETM formation.

BURCHARD und BAUMERT (1998) investigated the relative importance of different mechanisms in a numerical process study for a schematic estuary. They found that gravitational circulation and tidal pumping are the main processes responsible for the formation of the ETM. Moreover, there are also other important baroclinic processes. During ebb tide the fresh river water lies on top of more salty sea water which inhibits vertical mixing whereas during flood tide the water column is destabilized and there is an increase in vertical mixing (e.g. LANG et al. 1989). The term for this process, strain induced periodic stratification (SIPS), was coined by SIMPSON et al. 1990. Changes in vertical mixing efficiency (“tidal mixing asymmetry”) during times of stratification can lead to more efficient up-stream transport when sediment is transported further up in the water column compared to less efficient downstream transport when turbulence is damped by salinity stratification (JAY und MUSIAK 1994).

Simulated high SPM concentrations exceed 800 g/m^3 , which is consistent with observations (e.g. Fig. 2). During slack water the SPM concentration is reduced and suspended sediments are consequently deposited to the ground and eroded again during the following onset of higher current velocities and are then transported up- or downstream. The sediment concentration at one location therefore describes the sum of SPM advected from distant sources and locally eroded material as discussed in detail in GRABEMANN and KRAUSE (1989) based on measurements and in LANG et al. (1989) based on model results.

For average discharge conditions the ETM stretch of the Weser shows ebb dominance in current velocities evident both in measurements and modelling results (Fig. 4). Peak velocities are consistently higher during ebb tide compared to flood tide. For station Nordenham (Fig. 4, upper panel) modelled and measured current velocities match rather well; for station Rechtenfleth (Fig. 4, lower panel) modelled current velocities are consistently higher but show a comparable structure for flood and ebb tide.

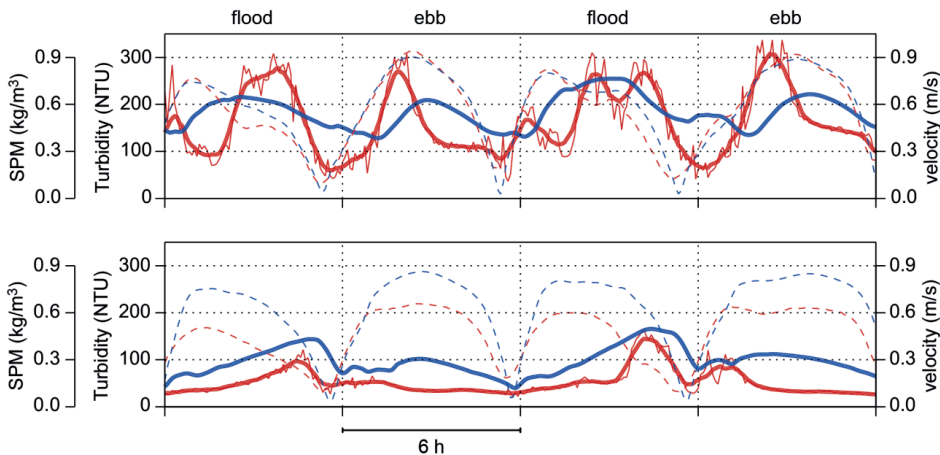


Figure 4: Time series of near-bottom modelled SPM concentration (solid blue line), modelled current velocity (dashed blue line), measured velocity (dashed red line) and measured turbidity (red) at stations Nordenham (km 55.8, upper panel) and Rechtenfleth (km 46.5, lower panel). The thin and thick red lines present the measured turbidity with and without small-scale variability, respectively.

Depending on the position of an observation point in relation to the ETM this leads to different characteristic patterns in SPM time series, as shown in Fig. 4. For average discharge conditions the station Nordenham is near the centre of the ETM (upper panel) and the station Rechtenfleth is near its landward margin (lower panel). In the centre of the ETM (Fig. 4, upper panel), the SPM concentration increases in phase with the current velocity. The signal during flood tide shows a characteristic bimodal form, especially in the measurements. The first peak is probably due to the erosion of local sediment sources and the second peak to advected material which was resuspended further downstream. During ebb tide, material is resuspended with increasing velocity and transported downstream. At the position further upstream (Fig. 4, lower panel), the SPM concentration peak sets in later during flood tide, probably presenting SPM advected from downstream, and early during ebb tide, probably presenting local erosion of sediments which are subsequently transported downstream. This is consistent with the cyclic deposition and erosion behaviour referred to above. A diurnal inequality of the SPM in the ETM exists but is generally not very strong.

Results from simulations and measurements may differ in detail, but they are consistent in the description of the characteristics of SPM concentrations. High flood tide and high ebb tide SPM values are comparable but the duration of high values is longer during flood tide than during ebb tide. This can be seen in the measurements as well as in the simulations. Thus, residual upstream transport of SPM can be expected due to higher sediment concentrations transported over a longer time during flood than during ebb tide.

The comparison of modelled and observed SPM concentration and turbidity shows a similar overall structure but the variability on shorter time scales is underestimated in the model. In nature sediments settle in the water column rapidly by e.g. flocculation and resuspension of flocs and this may lead to the highly variable behaviour observed. The model partly takes into account the effects of flocculation and the breaking up of flocs by treating the settling velocity of sediments as dependent on concentration and shear stress as proposed by MALCHEREK (1995). Yet, the observed variability of SPM concentration could not be fully reached.

4.2 Spring-neap variability

Tidal variations in the Weser estuary are dominated by semi-diurnal components (M_2 , S_2). At the tide gauge station “Alte Weser” (km 115), for example, the mean tidal range is about 2.9 m with a pronounced spring-neap difference of about 70 cm. The variation of the tidal range within a spring-neap-cycle leads to changes in current velocity and thus in bed shear stress. During spring tides higher bed shear stresses are expected and result in higher sediment concentrations (e.g. LANG et al. 1989).

As an example for the effect of an increase in tidal range two different time spans within the simulations are compared (Fig. 5). In order to minimize small-scale effects the model results are spatially averaged over the width of the navigational channel. The difference in tidal range between the two time spans is about 40 cm, which is roughly half the maximum spring-neap tide difference at station “Alte Weser”. The mean water level is also increased by about 20 cm.

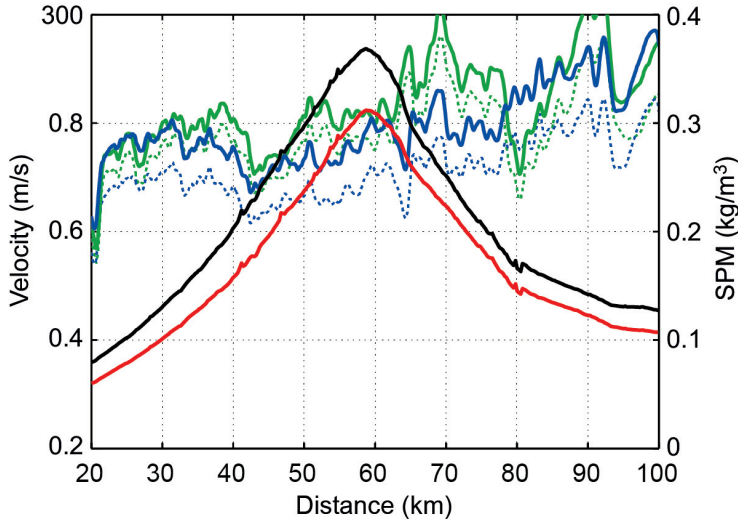


Figure 5: Transects of mean SPM concentrations for a situation with high (black line) and low (red line) tidal range, flood current velocities for high (solid blue line) and low tidal range (dashed blue line) and ebb current velocities for high (solid green line) and low tidal range (dashed green line). Current velocities are averages over ebb or flood tide.

The increase in tidal range (+11 %, average over km 20 - 100) leads to increased mean current velocities, flood velocities are affected more strongly (+13 %) than ebb velocities (+7 %) in this case. Due to higher current velocities mean SPM concentrations increase by about 20 %, thus the region with higher SPM concentrations is extended further up- and downstream. Taking into account that the spring-neap variability of the tidal range can be up to 70 cm at station “Alte Weser” at the mouth of the estuary, the variability of the SPM concentration can be expected to be higher than 20 %.

This assumption is corroborated by time series measurements at e.g. an individual location in the upstream part of the ETM (Fig. 6). In the simulations tidally averaged SPM concentrations are about 50 % higher during spring tide than during neap tide for the averaging time spans in Fig. 6. Similarly, tidally averaged measured turbidity is about 35 % higher during spring tides. For intratidal maximum SPM concentrations (turbidities) spring tide values exceed neap tide values by a factor of about 2 which is consistent with results given in GRABEMANN and KRAUSE 2001.

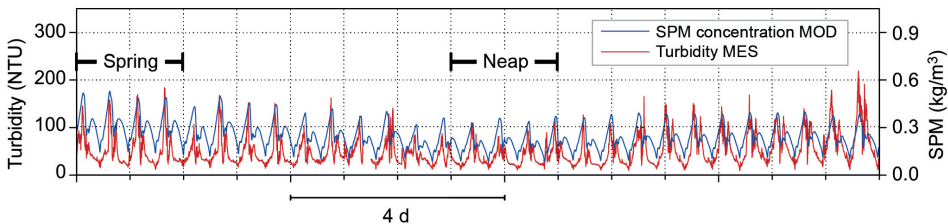


Figure 6: Time series of near-bottom measured turbidity (MES, red) and modelled SPM concentration (MOD, blue) at station Rechtenfleth (km 46.5). Averaging time spans for spring and neap tides are shown by bars.

Overall, significant differences between spring and neap tides exist in the Weser estuary. Different effects on flood and ebb tide velocities suggest changes in sediment dynamics, i.e. the flood to ebb ratio may change. This needs to be kept in mind, when planning or interpreting measurements or trying to obtain representative model results based on just a few tides.

4.3 River discharge-related variability

On longer time scales the redistribution of sediments in the system becomes important. Redistribution of sediments is the result of natural processes, such as tide induced residual upstream transport or the flushing of fines from the estuary during flood events, as well as of anthropogenic impacts, such as the dredging and disposal of sediments from the main navigation channel. Changes in ETM position related to river discharge are shown in Fig. 7.

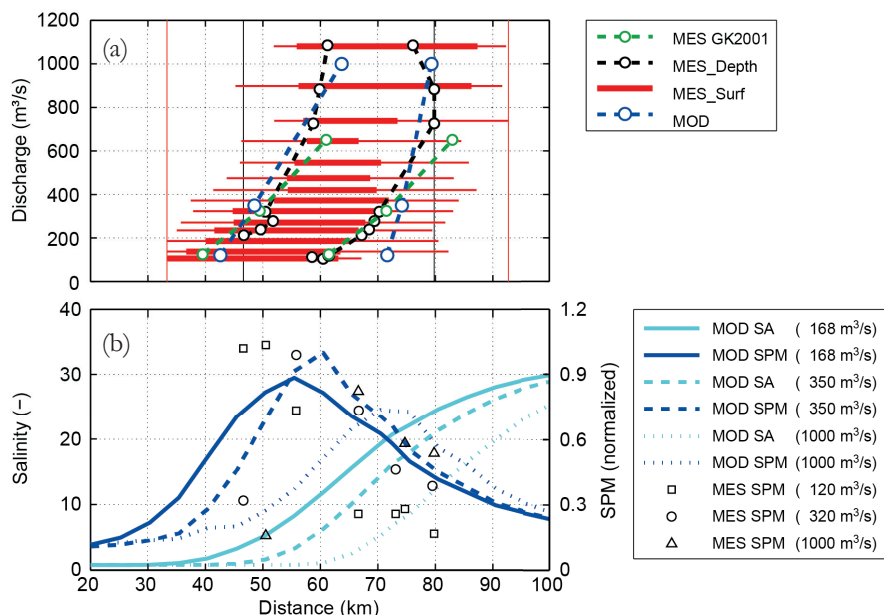


Figure 7: (a) ETM position for different river discharge conditions as obtained from turbidity measurements (MES GK2001: Results from GRABEMANN and KRAUSE (2001), MES_Depth: based on near-bottom data (see section 3.1)), MES_Surf: based on long-term near-surface monitoring data (see section 3.1)) and modelling results (MOD). Although error bars are only shown for MES_Surf based on 5 % and 95 % percentiles of measured turbidity; the other measurements and model results have similar uncertainties. The red and black vertical lines denote the up- and downstream limits of the near-surface and near-bottom measurements, respectively. (b) Tidally averaged salinity and SPM concentration from model results MOD (lines) and measurements MES (symbols). The vertical axis for SPM was normalized by medium river discharge conditions.

The ETM is shifted downstream for increasing river discharge. During low discharge the ETM occurs at about km 40 to 60, during high discharge it is more than 20 km further downstream. The shift of the ETM closely reflects the shift of the FSI. The close cou-

pling of FSI and ETM seen for the intratidal variability (Fig. 3) is also seen here (Fig. 7b). The impact of changes in river discharge depends on the hydrological condition. Under conditions with low river discharge the same change has a larger effect than under conditions with high river discharge. Thus the system is more sensitive to river discharge variations during times of low discharge showing a non-linear behaviour of ETM transition.

The near-bottom positions of the ETM (MES_Depth) generally corroborate the previous findings of GRABEMANN und KRAUSE (2001) with respect to changes of ETM position and its longitudinal extension with varying river discharge (Fig. 7a). MES_Depth suggests slightly less sensitivity of the ETM for high discharges. The positions based on the near surface long-term measurements of turbidity (MES_Surf) which comprise more river discharge conditions are in general comparable to the near-bottom ETM positions, but seem to be somewhat more extended upstream and have a larger longitudinal extent. The positions based on the measurements are likely biased by the vertical structure of the ETM. The region with highest near-bottom SPM (turbidity) in the longitudinal section is not necessarily the region with highest near-surface SPM (e.g. see Fig. 2). Near-surface and near-bottom measurements do not cover the same time span thus different forcing conditions (e.g. meteorological situations, river discharges) are covered, which may further complicate a direct comparison of ETM positions derived from different data sets.

In order to compare measurements with modelling results the ETM position was determined from the modelled SPM concentrations (Fig. 7b). A threshold SPM concentration of 0.6 was taken to determine the location of the ETM. The numerical modelling results show similar results as the measurements concerning the ETM position (MES and MOD in Fig. 7a). The upstream limit of the ETM for low and high river discharge is at about the same position along the river axis. The non-linear response of ETM transition to changes in river discharge is less pronounced in the model. The downstream limit of the ETM is further downstream in the model for low river discharge conditions.

The SPM concentration in the ETM can only be roughly compared between actual modelled SPM concentration (averaged over the width of the navigational channel) and measured turbidity as representative for SPM concentration (depth average at one location) (Fig. 7b). Even though the ETM positions and SPM concentrations are similar in simulations and measurements, they differ in details.

The model considers only the chosen quasi-stationary discharge conditions but omits transitions between different discharge conditions. The measurement data shown in Fig. 7b were analysed for specific discharge classes. In the measurements these classes contain the transitions between different discharge and environmental conditions. The interpretation is consequently restricted. The most frequent position of the ETM can be expected to be between km 45 and km 70 when considering that the river discharge is between 100 m³/s and 400 m³/s over 75 % of the time. This most frequent ETM position covers the mud stretch of the Weser found between km 55 and km 66.

Measurements indicate that river floods may have a longer lasting impact (GRABEMANN und KRAUSE 2001). SPM concentrations in the ETM after river floods (> 1,100 m³/s) are in some cases reduced and subsequently increase in the course of the following months thus indicating changes in local sediment sources. Account is not taken of the observed effects of high river discharges in terms of changes in the sediment inventory at the bed, such as changes in the amount of fine sediments. These effects should, however, be considered in following studies.

5 Summary and conclusions

The variability of the ETM on intratidal, spring-neap and river discharge-related (seasonal) time scales has been shown based on modelling results and measurements. The previously proposed description of suspended sediment transport within the ETM as a cyclic process (GRABEMANN and KRAUSE 1989, LANG et al. 1989) has been corroborated here. The intratidal ETM movement appears to be tightly coupled to the movement of the FSI for a given river discharge condition. On a fortnightly time scale a pronounced spring-neap variability of SPM concentration exists which modulates SPM concentrations. The increase of SPM concentration is almost uniform over the ETM region and the ETM can consequently be seen as extended further up- and downstream. On seasonal time scales the ETM will be strongly affected by changes in river discharge, which shifts the ETM together with the low salinity region of the mixing zone along the estuary depending on the discharge condition.

The determination of the position of the ETM from turbidity measurements appears to be reliable. However, the inference of SPM concentrations from turbidities is still limited by a number of uncertainties. The correlation of measured turbidity and SPM is not necessarily constant in time as assumed here, but may vary due to e.g. biological influences (e.g. phytoplankton). Moreover, it is assumed that measured tidal mean values for the two to three samples in a specific cross-section can be averaged to obtain average tidal mean SPM concentration for this cross-section. The numerical model delivers a more complete set of information on the sediment distribution, but is influenced by the model parameters chosen, such as the sediment fractions modelled and the choice of settling velocities.

Despite the uncertainties, the similarity between model and measurements on the different time spans considered here yields some confidence in the approaches taken. Thus, we are confident that the numerical model will allow more detailed simulations in the future in order to identify relevant processes further. As this study was focused on chosen quasi-stationary different river discharge conditions, the transition between different states will be a question of further research.

Two practical aspects of this study merit a brief mention. Firstly, the use of long-term measurements at the gauge stations to obtain the position of the ETM has been shown to be feasible, but is subject to large uncertainties. These uncertainties are expected to derive from strong natural variability, limitations of the analysis method and data limitations (e.g. device specific measurement accuracy). Currently turbidity can only be measured permanently at the edge of the fairway due to the requirements for safety and ease of navigation in restricted waterways. This limitation may be overcome in the future when plans of the WSA Bremerhaven to employ a Horizontal Acoustic Doppler Current Profiler (HADCP) have become operational. Secondly, even though the location of the ETM is highly variable on each of the different time scales considered here, a certain predictability exists. This may provide a useful element for a better description of the suspended sediment dynamics in the ETM and thus may contribute to the optimisation of sediment management in the Weser estuary.

6 Acknowledgements

The authors thank the German Waterways and Shipping Administration of the Federal Government (WSA Bremerhaven) for providing hydrodynamic and turbidity measurements. Assistance with graphics from B. Gardeike and W. Appel are gratefully acknowledged.

7 References

- AQUA VISION BV: Suspended sediment measurements in the Weser, June 2009. Technical report. Aqua Vision BV, 2009.
- BAW: Modellvalidierung UnTrim / SediMorph - Hydrodynamik und Schwebstofftransports des Jade – Weser – Ästuars. Bundesanstalt für Wasserbau, 93 p., 2009. from http://www.baw.de/downloads/wasserbau/mathematische_verfahren/Validierungsstudien/Modellvalidierung_Weser-GM_UnTRIM2007_v1.3.pdf
- BAW: Mathematical module SediMorph – Validation document, Bundesanstalt für Wasserbau, 77 p., 2005. from http://www.baw.de/downloads/wasserbau/mathematische_verfahren/pdf/vd-sedimorph.pdf
- BURCHARD, H. and BAUMERT, H.: The Formation of Estuarine Turbidity Maxima Due to Density Effects in the Salt Wedge. A Hydrodynamic Process Study. In: *Journal of Physical Oceanography*, Vol. 28, 309-321, 1998.
- CASULLI, V. and ZANOLLI, P.: High resolution methods for multidimensional advection–diffusion problems in free-surface hydrodynamics. In: *Ocean Modelling*, Vol. 10, 1-2, 137-151, doi: 10.1016/j.ocemod.2004.06.007, 2005.
- DE NIJS, M.A.J.; WINTERWERP, J.C. and PIETRZAK, J.D.: On harbour siltation in the fresh-salt water mixing region. In: *Continental Shelf Research*, Vol. 29, 1, 175-193, doi: 10.1016/j.csr.2008.01.019, 2009.
- DEUTSCHES GEWÄSSERKUNDLICHES JAHRBUCH: Weser und Emsgebiet 2010. 1.11.2009 - 31.12.2010. Niedersächsischer Landesbetrieb für Wasserwirtschaft, Küsten- und Naturschutz, 301 p., 2013.
- DIECKMANN, R.: Morphologische Strukturen im Weserästuars. In: *Deutsche Gewässerkundliche Mitteilungen*, Vol. 33, 3/4, 104-112, 1989.
- DOMS, G.; STEPPER, J. and ADRIAN, G.: Das Lokal-Modell LM. In: *promet*, Vol. 27, 3/4, 123-128, 2002.
- DYER, K.R.: *Estuaries: a physical introduction*. John Wiley and Sons, 1997.
- FESTA, J.F. and HANSEN, D.V.: Turbidity maxima in partially mixed estuaries: A two-dimensional numerical model. In: *Estuarine and Coastal Marine Science*, Vol. 7, 4, 347-359, doi: 10.1016/0302-3524(78)90087-7, 1978.
- GRABEMANN, I. and KRAUSE, G.: Transport processes of suspended matter derived from time series in a tidal estuary. In: *Journal of Geophysical Research*, Vol. 94, C10, 14373, doi: 10.1029/JC094iC10p14373, 1989.
- GRABEMANN, I. and KRAUSE, G.: On Different Time Scales of Suspended Matter Dynamics in the Weser Estuary. In: *Estuaries*, Vol. 24, 5, 688, doi: 10.2307/1352877, 2001.

- HOLZWARTH, I.; SCHULTE-RENTROP, A. and HESSER, F.: Auswirkungen klimabedingter Änderungen auf das Strömungs- und Transportverhalten deutscher Nordseeästuar. In: HAFENTECHNISCHE GESELLSCHAFT E.V. (ed.): Vorträge HTG-Kongress 2011. Würzburg, 275-282, 2011.
- IRION, G.; WUNDERLICH, F. and SCHWEDHELM, E.: Transport of clay minerals and anthropogenic compounds into the German Bight and the provenance of fine-grained sediments SE of Helgoland. In: Journal of the Geological Society, Vol. 144, 153-160, 1987.
- JAY, D.A. and MUSIAK, J.D.: Particle trapping in estuarine tidal flows. In: Journal of Geophysical Research, Vol. 99, C10, 20445, doi: 10.1029/94JC00971, 1994.
- LANG, G.: Zur Schwebstoffdynamik von Trübungszone in Ästuaren. Universität Hannover, Hannover, Institut für Strömungsmechanik und Elektron. Rechnen im Bauwesen, 113 p., 1990.
- LANG, G.; SCHUBERT, R.; MARKOFSKY, M.; FANGER, H.-U.; GRABEMANN, I.; KRASEMANN, H.L.; NEUMANN, L.J.R. and RIETHMÜLLER, R.: Data interpretation and numerical modeling of the Mud and Suspended Sediment Experiment 1985. In: Journal of Geophysical Research, Vol. 94, C10, 14381, doi: 10.1029/JC094iC10p14381, 1989.
- LANGE, D.; MÜLLER, H.; PIECHOTTA, F. and SCHUBERT, R.: The Weser Estuary. In: KURATORIUM FÜR FORSCHUNG IM KÜSTENINGENIEURWESEN (ed.): Die Küste. Archiv für Forschung und Technik an der Nord- und Ostsee. Heide i. Holstein, 275-287, 2008.
- MALCHEREK, A.: Mathematische Modellierung von Strömungen und Stofftransporten in Ästuaren. PhD thesis. Universität Hannover, Hannover, Institut für Strömungsmechanik und Elektron. Rechnen im Bauwesen, 203 p., 1995.
- OFFICER, C. B.: Physical dynamics of estuarine suspended sediments. In: Marine Geology, Vol. 40, 1-2, 1-14, doi: 10.1016/0025-3227(81)90039-6, 1981.
- RIETHMÜLLER, R.; FANGER, H.-U.; GRABEMANN, I.; KRASEMANN, H.L.; OHM, K.; BÖNING, J.; NEUMANN, L.J.R.; LANG, G.; MARKOFSKY, M. and SCHUBERT, R.: Hydrographic Measurements in the Turbidity Zone of the Weser Estuary. In: DRONKERS, J. and LEUSSEN, W. (eds.): Physical Processes in Estuaries. Berlin, Heidelberg, 332-344, doi: 10.1007/978-3-642-73691-9_18, 1988.
- SCHROTTKE, K.; BECKER, M.; BARTHOLOMÄ, A.; FLEMMING, B.W. and HEBBELN, D.: Fluid mud dynamics in the Weser estuary turbidity zone tracked by high-resolution side-scan sonar and parametric sub-bottom profiler. In: Geo-Marine Letters, Vol. 26, 3, 185-198, doi: 10.1007/s00367-006-0027-1, 2006.
- SEIFFERT, R.; HESSER, F.B.; SCHULTE-RENTROP, A. and SEIB, G.: Potential effects of climate change on the brackish water zone in German estuaries. In: HINKELMANN, R.-P., LIONG, Y., SAVIC, D., NASERMOADDELI, M.H., DAEMRICH, K.-F., FRÖHLE, P. and JACOB, D. (eds.): Understanding Changing Climate and Environment and Finding Solutions. Hamburg, 2012.
- SIMPSON, J.H.; BROWN, J.; MATTHEWS, J. and ALLEN, G.: Tidal Straining, Density Currents, and Stirring in the Control of Estuarine Stratification. In: Estuaries, Vol. 13, 2, 125, doi: 10.2307/1351581, 1990.

- TALKE, S.A.; SWART, H.E. DE and SCHUTTELAARS, H.M.: Feedback between residual circulations and sediment distribution in highly turbid estuaries: An analytical model. In: Continental Shelf Research, Vol. 29, 1, 119-135, doi: 10.1016/j.csr.2007.09.002, 2009.
- WELLERSHAUS, S.: Die Trübungswolke im Weser-Ästuar. In: Deutsche Gewässerkundliche Mitteilungen, 26, 1982.

Sediment Transport and Sediment Management in the Elbe Estuary

Holger Weilbeer

Summary

In this article the tidal Elbe serves as an example to show which kind of data, modelling and analysis tools are required for a qualitative and quantitative description of sediment transport in an estuary. These methods can be used to investigate sediment management options.

Keywords

Elbe, estuary, numerical model, suspended sediment measurements, dredging, sediment transport, sediment management

Zusammenfassung

Am Beispiel der Tideelbe wird gezeigt, welche Art von Daten, Modellierungs- und Analysewerkzeugen benötigt werden, um den Sedimenttransport in einem Ästuar qualitativ und auch quantitativ beschreiben zu können. Mit Hilfe dieser Methoden können Optionen für das Sedimentmanagement untersucht werden.

Schlagwörter

Elbe, Ästuar, numerisches Modell, Schwebstoffmessungen, Baggern, Sedimenttransport, Sedimentmanagement

Contents

1	Introduction	410
2	The Elbe estuary – a brief overview.....	411
3	Modelling system	414
4	Sediment transport in the Elbe estuary.....	415
4.1	Measurements	415
4.2	Model results	418
4.3	Monitoring of dredging activities.....	420
5	Application to sediment management tasks	421
5.1	Sediment management concept	421
5.2	Investigation of disposal sites.....	423
5.3	Modelling dredging activities	424

6	Outlook.....	425
7	References	425

1 Introduction

Estuaries are strongly influenced by tidal waves on the one hand and salt water, mixed water and freshwater zones on the other, and they transport large volumes of sediment along with their alternating currents. The deeper the water in fairways, the higher the tidal exchange volume and the higher the amounts of sediment that can be transported with the flowing water mass. As a result, dredging operations become more intensive. In Germany, for example, more than 45 million m³ of sediment material are dredged every year to maintain the required fairway depths. With over 40 million m³, the material dredged in sea waterways and seaports accounts for the major share of dredging operations. Considering these volumes it is clear that sediment transport processes in estuaries are of eminent importance. One of the main objectives is to stop the continuing increase in the amount of dredging material and rising dredging costs - even if the trend towards greater ship sizes continues unbroken.

Most of the dredged material is transported to temporary disposal sites in the estuary, meaning that the material remains in the system, thus influencing sediment transport rates and consequently also the estuary's morphological development. When choosing a disposal site, hydromorphological criteria as well as nature conservation aspects have to be considered. As a rule, the spreading of the relocated dredged material is considered as a desired effect, for instance, while resedimentation in dredged areas should be avoided since this would encourage repeated sediment and dredging cycles. By choosing suitable disposal sites and times, it might also be possible to promote beneficial morphological developments. The evolution of the Wadden Sea, for example, is extremely important as it compensates for the impact of the sea level rise.

An understanding of the hydrodynamic and morphodynamic influences in an estuary and knowledge about the relationships with water quality parameters are therefore an essential scientific prerequisite for the optimum management of sediment. An example is the upstream transport of sediments due to tidal pumping and the influence of baroclinic processes on the water flow and sediment transport in the estuary's gradient zone. Both are crucial factors in sediment transport and are the main cause of potential sediment cycles. Consequently, they need to be taken adequately into account when designing and implementing a sediment management strategy.

In this article the tidal Elbe serves as an example to show which kind of data, modelling and analysis tools are required for a qualitative and quantitative description of sediment transport processes in an estuary. These methods can be used to investigate sediment management options.

Section 2 provides a brief overview of the historic development of the Elbe estuary and section 3 describes the modelling system used in this study. Section 4 presents measurements and model results for sediment transport in the Elbe estuary. Section 5 then looks at specific model applications for sediment management tasks.

2 The Elbe estuary – a brief overview

The Elbe estuary is a very important German waterway. Its mouth is situated in the south-east of the German Bight, with the weir in Geesthacht defining the tidal limit. The entire length from the weir to the mouth, which has a width of approximately 15 km, is more than 160 km (Fig. 1).

Over the centuries, the Elbe estuary has been modified several times to meet the changing requirements of maritime traffic. Between 1860 and 1999 the fairway was deepened up to 10 m. Furthermore, a range of measures, such as the construction of the weir in Geesthacht, the cut-off of tributaries, the backfill of harbour basins, as well as diking and poldering, have been carried out in the last 50 years. Today the morphology of the Elbe estuary is characterised by a deep fairway leading to the Port of Hamburg and a complex system of islands, tributaries and branches in the landward section of the estuary as well as extensive tidal flats and tidal creeks in the seaward section.

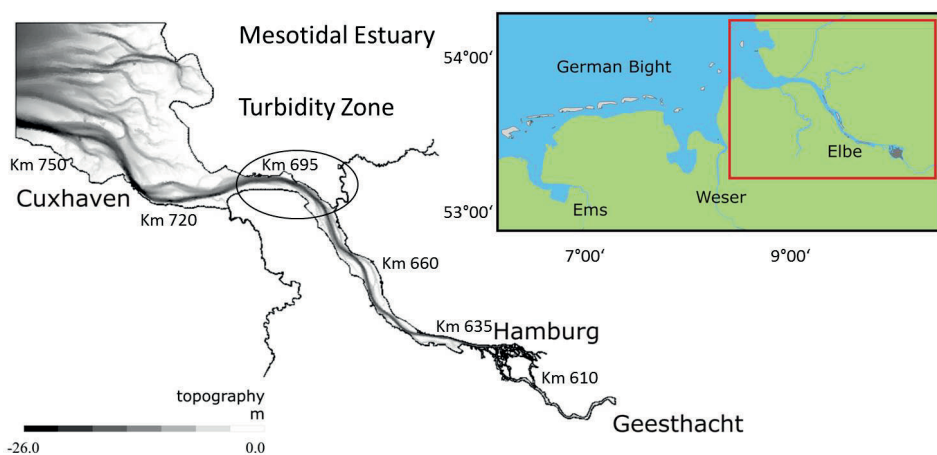


Figure 1: Geographic positions and denotations of the Elbe estuary.

Anthropogenic measures have given rise to changes in tidal characteristics and sediment transport processes. Fig. 2 shows the mean high water and the mean low water at a tidal gauge in St. Pauli, Hamburg, from 1900 to 2010. The tidal range has increased considerably (1 m in the last 35 years) due to a fall in the low water level and a rise in the high water level. The asymmetry of the tidal curve is enhanced, i.e. the flood current has become shorter but now reaches higher velocities, the slack tide between flood current and ebb current has become longer, and the ebb current has also become longer with smaller current velocities. This hydrodynamic behaviour is probably the main reason for the enhanced tidal pumping of sediment upstream. Sediment is transported upstream with the strong flood current, settles during the slack tide with less sediment mass being transported downstream with the weaker ebb current. The net transport of sediments depends on strength of the head water discharge (section 4.2).

Ongoing maintenance dredging of the channel has been necessary in order to guarantee the safety of shipping traffic. The amount of maintenance dredging has increased significantly since the last deepening in 1999, especially in the upper region of the estuary near Hamburg (Fig. 3). This graphic also shows a change in the management strategy for

fine sediments. Since 2008, all fine sediments dredged downstream of Hamburg have been disposed on sites located in the turbidity zone (Fig. 1) in order to enlarge sediment cycles. As a consequence the amount of dredging near Osteriff has increased.

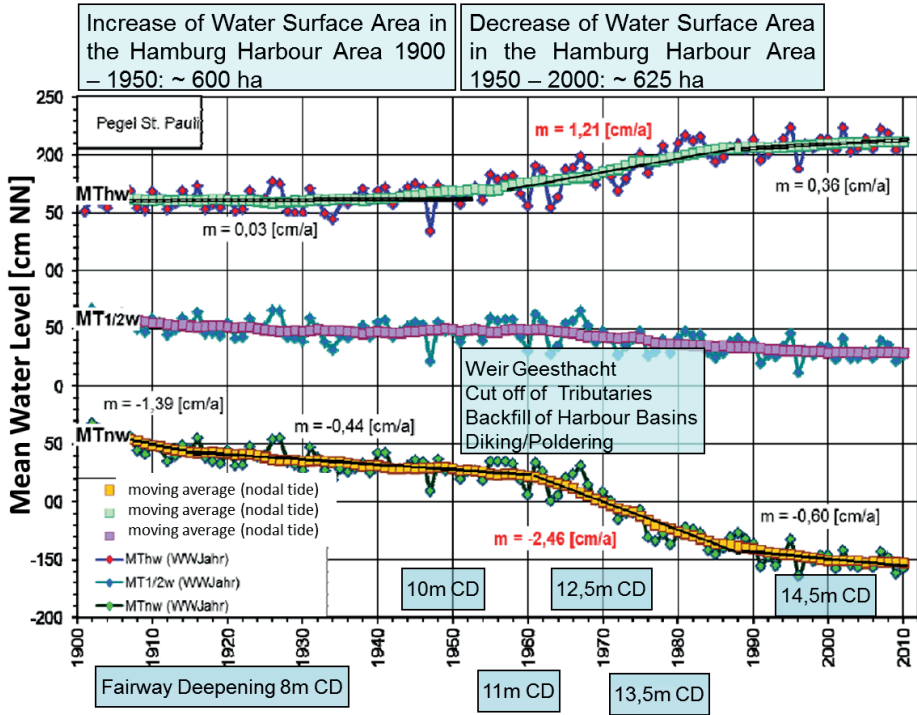


Figure 2: Mean high water and mean low water from 1900 to 2010 at tidal gauge in St. Pauli, Hamburg. Major anthropogenic measures are marked. Graphic from <http://www.portal-tideelbe.de/Projekte/FRA1999/index.html>, modified.

Another noticeable peak can be seen in a section in the outer estuary called “östliche Mittelrinne”. The amount of dredged sediments was doubled in 2008, and more sediment also needs to be dredged in the neighbouring sections. The reason for this strong increase can be found in the large-scale morphodynamics of the Outer Elbe caused by a chain of pronounced hydrological and meteorological events. In the winter season 2007/2008 the number of tidal high water events (Thw > 2.40 m NHN) was significantly larger than usual (BAW 2013). Thus the hydrodynamic load on the shallow areas in the Wadden Sea due to wave and current actions was higher and more sediment was moved.

Morphological development in the Outer Elbe is a very important issue, not only with respect to dredging amounts, but also for the evolution of the Wadden Sea as an important habitat and its meaning for coastal protection, and of course for the hydrodynamics of the whole tidal Elbe because of the dissipation of tidal energy in the outer area. The morphological development of the last 40 years is shown in Fig. 4. It is strongly influenced by the longitudinal dike “Kugelbake“ north of Cuxhaven. On the one hand, millions of cubic meters of sediment are lost in some areas and, on the other, millions of cubic meters of sediment must be dredged every year to maintain the fairway.

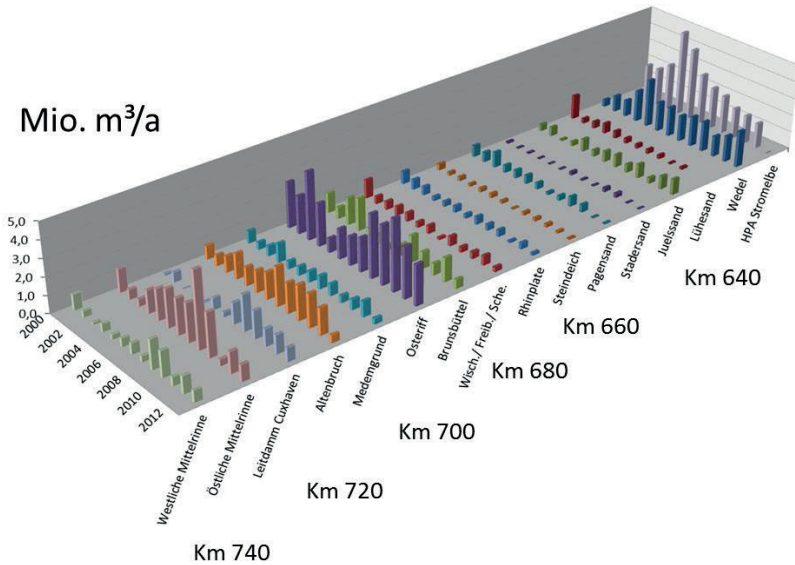


Figure 3: Amount of maintenance dredging in the Elbe estuary from 2000 to 2012. (Data from Baggerbüro Küste, GDWS-Nord).

All of these issues require monitoring, scientific investigation and system analysis of sediment transport processes using modern numerical methods. A better understanding of the cause-and-effect chain which has brought about these apparently anthropogenic driven changes to the estuary is required.

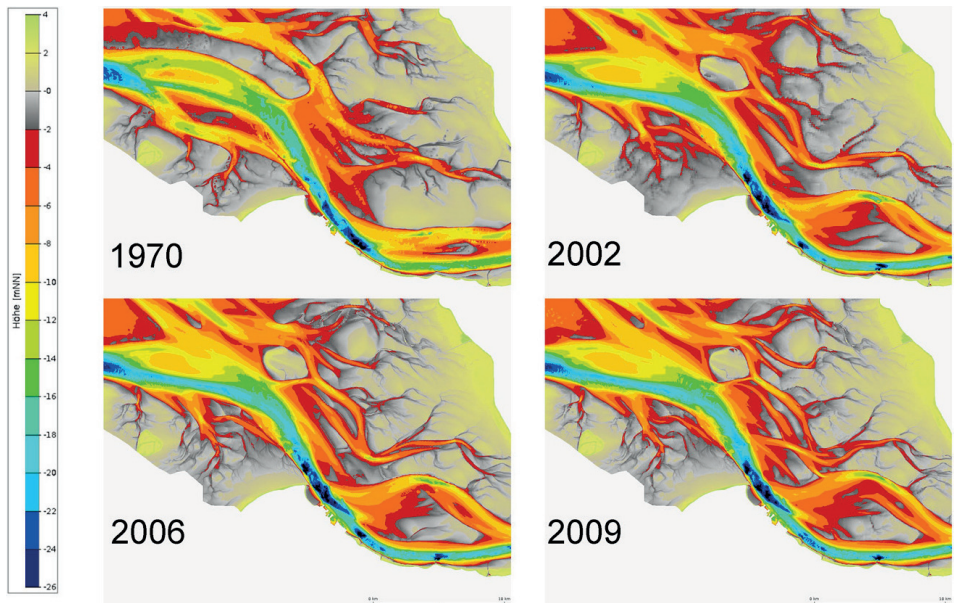


Figure 4: Morphological development in the Outer Elbe from 1970 to 2009.

3 Modelling system

The model runs described in this article are performed with the UnTRIM hydrodynamic and suspended transport model in combination with the SediMorph morphological model and – for some applications – in combination with the dredging module DredgeSim.

- UnTRIM is a computational model for solving a variety of two- and three-dimensional differential equations relating to hydrostatic and non-hydrostatic free-surface flow and transport in water bodies (CASULLI and WALTERS (2000), CASULLI and ZANOLLI (2002, 2005), LANG 2005).
- SediMorph is a software package for the two- or three-dimensional simulation of fractioned sediment transport processes within the bottom and at the bottom surface bodies (BAW 2005).
- DredgeSim can be used to take account of dredging and disposal actions in free surface flows. This allows the anthropogenic influence on sediment transport and morphology to be considered and maintenance strategies to be developed and evaluated focusing on different optimisation criteria (e.g. minimising dredging costs). DredgeSim can be used in two different modes. In each case the user has to define dredging and disposal areas. The date, time and amount of dredged material and its deposition is prescribed by the user in the time controlled maintenance mode. In this criterion controlled maintenance mode dredging is initiated according to prescribed dredge criteria, for instance if a deposition area in the shipping channel affects navigability. This simulation module was developed in cooperation with BAW and the University of the Armed Forces, Munich (MAERKER and MALCHEREK 2007).

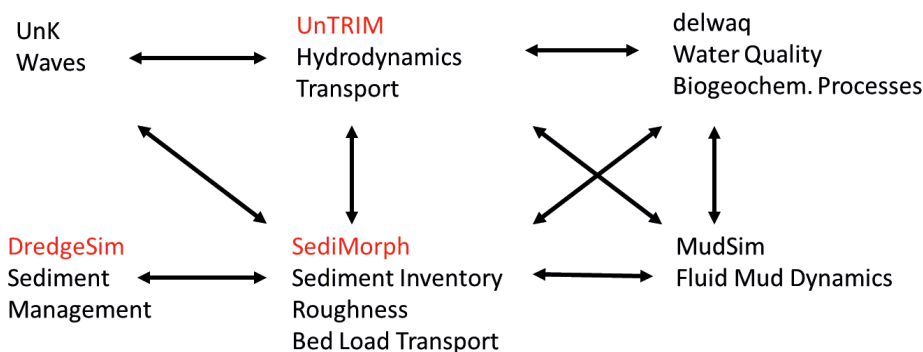


Figure 5: Simulation modules of the BAW modelling system. The most important modules used for this study are shown in red.

The interaction of the simulation modules used in the applications is shown schematically in Fig. 5. The modelling system contains all the necessary simulation modules which will enable it to be used as a tool for predicting estuary responses to proposed management options. Results presented in this article are produced with validated models from the Elbe estuary (BAW 2006, 2012).

4 Sediment transport in the Elbe estuary

4.1 Measurements

Field data of sediment concentrations and transport rates, which can be used for calibration and validation purposes, must be collected in special measurement campaigns. A medium-term field program was initiated in 2006 (and repeated in 2010 and 2011) with the aim of improving our understanding of the suspended sediment regime and of building up a database for validation of the numerical model.

The field data collection program covers the entire Elbe estuary and provides data on suspended solid concentrations and transport rates. Acoustic Doppler Current Profilers (ADCPs) are used for the measurements as these can provide data over (nearly) the whole depth range in a temporal and spatial resolution which is very suitable for numerical models. Some results of measurements along cross-sections are presented in this section. Further results and more detailed technical information can be found in MAUSHAKE and AARDOM (2007) and MOL (2007).

The measurements were carried out in autumn 2006. The head water discharge in this period was below 400 m³/s. A total of three cross-section measurements have been performed, each representing a characteristic hydrographic regime (Cuxhaven: marine zone; Rhinplatte: turbidity zone; Hamburg: fluvial zone). In total, the cross-section measurements consist of more than 200 ship-mounted crossings on three transects, each one covering the period of one tide with around 160 calibration sites and more than 300 water samples.

Some measured distributions of suspended sediment concentrations for three cross-sections are shown in Fig. 6. In each case, the maximum concentration during ebb and flood currents has been selected for each profile. Transport rates and transport fluxes can be computed directly from the collected datasets as ADCPs combine a current sensor and a SSC sensor in a single device which provides velocity and suspended sediment concentration profiles in the same area. Measured sediment concentrations, transport rates and velocities are shown as cross-section integrated values in Fig. 7.

Cross-section at Hamburg:

The maximum flood concentrations at the entrance to the Port of Hamburg (Hamburg profile) are much higher than the maximum ebb concentrations. Peak values of mean measured concentrations of more than 0.4 g/l are reached during flood, followed by a decrease to 0.05 g/l during slack water at high tide (Fig. 7). The ebb current is slower than the flood current owing to the significant tidal asymmetry in this part of the estuary. Thus the sediment concentrations during ebb are lower than those during flood and reach maximum values of 0.2 g/l. The concentrations again decrease to 0.05 g/l during slack water at low tide. The calculated sediment flux is a distinct indicator of the flood-dominated transport regime in this area: During flood current the transport of 27000 t suspended sediment was measured, during ebb current only 13000 t.

Cross-section at Rhinplatte:

In the turbidity zone of the Elbe estuary (Rhinplatte profile) the concentration in some areas sometimes increases to over 2 g/l, for example at the sides of the navigation channel (Fig. 6). Higher values probably occur near the bottom, but the measurement method is not valid for this reach. Thus the real sediment fluxes must be higher than

calculated fluxes based on measurements. Values of mean (cross-section integrated) measured concentrations of more than 0.6 g/l are reached during flood peak, followed by a decrease to 0.10 g/l during slack water at high tide (Fig. 7). The sediment concentrations during ebb are higher than during flood and reach maximum values of 0.7 g/l. This peak concentration at the end of the ebb current is probably caused by a muddy area located a few kilometres upstream of this cross-section. This does not necessarily indicate an ebb-dominated transport regime because the length of the cross-section navigable with the vessel was shorter during the ebb and thus lateral areas with lower sediment concentrations are not taken into account. During both flood and ebb current the transport of 130000 t suspended sediment was measured.

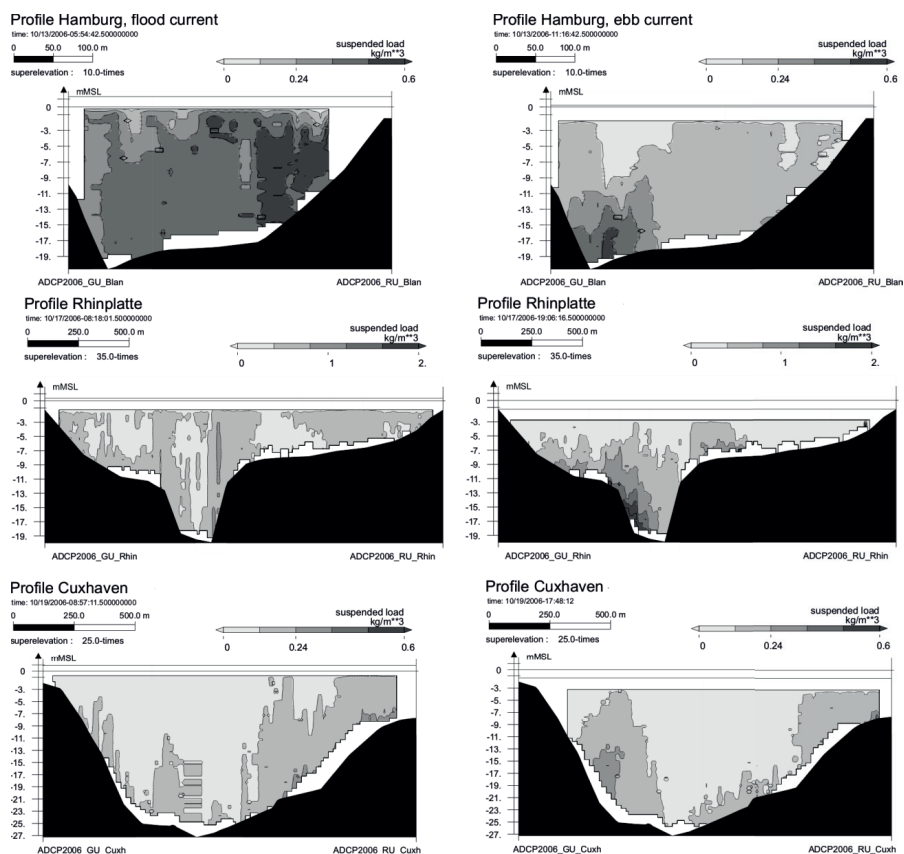


Figure 6: Maximum measured sediment concentrations at the cross-sections Hamburg/Blankenese, Glückstadt/Rhinplatte and Cuxhaven during flood and ebb current. The scale at the profile Glückstadt/Rhinplatte was adapted to the higher sediment concentrations in this area.

Cross-section at Cuxhaven:

The lowest concentrations were measured in the marine transect near Cuxhaven. The maximum of the ebb current is located in the western area of the profile and during flood the maximum current velocities occur at the eastern area of the profile. Thus the pattern

of suspended sediment concentration looks different (Fig. 6). Due to the high current velocities in this area the morphology is mainly affected by sand transport. The averaged measured sediment concentrations are small and vary between 0.02 g/l and 0.11 g/l with a tidal-averaged value of 0.07 g/l (Fig. 7). During flood current as well as ebb current the transport of 30000 t suspended sediment was measured.

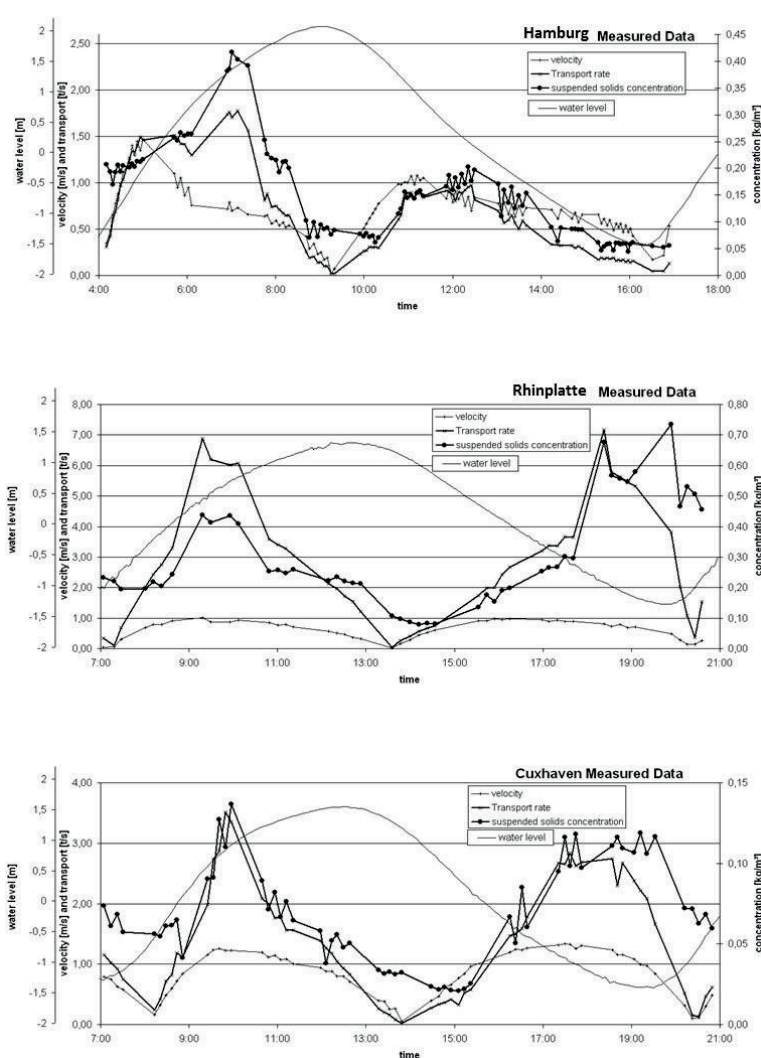


Figure 7: Measured current velocities, sediment concentrations and sediment fluxes at the cross-sections Hamburg/Blankenese (upper graph), Glückstadt/Rhinplatte (middle graph) and Cuxhaven (lower graph). The values are averaged over the cross-section area.

4.2 Model results

These data were used in a calibration process. The site-specific model was first calibrated using bathymetric and hydrologic conditions from 2006. During the calibration process the influence of settling velocity formulations was also investigated. This process cannot be described here in detail. One of the main findings was that none of the tested settling velocity formulations works well for the whole estuary. The model setup using two suspended sediment fractions each with constant settling velocities delivered the best results. However, flocculation processes, which are probably responsible for the strong decrease in sediment concentrations during slack tides, have not yet been considered satisfactorily in the model. Despite this weakness, mean sediment concentrations and transport rates calculated from the model are qualitatively and quantitatively in an acceptable range for the entire Elbe estuary, i.e. the model reproduces, in a broad sense, the general nature of sediment dynamics in the estuarine system.

Fig. 8 shows a comparison of measured and modelled current velocities and sediment concentrations at the cross-section Glückstadt/Rhinplatte. In general, measured values are more scattered and modelled values are smoother. The vertical distribution of sediment concentrations is more pronounced in the measurements. High concentrations near the bottom seem to be underestimated by the model, but on the other hand measured data are often not valid in this region.

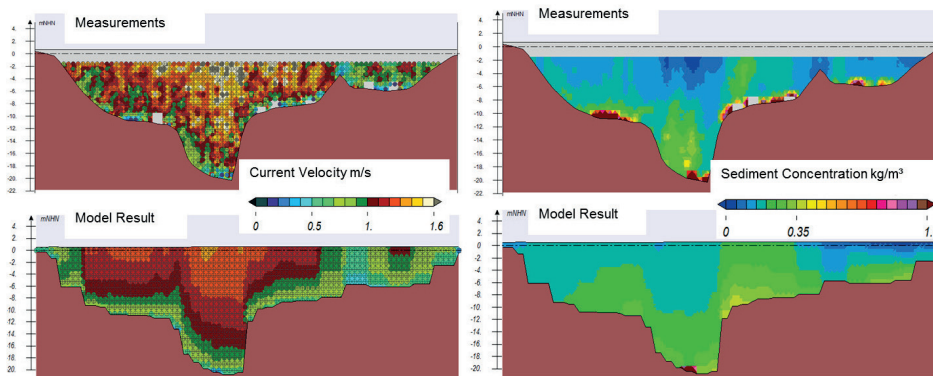


Figure 8: Elbe model 2006: Measured and modelled current velocities (left graph) and respective sediment concentrations (right graph) at the cross-section Glückstadt/Rhinplatte.

Results of measurements and model results for a similar setup of the Elbe model 2010 are shown in Fig. 9. Measured and modelled current velocities, sediment concentrations, discharges and sediment fluxes at the cross-sections at Elbe-Km 689 are averaged over the cross-section area. Note that with this calibration procedure the model ran already nearly 6 months until it was compared with measured data, i.e. the hydrologic history is inherent in the model results. Overall the model fits the measured data well. This model is used for the morphodynamic application described in section 5.3.

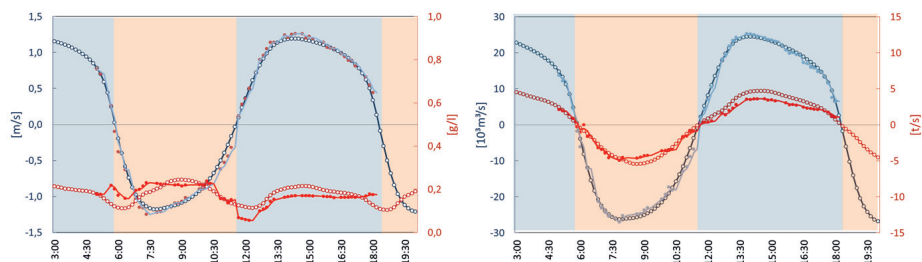


Figure 9: Elbe model 2010: Measured and modelled current velocities, sediment concentrations (left graph) and respective discharges, sediment fluxes (right graph) at the cross-sections at Elbe-Km 689. The values are averaged over the cross-section area.

In further specific model applications only the head water discharge is varied ($Q = 180, 720$ and $1260 \text{ m}^3/\text{s}$) in order to investigate the influence of head water discharge on hydrodynamic and sediment transport processes. All other model steering parameters, including initial conditions such as sediment and salinity distribution and other boundary conditions and values, were uniform for all model runs.

The model runs cover a four week simulation period (June 2nd to June 30th 2006). The analysis of the model results starts after nine days of simulation (June 11th 2006 to June 25th 2006). During this period (one spring-neap-cycle) all model results are stored every ten minutes. In several post-processing steps these data are analysed to calculate the minimum, mean and maximum values of water level, current velocities, salinities and sediment concentrations for each element. In addition, the sediment transport across defined cross-sections and along defined long-sections is calculated for each model run. This analysis provides a set of metrics which are useful to describe the system behaviour and provides a basis for comparison between model runs.

Fig. 10 shows on the right side suspended sediment concentrations along the fairway. These are time-averaged values of three-dimensional model results for one spring-neap-cycle. A turbidity maximum exists in all model runs. A higher fresh water discharge flushes the suspended sediments to the sea. Higher sediment concentrations occur in these runs. On the left side the ratio between the suspended sediment transport rates during flood current and during ebb current is shown. This value does not provide any information about quantities, but instead characterises the transport regime of suspended sediments. Together with the knowledge about absolute transport rates, this ratio constitutes an important criterion, for example for the assessment of dumping sites. The highest values of this ratio occur near the Port of Hamburg at low discharges.

There are two hydrodynamic reasons for this transport behaviour - baroclinic effects due to density gradients and tidal pumping, both indicated in Fig. 10. The influence of baroclinic processes on the sediment transport is high. The strong dominance of the near bed transport in flood direction between Cuxhaven and Brunsbüttel, which is also visible at higher head water discharges, may indicate further sediment cycles in the Elbe estuary. Furthermore the model runs for low or mean head water discharge predict distinct sediment transport in flood direction, at least upstream of Brunsbüttel. This transport characteristic is caused by tidal asymmetry, already described in section 2. Owing to these

transport characteristics fine sediments accumulate over the long term in this part of the Elbe and lead to an increase in the amount of maintenance dredging.

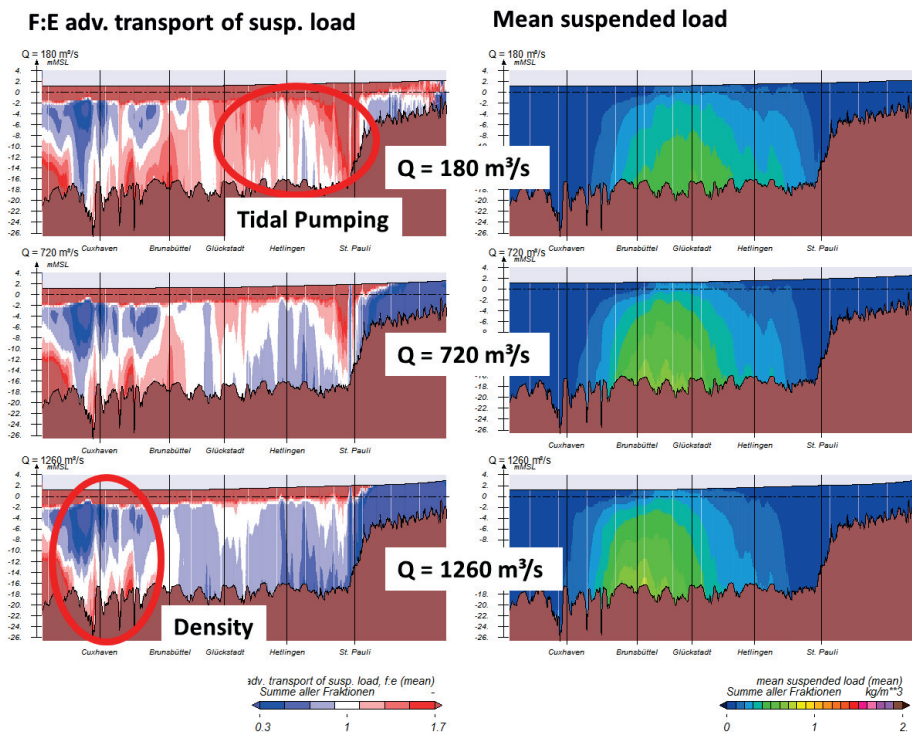


Figure 10: Flood/ebb (F:E) ratio of suspended load transport (left graph) and mean suspended load (right graph) for discharge $Q = 180 / 720 / 1260 \text{ m}^3/\text{s}$. 3D data, averaged over one spring-neap cycle. Specific features are marked by red circles.

4.3 Monitoring of dredging activities

Dredging and disposal actions lead to changes of morphology, of sediment concentrations and thus to changes in the net transport of sediments. The spreading of sediments and changes in sediment concentrations may offer economic and ecologic criteria for comparing and evaluating realistic dredging and disposal scenarios (location, tidal phase, sediment properties etc.). Detailed data of real dredging and disposal actions, or at least information about the applied sediment management strategy, are also needed for mid-term or long-term morphodynamic simulations.

Usually only information about the yearly amount of dredging volume for certain sections of the waterway are available (Fig. 3). A detailed spatial and temporal analysis of these data is not possible and this kind of data is therefore not appropriate for use in a numerical simulation.

Dredging data which can be used for a model run must describe the dredging and disposal action in great detail:

- A polygon to describe the dredging area
- Date and time of dredging
- Volume and density of dredged sediments
- A polygon to describe the disposal area
- Date and time of disposal
- Several identification numbers for a distinct description of the dredging cycle

If these data are available, dredging and disposal actions can be considered in detail during a numerical simulation. Since 2009, most of the dredging vessels working in the Elbe estuary have been equipped with the sensors needed for operational monitoring purposes and the data is now available for further investigations. If the morphodynamic model is only driven by dredging data, only that part of the bottom evolution becomes visible which is influenced by dredging operations. Fig. 11 shows dredge polygons near Osteriff and the resulting bed evolution based on monitoring data from the year 2010.

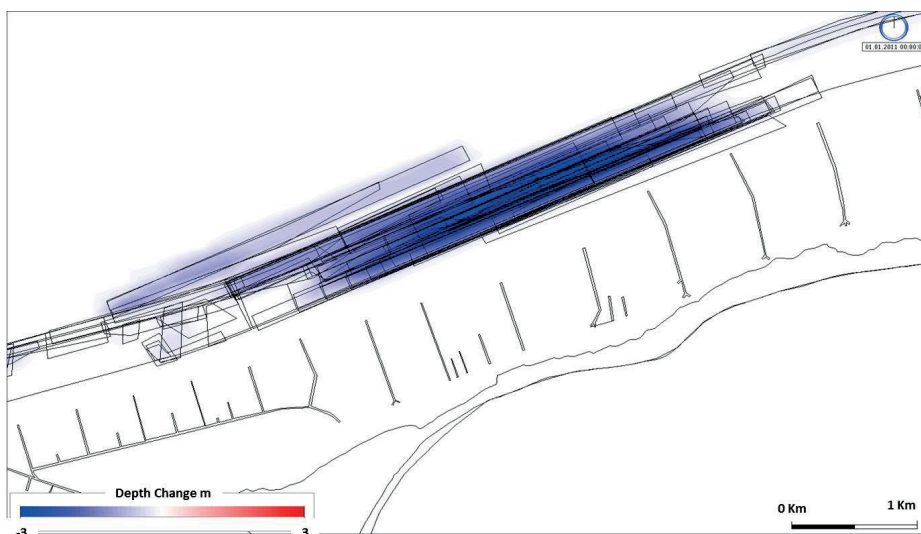


Figure 11: Dredge polygons near Osteriff and resulting bed evolution based on monitoring data from the year 2010.

5 Application to sediment management tasks

5.1 Sediment management concept

Currently, the maintenance concept for the Elbe estuary is a sediment management system combining different hydraulic engineering activities. It includes construction measures and optimised dredging actions and was developed in cooperation with all the associated authorities (HPA and WSV 2008). This concept is in a continuous process of ongoing developed and completion (ENTELMANN 2012, BAW 2013, BfG 2013).

Construction measures are mainly investigated to overcome the negative effects arising from flood dominated tidal characteristics and associated sediment transport. This can be achieved by creating a bigger tidal volume upstream and by increasing the dissipation of the incoming tidal energy. Possible measures include construction of hydraulic structures, the enlargement of shallow water areas in the Outer Elbe and the construction of additional tidally influenced areas in the upper part.

Further, optimised dredging and disposal strategies are aspired to reduce volumes of dredged material. This includes identifying and enlarging or destroying dredging cycles, where dredged material which is disposed in the estuary is transported back to dredging sites. This can be achieved by disposing of fine sediments in a more ebb-dominated transport regime. Coarse particles, in contrast, can be used in construction measures. Further, the influence of the head water discharge as well as the time-dependent change of the flow regime can be used to optimise dredging and even more disposal activities.

By constructing several sediment traps, the sediments are further forced to settle at certain stages to keep them out of critical areas. This enables the sedimentation processes to be steered in the estuary and the entry of fresh sediments in polluted harbour basins avoided.

Currently, most dredged material is disposed of within the estuary (Fig. 12). Furthermore, the Hamburg Port Authority has had temporary permission to dispose of a certain amount of fine sediments in the North Sea. As a result, around 1 million m³ of fine sediment was removed from the estuary every year between 2005 and 2011. A smaller amount, polluted by different contaminants which are transported and accumulating in the harbour from sources upstream, has to be treated and deposited landside. This management concept still requires the treatment and deposition of polluted sediments. The improvement of the water quality of the river Elbe and its sediments is still an important goal, and one which can only be fully achieved by stopping the emission of contaminations along the upstream tributaries. This is supported within the estuary by removing polluted sediments in the harbour.

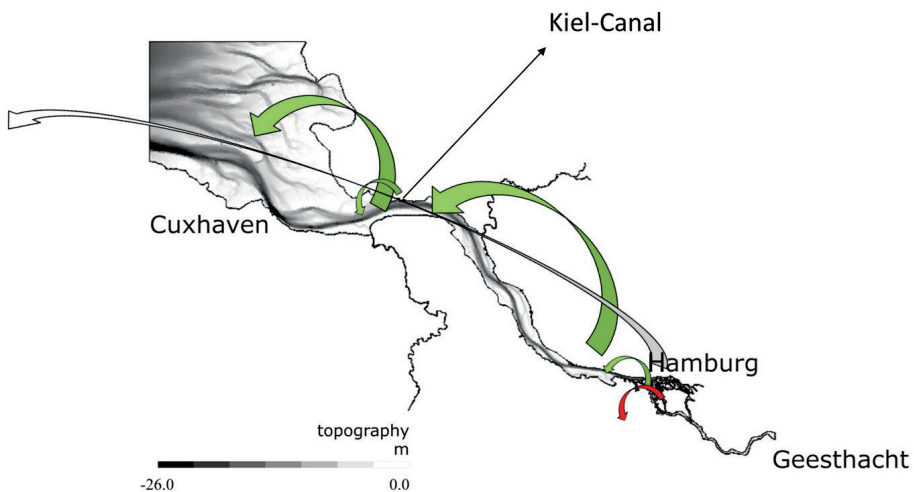


Figure 12: Schematic view of the management concept for fine sediments, applied 2005-2011. Red arrow indicate storage on land.

5.2 Investigation of disposal sites

The modelling system was applied to investigate the function of the disposal sites used in the Elbe estuary. The set-up of the model for this application is nearly identical to the studies described in section 4.2, but in addition to the initial sediment inventory three more sediment fractions are taken into account. These sediment fractions (fine, mean and coarse silt) have physical properties which are identical with the background inventory. These sediments are located at disposal sites and can be eroded and transported by the tidal current.

This kind of model application allows for detailed analysis of the transport behaviour of different types of sediments from different locations in the estuary. The spreading of the marked sediments shows the extent of influence of the investigated disposal site. This information, together with knowledge of dredging and disposal strategies, can be used to recognise sediment cycles.

This method was applied not only to all recent disposal sites in the Elbe estuary, but also to potential new sites, which may be more convenient (BAW 2012, 2013). An example from this investigation is the spreading of coarse silt from the disposal site at Elbe km 738 as shown in Fig. 13. The preferred transport direction is indicated by maximum sediment concentrations of coarse silt eroded from the disposal site. This is a proper site from a hydraulic engineering point of view because most of the sediments are transported in a south-east direction towards shallow areas, but not in the fairway, indicated by the black line. Thereby the formation of the Wadden Sea is supported, or at least the erosion of sediments from this region is compensated.

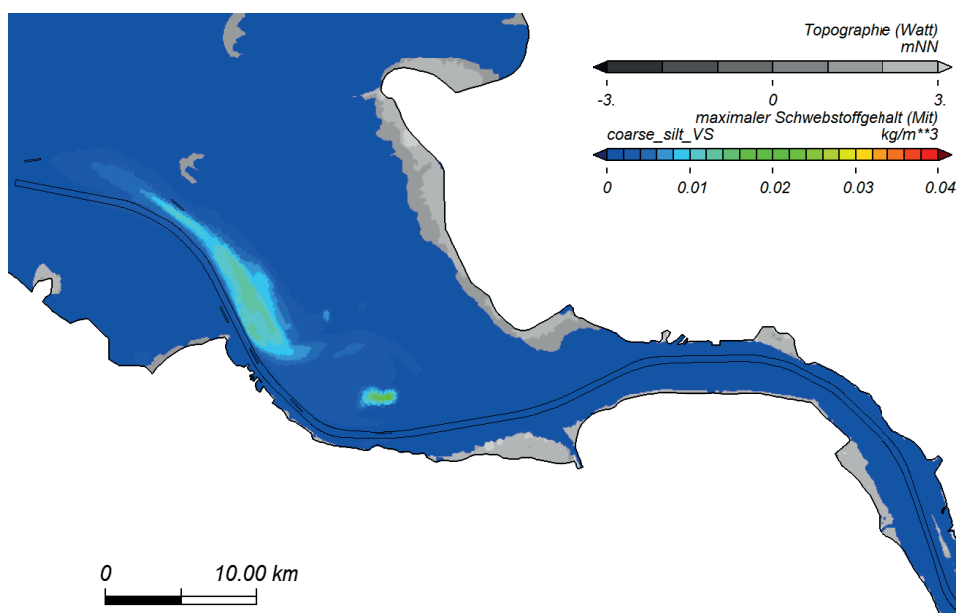


Figure 13: Spreading of fine sediments from the disposal site at Elbe km 738, indicated by maximum sediment concentrations of coarse silt eroded from the disposal site.

5.3 Modelling dredging activities

Finally the modelling system (section 3) was applied to simulate hydro- and morpho-dynamics for the year 2010, whereby all known dredging and dumping operations were included. Fig. 14 shows the modelled bottom evolution in the mouth of the Elbe estuary. Dredging sites as well as disposal sites are recognisable. Some larger scale morphological trends correspond well with observed changes (Fig. 15), but overall the model setup used for this run appears to overestimate erosion in some areas. Nevertheless the model is an indispensable tool for evaluating different sediment management strategies. It can be used to test management options, and the difference between two model runs shows the impact of the variation.

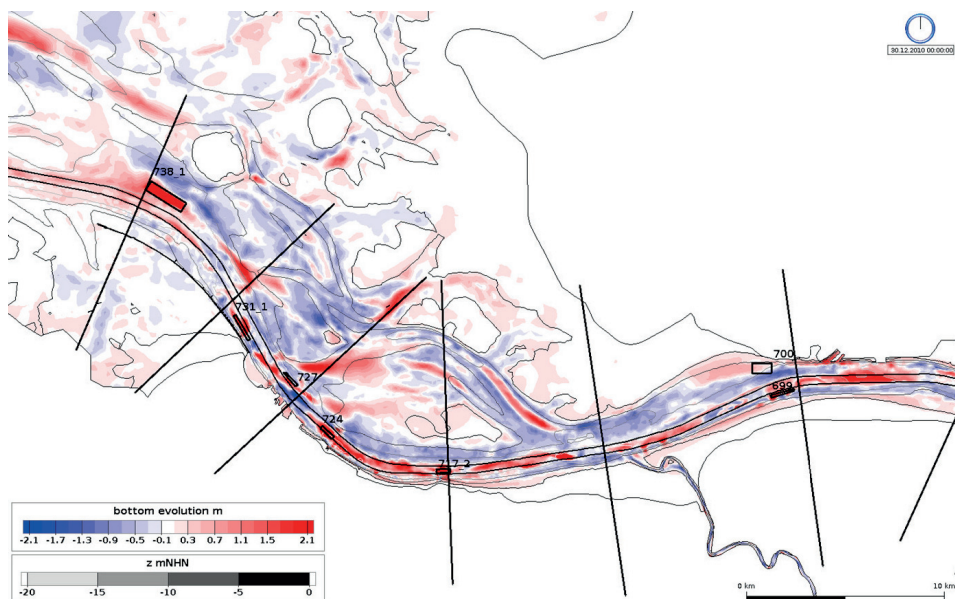


Figure 14: Modelled bottom evolution in the mouth of the Elbe estuary for the year 2010. Result of a three-dimensional model run. All known dredging and dumping operations are included. Dredging sites as well as disposal sites are recognizable. Black lines indicate the borders between dredging sections according to Fig. 3. Numbers denote stream kilometers.

Finally, Fig. 15 shows the difference in topography from the year 2011-2010. Dredging sites known from monitoring data are indicated as green polygons. The bottom evolution in the vicinity of the disposal sites is obviously influenced by disposal operations, as we have already seen in Fig. 14. However, some larger morphological trends also appear to be influenced by the disposal sites, e.g. the depositions are south-east of the disposal site at Elbe km 738 (Fig. 13).

We observe large morphological changes in the mouth of the Elbe estuary. The reasons for these changes need to be better understood given that the morphological state of the Outer Elbe has a strong impact on the tidal dynamics of the whole estuary. If possible proper morphological developments should be supported by a flexible and adaptive sediment management strategy.

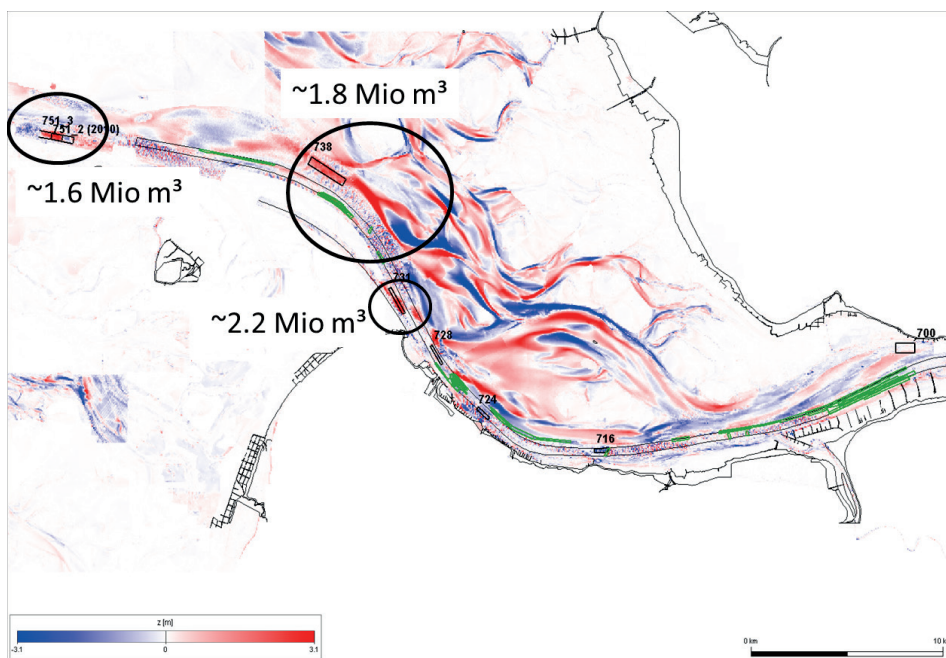


Figure 15: Difference topography for the year 2011-2010. Dredging sites are indicated as green polygons. The bottom evolution in the vicinity of the disposal sites is obviously influenced by disposal operations.

6 Outlook

Especially in the region of the North Sea estuaries, a profound understanding of sediment processes and expert sediment management are indispensable. It follows from the relationships discussed above that it is advisable to pursue an optimisation strategy for handling the dredged material which fulfils several purposes: minimising costs and dredging volumes, but also meeting other objectives. Optimised sediment management takes account of all the processes referred to above. At present, little is known about the long-term effects of the repeated removal of sediments. More scientific and practical basic knowledge is needed. Such knowledge would be of direct benefit for sediment management and would contribute to understanding the system. Hence, there is a need for further development of existing approaches. Given the permanent hydromorphological changes in estuarine systems due to both anthropogenic and natural influences, adapting and optimising sediment management strategies is a never-ending task.

7 References

BAW: Model validation and system studies for hydrodynamics, salt and sediment transport in the Elbe Estuary - Basic information for the River engineering and sediment management concept, Version 1.0, Hamburg, 2012.

- BAW: Handlungsoptionen zur Optimierung der Unterhaltungsstrategie im Mündungstrichter der Tidelbe, Hamburg, 2013.
- BAW: Validierung des Elbmodells. Bundesanstalt für Wasserbau, <http://www.zukunftelbe.de/Projektbuero/planaenderung/Downloads/h/h1/Anlage8.pdf>, 2006.
- BAW: Mathematical module SediMorph – Validation document, Bundesanstalt für Wasserbau, 77 p., http://www.baw.de/downloads/wasserbau/mathematische_verfahren/pdf/vd-sedimorph.pdf, 2005.
- BfG: Sedimentmanagement Tidelbe - Strategien und Potenziale - Systemstudie II. Ökologische Auswirkungen der Unterbringung von Feinmaterial. Band 1 (2), Endbericht. Im Auftrag des Wasser- und Schifffahrtsamtes Hamburg. Bundesanstalt für Gewässerkunde, Koblenz, BfG-1763, 2013.
- CASULLI, V. and WALTERS, R.A.: An Unstructured Grid, Three-Dimensional Model based on the Shallow Water Equations. *International Journal for Numerical Methods in Fluids*, 32, 331-348, 2000.
- CASULLI, V. and ZANOLLI, P.: Semi-Implicit Numerical Modelling of Non-Hydrostatic Free-Surface Flows for Environmental Problems, *Mathematical and Computer Modelling*, 36, 1131-1149, 2002.
- CASULLI, V. and ZANOLLI, P.: High resolution methods for multidimensional advection-diffusion problems in free-surface hydrodynamics. In: *Ocean Modelling*, Vol. 10, 1-2, 137-151, doi: 10.1016/j.ocemod.2004.06.007, 2005.
- ENTELMANN, I.: Optimierung von Unterhaltungsstrategien an der Tidelbe - Fragestellungen zum Sedimenttransport. In: *Dynamik des Sedimenthaushaltes von Wasserstraßen*. 14. Gewässermorphologisches Kolloquium der BfG, Koblenz, 2012.
- HPA and WSV – Hamburg Port Authority and Wasser- und Schifffahrtsverwaltung des Bundes: Strombau- und Sedimentmanagementkonzept für die Tidelbe. Hamburg/Kiel, <http://www.kuestendaten.de/publikationen/index.html>, 2008.
- LANG, G.: Mathematical model UnTRIM – Validation Document. Federal Waterways Engineering and Research Institute (BAW), <http://www.baw.de/vip/abteilungen/wbk/Methoden/hnm/untrim/PDF/vd-untrim.pdf>, 2005.
- MAERKER, C. and MALCHEREK, A.: DredgeSim – Erstellung der Grundversion eines Modul-pakets zur morphodynamisch-numerischen Simulation von Unterhaltungsmaßnahmen. Bericht im Auftrag der Bundesanstalt für Wasserbau, Institut für Wasserwesen, Universität der Bundeswehr München, 2007.
- MAUSHAKE, C. and AARDOM, J.: Suspended sediment measurements on the river Elbe using ADCP, *Underwater Acoustic Measurements 07 UAM07 proceedings*, Heraklion, Greece, 2007.
- MOL, J.: Suspended Sediment Measurements in the Elbe, AquaVison reports AV_DOC_070101, AV_DOC_070102 and AV_DOC_070301 contracted by BAW-AK, Hamburg, 2007.

Impact of Controlled Tidal Barrier Operation on Tidal Dynamics in the Ems Estuary

Dennis Oberrecht and Andreas Wurpts

Summary

River Ems estuary in the NorthWest of Germany is a partially mixed estuary, which exhibits strong accumulation of cohesive fines by means of fluid mud as a result of several deepening and straightening works that were conducted during the past decades. The driving phenomena are intensified baroclinic circulation which is extended inland by means of fluid mud induced baroclinic effects. Therefore, the turbidity zone consists of fluid mud deposits of several meters and extends throughout the whole tidally influenced reach up to the most downstream located weir. Strongly increased tidal asymmetry is present and results in short, but strong periods of flood flow in combination with weaker ebb flow over longer durations. The investigation presented here deals with a modelling approach to investigate a modified use of the Ems river barrage in order to influence the tidal wave propagation towards a more symmetric shape, while maintaining the tidal volume as much as possible. The aim is to reduce upstream sediment transport as well as turbidity and increase dissolved oxygen concentration, especially during periods of low fresh water discharge. The investigation shows decreased tidal asymmetry and influences on the baroclinic circulation in both, field measurements and also well reproduced by the numerical model as a result of the barrier operation. Also lower suspended sediment and higher dissolved oxygen concentrations in the lower Ems estuary are observed. The mode of the tidal barrier operation is subject to a hydro- and morphodynamic optimization procedure which is done by the numerical model described here.

Keywords

Ems estuary, tidal asymmetry, baroclinic circulation, tidal control, storm surge barrier, fluid mud

Zusammenfassung

Das Emsästuar im Nordwesten Deutschlands ist teildurchmisch und weist eine starke Ansammlung von kohäsiven Sedimenten in Form von Flüssigschlück auf. Diese ist auf die in der Vergangenheit durchgeführten Vertiefungen und Begradigungen des Flusses zurückzuführen. Im Wesentlichen wurde durch die flussbaulichen Maßnahmen die barokline Zirkulation intensiviert, deren räumliche Ausdehnung vergrößert und die Gezeitenasymmetrie gesteigert. In der Trübungszone des Ästuars bis hin zum Tidewehr findet man Flüssigschlück mit Mächtigkeiten bis zu mehreren Metern in der Wassersäule vor. Als Folge der Ausbauten ist zudem eine starke Asymmetrie entstanden, die eine kurze aber starke Flutströmung und eine lange und schwache Ebbströmung verursacht. Als Folge der verstärkten Ansammlung suspendierter Sedimente weist die Unterems insbesondere über die durch niedrige Oberwasserzuflüsse charakterisierten Sommermonate einen kritischen ökologischen Zustand auf. Die weiteren Nutzungsanforde-

rungen an das Gewässer erlauben jedoch keine Verflachung des Gewässers zur Herstellung der vormaligen Zustände. Die hier vorgestellte Untersuchung befasst sich mit der modelltechnischen Untersuchung einer veränderten Nutzung des Emsperrwerkes in Gandersum, um die Gezeitenasymmetrie zu beeinflussen. Durch eine temporäre Dämpfung des extremen Tidesiegs im ersten Drittel der Flut bei gleichzeitig möglicher Beibehaltung des Tidevolumen sollen die in dieser Tidephase sehr ausgeprägten, stromauf gerichteten Sedimenttransporte reduziert werden. Hiervon wird u.a. eine Verbesserung der Gewässergüte während Phasen niedrigen Oberwasserabflusses erwartet. Die numerischen Untersuchungen zeigen eine sehr gute Übereinstimmung im Vergleich mit den Ergebnissen mehrerer Naturversuche unter Einsatz des Emsperrwerkes.

Schlagwörter

Ems Ästuar, Tideasymmetrie, barokline Zirkulation, Tidesteuerung, Emsperrwerk, Flüssigschlick

Contents

1	Introduction	428
2	Model approach.....	430
3	Model calibration and validation	430
4	Results and observations.....	431
5	Conclusion.....	433
6	References	433

1 Introduction

In the present study a modified use of the storm surge barrier in Gandersum (GAN) is analyzed by means of hydrodynamic numerical results of estuarine flow behavior of the Ems estuary. A three-dimensional numerical model of the estuary was developed, calibrated and validated by means of data gathered from prototype tests involving the storm surge barrier in the years 2009, 2010 and 2012. This hydrodynamic study is carried out as a part of a hydro- and morphodynamic investigation focusing on changes of sedimentation rates as well as water quality improvements in the lower estuary, due to the modified use of the barrier. The Ems estuary (Fig. 1) is a partially mixed estuary in the NorthWest of Germany which partly also makes up the border to the Netherlands. The tidally influenced part of river Ems extends a total length of 110 km starting from the east Frisian island Borkum to the tidal weir in Herbrum with an average fresh water inflow of 78 m³/s. Due to deepening and straightening in past decades the flow behavior shifted to shorter but strong flood flow and weaker but longer ebb flow. This in turn led to massive accumulation of cohesive sediment, which has fluid mud exhibit complex interactions between suspended sediment and tidal currents like dynamic stratification and a non-Newtonian flow behavior in the lower parts of the water column. Further effects caused by the engineering measures are reduced shear and roughness which implies a less impeded propagation of the tidal wave through the estuary and resulted in higher high

water level as well as lower low water levels (HERRLING 2008). The tidal range at the mouth amounts 2.2 meters and increases upstream to 3.2 meters in Papenburg (PAP).

In order to analyze changes of tidal dynamics due to a modified use of the storm surge barrier at Gandersum, the barrage and a gate underflow parameterization have been implemented in the hydrodynamic model. The storm surge barrier was built in 2004 to protect the hinterland against flooding and consists of seven gates, where two gates for crossing vessels are used. Cross-section at the barrier is about 474 meters width, 13 % of which are blocked by piers, which corresponds to a net width of 414 meters. In order to influence the tidal dynamics closure scenarios during the prototype test from 2012 are exemplary considered here. Then up to 67 % of the cross-section was temporarily blocked by means of closing several gates.

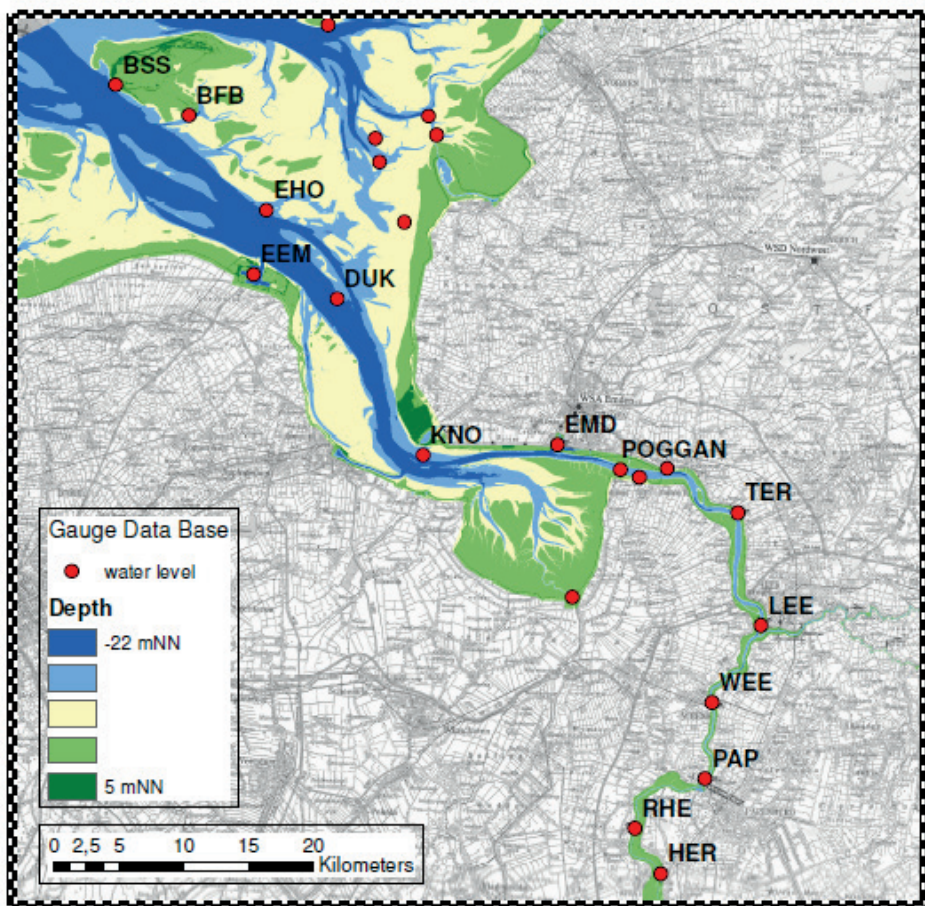


Figure 1: The Ems estuary. Map overlay shows bathymetry and water level and salinity gauge stations.

2 Model approach

A 3D structured grid, finite volume Delft3D model is applied to reproduce the hydrodynamic mechanisms and salt dynamics of the estuary. The specific time dependent mode of the barriers gates operation (cross sectional area is controlled by means of vertical gates with underflow) is implemented as a hydrodynamic energy loss approximation due to gate underflow in the numerical shallow water equation model. To reproduce vertical salinity gradients during slack times and baroclinic circulation pattern as well as turbulence situation of the estuary, a Prandtl-Mixing-Length model with a damping function after PERELS and KARELSE (1982) was implemented to solve the turbulence closure in the diffusion term of the Reynolds-averaged Navier Stokes equation and the vertical diffusivity parameterizations within the coupled advection-diffusion-equations for salt, temperature and suspended sediments.

3 Model calibration and validation

The study area extends from the east Frisian island Borkum up to the tidal barrier 110 km upstream in Herbrum (HER). The tributary river system of Leda and Jümme is also included in the model domain, mounding into the Lower Ems at Leerort. The model domain is represented by 51648 nodes and consists of 10 vertical layers. The lateral model boundaries follow the dike line and are fixed to 8 meters above mean sea level. The open boundary condition at the sea side of the model is implemented by tidal forcing of measured water level time series at station Borkum. Both inland boundaries (Herbrum and Leda) have been implemented as a discharge time series and for the transport of salt and temperature corresponding time series of nearby measurement stations were generated at all boundaries. For saline and temperature initial conditions throughout the model domain, average salinity and temperature values over simulation period were calculated and interpolated to all nodes.

For the investigations a four week simulation period was chosen in 2010. The first two weeks serve as a warm-up period and the remaining two weeks are then used for analysis. The simulation period starting at 10th March 2010 provides freshwater discharge decreasing from relatively high ($\sim 200 \text{ m}^3/\text{s}$) to lower values of $\sim 100 \text{ m}^3/\text{s}$. The calibration of the model and shown figures (2 & 3) of calibration is based on the time period of the prototype test 2012.

Fig. 2 shows a validation of measured and modelled water level differences across the tidal barrier during tidal control operation. The calibrated energy loss approximation enables the shallow water equation based model for sufficient reproduction of the barriers gates influence and hence the damping of the overall tidal dynamics due to the gates operation.

Fig. 3 shows a comparison of measured and calculated salinity differences time series between bottom and surface at location fairway ton 61 (in the “entrance” to lower Ems between Knock (KNO) and Emden (EMD), see Fig. 1). Sufficient reproduction of the flow and salt dynamics at this location is strictly required, since the upstream situation in river Ems is dominantly driven by the dynamics prevailing here, closely upstream of the flow splitting between Ems and Dollart (Fig 1). The large scale baroclinic circulation system is reproduced very well.

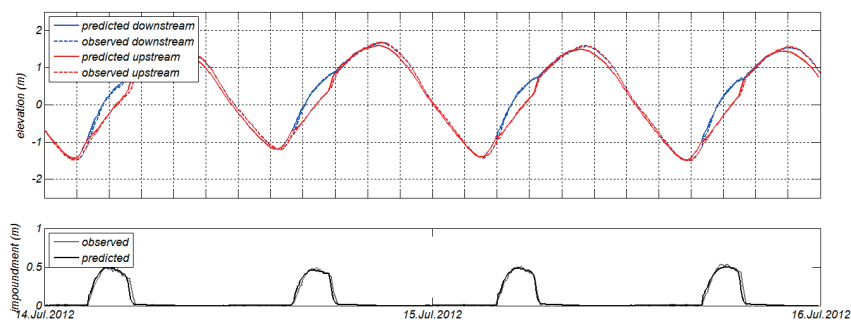


Figure 2: Upper panel shows comparison of measured and modelled water elevation time series during prototype test 2012 at Gandersum. Lower panel shows the corresponding water level differences between upstream and downstream position of the storm surge barrier.

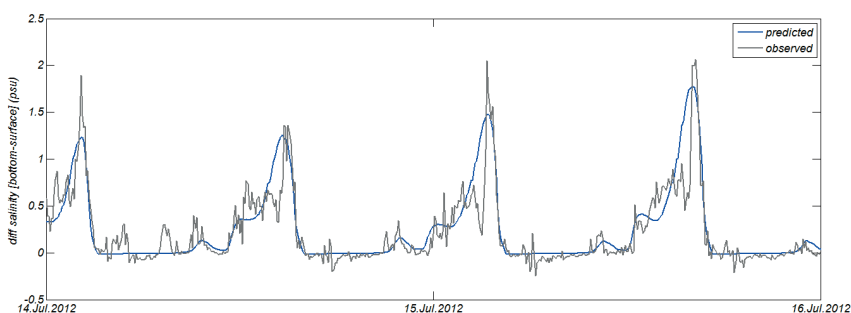


Figure 3: Comparison of vertical salinity difference between surface and bottom at station T61 close to Knock (KNO) during field test 2012.

4 Results and observations

The comparison presented here is based on modeled results of tidal dynamics with and without tidal control (reference state) for the same simulation period and with otherwise all model configuration kept identical. The tidal control scenarios are focused on a prototype test of 2012. During the test in 2012 all gates were closed except the main and secondary traffic gates located at the deepest part of the tidal channel. The other gates were temporarily closed, amounting of a reduction in flow cross-section around 67 %. Closing started at low water and reopening 2.5 hours after slack time before flood.

Fig. 4 shows the effect of the tidal control on the ratio of ebb to flood duration along the estuary. The change in tidal asymmetry is clearly visible from Emden to Weener. The step in Leerort is due to the inflow and outflow of Leda-Jümme River. The reduced tidal asymmetry shows a change to longer flood duration with weaker currents and shorter ebb duration with a stronger ebb flow.

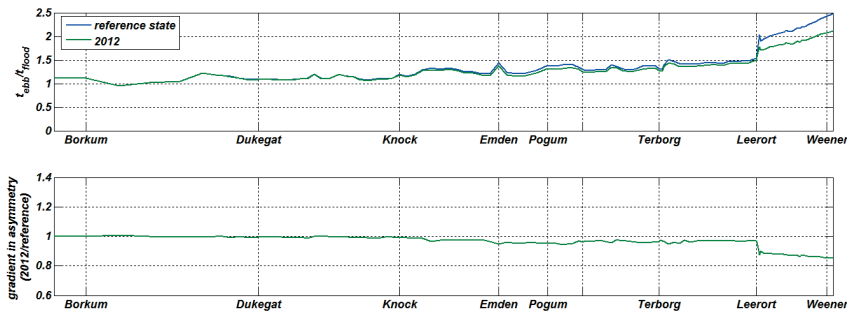


Figure 4: Upper panel shows tidal asymmetry based on modelled velocity measurements along the estuary. Lower panel shows the difference between tidal control and reference state.

Fig. 5 shows vertical salinity gradients as a proxy for baroclinic circulation intensity. Abscises shows time, ordinate shows longitudinal position starting from Eemshaven (EEM) to Oldersum (OLD, see Fig 1 for locations). This range roughly excludes the fluid mud dominated part of lower Ems, since there occur strong interaction phenomena of salinity transport and fluid mud.

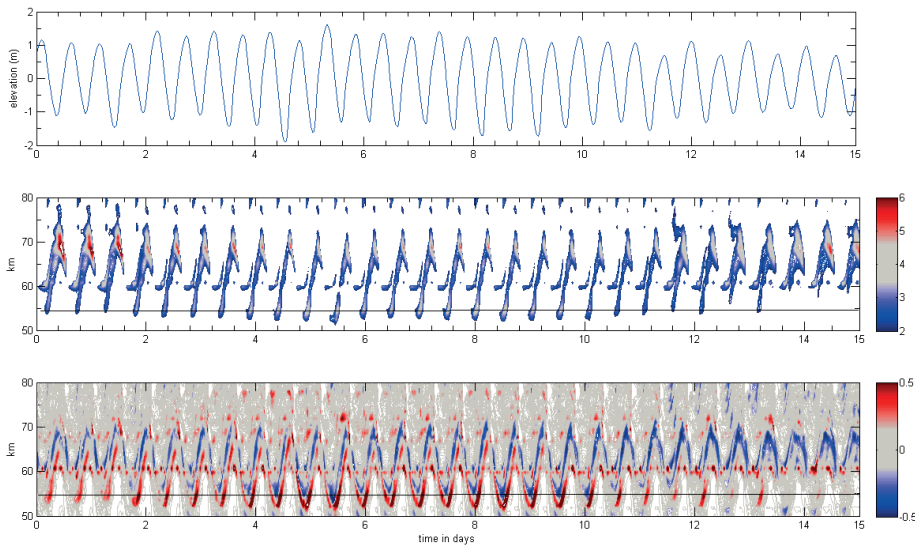


Figure 5: Upper panel shows water level at sea boundary, mid panel shows the vertical salinity gradient at reference model results in a longitudinal section and lower panel shows difference of reference and 2012 tidal control scenario. Black line indicates location of the storm surge barrier.

The location of the storm surge barrier in Gandersum is given by the horizontal black line at km 55. The vertical salinity gradient of reference state in middle panel of Fig 5 is shown. Mid panel of Fig 5 shows a vertical salinity gradient of 5-6 psu during slack time before flood at neap tide (days 0-4 + 11-15) around km 70. At spring tide (days 4-10) a

weaker gradient of 4-5 psu during slack before ebb compared to neap tide is observed. At slack time before ebb the strongest vertical salinity gradient appears at Gandersum by 0-2 psu during neap tide while at spring tide a gradient of 3-5 psu arises. Intensity of the vertical salinity gradient is mainly forced by the horizontal salinity gradient along the estuary and local turbulence intensity.

In comparison to reference state lower panel shows the difference with the tidal control scenario. Around Knock an increase of 0.3 psu during spring tide conditions combined with a reduction of stratification during ebb period was calculated. At neap tide occurs a significant reduction of vertical salinity gradient of 0.5 psu upstream of km 70, which causes in smaller baroclinic circulation zone during slack time before flood. During slack time before ebb at spring tide conditions a significant increase of salinity gradient of more than 0.5 psu combined with an upstream area by a clearly pronounced weakening of the gradient downstream. Weaker salinity stratification during ebb period can be observed as well. Calculations of tidal control have shown a reduction of tidal asymmetry at the surface in the baroclinic circulation zone. This statement is confirmed by measured data, which confirms the plausibility of the numerical model.

5 Conclusion

The numerical study which is presented here is part of a larger investigation aiming to improve the ecological situation of the lower Ems. This paper focusses on some hydrodynamic estuarine phenomena and how those are influenced by means of a new approach of tidal control by means of an alternative use of the existing storm surge barrier. The model is carefully adapted to the specific requirements of the physical problem (gate underflow in shallow water equation model, complex baroclinic forcing) and resolves this very well with respect to the relevant driving phenomena. A comparison of modeled tidal control and a reference state without tidal control is shown including changes and intensity of the vertical salinity gradient and baroclinic circulation pattern along the estuary. In comparison to reference state a change in flow behavior is observed due to the modified barrier operation. Tidal control by means of an adapted operation of the storm surge barrier shows to significantly reduce tidal asymmetry and influences the baroclinic mechanism as well. These parameters however are understood as only indicators regarding the major aim of positively influencing the sediment and ecological regime. Therefore in parallel the investigation continues towards an optimization of the operational mode based on sound morphodynamic calculations.

6 References

- HERRLING, G.: Comparison of the hydrodynamic regime of 1937 and 2005 in the Ems-Dollard estuary by applying mathematical modeling, NLWKN Coastal Research Station, 30 p., 2008
- PERELS, P.A.J. and KARELSE, M.: A two-dimensional laterally averaged model for salt intrusion in estuaries, Tech. Rep. 262, Waterloopkundig Laboratorium, Delft Hydraulics Laboratory, 1982

Simulation of High Suspended Sediment Concentrations and Options for a Reduction in the Lower Ems

Monika Donner and Oliver Stoschek

Summary

Estuaries with hyper-concentrated suspended sediment concentration (SSC) provide critical conditions for water management, channel shipping and ecological affairs. Due to the extreme situation of the Ems concerning the SSC, ecologists and water management authorities try to find solutions by different restoration measures, which aim to damp the hydrodynamic asymmetry and to reduce the suspended sediment concentration. Indicators especially for mobilization, resuspension and settling of fine cohesive sediments provide important benchmarks to evaluate restoration potential. Therefore hydro- and morphodynamic indicators like changes in flood and ebb currents, in flood- and ebb current gradients, net sediment flux and the shift of the turbidity zone were assessed. Especially indicators for fine sediments were selected to analyze the potential of meso-scale suspended sediment reduction.

Numerical simulations were performed to increase the Understanding of this estuary. But it shows limits to the existing physical approaches for cohesive sediment transport. For a performance of high suspended sediment concentrations two approaches, one with a simplified flocculation and typical hindered settling, and one with a new flocculation approach taking turbulence and salinity into account, were compared for the Ems Estuary. The hydrodynamic processes, salinity and suspended sediment transport were resolved by a numerical three dimensional finite volume model for the Outer and Lower Ems.

Considering the uncertainties already inherent in meso-scale simulations the long-term effects are difficult to anticipate. Based on an existing long-term approach for a tidal marsh river with cohesive sediments, first conclusions for a promising long-term concept in an estuarine environment are presented.

Keywords

hyper-concentrated suspended sediments, restoration measures, flocculation, indicators, long-term

Zusammenfassung

Ästuarie mit extrem hohen Schwebstoffkonzentrationen beeinträchtigen die wasserwirtschaftlichen Nutzungen, die Schifffahrt und die Gewässerökologie. Derzeit versuchen Ökologen und Wasserwirtschaftsbehörden Lösungen für die Ems in Form verschiedener Sanierungsvarianten, die die Tidesymmetrie abmindern und die Schwebstoffkonzentration absenken, zu finden. Indikatoren, die insbesondere für die Mobilisierung, die Resuspension und das Absinken von kohäsiven Sedimenten stehen, liefern für die Einstufung der Sanierungsvarianten wichtige Bewertungsgrößen. Hierzu wurden hydro- und

morphodynamische Indikatoren, wie die Veränderungen der Ebb- und Flutströmung, der Ebb- und Flutströmungsgradienten, des Nettosedimenttransports und die Verschiebung der Trübungszone bewertet. Insbesondere Indikatoren für Feinsedimente wurden gewählt, um eine mittelfristige Reduktion der Schwebstoffkonzentration zu bewerten.

Für die Prozessbeschreibung dieser Ästuarie wurden numerische Simulationen durchgeführt. Allerdings können bestehende physikalische Ansätze für kohäsive Sedimente nur bedingt angewandt werden. So wurden für die Abbildung hochkonzentrierter Schwebstofftransportprozesse zwei verschiedene Ansätze für die Ems gegenübergestellt: Ein Ansatz mit einem vereinfachten Flokkulationsterm und behindertem Absinken sowie ein neuer Flokkulationsansatz, der die Veränderung der Turbulenz und der Salinität mitberücksichtigt. Die Hydrodynamik, der Salz- und der Schwebstofftransport wurden dreidimensional mittels finiter Volumenmethode für die Außen- und Unterems aufgelöst.

Die hier durchgeführte Simulation mittelfristiger Tendenzen unterliegt bereits Unsicherheiten, so dass langfristige Tendenzen nur schwierig abzuschätzen sind. Auf Basis eines bestehenden Langzeitansatzes für tidebeeinflusste Marschgewässer mit kohäsivem Sediment werden erste Schlussfolgerungen für ein Langzeitkonzept in ästuariner Umgebung beschrieben.

Schlagwörter

Hochkonzentrierte Schwebstoffe, Sanierungsmaßnahmen, Flokkulation, Indikatoren, Langzeitverfahren

Contents

1	Introduction	437
2	Methodology	438
2.1	Numerical approach	438
2.2	Calibration and comparison of the different approaches	440
2.3	Assessment of restoration potentials	442
3	Results and discussion	443
3.1	Effect on hydrodynamics	445
3.2	Effect on suspended sediments	446
4	Conclusion	449
4.1	Restoration potential	449
4.2	General conclusion	450
5	Outlook	451
6	Acknowledgements	452
7	References	452

1 Introduction

Estuaries form a significant connection between marine and fluvial environments. Due to human pressure, especially the Ems Estuary was impaired inter alia by river regulations, deepening and reduced shallow water zones. The key reason for the high suspended sediment concentration in the Ems today was induced by the hydro- and morphodynamic changes due to the deepening of the Ems (WEILBEER 2005).

Hydrodynamic changes were indicated due to the reduction of the low tide and the increase in of high tide water level, thus the tidal range in Herbrum increased from 1 m up to 3.5 m within the last 70 years (JÜRGES and WINKEL 2003). In addition the asymmetry of flood and ebb increases the flood dominance with higher flood maximum currents while ebb currents are almost constant. The gradient of slack water to flood flow is up to 8 times steeper than, the gradient of slack water to ebb flow.

Currently the Ems estuary indicated a dramatic turbidity increase over the last 15 years: The annual averaged suspended sediment concentration rose from 1 g/l in 1992/93 (SCHUTTELAARS et al. 2009) up to 10 g/l in 2008/09 (NLWKN Aurich 2009) accompanied by an extreme shift of the estuarine turbidity maximum (ETM) to upstream locations. The historical progress of the annual averaged suspended sediment concentration demonstrates that during the 50^s the ETM was located in Emden with about 0.2 g/l. After deepening the Outer Ems (1975-76) the ETM was shifted upstream to Terborg with an increase to 0.4 g/l. In 2005 a broad-crested ETM with 1 g/l from Terborg to Papenburg was found. Especially from the mouth of the Lower Ems in the so-called Emden Fairway sediments are imported from the sea side during low and mean discharge events into the Ems Estuary. In addition fluid-mud layers evolve near the river bed. These fluid-mud layers in the upper part of the Lower Ems can be detected by extreme suspended sediment concentration gradients with 3 to 7 g/l/min.

Today ecologists and water management authorities are working together, like for example in the joint research project called "Perspective revitalized Lower Ems" in order to find solutions by restoration measures (Fig. 1) to reduce suspended sediment concentrations and to increase oxygen supply. Therefore different ideas of restoration elements were developed by water authorities, nature protection associations and international experts:

- Tidal polders (retention basins): Tidal polders, which are able to retard tidal volume and sediments and to reduce the tidal volume upstream of these polders.
- Shallow water zones including reactivated historical oxbows: Bifurcations and shallow-water zones on the foreland act like a macro-scale resistance due to the geomorphology. Due to the separation of flow, dissipation reduces currents and consequently the dynamics.
- Lengthening: An increased length of the Ems Estuary by a removal of the weir in Herbrum will change the tidal wave propagation and especially reduce the reflection of the tidal wave.
- Re-leveling: This increase of bed level stands for a reduction of water depth in the deep fairway between Leer and Papenburg, which will result in morphological effect due to a change of the width-to-depth ratio.
- Technical options with different regulations at the storm surge barrier (WURPTS 2012).

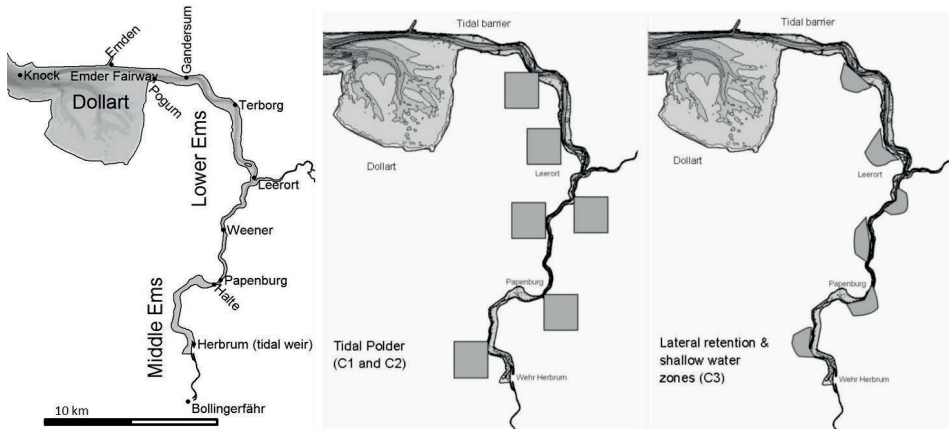


Figure 1: Overview for the Lower Ems (left), sketches of the restoration variants for the Ems Estuary, tidal polders (center) and shallow water zones (right).

This paper will only focus on effects of re-leveling, lengthening, tidal polders and lateral retention, with focus on restoration of the Ems estuary.

2 Methodology

In order to analyze the effect of restoration variants, at first the present situation of the Ems Estuary with its hydrodynamics and high suspended sediment concentrations were recovered by a numerical approach by taking two different approaches for the sediment transport into account.

2.1 Numerical approach

The numerical analysis is based on a three-dimensional resolution of the hydrodynamic processes, the salinity and suspended sediment transport for the Ems Estuary between Borkum and Bollingerfähr (Fig. 1). Therefore a finite volume method with a sigma layer approach in an unstructured grid (MIKE 3 FM) was applied. The hydrodynamics are solved based on the Reynolds-averaged Navier-Stokes equations, with a density coupled to the salinity transport. For the turbulence closure a $k-\epsilon$ approach in the vertical and the mixing length Smagorinsky approach with a coefficient of 0.28 in the horizontal direction was applied. The flow resistance effect of the almost frictionless riverbed, due to the cohesive and muddy sediments, was included based on a roughness approach according to Nikuradse with a roughness height between 0.5 and 5 mm in the supratidal area.

Two different methods (Mud Transport (MT) method and ECO Lab (EL) method) for the sediment dynamics were used and compared. Their main differentiator is the approach for settling velocities. The suspended sediment transport is solved for both methods with the 3d-advection-diffusion equation, taking hindered settling and cohesive sediment properties into account. Due to the presence and a high ratio of fine sand, silt and clay fraction, sand fractions and bed load transport play a less important role for the

suspended sediment dynamics, but will gain importance for the morphological changes (WEILBEER 2003).

The erosion rate is based on the formula according to PARTHENIADES (1965) for consolidated cohesive sediments:

$$S_{\text{ero}} = \beta_{\text{ero}} \left(\frac{\tau_0}{\tau_{\text{c,ero}}} - 1 \right) \quad \text{for } \tau_0 > \tau_{\text{c,ero}} \quad (1)$$

where β_{ero} is the erodibility factor [g/m²/s], $\tau_{\text{c,ero}}$ the critical erosion shear stress [N/m²], S_{ero} the erosion rate [g/m²/s], and τ_0 the bed shear stress [N/m²]. For both methods the general empirical erosion and deposition parameters were approximated based on empirical approaches, literature values and grain size distributions for the Ems, which were provided by the BAW and the NLWKN. The dry bulk density of the bed material was estimated based on an empirical approach according to Allersma (1988, in VAN RIJN 2007), which resulted in an interval of 170 to 1290 kg/m³ for the dry bulk density. The critical erosion shear stress was limited based on an approach according to ZANKE (1982) for soft and unconsolidated mud between 0.12 and 0.45 N/m². The erodibility factor was estimated based on the approach according to SCHWEIM (2005) taking the varying range of literature values from 0.01 up to 5 g/m²/s into account.

The deposition rate D is described according to KRONE (1962) by:

$$D = w_s \cdot c_b \cdot \left(1 - \frac{\tau_0}{\tau_{\text{c,dep}}} \right) \quad \text{for } \tau_0 \leq \tau_{\text{c,dep}} \quad (2)$$

where w_s is the settling velocity [m/s], c_b the near-bed concentration [g/m³], $\tau_{\text{c,dep}}$ the critical shear stress for deposition [N/m²], D the deposition rate [g/m²/s], and τ_0 the bed shear stress [N/m²]. The critical shear stress for deposition values are given by PARTHENIADES (1965) with 0.04 up to 0.15 N/m² and by LI et al. (1994) with 0.3 up to 0.5 N/m². For the Ems a constant value of 0.07 N/m² was applied.

For the MT method the settling velocities were based on an empirical flocculation approach according to BURT (1986) and a hindered settling for $c > c_{\text{hinder}}$ approach according to WINTERWERP (1999):

$$w_s = \begin{cases} \text{constant or linear} & \text{for } c < c_{\text{floc}} \\ k \cdot c^\gamma & \text{for } c_{\text{floc}} \leq c \leq c_{\text{hinder}} \\ w_{s,r} \frac{(1-\Phi_*) (1-\Phi_p)}{1+2.5\Phi} \quad \text{with } \Phi_p = \frac{c}{\rho_s}; \Phi_* = \frac{c}{c_{\text{gel}}} & \text{for } c > c_{\text{hinder}} \end{cases} \quad (3)$$

where w_s is the settling velocity [m/s], k and γ are coefficients [-], c sediment concentration [kg/m³], Φ the volumetric concentration of sediment [m³/m³], c_{floc} is the threshold concentration for the gelling point [kg/m³], ρ_s is the sediment density [kg/m³]. In the alternative EL method a new approach for the flocculation developed by NGUYEN (2010, 2012) was applied and compared to the MT method. This method is based on the same description and solution of the hydrodynamic as described above (MIKE 3 FM). Also the sediment transport (3d advection-diffusion), as well as erosion and deposition rates are computed analogous based on the approaches by PARTHENIADES (1965) and KRONE (1962). The difference is given by the settling velocity, which is taking the floc size, floc

density and drag coefficient into account under consideration of effects caused by salinity and turbulence; the computation of the settling velocity is based on the modified Stokes law:

$$w_s = (1 - \phi) \sqrt{\frac{4 \cdot (\rho_f - \rho_m) \cdot g \cdot D_f}{3 \cdot \rho_m \cdot C_{D,mt}}} \quad (4)$$

where w_s is the settling velocity under turbulence [m/s], ϕ the volumetric concentration of flocs in the mixture [m³/m³], ρ_f the floc density [kg/m³], ρ_m the density of sediment-fluid mixture [kg/m³], gravity acceleration [m/s²], D_f is the floc size [m], and $C_{D,mt}$ the drag coefficient of flocs [-]. The floc size is computed as a result of aggregation and breakup processes. So an increase of suspended sediment concentration leads to a higher probability of primary particle collisions, which is encouraging aggregation. High salinity is considered to support the formation of flocs as well by compression of the electric double layer of the particles and for this reason growing effect of van-der-Waals force. High turbulence will cause a breakup of flocs. Based on the floc size, the floc density is calculated subsequently. The drag coefficient depends on the shape and size of the primary particles or flocs and furthermore on the viscosity of the sediment-fluid mixture. Consideration of turbulence in the calculation of floc size and drag coefficient can be regarded to be a unique characteristic of the approach implemented in EL method.

2.2 Calibration and comparison of the different approaches

The numerical model was calibrated and validated against existing measurements for water levels, currents, salinity and suspended sediment concentrations (Fig. 2). Three summer events in 2008 with a low fluvial discharge (ca. 40 m³/s), a mean discharge (ca. 80 m³/s) and an annual mean flood discharge (ca. 110 m³/s) were taken into account. Winter events and storm surges are not relevant for the high turbidity in the Ems.

For quantifying the model performance the mean error (ME) was used. For water level and the tidal currents the ME was good with less than 0.12 m for the water level (0.05 to 0.24 m) and about 0.14 m/s for the currents (0.07 to 0.22 m/s). A delay appears in the phase between the simulated and measured tidal curve. The amplitude of the high tide is reproduced with variations below 10 cm (mean value) quite well, while the amplitude of the low tide is slightly overestimated with up to about 20 cm. The tidal asymmetry based on the water level gradient over the time is reproduced in the numerical model with a difference between simulated and measured gradients below 0.003 m/min, which is a very good result.

Due to the seasonal variability of the salinity at the sea boundary, which was derived by measured salinity time series at the station in Knock (Ems-km 51, Fig. 1), different boundary values between 30 and 32 PSU at Borkum were analyzed in a sensitivity study. For low fluvial discharges (MHQ to 40 m³/s), which are relevant for the high suspended sediment concentrations in the Ems estuary, the approach of 30 PSU at the sea side represented the measured salinity condition between Knock and Herbrum (Fig.1) with a mean error of 3.1 down to less than 0.01 PSU (Fig. 2).

The calibration of suspended sediment transport results in good accuracy with differences between measured and simulated suspended sediment concentrations of 0.2 up to

3.9 g/l (for MT method) and 0.3 up to 3.7 g/l (for EL method). The high delta of more than 3 g/l is for both methods generated by an underestimation of a local suspended concentration peak in the measured time series. The measured suspended sediment concentration in- and decreases during slack water at low tide from 5 g/l up to 40 g/l with a gradient of ± 7.8 g/l/min near Weener (Ems-km 7, Fig. 1) and ± 3.7 g/l/min near Papenburg (Ems-km 0, Fig. 1). Both measurement positions are located about 3 m above the river bed.

This peak concentration is only approximately resolved by the numerical model with significant lower amplitude. There might be three reasons for these temporary peak concentrations under minimal flow velocities near slack water:

- Suspended sediments are settling in the water column during slack water and due to hindered settling a very high concentrated near bed layer with an increasing thickness appears
- With the incoming flood flow very high concentrated near bed layer (fluid mud) is moved upstream and is accumulated between Weener and Papenburg.
- Suspended near bed sediments are re-suspended into the water column due to the high velocity gradient after slack water.

Apart from the concentration peaks upstream the tidal oscillation of the SSC is recovered by the numerical model (Fig. 2).

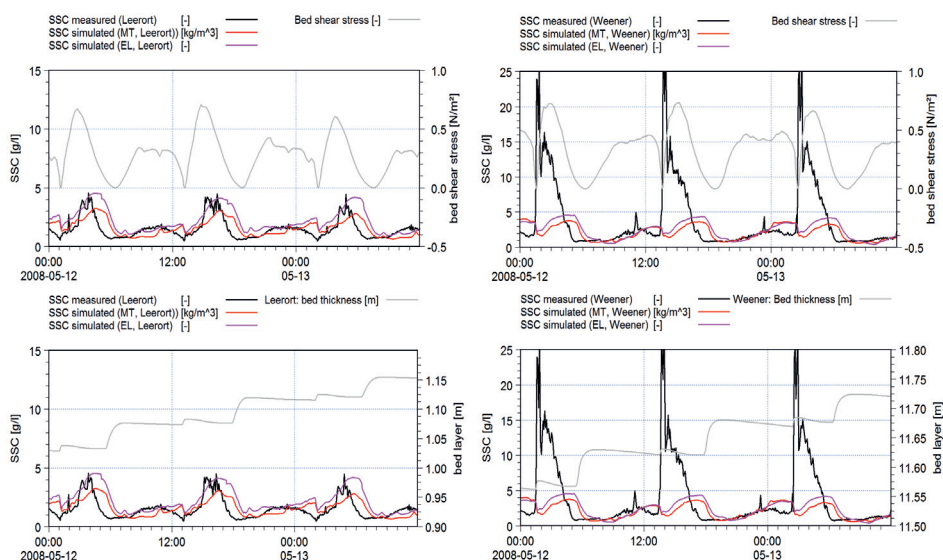


Figure 2: Comparison of simulated and measured time series in 2008 for suspended sediment concentrations at the Station in Leerort (Ems-km 14, left) and in Weener (Ems-km 7, right) in comparison with the simulated bed shear stress and the bed layer thickness, the measured data was provided by NWLKN Aurich (SSC).

The comparison between the two methods for the settling velocity showed, that the refined EL method is able to represent slightly higher suspended sediment concentrations especially during flood flow (see sharp peak in bed shear stress on the right side in Fig. 2). But both methods are not able to refigure the sharp increase and decrease of the

suspended sediment concentration in Weener. The reason for that can be found in the shear stress based erosion and deposition rate, which is used for both. Based on this approach the high concentrated suspension can only be refigured in the soft bed layer increase (here with a density of 360 kg/m^3). The reaction of the bed layer is represented immediately. The growth of the soft bed layer in both upstream locations is representative for the aggregation of fine soft sediment at the river bed. The morphological feedback due to this growth was not included.

2.3 Assessment of restoration potentials

For the assessment of the restoration variants and their shortcomings so-called key indicators for hydrodynamics and sediment transport, which are representative for fine sediments, were selected. Therefore indicators for flood dominance, tidal asymmetries, tidal range and sediment import were categorized based on their importance on fine sediment transport. The ranking of the indicators is based on the experience of different analyses as well as existing literature (e.g. LANG 2003).

One important objective is the reduction of flood flow, which postulates a reduction of sediment import. The longitudinal section of the maximum gradient ratio between flood and ebb currents represents a rough pointer for position of the ETM in the longitudinal section, with high ratios near the ETM. A reduction of the ratio of maximum currents (flood dominance) and an additional reduction in tidal range, especially a reduction in the upstream increase of both parameters, represent a damping of the hyper-synchronous character. The hydrodynamic key indicators for a restoration assessment are:

- Reduction of tidal asymmetry based on the net flow ratio below 1, which is describing the ratio between flood flow/ (ebb flow – fluvial inflow). This includes a decrease of flood flow as indicator for reduction of flood flow induced sediment transport and an increase of ebb flow.
- Reduction of ratio of maximum gradient between flood /ebb currents (dv/dt) in the main channel, which is an indicator for fine sediment transport acc. to DRONKERS (1986) and is relevant for the duration and intensity of re-suspension or sedimentation near slack water.
- Reduction of flood dominance based on the ratio of maximum flood/ ebb currents in the main channel below 1 (flood dominance with a ratio > 1), which is also representing the hyper-synchronous character of the Estuary and is an indicator for coarse sediment transport acc. to DRONKERS (1986).
- Increase of low tide as general indicator for an effect on the hydrodynamic behavior, which is resulting in a reduction of maximum flood currents and in an increase of maximum ebb currents.
- Decrease of tidal range by avoiding an increase of the tidal range from the mouth to upstream sections (hyper-synchronous character), which a general indicator for an effect on the hydrodynamic behavior.

The restoration effect is evaluated based on a change of the net sediment transport near the mouth and a shift of the ETM. An annual averaged sediment export at the mouth extended to upstream sections will reduce the suspended sediment concentration on larger time scales in the Lower Ems. Therefore a turn from sediment import to export in the Emden Fairway (which is corresponding with the mouth of Lower Ems) is an essential

change. Due to this export an accumulation of fine sediments in the fairway can be reduced and enables a change of the grain size distribution in the main channel. On the other hand local sediment import zones in upstream sections are regarded as less critical for the overall situation.

A reduction of the cross-sectional integrated and tidal averaged suspended sediment concentration with a downstream-shift of the ETM should be achieved. This shift indicates a lower sediment transport and consequently a lower mobilization or re-suspension of sediment due to reduced tidal dynamics. The downstream shift is consequently an indicator of a change to lower turbidities. Sediment key indicators for an assessment are:

- Decrease of net sediment import, with a turn to sediment export near the mouth to upstream sections based on a cross-sectional and tidal integrated sediment transport
- Downstream shift and reduction of the ETM based on a mean suspended sediment concentration by a cross-sectional and tidal averaged suspended sediment concentration
- Decrease of cross-sectional and tidal averaged suspended sediment concentration below a critical threshold according to ecologists with 100 mg/l for the fresh water section.

3 Results and discussion

The presented methods were applied to analyze the effect of tidal polder and lateral retentions by a combination of shallow-water zones and reactivated oxbows with the following scenarios:

- Scenario A1 includes a decrease of the water depth between Ems-km 14 up to 0 (Leer to Papenburg) from about -8 to -5 m NN to a constant level of -3.0 m NN (re-leveling). Here two sub-scenarios with the present sediments and with a sandy bed at the re-leveling area were compared
- Scenario B describes a lengthened Ems Estuary with a removed weir in Herbrum and a combination of two downstream polders, one at Ems-km 24 with 200 ha and Ems-km 12 with 400 ha. Both tidal polders are able to store a volume of about 18 million m³.
- Scenario C1 with six polders between Ems kilometer 23.5 up to -7 (7 km upstream of Papenburg) includes a restoration area of 1200 ha with polders between 400 and 50 ha and a tidal retention volume of about 29 Mio m³.
- Scenario C2 with nine polders between Ems kilometer 14 up to -6 (6 km upstream of Papenburg) includes a restoration area of 850 ha with polders between 150 and 50 ha and a tidal retention volume of about 14.2 Mio m³.
- Scenario C3 with eight bifurcations with shallow-water zones on the foreland between Ems kilometer 22 up to -7 (7 km upstream of Papenburg) including an area of 400 ha with new wetted areas between 130 and 30 ha with a tidal volume of about 10 Mio m³.

The re-leveling (Scenario A1) describes an artificial return to a historical bed level before deepening took place. This scenario would require an artificial channel between Ems-km 14 and 0 (Papenburg to Leer) for navigation. Due to this navigation channel downstream of Leer and upstream of Papenburg a deep river bed is necessary, which results in a bed slope between the navigation channel depth and the re-leveling section. This results in a

longitudinal section with a plateau between Ems-km 14 and 0. For the re-leveling two sediment types were analyzed: one with the actual grain size distributions (silty bed) and one with sand fractions (sandy bed).

The effect of lengthening was developed and analyzed in detail by SCHUTTERLAARS and DE JONGE (2011). They proved based on an analytical 1d-approach, which is simplifying the detailed geomorphology, but is taking the tidal propagation and cohesive sediment transport into account, that the location of the tidal weir has an effect on the location of the estuarine turbidity maximum. The most important outcomes of their study were: For the actual bed level (here 2005) including the weir at Herbrum the Ems estuary has a length which is close to the M2-tide resonance length, so the tidal wave has a standing wave character. Due to an upstream lengthening of more than 10 kilometer by removing the weir, the model predicted an ETM shift from Leer and Papenburg down to Emden. Similar but less significant effects were represented by a detailed numerical 3d-analysis for the Ems estuary of the BAW (ROLLENHAGEN 2011), which regarded a crest reduction of the weir in Herbrum from +1.8 m NN down to -0.5 m NN. This reduction of the weir height resulted in slight downstream reduction of the tidal averaged suspended sediment concentration and a very small shift of the ETM. Based on these experiences the lengthening was regarded in Scenario B with a full removal of the weir in Herbrum down to the bed level of about -1.5 m NN and was combined with two downstream polders in order to enhance the effect of ETM reduction and to reduce the tidal range by additional measures.

For tidal polders several parameters like the altitude of the bed, its size (volume and shape), position, form and type of the inlet are variable. In order to reduce these parameters, the following assumptions were made for all tidal polders: the polder bed was defined based on the mean low tide of the present situation, polders are connected perpendicular to the main channel, the length of the inlet is reduced to a few hundred meters and the form of the polder is simplified to a rectangle. Only position and size were varied, while the inlet width was narrowed downstream. Here a phase-shifted effect was achieved for the polders near and downstream of Leerort (Ems-km 14) with an inlet width of 30 to 40 % of the main channel width. For the upstream polders an in-phase inlet was used with about 50 to 70 % of the main channel width.

The lateral retention combines deep branches (outer bends) with a flat foreland, which is only wetted during high tide. Analogue to the polders several parameters like the width-to-depth-ratio, the altitude of the branch and the foreland bed, the position, form and types of branches are variable. Thus the following assumptions were made: the width of the branches varies between 75 to 90 % of main channel width, the altitude of the branches is about 1.5 m below the mean low tide, the altitude of foreland is about 1 m below the high tide and the position of the branches was based on historical oxbows.

All scenarios were simulated based on the above outlined numerical approaches for hydrodynamics, salinity and sediment transport by including the described restoration elements based on a short-term period, with measured tidal cycles from May 2008 at Borkum over about 3.5 weeks (MLW +1.27 m NN, MHW -1.97 m NN, tidal range 3.25 m at Knock) and a constant fluvial discharge of 88.11 m³/s (MQ) at the upstream boundary (Bollingerfähr). For the suspended sediment concentration and salinity 30 PSU and 0.02 g/l were defined at the sea side and 0.34 PSU and 0.05 g/l were set at the upstream boundary.

3.1 Effect on hydrodynamics

The hydrodynamics showed quite different effects for the scenarios: The re-leveling (A1) represented negative effect downstream of the re-leveling and positive effects at the re-leveling section and upstream: The negative effects downstream are characterized by a slight increase of the tidal range with a few centimeters, a reduction of the low tide and an increase of the high tide (Fig. 3). Additionally the maximum flood currents rose, which results in an increase of the flood dominance. At the re-leveling and upstream tidal range is reduced up to 1.4 m (A1, Fig. 3, top right).

The lengthening (B) showed an improvement for tidal water levels with a continuous reduction of the mean tidal range up to 1.1 m (Fig. 3, top right). All polder and shallow water zone scenarios showed a continuous reduction of the mean tidal range with up to 2 m (C1 and C2) and 0.8 m (C3). The maximum tidal range in the longitudinal section is slightly reduced to about 3.4 m for all scenarios (B, C1 to C3) and position of the maximum between Ems-km 10 to 40 is shifted downstream to Ems-km 30 to 40.

The polder and shallow water zone scenarios showed a reduction in flood dominance based on the ratio of maximum flood to ebb currents (Fig. 3, bottom left) by 30 % (C1), 25 % (C2) and 15 % (C3) between Ems-km 40 and 15 and by 20 % (C1, C2 and C3) between Ems-km 15 and -5. The local maximum of the flood dominance is decreasing from a flood-dominance ratio of 1.3 (present situation, Fig. 3) down to a slight ebb-dominance with about 0.9 (C1 and C2, Fig. 3), but is not shifted downstream. Only for scenario C3 the local maximum is shifted about 10 km downstream, but still remains flood dominant with 1.0 between Ems-km 10 to 20. The ratio of the maximum flood to ebb gradients, which has its maximum with 8.0 for the present situation near Papenburg (Ems-km 0, Fig. 3), is shifted downstream to Ems-km 20 to 40 for all scenarios. The reduction of the ratio due to the scenarios reaches 3.0 for C3, 2.5 for C2 and 2.0 for C1.

One important effect was represented by the net balance of flood/ ebb flow without fluvial discharge (here MQ) as a ratio for the tide-driven volume flow (Fig. 3, top right). The net flow ratio, which represents a peak value of factor 2.0 near Ems-km 0 (Papenburg) was shifted downstream with about 5 km by A1, but only a slight reduction to 1.6 (A1). For B no downstream shift appears, but the peak value is reduced to about 1 (Fig. 3). By C1 and C2 the peak of net flow ratio was shifted downstream with about 10 km and reduced to 1.0 (C1) and 1.1 (C2). For C3 the downstream shift increases to about 20 km and the peak value is reduced to 1 (Fig. 3).

Regarding the flood flow (volume/ duration), displayed in Fig. 3 (bottom left) in addition different effects of the extended polder section in C1 and the reduced upstream polders in C2 are obvious. Due to any tidal polder the tidal volume (flood and ebb volume) is increasing downstream due to an increasing wetted area (geomorphology) and reduced upstream. In addition the duration of the ebb and flood flow is slightly shifted to a more symmetric distribution (shortening of the ebb duration and lengthening of the flood duration). Thus downstream of tidal polders two different effects are superposed: an increase of flood volume as negative effect and an increase of flood duration as positive effect. In a certain distance downstream of the polders, the flood flow (volume / duration) represents a positive effect with a reduction in the flood flow. This reduction is extended in length and increasing in intensity, if tidal polders are shifted to upstream positions

(Fig. 3). This positive effect of upstream polders was also examined by ROLLENHAGEN (2011) and in a detailed analysis by CHERNETSKY (2012).

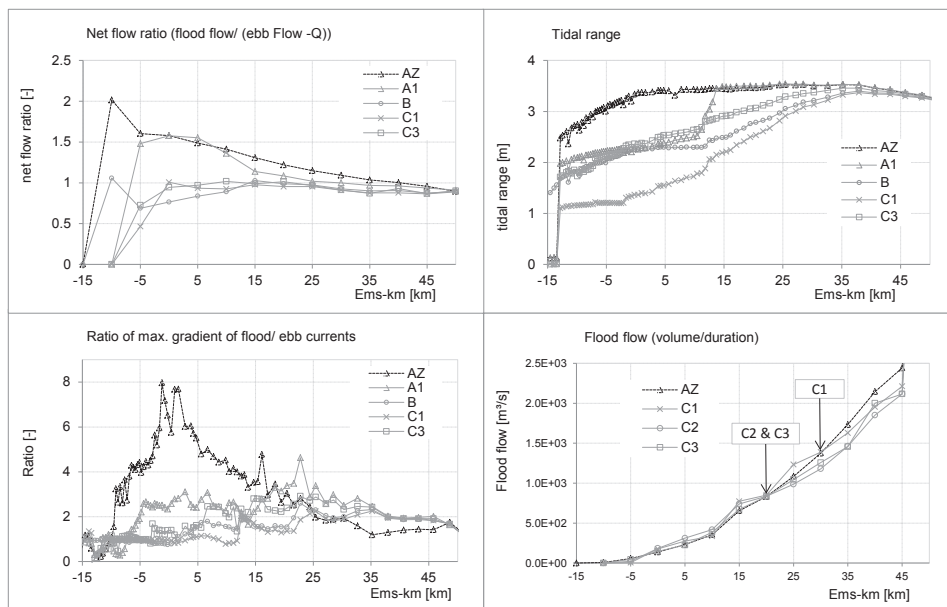


Figure 3: Longitudinal sections for the hydrodynamic indicators net ratio of flow (top left), tidal range (top right), ratio of maximum flood/ ebb currents (bottom left) and flood flow (bottom right) and for the present situation (AZ), for the scenario A1, B, C1, C2 (displayed for flood flow) and C3.

For hydrodynamics, the scenario C2 with a 30 % reduced and upstream shifted polder section represented the most positive effects on the tidal currents, tidal range and the tidal induced volume flow. The scenario C3 with its lateral retention has the smallest effects on the hydrodynamic side.

Scenario A1 showed shortcomings downstream, while the effects on tidal range and tidal currents were distinct in at the re-leveling and in upstream section. The main reason for this negative impact is the sharp increase in the bed level at the re-leveling, which is comparable to a fixed ground sill. So the tidal wave is reflected and tidal asymmetry is increasing in this downstream section. Upstream of the re-leveling, backwater effects with long-lasting reduced currents and significant reduced tidal water level oscillation appears. The rising low tide is induced by the elevation of the bed level and a reduction of the wetted area in the re-leveling section. This is also displayed by a reduction of the flood volume and ebb volume flow.

3.2 Effect on suspended sediments

For all scenarios sediment transport indicators like net sediment flux, a shift of the estuary turbidity maximum (ETM) and suspended sediment concentration (SSC, tidal averaged and cross-sectional integrated) were taken into account. An important indicator for a meso-scale change for the suspended sediment concentration was derived by the

extension and the intensity of sediment export from the mouth of the Ems estuary (Emder fairway). For the present situation at a mean fluvial discharge (MQ) an import near the mouth with about 2000 t/tide appears.

For the re-leveling (A1) the ETM is shifted downstream near to Ems-km 15, combined with a slight reduction of sediment import, but a lengthening of the import zone to upstream. The different sediments at the re-leveling (A1), silty sediments (like in the present situation) and sandy sediments (A1s), had only slight effects on the hydrodynamic behavior. With regard to the sediment dynamics the sediment types play an important role. For the silty river bed the ETM is shifted downstream from Ems-km -5 to Ems-km 15 with a strong increase from 3.2 g/l up to 4.5 g/l (A1). For a sandy bed at the re-leveling the import and export characteristics is the same, and also the estuary turbidity maximum is shifted downstream from Ems-km -5 to Ems-km 15, but with a decrease from 3.2 g/l up to 2.4 g/l (A1s). Additionally the natural water depth is higher than the proposed one. Therefore the re-leveling will be eroded and causes extra turbidity.

For the lengthening (B) the ETM is slightly reduced from 3.2 to 2.5 g/l, but shifted upstream by 5 km, but has a positive effect on the relevant sediment export over the Emder Fairway. The upstream shift of the ETM reveals two effects: the increase of tidal influence, which is already display in the hydrodynamic behavior, but also the mobilization of sediments upstream of the former weir at Ems-km -15. Due to the removal of the weir water level is tidal influence with a range of about 1.5 m (see Fig. 3). Consequently currents are increasing compared to former backwater currents to ebb-dominant currents. Upstream of the removed weir (Ems-km -15 to -20) only tidal water levels, but no flood currents (upstream velocities) appear anymore, so sediment is mobilized especially during low tide and higher currents (increase of about 200 %). These processes are increasing sediment concentration up to 0.9 g/l upstream of Ems-km -15 due to a short term mobilization of fine sediments there.

For tidal polders (C1, C2) and lateral retention (C3) the suspended sediment concentration on short-term is only slightly reduced, but the ETM is shifted downstream by 14 km with a reduction to 2.3 g/l (C1), by 16 km with a reduction to 2.7 g/l (C2) and by 5 km with a reduction to 2.0 g/l (C3). By C1 a reduced extension of sediment export up to about Ems-km 20, which was already analyzed for the hydrodynamics (see flood flow) with about 10000 t/ tide was initiated. For C2 and C3 this export is lengthened to Ems-km 15 with about 9000 t/tide (C2) and 8000 t/tide (C3).

The re-leveling scenarios based on the actual sediment characteristics demonstrated on short-term negative impacts on the sediment transport with an increase of the ETM. These high turbidities at the re-leveling are forced additionally by the discontinuity between the re-leveling and the downstream navigation section. The downstream shift of ETM is evaluated as a positive effect, which is representative for an improvement of the situation at the re-leveling and in upstream section. The increasing reach of the net sediment import from the Emder Fairyway indicates a medium-term worsening of the situation in the Ems, which fit together with the negative effect on the hydrodynamics in this section with an increasing flood dominance, tidal range and tidal asymmetry. For the sandy bed a reduction of the ETM but a comparable behavior of sediment dynamics including the same net sediment import and export zones were revealed.

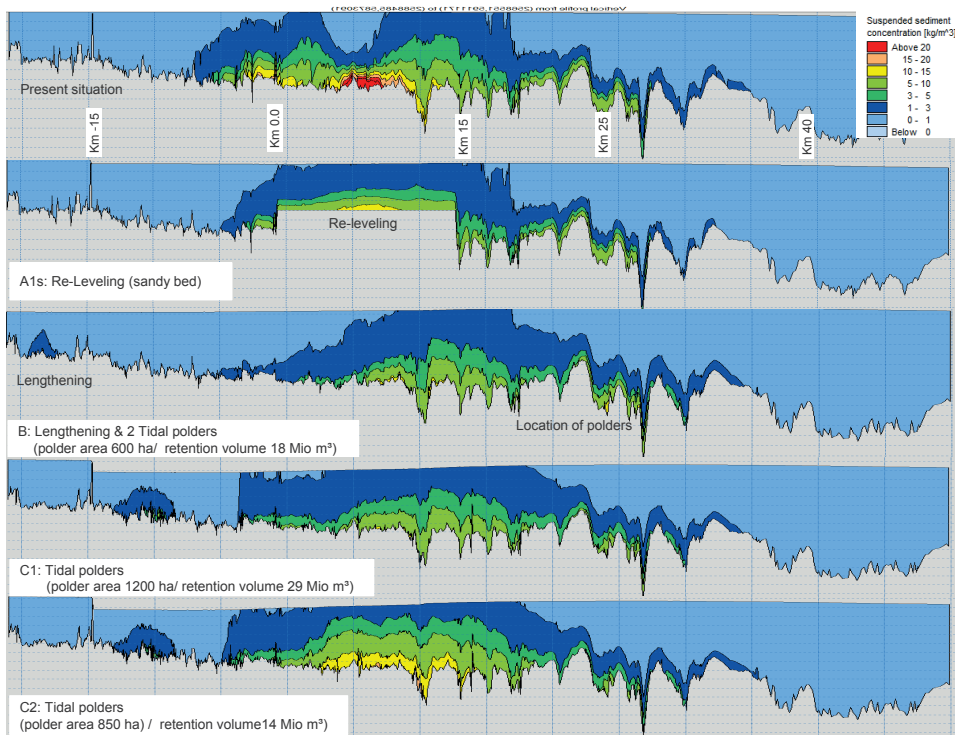
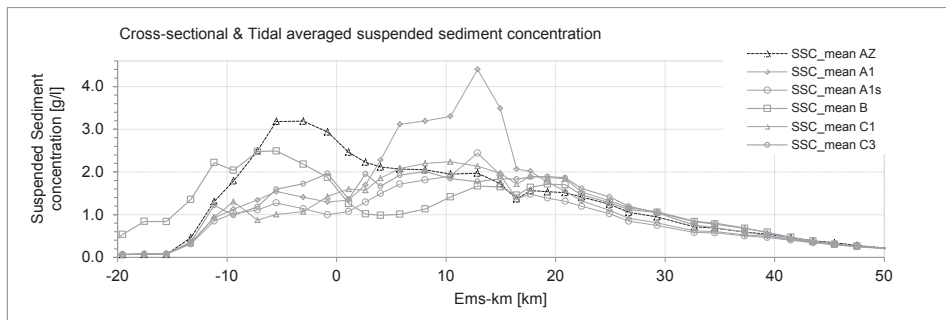


Figure 4: Longitudinal sections of cross-sectional averaged and tidal integrated suspended sediment concentration (top) and 2d-longitudinal sections of suspended sediment concentration in the river axis during high tide for the present situation (second figure), for the re-leveling with a sandy bed (A1s, 3th figure), for the lengthening and two tidal polders (B, 4th figure), for six tidal polders (C1, 5th figure) and for nine tidal polders (C2, 6th figure).

4 Conclusion

4.1 Restoration potential

For scenario A1 the re-leveled flow section, which can develop morphologically without any maintenances, provide an additional restoration potential for sediment trapping in this section. Due to the assumed sandy sediments at the river bed the ETM was reduced and shifted downstream with about 17 km, while the net sediment transport near the mouth is only slightly reduced, but lengthened to upstream sections. This import zone is evaluated as a strong negative impact for both (silty & sandy) scenarios, which stands for an on-going fine sediment import from sea side and worsening of turbidity. No changes in the sediment characteristic under assumed maintenance (preservation of the existing morphology) appear downstream of the re-leveling. Together the restoration potential and free development of the Ems at the re-leveling section of both scenarios resulted in low to moderate, keeping the above mentioned shortcomings in mind.

The lengthening of the Ems combined with the tidal polders near Emden show on short term deficits with an upstream shift and only a slight decrease of the ETM. The most positive effect, which will result in a medium-term reduction of fine sediments in the lower Ems, is shown in a turn from net sediment import to an export. Due to the negative effects of the mention upstream shift of the ETM the restoration potential of the analysed scenario was evaluated with low.

On short-term significant changes with a strong improvement of the hydrodynamic indicators were achieved for tidal polders and lateral retention variants. For the sediment dynamics a slight downstream shift of the ETM was achieved, but the suspended sediment concentration was not reduced below the defined critical threshold of 100 mg/l. But all scenarios showed a turn from sediment import to an export near the mouth, which is an indicator for a further improvement and reduction of the suspended sediment concentration. But this reduction is strongly linked to a morphodynamic change and changes in the composition of sediments, which should turn to coarser sediment fractions in the lower Ems. Due to anthropogenic pressures, like regular channel deepening for navigation, revetments at the banks and water management for the hinterland, only a small corridor of morphodynamic changes is feasible. As consequence new wetted areas like polders or shallow water zones with endorsed morphodynamic changes, provide an increased restoration potential (Tab. 1).

Together with the qualitative classification of the net sediment export to upstream sections, the short-term- shift and reduction of turbidity a meso-scale restoration potential was derived. The evaluation of the restoration potential on meso-scale, which is only provided in a qualitative way (Tab. 1), delivers the highest potential for scenario C2 due to the positive effect of the upstream polders, the extended net sediment transport and significant downstream shift of the ETM. The scenario C1 represents some shortcoming based on the negative effect of the polder near the mouth. In addition the sediment export is higher but does not extend as far as in the scenario C2 with the smaller upstream polders. In shallow water zones of the lateral retention areas (C3) sediments will accumulate and reduce the trapping effects on medium-term.

Table 1: Medium-term restoration potential of restoration variants for the Ems

Key indicator	Scenario A1s (re-leveling with sandy bed)	Scenario B (lengthening & tidal polders)	Scenario C1 (tidal polder)	Scenario C2 (tidal polder)	Scenario C3 (lateral retention)
Potential for a morphological development: area and section	re-leveling over 14 flow-km	Polder areas 600 ha, Lengthening over 9 flow-km	Polder areas 1200 ha over 31 flow-km	Polder areas 850 ha over 20 flow-km	Retention area 400 ha over 29 flow km
Net sediment transport (flood – ebb): Export from the mouth (intensity and extending)	Increase of sediment import in length up to Ems-km 35 with 800 t/tide	Extension up to Ems-km 20 with export 10.000 t/tide Negative effect of polder near the mouth	Extension up to Ems-km 20 with export 10000 t/tide Negative effect of the polder near the mouth	Extension up to Ems-km 15 with export 9000 t/tide No negative effect near the mouth	Extension up to Ems-km 15 with export 8000 t/tide No negative effect near the mouth
Downstream shift of the ETM: intensity and distance of the shift	Downstream shift with 17 km, reduction to 2.4 g/l	Upstream shift with 5 km, but reduction to 2.5 g/l	Downstream shift with 14 km, reduction to 2.3 g/l	Downstream shift with 16 km, reduction to 2.7 g/l	Downstream shift with 5 km, reduction to 2.0 g/l
Restoration potential	low	low	moderate	high	moderate

A powerful correlation between hydrodynamic changes, like the tidal range or flood dominance, and sediment transport like net sediment transport or ETM was not feasible. Thus an isolated interpretation of the restoration potential exclusively based on the hydrodynamic indicators, might deliver an insufficient priority variant.

4.2 General conclusion

The re-leveling which is acting like a fixed ground sill showed on short-term negative impacts on the hydrodynamics and sediment transport. Due to this bed level change a discontinuity appears. A simplified analysis of morphological stability of the re-leveling showed, that erosion of this ground sill will take place. Consequently this horizontal re-leveling will turn to a sloped shape. Positive effects on hydrodynamics are increasing and sediment concentration is strongly reduced due to the sandy river bed at the re-leveling.

The lengthening combined with two polders downstream, resulted in differing results, compared to the findings of previous studies. Thus a downstream shift of the ETM was examined by a 1d-approach of SCHUTTELAARS and DE JONGE (2011) and reduction without a significant downstream shift of the ETM was examined by a 3d-analysis by ROLLENHAGEN (2011). The reason for different results is based on different assumptions: here the weir was fully removed, which resulted in an extension of the tidal influenced estuary length. This tidal influence induces on short-term a mobilization of fine sediments near the former weir. This lengthening shifts the ETM to upstream sections, but also displayed a split into two separate diverging ETMs, which was also revealed in the 1d-analysis (SCHUTTELAARS and DE JONGE 2011). A newer 3d-analysis by JÜRGES

(2013) with a lengthening and shortening of the Ems estuary showed a similar behavior of hydro- and sediment dynamics as presented here.

Different locations, distributions as well as retention volume influence the retention and sediment trapping potential. Especially tidal polders (in C1, near Ems-km 25) near Emden as well as big polders along the river showed shortcomings on hydro- and sediment dynamics with an increase of flood dominance, due to an earlier slack water and ebb flow phase in the polder. Consequently a draining of the polder starts before slack water in main channel takes place, strengthens flood currents and amplifies local sediment import. But also big polders with more than 250 ha in upstream parts showed negative local effects with an increase of flood currents near the inlet accompanied by an erosion tendency, which is derived from the change from net sediment export downstream to sediment import upstream.

5 Outlook

The analysis on short-term does not deliver a final answer on the sustainability of restoration measures, but is indispensable to analyze shortcomings and allow an optimization of future restoration variants. Only for scenarios with a high restoration potential further analysis of long-term morphodynamic changes are recommended.

Therefore already central findings for a cohesive sediment dynamic system in DONNER and NEHLSSEN (2012) can be transferred to a long-term concept for the Ems estuary. The first requirement for any long-term concept is the availability of observational data on sediment dynamics and on morphological changes including dredged amounts and volumes. Only based on observed bed level changes any simulation of bed level change can be assessed. In addition different for example month-wise scenarios of fluvial discharge and tide need to be selected and combined in order to reproduce a typical annual cycle. A comparable long-term concept for an estuary with significant low suspended sediment concentrations (DONNER and NEHLSSEN 2012) already revealed, that any morphological speed-up combined with the strong non-linear behavior of all settling and erosion processes will be limited to very low factors. Thus for sediment concentrations up to 1 g/l the morphological speed-up was limited between 1 and 6 in order to avoid any overestimation of deposition at least in shallow water zones due to missing morphological feedback. Thus any long-term approach for the Ems estuary will be strongly limited to data and additional restrictions due to very high suspended sediment concentrations, results in non-linear behavior, which cannot be simplified to an almost linear behavior on short-term, which is feasible for sandy river beds.

Nevertheless an estimation of long-term effects on suspended sediments and sediment composition is necessary, to show if any restoration scenario is able to reduce sediment import and the extreme high suspended sediment concentrations on longer time scales. Thus already a further reduction and downstream shift of the ETM after a short time period might indicate a tendency to improve the situation in the Ems.

6 Acknowledgements

The Joint Research Project of WWF Germany, BUND, NABU and University of Technology in Berlin called “Perspective revitalized Lower Ems” (Perspektive Lebendige Ems) was funded by the DBU (Deutsche Bundesstiftung Umwelt) and BINGO (Niedersächsische Bingo-Umweltstiftung). We would like to thank the project team for their support and the project review group with water authorities and international experts for the fruitful discussions. Furthermore we would like to thank H.H. Nguyen for his research work on the effect of the effective floc density on settling velocities.

7 References

- BURT, T.N.: Field settling velocities of estuary muds. In *Estuarine Cohesive Sediment Dynamics*, A.J. Mehta. Ed, Springer-Verlag, 126-150, 1986.
- CHERNETSKY, A.: Trapping of sediment in tidal estuaries, PhD-Thesis, TU Delft, 2012.
- DONNER, M.; LADAGE, F.; STOSCHEK O. and NGUYEN H.H.: Methods and analysis tools for redevelopments in an estuary with high suspended sediment concentrations, Conference Proceedings, ICCE 2012; Santander, Spain, 2012.
- DONNER, M. and NEHLSSEN, E.: Impact analysis of anthropogenic stresses based on a morphodynamic long-term approach; Proceedings of IAHR 2012; München, Deutschland.
- DRONKERS, J.: Tidal Asymmetry and estuarine morphology, *Netherlands Journal of Sea Research* 20 (2/3), 117-131, 1986.
- JÜRGES, J. and WINKEL, N.: Ein Beitrag zur Tidedynamik der Unterems, Bundesanstalt für Wasserbau, Dienststelle Hamburg, Referat Ästuarsysteme II, Mitteilungsblatt der Bundesanstalt für Wasserbau Nr. 86, 2003.
- JÜRGES, J.: Grundsatzuntersuchung zur Verlängerung des Emsästuars, Bundesanstalt für Wasserbau, Dienststelle Hamburg, Vortrag im Rahmen des BAW Kolloquiums „Projekte und Entwicklungen für aktuelle Fragestellungen im Küstenwasserbau“ am 19.09.2013.
- KRONE, R.B.: Flume studies of the transport of sediment in estuarial processes, Hydraulic Engineering Laboratory and Sanitary Engineering Research Laboratory, Univ. of California, Berkeley, California, Final Report, 1962.
- LANG, G.: Analyse von HN-Modell-Ergebnissen im Tidegebiet, Mitteilungsblatt der Bundesanstalt für Wasserbau (Federal Waterways and Engineering Institute), Nr. 86, 2003.
- LI, Z.H.; NGUYEN, K.D.; BRUN-COTTAN, J.C. and MARTIN, J.M.: Numerical simulation of the turbidity maximum transport in the Gironde estuary, France, *Oceanologica Acta*, 1994.
- NGUYEN, H.H. and Chua, L.H.C.: A Simplified Physically-based Model for Estimating Effective Floc Density. *J. Hydraulic Engineering*, ASCE, doi: 10.1061/ASCE HY.1943-7900.0000355, 2010.
- NGUYEN, H.H.: Modelling the Transport of Fine Suspended Sediments, PhD-Thesis, Nanyang Technological University, Singapore, 2012.

- NLWKN Aurich: Emssperrwerk Gandersum Herbst – Probestau vom 27. bis zum 29.09.08 mit Überführung der CELEBRITY SOLSTICE von Papenburg nach Gandersum, Gewässerkundlicher Landesdienst, 2009.
- PARTHENIADES, E.: Erosion and deposition of cohesive soils, Proceedings of the American Society of Civil Engineers (ASCE), Volume 91 (HY1), 105-139, 1965.
- ROLLENHAGEN, K.: Untersuchungen zur Minderung des Schlickeintrags in die Unterems – Vergleich von Lösungsvarianten, presentation at the colloquium of the Federal Waterways and Engineering Institute, 22.09.2011, (www.baw.de).
- SCHUTTELAARS, H.M. and DE JONGE, V.: Influence of the length of an estuary on tidal motion and sediment trapping, unpublished, 2009.
- SCHWEIM, C.: Modellierung und Prognose der Erosion feiner Sedimente, PhD-Thesis, RWTH Aachen, 2005.
- SMAGORINSKY, J.: General Circulation Experiments with Primitive Equations, Monthly Weather Review, H. 91, 1963.
- TALKE, S.A. and DE SWART, H.E.: Hydrodynamics and Morphology in the Ems/Dollard Estuary: Review of Models, Measurements, Scientific Literature, and the Effects of Changing Conditions, University of Utrecht, IMAU Report # R06-01, 2006.
- VAN RIJN, L.C.: Manuel Sediment Transport Measurements in Rivers, Estuaries and Coastal Seas, Aqua Publications, Amsterdam, 2007.
- WEILBEER, H.: Numerical simulation and analyses of sediment transport processes in the Ems-Dollard Estuary with a three-dimensional model, Conference Proceedings, INTERCOH 2003, 2005.
- WINTERWERP, H.: On the Dynamics of High-concentrated Mud Suspensions, PhD-Thesis, TU Delft, 1999.
- WURPTS, A. and OBERRECHT, D.: A hydro-morphodynamic numerical study to reduce tidal asymmetry in the Ems Estuary, Germany, Conference Proceedings, ICCE 2012, Santander, Spain, 2012.
- ZANKE, U.C.E.: Grundlagen der Sedimentbewegung, Springer Verlag, Berlin, Heidelberg, 1982.

Investigations of Rheological Flow Properties Based on Lab Data of Fluid Mud Samples and an Extended Model Approach

Dennis Oberrecht and Andreas Wurpts

Summary

Fluid mud parameters like mass concentration, yield point and apparent viscosities are derived by means of fluid mud sampling along the tidal reach of river Ems and subsequent lab analysis regarding suspended sediment concentration, bulk density and rheological parameters. Equilibrium flow curves were obtained for every sample by means of constant-rate analysis with a high resolution lab rheometer. Comparisons of samples from different locations show good correlation between fluid mud mass concentration and yield point. A reliable method for yield point detection based on creep and recovery rheometer tests and a semi graphical approach was found to deliver the best results. In order to reproduce the large spread of viscosities occurring in reality, the Toorman model was extended by means of an empirical fit with respect to suspended sediment mass concentration. The comparison shows a good correlation between model results and measured constant-rate-test data. Also the thixotropic behavior due to weakening and strengthening as a result of disintegration and build-up of the internal floc structure is reproduced.

Keywords

fluid mud, Ems estuary, constant rate curves, yield point, rheological model

Zusammenfassung

Die Untersuchung befasst sich mit der Parametrisierung der kinematischen Eigenschaften von Flüssigschlück. Proben aus dem Ems-Ästuar wurden nach Konzentration, Bewegungsbeginn und Viskosität analysiert. Unter Einsatz eines hoch auflösenden Laborrheometers wurden Gleichgewichtslieflercurven unter Anwendung jeweils konstanter Scherraten erzeugt. Diese erlauben den Vergleich von Proben aus einer Vielzahl von Entnahmestellen und die Kalibrierung des von Toorman erweiterten nichtlinearen Fließmodells nach Worrall und Tuilani. Der Toorman-Ansatz wurde durch einen empirischen Fit zur Berücksichtigung der Suspensionskonzentration des Flüssigschlücks erweitert, um die große Bandbreite real auftretender Viskositäten abzudecken. Der Vergleich zwischen den gemessenen und den durch das erweiterte Modell berechneten Ergebnissen zeigt eine gute Übereinstimmung hinsichtlich der Reproduktion des thixotropen und nicht-Newton'schen Fließverhaltens von Flüssigschlück und insbesondere des Übergangs in den Gleichgewichtsbereich.

Schlagwörter*Flüssigschlick, Ems Ästuar, Constant-Rate Kurven, Fließgrenze, Rheologisches Modell***Contents**

1	Introduction	456
2	Fluid mud properties and dynamics.....	457
3	Rheological Approach.....	457
4	Experimental Setup	457
5	Comparison of lab data and extended model	459
6	Conclusion.....	461
7	References	461

1 Introduction

The Ems estuary is located in the NorthWest of Germany, connected to the border of the Netherlands. The estuary spreads out of a total length of 110 km starting from the east Frisian island Borkum to the tidal weir in Herbrum with an average fresh water inflow around 80 m³/s. The tidal range at the mouth is 2.2 meters and increases up to 3.2 meters in Papenburg. The estuary is important for the German and Dutch economy, since main harbors are located along the estuary (Eemshaven, Delfzijl, Emden and Papenburg) and a yard delivering large cruise-vessels several times a year resides in Papenburg. In order to satisfy the navigability needs engineering measures were applied in the past decades like deepening, canalization, groyne and tail fittings. Furthermore, a storm surge barrier in Gandersum nowadays protects the hinterland against flooding and allows raising the upstream water level for the initial passage of cruise ships from Papenburg to the open sea. The engineering measures led to massive changes in tidal dynamics, resulting in short, but strong periods of flood flow in combination with weaker ebb flow lasting over longer durations. HERRLING (2008) has shown an increased tidal range in the Lower Ems estuary in a comparison of data from 1937 and 2005. Furthermore HERRLING (2008) has shown, that the effect of deepening can be observed from Emden up to the tidal weir in Herbrum. In combination with the intensified baroclinic circulation this led to massive accumulation of fluid mud in the Lower Ems. As a result of the intensified flow dynamics and the high availability of suspended fines the sediment distribution along the estuary changed considerably, since a stratified system by means of a lutocline and a fluid mud layer of 2m -4m thickness below it can be found along the innermost 50km of the estuary. The obvious interactions between suspended sediment and the tidal currents become even more complicated because of the non-newton flow behavior within the fluid mud.

2 Fluid mud properties and dynamics

Fluid mud is a suspension of mainly cohesive fines (clay) some non-cohesive minerals like sand and other contents of biogenic origin. NASNER (2004) reports absolute mass concentrations up to 220 g/l and ignition loss ranging from 10 % to 20 % for several German tidal harbors. The complex rheological behavior of fluid mud is a result of the clay as well as the biogenic content by means of extracellular polymeric substances. The latter influencing the time dependent behavior even more than the electrostatic forces between clay particles.

The flow behavior of fluid mud ranges from Newtonian turbulent flow for low concentrations of suspended sediment to non-Newtonian, shear-thinning and thixotropic behavior with changes in viscosity by an order of magnitude and more. Due to the density difference to the less concentrated regions of the flow, dynamic stratification as a result of local damping of turbulent momentum exchange and turbulent mixing takes place, leading to lutocline formation.

3 Rheological Approach

Since fluid mud rheological behavior exhibits non-linear shear dependency as well as time dependency, none of the 'simple' rheological models like Bingham, Hershel-Bulkley etc. should be applied. We here focus on the TOORMAN (1997) Model and extend it with a straight-forward approach by means of an empirical fit of its model constants. In analogy with the model proposed by MOORE (1959), which based on describing the thixotropic behavior of clay suspension, WORRALL and TULLIANI (1964) extended their work by adding a yield stress term. TOORMAN (1997) gives a formulation with a more general equation of state, based on the Worrall and Tulliani model, which is independent on the rate equation and which can be applied to any flow history. For the thixotropic model and explicit shear stress description, Toorman gives the following equation which depends on yield stress, shear rate and degree of structure in suspension,

$$\tau = \lambda \tau_0 + (\mu_\infty + c\lambda + \beta \tau_0 \lambda_e) \dot{\gamma} \quad (1)$$

$$\lambda_e = \frac{\lambda_0}{1 + \beta \dot{\gamma}} \quad (2)$$

where $\beta = b/a$, a aggregation parameter, b structure break-down parameter, μ_∞ the Bingham viscosity, $c = \mu_0 - \mu_\infty$ and μ_0 is the initial differential viscosity. λ is the degree of structure in suspension, which basically covers the thixotropic behavior (0-fully broken, 1-fully structured). It is described by the following ordinary differential equation:

$$\frac{d\lambda}{dt} = -(a + b\dot{\gamma})(\lambda - \lambda_e) \quad (3)$$

4 Experimental Setup

In this study, fluid mud samples were taken in a longitudinal cross-section of the Lower Ems, as well as from the harbor of Emden. 20 Samples in the Lower Ems were taken in

August 2009 every 2 km during ebb phase, starting from the storm surge barrier in Gandersum up to the tidal weir in Herbrum and 5 samples were taken in the Emden tidal harbor. All samples were collected with a Ruttner-Sampler closely above the nautical bottom in the deep channel. Density measurements were carried out using a lab density meter (oscillating tube). For rheological parameters a Rheologica Stresstech HTHP rotational rheometer was used (lowest detectable stress level: 0.00125 mPa).

The yield point was investigated by stepwise increasing the shear stress and recording the corresponding shear rate. This measurement mode has to be started from a shear stress level well below the yield stress then being stepwise increased unless plastic motion dominates the process. Given a sufficiently sensitive rheometer even shear stress levels below the yield point result in (very small) shear so a decision has to be made which point within the shear curve is the 'real' begin of motion.

The yield point determination may depend on the problem itself and also the measurement equipment used. For fluid mud good results were obtained by means of a semi graphical procedure, the so called "tangent" method (METZGER 2006, Fig. 1). Applied at log scaled flow curves it allows reproducible determination of yield points which were consistently confirmed by creep-recovery-tests (FRANZ 2009).

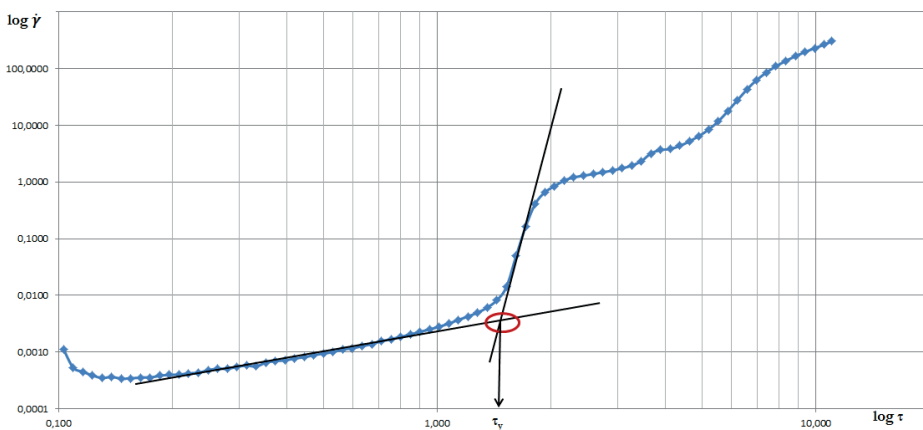


Figure 1: Example of the determination of the yield point with the tangent method (FRANZ, 2009).

Fig. 1 shows that (extremely low) shear exists already at the lowest stress level applied. Those low deformations during shear stress levels below the yield stress partly result from elastic deformation. The underlying conceptual model for pseudo plastic granular or aggregated suspensions includes an 'inner' structure formed by aggregated grains, flocks and EPS which contribute to the overall mechanical shear resistance of the suspension and which has to be overcome before relevant plastic flow takes place.

For a time- and shear-dependent pseudo plastic suspension like fluid mud due to thixotropy there exists an theoretically unlimited number of flow curves depending (amongst other parameters) on the current shear rate and shear history. Therefore an equilibrium state as described by Worrall and Tuliani is a meaningful quantity, which demands rate controlled measurements that are continued until the equilibrium state is reached.

Lab rheometers are usually stress controlled. This makes a regulator circuit necessary in order to control the system by means of a constant shear rate. The regulator's characteristics can significantly influence the equilibrium time of the experiment. Especially when applied to different shear rate values which can probably span over orders of magnitude, appropriate regulator settings can vary quite a lot.

The aforementioned conceptual model for granular or aggregated suspension directly allows for the application of the thixotropic rheological model suggested by Toorman. It is based on the equilibrium flow concept derived from Worrall and Tuliani and incorporates an equation of state which describes the structural 'inner' strength of the aggregated suspension.

Equation (3) is a rate equation for a structural integrity parameter that brings a time dependency into the apparent kinematic viscosity calculation. Parameter λ is reduced by shear and build up based on the amount of structure already available. The coefficients a (scaling the build-up rate) and b (scaling shear-induced destruction rate of internal structure) therefore have to be derived from constant rate experiments by evaluating the adaption time of the suspension. $\lambda = 1$ represents full structure, it is per definitional set to 1, which means that λ in this model may vary between 0 and 1. The increase and decay of λ is controlled by the rate equation.

5 Comparison of lab data and extended model

The aim of this rheological study is the determination of equilibrium flow curves of suspensions with widely varying density. In the first step the yield stresses of given suspensions were evaluated by flow curves obtained by predefined a shear stress ramp and applying the tangent method. All Bingham parameters like (pseudo) Bingham yield stress, initial differential viscosity and Bingham viscosity were determined after WORRALL and TULIANI (1964) by using these flow curves. We call those parameters Bingham-like, since high resolution measurements confirm the widely discussed aspect that a real Bingham Yield point is rather caused by insufficient measurement resolution than the real physics. Also, from a hydrodynamic point of view the singularity in the momentum equation due to an infinite viscosity at a Bingham – like yield point confirms this.

Comparison of Worrall and Tuliani parameter with respect to sample concentration can be seen in Fig. 2. TOORMAN (1997) modified the model, which describes thixotropic behavior of suspensions based on equilibrium flow curves. The equilibrium flow curves found by WORRALL and TULLIANI (1964) can be written as:

$$\tau_e = \lambda_0 \tau_0 + (\mu_\infty + \lambda_e) \dot{\gamma} \quad (4)$$

with τ_e the equilibrium shear stress. This equation for the equilibrium state in dependency of a given shear rate contains three empirical parameters (τ_0 , μ_∞ , c), which are characterized by analysis of the rheometer results of constant-rate curves.

The equilibrium structural parameter λ_e describes the degree of structure independent to shear rate in equilibrium state. Investigations of the behavior at transition to the equilibrium state after TIU (1974) is described in a first order equation:

$$\ln(\tau_y - \tau_{y,e}) = \ln(\tau_{y,i} - \tau_{y,e}) - kt \quad (5)$$

with t the time, which is between the start of measurement up to reaching the equilibrium by a constant shear rate ($d\lambda/dt=0$). By this equation, the analytical solution of the recovery rate parameter a and the break-down parameter b can be determined with $k = a + b\dot{\gamma} = a(1 + \beta\dot{\gamma})$.

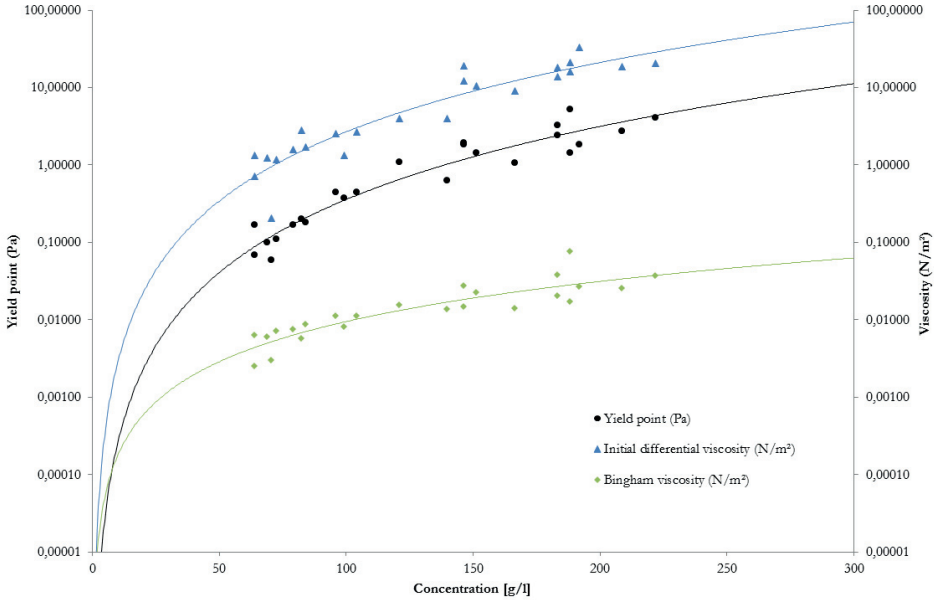


Figure 2: Graph illustrates comparisons of initial differential viscosity (blue), yield point (black) and Bingham viscosity (green) with respect to sample concentration.

After all parameters have been determined, fitting curves were calculated according to concentration of suspensions. The best fit for the concentration range from 63.5 g/l to 222 g/l is achieved with:

$$\mu_{\infty} = 3 \cdot 10^{-6} \cdot C^{1.72}$$

$$\mu_0 = 3 \cdot 10^{-6} \cdot C^{2.97}$$

$$\tau_y = 2 \cdot 10^{-7} \cdot C^{3.13}$$

Fig. 3 shows comparisons of measured shear stress by rheometer and calculated equilibrium flow curves by Tooman model. Comparison of calculated and measured equilibrium flow curves indicating a very well correlation at higher shear rates and an overestimating at low shear rates of calculated shear stresses by above equation (4), which is due to the inherent stronger internal damping of the rheometer at very low shear rates.

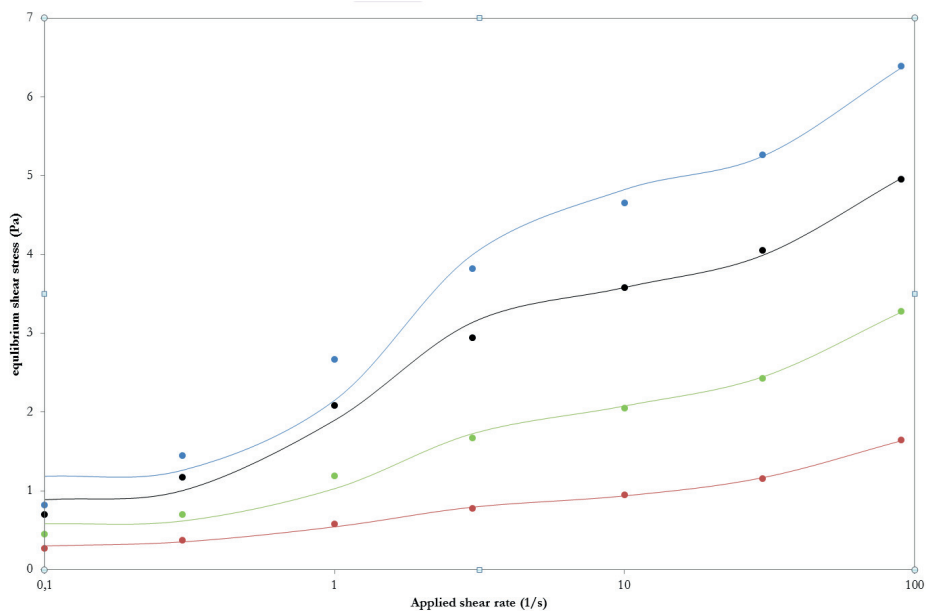


Figure 3: Comparison of calculated (dots) and measured (solid lines) equilibrium flow curves of 191 g/l (blue), 183 g/l (black), 139 g/l (green) and 99 g/l (red) in a log representation for the shear rate.

6 Conclusion

Based on fluid mud samples from river Ems and rheological lab analysis constants for the Toorman thixotropic rheological model were derived. In a straight forward empirical approach the model was extended in order to include the strong concentration dependency of fluid mud viscosity in real systems, spanning over an order of magnitude and more. The fitted model constants allow the model-based reproduction of the complex viscous behavior of fluid mud and especially its thixotropy dominated viscosity.

7 References

- FRANZ, B.: Rheologischer Vergleich von Flüssigschlicksuspension und synthetischer Tonmineralsuspension, Bachelor Thesis, Franzius-Institute LUH, 2009.
- HERRLING, G.: Comparison of the hydrodynamic regime of 1937 and 2005 in the Ems-Dollard estuary by applying mathematical modeling, NLWKN Coastal Research Station, 30 S., 2008.
- METZGER, G.: Das Rheologie Handbuch, s.l., Vicentz, 2006.
- MOORE, F.: The rheology of ceramic slips and bodies, Trans Brit Ceramic Soc., V 58, 470-494, 1959.
- NASNER, H.: Hydrodynamische und morphologische Vorgänge in Brackwasser beeinflussten Vorhäfen In-situ Messungen, Die Küste 68, 1-65, 2004.

TOORMAN, E.A.: Modelling the thixotropic behaviour of dense cohesive sediment suspensions. *Rheol. Acta*, 36, 56-65, 1997.

WORRAL, W.E. and TULLIANI, S.: Viscosity changes during the ageing of clay water suspensions. *Trans. Brit. Ceramic Soc.*, 63, 167-185, 1964.

A Numerical Model for Fluid Mud Dynamics in Estuarine Systems – Overview and Outlook

Denise Wehr

Summary

Fluid mud is a mixture of fine, mainly cohesive sediments, water and organic substances. The rheological behaviour of fluid mud is that of a non-Newtonian fluid; fluid mud is thus subject to its own dynamic compared to a water body with low suspended matter concentration. The occurrence of fluid mud in estuaries and coastal zones may vary spatially, from a few centimetres in layer thickness to river sections with fluid mud layers which are several kilometres long. The time variability of physical processes, such as the formation, transport and dissipation of fluid mud extends from a few seconds for turbulent mixing to months for creeping mud layers (MEHTA et al. 2014).

The progressive extension and development of coastal waterways has led to an increase in siltation and the formation of fluid mud in sections of estuarine shipping channels, ports and port approaches in recent decades. The need for a better understanding and profound knowledge of fluid mud dynamics has increased and new maintenance strategies and renaturation measures now need to be developed in estuaries and existing ones optimized. Numerical simulations contribute to the evaluation of such strategies.

This paper summarizes the current capabilities and performance of a newly developed three-dimensional numerical model for simulating fluid mud dynamics in estuarine systems. Further possible developments of the numerical model are presented. Important aspects are the interaction of rheology and turbulence in estuaries and the influence of biological parameters.

Keywords

Fluid mud, three-dimensional numerical model, cohesive sediment suspension, rheology, isopycnal model

Zusammenfassung

Flüssigschlick ist ein Gemisch aus feinen vorwiegend kohäsiven Sedimenten, Wasser und organischen Bestandteilen. Die rheologischen Eigenschaften sind die eines nicht-Newtonschen Fluides, somit unterliegt der Flüssigschlick einer eigenen Dynamik im Vergleich zum Wasserkörper mit geringer Schwebstoffkonzentration. Das Vorkommen von Flüssigschlick in Ästuaren und Küstenregionen kann sehr unterschiedliche räumliche Ausdehnungen von wenigen Zentimetern Schichtdicke zu kilometerlangen Flussabschnitten mit Flüssigschlickschichten annehmen. Gleichzeitig reicht die zeitliche Skala der physikalischen Prozesse wie die Entstehung, Transport und Resuspension von Flüssigschlick von Sekunden bei der turbulenten Durchmischung bis zu Monaten bei kriechenden Schlickschichten (MEHTA et al. 2014).

In den letzten Jahrzehnten hat der fortschreitende Ausbau von Seeschiffahrtsstraßen zu einer Zunahme der Verschlickung und Entstehung von Flüssigschlick in Bereichen der ästuarinen Schiffahrtsstraßen,

Häfen und Hafeneinfahrten geführt. Der Bedarf an fundierten Kenntnissen über die Flüssigschlickdynamik wächst, um neue Unterhaltungsstrategien und Renaturierungsmaßnahmen in Ästuaren zu entwickeln und bestehende zu optimieren. Numerische Modelle dienen als Werkzeug zur Beurteilung dieser Strategien und Maßnahmen.

In diesem Artikel werden die derzeitigen Möglichkeiten und die Leistungsfähigkeit eines neu entwickelten dreidimensionalen numerischen Modells zur Simulation der Flüssigschlickdynamik im ästuarinen Bereich zusammengefasst. Weiterhin werden Wege zur Weiterentwicklung des numerischen Modells aufgezeigt. Wichtige Aspekte sind hier Interaktion von Rheologie und Turbulenz in Ästuaren und der Einfluss von biologischen Parametern.

Schlagwörter

Flüssigschlick, 3D numerisches Modell, kohäsive Sedimentsuspension, isopyknisches Modell, Rheologie

Contents

1	Introduction.....	464
2	Strategy for simulating fluid mud dynamics.....	465
3	Achievements and applications of the three-dimensional numerical fluid mud model.....	467
4	Perspective.....	469
5	References.....	471

1 Introduction

Siltation in estuarine systems has increased in recent decades as shipping channels and harbours have been progressively developed and expanded. While cohesive suspended sediments are transported by turbulent currents, particles settle and accumulate on the bed in regions of quiescent flow or during periods of low currents, e.g. during slack water in tidal currents. Fluid mud then forms where there is an adequate supply of suspended matter. Fluid mud affects navigation and reduces the water quality. This increases the amount of maintenance required in estuarine waterways e.g. in the Ems estuary.

Fluid mud (high-concentration mud suspension) is a suspension consisting of mineral particles, organic substances, water and in some cases small amounts of gas. Owing to the cohesive properties of clay particles, the fraction of clay particles determines the specific flow behaviour of fluid mud. Fluid mud describes a state in which mud is capable of flowing in spite of very high concentrations of suspended matter in the range of several 10 g/l. The flow behaviour of fluid mud depends on the shear state and can be described as viscoelastic with a yield stress. By comparison, water is characterized as an ideal viscous Newtonian fluid. Fluid mud, being a non-Newtonian fluid, is therefore governed by a different rheology than clear water.

A profound understanding of the process of the formation, development and transport of fluid mud and the description of its rheological behaviour is required for the evaluation, planning and optimisation of construction work, maintenance work and activities

designed to reduce siltation. Today, the required detailed investigations and prognoses of the behaviour and reaction of water systems are supported by numerical modelling. This was the rationale for the initiation of the research project MudSim (03KIS66/67 - funded by the German Coastal Engineering Research Council (KFKI) under the auspices of the Federal Ministry of Education and Research (BMBF)). In recent years, a numerical model for simulating fluid mud dynamics (MudSim) has therefore been developed in cooperation between the Federal Waterways Engineering and Research Institute and Prof. A. Malcherek from the University of the German Armed Forces in Munich. A hydrodynamic numerical model in isopycnal coordinates has been extended to enable the simulation of fluid mud dynamics in coastal areas, estuaries and harbours. The MudSim model has been continually developed since then by the BAW. The fluid mud model is outlined in brief and a projection of future developments is provided in the following.

2 Strategy for simulating fluid mud dynamics

The numerical modelling of estuaries is carried out using three-dimensional models which take account of physical processes such as suspended sediment transport, salt transport, density-induced currents, and turbulence. These conventional models are based on the assumption of a Newtonian fluid. However, highly concentrated mud suspensions exhibit distinctly non-Newtonian behaviour and a module to simulate and predict the dynamics of fluid mud therefore had to be developed.

There is usually a strong density gradient in the transition zone between a fluid mud layer and the body of water above it. This transition zone is known as a lutocline. The two fluid layers exhibit very different flow behaviours and interact by virtue of the shear forces acting in the transition zone. A common approach is therefore to model the fluid mud as a two-dimensional, depth-averaged layer. Processes such as the formation and resuspension of fluid mud lead to changes in the density gradient and to the development of a system with multiple layers. For example, in the Ems estuary fluid mud layers of several meters in thickness appear in the maximum turbidity zone, especially during ebb tide as a result of tidal asymmetry. This was observed during a field survey in 2009 (see Fig. 1) during which multiple mud-suspension layers of different densities were detected.

An isopycnal approach, in which mud suspensions are resolved three-dimensionally by means of layers of constant density, has therefore been chosen for the numerical model to improve the resolution of such mechanisms and has proved to be promising. An existing three-dimensional hydrodynamic isopycnal model approach based on CASULLI (1997) was extended to model fluid mud dynamics. This model is called *MudSim*. The numerical method has the following characteristics:

- isopycnal discretization permits a three-dimensional resolution of the fluid mud body with a low degree of discretization and little computational effort
- the isopycnal approach resolves the density stratification and the velocity profile within the fluid mud body
- layer thicknesses vary with the transition to different states of suspension, thereby permitting simulation of the formation, resuspension, settling, and advective and gravitational transport of fluid mud

- the numerical implementation is based on a numerical discretisation in the vertical direction by ρ -layers, and in the horizontal direction by unstructured grids and in time
- interaction of the isopycnal layers is realized on the basis of momentum transfer, vertical mass transfer and interfacial shear stresses

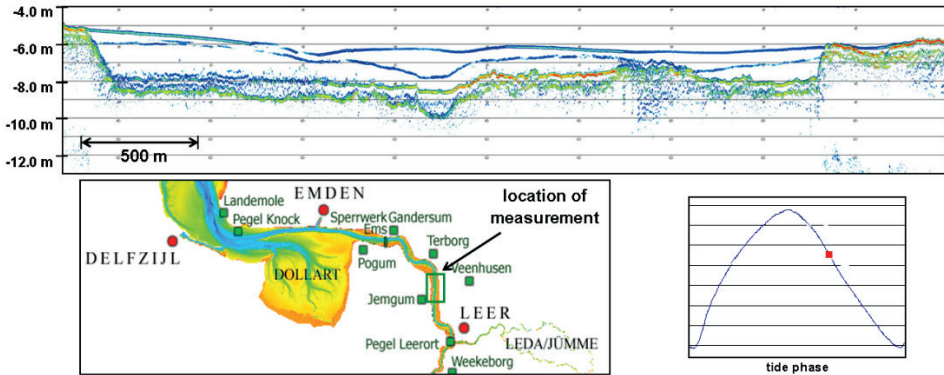


Figure 1: Multi-layer system of fluid mud detected by means of sediment echo sounding measurements (parametric sub-bottom profiler for shallow water) during an ebb tide. The longitudinal section is located between Terborg and Leer in the river Ems. The blue lines indicate strong density gradients and the horizon in red to yellow indicates the sediment bed. The field survey was carried out in July 2009 by the Federal Waterways Engineering and Research Institute (BAW).

It has also been extended to include an approximation of the inner stresses in a non-Newtonian fluid and by considering a parameterized approach for the description of the specific rheological behaviour of fluid mud.

A method is described for the integration of non-Newtonian flow behaviour in a numerical model based on the Reynolds-averaged Navier-Stokes equations. The model simulates the non-Newtonian flow of fluid mud by introducing a rheological viscosity to parameterize the rheology according to shear impact and particle concentration. The rheological model describes the structural break-up and recovery of aggregates in a mud suspension (outlined in MALCHEREK and CHA (2011) and in WEHR (2012)). The rheological viscosity is no longer a constant, such as the molecular viscosity, but is now a time-dependent and process-descriptive parameter. It is possible to apply different rheological models in this way. Internal friction and interfacial shear stresses are now related to the rheological behaviour of the mud suspension and are taken into account in the numerical solution.

The rheology of fluid mud is described as a viscoplastic shear-thinning fluid by applying a parameterized Worrall-Tuliani model (WORRALL and TULIANI 1964; KNOCH and MALCHEREK 2011; MALCHEREK and CHA 2011). This model considers a yield stress and the break-up and recovery of the microscopic structure (aggregates of cohesive sediments). These parameters are calculated as a function of the shear impact and solid volume concentration. The entire water column is modelled by adopting this approach, as it not only covers the non-Newtonian behaviour of high-concentration suspensions, but also the Newtonian behaviour of low-concentration suspensions and clear water. The shear-thinning behaviour has been studied phenomenologically and it was possible to

reproduce it in a study of the Ems river section from Rhede to the weir at Herbrum, in which stratified flow in a tidally-influenced system was investigated (WEHR 2012; WEHR and MALCHEREK 2012). The influence of rheological behaviour on high-concentration flow was analysed in a study of flow on an inclined plane (WEHR 2012; WEHR and MALCHEREK 2012). This effect was compared to the influence of gravitational forcing due to density differences, which has proved to be the dominant process for this test case.

Furthermore, major subprocesses of the fluid mud transport are taken into account by parameterizations in the MudSim model. Vertical transport processes, which lead to the formation and resuspension of fluid mud, are mainly governed by hindered settling and entrainment. This requires variation in the thickness of the density layers over time and in accordance with instantaneous mass transport rates.

The method for simulating fluid mud dynamics is presented in detail in WEHR (2012) as well as in WEHR and MALCHEREK (2012).

3 Achievements and applications of the three-dimensional numerical fluid mud model

Fluid mud dynamics under the influence of tidal currents has been investigated for two model domains: the Ems estuary and the Weser estuary in WEHR (2012) as well as in WEHR and MALCHEREK (2012):

- Fluid mud formation, advective and gravitational transport, and resuspension are periodic processes in tidal systems.
- Highly-stratified flow develops during slack water at high tide and during the ebb tide in the shipping channel.
- The rheological viscosities determined as a function of the shear rate and density yield plausible results and influence the velocities of the stratified flow.
- A qualitative comparison of simulated fluid mud formation and the observed development of the lutocline in the river sections of the Ems and Weser estuaries show similar results.

The latter aspect is presented in the following as a short representative result of simulating fluid mud dynamics with the MudSim model. The numerical model MudSim was applied on the river section Rhede to the weir Herbrum. The comprehensive description of the application and their results is presented in WEHR and MALCHEREK (2012). A characteristic result of the three-dimensional simulation with 16 density layers is shown. The sediment transport in this region is dominated by mud suspensions. The fine sediments are mainly carried into this region by tidal pumping. The fluid mud transport and development under tidal currents were evaluated qualitatively by comparing the simulation results with observations of the lutocline development according to WANG (2010). This is illustrated in Fig. 2. The observations were carried out over several tidal cycles at a specific location in the turbidity zone of the Ems estuary (Leerort). The simulation results are taken from a position between Rhede and Herbrum. Apart from these different locations, the hydrodynamic conditions are not the same in each case and only a phenomenological comparison is therefore possible. However, simulated and observed results both show the typical asymmetrical tide with high flood currents, long slack water at high tide as well

as a long ebb phase. The different freshwater discharge conditions in the simulations demonstrate the effect of variable hydrodynamic conditions. The observed lutocline was obtained from ADCP measurements by analysing the backscatter signal. A high backscatter gradient indicates a high-density gradient in the water column.

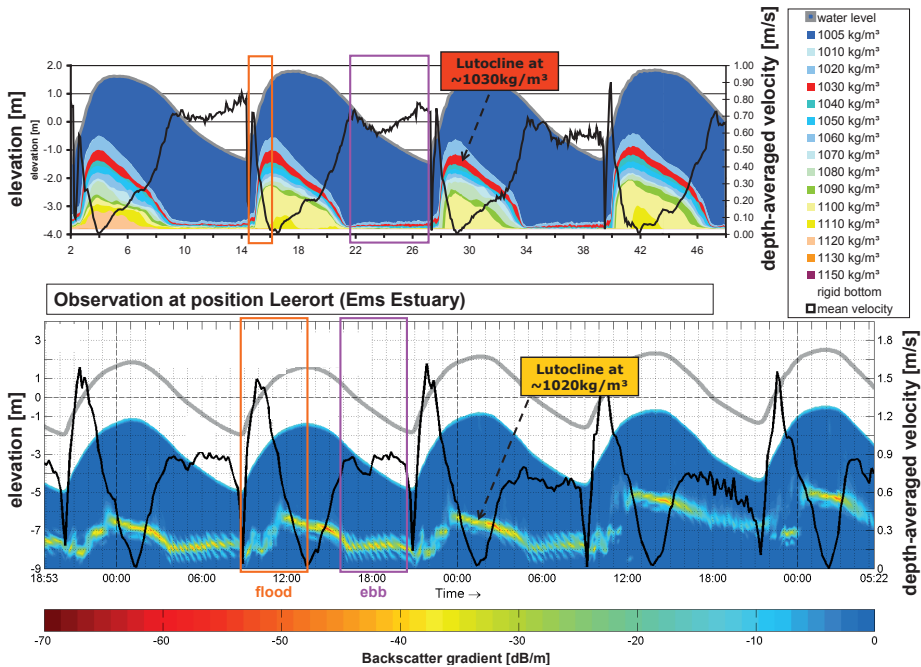


Figure 2: Tidal dynamics of the lutocline - comparison between simulation results (upper panel, simulation (1)) and observations based on 300 kHz ADCP measurements (lower panel). The density corresponding to the lutocline is 1030 kg/m^3 in the simulations. The lutocline is indicated by a high backscatter gradient in the measurements. The water level is indicated in grey and the depth averaged velocity in black. It should be noted that the simulated and measured data relate to different locations and different hydrological situations. However, the characteristic development of the lutocline is very similar (illustration of observations by courtesy of Wang (2010)).

The suspended matter concentration just below the lutocline is in the range of 30 kg/m^3 (density $\sim 1020 \text{ kg/m}^3$) during slack water at high tide, as reported by WANG (2010). The concentration increases downward to the bottom. The simulated density stratification is followed by the subsurface elevation of the density layers. The lutocline is defined as the transition between Newtonian and non-Newtonian behaviour and is accompanied by a sharp density gradient. This corresponds to the layer with a density of 1030 kg/m^3 in the simulations as indicated in red in the graphics.

The fluid mud suspension is entrained into the water column during the flood tide. The observations show low backscatter gradients over the entire water column. This mixing process is indicated in the model results by a rapid increase in the layer thicknesses (subsurfaces) of the mud suspensions. The increasing layer thicknesses result from higher concentration layers being mixed with lower concentration layers due to entrainment and horizontal transport. A highly-stable stratified system is then attained in both cases during slack water. The fluid mud is carried downstream with the ebb currents, which decreases

the lutocline elevation. The intensifying ebb velocities progressively lower the lutocline level as reflected in both the simulations and the observations. At the same time, the sharp transition between the fluid mud and the water body vanishes. The shapes of the simulated and observed lutoclines are very similar and reveal comparable reactions to the tidal flow, even though the mixing process should be intensified in the simulations.

These applications demonstrate that the developed numerical model approach permits the simulation of three-dimensional fluid mud dynamics. The developed numerical model is capable of simulating fluid mud dynamics in systems such as harbour basins and river sections where high-concentration flow and fluid mud formations dominate the system. Such simulations can contribute to classical 3D hydrodynamic and morphodynamic simulations of estuarine systems for evaluating sediment transport analysis and maintenance strategies.

4 Perspective

The presented numerical model applies an appropriate resolution of the fluid mud body using isopycnal layers. Each isopycnal layer represents a single phase fluid/suspension with a specific particle concentration and specific rheological properties. The isopycnal layer may become very thin or even attain zero thickness depending on the transport rate and the development of cohesive mud suspensions.

The three-dimensional isopycnal model is applied to the entire water column from the consolidated bed to the free surface in the presented model applications in WEHR (2012) and WEHR and MALCHEREK (2012). Simulations of the dynamics of highly-concentrated mud suspensions showed reasonable results. However, the numerical approach limits the flow to stable stratification. This assumption does not always apply in highly-turbulent flows with suspended sediments. In particular, the presence of suspended sediment transport and baroclinic processes may result in an unstable stratification in estuaries. Further investigations of the simulation of the low-concentrated water body are necessary to permit comprehensive modelling of estuarine systems. One possible way of arriving at a more sophisticated model of the water body is described in the following.

A solution can be achieved by coupling the isopycnal model with an existing and established three-dimensional hydrodynamic model such as UnTRIM (CASULLI and WALTERS 2000; CASULLI and LANG 2004), Telemac (HERVOUET and BATES 2000; ELECTRICITÉ DE FRANCE 2000) or Delft3D (LESSER et al. 2004; GERRITSEN et al. 2007). The isopycnal numerical model then functions as a module representing the fluid mud body. The suspended sediment and salt transport simulation is performed by the hydrodynamic model such as in WEILBEER (2014). The isopycnal fluid mud module would then become active in the case of fluid mud formation once the threshold from Newtonian to non-Newtonian flow or a specific mud concentration is exceeded. This module would only be activated in model domains with cohesive sediment accumulations, thereby reducing computational effort for large model domains with different transport regimes such as those in estuaries. This concept will require further developments, research and software engineering for the comprehensive modelling of estuarine systems. Communication between the models will require further investigations on software engineering as well as the description of physical processes. One aspect of the latter is outlined in the following.

The developments had focused so far on the interfacial and internal friction resulting from rheological behaviour. However, the internal shear stresses are also influenced by turbulence.

In nature, fluid mud flows become laminar as the turbulence is destroyed due to density stratification. On the other hand, their rheological behaviour changes from non-Newtonian to Newtonian as mud concentration decreases in the water body, with the possible creation of turbulence. Turbulence interacts with the suspended particles due to turbulence damping and buoyancy effects, which in turn influence the settling velocity. Thus, in the high-concentration, stratified areas, flow behaviour is characterised by the rheological viscosity whereas, in low-concentration mixed areas, the turbulent viscosity is dominant. Both rheology and turbulence are modelled with a similar conceptual model as described in WEHR (2012). They are taken into account through a viscosity and result in a deceleration of the average velocity with increasing viscosities (internal friction). However, their physical effect is contradictory. Whereas rheological viscosity leads to laminar and stratified flow as its magnitude increases, increasing turbulent viscosity, on the other hand, intensifies turbulent mixing and may cause unstable stratifications. Accordingly, research on the interaction between rheological and turbulent viscosity will be important for progressive fluid mud and suspended sediment transport modelling. The focus should be on the transitional area between fluid mud and dilute suspension as well as on the formation process and the resuspension of fluid mud as both quantities may reach considerable magnitudes during resuspension or entrainment. A general approach based on viscosity should combine rheology and turbulence modelling and take account of the solids concentration, shear conditions and structural mechanisms (e.g. flocculation) for the overall water body.

Improvement of the turbulence model will also affect the entrainment of fluid mud which is basically induced by turbulent interfacial shear stresses. Another aspect which would be worth investigating is the influence of fluid mud formation in large areas and of sizable thickness on the internal friction in estuarine systems. Turbulence will be damped during periods of high stratification and internal friction is built up by the rheological viscosity. The shear-thinning behaviour of fluid mud may then lead to relatively small rheological viscosities once the fluid mud moves with the tidal currents. Compared to the magnitudes of the rheological viscosities, the turbulent viscosities can reach much higher magnitudes in a turbulence-dominated system. This aspect and the reduced bottom friction of the water body flowing above the fluid mud body may lead to a larger tidal range in estuaries (see description of tidal dynamics in MALCHEREK (2010)).

Further process-based improvements and validation of the fluid mud model will require additional comparisons with laboratory studies and field measurements. Observation of the development of fluid mud involves measurements not only of the lutocline movement but also of density stratification below the lutocline and velocity distribution inside the fluid mud body. These types of measurement are the objects of ongoing research into highly dynamic systems as it is difficult to perform measurements in high-concentration suspensions. These measurements should enable specific observed phenomena to be related to physical processes. Physical processes are strongly related to the tidal cycle in tidal systems and it is therefore necessary to obtain continuous information in tidal systems (e.g. at least one tidal cycle).

The characteristic flow behaviour of fluid mud can be reproduced by considering a mud suspension comprised solely of cohesive sediments and water as realised in the presented model. However, there are several aspects from which we can learn and gain a better understanding of flow behaviour under different conditions. One important aspect is the influence of organic matter content and biological activity on the formation and flow behaviour of fluid mud. Initial investigations on the simulation of biochemical interactions in estuarine systems have been undertaken as part of the BAW project “Interaction of sediment transport and water quality in three-dimensional estuarine models” with the perspective of further research on the interaction between biological activity and sediment transport.

5 References

- CASULLI, V.: Numerical simulation of three-dimensional free surface flow in isopycnal co-ordinates. *International Journal for Numerical Methods in Fluids*, Vol. 25, 6, 645-658. doi: 10.1002/(SICI)1097-0363(19970930)25:6<645::AID-FLD579>3.0.CO;2-L, 1997.
- CASULLI, V. and LANG, G.: Mathematical model UnTRIM, Validation Document 1.0. The Federal Waterways Engineering and Research Institute (BAW), Hamburg, Germany. www.baw.de/downloads/wasserbau/mathematische_verfahren/pdf/vd-untrim-2004.pdf, 2004.
- CASULLI, V. and WALTERS, R.A.: An unstructured grid, three-dimensional model based on the shallow water equations. *International Journal for Numerical Methods in Fluids*, Vol. 32, 3, 331-348. doi: 10.1002/(SICI)1097-0363(20000215)32:3<331::AID-FLD941>3.0.CO;2-C, 2000.
- ELECTRICITÉ DE FRANCE: Telemac-2D validation document version 5.0. Note technique, Electricité de France, Direction des Etudes et Recherches, Chatou Cedex, France, 2000.
- GERRITSEN, H.; DE GOEDE, E.D.; PLATZEK, F.W.; GENSEBERGER, M; VAN KESTER, J.A.T.H.M. and UITTENBOGAARD, R.E.: Validation document Delft3D-FLOW - a software system for 3D flow simulations. Report X0356, M3470, Delft Hydraulics, The Netherlands, 2007.
- HERVOUET, J.M. and BATES, P.: The TELEMAC modelling system. *Hydrological Processes*, Vol. 14, 13, 2209-2210. doi: 10.1002/1099-1085(200009)14:13<2209::AID-HYP23>3.0.CO;2-6, 2000.
- KNOCH, D. and MALCHEREK, A.: A numerical model for simulation of fluid mud with different rheological behaviors. *Ocean Dynamics*, Vol. 61, 2-3, 245-256. doi: 10.1007/s10236-010-0327-x, 2011.
- LESSER, G.R.; ROELVINK, J.A.; VAN KESTER, J.A.T.M. and STELLING, G.S.: Development and validation of a three-dimensional morphological model. *Coastal Engineering*, Vol. 51, 8-9, 883-915. doi: 10.1016/j.coastaleng.2004.07.014, 2004.
- MALCHEREK, A.: *Gezeiten und Wellen - Die Hydromechanik der Küstengewässer. Praxis.* Vieweg + Teubner, Wiesbaden, Germany, 2010.
- MALCHEREK, A. and CHA, H.: Zur Rheologie von Flüssigschlick: Experimentelle Untersuchungen und theoretische Ansätze - Projektbericht. *Mitteilungen 111*, Universität

- sity of the German Armed Forces, Institute of Hydro Science, Munich, Germany, 2011.
- MEHTA, A., SAMSAMI, F., KHARE, Y. and SAHIN, C.: Fluid mud properties in nautical depth estimation." J. Waterway, Port, Coastal, Ocean Eng., Vol. 140, 2, 210–222, 2014.
- WANG, L.: Tide Driven Dynamics of Subaqueous Fluid Mud Layers in Turbidity Maximum Zones of German Estuaries, Dissertation, Fachbereich Geowissenschaften, University of Bremen, Germany, 2010.
- WEHR, D.: An isopycnal numerical model for the simulation of fluid mud dynamics, PhD-thesis, Mitteilungen 115, University of the German Armed Forces, Institute of Hydro Science, Munich, Germany, 2012.
- WEHR, D. and MALCHEREK, A.: Numerical simulation of fluid mud dynamics – The isopycnal model MudSim. Die Küste, 79, 2012.
- WEILBEER, H.: Sediment transport and sediment management in the Elbe estuary. Die Küste, 81, 2014.
- WORRALL, W.E. and TULIANI, S.: Viscosity changes during the ageing of clay-water suspensions. Trans British Ceramic Society, Vol. 63, 167-185, 1964.

Recent Developments in Hamburg's Coastal Protection

Jan-Moritz Müller and Gabriele Gönner

Summary

In 2012 Hamburg's government decided to raise the design water levels of the tidal River Elbe in the Hamburg region by about 0.80 m. As a consequence, the primary flood defences in the city have to be reinforced and heightened during the next 25-30 years. Prior to implementing the strengthening program for the dikes and sea walls, extensive design work has to be carried out, including wave simulations and the determination of free-board heights, resulting in new crest levels for the various coastal flood protection facilities in the city.

Keywords

flood protection in Hamburg, hydrodynamic loads, mathematical modelling, EurOtop, SWAN, design water levels

Zusammenfassung

Im Jahr 2012 hat der Senat der Stadt Hamburg neue Bemessungswasserstände für den Hamburger Bereich der Tideelbe beschlossen, die etwa 0.80 m über den bisher gültigen liegen. In den kommenden 25-30 Jahren werden die Hochwasserschutzanlagen erhöht und verstärkt werden müssen. Vorab sind jedoch umfangreiche Arbeiten zur Ermittlung des neuen Bemessungsseegangs und der neuen Freibordhöhen nötig, die zu den neuen Ausbauböhen der vielfältigen Flutschutzbauwerke Hamburgs führen.

Schlagwörter

Hochwasserschutz in Hamburg, hydrodynamische Belastung, mathematische Modellierung, EurOtop, SWAN, Bemessungswasserstände

Contents

1	Introduction	474
2	Strategy for the primary storm flood defence of Hamburg and HafenCity	474
3	Design water levels – multi-method approach	475
4	Wave modelling	476
5	Wave overtopping and dike profile	478
6	Implementation of the improvement program	478
7	References	479

1 Introduction

Rising sea levels are threatening coastal regions, especially cities located in estuaries and river deltas. Raising the height of the primary flood protection constructions such as sea dikes and barriers in city areas often causes problems due to the limited availability of space, financing and finding economic and environmentally sustainable solutions that provide on the one hand a very high safety standard and on the other, accommodate the different interests.

The city of Hamburg is located at the Elbe estuary, about 110 km away from the North Sea, from which this region of northern Germany is seriously threatened by storm surges. In addition to the storm surges, high river runoff from inland rivers into the Elbe should not be neglected. The river marshes can be threatened by both risks simultaneously. About 45% of the city is located in low lying areas, which without dikes, would be flooded by storm surges. The total surface of the low area protected by dikes is 342 km², with around 326,000 inhabitants living there.

Coastal flood protection in Hamburg is divided into three parts: public flood protection, consisting of flood protection walls and sea dikes, private flood protection, mainly applied as individual object protection in the HafenCity, and flood protection in the harbour area. The 103 km long public flood protection in Hamburg consists of 78 km of dikes, 25 km of sea walls and 86 other constructions inside the primary flood defences, such as pumping stations, locks and barriers. Since the water level in the Elbe estuary is influenced by the North Sea tides, the dikes along the River Elbe in Hamburg are classified as coastal protection.

2 Strategy for the primary storm flood defence of Hamburg and HafenCity

The height of Hamburg's flood protection constructions has been increased several times during the past decennia. When a new flood protection barrier is being built or an existing one significantly reinforced as part of a construction program, allowance must be made for a possible further increase of 0.80 m (extension capacity) in the future. This strategy enables the planners to extend the construction in an economical way.

In the 1990s, the Government of the City of Hamburg created a Masterplan to build a new residential and business district in an old harbour area that is no longer used for trading purposes. This Masterplan was approved by the Hamburg Senate in 2000. The new district, known as HafenCity, is located outside the area that is protected by the public flood defence. The buildings in this area need to be protected by individual object protection, such as flood gates, or they have to be built on artificially elevated ground. This safety concept is based on a high level of personal responsibility by the people living and working in this area. The new HafenCity district consists of two parts. One is situated around the Speicherstadt, which is characterized by old warehouses that were built at the end of the 19th century. The street level in this part is still on the same level as the old harbour area, and is below the current design water level. This area can become flooded so buildings have to be protected by individual object protection. The other part of HafenCity is built on artificially elevated ground which is high enough to stay dry during high storm tide water levels. No object protection is needed for the buildings on these higher levels. Some of these new buildings are connected to lower ground levels where

object protection is needed. The higher elevated streets are connected by evacuation bridges to areas that are protected by the public sea defence. During high storm tide water levels, people can safely leave the higher areas and cross into the safe city centre of Hamburg. The height of the artificially elevated dwelling mounts is determined just like all other flood protection facilities in Hamburg by taking into account the design water level and the local wave conditions. The freeboard at some places in the HafenCity could be reduced slightly by building stairs instead of vertical flood protection walls, as stairs reduce the amount of wave run up. The object protection on the buildings must be designed to withstand not only water pressure, but also ice loading and ice movement. Ice sheets on the River Elbe or in the harbour basins, and high water levels can occur at the same time so object protection along the HafenCity waterfront has to be extra robust up to a certain height to avoid damage to buildings in exposed places.

3 Design water levels – multi-method approach

The design water level is defined as the highest expected water level in a particular region for a certain period of time. It includes astronomical tides, wind surge, external surges and high river runoff. The design water level for the city of Hamburg is determined by the tidal gauge at Cuxhaven. The Cuxhaven values were determined by three methods. The different components that cause the highest storm surge water levels were combined non-linearly by a multi-method approach, which includes deterministic superposition, and numerical and statistical methods. Subsequently, the German Federal Waterways Engineering and Research Institute (BAW) transferred the Cuxhaven water level to Hamburg by a hydrodynamic-numerical model. In Hamburg, the design water levels along the River Elbe reach heights of between 7.90 m and 8.60 m above sea level (see Fig. 1). In the model simulations, a river runoff into the Elbe of 2200 m³/s was taken into account.

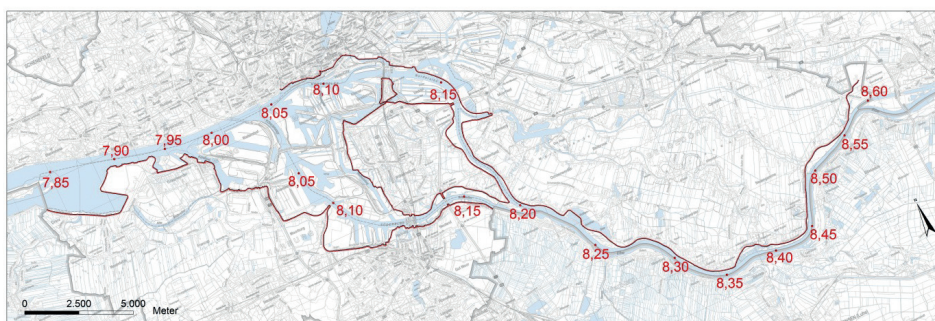


Figure 1: New design water levels for the River Elbe at Hamburg and primary flood protection (red line) (LSBG Hamburg).

Climate change and its consequences will have serious effects on the safety of people and economic values in coastal areas. These uncertainties necessitate new multi-dimensional protection concepts for the dimensioning of coastal protection facilities. In practice, a design level is verified by the required safety standard in a specific region. A probability of occurrence is associated with the design level. This value has to be compared to the required safety standard. If the safety standard for the calculated design level differs from

the analyzed safety standard for European metropolitan areas, the design level can be modified in order to ascertain the most effective coastal protection concept.

The developed approach to determine a new design water level for Hamburg involves detailed analysis of the highest single storm-surge components, springtides, external surge and wind surge. The analysis of the storm surge components showed that a combination of all components in their maximum observed value during the same storm surge event has not yet been observed. With regard to the aim to calculate physically feasible extreme events, hydrological feasibility in terms of combinations of all storm surge components have been investigated and found to be meteorologically and hydrologically feasible. As a result, the highest components from the different events are combined in the resulting extreme storm surge event, calculated by using the new approach, taking their non-linear interactions into account.

A multi-method approach has been developed for calculating the non-linear effects between the components. For this approach, alternatives for the calculation of extreme events were evaluated. It transpired that empirical, numerical and statistical methods present important and essential results, each possessing various restraints. In order to utilize the advantages and minimize the limitations and uncertainties, a multi-method approach was developed in which existing methods were exercised and brought together. Where several methods reach the same result, it can be considered reliable. Should the result be confirmed when comparing it with the safety standard for the research area, a basis is provided for spending millions of Euros of tax funding on coastal protection facilities. Examination of the storm surge curve is a special characteristic of this approach, which enables consideration of the whole storm surge run. The basic concept is to regard the results as ascertained only if they are proven by multiple, currently valid methods (GÖNNERT et al. 2013).

The climate factor is a reserve to maintain the safety standard for a defined period, normally for a further one hundred years. Also considered above all else in the climate factor is a rise in sea level, which in general is the most important influencing factor for future storm surge characteristics. Research analyses point out a huge range of sea level rise projections at the regional level up to the year 2100. An exploratory study analyzed these investigations in terms of a reference study (GÖNNERT et al. 2010). The regional scenarios for sea level rise in the North Sea range from just a few centimetres to 115 cm. Based on this information, the climate change factor must be specified in height for the investigation area; this will always be a technical as well as a specific political decision.

4 Wave modelling

The wave climate and the wave transformation in front of the primary sea defences in Hamburg were computed by the third-generation wave model SWAN (BOOIJ et al. 1999; RIS et al. 1999). Simulations were carried out for the design water level for different wind directions to get the critical wave conditions for every section of the sea defences in Hamburg.

Since the design water level is defined as the crest of the highest expected storm tide curve, currents were not taken into account. Areas in front of the primary sea defences that are on a lower level were assumed to be flooded. The following parameters have been extracted from the wave model at several points in front of the flood protection

structure: significant wave height, mean wave period, wave direction, directional spreading and water depth. A uniform wind field was used for all computations with a constant wind speed of 20 m/s and a direction ranging from 180° N to 360° N in sectors of 10 degrees. Westerly winds are mainly responsible for extremely high storm tide water levels in the Elbe estuary. The water level ranges from 7.90 m above sea level at the seaward boundary of the Hamburg part of the river Elbe, rising up to 8.60 m above sea level at the landward boundary near the city of Geesthacht. The water level surface data was taken from the calculations that were carried out by the German Federal Waterways Engineering and Research Institute.

It is assumed that no buildings exist on quays and polders in the harbour area because they might not exist at the time of the design storm surge. In this way, a conservative estimate of the extreme wave conditions is obtained, ensuring that the resulting protection works are safe, regardless of the possible future situation. Polder walls in the harbour area are schematized as walls with a height of 7.50 m above sea level. They are flooded with water levels of about 8.10 m above sea level to let them function as submerged breakwaters for the extreme wave conditions in the harbour area.

The harbour area is situated almost completely outside the primary sea defences of Hamburg, so it can become partially flooded during extreme storm tide water levels.

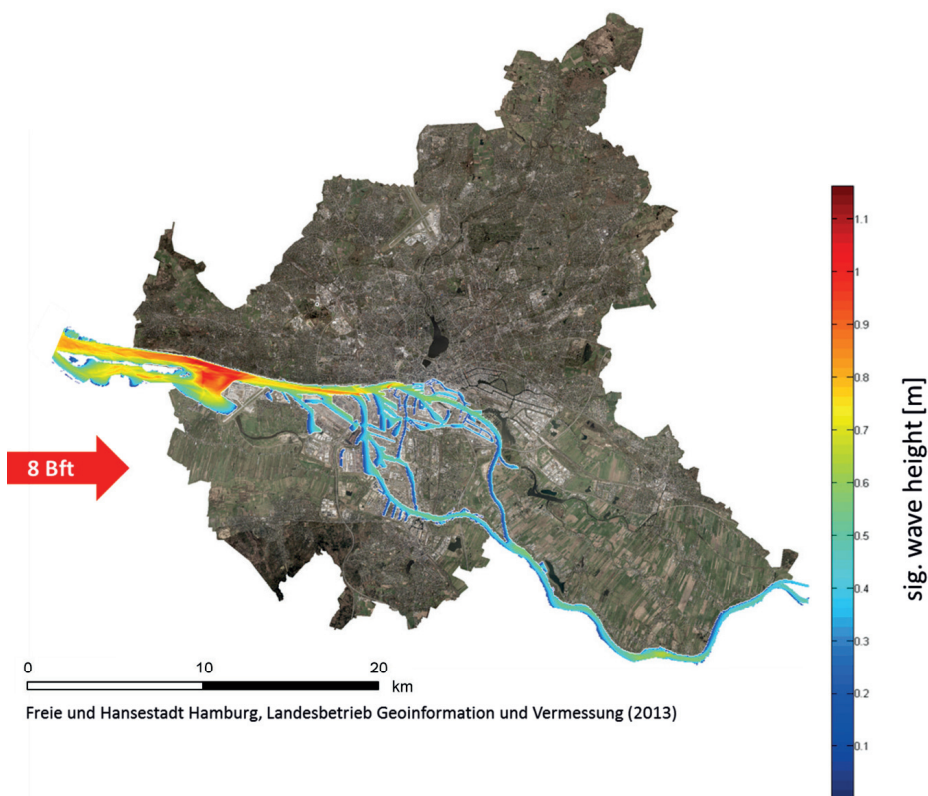


Figure 2: Wave climate in the tidal River Elbe in Hamburg for normal high tide and westerly winds.

5 Wave overtopping and dike profile

In Hamburg the EurOtop (EurOtop Overtopping Manual, 2007) approach was chosen to determine the freeboard of the public coast protection constructions. The allowance for wave overtopping on the dikes in Hamburg is 0.5 l/m/s. The minimum freeboard for dikes is fixed to 0.5 m and for vertical flood protection walls to 0.3 m.

Various Matlab-scripts were developed for calculating the necessary freeboard. The freeboard is calculated automatically by the scripts every 10 m along the public flood defence according to the orientation of the flood protection construction, the critical wave direction and wave height. The procedure determines whether the construction is a vertical concrete wall or a “green” sloping dike covered with grass. The results are stored in tables together with the latitude and longitude co-ordinates, dike-kilometer, critical wave conditions, local design water level, freeboard and the resulting crest height of the flood defence. The crest height is the final height that has to be guaranteed at each location and has to include a certain amount of height for possible settling.

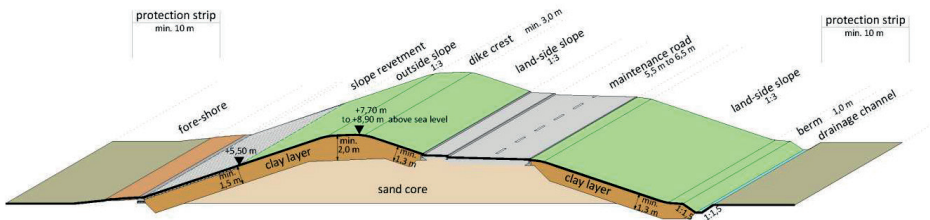


Figure 3: Typical dike profile in Hamburg.

A typical profile of a Hamburg sea dike is shown in fig. 3. The dike has grass-covered slopes on both sides with a gradient of 1:3. Open stones are placed on the lower part of the outer slope to protect the dike against ice loading and ice damage. Ice sheets on the River Elbe moved by tidal currents and water level changes could do considerable damage as their dimensions reach several. The dike profile also includes an asphalted road on the landward side to guarantee access to every place along the public sea defence during a severe storm surge event.

6 Implementation of the improvement program

Before the improvement program can begin, the order of the measures to be taken must be determined and a priority program developed. The various sections of the public flood defence were investigated according to their urgency for improvement, and criteria were defined. The first criterion was the difference in the existing height compared to the new design crest height. Another was the need for urgent maintenance on the dikes and sea walls. The vulnerability of the areas behind the sections was also taken into account. Thus it was possible to make a ranking of the urgency for raising and improving the various sections of the 103 km long public sea defence in Hamburg.

Prior to raising the height of the whole public sea defence structures in Hamburg, the height of the Hafencity extension area had to be calculated following the described

procedure. The elevated residential areas of this new district outside the flood protected part of the city are currently under construction. The time needed to build all the new dikes and sea walls of the public sea defence in Hamburg is estimated to be at least 25 to 30 years.

7 References

- BOOIJ, N., RIS, R.C. and HOLTHUIJSEN, L.H.: A third-generation wave model for coastal regions, Part I, Model description and validation, *J. Geophys. Res.* C4, 104, 7649-7666, 1999.
- EUROTOP OVERTOPPING MANUAL: Wave Overtopping of Sea Defences and Related Structures: Assessment Manual (*Die Küste* 73), 2007
- GÖNNERT, G. et al: Der Meeresspiegelanstieg. Ursachen, Tendenzen und Risikobewertung. *Die Küste*, Heft 76, 2010.
- GÖNNERT, G.; GERKENSMEIER, B.; MÜLLER, J.-M.: Ermittlung des Sturmflutbemessungswasserstandes für den öffentlichen Hochwasserschutz in Hamburg, *Berichte des Landesbetriebes für Straßen, Brücken und Gewässer*, Heft 12, 2012.
- Masterplan HafenCity; Freie und Hansestadt Hamburg, Bürgerschafts-Drucksache Nr. 16/3909.

For further information please visit: www.LSBG.Hamburg.de.

Model-Based Verification of Dikes along the West Coast of Schleswig-Holstein

Ulrich Winskowsky and Birgit Matelski

Summary

Every 10 to 15 years, the German Federal State of Schleswig-Holstein performs a safety check of its sea dikes. The regular check shall ensure that critical changes both to the structure and to the expected hydrological forces as a result of climate change are detected in time. While in the past wave run-up or debris edge measurements were used to determine the necessary wave parameters for the safety check, for the “Coastal Defence Master Plan 2012” of Schleswig-Holstein these parameters were calculated with a numerical wave model. An advantage of this method is that wave data in the required resolution for all dikes are established with a uniform procedure, regardless of natural data with frequent measurement errors. In the present paper this procedure is exemplified for the island of Pellworm.

Keywords

Sea dikes, safety check, wave model, design wave

Zusammenfassung

Alle 10 bis 15 Jahre führt das Land Schleswig-Holstein eine Sicherheitsüberprüfung seiner Seedeiche durch. Durch die regelmäßige Überprüfung soll sichergestellt werden, dass kritische Veränderungen sowohl am Bauwerk als auch bei den zu erwartenden Belastungen infolge der Klimaänderung rechtzeitig erkannt werden. Mussten in der Vergangenheit die für die Überprüfung erforderlichen Seegangparameter noch aus Wellenaufmessungen und Treibselmessungen ermittelt werden, so wurde für den „Generalplan Küstenschutz 2012“ des Landes Schleswig-Holstein der Seegang mit einem numerischen Seegangmodell berechnet. Das hat den Vorteil, einen an allen Deichstrecken mit einem einheitlichen Verfahren ermittelten Seegang in der erforderlichen Auflösung zur Verfügung zu haben, unabhängig von oftmals mit Messfehlern behafteten Naturdaten. Am Beispiel der Insel Pellworm wird das Verfahren vorgestellt.

Schlagwörter

Seedeiche, Sicherheitsüberprüfung, Seegangmodell, Bemessungsseegang

Contents

1	Introduction	482
2	Design wave evaluation	483
3	Boundary condition storm surge level	484

4	Boundary condition wind	484
5	Simulations	484
6	Wave parameters at the dike	485
7	Results	486
8	Outlook	488
9	References	489

1 Introduction

Schleswig-Holstein, the German Federal state between the North Sea and the Baltic Sea, has a coastline of 1105 kilometers in total. Nearly 430 km of that coast are protected by so-called state dikes (Fig. 1), a further 96 km by so-called regional dikes. State dikes have an accordingly high protective standard, safeguarding the hinterland against storm surges, often in interaction with other sea defenses (second dike line) or other flood protection systems (MELUR 2012). In general, regional dikes have a lower safety standard.

The west coast of Schleswig-Holstein is characterized by low lying marshland. Over a length of 228 km, the west coast is protected by state dikes, with a few exceptions. A further 131 km of state dikes can be found on the islands (71 km) and along the Elbe Estuary (60 km). In contrast, on the eastern coast of Schleswig-Holstein there are, with a total of 71 km, comparatively few state dikes.



Figure 1: Overview of Schleswig-Holstein with state dikes (black lines). (LKN-SH (Schleswig-Holstein Agency for Coastal Defense, National Park and Marine Conservation)).

The state dikes in Schleswig-Holstein are inspected regularly every 10 to 15 years regarding their protective standard, the last time in 2011 (MELUR 2012). For this dynamic dike safety system, established in the Coastal Defence Master Plan 2001, wave overtopping is used as a safety criterion. In the past, the regional run-up heights of waves were derived from debris edge measurements. The approach used from 2001 on has the advantage that, in addition to the water level and sea conditions, the local wave attack direction and the geometry of the seaward slope are also considered.

Allowing for the fact that small scale overtopping does not affect dike safety, Schleswig-Holstein accepts a maximum wave overtopping of two liters per meter and second. This value applies to dikes with an intact grass cover on the inland slope. For covered dikes, such as asphalt dikes, higher values are tolerated. If the calculated overtopping rate exceeds the permitted limit, dike strengthening becomes necessary.

For the Coastal Defence Master Plan 2001, an in-house developed method was used to calculate the wave parameters at the dike toe from wave run-up and debris edge measurements. These parameters were then interpolated to the entire dike stretch. As it turned out later, this method has some weaknesses. On the one hand, the debris edge measurements are not sufficiently reliable and on the other hand, the extrapolation over larger stretches is problematic (PROBST 2004).

The calculation of the wave overtopping rates has been carried out since 2008 on the basis of the deterministic method according to EUROTOP (2007). In the meantime, the EAK-method (EAK 2002) was also used, which, however, in comparison had lower overflow rates. Since then, the wave parameters required for this method are generated using a numerical wave model.

2 Design wave evaluation

The evaluation of the wave parameters for the safety check of the state dikes in 2012 was done using the spectral wave model SWAN (Simulating Waves Nearshore). The suitability of SWAN for the determination of sea states during storm events on the west coast of Schleswig-Holstein has already been described by MAI (2002) and NIEMEYER and KAISER (2003).

In the SWAN-simulations, all available physical processes that affect the sea in the computational area were considered. These include the energy input by wind, refraction, shoaling, depth-induced wave breaking and white capping, the nonlinear interactions between the waves (triad and quadruplet interaction) and bottom friction.

If the spatial resolution is high enough, SWAN can also take into account the influence of diffraction. Due to the size of the study area, however, this option could not be applied. In areas that are not exposed to the main attack direction of the swell, additional wave energy can be entered by diffraction. This effect must be considered when determining the design wave for areas which are shaded from wave action.

As a worst case scenario for the safety check of the dikes, a combination of a reference storm surge water level and the maximum possible wave was defined.

3 Boundary condition storm surge level

The storm surge water level used in the simulation was determined using a newly developed method which is based on the non-stationary and regional probability analysis (MELUR 2012). The resulting reference water level corresponds to a water level that statistically occurs once every 200 years (RHW200). Therefore, for each dike section a separate model run is required.

4 Boundary condition wind

Investigations of storm surge water levels and corresponding wind speeds and wind directions on the west coast of Schleswig-Holstein led to the conclusion that for the occurrence of the wind set-up in the case of reference water level the sector between SW and NW can be defined as the significant wind direction.

Regional wind measurements on the west coast were used to determine the highest expected wind speeds for these wind sectors. For example, the highest measured wind speeds (for the period from 1969 to 2011) and their directions are shown in Tab. 1, taken during a storm tide at the wind gauge on Hallig Hooe in the southern North Frisian Wadden Sea.

Table 1: Highest measured wind speeds for different wind directions during a storm tide at the wind gauge Hallig Hooe (DWD) for the period 1969-2011 (*gauge Husum (WSA Tönning); NHN: normal height null).

date	name	swl * [NHN+m]	wind	
			θ [-]	u [m/s]
24.11.1981	-	5.15	SW	26
08.01.2005	Freddy	3.46	WSW	25
03.12.1999	Anatol	5.37	W	29
03.01.1976	Capella	5.61	WNW	28
10.01.1995	-	4.37	NW	22

Based on these studies, the highest wind speed was determined to be 32 m/s for wind directions in the SW to NW sector. To prevent the risk of an underestimation of the design wave, the chosen wind speed value was set even higher than the measured values.

The choice for the highest wind speed on the west coast of Schleswig-Holstein has already proven to be true and not too high. During storm “Christian” on 28 October 2013, for example, the measured wind speed at the Hallig Hooe gauge was nearly 32 m/s, blowing from WSW.

5 Simulations

Due to the size of the study area, the number of dike sections and differing accuracy requirements on the model results, the simulations were performed with nested models with different expansion and grid width.

The model bathymetry in each case was based upon the latest available survey data. Fig. 2, for example, shows the procedure for the island of Pellworm.

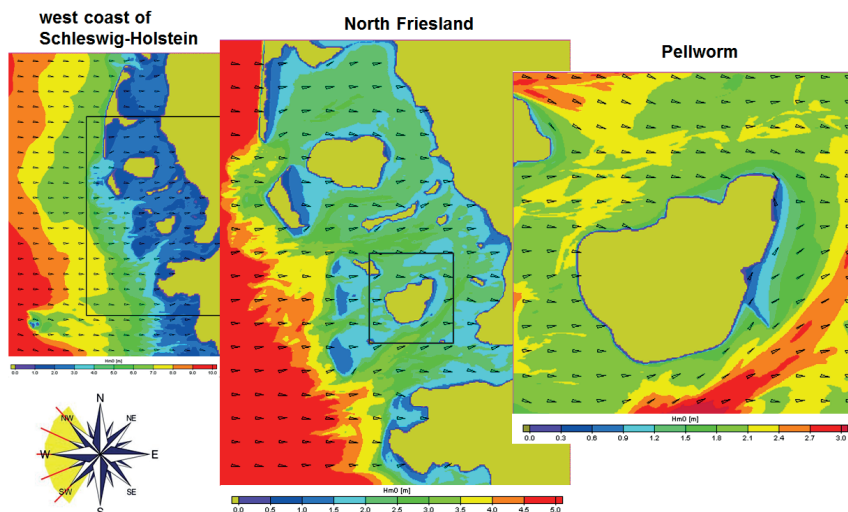


Figure 2: Simulated significant wave height and mean wave direction in the nested models for the scenario “wind from west”. (LKN-SH).

The boundaries of the parent model area (German Bight model) were set in such a way that the wave heights and wave periods at the edge had no influence on the simulated wave parameters in the area of the detailed models (dike section models). The waves in the Wadden Sea are already affected by the local wind. Therefore, the incoming waves only have a limited impact on this area.

Stationary simulations were performed, i.e., the water level and the wind field were assumed to be a temporal and spatial constant. The decisive wind sector between SW and NW was subdivided into five wind sections with an angle of 22.5° each. For each regionally different reference water level (RHW200), a total of five model runs had to be carried out.

6 Wave parameters at the dike

The calculation of wave run-up and wave overtopping by EUROTOP (2007) requires the wave parameters directly at the dike toe (The dike toe on dikes with a foreshore is the transition from the dike slope onto the foreshore, on dikes without a foreshore it is the transition onto the intertidal flats). On the west coast of Schleswig-Holstein, the elevation of the foreshore can reach up to NHN + 2 m. Thus, the dike toe is the decisive point for calculating the sea state.

Due to the fact that the safety check at the west coast of Schleswig-Holstein was usually performed at dike profiles with intervals of 500 m, the wave parameters (from the model calculations) at the dike toe were required for these profiles.

The wave model SWAN provides the option of producing wave parameters at specified altitudes on defined profiles. If it is assumed that the elevation of the dike toe of the dike without a foreshore lies at NHN + 1 m, while the toe of a dike with a foreshore is located at NHN + 2 m, the authoritative points can be automatically determined. For these points the wave parameters can be produced.

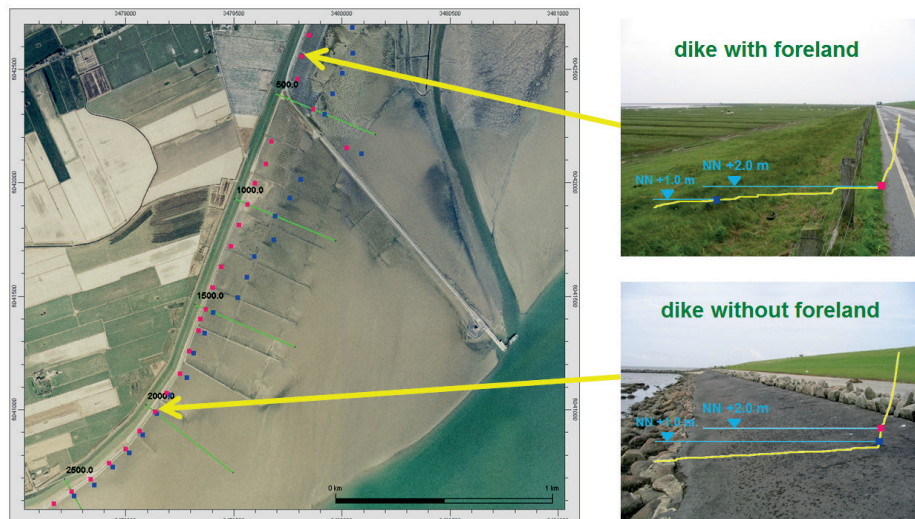


Figure 3: Locations for the design wave at the east side of the island Pellworm (red: NHN +2 m; blue: NHN +1 m; aerial photograph 2005). (LKN-SH).

Fig. 3 shows the exemplary result of this procedure for the east side of Pellworm with tidal flats, a tidal channel called Norderhever, a dam to the ferry dock and the harbor entrance to the old port of Pellworm. South of the dam to the deep-water ferry dock, the dike has no foreland over a distance of more than 1 km. At close range north and south of the dam, however, foreland has formed since the dam's completion in 1991.

As a criterion for the determination of the highest sea state from the simulation results for different wind directions, the amount of the expected wave run-up was used. The choice of the highest wave parameter, i.e. the worst combination of wave height, wave period and wave direction at each location of the dike profiles, was extracted from five results using the wave run-up formula by EUROTOP (2007).

7 Results

Fig. 4 shows the design wave, which was determined on the basis of the described simulations, for the state dike of the island of Pellworm. For the calculation of wave overtopping by EUROTOP (2007) the parameters significant wave height (H_{m0}) and average wave period ($T_{m-1.0}$) are needed. As expected, the design wave of the dike section at the south side of Pellworm is the largest. At the dike sections with a foreshore, the damping effect of the foreshore on the design wave is clearly noticeable.

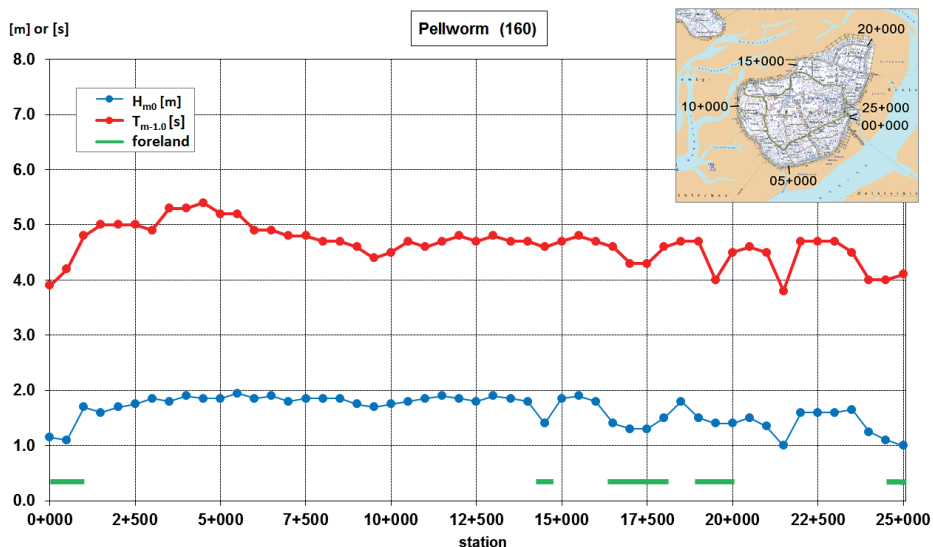


Figure 4: Model-based design wave for the safety check of the state dike of the island of Pellworm. (LKN-SH; top right: DTK50-V LVerGeo SH).

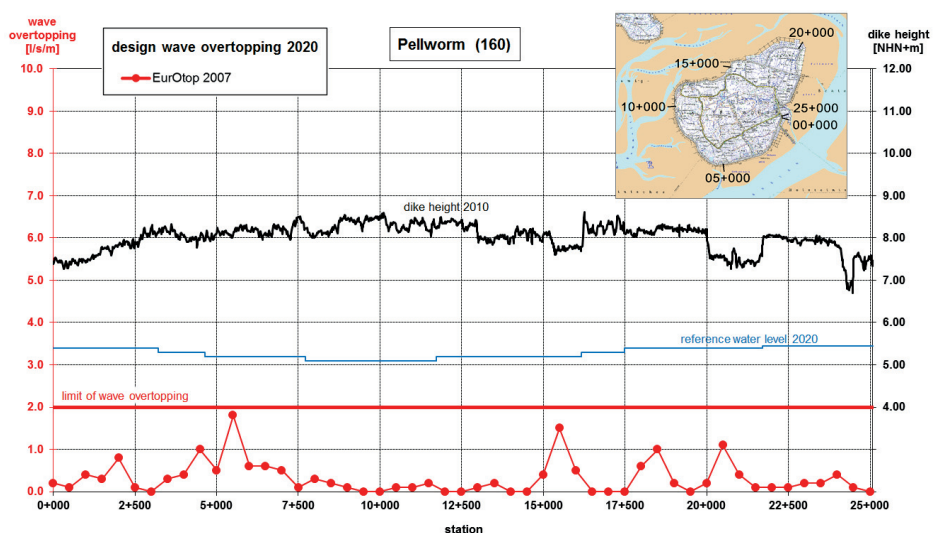


Figure 5: Design wave overtopping for the reference water level RHW200 at the state dike of the island of Pellworm. (LKN-SH; top right: DTK50-V LVerGeo SH).

Simulations of storm events (hindcasts) in the southern North Frisian Wadden Sea have shown that SWAN delivers good results for the wave height, compared to the measured data. The mean wave periods are a bit underestimated in the model. Since only little measured data for storm events is available, no reliable value for the deviation between model and natural period can be currently calculated. Additionally, the magnitude of the differences varies regionally. To avoid any risk of underestimation of the wave period, the

model-based periods were applied with a safety factor of 1.25 for the safety check. The results are, therefore, always on the safe side.

The result of the safety check in 2012 for the island of Pellworm is shown in Fig 5. Based on the calculated wave overtopping, the permitted overtopping of 2 l/s/m is not exceeded at any verified dike profile. So from a hydrological point of view, no dike strengthening is required for the island of Pellworm.

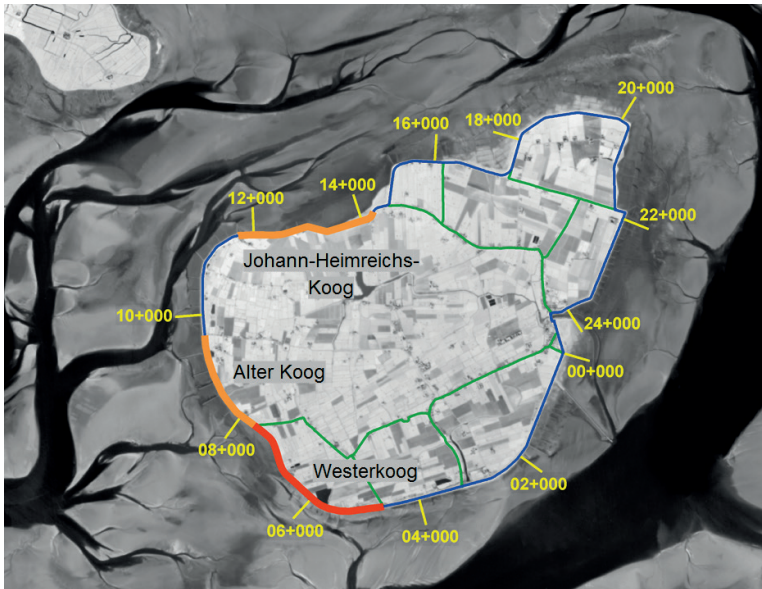


Figure 6: Planned dike strengthening on the island of Pellworm (red: urgent; blue-line: state dike; aerial photograph 2000). (LKN-SH).

However, apart from hydrological criteria, geotechnical (e.g., grass cover, dike material) and other criteria such as the presence of a second dike line determine the safety of state dikes as well. On the basis of these non-hydrological criteria, it was determined in the Coastal Defense Master Plan of 2012 that, for the dike section “Westerkoog”, an urgent strengthening is needed over a length of 3.1 km (Fig. 6). Further strengthening campaigns are needed at the sections “Alter Koog” and “Johann-Heimreichs-Koog”, respectively, over a total length of 4.5 km.

The safety check of the dikes on the east coast and at the Elbe Estuary was performed in a similar manner.

8 Outlook

Schleswig-Holstein will further investigate the safety status of the regional dikes in the coming years. Therefore, a method on the basis of combined probabilities for water level and waves will be applied.

9 References

- EAK 2002: Empfehlungen für Küstenschutzbauwerke. Die Küste, 65, 2002.
- EUROTOP: Wave Overtopping of Sea Defences and Related Structures: Assessment Manual, August 2007.
- MAI, S.: Seegangsausbreitung in Hever und Heverstrom. Mitteilungen des Franzius-Instituts für Wasserbau und Küsteningenieurwesen der Universität Hannover, 87, 98-141, 2002.
- MELUR: Generalplan Küstenschutz des Landes Schleswig-Holstein, Fortschreibung 2012.
- NIEMEYER, H. und KAISER, R.: Ermittlung des Bemessungsseegangs für Küstenschutzwerke und Randdünen mit Mathematischer Modellierung. Schlussbericht zum KFKI-Forschungsvorhaben „Bemessungsseegang“ KIS004, Niedersächsisches Landesamt für Ökologie, Forschungsstelle Küste, 2003.
- PROBST, B.: Dynamisches Deichsicherheitssystem in Schleswig-Holstein. In: GÖNNERT, G., GRASSL, H., KELLETAT, D., KUNZ, H., PROBST, B., VON STORCH, H., SÜNDERMANN, J. (Hrsg.): Klimaänderung und Küstenschutz, 29. und 30. November 2004, 223231, 2004.

Integrated Design of Sea- and Estuarine Dikes

Cordula Berkenbrink and Hans Dieter Niemeyer

Summary

The impact of the expected changes in the global climate will create an unknown challenge for coastal protection. The anticipated acceleration of the sea level rise in combination with an expected higher set-up of storm surges will create higher storm surge levels and stronger waves. Existing guidelines for the design of dike heights only consider hydrodynamic loads, whereas the resistance of the dike body or the dike covering has not been part of the design criteria up so far. Therefore, dikes had to be heightened according to the hydrodynamic loads. To achieve an economical and safe design, it is necessary to consider the hydrodynamic loads in more detail, together with the soil mechanic resistance of the dike material. That was the idea behind the integrated design concept developed in the project “Integrated Design of Sea- and Estuarine Dikes” of the German Coastal Engineering Research Council (KFKI), funded by the German Federal Ministry of Education and Research (BMBF). To establish the quantification of the soil mechanic characteristics, a detailed knowledge of the hydrodynamic loads is essential. This cannot be adequately achieved by way of empirical relationships. In order to match such requirements, the mathematical model OTT-1d of HR-Wallingford was developed, validated, calibrated and verified. Implementing the model for design practice, it was extended in such a way, that different roughness sections can be considered and the loads of the inner slope can be quantified. Finally, the integrated design concept is shown for one typical type of dike, for varying load scenarios at the coast and in an estuary of Lower Saxony, respectively.

Keywords

integrated design, hydrodynamic loads, wave overtopping, climate change, overtopping security

Zusammenfassung

Der Klimawandel und seine Folgewirkungen werden den Insel- und Küstenschutz vor erhebliche Herausforderungen stellen, da von stark wachsenden Beanspruchungen der Schutzwerke auszugehen ist. Beschleunigter Meeresspiegelanstieg, wachsender Stau von Sturmfluten bewirken einerseits höhere Bemessungswasserstände und andererseits höhere Wassertiefen, die wegen der Tiefenbegrenzung des Seegangs vor den Schutzwerken dessen Zunahme ermöglichen. Insofern ist von einem erheblichen Wachsen, der in den gängigen Bemessungsansätzen berücksichtigten hydrodynamischen Belastungen, auszugehen. Sie bestimmen bei der gegenwärtigen Bemessungspraxis allein die Dimensionierung von Deichen.

Im Sinne einer effektiveren Bemessung von See- und Ästuardeichen hinsichtlich Sicherheit und Wirtschaftlichkeit erscheint deshalb eine differenziertere Berücksichtigung der hydrodynamischen Belastungen in Verbindung mit der berücksichtigten bodenmechanischen Widerstandsfähigkeit der beim Deich verwendeten Erdbaustoffe unverzichtbar. Um diese Zielsetzung zu erreichen wurde ein entsprechendes Konzept für das Forschungsvorhaben „Integrierte Bemessung von See- und Ästuardeichen“ entwickelt, das

vom Kuratorium für Forschung im Küsteningenieurwesen (KFKI) gebilligt und vom Bundesministerium für Bildung und Forschung (BMBF) gefördert wurde.

Die Umsetzung des Forschungsvorhabens erfolgte einerseits durch eine Identifikation geeigneter bodenmechanischer Parameter zur Charakterisierung der Widerstandsfähigkeit der verwendeten Erdbaustoffe gegenüber den erfolgenden hydrodynamischen Belastungen. Sie wurden andererseits wesentlich differenzierter analysiert als mit den gegenwärtig genutzten empirischen Bemessungsansätzen möglich, um ein integriertes hydrodynamisch-bodenmechanisches Bemessungsverfahren entwickeln zu können. Hierfür wurde das bei HR Wallingford entwickelte mathematische Wellenauf- und -überlaufmodell OTT-1D genutzt. Es wurde verifiziert, kalibriert und für die Anwendung in der Bemessungspraxis dahingehend tauglich gemacht und optimiert, dass die hydrodynamischen Belastungen der Innenböschungen quantifiziert werden können und Baukörperabschnitte mit unterschiedlichen Rauheitsabschnitten berücksichtigt werden können. Im Anschluss wird das neuentwickelte integrierte hydrodynamisch-bodenmechanische Bemessungskonzept repräsentativ auf einen exponierten Seedeich und einen Ästuardeich in Niedersachsen angewendet. Mit Hilfe des differenzierten Bemessungsansatzes werden für diese Deiche die Potenziale an Belastungsreserven aufgezeigt, die sich bei seiner konsequenten Anwendung in Zukunft nutzen werden lassen, um einen Teil der aus Klimaänderungsfolgen herrührenden zusätzlichen Belastungen ohne weitere Erhöhungen von Deichen kompensieren zu können.

Schlagwörter

Insel- und Küstenschutz, integrierte Bemessung, Erdbaustoffe, Hydrodynamik, Bodenmechanik, Wellenüberlauf, Überlaufsicherheit, Klimaänderungsfolgen

Contents

1	Introduction and Motivation	492
2	Recent improvements in dike design in Lower Saxony, Germany	493
3	Integrated approach	494
3.1	Schematic representation	494
3.2	Description and modification of the mathematical model	495
4	Example for the integrated design	495
5	Potential for Compensation of Future Climate Change Impacts	498
6	Summary and Conclusions	499
7	Acknowledgements	500
8	References	500

1 Introduction and Motivation

Wave Overtopping is an important design criterion for coastal structures; in the past it has been the most common indicator for dike failure on the German coast. Knowing this, it is important to obtain reliable data for this hydrodynamic load in order to improve the safety of coastal structures against the background of rising sea levels and increased storm intensity. At present, the prediction of overtopping discharge is calculated by empirical formulae, which are limited to definite structures and wave conditions. They are

determined through hydraulic tests for defined wave and structure parameters. For geometries or wave conditions not examined in these hydraulic tests, these methods are not always reliable and lead to both over- and underestimations. Mathematical models are able to simulate wave overtopping more precisely than empirical relationships can, because the detailed geometry of the structure and the whole spectrum of the wave field can be considered and easily changed.

Project partners from the Institute of Soil Mechanics and Foundation Engineering of the University of Duisburg-Essen analysed the soil mechanical processes for a functional optimization of dike elements. An example is given to show the integration of the hydrodynamic loads and the soil mechanical resistance for an integrated design concept for dikes.

In situ investigations of dike overtopping security in the Netherlands documented that a dike could withstand overtopping rates up to 50 l/(m·s) without damage (Fig. 1) (VAN DER MEER et al. 2009). Therefore, in countries with lowlands like Germany or the Netherlands, ambitious research programs are carried out in order to intensify and increase the knowledge on wave overtopping security of dikes.



Figure 1: Inner slope of a dike in Delftzijl during in situ overtopping tests.

Aim of the project is to quantify the resistance of a dike through a comparison of local hydrodynamic loads with specific resistance parameters of the soil. Mechanical characteristics of construction material will be considered, based on data from other engineering sectors. The necessary safety standard can be optimized by connecting loads and load capacity. Furthermore, safety deficits on existing dikes can be localized in order to deploy a priority concept.

2 Recent improvements in dike design in Lower Saxony, Germany

The determination of design wave run-up for dikes has been seriously taken into consideration following the disastrous storm surge of February 1962, which had a death toll of more than 300 people (LÜDERS and LEIS 1964). But the lack of information of the local wave climate in the morphologically enormously differentiated coastal areas and estuaries initially only allowed for an empirical design. This design was oriented along data about wave run-up which had occurred during storm surges in the past. In order to provide sufficient security for the hinterland, estimates of design wave run-up have been carried

out by anticipating rather high values for long stretches as a whole (Fig. 2). Since 1976, measurements of flotsam benchmarks were not only used for the identification of wave run-up but also for its extrapolation for design conditions (NIEMEYER 1977), (NIEMEYER et al. 1995) allowing a more differentiated evaluation of design wave run-up (Fig. 2).

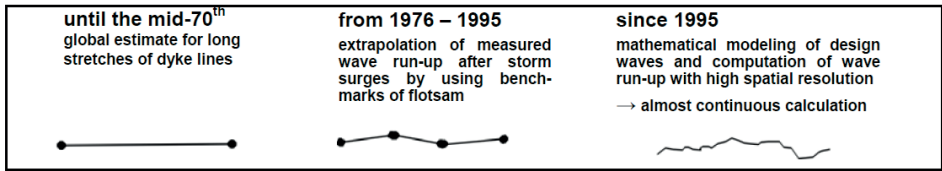


Figure 2: Changes in the evaluation of design wave run-up in Lower Saxony within the last decades (NIEMEYER et al. 2010).

Since 1997, design wave conditions are determined by applying the third generation full-spectral wave model SWAN (RIS, HOLTHUIJSEN and BOOIJ 1995) providing the input for modified wave run-up formulas (e.g. VAN GENT 1999) under consideration of an accepted overtopping rate of 3 % (NIEMEYER and KAISER 2001). Such detailed studies allow a much more differentiated determination of dike heights than before.

3 Integrated approach

3.1 Schematic representation

The research project “Integrated Design of Coastal and Estuarine Dikes” is aimed at the development of design procedures, under quantitative consideration of the detailed hydrodynamical loads, as well as the strength of the clay of dikes (Fig. 3).

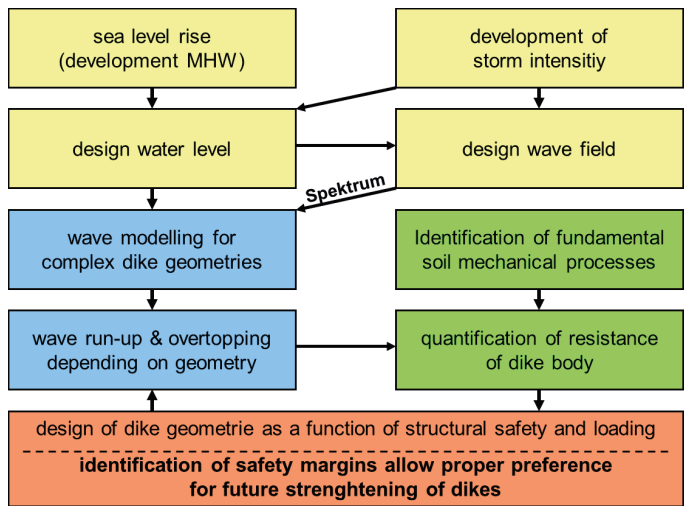


Figure 3: Design procedure.

For the evaluation of the design water level, as well as the design wave field, the design methods of the Federal State of Lower Saxony in Germany were used. Wave run-up, and

wave overtopping respectively, were calculated in more detail using mathematical modeling instead of empirical relationships. This has the advantage that nearly every structure and every wave field can be taken into account. Furthermore, the hydrodynamic loads can be identified at every point of interest for the soil mechanical functions.

3.2 Description and modification of the mathematical model

The mathematical model applied here is called OTT-1d developed by HR Wallingford (DODD et al. 1998) and is part of the ANEMONE group (Advanced Non-linear Engineering Models for the Nearshore Environment). It is based on the nonlinear shallow water (NLSW) equations, which describe the horizontal mass and momentum balance. They are solved explicitly using the finite volume method. The advantage of the OTT-1d model, in contrast to other similar NLSW-Models, is the use of the Godunov-type scheme. Water volumes can be treated equally in each computational node; that allows for the calculation of separated water volumes. The regeneration of waves by overtopping volumes in lee of the structure can also be modeled. Wave breaking is implicitly included by building a bore. The numerical waves steepen and form shocks with a vertical face. OTT-1d has very robust numerical solvers and runs efficiently and stable. The input parameters are reduced to a minimum.

Some modifications were necessary to be able to use the model for complex or real scale structures (BERKENBRINK et al. 2009). In a first step, the input and output parameters and the model domain were increased. Further, the still water level at the inner slope was reprogrammed to make calculation of hydrodynamic loads at the inner slope possible. Finally, the modified model is able to build up different roughness sections in the model domain. Previously, the roughness factor was assumed to be constant over the entire dike, resulting in the inability to model complex revetments. The accuracy of all those modifications has been verified through the output signals at the crest.

4 Example for the integrated design

Numerous tests were carried out during the project, which cannot all be introduced in this paper. A typical dike profile on the East Frisian coast in Lower Saxony was chosen as a representative example. It has a crest height of about 8.0 m above NN, an outer slope of 1:6 and an inner one of 1:3. The clay layer has a thickness of 1.5 m at the outer slope and crest and of 1.0 m on the inner slope (Fig. 4).

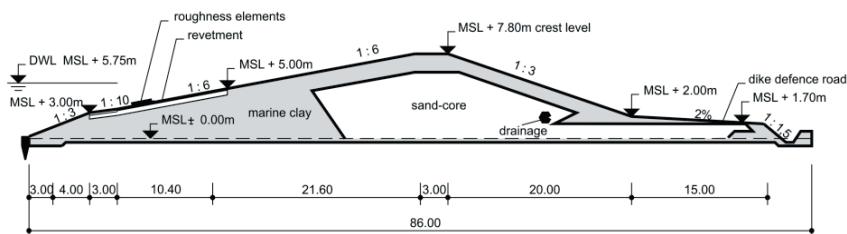


Figure 4: Dike profile at the East Frisian coast of Lower Saxony.

After creating a design procedure set-up, the dikes were tested in different scenarios of anticipated design water levels ranging from 5.0 m to 7.5 m above German Datum NN; with steps of 0.5 m. The present design water level is about 5.75 m above NN. For all these water levels between the the lowest and highest, design waves have been modeled by SWAN, (Fig. 5). The range of significant wave heights, energy periods and mean wave direction varies correspondingly as follows:

$$\begin{aligned}
 1.76 \text{ m} &\leq H_{m0} \leq 2.48 \text{ m} \\
 3.6 \text{ s} &\leq T_{m-1,0} \leq 5.4 \text{ s} \\
 310^\circ &\geq \theta_m \geq 303^\circ
 \end{aligned}$$

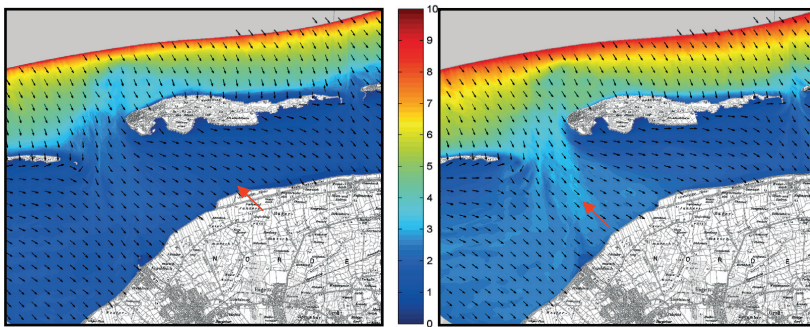


Figure 5: Significant Wave Heights [m] modeled by SWAN (left panel: supposed design water level: 5 m above German datum, right panel: anticipated design water level: 7.5 m above German datum) (BERKENBRINK et al. 2010).

The wave spectra at the toe of the dike at an exposed position for each anticipated design water level are used as boundary conditions for modelling wave run-up and overtopping on the dike (modelling was carried out by OTT-1d model).

The mean overtopping rates increase enormously with rising design water levels and wave parameters (Fig. 6), reaching a maximum of approximately 200 l/(s·m) for a design water level of NN+ 7.5 m. The present design water level leads to low mean overtopping rates. For higher overtopping rates, the tolerable design water level could be raised (see the tests in Delfzijl). The dike was able to bear 50 l/(s·m), amounting to a tolerable design water level of NN +6.7 m for this example. These mean overtopping rates, their corresponding layer thicknesses and velocities have been used in order to determine the capacity of a distinct clay quality.

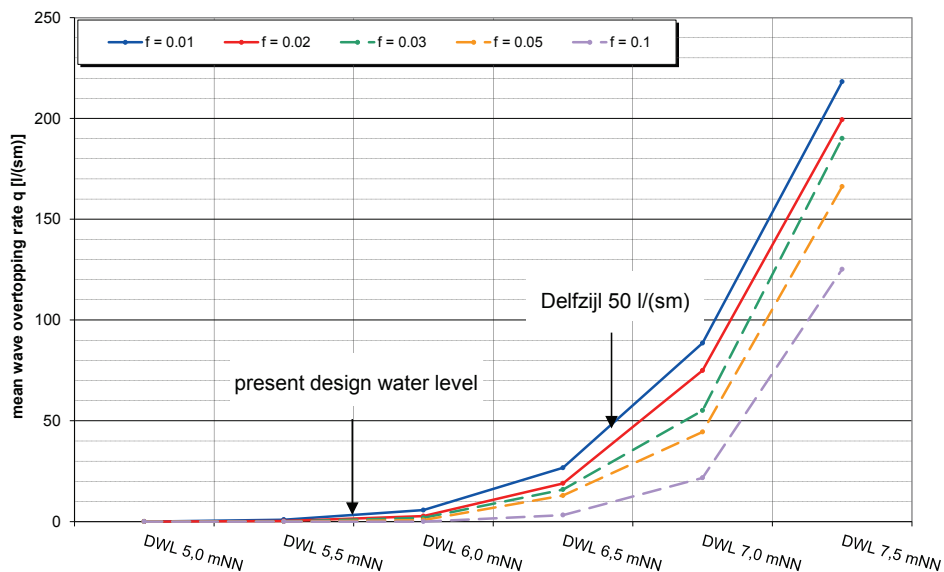


Figure 6: Mean Overtopping rates for different design level scenarios and roughness factors.

The hydrodynamic loads result in soil mechanical processes like erosion and infiltration. Because of this consistent wetting, the soil softens and loses its strength. The Inner slope is saturated with overtopping water and, in combination with the soil dead weight, the flow forces can initiate slope parallel sliding of the cover layer (Fig. 7). The sand-core is then defenseless against the following overtopping waves. Usually, the slope parallel sliding is signaled by fissures along the dike crest and a bulge at the inner toe (WEIBMANN 2003).



Figure 7: Slope parallel sliding.

With the hydrodynamic loads modeled by OTT-1d, the level of utilization for slope parallel sliding is calculated for different types of soil. They are categorized by WEIBMANN (2003), ranging from “less qualified” (Elisabethgroden 3.5) over “well qualified” (Elisabethgroden 9.0, Wustrow) up to “very well qualified” (Cäcilienroden I, II, Hohenkirchen (Fig. 8). Every type, except “Wustrow”, is clay. “Wustrow” is a marly soil. The safety against slope parallel sliding is given by the level of utilization $\alpha_s < 1$.

The “less qualified” soil is above that level, whereas the higher qualified soil is not. The resistance of the soil increases further with the grade of compression (Fig. 8).

The higher grade of compression results in a lower level of utilization, as there are less cavities and a lower level of saturation.

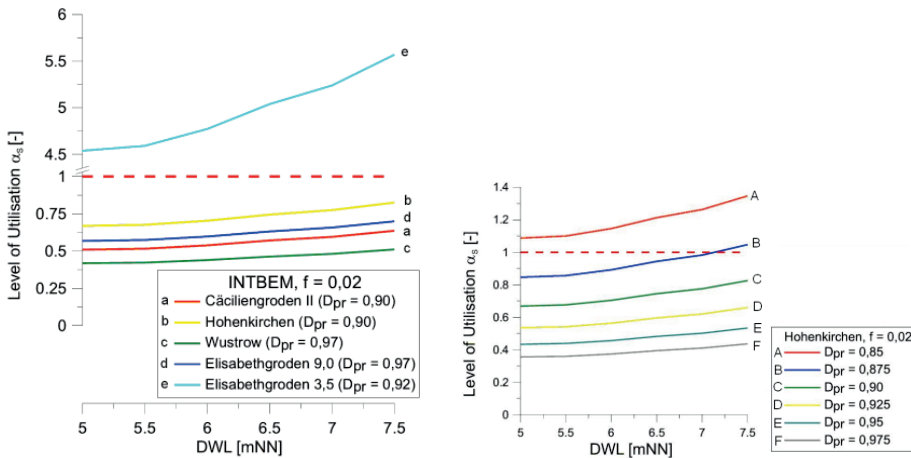


Figure 8: Safety against slope parallel sliding for different types of soil (RICHWIEN et al. 2010).

5 Potential for Compensation of Future Climate Change Impacts

The results of the research project highlight the fact that the clay covers of numerous dikes are capable of withstanding higher overtopping rates than presently assumed for their design levels. In order to quantify this enormous potential, the effect on the increase of an acceptable design water level in dependence of the overtopping tolerance is documented for both an exposed coastal and an estuarine dike (Fig. 9 and 10).

For the investigated exposed coastal dike, an increase of the design water level of more than 50 cm would be acceptable for a tolerable overtopping rate of 10 l/(m·s) and of nearly 70 cm for a tolerable overtopping rate of 15 l/(m·s) (Fig. 9) without requiring any strengthening of the structure. These values are not only based on the tests with the applied mathematical models; they are still remarkably lower than maximum values of the site tests in Delfzijl, during which no damage to the dike took place.

A similar result was achieved through the model tests for an estuarine dike with smaller wave attack (Fig. 10): An assumed tolerable overtopping rate of 10 l/(m·s) would allow an increase of the design water level of more than 50 cm and of more than 60 cm for an overtopping rate of 15 l/(m·s).

These examples highlight the benefits which are achievable through the application of an integrated design of coastal and estuarine dikes. Prerequisite for a reliable integrated design will be sufficient information about the relevant soil parameters of the clay covers implemented in the dikes. In relation to the expected cost of strengthening such structures, the benefits of a campaign to evaluate the soil parameters required for an integrated design are expected to be very high.

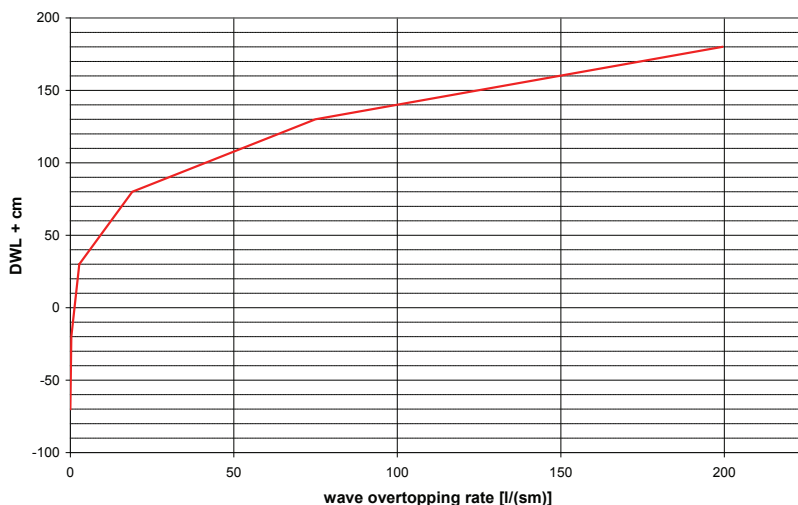


Figure 9: Cumulation of acceptable design water level increase in dependence of overtopping tolerance for an exposed coastal dike (NIEMEYER et al. 2010).

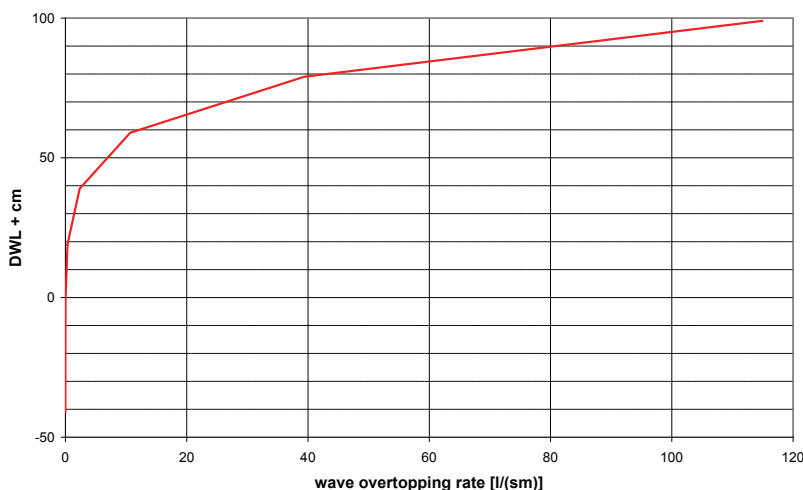


Figure 10: Cumulation of acceptable design water level increase in dependence of overtopping tolerance for an estuarine dike (NIEMEYER et al. 2010).

6 Summary and Conclusions

Aim of the project was the development of a new design concept for coastal and estuarine dikes. In addition to hydrodynamic loads, the detailed bathymetry in front of the dike and the quality of the implemented soil material will be considered quantitatively for the design. Thus, dikes can be dimensioned with improved safety and in a more economical

way. Safety reserves or safety deficits of existing dikes can be detected and quantified in order to highlight priorities for necessary reinforcements.

For the evaluation of the hydrodynamic loads, the mathematical model OTT-1d by HR Wallingford has been modified with respect to large scale conditions. The model considers the detailed geometry which allows the calculation of layer thickness, flow velocity, wave run-up and wave overtopping at every position of the structure. The hydrodynamic loads result in soil mechanical processes like erosion and infiltration. Because of this consistent wetting, the soil softens and its strength is reduced. The Inner slope is saturated with overtopping water and, in combination with the soil dead weight, the flow forces can initiate slope parallel sliding of the cover layer, which leaves the sand-core defenceless against the following overtopping waves. The overall resistance of the dike body is given by the level of utilisation for the loading cases for different types of soil.

There is an enormous potential for additional safety of coastal and estuarine dikes with respect to acceptable overtopping rates. The currently applied design procedures with their very conservative low overtopping tolerances require higher dikes than necessary. The research of the project should be intensified in the near future in order to establish new design procedures. Future results could lead to immediate and cost-saving countermeasures to counteract the effects of the accelerating rise in sea-levels.

7 Acknowledgements

The work presented here is part of the research project “Integrated Design of Sea- and Estuarine Dikes” (INTBEM) within the framework of the programme of the German Coastal Engineering Research Council (KFKI) and funded by the German Federal Ministry of Education and Research (BMBF) – project code: 03 KIS 061/062. We would like to thank our project partners Werner Richwien, Carsten Pohl and Lars Vavrina of the Institute of Soil Mechanics and Foundation Engineering of the University of Duisburg-Essen, and our colleagues from the Coastal Research Station (NLWKN), Ralf Kaiser and Markus Witting, for their support, inspiration and cooperation.

8 References

- BERKENBRINK, C.; KAISER, R. and NIEMEYER, H.D.: Prototype Overtopping Measurements and Model Verification. In: Proc. 31st Int. Conf. o. Coast. Eng. MC KEE SMITH, J. (Ed.), Bd. 4, Hamburg, 3009-3019, 2009.
- BERKENBRINK, C.; KAISER, R. and NIEMEYER, H.D.: Mathematische Modellierung hydrodynamischer Bealastungen von Deichen. Die Küste, Heft 77, KFKI (Ed.), Boyens & Co. KG, Heide i. Holstein, 2010.
- DODD, N.; GIARRUSSO, C.C. and NAKAMURA, S.: ANEMONE: OTT-1d – A User Manual. Report TR 50 - HR Wallingford, 1998.
- LÜDERS, K. and LEIS, G.: Niedersächsisches Deichgesetz – Kommentar. In: Wasser und Boden, Hamburg, 1964.
- NIEMEYER, H.D.: The Estimation of Design Wave Run-up on Sea Dykes in Consideration of Overtopping Security. Proc. 17th IAHR-Congress, Baden-Baden, 1977.
- NIEMEYER, H.D.; GÄRTNER, J.; KAISER, R.; PETERS, K.-H. and SCHNEIDER, O.: Estimation of Design Wave Run-up on Sea Dykes under Consideration of Overtopping

- Security by Using Benchmarks of Flotsam. In: Proc. 4th Conf. Coast. & Port Eng. i. Develop. Countr., Rio de Janeiro/Brazil, 1995.
- NIEMEYER, H.D. and KAISER, R.: Design Wave Evaluation for Coastal Protection Structures in the Wadden Sea. In: Proc. 4th Int. Symp. Ocean Wave Meas. & Analysis 2001. San Francisco. ASCE, Reston/Va., USA, 2001.
- NIEMEYER, H.D.; KAISER, R. and BERKENBRINK, C.: Increased Overtopping Security: A Potential for Compensating Future Impacts of Climate Change. In: Proc. 32nd Int. Conf. Coast. Eng. Shanghai/China 2010 (www.journals.tdl.org/icce/index.php/icce/issue/view/154/showToc).
- RICHWIEN, W.; POHL, C. and VAVRINA, L.: Bemessung von Deichen gegen Einwirkungen aus Sturmfluten. Die Küste, Heft 77, KFKI (Ed.), Boyens & Co. KG, Heide i. Holstein, 2010.
- RIS, R.; HOLTHUIJSEN, L.H. and BOOIJ, N.: A Spectral Model for Water Waves in the Nearshore Zone. In: Proc. 24th Int. Conf. Coast. Eng. Kobe/Japan. ASCE, New York, 1995.
- VAN GENT, M.: Wave run-up and Overtopping for Double Peaked Wave Energy Spectra. WL|Delft Hydraulics Report H 3351, 1999.
- VAN DER MEER, J.W.; STEENDAM, G.J.; DE RAAT, G. and BERNARDINI, P.: Further Developments on the Wave Overtopping Simulator. In: Proc. 31st Int. Conf. o. Coast. Eng., MCKEE SMITH, J. (Ed.). Bd. 4. Hamburg, 2957–2696, 2009.
- WEIBMANN, R.: Die Widerstandsfähigkeit von Seedeichbinnenböschungen gegenüber ablaufendem Wasser, Universität Duisburg-Essen, In: Mitteilungen aus dem Fachgebiet für Grundbau und Bodenmechanik, Heft 30, Glückauf Verlag, Essen, 2003.

XtremRisk – Integrated Flood Risk Analysis for Extreme Storm Surges at Open Coasts and in Estuaries: Key Results and Lessons Learned

H. Oumeraci, A. Kortenhans, A. Burzel, M. Naulin, D.R. Dassanayake, J. Jensen, T. Wabl, C. Mudersbach, G. Gönnert, S. Thumm, B. Gerkensteiner, P. Fröble, K.-F. Daemrich, E. Pasche and G. Ujeyl

Summary

A brief overview of the joint research project XtremRisk is given. The project has been focusing on developing/improving/expanding the knowledge, methods and models with respect to (i) physically possible extreme storm surge for current conditions and scenarios for climate change, (ii) failure mechanisms of flood defences, (iii) assessment of intangible losses (social and ecological) and their integration with direct/indirect economic losses, (iv) reliability analysis of flood defence systems and (v) SPR-based integrated flood risk analysis involving both tangible and intangible losses and its implementation for two selected pilot sites (representative for an open coast and an urban estuarine area in Germany). The key results are briefly summarised and the lessons learned for future flood risk studies are finally drawn.

Keywords

integrated risk analysis, SPR-Concept, extreme storm surge, flood defense structures and systems, reliability analysis, dike breach modelling, intangible and tangible flood losses, GIS-based spatial modelling

Zusammenfassung

Das Verbundprojekt XtremRisk wird zunächst kurz beschrieben. Schwerpunkte des Forschungsvorhabens waren die Entwicklung, Verbesserung und Erweiterung von Grundlagen, Methoden und Modellen hinsichtlich folgender Aspekte: (i) Physikalisch mögliche extreme Sturmfluten für verschiedene heutige und künftige Klimaszenarien, (ii) Versagensformen und -mechanismen von Hochwasserschutzwerken, (iii) Evaluation der intangiblen Flutschäden (soziale und Umweltschäden) sowie deren Aggregation mit direkten und indirekten Schäden in eine integrierten Risikoanalyse, (iv) Zuverlässigkeitsanalyse von Hochwasserschutzsystemen, (v) Implementierung der integrierten Risikoanalyse unter Berücksichtigung der tangiblen und intangiblen Schäden auf der Grundlage des bewährten SPR-Konzeptes (Source-Pathway-Receptor) am Beispiel von zwei ausgewählten Standorten an der deutschen Nordseeküste: Sylt repräsentativ für eine offenen Küste und Hamburg für ein urbanes Ästuar-Gebiet. Der Beitrag fokussiert lediglich auf einige Schlüsselergebnisse und die wichtigsten Lehren für künftige Forschungsvorhaben.

Schlagwörter

Integrierte Risikoanalyse, SPR-Konzept, extreme Sturmflut, Hochwasserschutzwerke und -systeme, Deichbruchmodellierung, Zuverlässigkeitsanalyse, intangible and tangible Flutschäden, GIS-basierte räumliche Modellierung

Contents

1	Introduction	504
2	Brief overview of overall project	505
2.1	Subproject 1 – Extreme storm surges	506
2.2	Subproject 2 – Reliability analysis and breach modelling of flood defences	507
2.3	Subproject 3 – Damage assessment/evaluation	507
2.4	Subproject 4 – Risk analysis/ risk evaluation	507
3	Key results and lessons learned	508
3.1	Risk sources	508
3.1.1	Key results	508
3.1.2	Lessons learned	510
3.2	Risk pathways	511
3.2.1	Key results	511
3.2.2	Lessons learned	512
3.3	Risk receptors	515
3.3.1	Key results	515
3.3.2	Lessons learned	517
3.4	Integrated risk assessment	518
4	Concluding Remarks	520
5	Acknowledgements	521
6	References	521

1 Introduction

Given the large uncertainties of the impact of climate changes on physically possible extreme storm surges and further unfavourable combinations of the loading conditions, as well as of the potential subsequent damages to be expected in the 21st century at open coasts and estuaries, it is obvious that an integrated reliability and risk analysis based on the Source-Pathway-Receptor (SPR) concept (OUMERACI 2004) represents the most appropriate approach to address this problem. Among the main obstacles for the practical implementation of such an approach are the remaining gaps of knowledge following the completion of the EU-FLOODsite project (KORTENHAUS and OUMERACI 2008), especially those associated with extreme storm surges, the failure mechanisms of flood defences, the intangible flood losses and their integration with tangible losses in a risk analysis.

With this background, the four -year project “XtremRisK”, funded by the German Federal Ministry of Education and Research (BMBF), was initiated in October 2008. It brought together three partners from different German universities (TU Braunschweig, fwu Siegen, TU Hamburg-Harburg, hereafter LWI, fwu and TUHH) and one partner from the Agency of Roads, Bridges and Water in Hamburg (LSBG) as well as the end-users of the prospective results for Hamburg (LSBG and HPA) and the Island of Sylt (Schleswig-Holstein Agency for Coastal Defence, National Park and Marine Conservation LKN) as cooperative partners.

After a very brief overview of the project and a brief summary of the key results, the lessons learned for future flood risk studies are finally drawn, also including recommendations for future priority R&D topics.

2 Brief overview of overall project

The XtremRisK project follows the SPR-based integrated risk analysis and management approach proposed by OUMERACI (2004) and FLOODsite (www.floodsite.net), but differs from previous similar flood risk projects in the sense that (i) it was intended to particularly focus on the extreme storm surge events which are physically possible at the present time and at the end of this century, (ii) it is based on a detailed modelling and reliability analysis of the failure of entire flood defence systems, including both man-made and natural barriers, (iii) the assessment of the tangible flood damages includes both direct and indirect losses, (iv) the assessment of the intangible losses includes both social losses (loss of life, cultural losses) and environmental losses, (v) both tangible and intangible losses are consistently considered and integrated to assess the overall flood losses in the risk analysis, including a consistent framework and methodology for admissible flood risks.

Two pilot sites, for which most of the required data already existed, were selected for the application of the developed methodologies, modelling tools and techniques, and, ultimately, for the practical implementation of the integrated risk analysis: for Hamburg, as a representative urban area in an estuary, and for the Island of Sylt, representative for an open coast.

The structure of the overall project (led by LWI) in four subprojects (SP1-SP4) follows the SPR-concept (Fig. 1) as they respectively address risk sources (SP1), risk pathways (SP2), risk receptors (SP3) and their integration in a risk analysis (SP4).

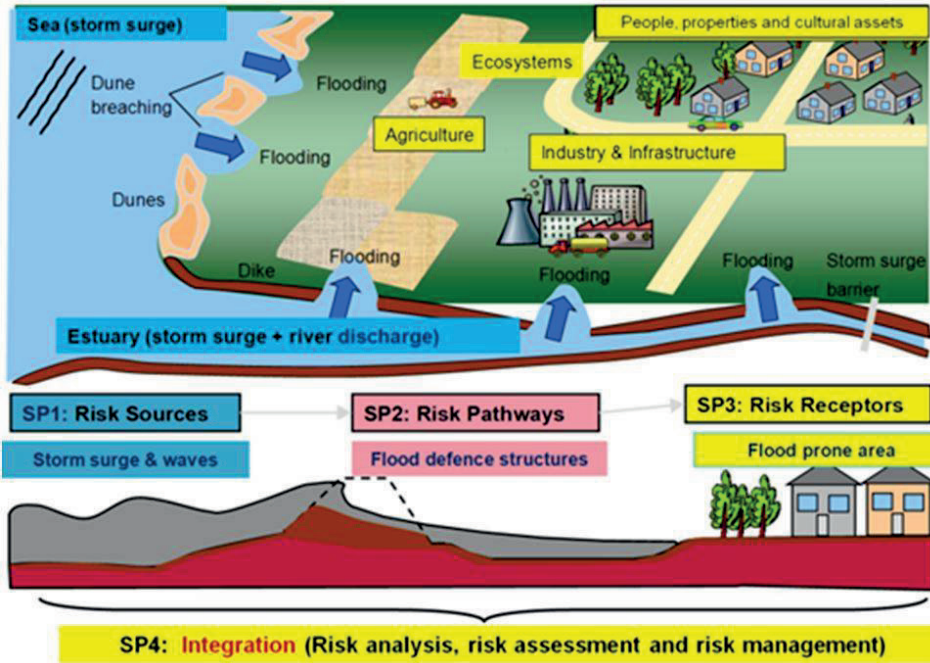


Figure 1: “Source-Pathway-Receptor” concept (SPR) and Subprojects (SP) in XtremRisk.

2.1 Subproject 1 – Extreme storm surges

Subproject 1 – Extreme storm surges (risk sources) is divided in SP1a, led by LSBG, and SP1b, led by fwu.

SP1a aims at the development of scenarios of the largest physically possible extreme storm surges for the selected pilot sites based on the analysis of field data (e.g. tidal gauge Cuxhaven) and numerical modelling by analysing all storm surge constituents (e.g. wind surge, tide and external surge) and their non-linear interactions as compared to their linear superposition (see Fig. 4).

SP1b aims at the determination of the exceedance probabilities of the extreme storm surge scenarios provided by SP1a. This is achieved through the development of a storm surge generator capable of reproducing entire parameterised storm surge curves combined with a multivariate statistical analysis of extreme storm surge water levels (field data and synthetic data obtained from storm surge generator). Joint probabilities of both peak values $h_{w,max}$ and fullness F of the extreme storm surge are determined using a bivariate Copula approach. A trivariate approach is required to also consider significant wave height H_s . The obtained joint probabilities are delivered to SP2 for the reliability analyses of the flood defences (risk pathways).

2.2 Subproject 2 – Reliability analysis and breach modelling of flood defences

Subproject 2 – Reliability analysis and breach modelling of flood defences (risk pathways) is led by LWI.

Based on the extreme storm surge scenarios developed in SP1, subproject 2 aims at the determination of the loading and the reliability analysis of all components of the flood defence systems for the two selected pilot sites. This will also comprise the full failure of these components, including breaching and breach development.

The ultimate goal will be the determination of a failure probability of the flood protection systems (and thus the flooding probability $P_{f,cond}$), which represents the first component of flood risk (defined in this project as the product of probability $P_{f,cond}$ and related consequences D). Moreover, the initial conditions at the breach location for the inundation modelling will also be determined, including the breach development and the final breach width and depth.

The results are delivered to SP3 for the numerical simulation of the flood inundation and the assessment of related damages in the two pilot sites.

2.3 Subproject 3 – Damage assessment/evaluation

Subproject 3 – Damage assessment and evaluation (risk receptors) is led by TUHH.

SP3 aims at the assessment of the direct and indirect economic losses in the two selected pilot sites. This is achieved through the combined application of numerical modelling for flood inundation, damage models for the assessment of direct damages to residential and commercial buildings, equipment and infrastructures, as well as an economic model for the indirect losses due to the disruption of economic and social activities as a consequence of the direct flood damages. The sole consideration of direct economic losses is, indeed, not sufficient in the case of extreme event related risks.

The direct damages are assessed at a micro scale level of one item (e.g. building) and extrapolated to a group of similar items at a meso-scale level. A cluster-based approach is used to aggregate the damages from the building level to the level of economic sectors in the entire pilot site considered, so that they can be implemented in an economic modelling framework at a macro-scale level.

The GIS-based direct and indirect economic damages are delivered to SP4 for the integration of all damage categories in a risk analysis.

2.4 Subproject 4 – Risk analysis/ risk evaluation

Subproject 4 – Risk analysis, risk evaluation and recommendations for risk mitigation (integration) is led by LWI.

SP4 primarily aims at bringing together all results from SP1–SP3 into an integrated flood risk analysis (see Fig. 1 and OUMERACI 2004) for the two pilot sites by considering the selected storm surge scenarios determined in SP1 for present (2010) and future climate conditions (2100). For this purpose, however, a proper methodology for the assessment of intangible losses (social, cultural and environmental losses), their GIS-based spatial modelling and their integration with the economic losses obtained from SP3 into

integrated risk maps is required. Therefore, a consistent GIS-approach (Cellbased Risk Assessment (CRA)) for the spatial modelling of risk needs to be developed. The CRA approach is also applied for the modelling of direct and indirect economic damages resulting from SP3, for the GIS-based mapping of the risk related to each damage category, and finally for the integration of all risk categories in an integrated risk map for the two pilot sites.

Moreover, the predicted flood risks for both conditions are evaluated based on tolerable risks estimated for each damage category in close collaboration with the prospective end-users of the results in the study areas. Finally, structural and non-structural mitigation measures are proposed to reduce predicted flood risks to a tolerable level.

The detailed analysis of the selected most appropriate mitigation measures in terms of technical and economic feasibility will possibly be conducted in a follow-up project, depending on the final outcome of discussions with the decision makers responsible for flood risk management at the two pilot sites.

3 Key results and lessons learned

3.1 Risk sources

3.1.1 Key results

A new approach combining empirical methods and numerical modelling to analyse the non-linear interaction between the storm surge constituents and to determine extreme storm surge scenarios has been developed and implemented for the study areas, including three main steps: (i) analysis of the highest event of each constituent and (ii) analysis of the interaction between tide and wind surge and the interaction between wind surge and external surge to (iii) calculate an extreme storm surge event based on the result of these analyses (GÖNNERT et al. 2012). Lower water levels are obtained by considering the non-linear effects between the storm surge constituents than those resulting from a linear superposition of constituents. This conclusion is, however, valid only for the data which have so far been analysed at the tidal gauge of Cuxhaven (continuous time series for more than 100 years). Moreover, the implementation of the proposed approach to the data of the tidal gauges in Hörnum (Sylt) has shown that it is also applicable to other areas (GÖNNERT et al. 2012). In order to better understand the relative contribution of the nonlinear effects and to check the validity of these important results, a PhD research programme for the implementation of a hybrid approach using hydrodynamic modelling and artificial neural networks was initiated, which is now nearing completion (see TAYEL and OUMERACI 2014).

A powerful and computationally efficient stochastic storm surge generator (SSSG) and an advanced Copula-based multivariate statistical analysis of extreme storm surge events (CMSA) have been developed and implemented for the two pilot sites.

The SSSG is capable to stochastically simulate a large number of storm surge scenarios (in the order of 107). It is based (i) on the observed storm surge water levels from the tidal gauges of Cuxhaven (Elbe estuary) and Hörnum (Sylt Island) which have been parameterised by means of 19 sea level parameters and 6 time parameters, (ii) the fitted parametric distribution functions to the data sets resulting from the parameterisation, (iii) the

consideration of parameter interdependencies and the application of empirical filter functions to avoid inconsistencies and (iv) Monte-Carlo-Simulations (MCS) using the fitted parametric distributions and different filter functions are applied. The capabilities of the SSG have been demonstrated by comparing synthetically generated storm surge curves (time series with a 1-minute resolution) with those obtained from observed data, from hydrodynamic models and from empirical analyses. More details are given in WAHL et al. (2011) and WAHL et al. (2012a, b).

In contrast to most of the previous studies where only the highest peak water level $h_{w,max}$ (S in Fig. 2) is considered to be the sole parameter to statistically represent the storm surge event, the CMSA in its bivariate version additionally considers the “fullness” F (Fig. 2) of the entire storm surge curve.

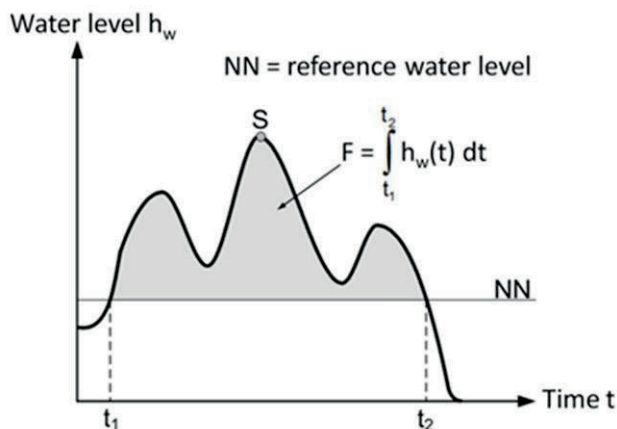


Figure 2: Storm surge curve with highest peak value S and “fullness” F (definition sketch) (modified from WAHL et al. 2011).

The “fullness” F may indeed be as crucial as $h_{w,max}$ for the stability of flood defences and flooding probability as it implicitly describes the residence time of the water levels from the reference water level NN to the maximum level $h_{w,max}$ (S). Therefore, the proposed CSMA and the obtained joint probabilities of $h_{w,max}$ and F as shown in Fig. 3 represent a significant advance in reliability and risk analysis.

By using a fully nested Archimedean Copula approach, the bivariate model is extended to a trivariate model which additionally accounts for the significant wave height H_s as one of the most important wave parameters.

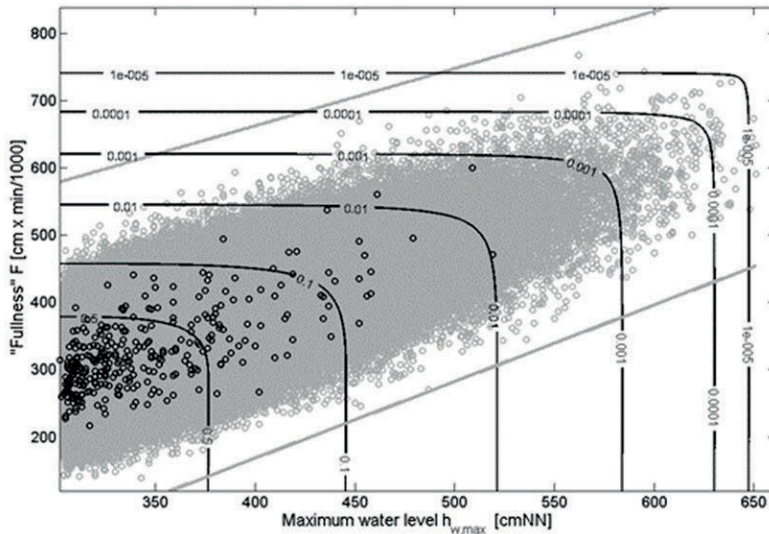


Figure 3: Joint probability of maximum water level and full-ness F (WAHL et al. 2011).

3.1.2 Lessons learned

Many of the conventional bivariate approaches available suffer from restrictions and constraints regarding the underlying data sets in terms of dependence or marginal distributions. Unlike the conventional models, Copula-based approaches are more flexible and able to handle dependent parameters with mixed marginal distributions.

Therefore, the proposed CSMA can be extended to account for further storm surge wave parameters. Moreover, Copula functions represent a promising alternative to address further classes of multivariate problems. The major issue, however, remains the considerable uncertainties associated with higher dimensional Copula-based models.

The attempt made in this study by considering only two sources of uncertainties, namely the Copula parameter θ and the stochastically generated synthetic storm surge data by using filter functions, has shown that the latter source is much more crucial and that the uncertainties can only be reduced through an improved physical understanding of the relative contributions of the storm surge constituents and their non-linear interactions (Fig. 4), the underlying formative factors, including their variability range and their limits compatible with the physical laws.

For this purpose, a consistent modelling strategy with proper models and proper uncertainty analyses will be required to predict the effects of climate/ geophysical/ morphological inter-decadal changes on the joint probability distributions of storm surge water levels and waves, including joint design extremes. A first step in this direction has been made by TAYEL and OUMERACI (2014) with the implementation of a combined 2D-hydrodynamic model and recurrent artificial neural network (ANN) to improve the understanding of the non-linear interaction between the storm surge constituents in the German Bight as illustrated by Fig. 4. The results are very encouraging, as they show that the developed hybrid modelling approach is efficient in the sense of its capabilities to

capture the overall relative contribution of the non-linear interaction between the storm surge constituents as compared to their linear superposition – and, thus, to predict extreme storm surges. As found by GÖNNERT et al. (2012) linear superposition generally results in higher water levels, but under certain circumstances which are still not fully clarified, the nonlinear effects may result in higher water levels (TAYEL and OUMERACI 2014).

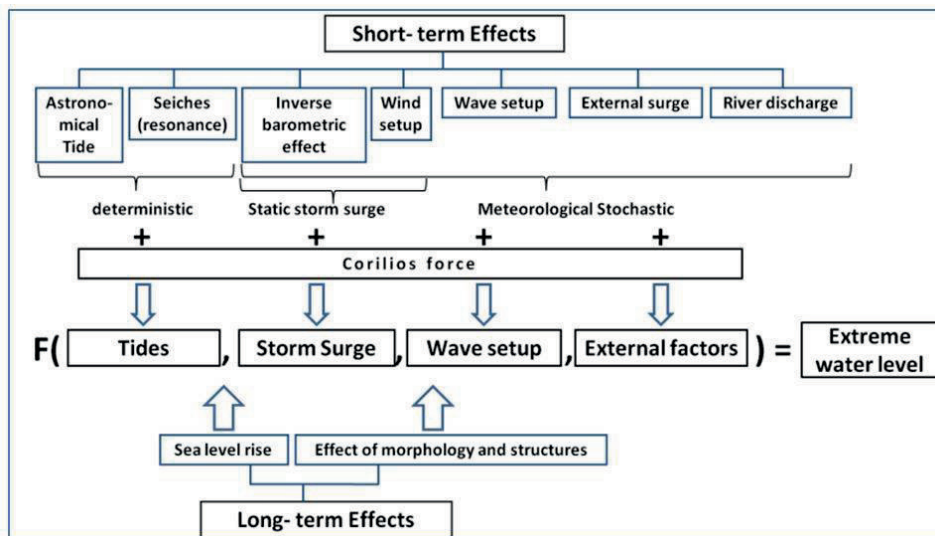


Figure 4: Storm surge constituents and their non-linear interactions (TAYEL and OUMERACI 2012).

3.2 Risk pathways

3.2.1 Key results

Based on the knowledge and modelling tools developed in previous projects such as FLOODsite (www.floodsite.net) and further improved/extended in XtremRisK, a reliability analysis of the linear flood defences such as sea dikes, coastal dunes and flood walls is performed for the two pilot sites. As a result, a probability of flooding P_f is obtained for the different extreme storm surge scenarios provided by SP1. This also includes (i) breach modelling for sea dikes by using the models developed by TUAN and OUMERACI (2010, 2011) and STANCZAK and OUMERACI (2012) for a dike breach initiated respectively by wave overtopping/overflow on the inner dike slope and by breaking wave impact on the outer slope and (ii) dune erosion and breaching by using the “X-Beach” code.

As the defence lines in the pilot sites consist of different types of structures which are commonly non-homogeneous along their entire length, a segmentation was performed into approx. 300 homogeneous sections in terms of both loading and resistance properties. For each section, about 80 parameters were required for the 35 limit state equations (22 LSE for dikes, 8 LSE for flood walls and 5 LSE for dunes) used to perform

the reliability analysis. Most of the LSEs considered were taken from the previous studies, including some modifications and further developments in this project.

Beside the commonly applied limit state equations for dune erosion, additional limit state equations for cross-shore profile response of dunes due to wave impact and overwash by applying available analytical models are also included. Moreover, the common approach for the LSE, which compares the admissible wave overtopping/overflow rate q_{adm} with the actual wave overtopping/overflow rate q has been modified to, instead, consider the admissible volume V_{adm} and actual volume V (Equation 1)

$$V = \sum_{i=1}^{n,m} V_i = \sum_{i=1}^{n,m} q_i \cdot t_i \cdot l_i \quad (1)$$

with: t_i = time [s]; l_i = length of flood defence section [m]; n = number of time steps [-]; m = number of sections [-]. The consideration of time-dependent volumes has substantial advantages, as it represents a better approximation of the time-dependent process (unsteady conditions) and related failure mechanisms over the entire storm surge time history. Moreover, the storage capacity of the hinterland is taken into account in contrast to the common approach based on overtopping discharges. In fact, exceedance of the critical overtopping discharge might occur for a short period at the peak of the storm surge, but should not necessarily result in flooding. More details are given in NAULIN et al. (2012a, b). Due to the deficiencies of the available state of the physical knowledge, which is still very limited regarding the time dependency of the failure modes and their spatial correlation along the entire defence line, the reliability analysis could not fully consider the effect of time and the so-called “length effect”, i.e. the failure modes were considered more or less separately for each section of the segmented defence line. Despite these simplifications, and though only conventional fault tree analyses have been performed without taking into account (i) the *duration* of the failure mechanisms as well as their *time sequencing* and *actual links* and (ii) the failure modes, which are hardly amenable to common limit state equations (e.g. failures of moveable barriers due to human and organisation errors), the results have clearly revealed the relative contributions of each failure mode to the probability of the top event (flooding), and, thus, have also provided valuable indications on the priority issues which need more elaboration and more R & D efforts. Traditional hierarchical reliability models such as fault/event trees and reliability block diagrams are neither capable of capturing the causality of failures, nor their interactions in time and space (ZIO 2009). For this purpose, new agent based modelling approaches are emerging which are capable of using the existing knowledge and models on the environmental loads and material properties to identify and model potential failures and their mutual interactions, including cascading effects (MACAL and NORTH 2010).

3.2.2 Lessons learned

In spite of the aforementioned and further simplifications required to make the reliability analysis practically feasible for entire flood defence systems, the obtained failure probabilities of the flood defence components/sections and the related conventional fault trees substantially contribute to identifying the weak links and to prioritising the issues being candidates for further detailed investigations. This also applies to risk mitigation for related possible structural countermeasures. Moreover, it was found that the performance of

an entire defence system is much too complex to be addressed efficiently by current modelling approaches and by conventional reliability/fault tree analyses. This complexity is significantly increased by the high degree of temporal and spatial variability of the load and resistance parameters affecting the failure modes, as well as by their interaction for a single defence component and for an entire flood defence system.

Therefore, an *appropriate modelling approach* is needed which is capable of coping with the complex failure mechanisms in time and space, including all interactions between the components of the defence system and the integration of the expected damages directly caused by the flood propagation. Such a modelling approach might be obtained by coupling system dynamic models to cope with the time dependent processes and GIS-based approaches to cope with spatial modelling. Such an approach will also enable the simulation of the performance of the entire defence system over the intended design life time, and, thus, to also explicitly account for the long-term change of the failure probabilities which would necessarily result from the long-term changes in load and resistance parameters. This issue is particularly crucial for probability discounting, as optimisation can only be achieved by considering life-cycle costs.

Time-dependent reliability analysis: A structured approach to define statistical models for time-dependent processes of flood defences and a sophisticated modelling framework including hierarchical and stochastic process models have been proposed by BUIJS et al. (2009). This is indeed a very promising approach which may provide new insights into the time-dependent behaviour of flood defence structures, especially for failures associated with deterioration processes. However, the scientific knowledge available yet on the physical processes underlying time dependent failure mechanisms and their mutual interactions over time is still too poor to efficiently apply this or any other sophisticated time dependent reliability approach on realistic flood defence components and systems in engineering practice. Reliance upon sophisticated modelling approaches without sufficient knowledge on the underlying physical processes, deterioration mechanisms and other time dependent failure modes and their interaction might indeed represent an *additional hazard* which may substantially contribute to increase flood damages and losses. The practical implementation of modelling approaches enabling, for instance, the development of time-dependent fragility curves and their embedment in the reliability analysis of an entire flood defence system needs to proceed with the results of basic research on the most relevant underlying physical processes. Iterative refinements, based on these results and upon sensitivity analysis of the entire system, to each of these processes will also be required.

In a longer term, an improved understanding of the interactions between the diverse failure modes, the temporal and spatial correlation between the sections along a defence line and between the different components of the entire defence system is needed to overcome the drawbacks of conventional fault tree analysis. The latter is rather based on engineering judgment and therefore subjective, as the outcome is strongly dependent on the expertise and skills of the analyst. Moreover, advanced fault trees or other alternative tools will be needed to account for the time duration, the time sequencing and the actual links in space and time of the failure mechanisms within and along each defence component, as well as within entire flood defence systems. These will significantly help moving the conventional analysis from art to science, from a fragile and very sensitive tool to a more robust and widely affordable approach for practitioners. In this respect,

the feasibility of integrated system dynamic models and GIS-approaches to develop a modelling framework capable of coping with space and time dependent processes and interactions needs to be examined.

Moreover, time-dependent fault trees or other alternative integrating tools must also include failure modes which are not or hardly amenable to common limit state equations (e.g. failures of moveable barriers due to human and organisational errors). For this purpose, a “quantification” of the failure probability by elicitation of expert opinions and/ or simulations may considerably improve confidence. Particularly in cases where the load and resistance parameters are time dependent and where the time duration of the failure mechanisms, as well as their time sequencing and links, are important, the final outcome of a conventional fault tree may be largely on the unsafe side.

Spatial variability and length effects. The different failures mechanisms are commonly assessed by considering a representative cross section of each segment resulting from a segmentation of the entire defence line. It is, therefore, obvious that the probability of failure will increase with the length of the defence lines, due to the spatial variability of both load and resistance terms of the limit state equations, as well as to the fact that “a chain is as strong as its weakest link” (*length effect*). The higher the spatial variability (i.e. shorter auto-correlation distances) of the load (e.g. waves and water levels) and resistance parameters (e.g. soil parameters), the higher the length effect. The relative contribution of the resistance parameters (e.g. soil properties) to the length effect are generally much higher due to their larger heterogeneity along the defence line as compared to that of the load parameters, which are commonly characterized by much larger correlation distances. The multiple breaches, which occurred as a result of weak spots along the defence lines in New Orleans during hurricane Katrina, have shed more light on the importance of these issues. Moreover, the resistance-dominated failure mechanisms generally govern the length effect and failure probability of a single segment and of the entire defence line may differ by more than two orders of magnitude (VRIJLING et al. 2011). A consistent framework for the modelling of the continuous spatial variability of soil parameters using random field theory already exists and has gained distinct importance in recent years, as spatial variability of soils represents one of the main damage (failure) sources of built-up systems in civil engineering (VROUWENVELDER 2006). Discrete spatial variability (e.g. weak spots) can be incorporated into modelling by using conditional probability based on scenarios (VRIJLING et al. 2011).

The large uncertainties associated with the spatial variability of the resistance parameters along the defence lines (heterogeneity in terms of shear strength, hydraulic permeability and soil layer thickness, weak spots at transitions and those caused by burrowing animals, etc.) are not only inherent (aleatory), but also epistemic in the sense that they exist due to the lack of measurement/observation data and are continuously and discretely changing over time. They represent the main obstacles to plausibly account for the length effect in the reliability analysis of entire flood defence systems. Targeted aerial reconnaissance, using infra-red and further geophysical surveys, can be used as a first step in detecting possible weak spots. In the long term, a consistent and systematic monitoring strategy will be required.

It should be kept in mind, that the omission or improper consideration of the aforementioned aspects (time dependence and spatial variability of the failure mechanisms and their interaction, single point structures), which is common in the current reliability

analyses of flood defences, generally leads to lower predicted values of flooding probabilities, i.e. to results on the unsafe side.

3.3 Risk receptors

3.3.1 Key results

Substantial results were achieved in the development/implementation of new approaches for the assessment of both *tangible and intangible losses*, as well as for their aggregation in an integrated risk analysis.

Tangible losses: The main achievements are related to the development of new methods for the micro-scale assessment of direct economic damages (caused by the physical contact of assets with water) based on actual market prizes and for their aggregation at a meso-scale level, as well as for the assessment of indirect economic losses (caused by disruption of economic and social activities as a consequence of direct flood damages).

The focus is placed on residential buildings, as well as on commercial and industrial assets, but damages to infrastructure and agriculture are also considered. As a main input hydraulic parameter for damage calculation, the flood depth obtained from inundation modelling using MIKE21 is applied for the development of asset-based depth-damage functions (data obtained from building inspections, photos and floor plans of the buildings). Inundation modelling is based (i) on the storm surge scenarios provided by SP1 and (ii) on the overtopping/overflow volumes or the initial conditions resulting from dike breaches provided by SP2. The micro-scale approach is mainly based on damage assessment using the Flood Resilient Tool (FloReTo) for sample type buildings (e.g. for residential assets defined by the type of building, the occupancy of the ground floor and the wall construction) (UJEYL et al. 2011, 2012). The calculated damages and the inundation depths are brought together using GIS-based spatial modelling (see Section 4) using the “develop depth-damage”- functions. A comparative analysis with commonly used meso-scale approaches is also performed to underpin the benefit of the proposed approach (e.g. for deriving efficient risk mitigation measures).

Based on the results of a literature study, the Adaptive Regional Input-Output (ARIO) model proposed by HALLEGATTE (2008) was identified as the most appropriate approach for the assessment of the indirect economic losses which result from production interruption and service losses in the housing sector. Its implementation for the pilot site in Hamburg has shown how indirect losses are related to the direct damages. It was found that the former remain negligibly small (even negative) for direct losses below a certain level, but increase nonlinearly with direct losses following exceedance of this level. The latter indicates the existence of a threshold in the coping capacity of economic systems. For the pilot site in Hamburg, the threshold was found to be about 2.5 billion Euros (UJEYL and KOWALEWSKI 2012). The corresponding values obtained by HALLEGATTE (2008) for Louisiana are 50 billion and 200 billion U.S. \$, respectively (Fig. 5).

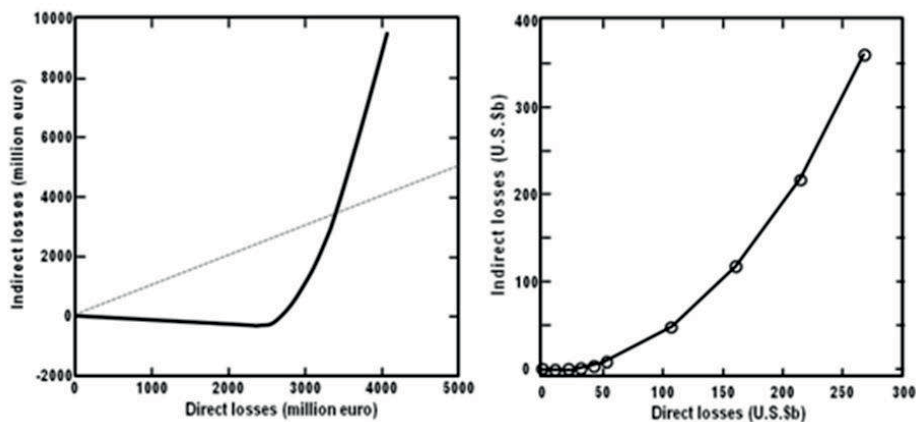


Figure 5: Indirect economic losses in terms of value-added losses vs. direct losses for Hamburg (UJEYL and KOWALEWSKI 2012, left) and for Louisiana (HALLEGATTE 2008, right).

Intangible Losses: The results of a comprehensive state of the art report (DASSANAYAKE and OUMERACI 2010) have revealed the gaps in the methodologies available (i) to assess the social losses (loss of life/injuries and cultural losses) and environmental losses incurred by floods and (ii) to integrate them with the tangible losses in a risk analysis. Moreover, the results have particularly contributed to identify the lack of appropriate methodologies for the evaluation of both cultural and environmental losses, as well as for their integration with other losses in risk analysis. Therefore, a systematic framework and methods for the assessment of intangible losses and their integration with tangible losses have been developed and implemented for the two pilot sites (DASSANAYAKE et al. 2012; BURZEL et al. 2012).

Within this framework, the model proposed by PENNING-ROWSELL et al. (2005) for the assessment of loss of life and human injuries caused by river floods is applied by taking into account both flow depth and velocity, as well as the characteristics of the population at risk (number, age, etc) and those of the flood-prone areas. Since this model has, as yet, been applied for river floods only, the model proposed by JONKMAN (2007) is also applied for comparison.

For the evaluation of cultural losses, however, a new methodology based on physical damages due to flooding and the cultural values of the assets is developed (DASSANAYAKE et al. 2011a). The estimation of direct physical damages to cultural assets is based on both flow depth and flow velocity. The cultural value of the different types of assets (heritage and non-heritages assets) is assessed by considering their historical (HS) and societal significance (SS). The results are then integrated into a cultural loss assessment matrix (CLAM) by using a five-point score scale, varying from very low (1) to very high (5). The spatial analysis of social losses was successfully performed in ArcGIS for the pilot site in Hamburg (BURZEL et al. 2012).

For the environmental losses, a two-step ecosystem services-based approach is proposed by making use of the classification of the ecosystem services developed by the Millennium Ecosystem Assessment in 2005, which is modified in the sense that supporting services are omitted so that only Provisioning Services, Regulating Services and Cultural Services are considered in order to avoid double-counting. The identification

of the ecosystems at risk and their services (1st step) is based on the analysis of CORINE land cover data and further available knowledge. The assessment of their changes (measured in percentage) induced by inundation (2nd step) is performed by considering flood depth, velocity and duration as well as salinity obtained from numerical modelling. The approach has already been implemented for the pilot site Sylt. Spatial modelling of the losses is performed based on the Cellbased Risk Assessment (CRA) approach (BURZEL and OUMERACI 2011).

Integration of tangible and intangible losses: As the different loss categories are measured in different units (economic losses in Euro, loss of life and injuries in number of people, cultural losses in a five-point score and environmental losses in a percentage) a consistent integration methodology had to be developed. This was developed within a GIS-based multi-criteria analysis (MCA) framework. The methodology is performed in 8 steps (1 - Problem definition, 2 - evaluation criteria, 3 - selection of spatial units and grid size, 4 - criteria evaluation, 5 - criterion weights, 6 - decision rules, 7 - ranking of alternatives, 8 - sensitivity analysis) and has the following objectives (i) integration of all tangible and intangible losses into a single score scale of 0 to 1, (ii) aggregation according to their relative significance and (iii) determination of the severity of the total flood loss within the study area as a final result in a score between 0 and 1, allocated to each GIS-grid cell. Among the several MCA approaches, multi-attribute utility theory (MAUT) is selected for step 6 and a pairwise comparison method for criterion weighting in step 5 (DASSANAYAKE et al. 2011b). This methodology has been implemented in the pilot sites and represents one of the most important achievements within the risk receptor part of the project (DASSANAYAKE et al. 2012; BURZEL et al. 2012).

3.3.2 Lessons learned

The results have shown that *the assessment of the direct economic losses* at a micro-scale level and their aggregation to a meso-scale, though requiring more data and efforts, is worthwhile, as compared to the common meso-scale assessment. Moreover, results have also clearly indicated (i) why the value of direct losses cannot represent a sufficient indicator for the severity of the losses and for decision making related to risk mitigation measures and (ii) why a consistent consideration of indirect economic losses and intangible losses, as well as their consistent aggregation, is crucial for the outcome of the integrated risk analysis. The results of *the indirect economic loss assessment* highlight the main difficulties in defining, measuring and predicting these costs as a function of the direct costs, and emphasize the need for a better understanding of the most important underlying economic mechanisms and market related processes in the recovery and reconstruction phase after an extreme flood event. This particularly includes abnormal solidarity and assistance at regional/national/international levels, as well as further governance/ political processes, which are not considered in the current assessments (HALLEGATTE 2008). Moreover, a better insight into the relationships between the mechanisms of the financial and business sectors and those of a natural disaster may help to better understand the underlying governing processes and the difficulties in assessing the impact of natural disasters based on macro-economic data.

Regarding *the intangible loss assessment*, beside the final results of the evaluation of the loss categories measured in different units and the severity of flood losses expressed in a

score scale between 0 and 1 for each GIS-grid cell, it would also be desirable to define all the losses on a monetary scale based on the life quality index (LQI). This is important for the decision -making process, based on a cost/benefit analysis (CBA), but also to improve CBA-based assessments of the benefits resulting from different options for risk mitigation measures. A first encouraging attempt in the direction of an LQI-based approach for the assessment of statistical value of life (VSL) is in progress (DASSANAYAKE and OUMERACI 2012).

For the *determination of criterion values and weights* within MCA, a structured procedure should be developed to also include the opinions of experts and of the affected citizens within the flood prone areas. The latter group is also particularly relevant in determining the relative importance of the different loss categories. The multiplicity of terms to characterize the diverse categories of losses caused by extreme events, as well as the diversity of assessment methodologies and underlying assumptions, not only reflect the confusion in the published literature, but also make the selection of an appropriate methodology and a meaningful comparison or aggregation of the published results extremely difficult. The selection of the adequate methodology and the proper degree of detail of the analysis primarily depends on the purpose of the loss assessment (insurance, risk mitigation measures, etc.). Moreover, the difficulties are significantly increased by the inherent multidimensionality of the impact of extreme events and their significant redistributive effects, as well as by the large uncertainties involved, which are rarely assessed. Therefore, a *harmonization within the risk analysis community*, possibly at transdisciplinary and transnational levels, is urgently needed. Such a harmonization is expected to significantly contribute to the evaluation of the very large uncertainties, which currently represents the most critical bottleneck in any integrated risk assessment. These uncertainties are primarily due to the lack of sufficient knowledge on the interaction between the socio-economic dynamics and the impact dynamics of natural disasters, but also to insufficient data and inconsistent assessment methodologies.

3.4 Integrated risk assessment

The overall project was completed at the end of 2012, including the integration of the results from subprojects 1-3 in the risk analysis for different extreme storm surge scenarios, the risk evaluation and subsequent recommendations for possible mitigation measures for the two pilot sites. Some of the results related to the developed integration methodology are summarised below.

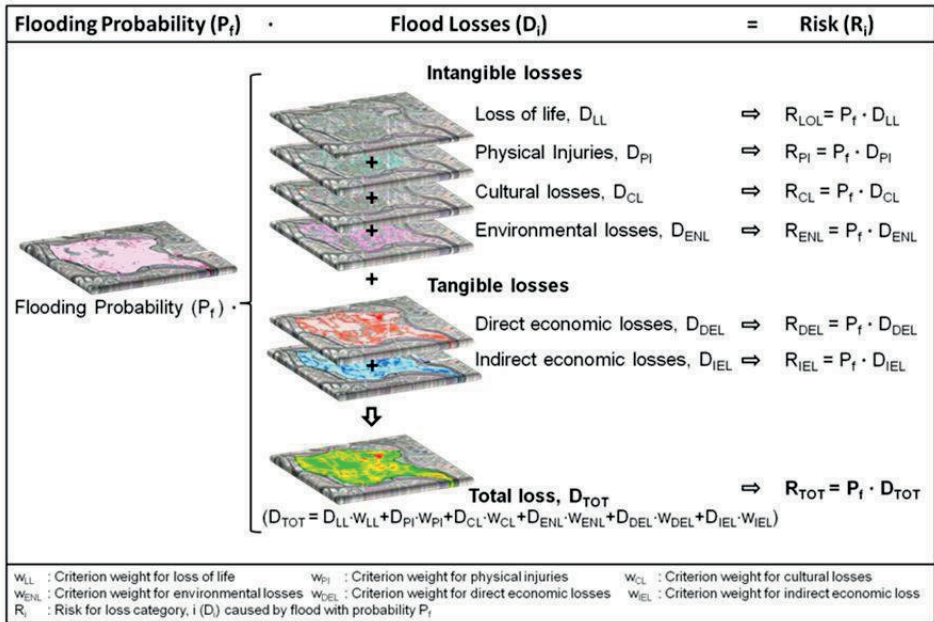


Figure 6: Risk related to the different categories of losses and their aggregation in the integrated risk analysis (modified from DASSANAYAKE et al. 2012a).

Cellbased Risk Assessment (CRA): A GIS-based approach has been developed as a flexible and robust framework for the spatial modelling of the different categories of flood losses, as well as for their aggregation in the integrated risk analysis. Due to the considerable spatial variability of the characteristics of both hazard and vulnerability in the flood prone areas of both selected pilot sites, the GIS raster concept, which has often been used in the past, is inadequate (e.g. only one attribute can be stored in one raster file). Therefore, a polygon-based concept for spatial risk analysis has been developed, which makes use of the advantages of both raster and polygon concepts. For the CRA based analysis, the flood prone area is subdivided into uniform polygons (cells) of a given size, which primarily depends on the size of the study area and the scale of the assessment. These cells form a uniform grid and are, therefore, termed as grid cells. Resolutions of 100 m, 50 m and 10 m have been applied in the pilot sites. Comprehensive geoprocessing workflows are developed in a modular structure using the Model Builder environment in ArcGIS, thus making the model highly flexible and adaptive to any study area and resolution.

The CRA is performed in three main steps: (i) conversion of all irregular shaped input data into the assigned compartment, (ii) application of the selected model to all cells within the investigation site, and (iii) visualisation of the results on a spatial basis. The CRA approach has successfully been applied for the modelling of tangible losses (direct and indirect economic damages) and intangible losses (loss of life and human injuries, cultural losses and environmental losses) for different scenarios as described in Section 3.3 above.

Integration of tangible/intangible losses and GIS-mapping: Using the MCA based approach developed by DASSANAYAKE et al. (2011b) (see Section 3.3 above) for the integration of the different losses, the CRA approach is applied to generate flood maps, maps for each

category of losses and for aggregated losses, as well as related risk maps, by combining flood maps and loss maps (Fig. 6). Particularly the risk maps for each loss category, together with the aggregated risk maps, which are obtained for different extreme storm surge scenarios, build the primary basis for the evaluation of the predicted risk as compared to tolerable risk, and finally for the recommendations of possible risk reduction measures for both considered pilot sites. For this purpose, a consistent and transparent framework, including the required methodology and tools to assess tolerable risks, is required.

4 Concluding Remarks

One of the key features of the XtremRisk project, which started 2008 and was completed at the end of 2012, is the level of detail which has been kept at the highest mark (practically feasible within the time frame of the project) for the analysis of the risk sources (e.g. effect of non-linear interaction of constituents on extreme storm surge), risk pathways (e.g. failures modes of flood defences and failure probabilities) and risk receptors (e.g. consideration of different categories of tangible and intangible flood damages) given the available knowledge/models and the available time/resources for further/new developments. Therefore, it is believed that this study represents one of the most process-based integrated risk analyses of coastal floods induced by storm surges with sample applications at two pilot sites, selected to represent an open coast and an urban estuarine area. This high level of detail was necessary in order to better identify not only the deficiencies of the current knowledge/models and the prioritization of further research, but also to find out where, how and to which degree simplifications over the entire risk analysis process are possible without losing sight of the essentials. Moreover, this study might also help to better assess the outcome of simplified or holistic approaches, such as those proposed in the joint HoRisk project (SCHÜTTRUMPF et al. 2012) and in the EU-THESEUS project (NARAYAN et al. 2013; ZANUTTIGH et al. 2013).

Beside closing the most relevant knowledge gaps which have been identified in the sections above, the ultimate challenge will be the simplification of the process, as much as reasonably practicable, i.e. without losing any important issue, so that the proposed integrated risk analysis methodologies and tools will be comprehensible and affordable by practitioners and further prospective decision makers (e.g. for the implementation of the EU flood directive). Making the best use of the outcome of the joint projects XtremRisk, HoRisk and THESEUS (ZANUTTIGH et al. 2013), it is intended to initiate a new R & D project in 2015 with the ultimate objective of developing a Living Decision Support System (LDSS) with a modular tiered structure for the three decision levels commonly encountered in engineering practice: the feasibility, preliminary and detailed levels. As a result, an integrated coastal flood risk assessment as a flexible and robust tool will be obtained, which can be used for risk-based design, safety assessment and monitoring/maintenance of flood defence systems, as well as for efficient flood risk management in coastal and estuarine areas. A particular focus will be placed on the damages to the so-called critical infrastructures in coastal areas. Such complex systems are generally designed to withstand events and threats such as storm surges and coastal flooding, which are predictable through existing modelling tools and in line with existing design standards for such conditions. However, for extreme low probability events, which are difficult to

predict, a 100 % protection is neither technically nor economically feasible, so that these events generally result in catastrophic damages and losses, if a consistent and robust set of countermeasures are not provided. The efficiency of the types of countermeasures depends on the degree of complexity of the system considered together with its components (sub-systems) and its nesting in larger systems at regional, national and international scales, but also on the type, magnitude and frequency of the extreme event, the type and importance of critical infrastructure, the type and relative importance of possible cascading effects, the categories and magnitudes of potential losses (economic, social and environmental) and the local risk culture (risk acceptance). Critical infrastructures nested in their environment are highly complex and non-linear systems in the sense that the collective behaviour of their constituents entails emergence of properties that can hardly, if not at all, be inferred from properties of the constituents. This has significant implications on the conceptual and theoretical framework for the generation of the knowledge base, the methodologies, the modelling approaches and further analysis tools/techniques to understand the basic functioning of complex systems aimed at minimising the risk in the case of unexpected extreme hazards. These, together with the outcome of the aforementioned completed and further related projects, will build the basis for the new 3-stage LDSS. Whether the LDSS will be developed within an Agent-Based Modelling (ABM) framework or within a more conventional framework is still to be clarified. In both cases, a synergetic transnational partnership and collaboration would be desirable.

5 Acknowledgements

The XtremRisK project was funded by the German Federal Ministry for Education and Research (BMBF) through the project management of Projektträger Jülich (Grant number No. 03F0483A). The support of the local authorities LSBG and HPA for the pilot site in Hamburg and LKN for the one in Sylt are also gratefully acknowledged.

6 References

- BUIJS, F.A.; HALL, J.W.; SAYERS, P.B. and VAN GELDER, P.H.A.J.M: Time-dependent reliability analysis of flood defences. In: Reliability Engineering and System Safety 94, 1942-1953, 2009.
- BURZEL, A. and OUMERACI, H.: Development of a Framework for the Spatial Modelling of Extreme Risks and the Consideration of Risk Acceptance: Progress Report. Leichtweiß-Institute, TU Braunschweig, 2011.
- BURZEL, A.; DASSANAYAKE, D.R. and OUMERACI, H.: Spatial Modelling of tangible and intangible Losses in Integrated Risk Analysis – Results of the XtremRisK Proc. 2nd European Conference on FLOODrisk Management, Rotterdam, 2012.
- DASSANAYAKE, D.R. and OUMERACI, H.: Framework and Methods for the Evaluation of Intangible Losses and their Integration in Coastal Flood Risk Analysis. State of the Art Report. Leichtweiß-Institute, TU Braunschweig, 80 p, 2010.
- DASSANAYAKE, D.R.; BURZEL, A.; KORTENHAUS, A. and OUMERACI, H.: Evaluation of cultural losses due to coastal floods. XtremRisK Progress Report. Leichtweiß-Institute, TU Braunschweig 38 p, 2011a.

- DASSANAYAKE, D.R.; BURZEL, A. and OUMERACI, H.: Integration of Tangible and Intangible Flood Losses: A GIS Based Multicriteria Analysis (MCA) Approach. XtremRisK Progress Report. Leichtweiß-Institute, TU Braunschweig, 40 p, 2011b.
- DASSANAYAKE, D.R.; BURZEL, A. and OUMERACI, H.: Intangible Flood Losses: Methodologies for their Evaluation and Integration in Flood Risk Analysis. Proc. 2nd European Conf. on FLOODrisk Management, Rotterdam, 2012a.
- DASSANAYAKE, D.R. and OUMERACI, H.: Value of statistical life based on life quality index. Progress Report. Leichtweiß-Institute, TU Braunschweig, 2012b.
- GÖNNERT, G. and SOSSIDI, K.: A new approach to calculate extreme storm surges: Analyzing the interaction of storm surge components. In: BENASSAI, G., BREBBIA, C.A. and RODRIGUEZ, G.R. (Eds.): Coastal Processes II. Southampton, pp.139-150, 2011.
- GÖNNERT, G.; THUMM, S. and GERKENSMEIER, B.: Empirical analyses of extreme storm surges – Results of the XtremRisK project. Proc. 2nd European Conf. on FLOODrisk Management, Rotterdam, 2012.
- GÖNNERT, G. and GERKENSMEIER, B.: A 2-method-concept to approach extreme storm surge events – Combination of deterministic empirical and numerical methods. Proc. 10th Intern. Conf. Hydroinformatics, Hamburg, Germany, 2012.
- HALLEGATTE, S.: An adaptive regional input-output model and its application to the assessment of the economic cost of Katrina. In: Risk Analysis, Vol. 25, No. 3, 779-799, 2008.
- KORTENHAUS, A. and OUMERACI, H.: Flood risk analysis and management in Europe – The way ahead. Proc. of the 31st Intern. Conf. Coast. Eng. (ICCE), ASCE, Hamburg, Germany, 2008.
- MACAL, C.M and NORTH, M.J: Tutorial on agent-based modelling and simulation Journal of Simulation 4, 151-162, 2010.
- NARAYAN, S. et al.: The SPR systems model as a conceptual foundation for rapid integrated risk appraisals: Lessons from Europe. In: Coastal Engineering 87, 15-31, 2014 (<http://dx.doi.org/10.1016/j.coastaleng.2013.10.021>).
- NAULIN, M.; KORTENHAUS, A. and OUMERACI, H.: Reliability Analysis and Breach Modelling of Flood Defences in an Integrated Risk Analysis – Results of the XtremRisK Project. Proc. 2nd European Conf. on FLOODrisk Management, Rotterdam, 2012.
- OUMERACI, H.: Sustainable coastal flood defences: Scientific and modelling challenges towards an integrated risk-based design concept. Proc. First IMA Intern. Conf. on Flood Risk assessment, University of Bath, UK, 9-24, 2004.
- PENNING-ROWSELL, E.C.; FLOYD, P.; RAMSBOTTOM, D. and SURENDRAN, S.: Estimating Injury and Loss of Life in Floods: A Deterministic Framework. Natural Hazards 36, 43-64, 2005.
- SCHÜTTRUMPF, H.; BACHMANN, D.; GIER, F.; GRIMM, C. and WÖFFLER, T.: Vulnerability and Risk Assessment of the coastal zone in a changing environment. 26th Umbrella Symposium for the Development of Joint Cooperation Ideas “Sustainable Urban Development” 2012, Haifa, Israel, 2012.
- TAYEL, M. and OUMERACI, H.: Prediction of extreme storm surge water levels using recurrent artificial neural networks. Proc. 10th Intern. Conf. Hydroinformatics, Hamburg, Germany, 2012.

- TAYEL, M. and OUMERACI, H.: A hybrid approach using hydrodynamic modelling and artificial neural networks for extreme storm surge prediction (submitted this issue), 2014.
- UJEYL, G. and KOWALEWSKI, J.: Estimating Direct and Indirect Damages from Storm Surges: The Case of Wilhelmsburg/Hamburg. Proc. 10th Intern. Conf. Hydroinformatics, Hamburg, Germany, 2012a.
- UJEYL, G.; FRÖHLE, P. and PASCHE, E.: Evaluating direct damages of residential and commercial assets on a micro scale – Results of the XtremRisK Project. Proc. 2nd European Conf. on FLOODrisk Management, Rotterdam, 2012b.
- VROUWENVELDER, A.C.W.M.: Spatial effects in reliability analysis of flood protection systems. IFED Forum 2006, Lake Louise, Canada, 2006.
- WAHL, T.; MUDERSBACH, C. and JENSEN, J.: Assessing the hydrodynamic boundary conditions for risk analyses in coastal areas: a stochastic storm surge model. Nat. Hazards Earth Syst. Sci., 11, 2925-2939, 2011.
- WAHL, T.; MUDERSBACH, C. and JENSEN, J.: Assessing the hydrodynamic boundary conditions for risk analyses in coastal areas. Nat. Hazards Earth Syst. Sci., 12, 495-510, 2012a.
- WAHL, T.; MUDERSBACH, C. and JENSEN, J.: Statistical assessment of storm surge scenarios within integrated risk analyses – Results of the XtremRisK project. Proc. 2nd European Conf. on FLOODrisk Management, Rotterdam, 2012b.
- ZANUTTIGH, B. et al.: THESEUS decision support system for coastal risk management, Coast. Eng. 2013 (<http://dx.doi.org/10.1016/j.coastaleng.2013.11.013>).
- ZIO, E.: Reliability engineering: Old problems and new challenges. In: Reliability Engineering and System Safety 94, 2, 125-141, 2009.

A Consistent Return Level Assessment Considering Present Day and Future Mean Sea Level Conditions

Arne Arns, Jürgen Jensen and Thomas Wahl

Summary

This paper presents the result from combining statistical and numerical models to assess return levels and return periods of extreme water levels under current and possible future mean sea level conditions. As water level records are limited in some parts of the study area, the proposed method is based on a numerical multi-decadal model hindcast of water levels for the whole of the North Sea. Predicted water levels from the hindcast are bias-corrected using the information from the available tide gauge records. These bias-corrected water levels are then used to calculate return water levels for the entire coastline of Schleswig-Holstein. Additionally, the impact of sea level rise on extreme water levels is investigated using the same numerical model and conducting a second hindcast that considers the same atmospheric forcing but adding +0.54 m to the MSL to explore the effects of SLR on storm surges in the investigation area. At most locations, the second model run leads to changes in the storm surge and return water levels that are significantly different from the changes in MSL alone.

Keywords

storm surges, numerical modelling, statistical assessment, sea level rise, return levels

Zusammenfassung

Dieser Beitrag zeigt die Kopplung statistischer und numerischer Modelle zur Ermittlung der Höhen und Häufigkeiten extremer Wasserstände. Die Untersuchungen erfolgten am Beispiel der Schleswig-Holsteinischen Nordseeküste. Da die zur Verfügung stehenden Wasserstandsaufzeichnungen in einigen lokalen Bereichen des Untersuchungsgebietes limitiert sind, wurden die benötigten Wasserstandsinformationen mit Hilfe eines hydrodynamisch-numerischen Modells generiert. Die modellgenerierten Wasserstände wurden mit den Wasserstandsinformationen an den vorhandenen Pegelstandorten Bias korrigiert. Die Bias korrigierten Modellwasserstände wurden anschließend für die statistische Ermittlung extremer Wasserstände entlang der gesamten Küstenlinie Schleswig-Holsteins verwendet. In einem weiteren Modelllauf wurde der Einfluss eines möglichen Meeresspiegelanstiegs von 0,54 m auf Extremwasserstände untersucht. In den meisten Bereichen zeigt dieses Szenario einen Anstieg in den Extremwasserständen, der signifikant über den Anstieg des mittleren Meeresspiegels hinaus geht.

Schlagwörter

Sturmfluten, numerische Modellierung, statistische Analysen, Meeresspiegelanstieg, Wiederkehrintervalle

Contents

1	Introduction	526
2	Data and study area	527
3	Return level assessment	529
4	Methods	529
4.1	Numerical model setup	529
4.2	Bias-correction.....	531
4.3	Validation	533
4.4	SLR run.....	533
5	Results.....	534
5.1	Present day return levels	534
5.2	Changes in return periods in the SLR scenario.....	534
6	Summary and discussion.....	536
7	References	537

1 Introduction

Storm surges are among the most hazardous geophysical risks in coastal regions and are often associated with significant losses of life and property (VON STORCH 2012). The North Sea, and the German coastline in particular, has a long history of severe storm surges. For example, a large storm occurred in the German Bight in 1962 and more than 300 people lost their lives (BÜTOW 1963; VON STORCH and WOTH 2006). It is thus essential that the flood risk is accurately evaluated and defences are upgraded where necessary (COLES and TAWN 2005; HAIGH et al. 2010a).

The design of coastal defences is often based on some form of statistical models (DIXON and TAWN 1994). These models are mostly based on extreme value statistics, a special discipline in probability theory that deals with rare events, such as coastal floods (COLES 2001). Over the last five decades, several different extreme value analysis (EVA) methods for estimating the heights (i.e. return levels) and occurrence probabilities (i.e. return periods) of extreme water levels have been developed (see HAIGH et al. 2010a for an overview). There is, however, currently no universally accepted method available. Instead, different methods have been applied on transnational but also on national scales resulting in a heterogeneous level of protection. Therefore, it is difficult to assess the level of protection offered by defences across the different states. To provide coastal protection of consistent standard, design levels need to be consistently calculated based on an objectively defined model setup.

Furthermore, an accurate assessment of return water levels using traditional extreme value analysis methods requires records of sufficient length (> 30 years; HAIGH et al. 2010a), indicating one of the largest pitfalls of extreme value models, as the availability of measured water levels is limited in many regions. In the German Bight, multi-decadal records of high and low waters exist at several sites, but for some regions (e.g. at some small islands in the German Wadden Sea) no or only very short and incomplete time series exist. In practical applications it is often assumed that at-site (i.e. using local water

level records from a tide gauge station) estimates can be transferred to un-gauged surroundings. Nevertheless, water levels in the German Bight can differ significantly between stations as they are strongly influenced by shallow water effects and the complex topography of the coastline (see e.g. JENSEN and MÜLLER-NAVARRA 2008). Simply transferring information about the likelihood of extreme water level events from gauged to surrounding un-gauged sites is thus highly debatable and can cause erroneous return level estimates. Thus, more elaborate procedures to adequately transfer water level information are required

The return water level assessment is not only uncertain regarding the heterogeneous assessment procedures or the limited water level information but also with respect to possible future projections related to climate change. Recent analyses highlight that global MSL rose by 3.2 mm/year from 1971 to 2010. As consequence from an increased ocean warming and the increased loss of mass from glaciers and ice sheets, future rates of sea level rise (SLR) are expected to very likely exceed those observed during 1971 to 2010 (IPCC 2013). Until now, most coastal protection strategies assumed that changes in extreme water levels during the 21st century will be dominated by changes in MSL and design water levels were raised by exactly the same amount of the projected SLR (SMITH et al. 2010). These results are limited to the assumption of a similar long-term behaviour between mean and extreme water levels. For the German Bight, however, MUDERSBACH et al. (2013) showed that trends in extreme high water levels differed significantly from those in MSL from the mid-1950s to approximately 1990, indicating the presence of non-linear interactions between the different sea level components (i.e. MSL, tide, surge). This is contrary to most other locations around the world, where observed changes of extremes were found to be equal to those of the MSL. In order to plan adequate adaptation strategies to cope with climate change challenges it is thus essential that reliable projections of extreme water level changes become available.

2 Data and study area

The methodologies and results presented hereafter were developed in the ‘*ZukunftHallig*’ research project investigating the future development of the North Frisian Halligen. The Halligen are small low lying islands located off the coastline of Schleswig-Holstein (the most northern federal state) in Germany (see the blue shaded areas in Fig. 1b). The Halligen are surrounded by the North Frisian Wadden Sea which was added to UNESCO’s World Heritage List in 2009.

For the analyses a number of tide gauges along the coastlines of the United Kingdom (UK), the Netherlands (NL), France (FRA) and Germany (GER) (see Tab. 1) are used and their locations are shown in Fig. 1. All water level records are referred to the German reference datum ‘Normalhöhennull’ (NHN). To calibrate a numerical model, high resolution tide gauge data from the inner North Sea were used, covering the British East Coast, the English Channel, the Dutch coastline and the German Bight. The calibration was performed using the storm surge event of November 1st, 2006. For the bias-correction of the model output, high water levels for the period from 1970 to 2009 from all German Bight tide gauges except Pellworm Harbour were used; the water level record of Pellworm Harbour was used for validation purposes.

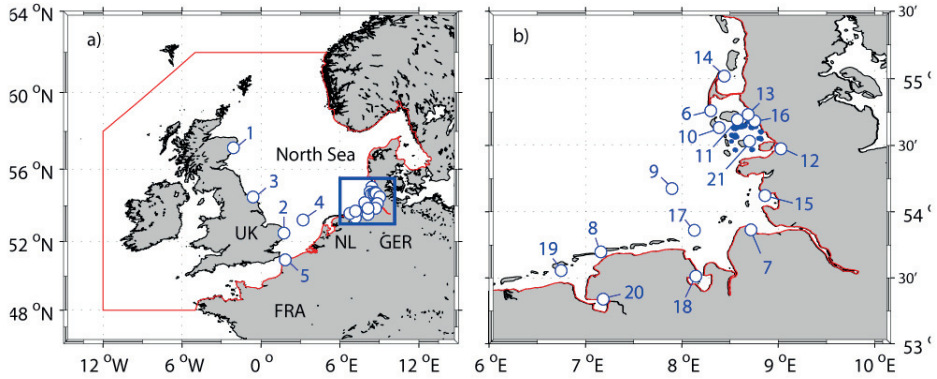


Figure 1: Study area with a) tide gauges in the entire model domain and b) tide gauges in the German Bight.

Table 1: Tide gauges used to calibrate, correct and validate the model output. The (*) indicates that tidal high and low waters are available; at all other stations, high resolution values (1-minute) were used. The marker (✓) indicates in which computational step the data was used.

#	tide gauge location (label)	country	years	availability [%]	cal.	cor.	val.
1	Aberdeen (ABE)	UK	2006	100	✓	-	-
2	Lowestoft (LOW)	UK	2006	100	✓	-	-
3	Whitby (WHI)	UK	2006	100	✓	-	-
4	K 13a Platform (K13)	NL	2006	100	✓	-	-
5	Calais (CAL)	FRA	2006	89.6	✓	-	-
6	Hörnnum (HOR)	GER	2006 1970-2009	98.9 100*	✓ -	- ✓	- ✓
7	Cuxhaven (CUX)	GER	1970-2009	100*	✓	✓	✓
8	Norderney (NOR)	GER	1970-2009	100*	✓	✓	✓
9	Helgoland (HEL)	GER	1970-2009	100*	-	✓	✓
10	Wittdün (WIT)	GER	1970-2009	100*	-	✓	✓
11	Wyk (WYK)	GER	1970-2009	100*	-	✓	✓
12	Husum (HUS)	GER	1970-2009	100*	-	✓	✓
13	Dagebüll (DAG)	GER	1970-2009	100*	-	✓	✓
14	List (LIS)	GER	1970-2009	100*	-	✓	✓
15	Büsum (BUS)	GER	1970-2009	100*	-	✓	✓
16	Schlüttsiel (SCH)	GER	1970-2009	100*	-	✓	✓
17	LT Alte Weser (LTA)	GER	1970-2009	100*	-	✓	✓
18	Wilhelmshaven (WIL)	GER	1970-2009	100*	-	✓	✓
19	Borkum FB (BOR)	GER	1970-2009	100*	-	✓	✓
20	Emden (EMD)	GER	1970-2009	100*	-	✓	✓
21	Pellworm Hafen (PEL)	GER	1970-2009	100*	-	-	✓

3 Return level assessment

A recent assessment on the general performance of the two main direct extreme value analysis methods (i.e. the block maxima (BM) method and the peaks over threshold (POT) method) and their applicability to water level records in the German Bight was conducted in a companion study by ARNS et al. (2013). The return level and return period assessment in this paper is based on these recommendations. Results from that study showed that the POT method generally yields better results than the BM method if the model set-up is carefully chosen. The POT method is based on the assumption that the sample (i.e. all values above a threshold) is characterized by the generalized Pareto distribution (GPD). The POT sample is created choosing all values of a record that exceed a predefined threshold. The threshold selection is often subjective and this can potentially lead to different outcomes, especially when comparing the results from many sites along a coastline. In analyzing different threshold selection criteria, ARNS et al. (2013) showed that the 99.7th percentile leads to stable and consistent results in the German Bight. Furthermore, it was shown that the storm surge of 1976 has to be included in the statistical analyses; this event was the highest one ever recorded in large parts of the German Bight. The approach recommended by ARNS et al. (2013) for estimating return levels in the German Bight with minimal subjectivity comprises the following steps:

- Use a high water peak time series starting in 1976 or earlier as input data.
- Create a stationary dataset using a 1-year moving average trend correction of the high water peaks.
- Create a sample from all 99.7th percentile threshold exceedances of the high water peaks.
- Use the extremal index for declustering.
- Fit the GPD to the extreme value sample.
- Use the maximum likelihood estimation (MLE) for parameter estimation (see. e.g. SMITH 1986; HOSKING and WALLIS 1987).

4 Methods

4.1 Numerical model setup

To generate continuous water levels for the entire German Bight, a 40-year hindcast for the period from 1970 to 2009 was conducted with a process-based hydrodynamic numerical model. A two-dimensional, depth-averaged barotropic tide-surge model of the entire North Sea has been configured using the Danish Hydraulic Institute's (DHI) Mike21 FM (flexible mesh) model suite. The software is based on the numerical solution of the incompressible Reynolds averaged Navier-Stokes equations; the spatial discretization is achieved using a flexible mesh. The model was configured within a coastline provided by the National Oceanic and Atmospheric Administration (NOAA) with a resolution of 1:250.000 km (http://www.ngdc.noaa.gov/mgg_coastline/). The resolution of the coastline was resampled to 30 km along the open boundaries, increasing to 10 km in the northern- and southern-most parts of the European mainland coastline. In between these locations (Scandinavia, the Netherlands, Belgium, France), the resolution was successively resampled until reaching a maximum resolution of 1 km in the German Bight.

The bathymetric data, interpolated onto the model grid (see Fig. 2), was obtained from various sources. In the northern part of the German Bight, high resolution (~ 15 m) survey maps of the Wadden area provided by the Schleswig-Holstein Agency for Coastal Defence, National parks and Marine Conservation (LKN-SH) were used. In this particular area, the Halligen are located. To account for influences on currents resulting from these small islands, a Digital Elevation Model (DEM) covering all of the ten existing Halligen was integrated into the model. The DEM was also provided by the LKN-SH. In the remaining parts of the German Bight, a bathymetric dataset with a resolution of 1 nautical mile provided by the Federal Maritime and Hydrographic Agency (BSH) was interpolated onto the grid. Apart from the German Bight, the General Bathymetric Chart of the Oceans (GEBCO) data provided by the British Oceanographic Data Centre (BODC) with global coverage and a resolution of 0.5° was used. All datasets were corrected to the German reference datum NHN.

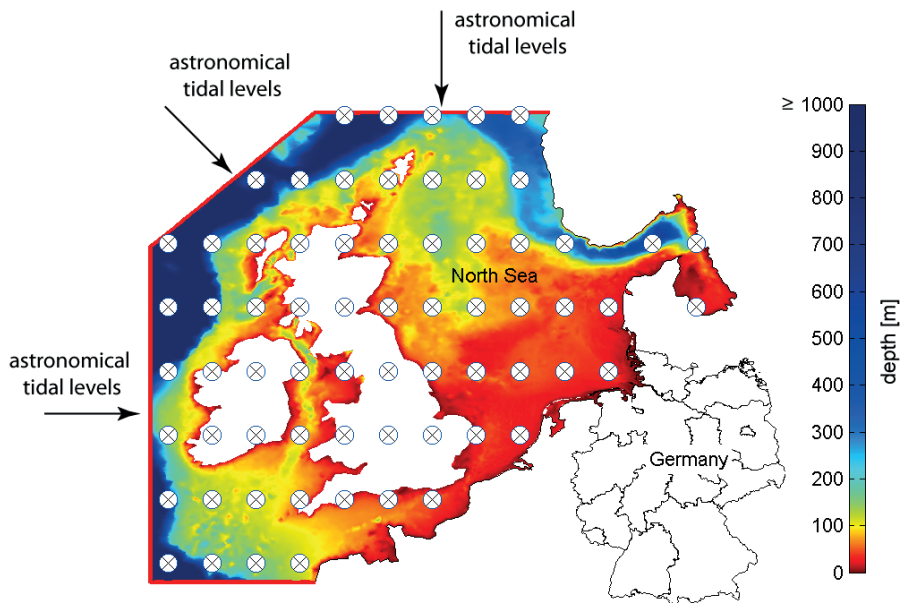


Figure 2: Model domain (outer boundary), bathymetry (according to the legend) and locations of atmospheric (crosses) and tidal (red line) boundary conditions.

At the open boundaries, the model was driven by astronomical tidal levels (see Fig. 2). These were derived from a global tide model provided by MIKE21 (DHI), including the eight primary harmonic constituents (K_1 , O_1 , P_1 , Q_1 , M_2 , S_2 , N_2 und K_2 , see e.g. ANDERSEN 1995). Additionally, the Mean Sea Level (MSL) was considered using an index-time series for the entire North Sea from WAHL et al. (2013); the time series was derived using data from 30 tide gauges located around the North Sea basin. As each year of the considered 40- year hindcast was run separately, the MSL at the open boundaries was adjusted according to the annual average MSL values from the index time series.

The surge component was generated by forcing the model with mean sea level pressure fields and u and v components of 10 m wind fields provided by the Cooperative Institute for Research in Environmental Sciences (CIRES) 20th Century Project (COMPO et

al. 2011) of the Earth System Research Laboratory, US National Oceanic & Atmospheric Administration (NOAA). These fields are available with a spatial resolution of 2° and a temporal resolution of 6 hours (3 hours in the forecast).

The model was run for each year with a two day warm up period (using longer warm up periods did not show any changes) and results were stored at an interval of 10 minutes for every model grid point. A calibration was performed by using a stepwise variation of the bed resistance and comparing the simulated and observed water levels. For this purpose, the storm surge of the 1st November 2006 was used. Simplified, constant Manning's n-values were used spatially across the entire model domain. The evaluation of the models performance was conducted using the *Coefficient of determination* (r^2), the *Index of agreement* (d) and the *Root Mean Squared Error* (RMSE) (see KRAUSE et al. 2005 for a description of different efficiency criteria). The calibration results are shown in Tab. 2, highlighting that the overall agreement was highest along the UK coastline. Slightly higher differences occurred in the German Bight and are most probably attributed to using one representative bed resistance instead of defining regions of different resistances as well as from shallow water effects that occur in this region and which are possibly not captured properly by the model.

Table 2: Efficiency criteria based on the models best fit.

Criteria	ABE	WHI	LOW	CAL	K13	HÖR	CUX	NOR
r^2 [-]	0.97	0.95	0.86	0.94	0.85	0.91	0.88	0.89
d [-]	0.99	0.99	0.96	0.98	0.96	0.98	0.96	0.97
RMSE [cm]	13.26	19.76	17.25	33.20	14.61	16.64	31.08	21.92

4.2 Bias-correction

The calibration exercise allowed us to minimize the differences between the observed and the modelled water levels (bias) at individual stations but there are still some differences present. The possible sources of such differences are multifarious including the parameterization that is conducted in the model set-up, allowing for a range of different strategies. Furthermore, all water level observations are prone to natural and anthropogenic influences that cannot entirely be captured by a numerical model. For instance, the wind fields that were used have a temporal resolution of 3 hours and a spatial resolution of 2°; for simulating storm surges, this might be too coarse in order to capture all local meteorological effects. The bias can also be attributed to input deficiencies e.g. resolution or scaling effects. With regards to extreme value analyses, this bias can produce large discrepancies in return water level estimates, particularly at higher return periods.

Thus, the modelled water levels are corrected prior to performing the extreme value analysis. The bias correction can be assumed as a function to transfer the modelled variable into a corrected variable (PIANI et al. 2010). This function is created by describing the differences between a pair of variables (e.g. observed and modelled water levels at a tide gauge station) with a parametric or a non-parametric fit (MUDELSEE et al. 2010). In this paper, we use a bias correction method (for more details see ARNS et al. 2013 and ARNS et al., in review) to derive reliable water level data covering the entire German Bight and the period 1970 to 2009, i.e. a period where many tide gauge records exists. A non-parametric transfer function for each individual year of the 40-year hindcast is used.

The bias correction is based on three computational steps. Firstly, high water levels of observed x_o and modelled water levels x_m are computed and sorted in ascending order. Secondly, the differences (bias) between the cumulative distribution functions (CDF) of observed $Q(x_{o,j,s})$ and modelled $Q(x_{m,j,s})$ high waters at tide gauge station s and for year j are calculated as follows:

$$B_{c,j,s} = Q(x_{o,j,s}) - Q(x_{m,j,s}) \tag{1}$$

The differences ($B_{c,j,s}$) are added to the distributions of the modelled high waters $Q(x_{m,j,s})$ in order to eliminate the bias at each individual station; the resulting values correspond to the high waters derived from tide gauge records:

$$Q(x_{o,j,s}) = B_{c,j,s} + Q(x_{m,j,s}) \tag{2}$$

This procedure can be used to eliminate the bias at each gauged station and for each period where observational data is available. Fig. 3b exemplarily shows the distributions of observed (black line) and modelled (red line) high waters using the Hörnum tide gauge station as a case study. The bias, i.e. difference between the two distributions according to Equation (1), is shown as blue line. Any bias having a probability between 0 and 1 yields a value to correct the modelled data. For instance, the correction for $Q(x = 0.2)$ amounts to $\Delta h = 4.95$ cm.

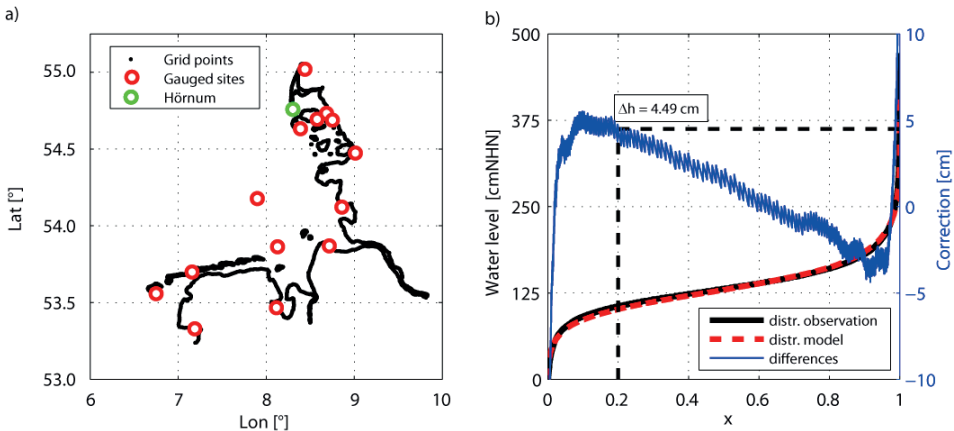


Figure 3: Example of performing the bias-correction (adapted from Arns et al. 2013) with: a) showing all grid-points (black) and tide gauges (red) of the model along the coast; b) the distributions of observed (black) and modelled (red) high waters for Hörnum tide gauge.

Fig. 3a shows all grid-points (black dots) of the model along the coast for which water level time series are available from the 40-year hindcast tide gauge locations are shown as red circles. This figure indicates that the model also generates water levels between the gauged sites highlighting that the bias-correction needs to be transferred to these locations. In the third stage, the bias-correction is thus interpolated from all 15 tide gauge stations envisaged for correction purposes (see the correction (cor.) column in Tab. 1) to the locations between the gauged sites. The interpolation is performed for each year individually using the *Inverse Distance Weighted* (IDW) method (e.g. MCMILLAN et al. 2011).

4.3 Validation

For validation purposes, the methodology described above is applied to 15 validation sites that are listed in Tab. 1 (see the validation (val.) column). From this list, Pellworm Harbour is the only tide gauge station that has not been used for the correction. Instead it has been removed from the pool of tide gauge records considered for correction purposes, so that the modelled water levels of Pellworm Harbour are adjusted using the bias-correction that has been interpolated from neighbouring stations. The overall performance of the methodology is assessed using the same efficiency criteria as in Sect. 4.2. In Fig. 4, the red dots show the comparison of observed and modelled water levels at individual stations; the blue dots show the comparisons of observed vs. modelled and bias-corrected water levels. As expected, the bias-correction increases the *coefficient of determination* r^2 at all stations (including Pellworm Harbour), reaching values of $r^2 \approx 1$ [-] (Fig. 4a). Fig. 4b shows a similar effect for the *index of agreement* d . At all stations, the d is improved to $d \approx 1$ [-]; the improvement at Wittdün, Wyk and Dagebüll is small, as the *index of agreement* was already high at these stations before the bias-correction was applied. In summary, the validation shows that high water levels derived from numerical model simulations are very well represented when the bias-correction is applied. A more sophisticated verification can be found in ARNS et al. (2013), concluding that the above presented bias-correction is suitable to be used with modelled water levels in the German Bight, which are envisaged to serve as input for extreme value analyses, especially in un-gauged areas.

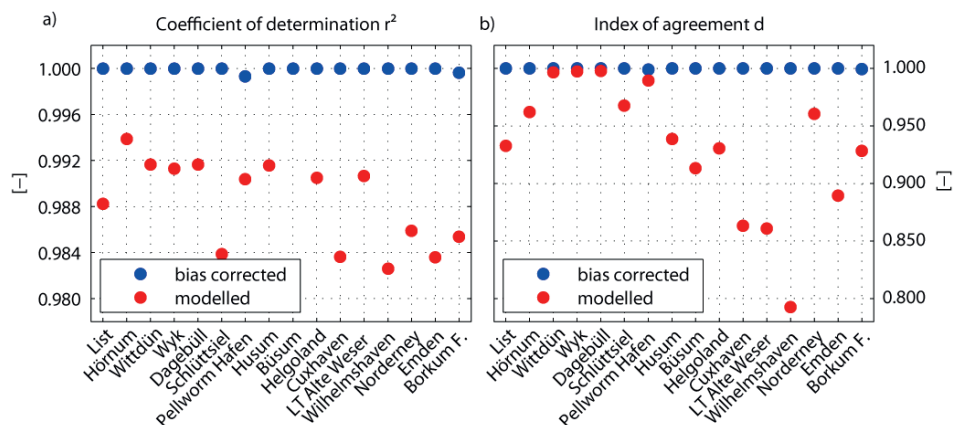


Figure 4: Compilation of efficiency criteria applied to 16 stations (taken from ARNS et al. 2013).

4.4 SLR run

A scenario run was conducted to examine how SLR might affect extreme water levels in the future, hereafter referred to as SLR scenario run. Regional MSL projections have recently been published in the AR5, but the model resolution is still relatively coarse for marginal seas such as the North Sea. To account for changes in MSL the global projections given in the AR5 are used, reporting that SLR will very likely exceed the observed rates during 1971 and 2010 due to increased ocean warming and increased loss of mass

from glaciers and ice sheets. Based on climate projections in combination with process-based models they state that global MSL rise for 2081–2100 relative to 1986–2005 will likely be in the range of 0.26 to 0.82 m including uncertainties. This range covers four different Representative Concentration Pathways (RCPs) allowing for possible future climates, each of which is considered possible depending on how much greenhouse gas is emitted in the upcoming decades. For the SLR scenario the average of all four RCPs is used with $z = 0.5$ m and it is assumed that this is the global MSL rise by 2100.

Additionally, vertical land movements in the German Bight are considered as derived from the glacial isostatic adjustment (GIA) model of PELTIER (2004) which were downloaded from the website of the Permanent Service for Mean Sea Level. In the study region, GIA amounts to ~ 0.44 mm/year on average (closest point to the study region: Lon. 8; Lat. 54.4). Assuming that vertical trends describe ongoing (at least until 2100) long-term processes, SLR projection and GIA influence can be summed up to a relative mean sea level (RMSL) rise scenario of +0.54 m. This projection is assumed to be valid for the entire study region.

Currently, changes in atmospheric circulation and storminess are controversially discussed (see e.g. WEISSE and VON STORCH 2009 and references therein). In the light of these competing results, the SLR scenario used here assumes that wind conditions (speed and directions) do not change. Instead, the SLR scenario runs are conducted using the same meteorological forcing from 1970 to 2009, i.e. the SLR scenario run considers all boundary conditions to remain as described in Sect. 4.1 but assuming the MSL to have increased by an additional +0.54 m. This increase is added to the observed MSL between 1970 and 2009. Hence, the effects of SLR on storm surge water levels can directly be compared. It is noted that changes in storminess may additionally increase future storm surge water levels in the German Bight (WOTH et al. 2006).

5 Results

5.1 Present day return levels

Following the bias correction stage, extreme value analyses were conducted for the whole North Sea coastline of Schleswig-Holstein (north-eastern German Bight). For this stretch of coastline, the model provides water level time series at about 900 coastal grid points that are located approximately every kilometre (i.e. the mean distance). All return water levels are estimated using the approach recommended in Sect. 3 (see ARNS et al. 2013 for details). Fig. 5 schematically shows present day water levels with a return period of 200 years for the entire coastline of Schleswig-Holstein including the un-gauged islands and Halligen areas. This information can be used as a basis for the design of protection measures and is also useful for risk analyses in un-gauged regions like the Halligen.

5.2 Changes in return periods in the SLR scenario

This section investigates changes in return periods of extreme water levels due to a SLR of 0.54 m along the entire coastline of Schleswig-Holstein (a federal state in Germany). Fig. 6 shows the samples and the theoretical distributions of a) the control run, b) the control run simply superimposed by the considered SLR, and c) the SLR scenario run,

explaining how changes in return periods were assessed. Furthermore, this figure highlights that future extreme water levels could be notably larger than expected from SLR alone (for more details see ARNS et al., in review).

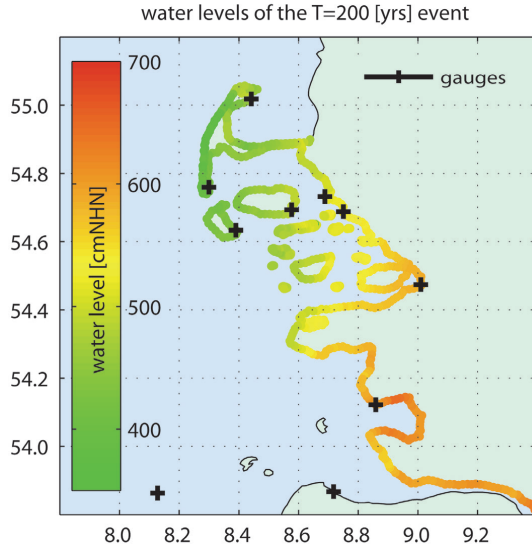


Figure 5: Return water levels along the coastline of Schleswig-Holstein.

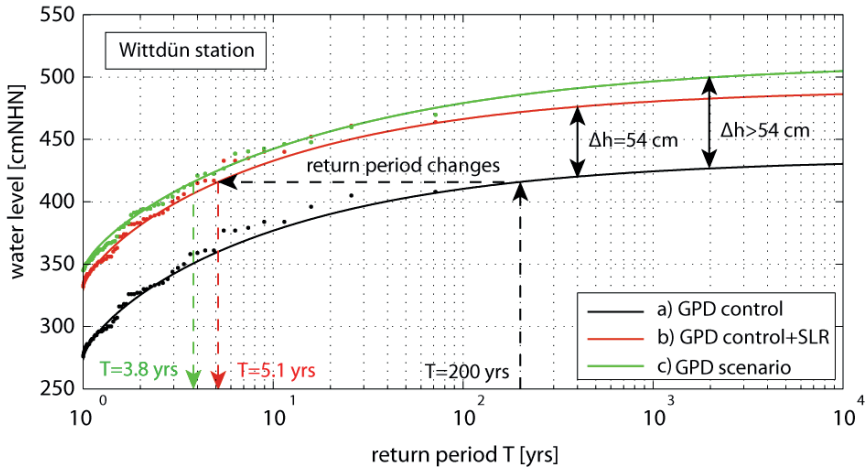


Figure 6: Present day return water levels at tide gauge Wittdün (a) and the effect of SLR when using the MSL-Offset method (b) or the numerical model simulations (c).

Fig. 7 shows the return periods from the SLR scenario run calculated on basis of the current state 200 year return levels for the entire coastline of Schleswig-Holstein. The figure indicates that water levels that currently have a return period of 200 years considerably reduce to return periods of down to 3 years in the SLR scenario. The figure further highlights the spatially inconsistent feedback showing the largest return period changes in the most westerly parts (e.g. the larger islands), but partly also along the mainland coastline.

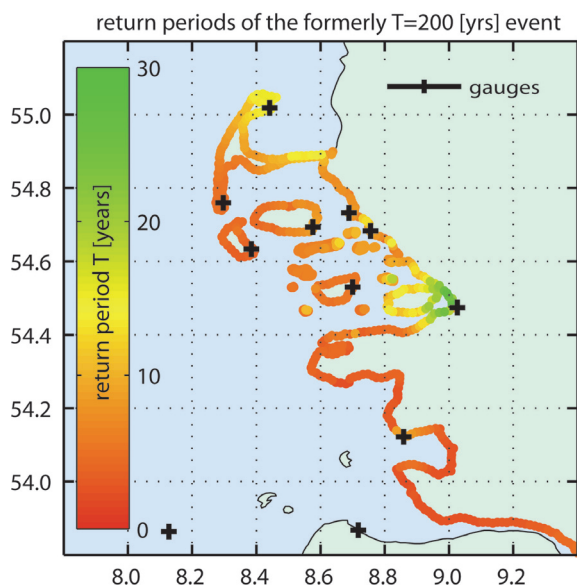


Figure 7: New return periods as a result of the SLR scenario run; the return periods are referred to the water levels of the former 200-years water levels.

6 Summary and discussion

This study uses a combination of numerical and statistical methods to estimate present day return water levels at sites where only little or even no measured water level data is available. A similar method has recently been applied along different stretches of coastlines around the globe (see e.g. HAIGH et al. 2013). This approach was adopted and modified to satisfy the characteristics along the entire coastline of Schleswig-Holstein in northern Germany. It is shown that water levels derived from a hydrodynamic model can be used to calculate reliable return water levels. Regions with no or only few tide gauge stations can especially benefit from this approach. However, a precondition is to adequately correct the bias that is generated with the numerical simulations. The bias-correction is performed first at each individual station where water level observations exist. Then the correction is transferred to the neighbouring sites points using an *Inverse Distance Weighting* interpolation method. As a result, regionalized return water levels at ungauged sites are obtained, that account for locally confined coastal attributes. An assessment showed that return water levels that are estimated using the approach presented in this paper are highly consistent with the return water levels from at-site analyses.

To account for possible future changes we also investigated the impact of a 0.54 m SLR on future extreme water levels along the coastline of Schleswig-Holstein (a federal state in Germany). The study shows that future extreme water levels could be significantly larger than expected from SLR alone. These differences are mainly caused by changes in shallow water and frictional effects, altering the tidal component of the total water levels (for more details see ARNS et al., in review). Furthermore it is shown that return levels of extreme water levels will considerably reduce, i.e. a water level of given

return period occurs more frequently in future as e.g. the 200 year return level, which will be 3 year return level in the SLR scenario.

A combination of individual parts of this paper can be used to objectively and reliably estimate regional to local return levels for current and future SLR conditions. These methodologies enable to estimate return levels for an entire coastline helping to obtain water level information in un-gauged areas. The results can be used for the design of coastal defences or for risk analyses.

7 References

- ANDERSEN, O.B: Global ocean tides from ERS 1 and TOPEX/POSEIDON altimetry, *Journal of Geophysical Research*, Vol. 100, 1995.
- ARNS, A.; WAHL, T.; HAIGH, I.D.; JENSEN, J. and PATTIARATCHI, C.: Estimating extreme water level probabilities: A comparison of the direct methods and recommendations for best practise, *Coastal Engineering*, Vol. 81, 2013.
- ARNS, A.; WAHL, T.; DANGENDORF, S. and JENSEN, J.: The impact of sea level rise on extreme water levels in the northern part of the German Bight, *Coastal Engineering*, under review.
- ARNS, A.; WAHL, T.; DANGENDORF, S.; MUDERSBACH, C. and JENSEN, J.: Ermittlung regionalisierter Extremwasserstände für die Schleswig-Holsteinische Nordseeküste. *Hydrologie und Wasserbewirtschaftung*, HW57, 2013.
- BÜTOW, H.: Die große Flut in Hamburg: Eine Chronik der Katastrophe vom Februar 1962. Verlag: Hansstadt, 1963.
- COLES, S.: *An Introduction to Statistical Modeling of Extreme Values*. Springer Verlag, London, 2001.
- COLES, S.G. and TAWN, J.A.: Bayesian modelling extreme surges on the UK east coast. *Phil.Trans. Roy. Soc. A: Mathematical, Physical and Engineering Sciences*. 363, 1387-1406, 2005.
- COMPO G.B.; WHITAKER, J.S.; SARDESHMUKH, P.D.; MATSUI, N.; ALLAN, R.J.; YIN, X.; GLEASON, B.E.; VOSE, R.S., RUTLEDGE, G.; BESSEMOULIN, P.; BRÖNNIMANN, S.; BRUNET, M.; CROUTHAMEL, R.I.; GRANT, A.N.; GROISMAN, P.Y.; JONES, P.D.; KRUK, M.C.; KRUGER, A.C., MARSHALL, G.J.; MAUGERI, M.; MOK, H.Y.; NORDLI, Ø.; ROSS, T.F.; TRIGO, R.M.; WANG, X.L.; WOODRUFF, S.D. and WORLEY, S.J.: The twentieth century reanalysis project. *Q J Roy Meteor Soc* 137:1-28, doi: 10.1002/qj.776, 2011.
- DIXON, M.J. and TAWN, J.A.: Extreme sea-levels at the UK A-class sites: site-by-site analyses. Proudman Oceanographic Laboratory Internal Document No. 65, 1994.
- HAIGH, I.D.; NICHOLLS, R. and WELLS, N.: A comparison of the main methods for estimating probabilities of extreme still water levels. *Coastal Engineering* 57, 838-849, 2010a.
- HAIGH, I.; NICHOLLS, R. and WELLS, N.: Assessing changes in extreme sea levels: application to the English Channel, 1900-2006. *Continental Shelf Research* 30, 1042-1055, 2010b.
- HOSKING, J.R.M. and WALLIS, J.R.: Parameter and quantile estimation for the generalized Pareto distribution. *Technometrics* 29, 339-349, 1987.

- IPCC: Summary for Policymakers. In: STOCKER, T.F.; QIN, D.; PLATTNER, G.-K.; TIGNOR, M.; ALLEN, S.K.; BOSCHUNG, J.; NAUELS, A.; XIA, Y.; BEX, V. and MIDGLEY, P.M. (eds.): *Climate Change 2013: The Physical Science Basis. Contribution of Working Group I to the Fifth Assessment Report of the Intergovernmental Panel on Climate Change*. Cambridge University Press, Cambridge, United Kingdom and New York, NY, USA, 2013.
- JENSEN, J. and MÜLLER-NAVARRA, S.: Storm surges on the German Coast. *Die Küste*, 74, 92-125, 2008.
- KRAUSE, P.; BOYLE, D.P. and BÄSE, F.: Comparison of different efficiency criteria for hydrological model assessment. *Adv. in Geosc.*, Vol. 5, 89-97, 2005.
- MCMILLAN, A.; BATSTONE, C.; WORTH, D.; TAWN, J.; HORSBURGH, K. and LAWLESS, M.: Coastal flood boundary conditions for UK mainland and islands. Project: SC060064/TR2: Design sea-levels. Environment Agency of England and Wales, 2011.
- MUDELSEE, M.; CHIRILA, D.; DEUTSCHLÄNDER, T.; DÖRING, C.; HAERTER, J.; HAGEMANN, S.; HOFFMANN, H.; JACOB, D.; KRAHE, P.; LOHMANN, G.; MOSELEY, C.; NILSON, E.; PANFEROV, O.; RATH, T. and TINZ, B.: Climate Model Bias Correction und die Deutsche Anpassungsstrategie. *Mitteilungen Deutsche Meteorologische Gesellschaft*, 2-7 (in German), 2010.
- MUDERSBACH, C.; WAHL, T.; HAIGH, I.D. and JENSEN, J.: Trends in extreme high sea levels along the German north sea coastline compared to regional mean sea level changes. *Continental Shelf Research* (in press). ISSN 0278-4343. <http://dx.doi.org/10.1016/j.csr.2013.06.016>, 2013.
- PELTIER, W.R.: Global Glacial Isostasy and the Surface of the Ice-Age Earth: The ICE-5G(VM2) model and GRACE. *Ann. Rev. Earth. Planet. Sci.* 2004. 32, 111-149, 2004.
- PIANI, C.; HAERTER, J.O. and COPPOLA, E.: Statistical bias correction for daily precipitation in regional climate models over Europe. *Theor. Appl. Climatol.*, Vol. 99, 187-192, 2010.
- SMITH, R.L.: Extreme value theory based on the r largest annual events. *Journal of Hydrology* 86, 27-43, 1986.
- SMITH, J.M.; CIALONE, M.A.; WAMSLEY, T.V. and MCALPIN, T.O.: Potential impact of sea level rise on coastal surges in southeast Louisiana. *Ocean Engineering*, Vol. 37, 37-47, 2010.
- VON STORCH, H. and WOTH, K.: Storm surges - the case of Hamburg, Germany. ESSP OSC panel session on "GEC, natural disasters, and their implications for human security in coastal urban areas". Available online: <http://www.safecoast.nl/editor/databank/File/hamburg-storms.pdf>. Last visited 26.1.2012, 2006.
- VON STORCH, H.: Storm Surges: Phenomena, Forecasting and Scenarios of Change. *Proceeding of the International Union of Theoretical and Applied Mechanics (IUTAM)*, 2012.
- WAHL, T.; HAIGH, I.D.; WOODWORTH, P.L.; ALBRECHT, F.; DILLINGH, D.; JENSEN, J.; NICHOLLS, R.J.; WEISSE, R. and WÖPPELMANN, G.: Observed mean sea level changes around the North Sea coastline from 1800 to present, *Earth-Science Reviews*, Vol.124, 51-67, <http://dx.doi.org/10.1016/j.earscirev.2013.05.003>, 2013.

- WEISSE, R. and VON STORCH, H.: Marine Climate and Climate Change: Storms, Wind Waves and Storm Surges. Springer-Verlag, Berlin Heidelberg New York, 2009.
- WOTH, K.; WEISSE, R.; VON STORCH, H.: Climate change and North Sea storm surge extremes: An ensemble study of storm surge extremes expected in a changed climate projected by four different regional climate models. Ocean Dyn., Vol. 56, 3-15, 2006.

Investigating Impacts of Climate Change on the Weser Estuary

Anna C. Zorndt and Torsten Schlurmann

Summary

According to the Intergovernmental Panel on Climate Change, global climate change will have profound impact on our environment. This applies to estuaries in particular, as they are not only influenced by changes in the meteorological conditions, but also by the mean sea level rise, changes in river runoff regimes and possibly more intense storm surges. As this makes impact studies in estuaries rely on impact studies of neighboring systems such as watersheds or adjacent shelf seas, uncertainties may accumulate. This complicates to derive reliable projections for planners and decision makers. This contribution describes a work package of a joint climate impact project of the German state Lower Saxony. The aim of the project is to investigate impacts on hydrodynamics and salinities of the Weser estuary. The impact model used in the study is a 3D hydrodynamic modelling tool. The article focuses among others on results and discussion of a mean sea level rise scenario.

Keywords

hydrodynamic modelling, climate impact, Weser estuary, salinity intrusion, tidal dynamics

Zusammenfassung

Dem Intergovernmental Panel on Climate Change zufolge wird der globale Klimawandel in der Zukunft weitreichende Folgen für unsere Lebensumwelt haben. Dies gilt insbesondere für Küstenbereiche wie Ästuarare, da sie nicht nur durch meteorologische Änderungen, sondern auch durch den Anstieg des mittleren Meeresspiegels, Änderungen im Abflussregime und möglicherweise auch durch verstärkte Sturmfluten gefährdet sind. Da Impaktuntersuchungen in Ästuaren demnach von Impaktstudien in benachbarten Systemen wie beispielsweise der Einzugsgebiete oder angrenzender Meeresgebiete abhängen, addieren sich Unsicherheiten. Dies erschwert die Ableitung von belastbaren Projektionen für politische Entscheidungsträger und Planer. Dieser Beitrag beschreibt ein Teilprojekt des Klimafolgenforschungsprojektes KLIFF des Landes Niedersachsen, welches sich mit den Folgen für die Hydrodynamik und die Salzgehalte im Weserästuar befasst. Als Impaktmodell kommt ein 3D hydrodynamisch-numerisches Modell zum Einsatz. Schwerpunkt des Beitrags sind unter anderem Ergebnisse und Diskussion eines Szenarios mit einem mittleren Meeresspiegelanstieg.

Schlagwörter

Hydrodynamische Modellierung, Klimafolgen, Weserästuar, Salzintrusion, Tidedynamik

Contents

1	Introduction	542
2	Salinity and hydrodynamics of the Weser Estuary in its present state.....	543
3	Methods.....	544
3.1	Modelling tool.....	544
3.2	Weser estuary model.....	545
3.3	Computation of investigated tidal characteristics.....	545
4	Investigation of a mean sea level rise scenario.....	546
4.1	Experimental design	546
4.2	Investigated scenario	547
4.3	Results.....	547
5	Summary and discussion.....	548
6	References	550

1 Introduction

The salinity distribution and the hydrodynamics of the Weser estuary are influenced by the tides in the German Bight, the runoff from the watershed, meteorological influences such as wind- or storm events and the geometry of the estuary. Climate change may impact the Weser directly by change of the meteorological forcing but mainly indirectly by changes in neighboring systems like the North Sea or the watershed, which provide important boundary conditions of the estuary (see Fig. 1).

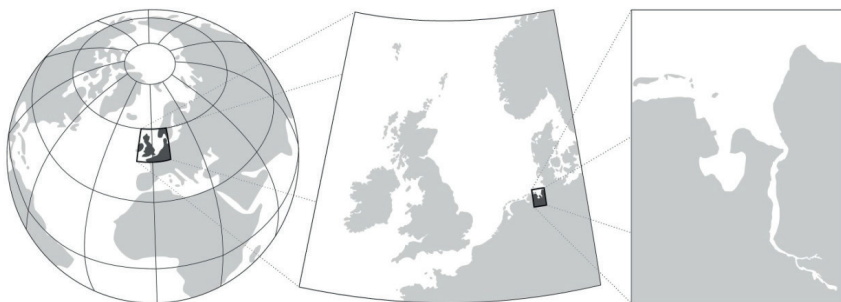


Figure 1: Global climate changes impact the Weser estuary mostly by changes of other systems like the North Sea, which poses a challenge to climate impact research.

Research has been undertaken in the last decades by the German state Lower Saxony (projects KLIMU and KRIM, e.g. SCHIRMER and SCHUCHARDT 2001) and currently by the Federal Ministry of Transport, Building and Urban Affairs (KLIWAS, see SEIFFERT et al., this volume) to investigate possible impacts of climate change on the Weser. Yet there is still uncertainty on both the side of the changed forcing as well as on the side of the system's response. Coastal planners and decision makers however are in need of reliable projections, as adaptation measures need to be envisaged well in advance in order to be prepared for the challenges ahead. This has motivated the Ministry for Science and

Culture of Lower Saxony to investigate impacts of climate change on the Weser estuary as part of yet another interdisciplinary research program launched in 2009 (KLIFF – www.kliff-niedersachsen.de).

To investigate changes of the salinity distribution and hydrodynamics of the estuary, a 3D model was built up and validated with observations of past events. With help of scenario simulations, possible impacts of climate change on today's state of the Weser estuary with its natural seasonal, periodic and meteorologically induced variations were investigated. To achieve more reliable projections, the attempt was made to decrease or at least quantify the uncertainty of the projections induced by internal variability of the system and the boundary condition uncertainty.

The study was carried out in strong collaboration with partners investigating climate change impact on the adjacent watersheds of the estuary (e.g. KREYE et al. 2010) and the groundwater (e.g. YANG et al. 2013).

In this contribution, an introduction on the hydrodynamics and salinity intrusion of the Weser estuary in its current state is provided in Section 2. Methods are described in Section 3. The main part of this contribution focuses on results of a simple mean sea level rise scenario which is described in Section 4, followed by a summary and discussion in Section 5.

2 Salinity and hydrodynamics of the Weser Estuary in its present state

A detailed study of the hydrodynamics of the Weser Estuary in the present state was carried out within this study. Here, a short summary is presented. In today's state, the tidal range of the estuary amounts to approximately 2.8 m in the outer estuary (Leuchtturm Alte Weser) and then continuously increases upstream toward a maximum of 4.10 m at the weir in Bremen. The tidal dynamics of the estuary are influenced by astronomical periodic variations such as the spring-neap cycle. Further upstream, they are also influenced by the runoff. The runoff however, inflowing at the weir from the Mittelweser and also from smaller adjacent catchments, underlies strong seasonal variations. The long-term mean amounts to approximately $324 \text{ m}^3 \text{ s}^{-1}$ (1990-2010). The lowest monthly means occur in September, the highest in March ($166 \text{ m}^3 \text{ s}^{-1}$ and $564 \text{ m}^3 \text{ s}^{-1}$, extremes of $74 \text{ m}^3 \text{ s}^{-1}$ and $2190 \text{ m}^3 \text{ s}^{-1}$, respectively).

The position of the mixing zone between freshwater and seawater varies in relation of those values. It can be described by the distance of the tidally averaged 2- and 10 psu isohalines from the tidal weir in Bremen (P_{12} , P_{110}). During average runoff conditions, which occur in spring or autumn after or before the increased winter high water, the 2 psu isohaline is found at a distance of approximately 57 km from the tidal weir as can be seen in Fig. 2 ($P_{12} = 57 \text{ km}$, $P_{110} = 70 \text{ km}$). In the summer when runoff is typically very low, it intrudes further upstream the estuary so that $P_{12} = 52 \text{ km}$ for $Q = 200 \text{ m}^3 \text{ s}^{-1}$. During the high waters occurring in winter, a displacement downstream can be observed (e.g. $P_{12} = 73 \text{ km}$ for $Q = 1800 \text{ m}^3 \text{ s}^{-1}$).

An important indicator for sediment dynamics and the position of the estuarine turbidity maximum is the residual current velocity, which is shown in Fig. 2 (bottom) for average runoff conditions. In the upstream river reach up to a distance of approximately 57 km from the tidal weir, the vertical structure of the residual flow is mostly uniform. Downstream from here however, the bottom residual current velocity turns and becomes

landwards directed. In parallel to the position of the mixing zone, this null point of bottom residual current velocity is displaced down- or upstream with varying runoff.

The local variations of the salinity due to the tides are close to zero at seaward and the upstream ends of the mixing zone and increase toward the centre of the mixing one up to values of 12 psu. Simulations show that the vertical stratification also varies with runoff and the tides. During higher runoff and increasingly in neap conditions, stratification establishes with higher salinity in the lower and reduced salinity in the upper water column. This is observed especially during ebb current and has been described in literature as strain induced periodic stratification (SIMPSON et al. 1990).

In a prior publication of the authors, the impact of storms on salinity intrusion was investigated (ZORNDT et al. 2012). The investigation was based on past storm events and scenario storms which were extracted from North Sea model runs of project partners (GASLIKOVA et al. 2012). The simulations showed that depending on duration and intensity of the storm surge, a storm event can move the mixing zone up to 30 km further upstream.

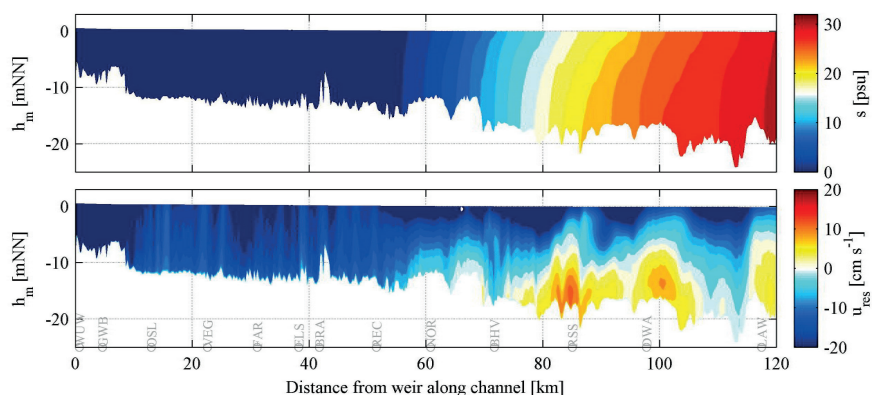


Figure 2: Salinity (top) and residual current velocity (bottom) along the river kilometre line, averaged over a spring-neap cycle of a simulation during average runoff conditions (MQ, see Section 4.1). Seawards directed current is defined to be negative (blue) landwards positive (red).

3 Methods

3.1 Modelling tool

The modelling tool employed in this project has been developed by ZHANG and BAPTISTA (2008). It solves the Reynolds averaged Navier-Stokes equations with shallow water assumption and Boussinesq approximation. SELFE is a semi-implicit Eulerian-Lagrangian finite-element model based on a Galerkin finite element framework with linear shape functions for elevation. Terrain-following hybrid vertical coordinates are used. For turbulence closure, several one- or two equation models can be chosen. Being an open-source community tool, it provides several additional modules for studying among others tsunami inundation, sediment transport, oil spill or water quality. The modelling system is parallelized using domain decomposition. For a more comprehensive description, see ZHANG and BAPTISTA (2008).

3.2 Weser estuary model

The computational domain encompasses an area of 2,140 km² and contains 191,111 vertices and 372,708 elements. In the North, it stretches out to a latitude of approx. 54°. The domain boundaries follow the main dike protection lines and ends in the South at the tidal weir (see Fig. 1, right). The model partly incorporates tributaries mouting into the estuary. The river Hunte is modeled up to the city of Oldenburg and the smaller tributaries Hamme and Wümme reach up to Ritterhude and Niederbrockland, respectively.

To construct the bathymetry, data sets from multi- and single beam soundings as well as airborne data and a digital land model of Lower Saxony were used, which were provided by agencies of the Waterways and Shipping Administration of the German Federal Government and the land of Lower Saxony. The majority of data stems from surveys between 2006 and 2010. Thus, this period has been defined as the model's reference state.

The model is forced by water surface elevation at the Northern open boundary to the German Bight, freshwater input at the open boundaries of Ritterhude, Niederbrockland, Hunte, Ochtum, Geeste and Bremen as well as wind forcing over the wind. The model was calibrated based on a period in April 2009 characterized by medium runoff. It was validated by simulation of periods with varying runoff. In Fig. 3, a comparison between observed and simulated time series is presented for a validation period from winter 2003, in which a peak runoff value of 2190 m³ s⁻¹ was observed.

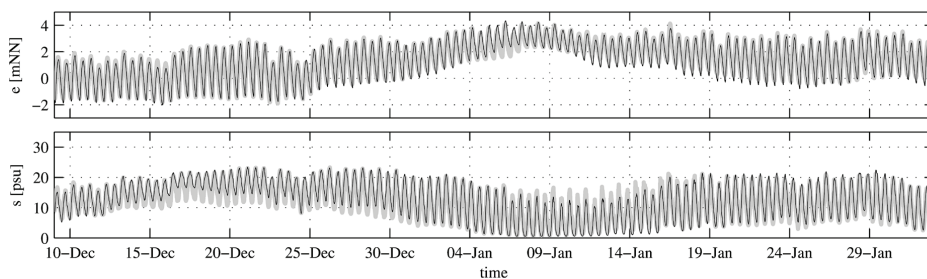


Figure 3: Observed (gray) and simulated (black) time series of elevation at the weir (top) and salinity at a station 85 km from the weir (bottom) for a validation period.

The skill of Murphy (1988) and the root mean squared error were used to quantitatively evaluate the model's ability of reproducing measured water surface elevation, current velocity and salinity. Average skill values amount to 0.95 for water surface elevation, 0.89 for salinity and 0.80 for current velocity, based on two validation periods and with 12 evaluated stations each, which partly consisted of up to three measuring devices distributed over the water column.

3.3 Computation of investigated tidal characteristics

The results presented in this contribution were derived with the following automated steps: The extracted simulated time series of 30 min. resolution were upscaled to 10 min. with spline interpolation. Salinity and current velocity time series were depth averaged for

most of the results presented here. Current velocity vectors were rotated into the main channel direction and only the main current direction was further evaluated, flood current defined as positive. Time series were split up into single tides. Beginning and end of each tide were defined to be low water for water surface elevation, lowest salinity for salinity and slack point after ebb for main current velocity. Tidal characteristics (TC) were calculated for each tide. Presented here are tidally averaged water level (MW), high water (HW), low water (LW), tidal range (TR), tidally averaged salinity (S_M), tidal salinity maximum (S_{MAX}) and residual of the current velocity in main channel direction (U_{RES}). The tides between reference and scenario runs were matched and differences between the tidal characteristics (ΔTC) were computed for each tide.

4 Investigation of a mean sea level rise scenario

4.1 Experimental design

As mentioned in the introduction, attention was paid to decrease the uncertainty of the projections induced by internal variability of the system. In climate impact studies investigating the impact of changes in meteorological conditions directly (e.g. wind on storm surges as in GASLIKOVA et al. 2012), this can be solved by simulation of data from global climate model runs with varying initial conditions.

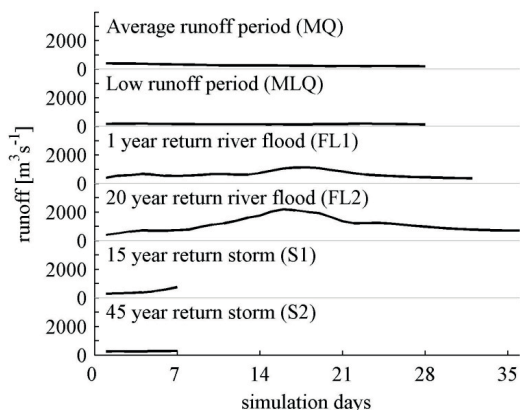


Figure 4: Representation of the reference state.

In this impact study however, the most dominant cause for change is not the impact of the meteorological forcing directly, but changes in boundary conditions from other systems such as the North Sea or the watershed. Due to limited information on the transient changes of the boundary conditions and limited numerical capacity, the impact simulations of this study are limited to shorter time periods. When this is the case, the simulated time slices should be chosen in a way to best capture the whole variability of the present state. In this respect, this study adapts the approach of projects like KRIM or KLIMU (e.g. GRABEMANN et al., 2001) and tests the investigated scenarios on a set of simulations each representing different characteristic situations in the reference state. The simulations are based on past events with boundary conditions generated from

measurements. The choice of simulations is based on the analysis of the present state (see Section 2). In total, six periods were chosen which represent typical periods of average runoff (MQ), low runoff (MLQ) and river floods with return values of approximately one and 20 years as well as storm surges (Fig. 4). This contribution however focuses only on results derived from the first four periods.

4.2 Investigated scenario

This contribution focuses solely on the results of a simple mean sea level rise (MSLR) scenario, which is considered a “likely” scenario. The investigated MSLR is 0.74 m which is based on the 5th assessment report of the Intergovernmental Panel on Climate Change (IPCC) and is there presented as the “most likely” value for global rise in 2100, assuming the representative concentration pathway RCP8.5 (IPCC 2013). In addition to this, a high end scenario was tested in this project which is not shown here. The MSLR is added to the time series for water surface elevation at the open North Sea boundary as a constant. This simplified approach is further discussed in Section 5. Neither taken into account in the results presented here are salinity changes at the open boundaries. Gradual changes of bathymetric and bottom roughness due to altered sedimentation patterns in the domain itself or changed roughness are to be expected, but not considered in the results presented here.

4.3 Results

The simulations of the reference state (see Section 4.1) were repeated with boundary conditions adapted to the investigated scenario (see Sec 4.2). Box- and whisker plots of the computed ΔTC (see Section 3.3) are presented in Fig. 5 and 6. This contribution only presents results for three focus regions in the study region. The focus region BHV is located just north of the entrance to the narrow Unterweser reach of the estuary at Bremerhaven approximately 75 km from the tidal weir. It is characterized by a highly variable salinity depending on the tidal phase and the runoff. The focus region BRA is located at the latitude of the city of Brake in the inner estuary (45 km distance from weir) and is at today’s beginning of the brackish water zone, meaning that salinities are mostly below 1 psu except for summer and autumn when they can hit peaks of 5 psu during high tide. The focus region HB is located in the tidal freshwater reach about 15 km from the weir.

The results presented in Fig. 5 illustrate that the investigated scenario of 0.74 m of MSLR at the open boundary leads to a change in tidal dynamics. In the upstream part of the inner estuary, an increase of the M2 and M4 tidal constituent amplitudes (not shown here) leads to increase of tidal range TR. In focus region HB, this increase amounts to approximately 15 cm (Fig. 5d). The increase in TR goes along with a decrease of the tidal low water LW relative to the imposed MSLR (Fig. 5c). The tidal high water (Fig. 5b) is less affected and the roughly corresponds to the imposed MSLR. The increase in mean water level (Fig. 5a) is lower than the imposed MSLR, which is again more pronounced upstream the estuary. All in all, the computed ΔTC s are similar for the four representations of the reference state MQ, MLQ, FL1 and FL2.

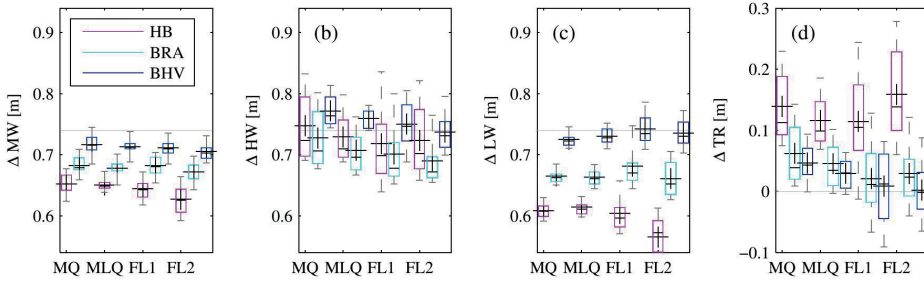


Figure 5: Computed differences ΔTC for water surface elevation between the MSL 0.74 m scenario- and the reference simulations for three focus areas. The boxes and whiskers indicate 25/75 % and 10/90 % percentiles, respectively, medians are shown as (-), means as (+).

The salinity is also affected by the scenario which is shown in Fig. 6. Generally, the mixing zone between salt and fresh water (see Fig. 2) intrudes further upstream the estuary (not shown here, see for example SEIFFERT et al., this volume). This leads to an increase of salinity upstream the estuary. The average salinity S_M increases by approx. 2 psu in focus region BHV (Fig. 6a). This applies to the simulations of average and low runoff and also to periods of river floods. In the focus region BRA, only a very small increase of S_M can be observed, but the tidal maximum salinity S_{MAX} increases by almost 1 psu during the MNQ simulation (Fig. 6b). This shows that especially during low runoff conditions in summer, increased salinity may be a problem for use of estuarine water in this region.

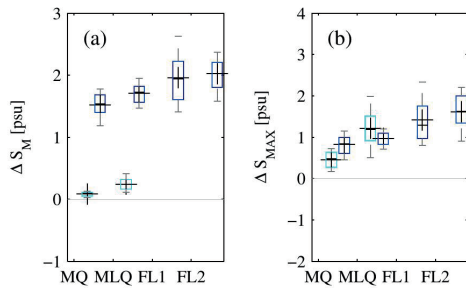


Figure 6: Continued from Figure 5 for salinity.

The changes in tidal dynamics are accompanied by changes in the current velocities in main channel direction. The simulations reveal that the intensity of the flood current is strengthened in comparison with the ebb current velocities (not shown here).

5 Summary and discussion

The aim of the project presented here is to investigate impacts of climate change on hydrodynamics and salinities of the Weser estuary, Germany. A 3D hydrodynamic model of the estuary was built up and validated successfully. To describe the present state of the estuary and best capture internal natural variability, a set of simulations was chosen all representing different characteristic periods of the current state such as river floods, average and low runoff and storm surges. A simple scenario with a MSLR of 0.74 m was

simulated and characteristic values of the scenario simulations were compared to those of the reference simulations.

Results show that the overall rise in mean water level is accompanied with changes in the tidal dynamics. In particular, an increase in tidal range with a fall of the low water levels as well as an increase of flood in relation to ebb current can be observed. The salinity in the inner estuary increases. There is a general tendency towards an upstream displacement of the mixing zone and null point of bottom residual current velocity. The reason for the upstream displacement may be the intensification of flood current due to decrease of dissipation.

To put the results into perspective and derive meaningful information for practitioners and decision makers, it is crucial to shortly discuss the uncertainties of the investigated scenario and comment on the confidence of the results. According to the IPCC (2013) it is "virtually certain" that the rate of global mean sea level rise (GMSLR) has accelerated during the last centuries and future rise rates are „very likely“ to exceed those observed in the last years. Projections for the GMSLR until 2100 are presented for different representative concentration pathways (RCPs), all providing a likely range and an average. This project focuses on RCP8.5, assuming a continued rise in greenhouse gas emissions. From the range of likely GMSLR values given for this scenario, the most likely one is chosen. On the global scale, this value can be assigned a "medium confidence" for RCP8.5 (IPCC 2013), but it should be mentioned that the confidence decreases drastically when the GMSLR is projected directly to the boundary condition of the Weser due to two reasons: To begin with, there is evidence that the GMSLR will not be distributed evenly on the globe. However, adapting the global projection is not possible due to limited knowledge on these processes. Secondly, there is evidence that the tidal dynamics (TDs) in the North Sea will change which might lead to higher or lower tidal range in the German Bight. The impact of MSLR on the North Sea TDs has recently been investigated in some studies but the most reliable results are still provided by PLÜB (2004) due to better resolution of the Wadden Sea area. However, PELLING et al. (2013) have shown with a simplified experimental design that TD changes mainly depend on the energy dissipation induced by the flat Wadden Sea areas of the German Bight. This indicates that changes in sedimentation patterns and possibly coastline changes will play an important role for the future changes in TDs under a MSLR. Therefore, it can be argued that not deforming the tidal signal at the German Bight inherits the same amount of boundary condition uncertainty as deforming it without further investigating TD changes in the North Sea. Furthermore, as mentioned in Section 4.2, changes in sedimentation patterns can be expected to occur within the Weser just as they will within the North Sea. As bathymetry and roughness can be considered boundary conditions in this respect, this leads to further boundary condition uncertainty which will be investigated in further research within this project.

Despite these uncertainties in scenario and boundary conditions, the results derived from the scenario presented here can be seen as a best estimate at the time, assuming that greenhouse emissions do not decline. As mentioned earlier, the investigations will be complemented by a high end scenario and further investigations aiming for quantifying uncertainties induced by boundary conditions.

6 References

- GASLIKOVA, L.; GRABEMANN, I.; and GROLL, N.: Changes in North Sea storm surge conditions for four transient future climate realizations. *Natural Hazards*, Vol. 66(3), 1501-1518, 2012.
- GRABEMANN, H.-J.; GRABEMANN, I., HERBERS, D. and MÜLLER, A.M.: Effects of a specific climate scenario on the hydrography and transport of conservative substances in the Weser estuary, Germany: a case study. *Climate Research*, Vol. 18, 77-87, 2001.
- IPCC, 2013: Summary for Policymakers. In: STOCKER, T.F.; Qin, D.; PLATTNER, G.-K.; TIGNOR, M.; ALLEN, S.K.; BOSCHUNG, J.; NAUELS, A.; XIA, Y.; BEX, V. and MIDGLEY, P.M. (eds.): *Climate Change 2013: The Physical Science Basis. Contribution of Working Group I to the Fifth Assessment Report of the Intergovernmental Panel on Climate Change*. Cambridge University Press, 2013.
- KREYE, P.; GOCHT, M.; FÖRSTER, K.: Entwicklung von Prozessgleichungen der Infiltration und des oberflächennahen Abflusses für die Wasserhaushaltsmodellierung. *Hydrologie und Wasserbewirtschaftung*, Vol. 5, 268-27, 2010.
- MURPHY, A.H.: Skill Scores Based on the Mean Square Error and Their Relationships to the Correlation Coefficient. *Monthly Weather Review*, Vol. 16, 2417-2424, 1988.
- PELLING, H.E.; GREEN, J.M., and WARD, S.L.: Modelling tides and sea-level rise: To flood or not to flood. *Ocean Modelling*, Vol. 63(0), 21-29, 2013.
- PLÜB, A.: Nichtlineare Wechselwirkung der Tide auf Änderungen des Meeresspiegels im Übergangsbereich Küste/Ästuar am Beispiel der Elbe. In: GÖNNERT, G.; GRASSL, H.; KELLETAT, D.; KUNZ, H.; PROBST, B.; VON STORCH, H. and SÜNDERMANN, J. (eds): *Klimaänderung und Küstenschutz*. Universität Hamburg, 129-138, 2004.
- SCHIRMER, M. and SCHUCHARDT, B.: Assessing the impact of climate change on the Weser estuary region: an interdisciplinary approach. *Climate Research*, Vol. 18, 133-140, 2001.
- SIMPSON, J.H.; BROWN, J.; MATTHEWS, J. and ALLEN, G.: Tidal straining, density currents, and stirring in the control of estuarine stratification. *Estuaries*, Vol. 13, 125-132, 1990.
- YANG, J.; GRAF, T.; HEROLD, M. and PTAK, T.: A fully coupled surface-subsurface approach to simulate flow dynamics in coastal aquifers. *Journal of Contaminant Hydrology*, Vol. 149, 61-75, 2013.
- ZHANG, Y.J. and BAPTISTA, A.M.: SELFE: A semi-implicit Eulerian-Lagrangian finite-element model for cross-scale ocean circulation. *Ocean Modeling*, Vol. 21, 71-96, 2008.
- ZORNDT, A.C.; SCHLURMANN, T. and GRABEMANN, I.: The influence of extreme events on hydrodynamics and salinities in the Weser estuary in the context of climate impact research. *Proceedings of the International Conference on Coastal Engineering*, Vol. 33, 2012.

Investigating Climate Change Impacts and Adaptation Strategies in German Estuaries

Rita Seiffert and Fred Hesser

Summary

Due to sea level rise, estuaries are particularly affected by climate change. Besides sea level rise, changes in precipitation resulting in changing fresh water discharge and changes in storm activities can also have an impact on estuaries. The Elbe, Jade-Weser and Ems estuaries located in the German Bight (North Sea) are not only important ecosystems, they are also used as waterways. We need to know how climate change affects the estuaries in order to develop adaptation strategies. Generally, it is difficult to project climate change impacts on a local scale. The uncertainties involved can become very large. In this paper we describe an approach to determining the impacts of local climate change and to the investigation of adaptation measures without getting lost in the large range of uncertainty. First, we identify the main drivers which are assumed to be altered by climate change. In the next step we carry out sensitivity studies in which the main drivers are varied. For the sensitivity studies we use 3D-hydrodynamic numerical models. To test possible adaptation measures we repeat selected simulations which then include different adaptation measures. The results on local climate change impacts suggest that today's challenges are likely to become more acute. Higher salinities, increased upstream sediment transport, and higher water levels during storm surge must be expected. Adaptation measures can reduce these effects.

Keywords

hydrodynamic numerical model, uncertainties, sensitivity study, sea level rise, fresh water discharge, waterways, tidal dynamic, salt transport, sediment transport, storm surge

Zusammenfassung

Aufgrund des Meeresspiegelanstiegs sind Ästuarie besonders durch den Klimawandel betroffen. Neben dem Meeresspiegelanstieg können auch Änderungen im Niederschlag, die den Oberwasserzufluss beeinflussen, und veränderte Sturmverhältnisse Auswirkungen auf die Ästuarie haben. Die Ästuarie Elbe, Jade-Weser und Ems werden als Wasserstraßen genutzt und bilden wichtige Ökosysteme. Voraussetzung für die Entwicklung von Anpassungsoptionen ist das Verständnis darüber, wie sich der Klimawandel auf die Ästuarie auswirkt. Im Allgemeinen ist es schwierig die Folgen des Klimawandels auf lokaler Ebene abzuschätzen, da die Unsicherheiten groß werden können. In diesem Artikel beschreiben wir eine Herangehensweise, wie lokale Folgen des Klimawandels und Anpassungsoptionen trotz großer Unsicherheiten analysiert werden können. Im ersten Schritt identifizieren wir die Haupteinflussfaktoren, die voraussichtlich durch den Klimawandel beeinflusst werden. Anschließend führen wir Sensitivitätsstudien durch, in denen die Haupteinflussfaktoren variiert werden. Dafür verwenden wir 3D-hydrodynamisch-numerische Modelle. Um Anpassungsoptionen zu untersuchen, wiederholen wir ausgewählte Simulationen unter

Berücksichtigung verschiedener Anpassungsmaßnahmen. Die Ergebnisse zu den Folgen des Klimawandels deuten darauf hin, dass sich Herausforderungen, die schon heute bestehen, vergrößern werden. Es muss mit höheren Salzgehalten, einem verstärkten Transport von Sedimenten nach stromauf und höheren Sturmflutscheitelwasserständen gerechnet werden. Die untersuchten Anpassungsmaßnahmen zeigen, dass sie die Auswirkungen reduzieren können.

Schlagwörter

Hydrodynamisch-numerisches Modell, Unsicherheiten, Sensitivitätsstudien, Meeresspiegelanstieg, Oberwasserzufluss, Wasserstraße, Tidedynamik, Salztransport, Sedimenttransport, Sturmflut

Contents

1	Introduction	552
2	Method.....	553
3	Results of sensitivity studies	555
3.1	Local climate change impacts.....	555
3.2	Development of adaptation strategies	558
4	Discussion and conclusions	560
5	Acknowledgements.....	561
6	References	562

1 Introduction

Increasing atmospheric greenhouse gas concentrations lead to changes in climate. Climate change affects people and wildlife almost everywhere. Due to global sea level rise, coastal areas in particular are affected. The Elbe, Jade-Weser, and Ems estuaries, located in the German Bight (North Sea), form important ecosystems which provide unique conditions for wildlife. They are also used as waterways and represent important economic factors. Climate change might restrict estuaries in their function as waterways. For the development of adaptation strategies we need to know how climate change will affect the estuaries. Climate change may, for example, impact tidal dynamics, salt transport, transport of sediments, and extreme water levels in the event of storm surges.

To date, few studies have investigated the local impacts of climate change and adaptation strategies in the estuaries of Elbe, Jade-Weser or Ems. GRABEMANN et al. (2001) explore the impact of climate change on the hydrography and water quality of the Weser estuary. They simulate one climate scenario using a 1-dimensional water quality and transport model. PLÜB (2004) studies the effects of sea level rise on tidal dynamics in the Elbe estuary. He carries out simulations with different sea level rises using a 3D-hydrodynamic numerical model. His analysis concentrates on water levels. ZORNDT and SCHLURMANN (2014) investigate the effects of sea level rise in the Weser estuary (see this volume). They also use a 3D-hydrodynamic numerical model. Their analyses focus on changes of characteristic numbers of water level and salinity. Other studies on climate change impacts and adaptation strategies in the German estuaries concentrate on storm

surge protection (LIEBERMANN et al. 2005; GROSSMANN et al. 2006). Studies of climate change impacts in the Elbe, Jade-Weser, and Ems estuaries that focus specifically on the needs of navigation are not available.

Within the framework of the research project KLIWAS (Impacts of climate change on waterways and navigation - Searching for options of adaptation) we investigate potential climate change impacts on German estuaries and develop adaptation strategies with regard to the needs of navigation. The overall KLIWAS project considers both coastal and inland waterways in Germany. With a chain of models (e.g., global climate models, regional climate models, hydrological models, and hydrodynamic models) the global climate change signal is downscaled step by step to the local waterways.

The outcomes at the end of this downscaling process are in many cases difficult to interpret because the uncertainties attached to them are large. All models represent nature in a simplified way. Additionally, boundary conditions contain assumptions and are taken from other models or observations that do not represent nature in a perfect way either. For this reason the uncertainties become larger at each step of the downscaling process. At the end of the downscaling process the uncertainties attached to local climate change signals can be large (WILBY and DESSAI 2010; CARTER et al. 2007). Hence it is difficult to determine the local impacts of climate change on small regions such as estuaries.

LOWE et al. (2009) describe one way of dealing with these uncertainties. They develop adaptation strategies for storm surge protection in the Thames estuary in relation to sea level rise. A key idea of their approach is to define threshold levels of sea level rise up to which different adaptation strategies would work. Although they do not know how high sea level is rising, they prepare an adaptation plan for different potential scenarios. This adaptation plan must also include time horizons for planning and implementing the adaptation measures. KWADIJK et al. (2010) describe a similar approach. They introduce the concept of adaptation tipping points. Adaptation tipping points are points in time at which, in the face of climate change, existing measures will no longer be able to meet their objectives. The aim of applying the concept of adaptation tipping points is to determine the amount of climate change and rise in sea level an existing measure will be able to cope with. A sensitivity study is performed to identify adaptation tipping points.

We also carry out sensitivity studies. Whereas LOWE et al. (2009) and KWADIJK et al. (2010) mainly concentrate on the development of adaptation strategies, we combine the investigation of local impacts and the development of adaptation measures. This paper describes a method for using hydrodynamic numerical models to explore climate change impacts on small regions such as estuaries and for the development of adaptation strategies. We present the main findings of different sensitivity studies in the results section of this paper.

2 Method

For the simulation of hydrodynamic processes we use the hydrodynamic numerical model UnTRIM (CASULLI and WALTERS 2000; CASULLI and LANG 2004) in the version of UnTRIM2007 coupled with the morphological model SediMorph (MALCHEREC et al. 2005). UnTRIM is a semi-implicit finite difference model. It solves the three-dimensional shallow water equations and the transport equations of salt, heat, and suspended sediments on an unstructured grid. SediMorph computes the sedimentological processes at

the alluvial bed of the estuaries. We use it in a mode in which morphodynamic changes of water depths are not simulated. For each estuary we apply an individually calibrated model. The resolution in space and time, the size of the model domain, and the length of the time period simulated depend on the question focused on. The horizontal resolutions of the unstructured grids vary from a few metres to several hundreds of metres. The time periods simulated range from a few days to several months. Compared with climate simulations, which usually simulate several decades, our simulation time periods are rather short. These short simulation time periods are possible, because the modelled processes respond rapidly to changes of external drivers.

To explore possible climate change impacts on the estuaries we carry out several sensitivity studies. In a first step we identify the main drivers that are presumably affected by climate change. The main drivers of the local system are the most important external parameters forcing the local processes. They affect the characteristics of water levels, current velocities, salt transport, and sediment transport. The main drivers are sea level and the tidal signal in the North Sea, fresh water discharge, and wind. The bathymetry of the estuary also determines the hydrodynamics, but future changes in bathymetry are difficult to estimate. Changes in bathymetry are inhomogeneous in space and determined by anthropogenic activities such as dredging and dumping of sediments as well as by natural processes. For this reason we keep the bathymetry constant. Sea level, fresh water discharge, and local wind are varied both separately and in combination. They are modified within the range of expected possible future climate values. Sea level is rising due to climate change. Long periods with little precipitation in the catchment area can result in long-lasting low fresh water discharge. On the other hand, extremely high precipitation can lead to very high fresh water discharge. Wind affects the estuary mainly during storm surges. Higher wind velocities would increase highest water levels.

A sensitivity study consists of the simulation of the reference state and of one or more scenarios in which the main drivers are varied. The comparison of the scenarios and the reference state reveals how water levels, currents, salinity, and sediment transports react to changed boundary conditions. Thresholds can be identified that cause increased vulnerability. In the next step we investigate the efficacy of different adaptation measures. We repeat selected simulations of the sensitivity studies. This time, however, we include adaptation measures in the numerical model (Fig. 1). This approach presents a direct way to test and compare the adaptation measures.

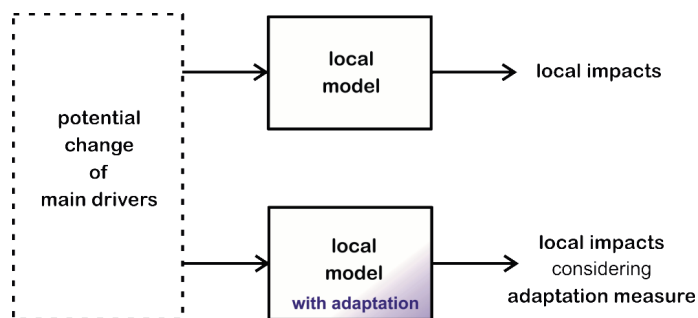


Figure 1: Schematic diagram of the investigation of local climate change impacts and adaptation measures, adapted from SEIFFERT et al. (2013).

3 Results of sensitivity studies

3.1 Local climate change impacts

In one of the sensitivity studies we vary sea level in the North Sea to investigate the impacts of sea level rise on tidal dynamics. We increase sea level in the North Sea by 80 cm. This value lies within the range of estimates for sea level rise in the North Sea up to the end of this century (GÖNNERT et al. 2009). The choice of 80 cm does not imply that this value is more likely than other values. It is well suited for our purpose of investigating the main processes involved when sea level rises. A detailed description of the simulations carried out for this sensitivity study can be found in HOLZWARTH et al. (2011). The study shows that water levels in the interior of the estuaries do not just increase uniformly due to sea level rise. Tidal dynamics change. In most parts of the estuaries high water levels rise more than low water levels (Fig. 2). Thus the tidal range is larger in the model simulations that include sea level rise. The shape of the tidal curve is changed. Flood current velocities increase more strongly than ebb current velocities in many parts of the estuaries. There is an increase in the ratio of flood current velocity to ebb current velocity (Fig. 3). Due to the larger ratio of flood current velocity to ebb current velocity more sediment is transported in the upstream direction. An exception is the upper part of the Lower Ems. In this part the ratio of flood current velocity to ebb current velocity decreases.

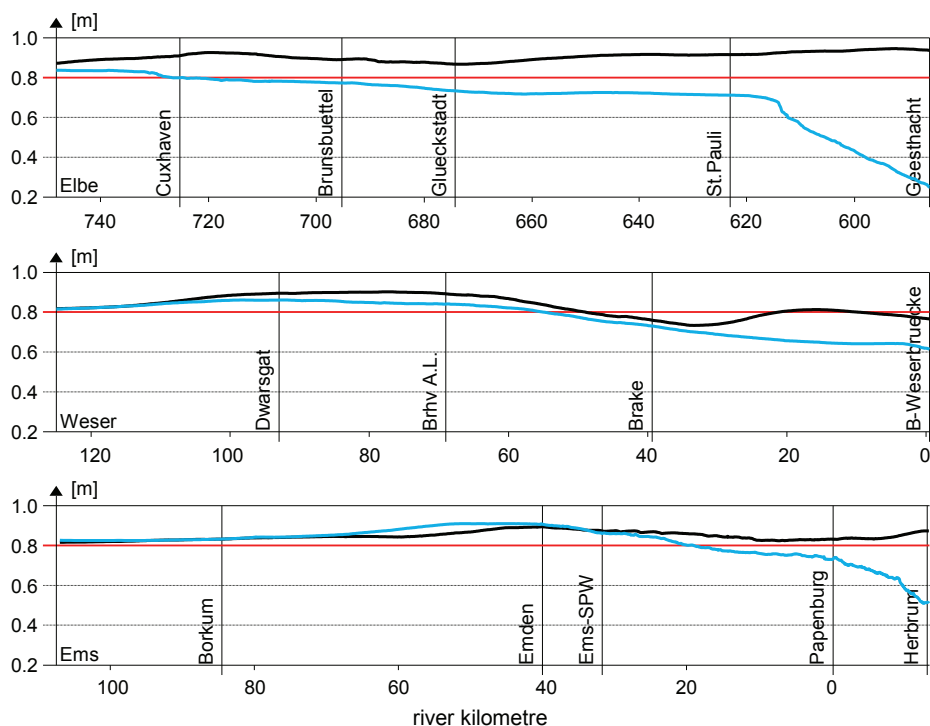


Figure 2: Change of mean high water levels (black) and mean low water levels (blue) due to a sea level rise of 80 cm along the fairways of the estuaries Elbe, Weser, and Ems.

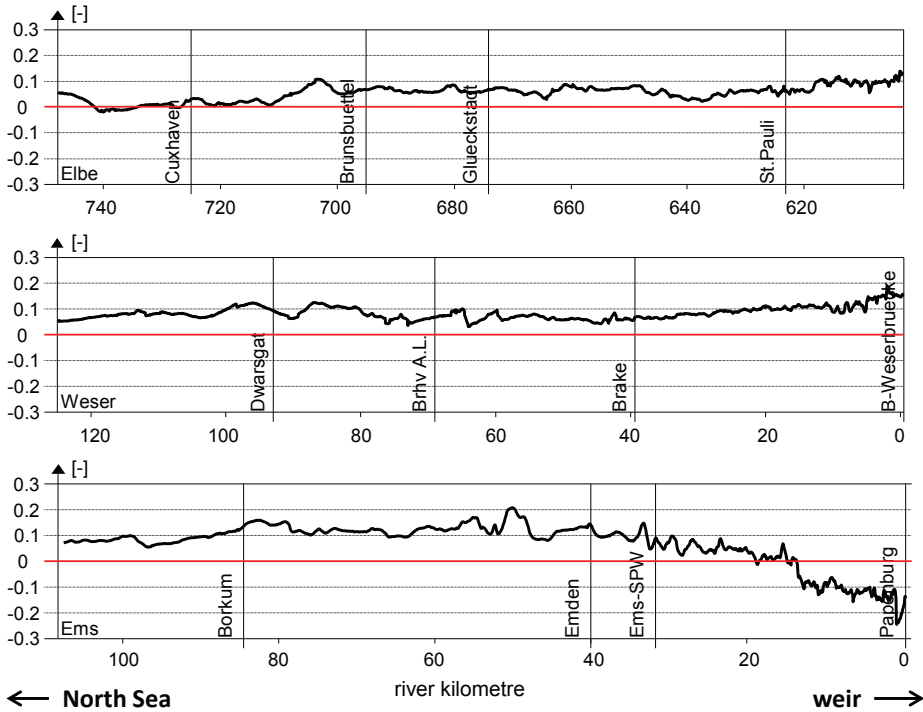


Figure 3: Change of the ratio flood current velocities (mean) to ebb current velocities (mean) due to a sea level rise of 80 cm along the fairways of the estuaries Elbe, Weser and Ems.

In another study we investigate the intrusion of salt into the estuaries in the event of long-lasting low fresh water discharge and sea level rise (SEIFFERT et al. 2012). Long-lasting low fresh water discharge is assumed, since periods with little precipitation in the catchment area can result in low fresh water discharge (NILSON et al. 2014). In different simulations with and without sea level rise fresh water discharge is held constant over several weeks, first at the mean measured freshwater discharge (MQ) and then at the mean of the lowest discharge measured per summer half-year (SoMNQ). The results of this study show that both low fresh water discharge and sea level rise generally lead to higher salinities in the inner estuary (Fig. 4). In comparison, long-lasting low fresh water discharge can have a much larger effect on salinities than a sea level rise of 80 cm. The combination of both results in the highest salinities. Changes in sea level and fresh water discharge, however, act and last on different time scales. Whereas fresh water discharge fluctuates on rather short time scales and leads to short term increases in salinity, mean sea level rises very slowly but leads to permanent changes.

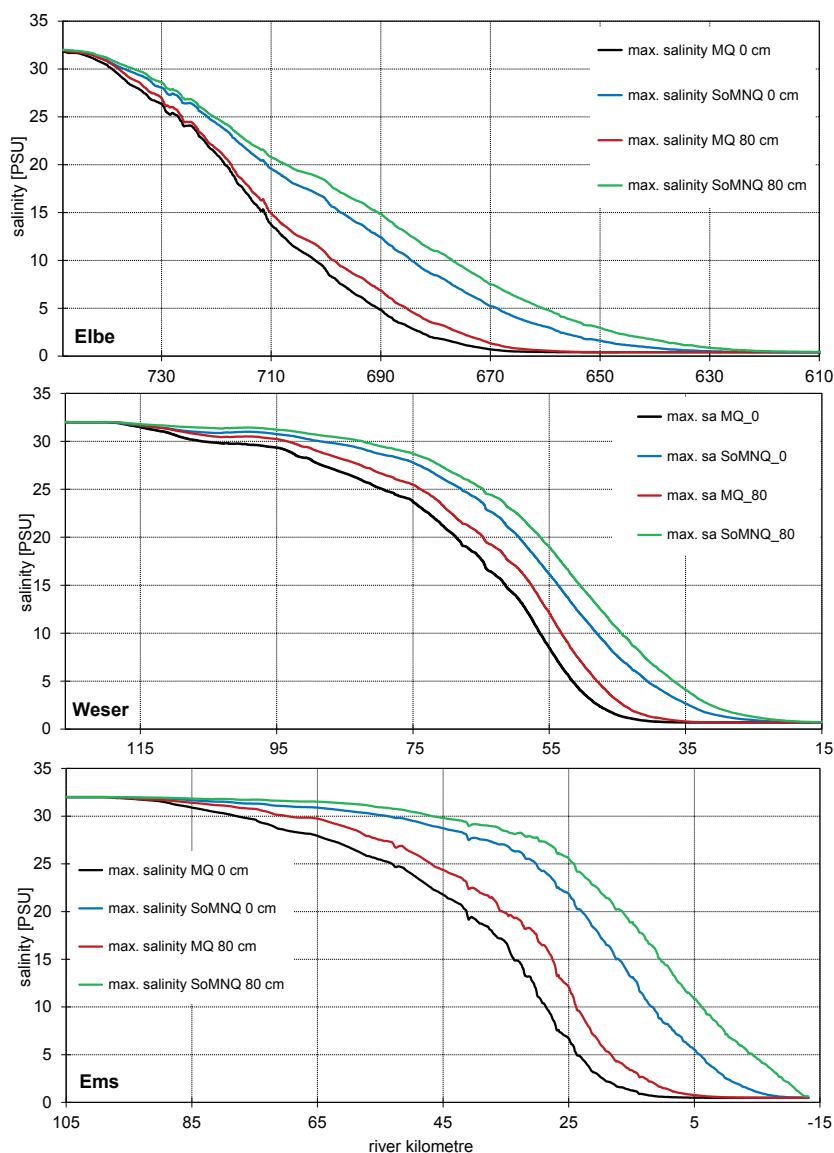


Figure 4: Maximum salinity (averaged over one spring-neap cycle) along the fairways. Black: mean fresh water discharge (MQ). Red: mean fresh water discharge and a sea level rise of 80 cm. Blue: low fresh water discharge (SoMNQ). Green: low fresh water discharge and a sea level rise of 80 cm.

The results of a sensitivity study on climate change impacts in the case of storm surges are shown in RUDOLPH (2014) in this volume. In this sensitivity study historical storm surges are simulated with different sea level rises, wind velocities, and high freshwater discharge. The study shows that the effects of sea level rise reach far into the interior of the estuaries. The highest water levels in the inner estuary are approximately increased by

the sea level rise that is applied at the mouth of the estuary. Higher wind velocities would increase highest water levels, too. In the upper part of the estuary fresh water discharge dominates highest water levels.

3.2 Development of adaptation strategies

The sensitivity studies referred to above show that climate change is likely to amplify the challenges we are already facing today. Higher salinities, increased upstream sediment transport, and higher water levels during storm surge must be expected. The aim of investigating adaptation strategies is to check and improve existing measures as well as to develop new adaptation measures. An adaptation strategy can include different possibilities. With respect to the maintenance of waterways, for example, sediment management in the estuaries could be adapted. Hydraulic engineering structures are another potentially suitable adaptation response. We investigate exemplarily different measures.

In the Ems estuary a groundsill at the storm surge barrier near Gandersum is discussed. Numerical simulations suggest that a groundsill could decrease sediment import from the North Sea. This would then reduce the necessary dredging effort. Using the approach described above (Fig. 1) we test whether the groundsill would still work under climate change. We find that it is still effective when sea level rises and fresh water discharge is low (SEIFFERT et al. 2014).

Storm surge barriers provide protection against storm surges. Today the storm surge barrier in the Ems estuary near Gandersum protects the hinterland against the extreme water levels which occur during storm surge. To test how the storm surge barrier works under future climate conditions, we carry out a sensitivity study with different sea level rises and fresh water discharges (RUDOLPH et al. 2012). The results show that the barrier effectively protects the hinterland up to a certain level of sea level rise (Fig. 5).

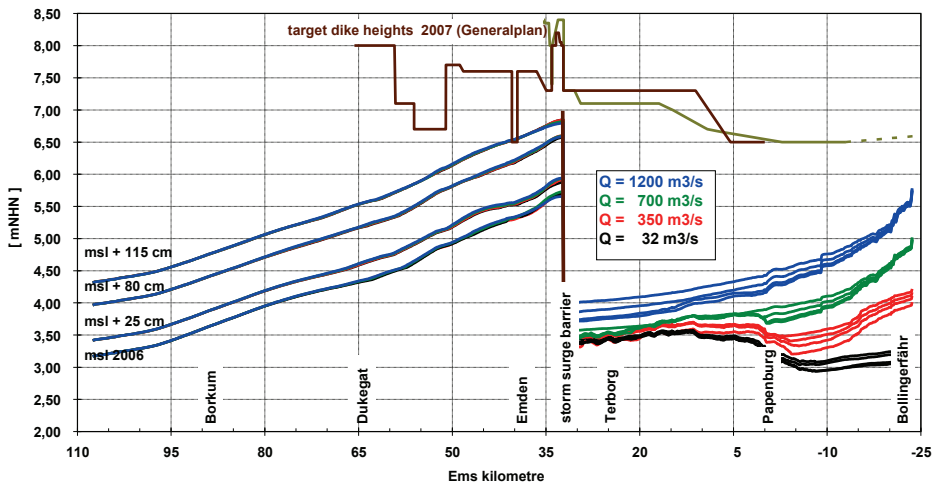


Figure 5: Highest water levels along the fairway of the Ems estuary for different mean sea level (msl) rises and fresh water discharges (Q). The storm surge barrier is closed when the water level reaches NHN +3.50 m at the barrier.

Similar to the barrier in the Ems estuary a storm surge barrier in the mouth of the Weser estuary can be an option. Our simulations with and without barrier and sea level rise show that a storm surge barrier near Bremerhaven would effectively protect the areas in the upstream direction of Bremerhaven (SEIFFERT et al. 2014). Sea level rise has no effect on water levels upstream of the barrier when the barrier is closed (Fig. 6). Coastal areas seaward of the barrier are still exposed to sea level rise. Additionally, the barrier itself can affect highest water levels on the seaward side. Depending on the closing time of the barrier a surge wave can be released. A surge wave develops if the closing time coincides with pronounced flood current velocities.

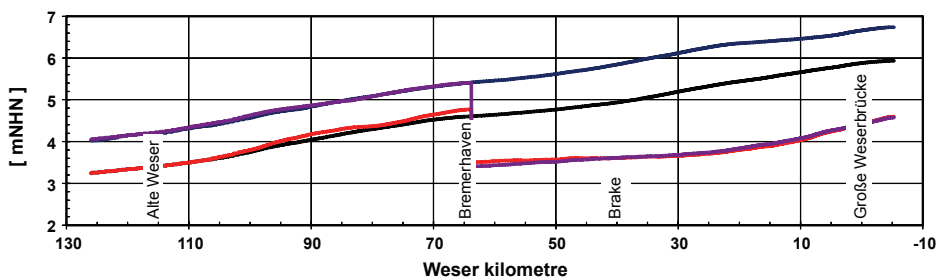


Figure 6: Highest water levels along the fairway of the Weser estuary of the simulated storm surge on 1 November 2006 (black), with 80 cm sea level rise (blue), with storm surge barrier (red), with 80 cm sea level rise and with storm surge barrier (purple).

Storm surge barriers completely block the entrance of estuaries during storm surges. Alternatively, measures could be taken to narrow the mouth of the estuary (SEIFFERT et al. 2014). This would dampen storm surges entering the estuary. Measures narrowing the mouth would have less impact on navigation. Furthermore they could also have positive effects on sediment transport under normal tidal conditions (KLÖPPER 2013). Fig. 7 shows two measures in the mouth of the Elbe estuary: an island located in the outer area of the mouth and a dam closer to the inner area of the mouth. The height of both measures is NNH +10 m.

Fig. 8 shows the results of simulations of the storm surge on 1 November 2006 with and without these two measures. The island has almost no effect on highest water levels. On the contrary, the dam reduces highest water levels along the whole estuary upstream of the measure by around 20 cm. The dam is more effective because the actual flow cross section is narrowed much more by the dam than it is by the island further out to sea. Generally, the more the measure narrows the cross section, the greater the reduction in highest water levels. Compared with a storm surge barrier, which blocks incoming storm surges completely, the dam only partly reduces the impact of sea level rise.

The measures also influence current velocities. In the area of the fairway near the dam current velocities are considerably increased. High current velocities can result in intensified erosion rates and affect navigation.

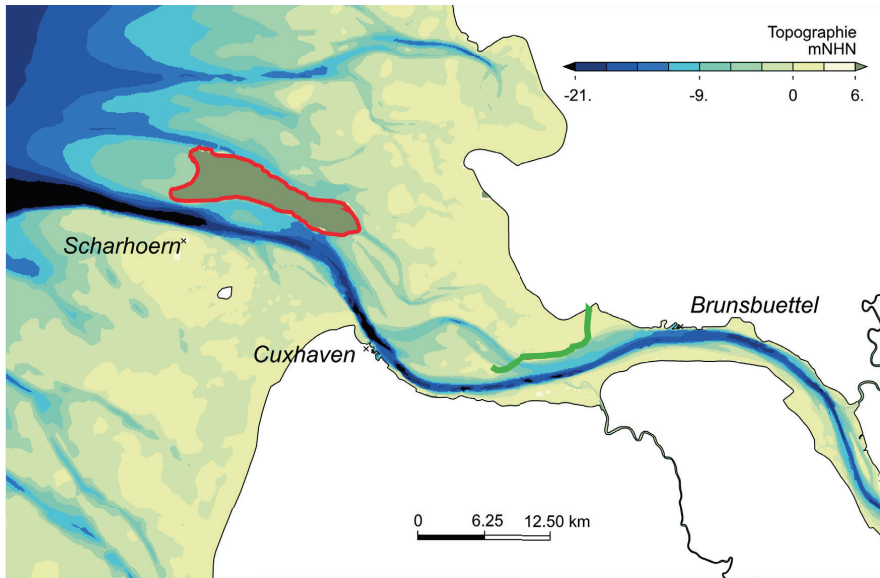


Figure 7: Mouth of the Elbe estuary with two different measures narrowing it: an island located in the outer area of the mouth (red) and a dam located closer to the inner area of the mouth (green).

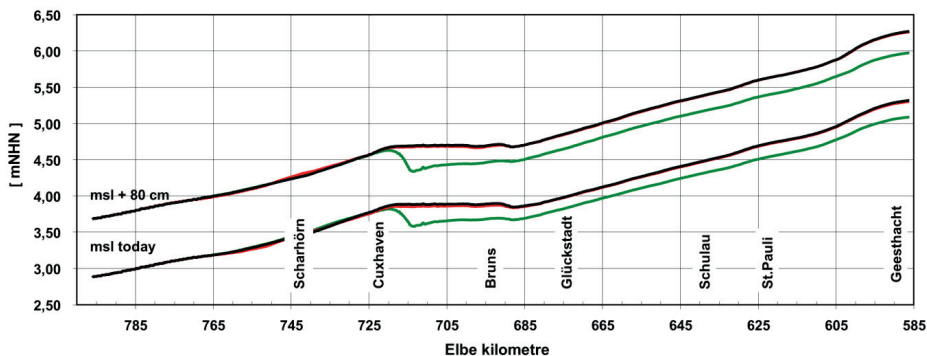


Figure 8: Highest water levels along the fairway of the Elbe estuary of the simulated storm surge on 1 November 2006 with and without sea level rise of 80 cm, black: no narrowing measures, red: with island, green: with dam.

4 Discussion and conclusions

In this paper we have shown how hydrodynamic numerical models can be used to investigate climate change impacts and adaptation strategies on a local scale. The challenge is to investigate climate change impacts in a specific local system without getting lost in the large range of uncertainties. Sensitivity studies help us to gain a better understanding of the processes involved. They produce clear if-then-statements which are easy to understand. Of course, uncertainties are not actually reduced by the formulation of if-then-

statements. By definition, each if-then-statement is based on an assumption. Typically, no or little extra information about the likelihood of an assumption being correct is given. The probability of an assumption being correct is simply not known. For example, we do not know how far the sea level will have risen in the North Sea by the year 2100. Therefore, it is not possible to make a forecast, for example, about the increase of the tidal range by the value x at year 2100. Sensitivity studies reveal whether we should expect an increase or decrease and provide us with some idea about the order of magnitude of changes. Thus, it is not important what particular assumption we make for single simulations.

The length of numerical simulations carried out can be kept short since estuarine processes respond rapidly to changes in external conditions. The response time of morphodynamic processes is an exception. The simulation of long-term morphodynamic processes, however, is associated with a high degree of uncertainty. The models require further development in order to produce feasible results. This is one reason why we keep the bathymetry static in all simulations. This does mean, however, that we do not take account of the feedback processes connected to morphodynamic processes. For example, the sensitivity study that explores the effects of sea level rise implies an increased transport of sediments from the North Sea into the estuaries due to sea level rise. This means more sediment is deposited in the estuaries. To ensure safety and efficient navigation more dredging effort might be the consequence. Based on the assumption of no dredging activities, more deposition would lead to shallower water depths. The water depth, in turn, influences tidal dynamics and thereby sediment transport. Long-term morphodynamic simulations will be needed in future studies in order to include the feedback processes associated with morphodynamic processes.

The adaptation measures presented in this paper are first suggestions about what such measures could be and how they can be tested using hydrodynamic numerical models and sensitivity studies. The results of this study lay the groundwork for further investigations. Such further investigations should not only include optimisation with regard to hydraulic effectiveness but should also consider impacts on other sectors, e.g. ecology. Generally, preference should be given to the development of cross-sectoral adaptation strategies. However, impacts on other sectors must be investigated and taken into account at the very latest as soon as serious consideration is given to applying an adaptation measure.

5 Acknowledgements

This work has been carried out within the research programmes KLIWAS 'Impact of climate change on waterways and navigation' and KLIMZUG-Nord 'Regional strategies concerning climate changes in the metropolitan area of Hamburg'. KLIWAS was financed by the German Federal Ministry of Transport, Building and Urban Development; KLIMZUG-Nord is supported by the German Federal Ministry of Education and Research, the city of Hamburg, and the metropolitan area of Hamburg. We thank all co-workers of the KLIWAS/KLIMZUG-Nord team at the Federal Waterways Engineering and Research Institute in Hamburg for their support and for carrying out some of the simulations. Special thanks go to Annette Büscher, Ayla Johanna Bockelmann, Ingrid Holzwarth, Elisabeth Rudolph, Annkathrin Rinnus, and Norbert Winkel.

6 References

- CARTER, T.R.; JONES, R.N.; LU, X.; BHADWAL, C.; CONDE, C.; MEARN, L.O.; O'NEILL, B.C.; ROUNSEVELL, M.D.A. and ZUREK, M.B.: New Assessment Methods and the Characterisation of Future Conditions. In: PARRY, M.L., CANZIANI, O.F., PALUTIKOF, J.P., LINDEN, P.J. VAN DER and HANSON, C.E. (eds.): *Climate Change 2007: Impacts, Adaptation and Vulnerability. Contribution of Working Group II to the Fourth Assessment Report of the Intergovernmental Panel on Climate Change*. Cambridge, 133-171, 2007.
- CASULLI, V. and LANG, G.: *Mathematical Model UnTRIM Validation Document*. Technical Report. Bundesanstalt für Wasserbau Dienststelle Hamburg (BAW), http://www.baw.de/downloads/wasserbau/mathematische_verfahren/pdf/vd_unt_rim-2004.pdf, 2004.
- CASULLI, V. and WALTERS, R.A.: An unstructured grid, three-dimensional model based on the shallow water equations. In: *International Journal for Numerical Methods in Fluids*, Vol. 32, 3, 331-348, 2000.
- GÖNNERT, G.; JENSEN, J.; STORCH, H. VON; THUMM, S.; WAHL, T. and WEISSE, R.: *Der Meeresspiegelanstieg Ursachen, Tendenzen und Risikobewertung*. *Die Küste*, 76, 225-256, 2009.
- GRABEMANN, H.-J.; GRABEMANN, I.; HERBERS, D. and MÜLLER, A.: Effects of a specific climate scenario on the hydrography and transport of conservative substances in the Weser estuary, Germany: a case study. In: *Climate Research*, Vol. 18, 77-87, 2001.
- GROSSMANN, I.; WOTH, K. and STORCH, H. VON: Localization of Global Climate Change: Storm Surge Scenarios for Hamburg in 2030 and 2085. *Die Küste*, 71, 169-182, 2006.
- HOLZWARTH, I.; SCHULTE-RENTROP, A. and HESSER, F.: Auswirkungen klimabedingter Änderungen auf das Strömungs- und Transportverhalten deutscher Nordseeästuare. In: *Hafentechnische Gesellschaft e.V. (ed.): Vorträge HTG-Kongress 2011*. Würzburg, 275-282, 2011.
- KLÖPPER, M.: Dissipating Tidal Energy in the Mouth of the Elbe Estuary. In: *Hamburg Port Authority (HPA) and Flemish government, Department of Mobility and Public Works (MOW) (eds.): Joint Study on Mitigation Measures in the Estuary Mouth (Scheldt & Elbe)*. by HPA and MOW Jun. 2013. Bundesanstalt für Wasserbau Dienststelle Hamburg (BAW); Svasek Hydraulics, 2013.
- KWADIJK, J.C.J.; HAASNOOT, M.; MULDER, JAN P.M.; HOOGVLIET, MARCO M.C.; JEUKEN, AD B.M.; VAN DER KROGT, ROB A.A.; VAN OOSTROM, NIELS G.C.; SCHELFHOUT, H.A.; VAN VELZEN, EMIEL H.; VAN WAVEREN, H. and DE WIT, MARCEL J.M.: Using adaptation tipping points to prepare for climate change and sea level rise: a case study in the Netherlands. In: *Wiley Interdisciplinary Reviews: Climate Change*, Vol. 1, 5, 729-740, doi: 10.1002/wcc.64, 2010.
- LIEBERMANN, N. VON; GRABEMANN, I.; MÜLLER, A. and OSTERKAMP, S.: Vergleichende Abschätzung von Effektivität und Nebenwirkungen verschiedener Reaktionsvarianten des Küstenschutzes an der Unterweser gegenüber einer Klimaänderung. In: *SCHUCHARDT, B. (ed.): Klimawandel und Küste. Die Zukunft der Unterweserregion*. Berlin [u.a.], 243-254, 2005.

- LOWE, J.A.; HOWARD, T.; PARDAENS, A.; TINKER, J.; JENKINS, G.; RIDLEY, J.; HOLT, J.; WAKELIN, S.; WOLF, J.; HORSBURGH, K.; REEDER, T.; MILNE, G.; BRADLEY, S. and DYE, S.: UK Climate Projections Science Report: Marine and Coastal Projections. Met Office Hadley Centre, 95 p., 2009.
- MALCHEREK, A.; PIECHOTTA, F. and KNOCH, D.: Mathematical Module SediMorph Validation Document. Technical Report. Bundesanstalt für Wasserbau (BAW), http://www.baw.de/downloads/wasserbau/mathematische_verfahren/pdf/vd-sedimorph.pdf, 2005.
- NILSON, E.; KRAHE, P.; LINGEMANN, I.; HORSTEN, T.; KLEIN, B.; CARAMBIA, M. and LARINA, M.: Auswirkungen des Klimawandels auf das Abflussgeschehen und die Binnenschifffahrt in Deutschland. Schlussbericht KLIWAS-Projekt 4.01. Bundesanstalt für Gewässerkunde (BfG) und KLIWAS Koordination, Bundesanstalt für Gewässerkunde (BfG), Koblenz, (KLIWAS Schriftenreihe, KLIWAS-43/2014), doi: 10.5675/Kliwas_43/2014_4.01, 2014.
- PLÜß, A.: Nichtlineare Wechselwirkung der Tide auf Änderungen des Meeresspiegels im Übergangsbereich Küste/Ästuar am Beispiel der Elbe. In: GÖNNERT, G., GRABL, H., KELLETAT, D., KUNZ, H., PROBST, B., STORCH, H. von and SÜNDERMANN, J. (eds.): Klimaänderung und Küstenschutz. Universität Hamburg, 129-138, 2004.
- RUDOLPH, E.: Storm surge studies in the estuaries Elbe, Jade-Weser and Ems. *Die Küste*, 81, 2014.
- RUDOLPH, E.; SCHULTE-RENTROP, A.; SCHÜBLER, A. and JOHANNSEN, A.: Storm Surges in the Elbe, Jade-Weser, and Ems Estuaries - A Sensitivity Study against the Backdrop of Climate Change. In: Federal Ministry of Transport, Building and Urban Development (ed.): KLIWAS Impacts of Climate Change on Waterways and Navigation in Germany. 131-135, 2012.
- SEIFFERT, R.; HESSER, F.; BÜSCHER, A.; FRICKE, B.; HOLZWARTH, I.; RUDOLPH, E.; SEHILL, A.; SEIB, G. and WINKEL, N.: Auswirkungen des Klimawandels auf die deutsche Küste und die Ästuar. Mögliche Betroffenheiten der Seeschiffahrtsstraßen und Anpassungsoptionen hinsichtlich der veränderten Hydrodynamik und des Salz- und Schwebstofftransports - Schlussbericht KLIWAS-Projekt 2.04/3.02 (KLIWAS Schriftenreihe, 36), doi: 10.5675/Kliwas_36/2014_3.02, 2014.
- SEIFFERT, R.; RUDOLPH, E. and WINKEL, N.: Investigating Impacts and Developing Adaptation Strategies on Local Scale - An Example. In: Impacts World 2013 Conference Proceedings. Potsdam, 580-587, 2013.
- SEIFFERT, R.; HESSER, F.B.; SCHULTE-RENTROP, A. and SEIB, G.: Potential effects of climate change on the brackish water zone in German estuaries. In: HINKELMANN, R.-P., LIONG, Y., SAVIC, D., NASERMOADDELI, M.H., DAEMRICH, K.-F., FRÖHLE, P. and JACOB, D. (eds.): Hydroinformatics 2012.
- WILBY, R.L. and DESSAI, S.: Robust adaptation to climate change. In: *Weather*, Vol. 65, 7, 180-185, doi: 10.1002/wea.543, 2010.
- ZORNDT, A.C. and SCHLURMANN, T.: Investigating impacts of climate change on the Weser Estuary. *Die Küste*, 81, 2014.

Evaluation of Coastal Protection Strategies in Respect of Climate Change Impacts

Hanz Dieter Niemeyer, Cordula Berkenbrink, Anne Ritzmann, Heiko Knaack, Andreas Wurpts and Ralf Kaiser

Summary

The expected change of global climate will create impacts being an unknown challenge for coastal protection: Both, accelerated sea-level rise and stronger storms create higher set-ups of storm surges and stronger waves. Moreover, the adaption of intertidal areas in the coastal areas might be delayed providing larger water depths in front of coastal structures allowing again the occurrence of stronger waves. The question, if coastal lowlands could remain safe against the sea is of increasing importance. Alternatives to the presently exercised strategy of Keeping the Line of protection are discussed with reference to historical experience. For a quantitative comparison mathematical modelling of hydrodynamic loads for designing coastal protection structures is carried out for distinct scenarios of boundary conditions to be expected as consequence of climate change until the year 2100. As a final result protection by Keeping the Line is found to be the most favourable strategy in respect of both, safety and effectiveness. Based on these findings the adaptation strategy for coastal protection to climate change effects until 2100 was implemented by the State Government of Lower Saxony in 2013.

Keywords

coastal protection strategies, climate change impacts, accelerated sea level rise, storm surges, design

Zusammenfassung

Die zu erwartenden Folgewirkungen des globalen Klimawandels werden an den Insel- und Küstenschutz erhebliche Anforderungen von bisher nicht erlebtem Maß stellen: Beschleunigter Meeresspiegelanstieg und stärkere Sturmintensität führen zu höheren Staus bei Sturmfluten mit größeren Wassertiefen vor Schutzwerken, mit denen wiederum eine stärkere Seegangbelastung einhergeht. Darüber hinaus wird es eine verzögerte und abnehmende Anpassung von Watten an beschleunigte Anstiegsraten des Meeresspiegelanstiegs geben, die zu einer weiteren Vergrößerung der Wassertiefen und damit auch zu verstärkten Seegangbelastungen führen. Es stand daher zur Debatte, wie künftig der Insel- und Küstenschutz auszurichten sei, um den zu erwartenden Herausforderung erfolgreich und zugleich effektiv begegnen zu können. Deshalb wurden Alternativen zu der bisher traditionell seit Jahrhunderten angewandten Strategie linienhafter Schutz untersucht. Mit vergleichbaren Randbedingungen wurden in quantitativer Form die Konsequenzen alternativer Strategien im Vergleich zum linienhaften Schutz mit dem Maßstab gleicher Sicherheit für die zu schützenden Niederungsgebiete aufgezeigt, um eine objektive Evaluierung zu ermöglichen. Diese vergleichenden Untersuchungen mit alternativen Strategien haben eindeutig belegt, dass die Strategie linienhafter Schutz optimal hinsichtlich Sicherheit und Kosteneffizienz ist. Daher ist die

Strategie linienhafter Schutz Grundlage der in Niedersachsen von der Landesregierung eingeführten Anpassungsstrategie an Klimaänderungsfolgen bis 2100 geworden.

Schlagwörter

Küstenschutz-Strategien, Klimaänderungsfolgen, beschleunigter Meeresspiegelanstieg, Sturmfluten, Bemessung

Contents

1	Introduction	566
2	Chosen boundary conditions for the evaluation.....	567
2.1	Scenarios	567
2.2	Modelling.....	568
2.3	Resulting loads on the dykes	569
3	Evaluation of alternative strategies	569
3.1	Retreat	570
3.2	Accommodation.....	571
3.3	Set-Back	573
3.4	Combined Protection	574
4	Summary and Conclusions	575
5	Acknowledgements.....	575
6	References	576

1 Introduction

Changes in global climate and the consequently resulting acceleration of sea-level rise require a thorough re-evaluation of coastal protection strategies in many parts of the world. This yields also for the lowlands at the southern North Sea coast which are protected by a line of dykes since about 1,000 years. The anticipation of an accelerated sea-level rise due to global warming has raised the question if this strategy of Keeping the Line will still be appropriate or if alternatives should seriously be taken into consideration. This yields the more since furthermore a number of secondary effects of climate change will lead to stronger loads on coastal protection structures: increasing intensity of storms and consequently higher set-ups of storm surges (WOTH 2005) create as well larger water depths in front of coastal structures as the delayed adaptation of tidal flat levels to an accelerating sea-level rise (MÜLLER et al. 2007). Since wave heights and periods on tidal flats are strongly depth-controlled (NIEMEYER 1983; NIEMEYER and KAISER 2001) any increase of local water depth is accompanied by corresponding higher wave loads on coastal structures.

This contribution provides results on the evaluation of coastal protection strategies gained within the research theme A-KÜST in the framework of the KLIFF program for the German Federal State of Lower Saxony. KLIFF focuses on adaptation to climate

change effects and covers the topics agriculture, forestry and water management. A-KÜST is targeted at the evaluation of distinct coastal protection strategies like the historically practiced ones as well as those being discussed in earlier research projects (NIEMEYER 2005a, 2005b, 2010).

Major aim of the project is to compare alternative strategies with a methodical approach being in tune with the design practice due to the Lower Saxon Dyke Act. The alternative strategies are on the one hand the ones being already practiced in history like Retreat and Accommodation and on the other hand variations of Protection such as Set-Back or Combined Protection (Fig. 1). They have been compared with Keeping the Line as the traditional execution of the strategy Protection (NIEMEYER 2005a, 2005b, 2010).

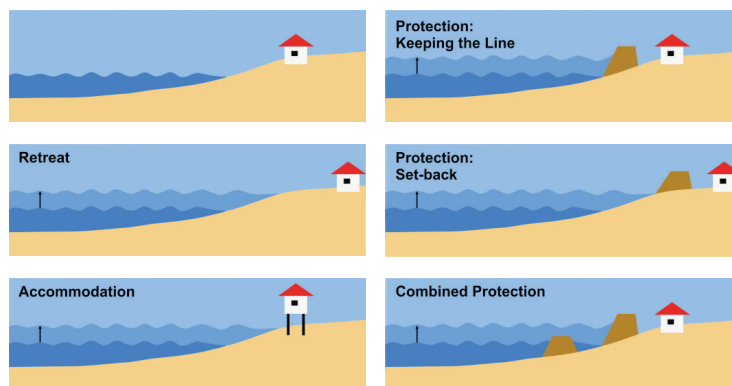


Figure 1: Alternative coastal protection strategies in response to sea-level rise (IPCC 1990) and adapted from COMCOAST (2007); (NIEMEYER 2005a, 2005b).

2 Chosen boundary conditions for the evaluation

As boundary conditions for the evaluation of coastal protection strategies design water levels and wave climate have been simulated for the southern North Sea for the present design conditions and for scenarios being both reliable and pessimistic for future climate change effects. On that basis hydrodynamic loads on coastal protection structures have been analysed by mathematical modelling for the test region Ems-Dollard estuary. The evaluation of hydrodynamic loads has been exercised with the same methodology and spatial resolution as applied for the actual design procedure for coastal protection structures in Lower Saxony.

2.1 Scenarios

Three scenarios for the development of hydrodynamic loads in the Dollard region till the end of the century were established (Fig. 2): the first one represents the actual design conditions with a safety measure for the design water level of 0.5 m created by a static water level rise of 25 cm – corresponding to measured one of MHWL at the southern North Sea coast during the last centuries – and an additional set up of 25 cm of storm surges due to higher gale forcing. For the second scenario the safety measure for the design water level has been increased to 1.0 m by a combination of a static water level rise

of 65 cm, which is in the same order of magnitude as the upper limit of sea level rise by IPCC (2007). Furthermore an increase of the set-up of storm surges of 35 cm due to stronger forcing by wind has been added in accordance with earlier investigations (WOTH et al. 2006) and recent ones in the framework of the research theme A-KÜST by the HZG Institute for Coastal Research (WEISSE et al. 2012). The third scenario is a pessimistic one with an increase of the safety measure for the design water level of 1.5 m due to an increase of the static water level of 100 cm and a heightening of the surge set-up of 50 cm by stronger storms. Since water depths as well as wind forcing increases for all three scenarios a corresponding growth of wave heights and periods is implemented.

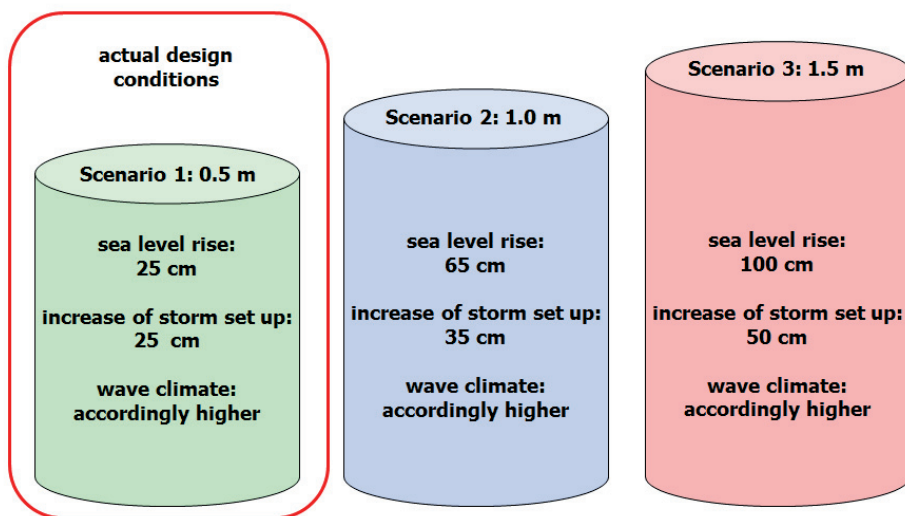


Figure 2: Scenarios for increasing design water levels.

2.2 Modelling

Modelling of the water level in the area of the Ems estuary was carried out by using a hierarchical cascade of three nested 2D-hydrodynamic models applying DELFT-3D with increasing resolution: the coarse Continental Shelf Model covering the whole North Sea and adjacent parts of the Atlantic, a model of the German Bight and a model of the Ems-Dollard estuary with a resolution of about 120 m (Fig. 3). The increase of sea level was implemented by adding the value respectively to the scenario on the water levels. The increase of surge however was effected by an increase of the respectively wind speed over the whole model cascade on the basis of a real storm surge from November 9th 2007 and adjusted for each scenario to the gauge Borkum at the entrance of the estuary.

Waves in front of the dykes were calculated applying the mathematical wave model SWAN coupled to the tidal model Delft-3D in two nested models considering the increased water levels of the scenarios and according wind conditions. The resolution of the inner model was 30 – 10 m. As offshore boundary of the outer model a JONSWAP spectrum with $H_{m0} = 10$ m, $T_p = 15$ s and a mean $Dir = 315^\circ$ was applied according to actual design practice in Lower Saxony (NIEMEYER 2001).

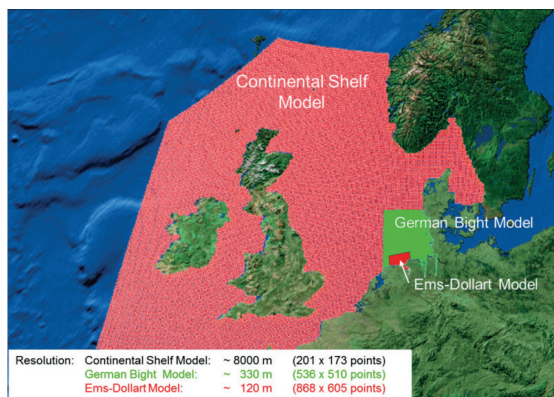


Figure 3: Model cascade.

2.3 Resulting loads on the dykes

Modelled peak water levels ascend considerably from the North Sea into the Ems-Dollard estuary (Fig. 4). For the chosen scenarios the increase intensifies the more the higher the absolute levels: e.g. for scenario one the safety measure of 0.5 m for the design water level at the gauge Borkum cause an increase of the design water levels of approximately 0.6 m in the inner part of the estuary.

Local wave conditions are strongly fluctuating according to coastline exposition to wind direction. Due to increasing wind velocities and growing water depths significant wave heights mount up by a magnitude of up to some decimetres and a gain in wave energy periods of up to approximately 0.5 s.

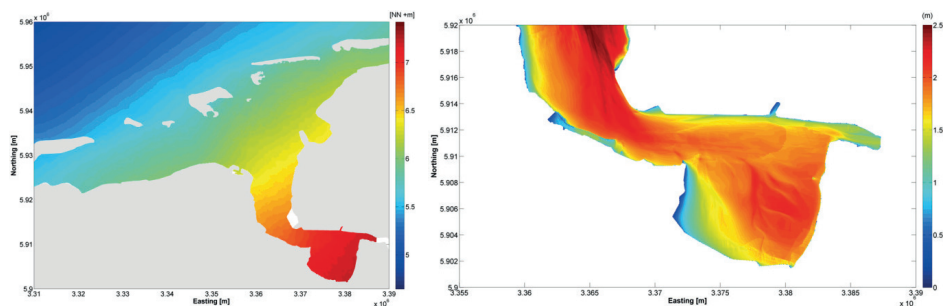


Figure 4: Left: Peak water levels for scenario 2. Right: Significant wave heights H_{m0} [m] for scenario 2.

3 Evaluation of alternative strategies

The present strategy for coastal protection in Germany is specified as Keeping the Line: In response to increasing hydrodynamic loads strengthening of the existing line of protection structures is performed (Fig. 5). The extension of the protected lowlands covers 14 % of the state and is inhabited by about 1.200000 people (REGIERUNGSKOMMISSION KLIMASCHUTZ 2012). Moreover, the safety against storm surges for a large number of

people living in the neighbouring federal states of Bremen and Hamburg and in the Dutch province Groningen depends on coastal protection. Without any protection they all would lose their homes and economic basis. The question in respect to climate change is, if the actual exercised strategy of Keeping the Line will remain feasible and if other strategies would be preferable. The results of that evaluation are presented here.

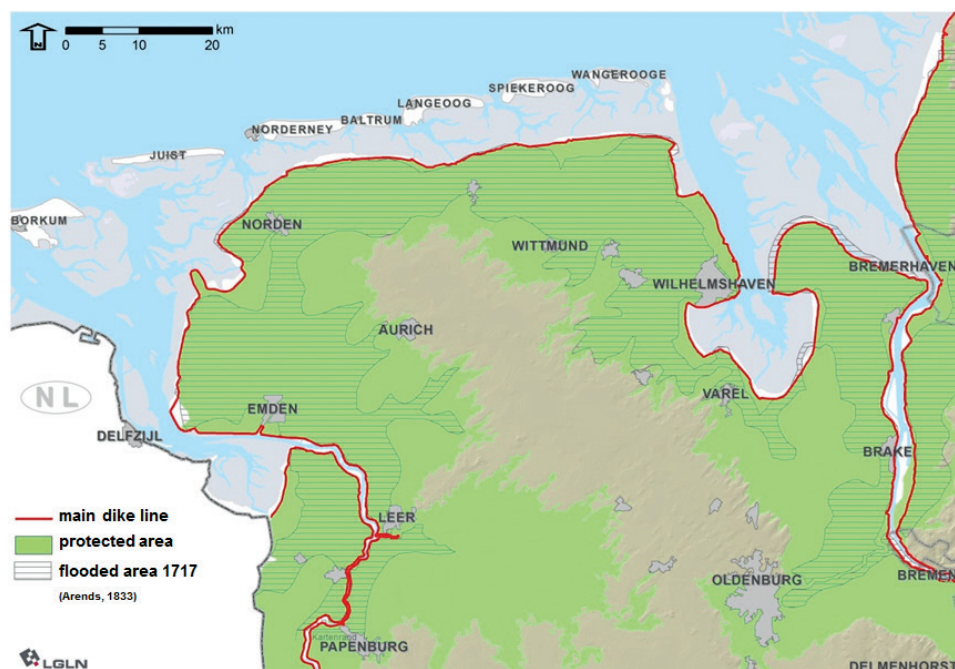


Figure 5: Protected lowlands in the western part of Lower Saxony (RITZMANN and NIEMEYER 2011).

3.1 Retreat

A retreat from all coastal areas being endangered by storm surges would induce enormous losses. A resettlement of the coastal population into areas being safe from inundation due to storm surges without any requirement of protection against storm surges would furthermore create a large burden for both, individuals and society. The extension of those areas becoming uninhabitable without protection against storm surges is enormous which is clearly demonstrated by those areas being nowadays designated by the Lower Saxon Dyke Act as protected coastal protection structures (Fig. 5). The vulnerability against very high storm surges in case of a non-effective coastal protection scheme is highlighted by the flooding due to the catastrophic Christmas Surge in 1717 as documented by ARENDS (1833) and edited by Hans Homeier (FORSCHUNGSSTELLE KÜSTE 1980) (Fig. 5). A storm surge with a similar gale forcing would nowadays flood even larger areas since the MHWL is about 0.75 m higher due to sea level rise (Fig. 6).

Abandoning coastal protection for the lowlands of Lower Saxony would not only affect the loss of homes and economic basis of the people living here, but also endanger an

almost equal number in neighbouring states being indirectly dependent on the Lower Saxon coastal protection system. Furthermore, the cultural heritage of the lowlands like e.g. medieval churches or prehistoric stone graves would be lost forever. Comparing the cost saving aspects due to a total withdrawal from coastal protection with the implicit enormous economic and cultural losses, this alternative is regarded as highly unfavourable. The effect of Retreat in respect of corresponding losses is sufficiently highlighted by the coastal flood prone areas as designated by the Lower Saxon Dyke Act. The impacts of future climate change simply evaluated by adding anticipated higher sea levels of 0.5 m and 1.0 m above present design water level (Fig. 6).

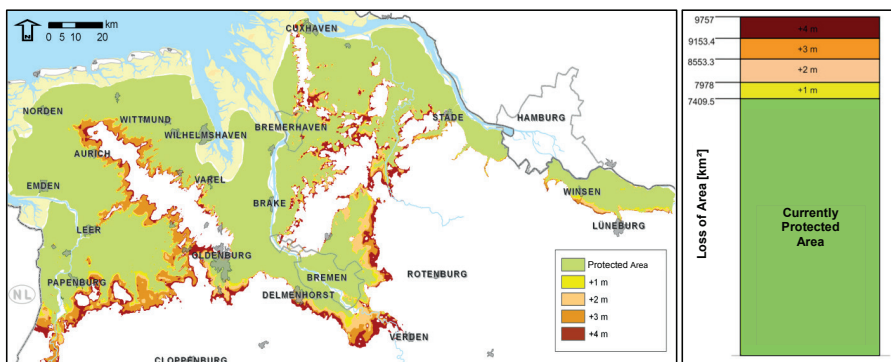


Figure 6: Abandoned land due to execution of the strategy Retreat from storm surge endangered areas (RITZMANN and NIEMEYER 2011).

3.2 Accommodation

Accommodation in the lowlands requires the creation of numerous protected islands with settlements and industrial areas in the lowlands along the coast and tidal estuaries. The use of the former dwelling mounds is deficient for safety against storm surges since the level of their surface is nowadays too low in respect of storm surge levels due to the sea-level rise which has taken place since their erection. A further heightening is only possible for a few ones without settlements and buildings. Most of the dwelling mounds are densely covered with buildings (Fig. 7).

Any rising of the level of inhabited dwelling mounds would require the dismantling and reconstruction of the existing infrastructure. The creation of well-chosen areas being protected by rings of surrounding dykes is therefore regarded as more appropriate for economic reasons. This yields the more since adaption of level heights of dwelling mounds to rising water levels would become repeatedly necessary in the future and would be again more costly than strengthening of dykes.

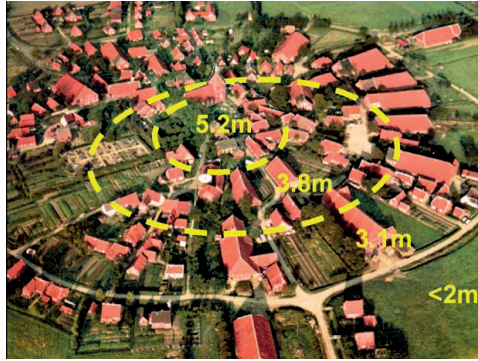


Figure 7: Dwelling mound village of Rysum in East Frisia with marker lines for existing levels above German datum; actual design water level in the area is about 6.5 m above German datum (RITZMANN and NIEMEYER 2012).

A schematic example of an area with low population density highlights the enormous efforts being necessary to create those safe havens against storm surges in the lowlands (Fig. 8). Major advantage of the strategy Accommodation is the anticipation of a significantly reduced length of the dyke line. In the investigated area of western East Frisia in Lower Saxony this would be only achieved if solely the settlements with more than 20.000 inhabitants experienced a protection against storm surges by surrounding dykes. But compared to the size of the protected area the economical aspect is not given (Fig. 9).

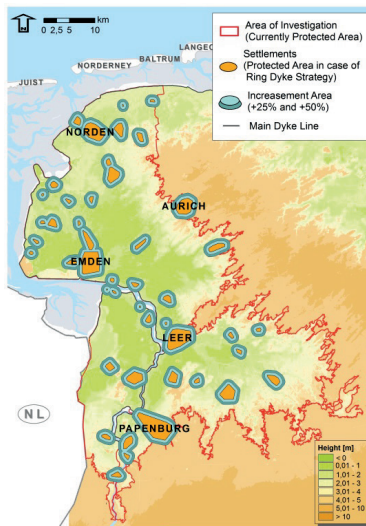


Figure 8: Dyke rings for large settlements and commercial sites (RITZMANN and NIEMEYER 2012).

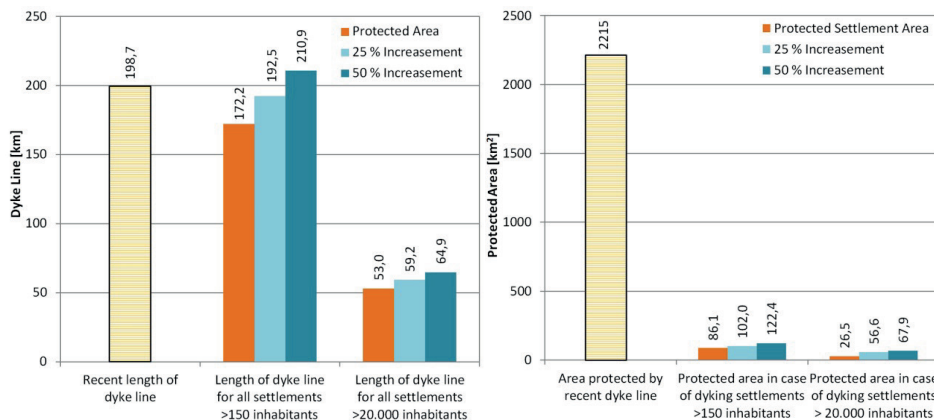


Figure 9: Comparison of the strategies Accommodation by dyke rings and Protection by Keeping the Line. Left: Length of the necessary dyke line. Right: Protected area (RITZMANN and NIEMEYER 2012).

Furthermore infrastructure like e.g. roads, railways or transmission links of energy between the safe havens would be more vulnerable against the impact of storm surges and would require much higher maintenance costs than in protected areas. Already a rough comparison makes it evident that Accommodation as an alternative coastal protection strategy for dealing with an accelerating sea-level rise will require high investments corresponding with enormous economic losses due to the abandonment of smaller settlements and agricultural revenues on the one hand and increasing maintenance costs of infrastructure after flooding due to storm surges. For areas like the lowlands at the Lower Saxon coast the strategy Accommodation is therefore extremely unfavourable in comparison to protection of the areas in total.

3.3 Set-Back

Other options which are discussed as alternative strategies are modifications of protection like Set-Back or realignment by erecting a new protection line in a larger distance from the coastline creating a belt of salt marshes with the aim of a stronger attenuation of waves (COMCOAST 2007). But that concept neglects that in embanked areas no longer sedimentation could take place after earlier embankments of salt marshes. Whereas the salt marshes in front of the dykes could grow furthermore, the embanked ones remained at the level before their embankment. Therefore the gradient of the surface level is declining from the present coastline inland leading to lower surface levels the more away from the sea. After a Set-Back of dyke line water depths in front of a dyke in a certain distance from the present coastline will increase. Consequently, wave loads on the dyke will be higher than at the present coastline. An example of a Set-Back of 3.5 km at the Dollard Bay makes evident by wave modelling that for design conditions significant wave heights increase by approximately 15 % and energy periods by approximately 8 % (Fig. 10) which furthermore results in an increase of wave run-up of approximately 20 %.

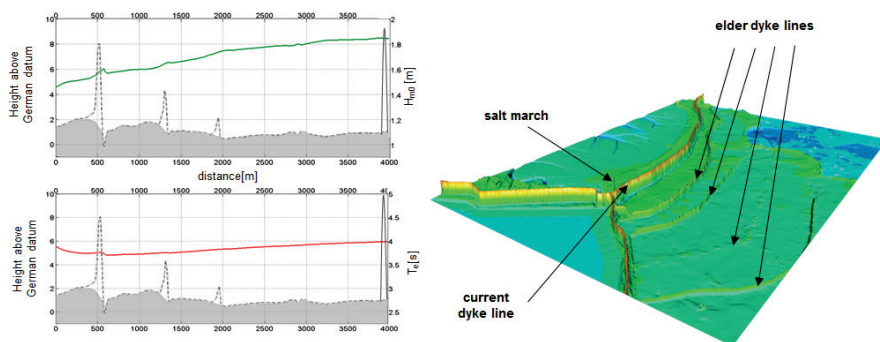


Figure 10: Left: Increase of significant wave height (top) and energy period (bottom) after Set-Back of a dyke. Right: Set-Back of dyke lines in the past (KAISER et al. 2010).

Already this simple example highlights that the Set-Back of a dyke line in coastal lowlands has no advantages: wave loads are higher and require a higher structure for protection against storm surges than at the present coastline. Furthermore, that strategy would demand enormous efforts for the construction of a totally new dyke line landward of the existing one and the necessary compensation of the private land owners according to existing law. An unquestionable advantage being achieved by a Set-Back of a dyke line would be the creation of large areas of salt marshes which are regarded as highly valuable with respect to ecology. But in respect of coastal protection a Set-Back of dyke lines is unfavourable in regard of safety and economics.

3.4 Combined Protection

Another alternative for protection of the hinterland is the two-line strategy: a combination of two structures for coastal protection: the most seaward one with the aim to act as a submerged breakwater and in a certain distance another one being sufficiently high to keep storm surges levels at bay. This assumption is mainly based on observations of wave damping in the shelter of summer dykes during lower storm surges. But observations during higher storm surges highlighted their decreasing effectiveness due to higher water levels (NIEMEYER and KAISER 1998, 2001). Mathematical wave modelling has proved this result to a much further extent (NIEMEYER and KAISER 1998, 2001): Even for present design conditions the effect of the existing summer dykes as submerged breakwaters are reduced to small insignificant numbers (Fig. 11) which are even insufficient to justify the maintenance of summer dykes.

In order to create submerged breakwaters being even effective for an accelerating sea-level rise, significantly higher efforts would be required than the maintenance or construction of structures with dimensions like the nowadays existing summer dykes: Investment costs will be very high since the construction must be strongly armoured in order to avoid its destruction by overflow during a storm surge leading to strong wave attack on the second dyke which is highly vulnerable against wave attack would then endanger the whole protected hinterland.

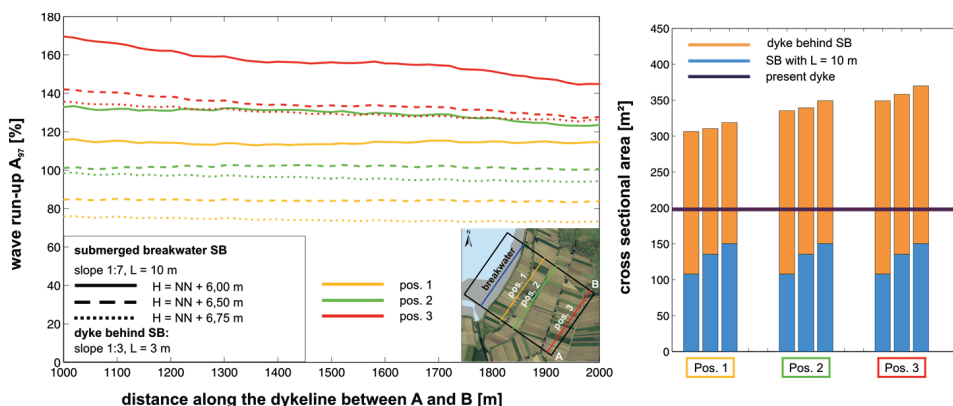


Figure 11: Left: Wave run-up at dykes behind a submerged breakwater. Right: needed cross sectional area for a conventional dyke due to Keeping the Line compared to Combined Protection (NIEMEYER et al. 2011b).

Combined Protection with two lines of structures is not expected being safer than the line protection with one single structure as practiced since 1000 years. Moreover, this alternative strategy will require higher investment costs and probably also an increase of maintenance costs in comparison with the traditional one.

4 Summary and Conclusions

Global climate change and its anticipated impacts like e.g. acceleration of sea-level rise or higher set-up of storm surges require a thorough and reliable evaluation of coastal protection strategies. This work provides investigation results carried out in the research theme A-KÜST being a constituent of the research framework KLIFF in the German Federal State of Lower Saxony. The evaluation is carried out by means of mathematical models and aimed at the reproduction of real world conditions both for hydrodynamic loads on structures and their design. The results are representative for the lowlands coasts at the southern North Sea and are transferrable for coasts with similar boundary conditions worldwide.

Since about 1000 years the lowlands at the Lower Saxon lowland coast is protected by a single dyke line which is also common practice at other lowland coasts at the southern North Sea. In the past, these protection structures have been strengthened in response to increasing hydrodynamic loads. The evaluation of distinct strategies has highlighted that these strategy will also be preferable in future, even for the enormous increase of hydrodynamic loads to be expected by climate change impacts until 2100.

Based on this results an adaption strategy for coastal protection has been developed and afterwards been implemented by the State Government of Lower Saxony in 2013.

5 Acknowledgements

The research on alternative coastal protection strategies is carried out jointly by the Coastal Research Station of the Lower Saxony Water Management, Coastal Defence and Nature Conservation Agency as lead partner with the following partner institutions in the

framework of the project A-KÜST: Helmholtz Centre Geesthacht-Institute for Coastal Research, Coastal Research Laboratory/Kiel University, Institute for Communication on Environmental Problems/Leuphana University Lüneburg. The research theme A-KÜST is part of the KLIFF-programme (Research on Effects of Climate Change) being launched and sponsored by the Lower Saxon Ministry for Science and Culture.

6 References

- ARENDS, F.: Physische Geschichte der Nordseeküste und deren Veränderungen durch Sturmfluthen seit der Cymbrischen Fluth bis jetzt. Emden, 1833.
- COMCOAST: The future of flood risk management. www.comcoast.org, 2007.
- FORSCHUNGSSTELLE KÜSTE: Reisefibel. Forschungsstelle Küste, Norderney, 1980.
- IPCC (Intergovernmental Panel on Climate Change): Strategies for adaption to sea-level rise. Executive Summary of the Coastal Zone Management Subgroup. Intergovernmental Panel on Climate Change – Response Strategies Working Group. The Hague/The Netherlands, 1990.
- IPCC (Intergovernmental Panel on Climate Change) SOLOMON, S.; QIN, D.; MANNING, M.; CHEN, Z.; MARQUIS, M.; AVERYT, K.B.; TIGNOR, M. and MILLER, H.L. (Eds.): Summary for Policymakers. Climate Change 2007: The Physical Science Basis. Contribution of Working Group I to the Fourth Assessment Report of the IPCC. Cambridge University Press, United Kingdom and New York, NY, USA, 2007.
- KAISER, R.; KNAACK, H.; MIANI, M. and NIEMEYER, H.D.: Examination of Climate Change adaptation strategies for Coastal Protection. In: MCKEE SMITH, J. and LYNETT, P. (Eds.): Proceedings of the 32nd International Conference on Coastal Engineering 2010, Shanghai, 2010 (<http://journals.tdl.org/icce/index.php/icce/issue/view/154/showToc>).
- MÜLLER, J.-M.; ZITMAN, T.; STIVE, M. and NIEMEYER, H.D.: Long-Term Morphological Evolution of the Tidal Inlet “Norderneyer Seegat”. In: MCKEE SMITH, J. (Ed.): Proceedings of the 30th International Conference on Coastal Engineering, San Diego 2006, World Scientific, New Jersey, 4035-4046, 2007.
- NIEMEYER, H.D.: Über den Seegang an einer inselgeschützten Wattküste. BMFT – research report. MF 0203, 1983.
- NIEMEYER, H.D.: Sturmflutschutz an Niederungsküsten – sind alternative Strategien sinnvoll? In: FANSA, M. (Ed.): Kulturlandschaft Marsch, Natur – Geschichte – Gegenwart. Isensee-Verl., Oldenburg, 204-213, 2005a.
- NIEMEYER, H.D.: Coastal protection of Lowlands: Are alternative strategies purposeful for changing climate? In: Proceedings of the 14th Biennial Coastal Zone Conference, New Orleans/Louisiana, 17-21, 2005b.
- NIEMEYER, H.D.: Protection of Coastal Lowlands: Are Alternative Strategies a Match to Effects of Climate Change? In: Proceedings of 17th IAHR-APD Conference, Auckland/New Zealand, 811-820, 2010.
- NIEMEYER, H.D. and KAISER, R.: Modeling of Effectiveness of Wave Damping Structures in Wadden Sea Areas. In: Proceedings of 5th International Workshop on Wave Hindcasting and Forecasting. Melbourne/Florida, 231-238, 1998.

- NIEMEYER, H.D. and KAISER, R.: Hydrodynamische Wirksamkeit von Lahnungen, Hellern und Sommerdeichen. In: KFKI (Ed.): Die Küste, Heft 64, Boyens & Co. KG, Heide i. Holstein, 15-60, 2001.
- NIEMEYER, H.D.; KAISER, R.; KNAACK, H.; DISSANAYAKE, P.; MIANI, M.; ELSEBACH, J.; BERKENBRINK, C.; HERRLING, G. and RITZMANN, A.: Evaluation of Coastal Protection Strategies for Lowlands in Respect of Climate Change. In: VALENTINE, E.M.; APELT, C.J.; BALL, J.; CHANSON, H.; COX, R.; ETTEMA, R.; KUCZERA, G.; LAMBERT, M.; MELVILLE, B.W. and SARGISON, J.E. (Eds.): Proceedings of the 34th World Congress of the International Association for Hydro-Environment Research and Engineering: 33rd Hydrology and Water Resources Symposium and 10th Conference on Hydraulics in Water Engineering. Barton, A.C.T.: Engineers Australia, 1218-1225, 2011a.
- NIEMEYER, H.D.; BERKENBRINK, C.; MIANI, M.; RITZMANN, A.; DISSANAYAKE, P.; KNAACK, H.; WURPTS, A. and KAISER, R.: Coastal Protection of Lowlands: Are Alternative Strategies a Match to Effects of Climate Change? In: SCHÜTTRUMPF, H. and TOMASSICCHIO, G.R. (Eds.): Proceedings of the 5th International Short Conference on Applied Coastal Research, 299-307, 2011b.
- NIEMEYER, H.D.; KAISER, R.; BERKENBRINK, C.; KNAACK, H. and WURPTS, A.: Evaluierung alternativer Küstenschutz-Strategien in Niedersachsen. Wasser und Abfall 14, Nr. 7/8, 21-26, 2012.
- REGIERUNGSKOMMISSION KLIMASCHUTZ – Niedersächsisches Ministerium für Umwelt, Energie und Klimaschutz: Empfehlung für eine niedersächsische Strategie zur Anpassung an die Folgen des Klimawandels, 49-57; 147-144; 180-181, 2012 (<http://www.umwelt.niedersachsen.de/klimaschutz/aktuelles/107128.html>).
- RITZMANN, A. and NIEMEYER, H.D.: Gebietsverluste bei der Strategie Rückzug als Reaktion auf Klimaänderungsfolgen im niedersächsischen Tidegebiet. Forschungsbericht 02/2011, NLWKN-Forschungsstelle Küste, 2012 (unveröff.).
- RITZMANN, A. and NIEMEYER, H.D.: Gebietsverluste bei der Strategie Anpassung als Reaktion auf Klimaänderungsfolgen im niedersächsischen Tidegebiet, Forschungsbericht 02/2012, NLWKN- Forschungsstelle Küste, 2012 (unveröff.).
- WEISSE, R.; VON STORCH, H.; NIEMEYER, H.D. and KNAACK, H.: Changing North Sea Storm Surge Climate: An Increasing Hazard? *Ocean & Coastal Management*, Vol. 68, 58-68. doi: 10.1016//j.ocecoaman.2011.09.005, 2012.
- WOTH, K: North Sea storm surge statistics based on projections in a warmer climate: How important are the driving GCM and the chosen emission scenario? In: *Geophysical Research Letters*, Vol. 32, doi: 10.1029/2005GL023762, 2005.
- WOTH, K; WEISSE, R. and v. STORCH, H.: Climate Change and North Sea Storm Surge Extremes: Ensemble Study of Storm Surge Extremes Expected in a Changed Climate Projected by Four Different Regional Climate Models. *Ocean Dynamics*, Vol. 56, 3-15, 2006.

Authorindex

Arns Arne

Universität Siegen, Forschungsinstitut Wasser und Umwelt, Abteilung Wasserbau und Hydromechanik
arne.arns@uni-siegen.de

Behrens Arno

Helmholtz-Zentrum Geesthacht
arno.behrens@hzg.de

Berkenbrink Cordula

Nds. Landesbetrieb für Wasserwirtschaft, Küsten- und Naturschutz
cordula.berkenbrink@nlwkn-ny.niedersachsen.de

Beyer Ronny

Wasser- und Schifffahrtsamt Hamburg
ronny.beyer@wsv.bund.de

Brecht Benedict

Deutscher Wetterdienst
benedict.brecht@dwd.de

Brüning Anja

DHI-WASY GmbH
abu@dhigroup.com

Brüning Thorger

Bundesamt für Seeschifffahrt und Hydrographie Hamburg
thorger.bruening@bsh.de

Burchard Hans

Institut für Ostseeforschung Warnemünde IOW
hans.burchard@io-warnemuende.de

Burzel Andreas

Deltares, Inland Water Systems
andreas.burzel@deltares.nl

Daemrich Karl-Friedrich

Leibniz Universität Hannover
schlurmann@fi.uni-hannover.de

Dassanayake Dilani R.

Technische Universität Braunschweig, Leichtweiß Institut für Wasserbau
dilani.dassanayake@tu-braunschweig.de

Dick Stephan

Bundesamt für Seeschifffahrt und Hydrographie Hamburg
stephan.dick@bsh.de

Donner Monika

DHI-WASY GmbH, Hydrodynamics and Coastal Engineering
mod@dhi-wasy.de

Elsebach Johanna

Nds. Landesbetrieb für Wasserwirtschaft, Küsten- und Naturschutz
postfach@nlwkn-ny.niedersachsen.de

Frank Helmut

Deutscher Wetterdienst
helmut.frank@dwd.de

Fröhle Peter

Technische Universität Hamburg-Harburg, Institut für Wasserbau
froehle@tuhh.de

Gaslikova Lidia

Helmholtz-Zentrum Geesthacht
lidia.gaslikova@hzg.de

Gerkenmeier Birgit

Freie und Hansestadt Hamburg, Landesbetrieb Straßen, Brücken und Gewässer
birgit.gerkenmeier@lsbg.hamburg.de

Geyer Beate

Helmholtz-Zentrum Geesthacht
beate.geyer@hzg.de

Gönnert Gabriele

Freie und Hansestadt Hamburg, Landesbetrieb Straßen, Brücken und Gewässer
Gabriele.Goennert@lsbg.hamburg.de

Goseberg Nils

Leibniz Universität Hannover, Franzius-Institut für Wasserbau, Ästuar- und
Küsteningenieurwesen
goseberg@fi.uni-hannover.de

Grabemann Iris

Helmholtz-Zentrum Geesthacht
iris.grabemann@hzg.de

Gräwe Ulf

Institut für Ostseeforschung Warnemünde
ulf.graewe@io-warnemuende.de

Groll Nikolaus

Helmholtz-Zentrum Geesthacht
nikolaus.groll@hzg.de

Hammrich Arne

DHI-WASY GmbH
arh@dhi-wasy.de

Hein Birte

Bundesanstalt für Gewässerkunde
birte.hein@bafg.de

Herrling Gerald

MARUM - Zentrum für Marine Umweltwissenschaften, Universität Bremen
gherrling@marum.de

Hesser Fred

Bundesanstalt für Wasserbau
fred.hesser@baw.de

Heyer Harro

Bundesanstalt für Wasserbau
holger.rahlh@baw.de

Holtermann Peter

Institut für Ostseeforschung Warnemünde
peter.holtermann@io-warnemuende.de

Jandt Simon

Bundesamt für Seeschifffahrt und Hydrographie Hamburg
simon.jandt@bsh.de

Janssen Frank

Bundesamt für Seeschifffahrt und Hydrographie Hamburg
frank.janssen@bsh.de

Jensen Jürgen

Universität Siegen, Forschungsinstitut Wasser und Umwelt, Abteilung Wasserbau und Hydromechanik
jensen@fb10.uni-siegen.de

Kaiser Ralf

Nds. Landesbetrieb für Wasserwirtschaft, Küsten- und Naturschutz
ralf.kaiser@nlwkn-ny.niedersachsen.de

Kastens Marko

Bundesanstalt für Wasserbau Hamburg
marko.kastens@baw.de

Kirchesch Volker

Bundesanstalt für Gewässerkunde
volker.kirchesch@bafg.de

Kleine Eckhard

Bundesamt für Seeschifffahrt und Hydrographie Hamburg
eckhard.kleine@bsh.de

Klingbeil Knut

Institut für Ostseeforschung Warnemünde
knut.klingbeil@io-warnemuende.de

Knaack Heiko

Nds. Landesbetrieb für Wasserwirtschaft, Küsten- und Naturschutz
heiko.knaack@nlwkn-ny.niedersachsen.de

Komo Hartmut

Bundesamt für Seeschifffahrt und Hydrographie Hamburg
harmut.komo@bsh.de

Konietzky Heinz

Technische Universität Bergakademie Freiberg, Institut für Geotechnik
heinz.konietzky@ifgt.tu-freiberg.de

Koppe Roland

Alfred-Wegener-Institut, Helmholtz-Zentrum für Polar und Meeresforschung
roland.koppe@awi.de

Kortenhaus Andreas

Technische Universität Braunschweig, Abt. Hydromechanik und Küsteningenieurwesen
a.kortenhaus@tu-bs.de

Kösters Frank

Bundesanstalt für Wasserbau
frank.koesters@baw.de

Krämer Knut

Leibniz Universität Hannover, Franzius-Institut für Wasserbau, Ästuar- und Küsteningenieurwesen
kraemer@fi.uni-hannover.de

Kristandt Jana

Nds. Landesbetrieb für Wasserwirtschaft, Küsten- und Naturschutz
jana.kristandt@nlwkn-nor.niedersachsen.de

Lehfeldt Rainer

Bundesanstalt für Wasserbau
rainer.lehfeldt@baw.de

Lojek Oliver

Leibniz Universität Hannover, Franzius-Institut für Wasserbau, Ästuar- und Küsteningenieurwesen
lojek@fi.uni-hannover.de

Malcherek Andreas

Universität der Bundeswehr München, Institut für Wasserwesen
andreas.malcherek@unibw-muenchen.de

Maßmann Silvia

Bundesamt für Seeschifffahrt und Hydrographie Hamburg
silvia.massmann@bsh.de

Matelski Birgit

Landesbetrieb für Küstenschutz, Nationalpark und Meeresschutz Schleswig-Holstein
Husum
birgit.matelski@lkn.landsh.de

Melles Johannes
Bundesamt für Seeschifffahrt und Hydrographie Hamburg
johannes.melles@bsh.de

Menzenhauer-Schuhmacher Inge
Bundesamt für Seeschifffahrt und Hydrographie Hamburg
inge.menzenhauer-schuhmacher@bsh.de

Meyer Elke
Helmholtz-Zentrum Geesthacht
elke.meyer@hzg.de

Milbradt Peter
smileconsult GmbH
milbradt@smileconsult.de

Mittelbach Livia
Bundesanstalt für Wasserbau
livia.mittelbach@baw.de

Mudersbach Christoph
Hochschule Bochum
christoph.mudersbach@hs-bochum.de

Müller Jan-Moritz
Freie und Hansestadt Hamburg, Landesbetrieb Straßen, Brücken und Gewässer
jan-moritz.mueller@lsbg.hamburg.de

Naulin Marie
Bundesanstalt für Wasserbau
marie.naulin@baw.de

Neumann Lothar
Wasser- und Schifffahrtsamt Hamburg
lothar.neumann@wsv.bund.de

Niemeyer Hanz Dieter
Nds. Landesbetrieb für Wasserwirtschaft, Küsten- und Naturschutz
andreas.wurpts@nlwkn-ny.niedersachsen.de

Oberrecht Dennis
Nds. Landesbetrieb für Wasserwirtschaft, Küsten- und Naturschutz, Norderney
dennis.oberrecht@nlwkn-ny.niedersachsen.de

Orths Axel
Wasser- und Schifffahrtsamt Cuxhaven
axel.orths@wsv.bund.de

Oumeraci Hocine
Technische Universität Braunschweig, Leichtweiß Institut für Wasserbau
h.oumeraci@tu-braunschweig.de

Pasche Erik †

Technische Universität Hamburg-Harburg, Institut für Wasserbau
froehle@tuhh.de

Plüß Andreas

Bundesanstalt für Wasserbau
andreas.pluess@baw.de

Pohl Martin

Bundesanstalt für Wasserbau
martin.pohl@baw.de

Precht Elimar

DHI-WASY GmbH
epr@dhigroup.com

Putzar Bert

Universität der Bundeswehr München, Institut für Wasserwesen
bert.putzar@unibw.de

Ritzmann Anne

Nds. Landesbetrieb für Wasserwirtschaft, Küsten- und Naturschutz
anne.ritzmann@nlwkn-ny.niedersachsen.de

Rudolph Elisabeth

Bundesanstalt für Wasserbau
elisabeth.rudolph@baw.de

Schäfer Angela

Alfred-Wegener-Institut, Helmholtz-Zentrum für Polar und Meeresforschung
angela.schaefer@awi.de

Schlurmann Torsten

Leibniz Universität Hannover, Franzius-Institut für Wasserbau, Ästuar- und
Küsteningenieurwesen
schlurmann@fi.uni-hannover.de

Schöl Andreas

Bundesanstalt für Gewässerkunde
schoel@bafg.de

Schubert Reiner

Bundesanstalt für Wasserbau
reiner.schubert@baw.de

Schulze Peter

Bundesanstalt für Wasserbau
peter.schulze@baw.de

Schulz-Stellenfleth Johannes

Helmholtz-Zentrum Geesthacht, Zentrum für Material- und Küstenforschung
johannes.schulz-stellenfleth@hzg.de

Schuster Dagmar
Hamburg Port Authority
arh@dhi-wasy.de

Seiffert Rita
Bundesanstalt für Wasserbau
rita.seiffert@baw.de

Seiß Guttram
Bundesanstalt für Wasserbau
guntram.seiss@baw.de

Stanev Emil
Helmholtz-Zentrum Geesthacht, Zentrum für Material- und Küstenforschung
emil.stanev@hzg.de

Staneva Joanna
Helmholtz-Zentrum Geesthacht, Zentrum für Material- und Küstenforschung
joanna.staneva@hzg.de

Stoschek Oliver
DHI-WASY GmbH, Hydrodynamics and Coastal Engineering
ost@dhi-wasy.de

Tayel Mohamed
Leichtweiß-Institut für Wasserbau, Abt. Hydromechanik und Küsteningenieurwesen
m.tayel@tu-braunschweig.de

Thumm Sigrid
Freie und Hansestadt Hamburg, Landesbetrieb Straßen, Brücken und Gewässer
sigrid.thumm@lsbg.hamburg.de

Ujeyl Gehad
Institut für Wasserbau, Technische Universität Hamburg-Harburg
gehad.ujeyl@tu-harburg.de

Umlauf Lars
Institut für Ostseeforschung Warnemünde
lars.umlau@io-warnemuende.de

Valerius Jennifer
Bundesamt für Seeschifffahrt und Hydrographie Hamburg
jeniffer.valerius@bsh.de

Wahl Thomas
Universität Siegen, Forschungsinstitut Wasser und Umwelt, Abteilung Wasserbau und Hydromechanik
thomas.wahl@uni-siegen.de

Wehr Denise
Bundesanstalt für Wasserbau
denise.wehr@baw.de

Weilbeer Holger
Bundesanstalt für Wasserbau
holger.weilbeer@baw.de

Weisse Ralf
Helmholtz-Zentrum Geesthacht
ralf.weisse@hzg.de

Winskowsky Ulrich
Landesbetrieb für Küstenschutz, Nationalpark und Meeresschutz Schleswig-Holstein
Husum
ulrich.winskowsky@lkn.landsh.de

Wurpts Andreas
Nds. Landesbetrieb für Wasserwirtschaft, Küsten- und Naturschutz
andreas.wurpts@nlwkn-ny.niedersachsen.de

Wyrwa Jens
Bundesanstalt für Gewässerkunde
wyrwa@bafg.de

Zeiler Manfred
Bundesamt für Seeschifffahrt und Hydrographie Hamburg
manfred.zeiler@bsh.de

Zorndt Anna
Leibniz Universität Hannover, Franzius-Institut für Wasserbau, Ästuar- und
Küsteningenieurwesen
zorndt@fi.uni-hannover.de